SANDIA REPORT
SAND2012-0040
Unlimited Release
Printed January 2012

Protection Characteristics of a Faraday Cage Compromised by Lightning Burnthrough

Larry K. Warne, Roy E. Jorgenson and Rebecca S. Coats
Electromagnetic Theory Dept.
Leonard E. Martinez, John M. Jojola and Sandra L. Montoya
Electromagnetic Effects Dept.
Kimball O. Merewether
Weapon Surety & EM Engineering Dept.
Edward Bystrom
Sensing & Imaging Technologies Dept.

Prepared by
Sandia National Laboratories
Albuquerque, New Mexico 87185 and Livermore, California 94550

Sandia National Laboratories is a multi-program laboratory managed and operated by Sandia Corporation, a wholly owned subsidiary of Lockheed Martin Corporation, for the U.S. Department of Energy's National Nuclear Security Administration under contract DE-AC04-94AL85000.

Issued by Sandia National Laboratories, operated for the United States Department of Energy by Sandia Corporation.

Available to DOE and DOE contractors from
U.S. Department of Energy
Office of Scientific and Technical Information
P.O. Box 62
Oak Ridge, TN 37831

Telephone: (865) 576-8401
Facsimile: (865) 576-5728
E-Mail: reports@adonis.osti.gov
Online ordering: http://www.osti.gov/bridge

Available to the public from
U.S. Department of Commerce
National Technical Information Service
5285 Port Royal Rd.
Springfield, VA 22161

Telephone: (800) 553-6847
Facsimile: (703) 605-6900
E-Mail: orders@ntis.fedworld.gov
Online order: http://www.ntis.gov/help/ordermethods.asp?loc=7-4-0#online

SAND2012-0040
Unlimited Release
Printed January 2012

Protection Characteristics of a Faraday Cage Compromised by Lightning Burnthrough

Larry K. Warne, Roy E. Jorgenson, and Rebecca S. Coats
Electromagnetic Theory Dept. 01652

Leonard E. Martinez, John M. Jojola, and Sandra L. Montoya
Electromagnetic Effects Dept. 01653

Kimball O. Merewether
Weapon Surety & EM Engineering Dept. 0433

Edward Bystrom
Sensing & Imaging Technologies Dept. 01535

Sandia National Laboratories
P. O. Box 5800
Albuquerque, NM 87185-1152

Abstract

A lightning flash consists of multiple, high-amplitude but short duration return strokes. Between the return strokes is a lower amplitude, continuing current which flows for longer duration. If the walls of a Faraday cage are made of thin enough metal, the continuing current can melt a hole through the metal in a process called burnthrough. A subsequent return stroke can couple energy through this newly-formed hole. This LDRD is a study of the protection provided by a Faraday cage when it has been compromised by burnthrough. We initially repeated some previous experiments and expanded on them in terms of scope and diagnostics to form a knowledge baseline of the coupling phenomena. We then used a combination of experiment, analysis and numerical modeling to study four coupling mechanisms: indirect electric field coupling, indirect magnetic field coupling, conduction through plasma and breakdown through the hole. We discovered voltages higher than those encountered in the previous set of experiments (on the order of several hundreds of volts).

Intentionally Left Blank

Contents

Figures

Tables

Intentionally Left Blank

Protection Characteristics of a Faraday Cage Compromised by Lightning Burnthrough

1 INTRODUCTION

A lightning flash can be comprised of several high-amplitude, short-duration return strokes. Between the return strokes, a lower amplitude but longer duration current, called the continuing current, can flow through the lightning channel. Figure 1 taken from a report by Fisher [1], shows the average value and the one-percentile level of some lightning parameters. An undamaged Faraday cage protects components in its interior from the high voltage caused by the electric charges and rapid current rise rate of the first return stroke. If the walls of a Faraday cage are made of thin enough metal, the continuing current can melt a hole on the order of one to two cm in diameter through the metal in a process called burnthrough. A subsequent return stroke can then couple energy to a cable that happens to be in the vicinity of the newly-formed hole, which guides the energy to the sensitive components. Figures 2, 3, and 4 show three different scenarios for creating differential mode current on a cable system; the first has a connection to chassis ground and the next two are floating cable systems.

Table 2
Recommended Direct-Strike Lightning Environment for Future STSs

ABNORMAL LIGHTNING ENVIRONMENTS

A lightning strike directly to the warhead or to equipment associated with the warhead is considered a credible possibility. The lightning could be of either the cloud-to-ground or cloud flash (intracloud, intercloud, or cloud-to-air) type. Extreme (1% frequency of occurrence) and median (50%) values are given below for those cloud-to-ground flash parameters considered to constitute the most important threats to the weapon. Corresponding cloud flash parameters fall within the envelope defined below and are therefore not separately listed.

RETURN STROKE PARAMETERS[1]	1%	50%
a. Peak Current (kA)	200	30
b. Time to Peak (μs)	0.1-15	3
c. Max. Rate of Current Rise (kA/μs)	400	150
d. Time to Decay to Half Peak (μs)	10-500	50
e. Amplitude of Continuing Current[2] (A)	30-700	150
f. Duration of Continuing Current (ms)	500	150
FLASH PARAMETERS		
a. Number of Strokes	>20	4
b. Interstroke Interval (ms)	10-500	60
c. Total Flash Duration (ms)	30-1000	180
d. Total Charge Transfer (C)	350	15
e. Action [$\int i^2 dt$] ($A^2 \cdot s$)	3×10^6	5×10^4

[1]The entire cloud-to-ground discharge may be comprised of multiple individual major current pulses. These are known as return strokes or, simply strokes.

[2]Continuing currents can occur between individual strokes, following the final stroke in a flash, or both.

Figure 1. Parameters of a lightning flash

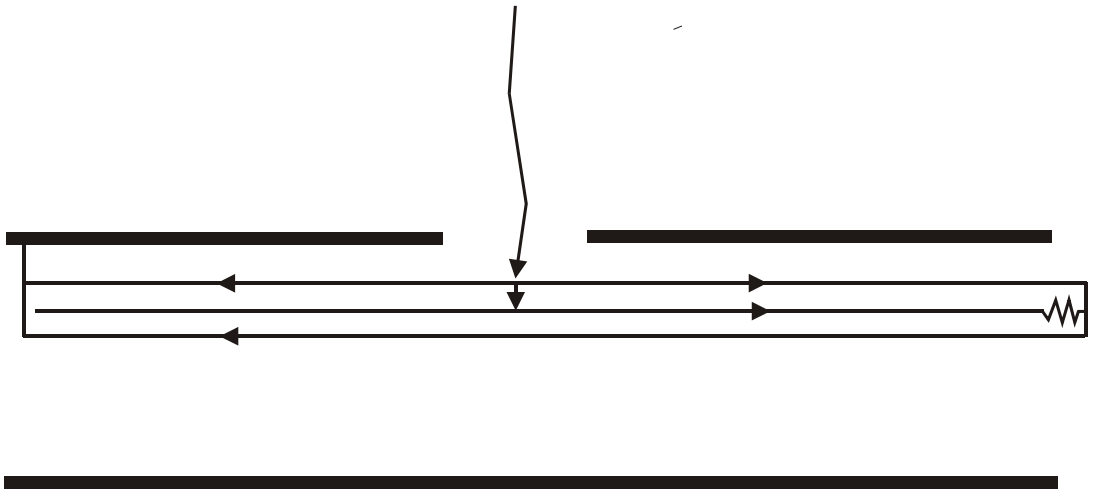

Figure 2. Conceptual coupling to a cable in the vicinity of a hole with a chassis ground at one end of the cable. It is assumed that the center conductor and shield are connected at the burnthrough hole due to heating and melting of the insulation.

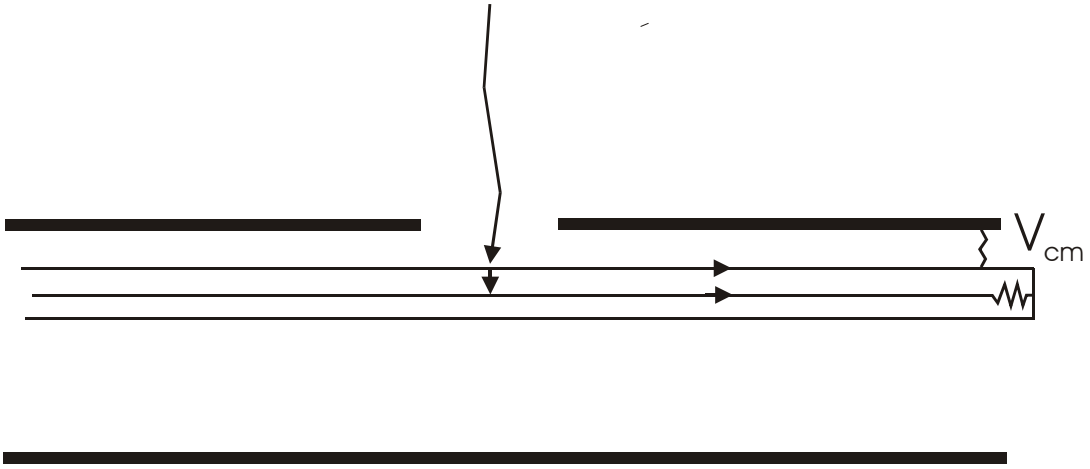

Figure 3. Conceptual coupling to a cable in the vicinity of a hole with no initial connection to chassis ground. The induced potential is assumed to rise in potential until a discharge forms to chassis ground somewhere along the cable. It is again assumed that the center conductor and shield are connected at the burnthrough hole due to heating and melting of the insulation.

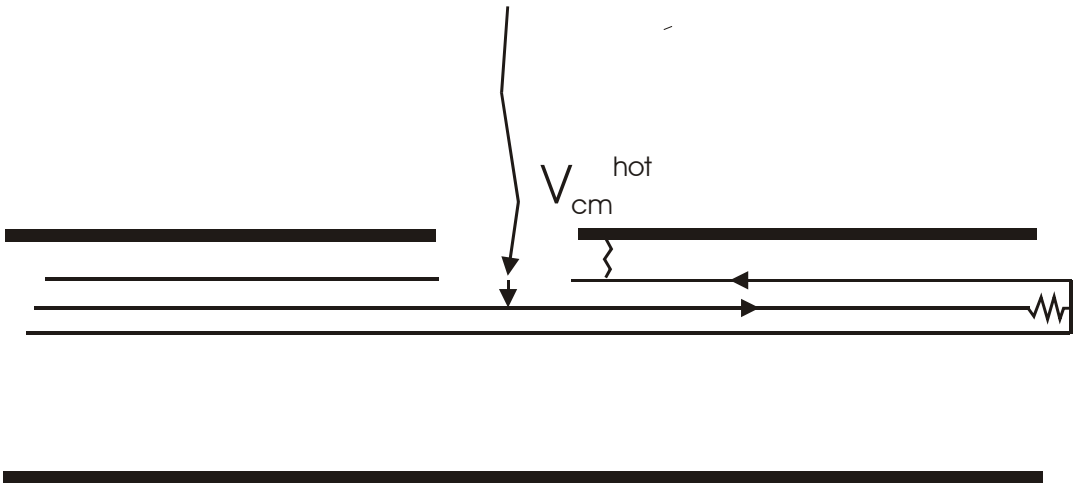

Figure 4. Conceptual coupling to a cable in the vicinity of a hole with no initial connection to chassis ground. The shield is assumed to be burned away at the location of the burnthrough hole and a connection to chassis is formed due to heating of the insulation near this location.

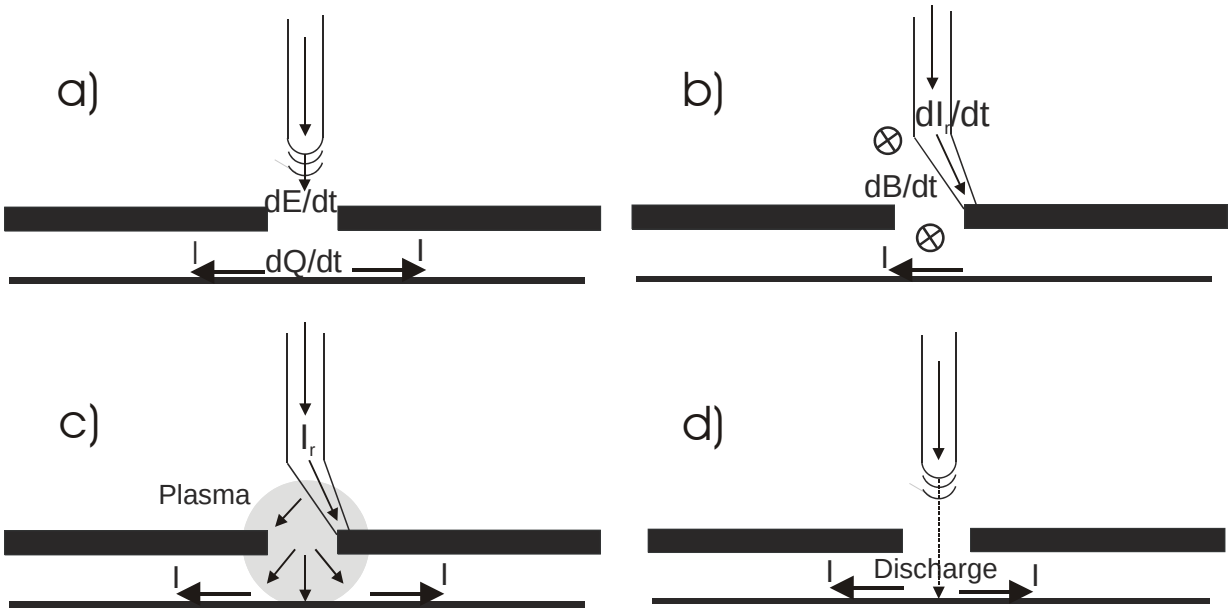

Figure 5. Coupling mechanisms through burnthrough hole.

This LDRD is a study of the protection provided by a Faraday cage after it has been compromised by lightning attachment and burnthrough. When a second return stroke occurs, the electric or magnetic field due to the stroke can get through hole with some attenuation and induce a stimulus on the inside cable. Also, the second return stroke could fail to attach to the sides of the hole but breakdown to the cable inside. This situation is complicated by the fact that the melting process during the continuing current heats the air in the vicinity of the hole causing a hot plasma to form of complex composition. There are thus four coupling mechanisms: indirect field coupling (a and b mechanisms in Figure 5) by means of time changing electric and magnetic fields, and direct coupling (c and d mechanisms in Figure 5) by plasma conduction through the burnthrough hole or discharge formation through the burnthrough hole.

This LDRD is not concerned with studying the formation of the hole. From experiment, we know that Faraday cage materials and often will experience burnthrough. We also know the approximate size of the holes – one to two cm in diameter. The focus instead is on the coupling event during a subsequent return stroke as illustrated in Figure 6 to better assess the subsequent hazards to electrical devices posed by burnthrough holes in metallic barriers.

2 ORIGINAL COUPLING EXPERIMENTS

Lightning penetration of metallic barriers is an area of interest in the aircraft industry [2], and other applications [4], [5], [7]. Attempts have been made to model these burnthrough events [3], and many models addressing similar physics have been motivated by welding [6], as well as here at Sandia [7]. By contrast, work on electrical penetration and coupling from subsequent lightning return strokes has received less attention. In the 1994 experiments a series of measurements were performed in order to determine the voltage seen on an object located behind a 0.047 inch thick aluminum coupon struck by lightning [8]. The experiments were performed in the Sandia Lightning Simulator. Figures 7 and 8 show the fixture and test setup used in the original 1994 experiment. Various combinations of return strokes and continuing current were tried. The following sub-sections summarize the results for each configuration. We include information from laboratory notes on the experiment and the actual saved coupons, to augment the information found

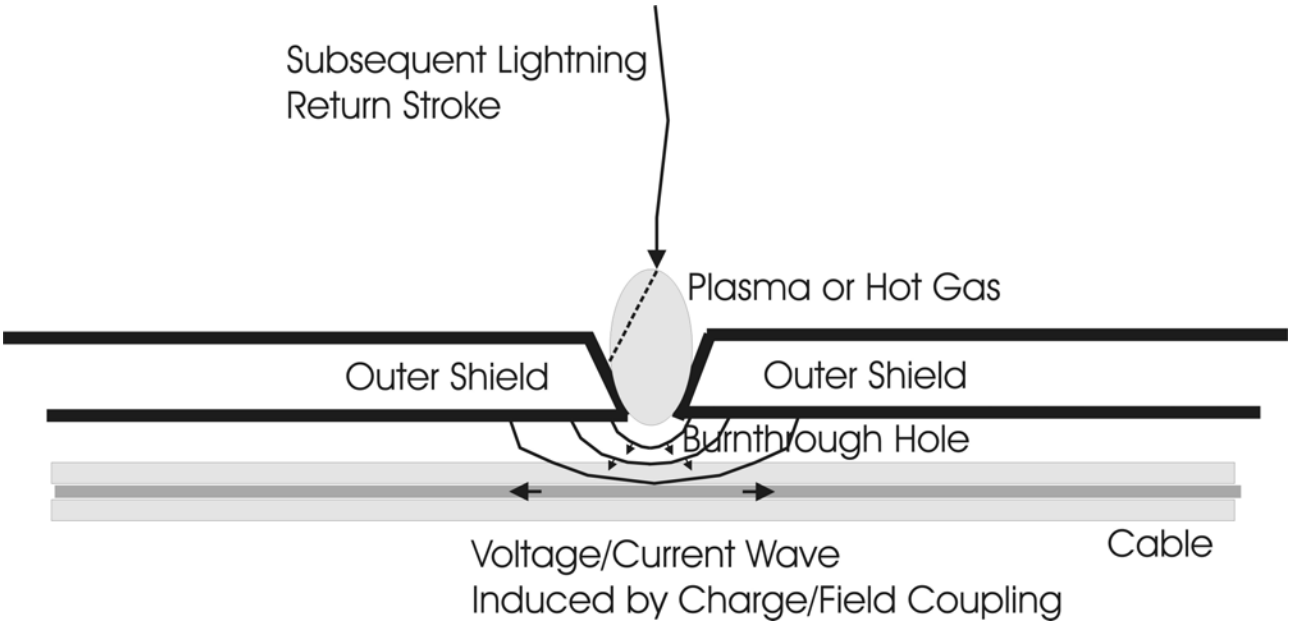

Figure 6. Coupling after burnthrough.

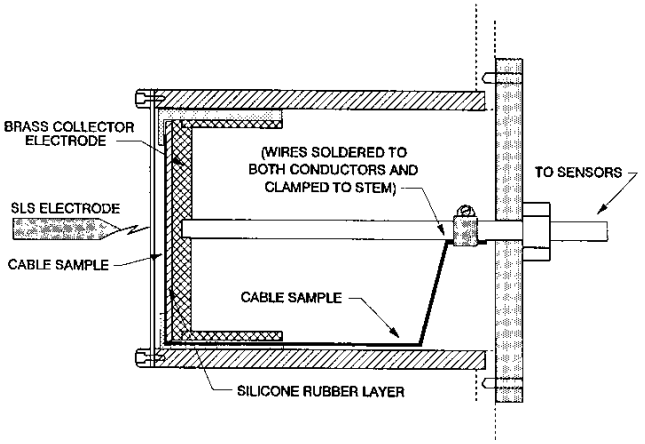

Figure 7. Apparatus used in 1994 experiment.

in [8].

2.1 Voltage from a Single Return Stroke

Table 1 shows the collector response due to a single return stroke that has a peak current Ip. A hole, 0.125 inches in diameter, was pre-drilled through the coupon. The electrode was 0.25 inches in diameter and made of tungsten. The gap between electrode and coupon was set at 0.25 inches for all the shots. The collector electrode was floating. The distance between the collector electrode and the coupon was varied and is labeled "h" in the table. The collector charge was measured and the collector voltage was derived from it using measured values of the collector capacitance (nominally 85 pF).

There is minimal damage to the coupon due to the single return stroke – just a bit of aluminum splatter. The hole doesn't increase in size at all. Note that the charge remains the same as the collector is moved 0.2 and 0.4 inches away from the hole, but drops precipitously when the collector moves 0.8 inches away. If the charge from the electrode is constant between shots, this implies that the charge entering the hole is now being deposited on the coupon rather than on the collector. As we move the collector away from the coupon, the capacitance between the top of the collector and the coupon decreases. The capacitance between the sides of the collector and the sides of the instrumentation chamber walls should be constant and dominant and therefore one would expect the voltage of the floating collector electrode to decrease as it is recessed away from the coupon.

2.2 Voltage from a Return Stroke Followed by Continuing Current

Table 2 shows the collector response due to a single return stroke that has a magnitude Ip followed by continuing current that has an initial magnitude Icc and exponential decay. The continuing current lasted about a second. The electrode was a 0.156 inch diameter pointed tungsten electrode. The gap between electrode and coupon was 0.25 inches. The collector electrode was floating. The distance between the collector electrode and the coupon was varied and is labeled "h" in the table. The charge is measured; the voltage is derived.

Ip should have no effect on the size of the burnthrough hole because the experiments summarized in 2.1 show that the return strokes by themselves do minimal damage to the coupon. Therefore, all damage to the coupon should be due to the continuing current. Ip should not have an effect on the measured

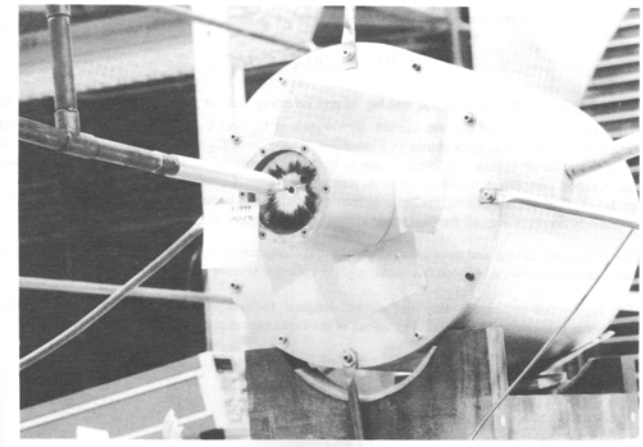

Figure 8. Original 1994 test setup.

Shot ID	Ip (kA)	h (in.)	Charge (nC)	Voltage (V)
1971	43	0.2	8.7	102
1972	50	0.4	8.0	94
1973	50	0.8	0.3	4

Table 1. Voltage due to single return stroke with pre-drilled hole

charge either, because the hole hasn't yet been formed when the return stroke is present and there is no mechanism for charge transfer. The information on Ip should not play a role, therefore, in the size of the hole or in the charge transfer. Icc forms the hole and transfers the charge. The initial return stroke was needed in the experiment to establish the arc path that the continuing current follows.

The voltage of the collector is seen to oscillate. When the coupon is breached, the voltage on the collector spikes negative (this is what was recorded in the table). Then the voltage starts to oscillate slowly between positive and negative values, in ever-decreasing excursions from zero.

2.3 Voltage from Two Return Strokes and Continuing Current

Table 3 shows the collector response due to two return strokes with continuing current between them. Ip1 is 50 kA, Icc is initially 500 A and decaying exponentially, Ip2 is 100 kA. The time between return strokes is 100 ms. The report does not specify the gap distance between electrode and coupon nor does it give any characteristics of the electrode. The collector electrode is floating. The distance between the collector electrode and the coupon is labeled "h" in column 2 of the table.

Like in 2.2, the initial return stroke should have no effect on the results, so the only difference between Tables 2 and 3 is the presence of a second return stroke. The oblong characteristics of the holes in the coupon is somewhat puzzling (In one case, (Shot 1999) there are even two holes through the coupon.). In the Sandia Lightning Simulator, continuing current is supplied by a generator, independent of the return strokes, which are supplied by two Marx banks. Continuing current not only flows between the two return strokes, but also can flow after the second return stroke until it self extinguishes. One could imagine, therefore, that the second return stroke physically moves the continuing current arc root, which then continues to flow and melt the coupon in a new location. This behavior could pertain to actual lightning if the subsequent return strokes move the arc root to new locations, then the continuing current portion of the flash would have the opportunity to burn multiple holes in the Faraday cage.

The voltage waveforms associated with Table 2 show that whenever the coupon burns through, there is a sharp spike of negative voltage that slowly becomes positive and then slowly oscillates around zero, finally decaying to zero after about 50 ms. When the collector is 0.4 inches away from the coupon, the negative voltages are 18, 27, 28 and 21 volts and when the collector is 0.8 inches away, the negative voltages are 15, 27, 11, and 8 volts. In the waveforms associated with Table 3 we would expect to see the same behavior when burnthrough occurs. No voltage spikes are evident in the Shot 1994 and 1996 waveforms when h = 0.4. When we move the collector away to h = 0.8 inches we see a positive 10 volt spike in shot 1992. Moving even further away to h = 1.2 inches we note well-defined voltage spikes. Shot 1999 has the expected negative polarity. Shot 2000 has a large (50 volt) positive voltage spike.

2.4 Current from Return Strokes and Continuing Current

Table 4 shows the collector response due to either one or two return strokes having a magnitude of Ip1 for the first and Ip2 for the second. Continuing current, having an initial magnitude Icc and exponential decay occurs after the first return stroke. The electrode for this series was not described. The gap between

Shot ID	Ip (kA)	Initial Icc (A)	h (in.)	Charge (nC)	Voltage (V)	Hole diameter (in.)
1978	49	445	0.2	<0.35	<4.1	0.50
1981	46	426	0.2	1.8	21.4	0.55
1982	51	421	0.2	4.0	47.2	0.60
1993	49	452	0.4	1.3	18.2	0.57
1995	50	453	0.4	1.9	26.6	0.52
2003	50	468	0.8	1.0	15.0	0.58
2004	50	456	0.8	1.8	27.0	0.50
2001	51	468	1.2	1.1	16.0	0.70
2002	41	461	1.2	1.8	31.3	0.42
1985	98	510	0.2	4.8	56.6	0.80
1986	92	430	0.2	6.5	76.7	0.54
1987	83	510	0.4	2.0	28.0	0.70
1988	92	510	0.4	1.5	21.0	0.60
1989	93	500	0.8	0.7	10.5	0.65
1990	90	510	0.8	0.5	7.5	0.70

Table 2. Voltage due to return stroke, continuing current

Shot ID	h (in)	V (volt)	Hole Dimensions (in.)
1994	0.4	176	0.7 x 0.9
1996	0.4	109	0.5 x 1.0
1991	0.8	23	0.5 x 0.5
1992	0.8	30	0.5 x 0.3
1999	1.2	16	2 circular holes 0.3
2000	1.2	64	0.4 x 0.7

Table 3. Voltage due to return stroke, continuing current and return stroke

Shot ID	Ip1 (kA)	Ip2 (kA)	Icc (A)	h (in.)	CVR (A)	CVT (A)	Hole Dimensions (in.)
3426	53	NA	472	0.2	70	139	1.0
3427	56	NA	lost	0.2	77	45	0.9
3428	53	NA	482	0.2	52	lost	1.0
3832	50	NA	519	0.2	39	clipped	1.35
2056	51	107	490	0.4	75		0.5 x 0.75
2057	54	109	480	0.4	105		0.42
2058	50	92	500	0.8	95		0.45
2059	52	111	500	0.8	25		0.4
2060	50	109	500	0.8	83		0.47
2061	54	108	500	0.8	102		0.84 x 0.4
2064	55	116	500	1.2	65		0.5 x 0.7
2062	46	120	500	1.2	<2		0.54 x 0.8
3855	53	88	500	0.2	0	0	1.32

Table 4. Short circuit current due to return stroke, continuing current and return stroke

electrode and coupon was 0.25 inches. The collector electrode was grounded through a CVR. The distance between the collector electrode and the coupon is labeled "h" in the table. The last row (Shot 3855) has a sheet of rubber installed between the back of the coupon and the front of the collector, which prevents current from flowing onto the collector.

The holes in more than half the cases were much larger than the 0.4 to 0.6 inch diameter seen in the previous tables. The only difference between these cases and those in the previous tables are that here we ground the collector where previously the collector was floating. In the last row, since current is not allowed to flow to the collector, we would expect the configuration to be similar to that of the floating electrode. Within this series, Shot ids 2057 through 2060 show reasonably-sized holes.

Table 5 was measured under the same circumstances as Table 4 except that the distance from electrode to coupon is 1.0 inch. This series of tests was done because with the 0.25 inch electrode-coupon spacing, the electrode would often end up inside the coupon hole because of coupon bulging. The concern was that this was artificially enhancing the level of Isc. The last row of Table 5 is with a rubber insulator installed behind the coupon, which prevents current from flowing onto the collector.

Figure 9 shows a typical short circuit collector current waveform. Notice the relatively slow rise rate.

2.5 Voltage on a Flat Cable from a Return Stroke and Continuing Current

Table 6 shows the voltage seen on a flat cable that passes behind the coupon. Between the cable and the collector is a sheet of rubber to keep charge from flowing directly to the collector. In column 4 "h" is the distance between coupon and collector. The measured voltage is due to the continuing current because the second return stroke did not occur. The hole sizes in this case are uniformly larger than expected. The electrode is 0.25 inch diameter, pointed and made of tungsten. It is located 1.0 inch from coupon.

3 SUMMARY OF PRESENT EXPERIMENTS

Both high level and laboratory scale experiments were conducted and formed a significant part of the project. The appendix contains detailed descriptions of these experiments beginning with the initial plans for each of the five rounds of experiments. Also included is a detailed description of the equipment used in

Shot Id	Ip1 (kA)	Ip2 (kA)	Icc (A)	h (in)	CVR (A)	CVT (A)	Hole Dimensions (in.)
3833	46	NA	534	0.4	53	Clipped	1.3 x 1.7
3834	55	NA	556	0.4	122	8	1.3 x 1.5
3844	55	94	550	0.2	238	157	1.1
3848	55	89	500	0.2	164	169	1.3
3853	50	88	500	0.2	307	241	1.0 x 1.3
3854	49	83	500	0.2	55	44	1.1 x 1.4
3835	56	NA	541	0.4	0	0	2.1 x 1.5

Table 5. Short circuit current due to return stroke, continuing current and return stroke

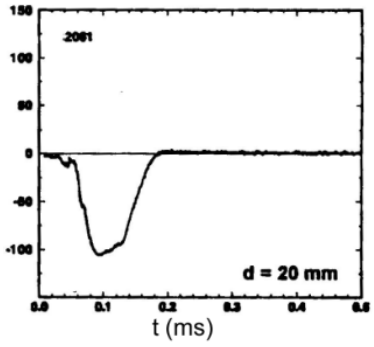

Figure 9. A typical interior collector current waveform in original 1994 experiments.

Shot Id	Ip1 (kA)	Icc (A)	h (in.)	Measured Voltage (V)	Hole Dimensions (in.)
3433	53	464	0.2	Noise	1.4 x 1.2
3434	54	463	0.2	37	1.5 x 1.3
3435	54	455	0.2	41	1.2
3840	56	494	0.2	39	1.4 x 1.3
3841	42	497	0.2	41	1.9 x 1.7
3842	52	509	0.2	46	2.0 x 1.4

Table 6. Voltage on cable due to return stroke and continuing current

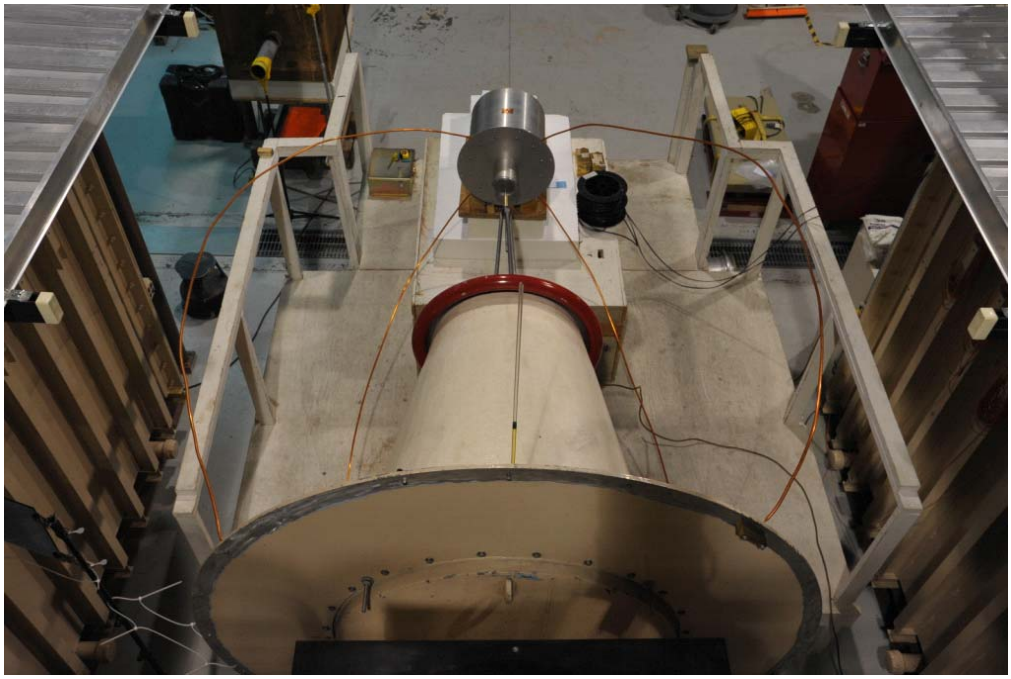

Figure 10. Experimental setup (metallic object) in the Sandia Lightning Simulator.

the experiments. The high level experiments were conducted in the Sandia Lightning Simulator shown in Figure 10. Figures 11 and 12 show the continuing current output and return stroke impulses. The lower level experiments were conducted using several pulsers: PTX pulser, PASD pulser, and Velonex pulser.

This section summarizes the questions being asked in the plan and the results of each of the experiments. This summary thus presents the information gained from the experiments and acts as an introduction to the detailed appendix as well as to the subsequent modeling and comparison sections for each of the penetration mechanisms. Figure 13 shows the damaged coupon barrier after an experiment. Because the continuing current continues to flow after the interval containing the return strokes, there is often additional hole enlargement at the end of an experiment.

3.1 Round One: Repeat of Original Experiments, Severe Continuing Current Duration & Indirect Coupling

The objective of the first round of experiments was to repeat the original tests from 1994 but add high speed photography. During the course of the planning some additional experiments were added to address extreme one-percentile duration continuing current (500 ms with a 500 A peak decaying exponential corresponds to the approximate negative return stroke one-percentile charge transfer in Cianos and Pierce [9]) in addition to the nominal interstroke intervals (100 ms) used in the original experiments. Figure 14 shows the return stroke impinging on the experimental fixture. The barrier coupon had a thickness of 0.05 inches. Figure 15 shows the interior collector current with a 0.8 inch spacing from barrier coupon to collector surface and a 100 ms interval between return strokes. The first stroke was nominally 50 kA and the second return stroke was nominally 100 kA. The continuing current had a nominal peak level of 500 A followed by an exponential decay. Figure 15 is to be compared to the original experiment of Figure 9, where it can be seen that both the peak level and rise rate are fairly well repeated in the recent experiments. Unlike the original experiments in 1994, high speed photography was used in the new experiments so that we can correlate observed barrier damage with recorded electrical signals. Figure 16 shows a single frame

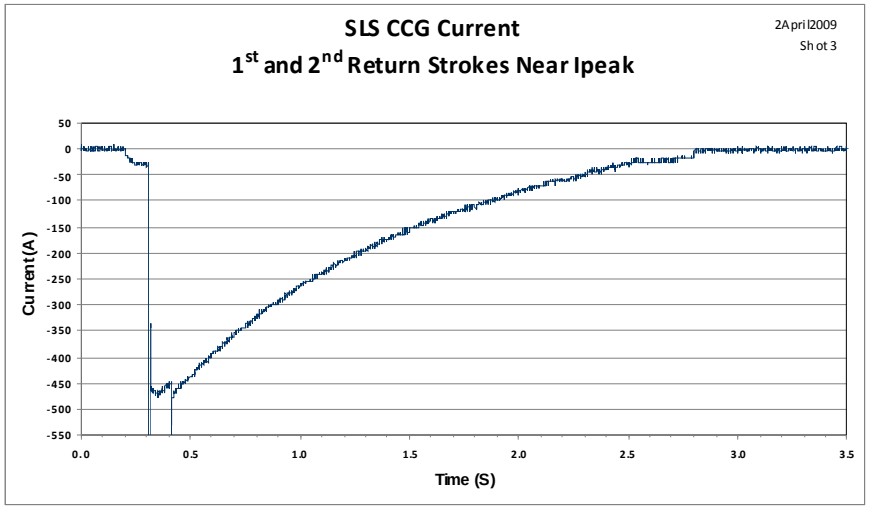

Figure 11. Continuing current waveform from Sandia Lightning Simulator with two return strokes shown as negative impulses.

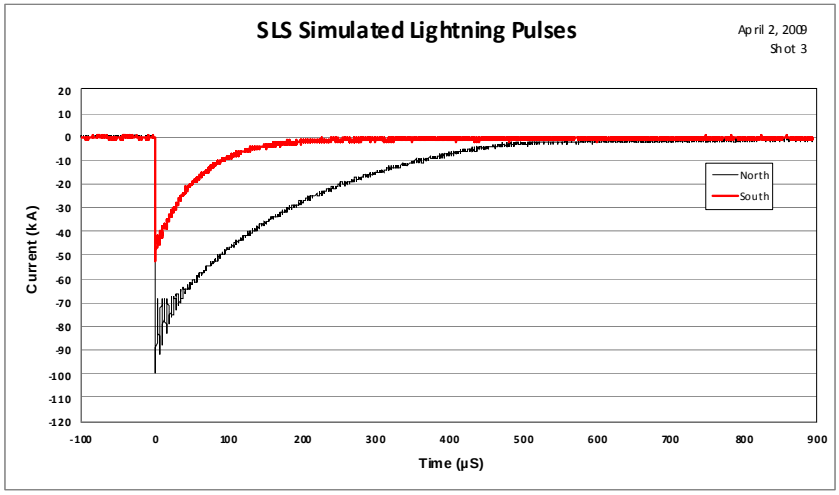

Figure 12. Typical first (red - south tank) and second (black - north tank) return strokes from Sandia Lightning Simulator.

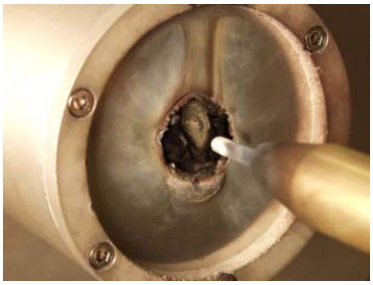

Figure 13. Final damage to barrier coupon and interior after a shot.

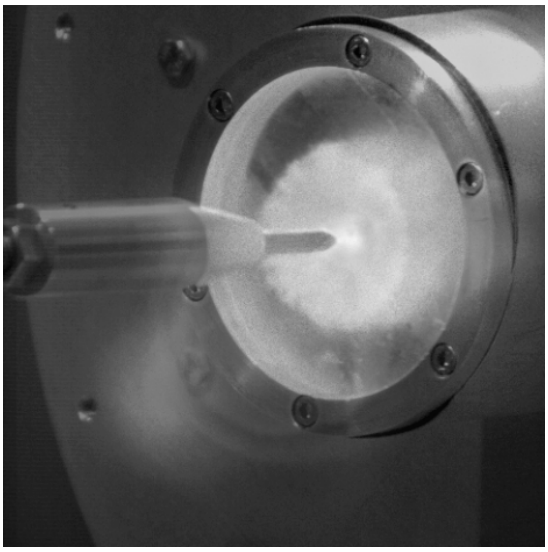

Figure 14. Double exposure showing hardware setup and return stroke.

from the high speed photography just before the second return stroke impinges on the barrier near 100 ms into the experiment. The exterior movies showed a definite penetration appearing near 180 ms into the event. The second return stroke creates a hole penetration, indicating that the barrier material has been softened up by the preceding continuing current, since a return stroke alone produces no hole. The slow rise rate of the collector short circuit current in this 100 ms experiment is thought to result from the time required to create the hole during the second return stroke interval.

An experiment with a 500 ms interval between the two return strokes was imaged just before the second return stroke in the high speed frame of Figure 17. An obvious circular hole of approximately 0.5 inch diameter has already been created before the second return stroke hits. Figure 18 shows a single frame near 500 ms and the flash of light from the second return stroke. Figure 19 shows a high speed frame illustrating the enlargement of the barrier hole just after the second return stroke at 500 ms into the experiment. Figure 20 shows the collector short circuit current in the experiment with a 500 ms interval between return strokes. Notice the larger amplitude and, in particular, the shorter rise time of the current in this case.

Figure 21 shows a predrilled hole of 0.5 inch diameter which was subjected to a single return stroke. Figure 22 shows the short circuit current for the predrilled hole case. Notice the similarity with the 500 ms duration burnthrough event short circuit current in Figure 20. Figure 23 shows the corresponding open circuit voltage for the predrilled 0.5 inch hole subjected to a single return stroke.

Experiments focused on the indirect field coupling mechanisms were also carried out in round one. Figure 24 shows the setup for the magnetic field indirect coupling experiment to a stripline cable with a 0.5 inch predrilled hole in the coupon barrier (measurements were also made on a circular cable or wire). The Velonex pulser was used to drive these low level magnetic experiments with a peak time derivative of the drive current of 0.83 kA/microsecond. The two limiting excitations of the hole were used for the magnetic indirect coupling experiments. Figure 25 shows the vertical excitation (current normal to the plane containing the hole). The other limiting case was horizontal excitation (current parallel to the plane containing the hole). Figure 26 shows the results for the vertical drive. The effective value of the short circuit magnetic field driving the hole is the constant value that produces the proper interior dipole field of the hole with the actual varying field of the line source (in the vertical case this is simply the center value of the line source field). Figure 27 shows the results for the horizontal drive. A linear combination of these

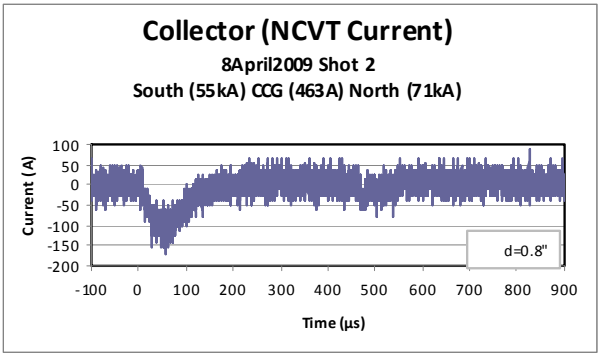

Figure 15. Interior collector short circuit current for a double return stroke and 100 ms interstroke interval continuing current experiment.

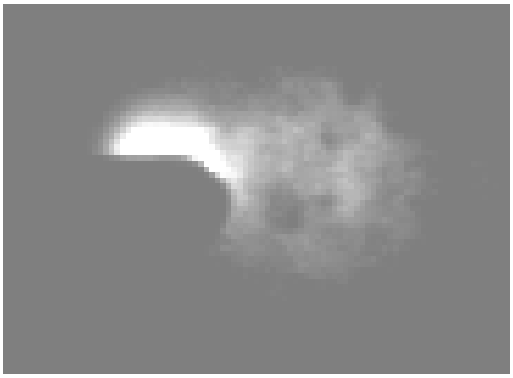

Figure 16. A single frame of the high speed photography near 100 ms into the event (just before the second return stroke hits), not showing any obvious penetration of the barrier coupon.

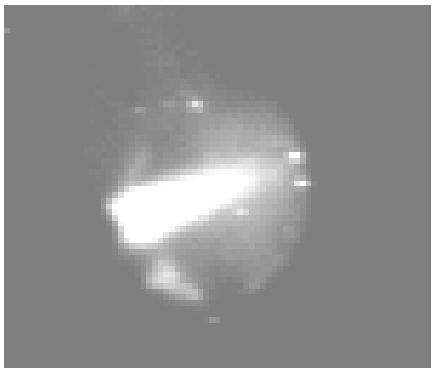

Figure 17. A high speed frame near 500 ms (just before the second return stroke in this experiment) showing an obvious penetration before the second return stroke.

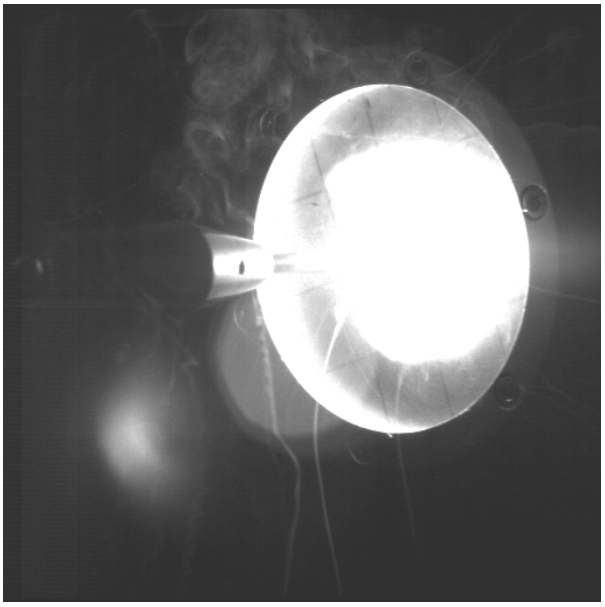

Figure 18. Flash of light from second return stroke near 500 ms.

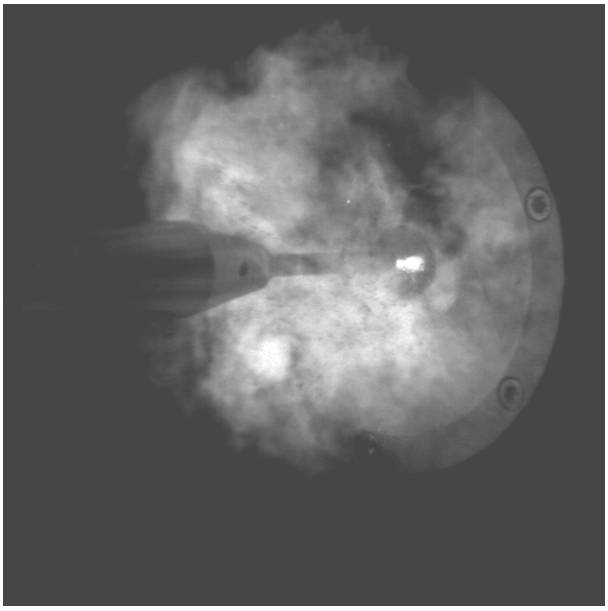

Figure 19. The hole in the barrier at the end of the second return stroke at 500 ms into the experiment.

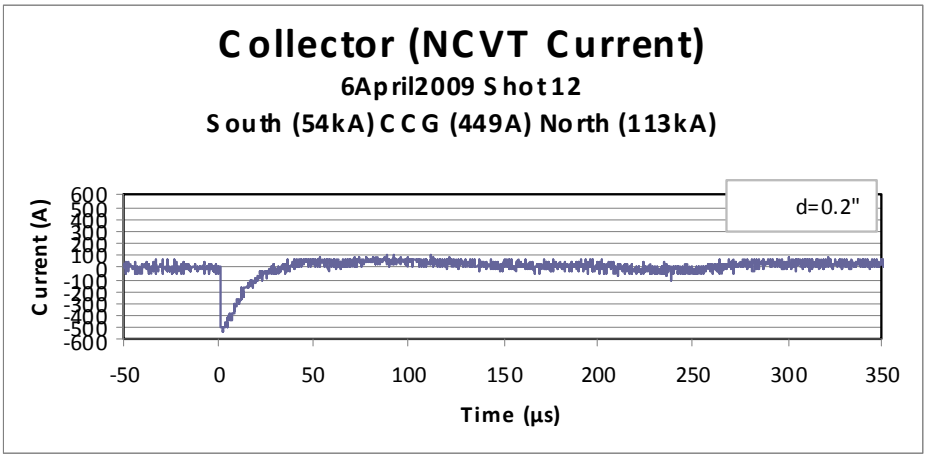

Figure 20. Collector short circuit current for the case of a 500 ms interstroke interval.

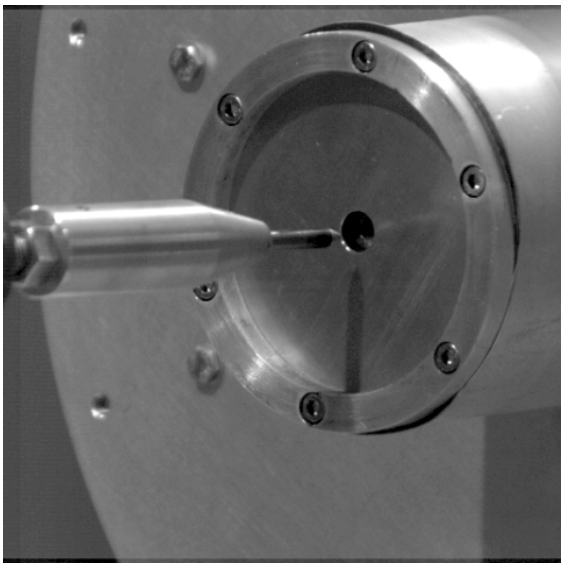

Figure 21. Predrilled 0.5 inch diameter hole in coupon barrier to simulate burnthrough hole.

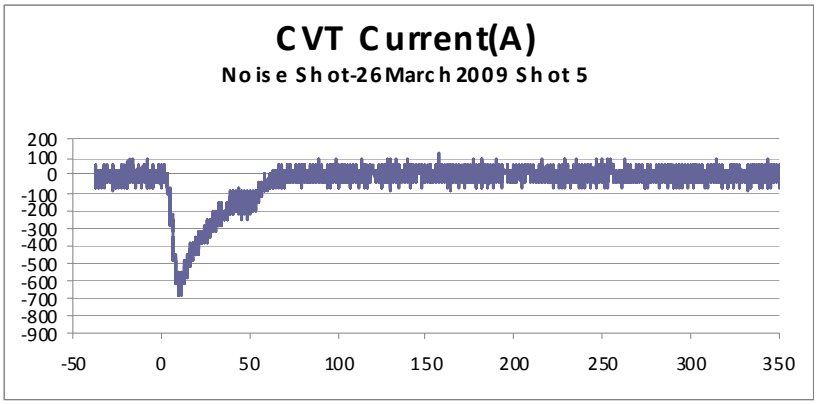

Figure 22. The collector short circuit current for a coupon barrier with a 0.5 inch predrilled hole.

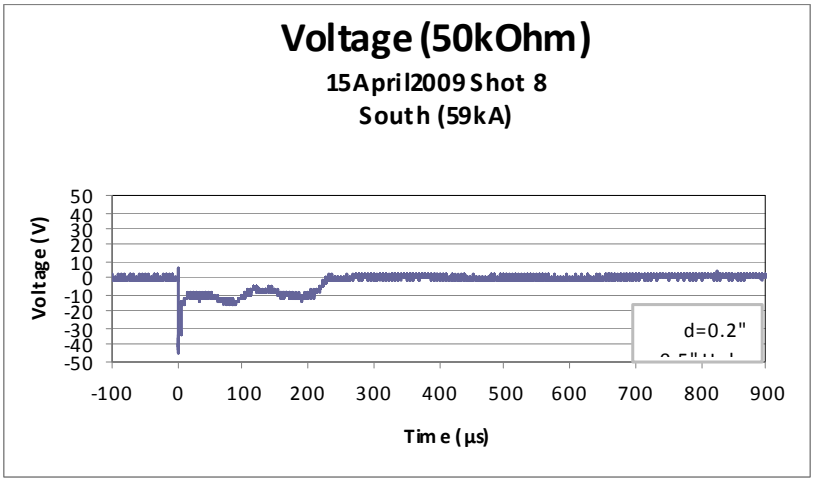

Figure 23. Open circuit voltage for the 0.5 inch predrilled hole subjected to a single return stroke.

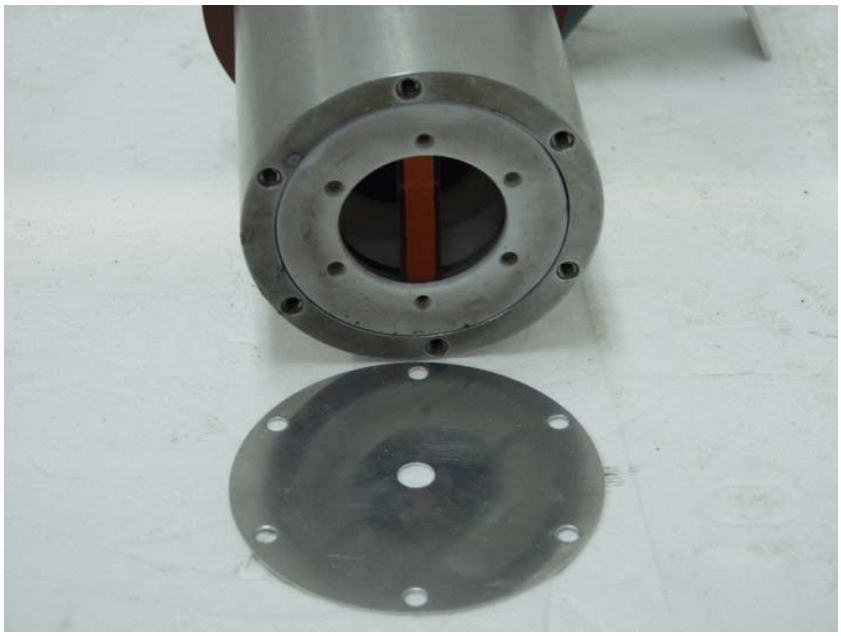

Figure 24. Stripline cable used in indirect magnetic field coupling experiment.

two orientations would make up a more realistic attachment configuration, but separately they illustrate the behavior, and the horizontal case bounds the response. Note that the horizontal response, when scaled to a drive level representing severe lightning of 400 kA/microsecond, yields about 320 V for the interior level.

Figure 28 shows the interior setup for the electric field indirect coupling, which used the piston collector. Figure 29 shows the exterior of the setup with the rod-to-plane drive setup. The PASD pulser was used in this case with a drive having a voltage time derivative peak of 3 kV/nanosecond and a voltage value of 4.6 kV (at the first interior peak response). Figure 30 shows the electric field coupling results. The limits for the time derivative of the electric field in natural lightning are not as well known, but if we use the facility level of 2 x 800 kV (assuming we have artificially inhibited ionization phenomena) this scales to 225 V interior level.

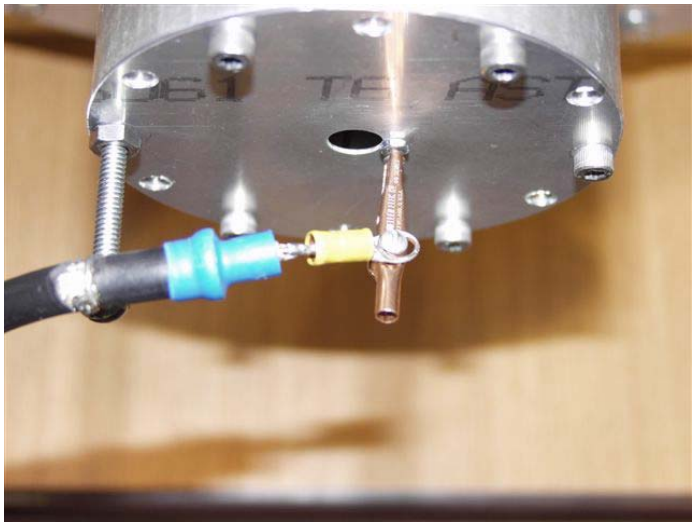

Figure 25. Vertical current excitation of hole for magnetic coupling.

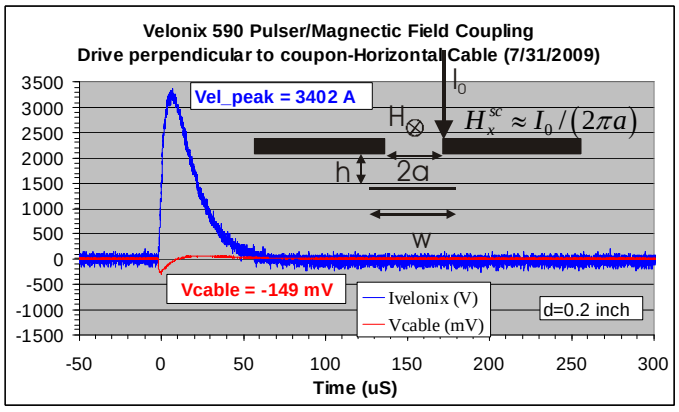

Figure 26. Indirect magnetic coupling for the vertical current drive. The blue curve is the Velonix drive current waveform and the red curve is the open circuit voltage on the cable. The inset shows the geometry (the cable was artificially rotated by ninety degrees from maximal coupling to show the cross section).

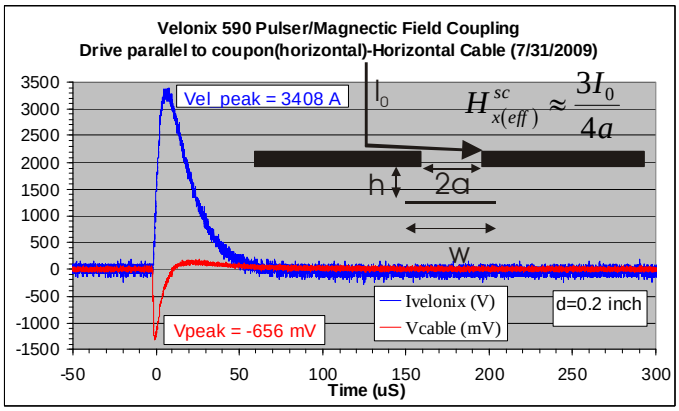

Figure 27. Indirect magnetic coupling for the horizontal current drive. The blue curve is the Velonix drive current waveform and the red curve is the open circuit voltage on the cable. The inset shows the geometry (the cable was artificially rotated by ninety degrees from maximal coupling to show the cross section).

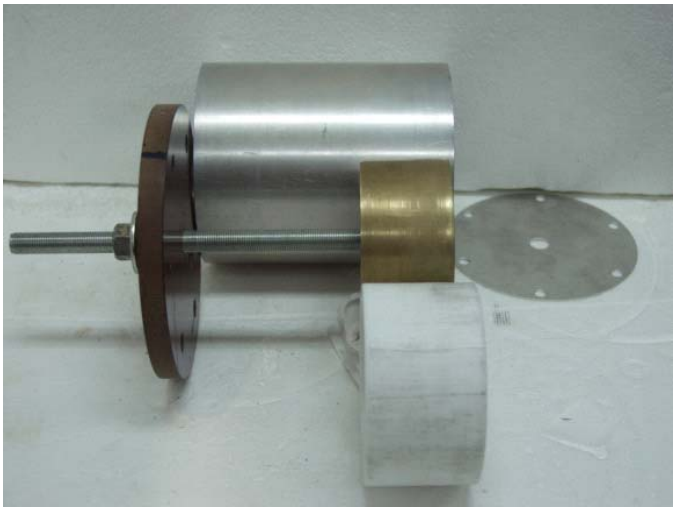

Figure 28. Interior hardware for the indirect electric coupling measurement.

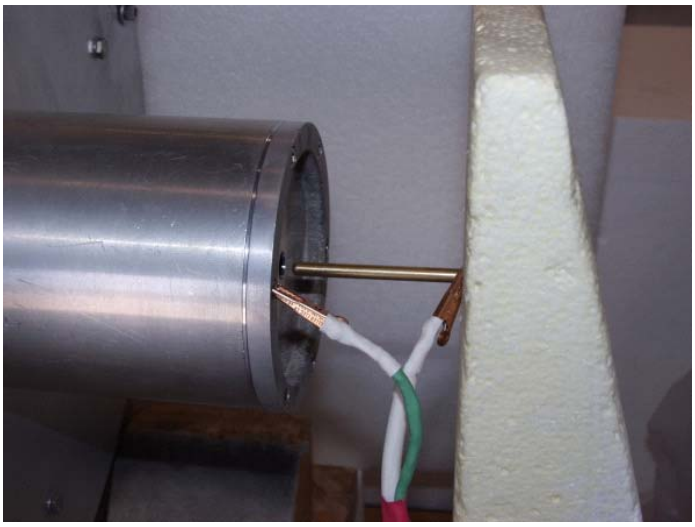

Figure 29. Indirect electric field coupling experiment with exterior rod-to-plane geometry.

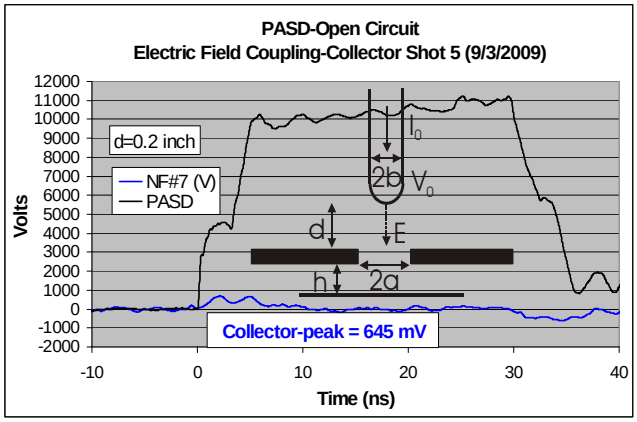

Figure 30. Indirect electric field coupling results. The black curve is the voltage drive of the PASD pulser. The blue curve is the interior response voltage.

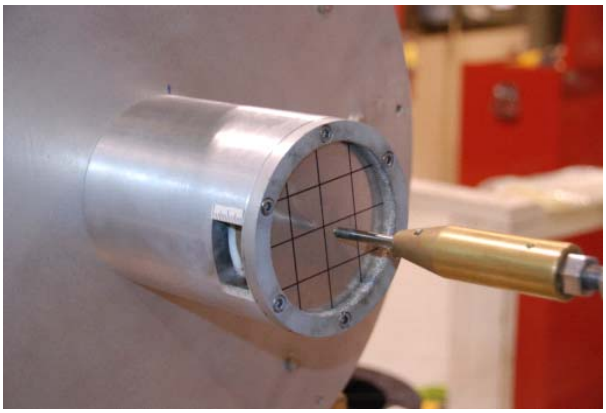

Figure 31. Interior high speed photography was enabled by the insertion of a slot in the side of the enclosure barrier as shown.

3.2 Round Two: Multiple Return Strokes & Interior Penetration

The round two experiments had two main objectives. The first objective was to perform interior high speed photography in an attempt to observe the timing of the first barrier penetration (first light). The second objective to address the issue of multiple return strokes in a lightning flash. This second objective was addressed by using a starter wire to initiate the discharge to the coupon barrier, allowing us to reserve the two return stroke capability of the Sandia Lightning Simulator for later in the flash (after the continuing current has softened up the coupon barrier). The starter wire initiates the discharge and then quickly vaporizes. The continuing current is then followed by two return strokes after 400 ms and 500 ms, respectively, from the beginning of the experiment. The first return stroke enlarges the hole size and the second causes coupling. Although the lightning flash may consist of many return strokes [1] their severity must conform with the severe action (integral of the square of the current over time) of the entire flash. This means that each individual return stroke will be smaller than severe levels for an individual stroke.

Figure 31 shows the slot that was introduced in the enclosure barrier to enable interior photography during the burnthrough event. Checks were made on the electrical coupling levels to the interior through the slot to get a feel for the new noise floor levels. Figure 32 shows the early interior penetration (first light) at about 25 ms into the burnthrough event. The exterior photography showed clear evidence of a penetration at 180 ms, but apparently there are smaller penetrations in existence much earlier in time. Figure 33 shows a case where a return discharge has formed (toward the bottom of the figure) between the collector and the coupon barrier, in addition to the main discharge to the collector (center of the figure), which was associated with a floating collector.

Figure 34 shows the starter wire arrangement. Figure 35, shows the drive current waveform using the starter wire, where the two return stroke impulses occur later in the experiment. Figure 36 shows the results for the short circuit collector current in a starter wire experiment. Figure 37 shows the interior open circuit collector voltage in a starter wire experiment.

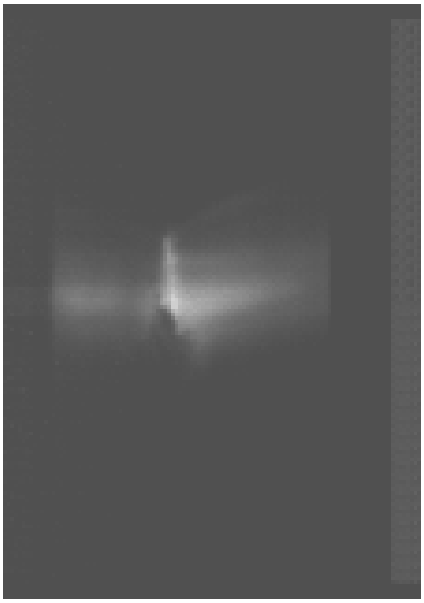

Figure 32. First light on the interior was observed in the high speed photography at about 25 ms into the experiment.

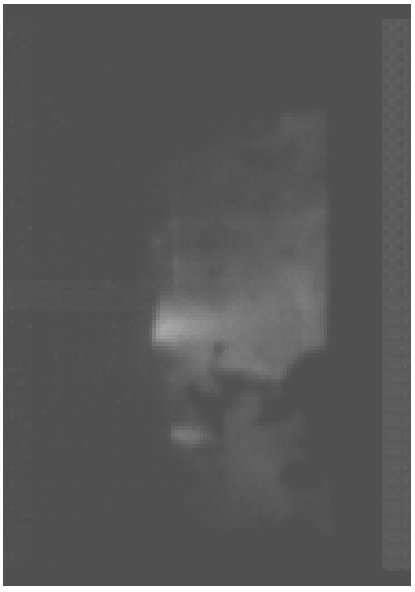

Figure 33. An example of a return discharge from collector to coupon on interior (bottom of figure) in addition to the main discharge to the collector (center of figure).

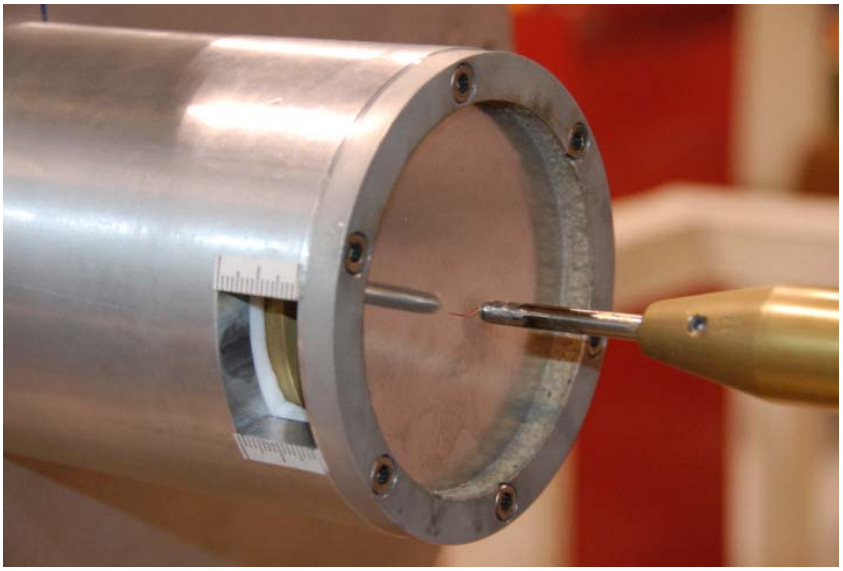

Figure 34. Starter wire to initiate discharge to coupon barrier.

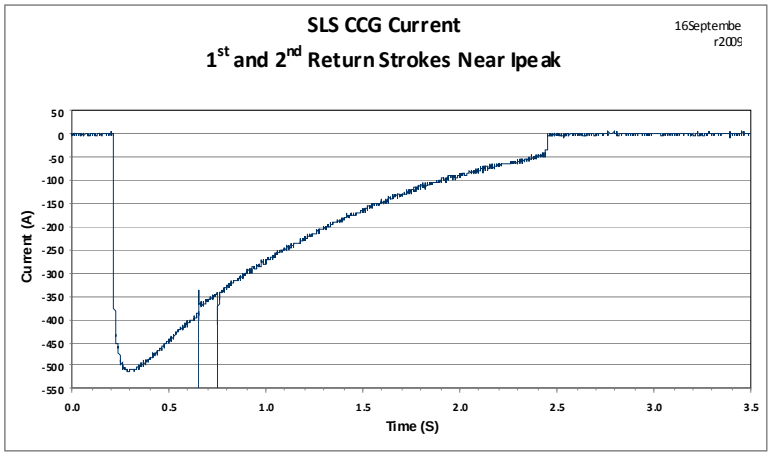

Figure 35. Continuing current waveform initiated by a starter wire with the two return stroke impulses later in the event.

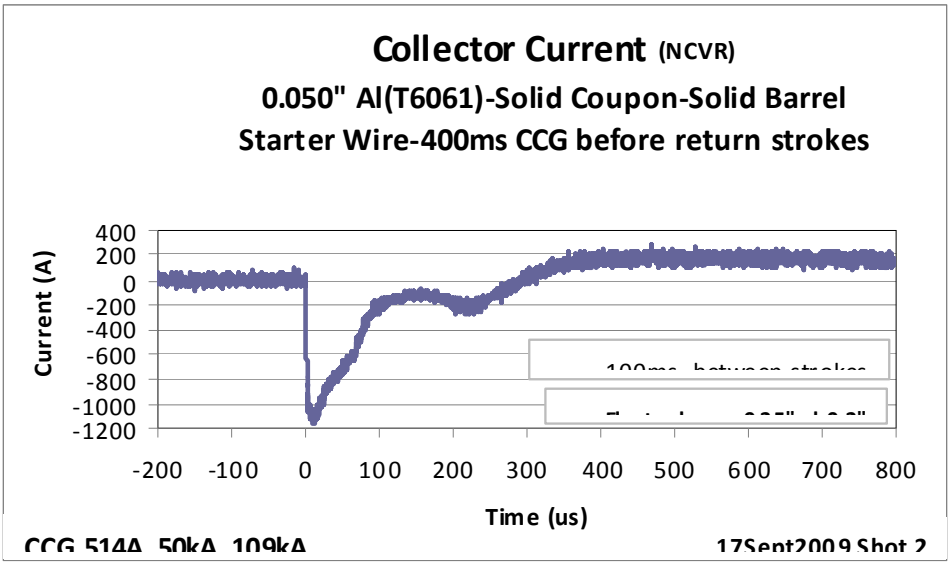

Figure 36. Interior short circuit collector current when a starter wire is used to initiate the discharge.

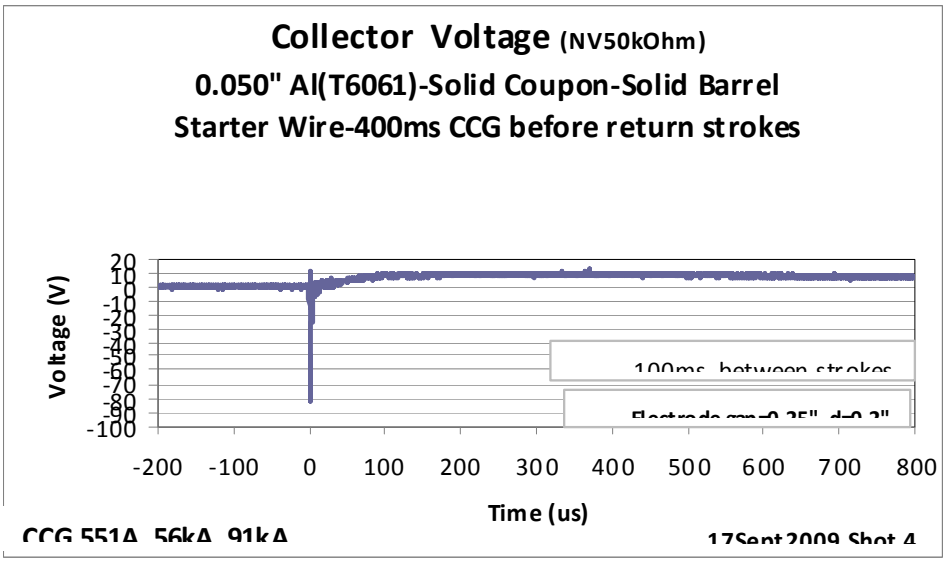

Figure 37. Interior open circuit collector voltage in a starter wire experiment.

Figure 38. Split probe concept.

3.3 Round Three: Plasma Current Distribution, Interior Attachment Test & Exterior Field

The round three experiments had two primary objectives. The first objective was to examine the plasma current distribution by means of various direct measurement probes. The radial size of the plasma is of interest both for the continuing current phase, the return stroke phase, as well as for the transition between them. The second objective was to examine the conditions required on cathode position to develop a discharge attachment to the interior collector.

Figures 38 and 39 show the split probe. This type of probe was used in welding arcs by Nestor [10]. As the arc moves over the probe surface across the cut the current distribution on the two halves of the probe vary, and this information can be used to construct the current profile. In the steady state welding arcs the position of the discharge column was controlled and was stable. One of the problems here is the transient nature of the arc and uncontrolled variations in position. Another problem is the size of the probe inductance, caused by the connections to the current viewing resistors (CVRs) used to monitor the current in each half, which prohibited its use with the return stroke. Consequently this probe was only used on the continuing current phase and indicated that the plasma column radius was in a range consistent with free burning arc model predictions [11].

Figures 40 and 41 show the ring probe. This probe consisted of a series of brass rings, the current on each being monitored by a current viewing resistor. The wiring paths were made as short as possible to smaller power current viewing resistors (since the current is split up) to minimize inductance. Since each ring is being individually monitored, the interpretation of the response is simple in principle. This probe was only used for the return stroke because the heating associated with the continuing current was thought to be too intense for the insulation. Figure 42 shows the currents measured during a return stroke experiment. The radial spreading of the current is indicated except for the behavior of the second channel or ring. Evidence of arcing in the CVR connections lead to questions about the validity of these measurements.

Figures 43 and 44 show the groove probe, which was introduced to minimize inductance and provide a more robust measurement. Each groove provides a voltage response that must be inverted to determine the radial current distribution. Figure 45 shows an example of such responses for a single return stroke. Figure 46 shows the screen box used to house the scope for recording the multichannel information associated with the probe. This probe was also inverted in direction (grooves facing out) to reduce heating of the groove areas. The return stroke expansion backed out of the groove responses appeared to be consistent with hydrodynamic channel expansion predicted by models discussed below. The transition between continuing current and return stroke was attempted but damage to the grooves was observed even in the inverted

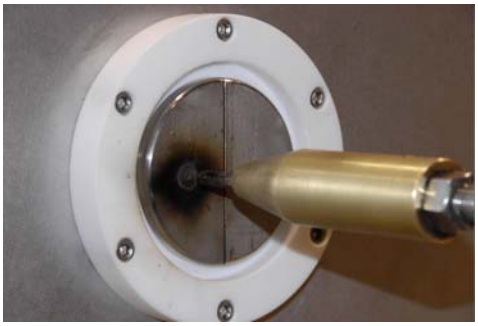

Figure 39. Split probe in use during continuing current.

configuration.

The second objective was to ascertain how close the cathode rod would have to come to the collector in order to create a large interior voltage. Figure 47 shows the setup. When this experiment was first run no large interior voltage was observed. It was then noted that the Sandia Lightning Simulator voltage rise occurred earlier in time than the current rise and the measurement triggering was changed to the laser triggering of the Marx banks. This triggering was used on all later measurements and was an important change to make certain that no interior voltage spikes were overlooked. Figure 48 shows the results of this experiment when the cathode was actually moved inside the hole edge. Thus large, short duration, voltages can be observed on the interior in extreme cases (cathode protruding inside the barrier).

Figure 40. Ring probe concept.

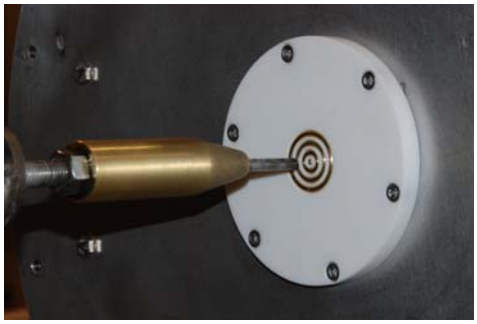

Figure 41. Ring probe in experiment.

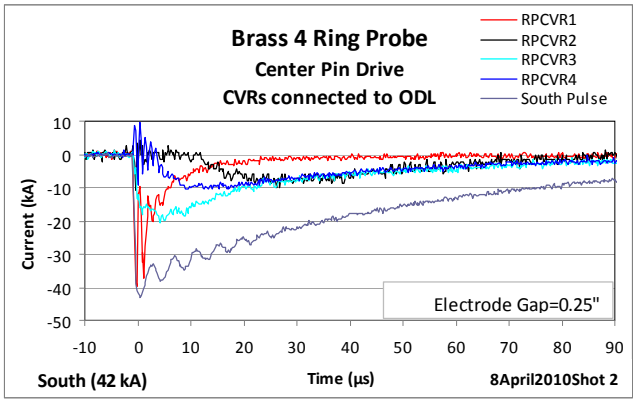

Figure 42. Currents from the ring probe during a return stroke.

Figure 43. Groove probe concept.

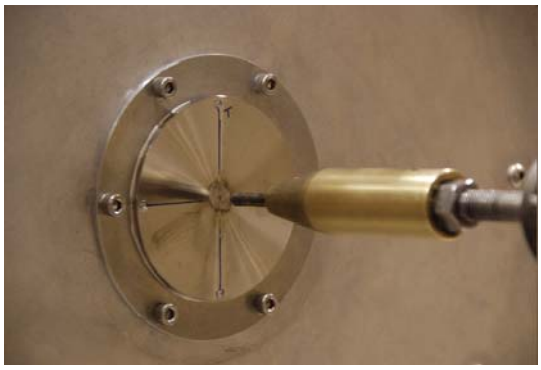

Figure 44. Groove probe setup.

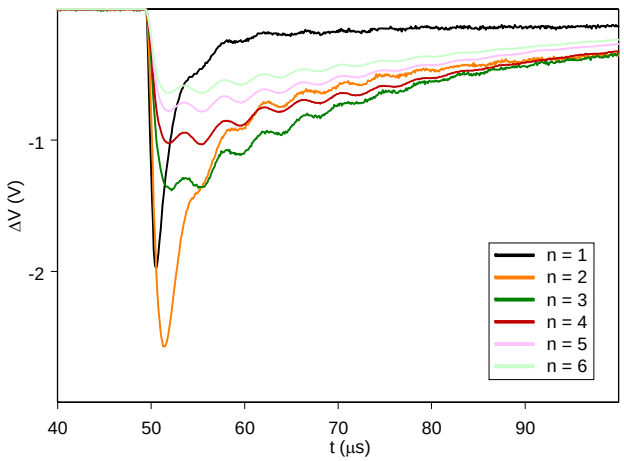

Figure 45. Measurements of the groove probe voltages during a return stroke.

Figure 46. Screen box for housing scope to record multichannel responses of the groove probe.

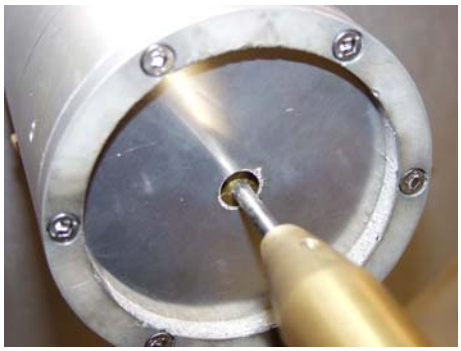

Figure 47. Predrilled hole used for Sandia Lightning Simulator discharge to collector experiment.

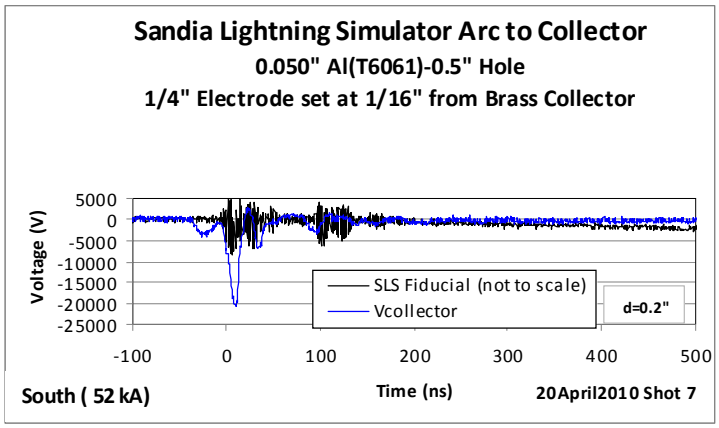

Figure 48. Early time open circuit voltage measurement of Sandia Lightning Simulator experiment.

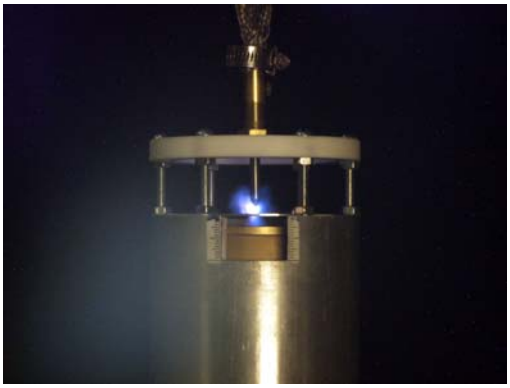

Figure 49. The cathode was positioned exterior to the predrilled barrier hole.

3.4 Round Four: Breakdown Attachment Experiments & Early Time Cable Voltage

The conditions to establish a discharge to the interior collector through a predrilled hole were explored in a more systematic manner by using a medium level pulser (the PTX pulser with a rise time in the 100s of ns) and recording interior voltages as a function of rod tip position. Figure 49 shows the rod tip external to the barrier. Figure 50 shows the corresponding interior collector voltage (blue curve) is quite small (right V scale). Figure 51 shows the rod tip position even with the barrier hole. Figure 52 shows the corresponding voltage (blue curve) is relatively large (right kV scale) in this case.

A second objective of round four was to measure the early time (motivated by the preceding attachment experiment of round three) open circuit voltage induced on a cable collector during a burnthrough experiment. Figure 53 shows the stripline cable collector. Figure 54 shows the recorded cable collector open circuit voltage. This value is larger than previously observed in burnthrough experiments. Figure 55 shows the damage after the cable experiment. The presence of the insulator behind the cable (used to avoid arcing to the piston collector that is holding the cable in place) is thought to increase the hole size in the coupon barrier by preventing a stable continuing current arc from forming to the piston collector (the cable collector burns away during the experiment).

The probes external to the damage of the previous experiment were used to monitor the electric field in the vicinity of the barrier penetration. Figure 56 shows a measurement setup where the electric field was monitored when a single return stroke in the Sandia Lightning Simulator impinges on the rod (with one inch spacing from the barrier plane). One probe is a short calibrated monopole and the other is a commercial electric field sensor. Figure 57 shows the electric field response of the two probes. The peak value is just over 4.3 kV/cm (this level, without ionization, would correspond to about a 68 kV cathode voltage, which is less than one tenth the incident wave level; this field level is also near the sustaining field for streamers in air).

3.5 Round Five: Multiple Return Strokes, Severe Charge Transfer & Early Time Voltages

The main objective of round five was to examine the early time open circuit voltage during starter wire - two stroke burnthrough experiments, with very severe charge transfer levels. The dual return strokes were delayed in some of these experiments to capture the one-percentile charge transfer levels of the Fisher-Uman specification (note that here we are using negative lightning) [1]. Figure 58 shows the hole size at 900 ms

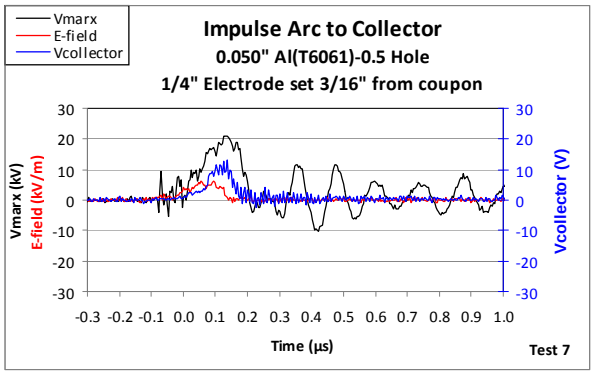

Figure 50. The interior collector voltage (blue curve) with the rod tip positioned exterior to the barrier. The black curve is the drive voltage at the pulser. The red curve is an uncalibrated electric field recording at the barrier.

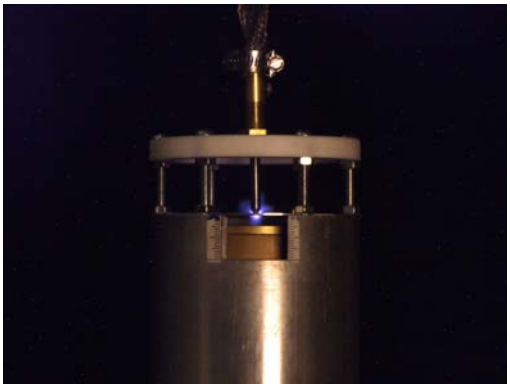

Figure 51. The cathode was positioned even with the predrilled barrier hole.

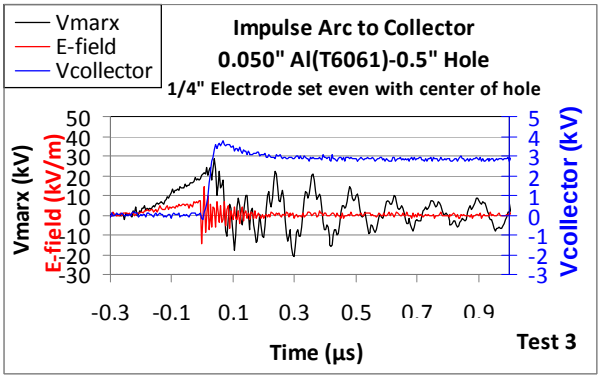

Figure 52. The interior collector voltage (blue curve) with the rod tip positioned even with the barrier. The black curve is the drive voltage at the pulser. The red curve is an uncalibrated electric field recording at the barrier.

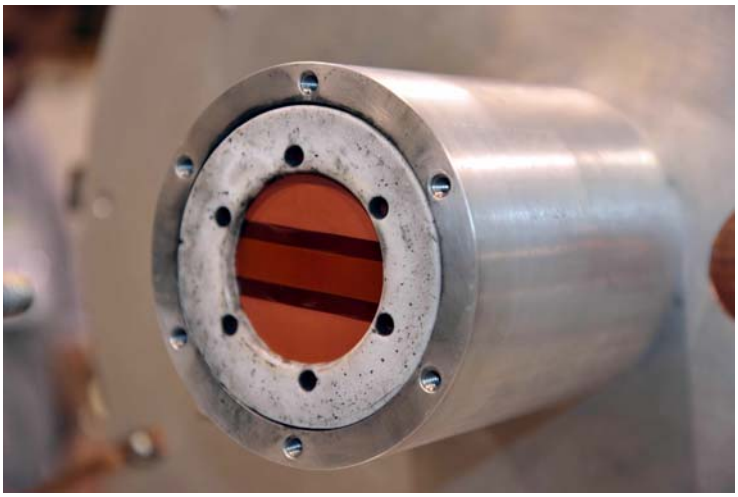

Figure 53. Stripline cable collector.

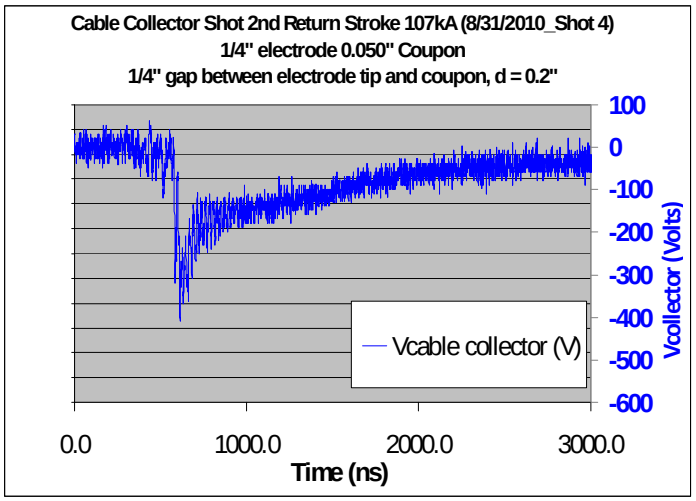

Figure 54. Early time voltage peak for cable collector induced by second return stroke in a burnthrough experiment using the Sandia Lightning Simulator.

Figure 55. Damage observed after cable collector burnthrough experiment.

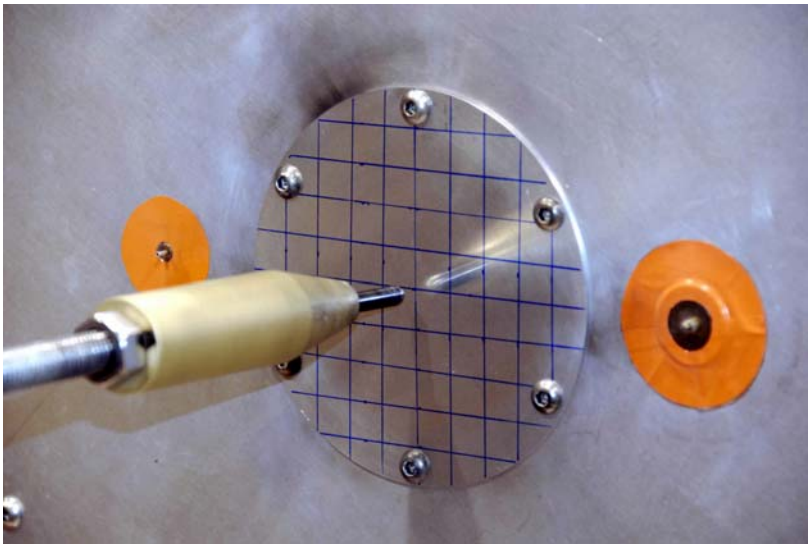

Figure 56. Two electric field probes used to monitor the electric field near the cathode during an experiment in the Sandia Lightning Simulator.

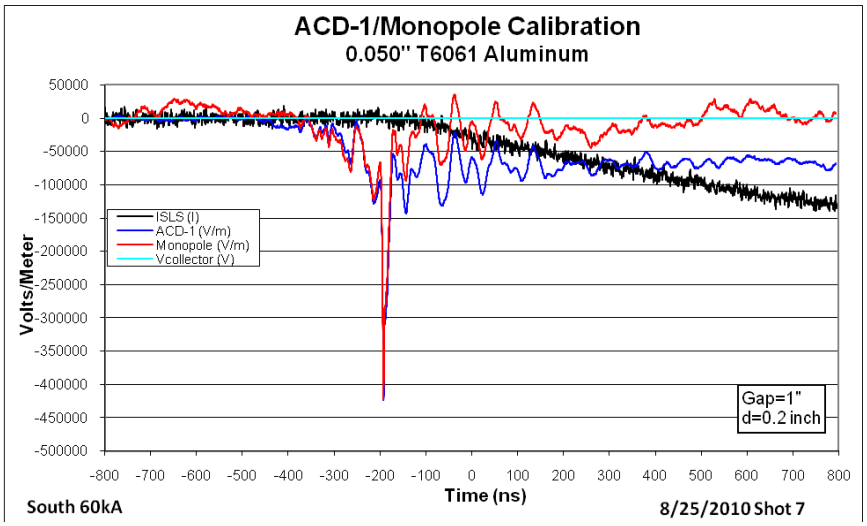

Figure 57. Electric field response on the barrier plane from the two electric field probes.

Figure 58. Larger hole associated with severe charge transfer level.

when the first return stroke hits. Figure 59 shows the current drive and charge transfer (dashed curve) used in this starter wire burnthrough experiment. Figure 60 shows the open circuit voltage from this starter wire burnthrough experiment with very severe level of continuing current charge transfer. This level is larger than previous experiments using the piston collector by about a factor of 2-3. Figure 61 shows the damage in the aftermath of the starter wire experiment. Figure 62 illustrates some possible current return paths when a burnthrough experiment is conducted using a floating collector configuration (for open circuit voltage measurement) that have been motivated by interior photography showing return discharges to the coupon barrier. Figure 63 shows the starter wire setup in these experiments. Figure 64 shows the current drive and charge transfer for a starter wire experiment using a cable collector (this is somewhat less severe charge transfer than the preceding piston experiment). Figure 65 shows the open circuit voltage on the cable collector for this starter wire experiment. Notice that the interior voltage level is the largest show. If the charge transfer level was made as large as the preceding piston collector experiment is not too hard to imagine the voltage becoming even somewhat larger. Figure 66 shows the damage after the cable collector experiment.

Other experiments were planned (and some were begun) in round five but time constraints limited how many could be completed. These others included the assessment of the dynamic source impedance of the coupling as well as the most severe return stroke amplitudes (200 kA) that can be provided by the Sandia Lightning Simulator.

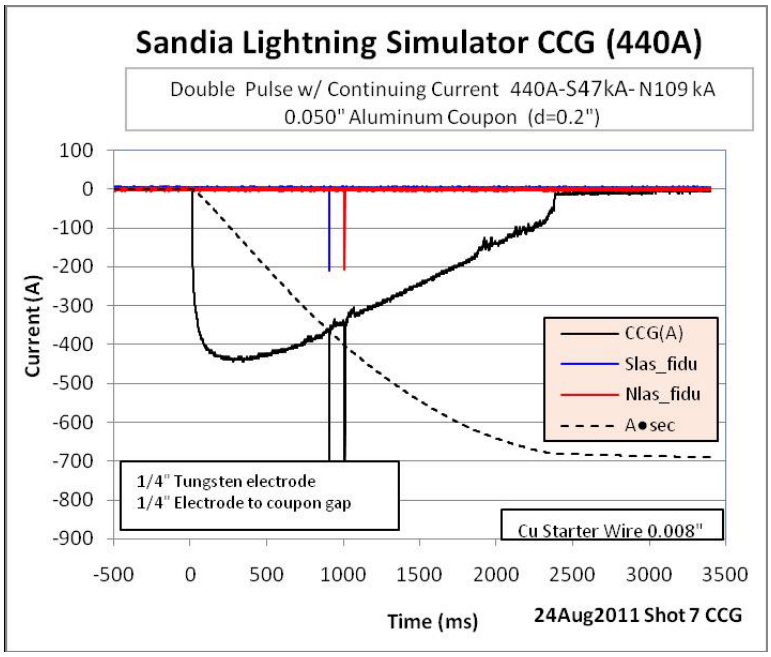

Figure 59. Continuing current waveform with return stroke impulses and charge transfer (dashed curve) for a starter wire - multiple return stroke experiment using the piston collector.

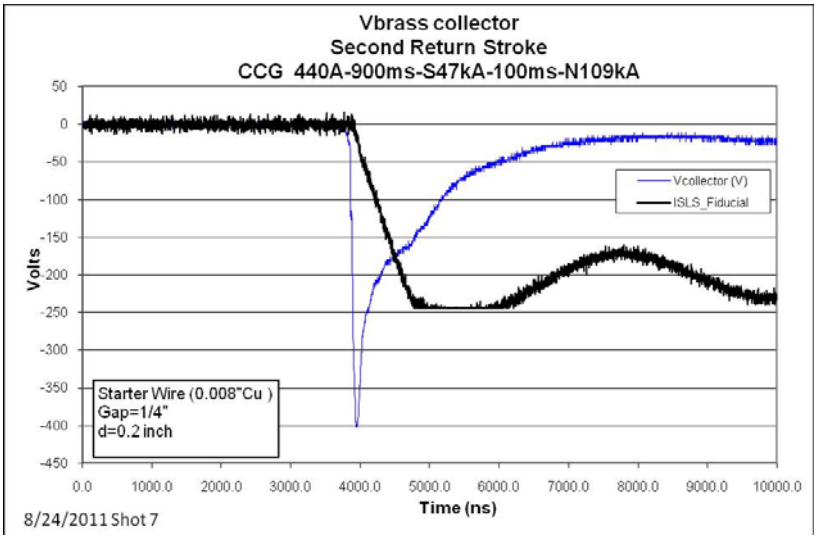

Figure 60. Open circuit voltage on piston collector for starter wire burnthrough experiment with very severe level of continuing current charge transfer by return stroke time interval.

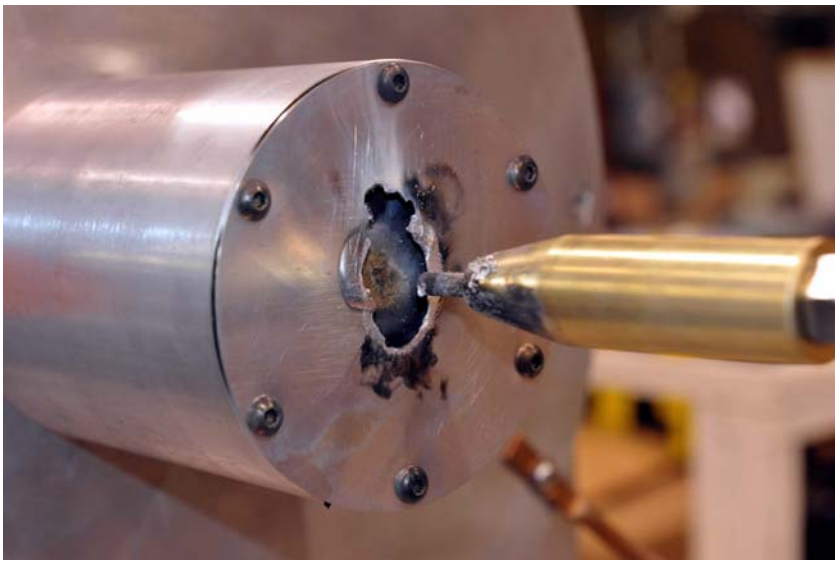

Figure 61. Damage from starter wire piston collector experiment with very severe continuing current charge tranfer.

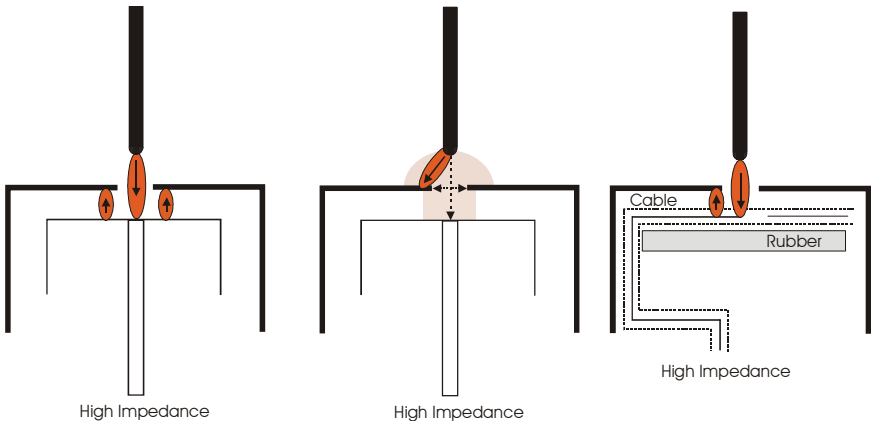

Figure 62. Current return configurations with floating collector.

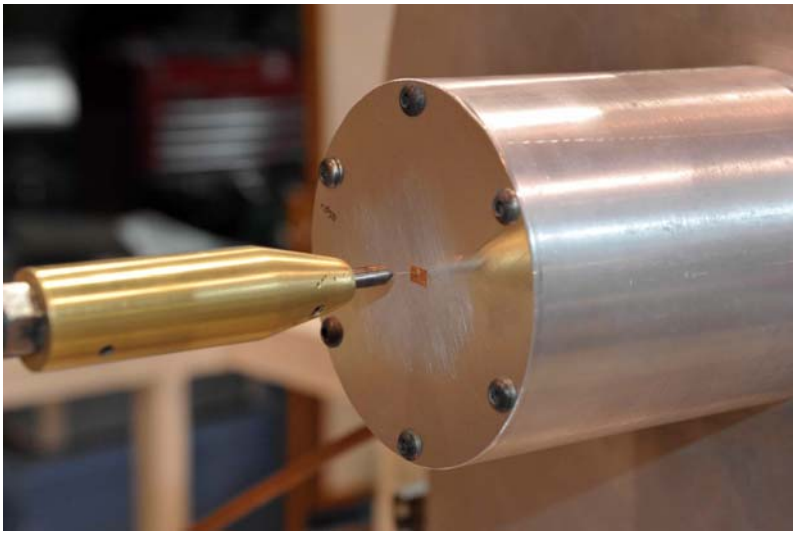

Figure 63. Starter wire setup for cable collector burnthrough experiment.

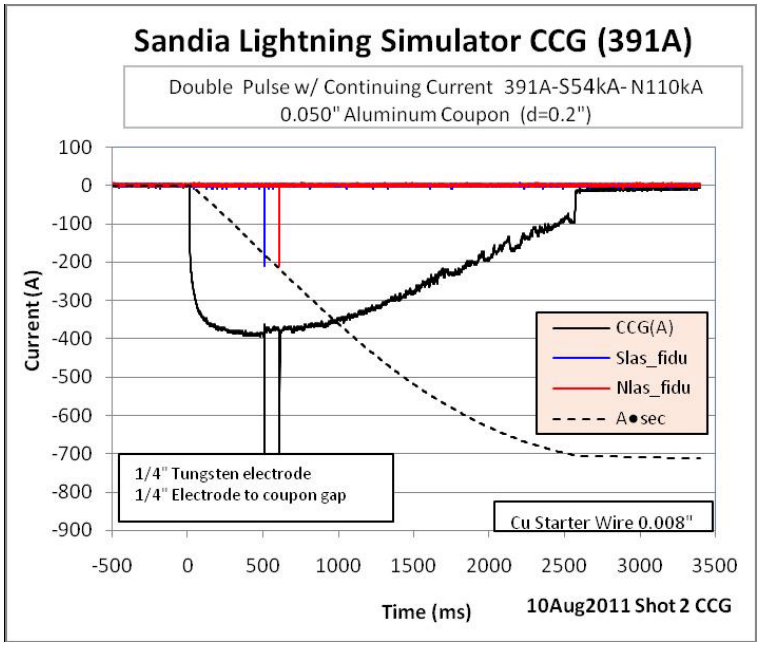

Figure 64. Continuing current waveform and return stroke impulses used in a cable collector burnthrough experiment. The dashed curve shows the charge transfer.

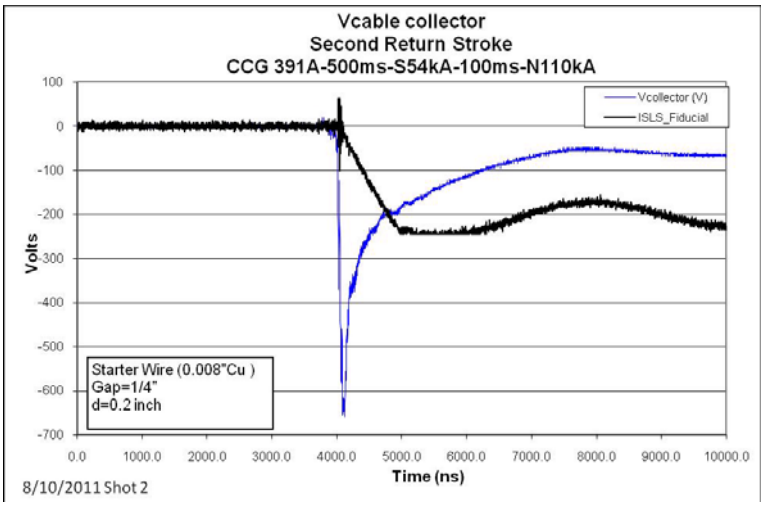

Figure 65. Open circuit voltage on cable collector using starter wire initiation and double return strokes with severe charge transfer.

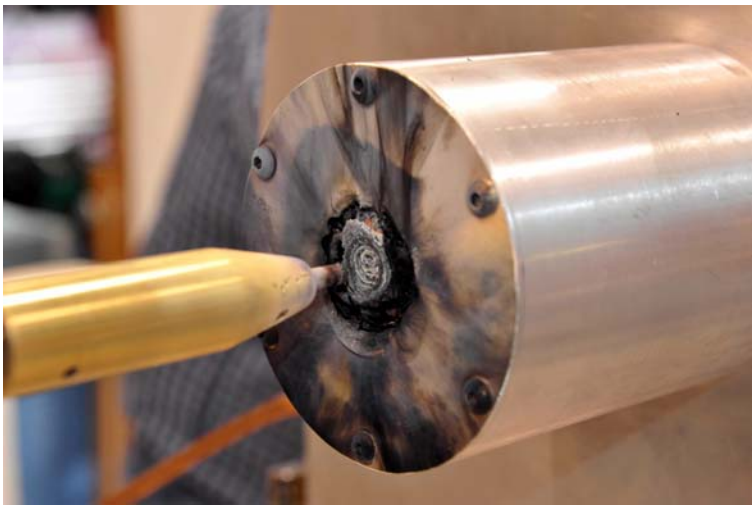

Figure 66. Damage in starter wire and cable collector burnthrough experiment.

4 INDIRECT COUPLING MECHANISMS

It is important to understand field coupling levels to interior cables to establish linear baseline levels that exist independent of ionization pathways that may be formed during the direct discharge. This section estimates the induced sources for magnetic field and electric field coupling to interior cables. We take the approach here of decomposition of the problem into exterior field, aperture penetration, and cable coupling, but carefully insert relevant practical (and interesting) details necessary for comparison to the experiments.

4.1 Magnetic Field Coupling

The magnetic field coupling problem to the interior cable is now formulated.

4.1.1 Reciprocity Formulation of Cable Voltage Source

The magnetic flux penetrating the hole induces an equivalent voltage source on the common mode (cable to enclosure) transmission line formed by the cable with respect to the chassis ground of the enclosure. We follow Latham's reciprocity approach [12] to determine the equivalent voltage source in terms of the exterior drive field, the hole properties, and the interior transmission line. We define an auxiliary magnetic scalar potential ϕ_m^0 as the potential that is generated by the common mode current I_0 on the cable (with return $-I_0$ on the enclosure formed by an image of the cable) with the hole shorted. This potential satisfies Laplace's equation

$$\nabla^2 \phi_m^0 = 0$$

where the auxiliary field is

$$\underline{H}^0 = -\nabla \phi_m^0$$

This potential is associated with a current I_0 on the center conductor and a current $-I_0$ on the surface of the auxiliary shield S_0. The boundary conditions are the vanishing of the normal component of the magnetic field on the metallic surfaces of the enclosure and the cable or

$$\frac{\partial \phi_m^0}{\partial n} = 0$$

Because there is a current I_0 in the region where ϕ_m^0 is defined, there is a branch surface J from the cable conductor out to the enclosure conductor on which the potential jumps by I_0; this branch surface can be taken to connect a curve (in the simplest case a line) along the wire surface to the interior enclosure plane away from the hole location. We denote the two sides of the jump surface by J_+ and J_- where J_+ is the side determined by applying the right hand rule to the cable (I_0 in the thumb direction and fingers emanating from J_+).

The actual problem with the hole has magnetic potential ϕ_m^h satisfying Laplace's equation

$$\nabla^2 \phi_m^h = 0$$

with current I_0 in the center conductor. The boundary conditions are

$$\frac{\partial \phi_m^h}{\partial n} = 0$$

on the enclosure with the hole (excluding the hole) and on the cable surface. The difference potential can be defined

$$\phi_m = \phi_m^h - \phi_m^0$$

also satisfying

$$\nabla^2 \phi_m = 0$$

but in this case having no jump surface J since there is no net current on the cable for the difference problem. Now we can write

$$\nabla \cdot \left(\phi_m^0 \nabla \phi_m - \phi_m \nabla \phi_m^0 \right) = \phi_m^0 \nabla^2 \phi_m - \phi_m \nabla^2 \phi_m^0 = 0$$

Integration over the interior volume and using the divergence theorem (Green's theorem) gives

$$\int_V \nabla \cdot \left(\phi_m^0 \nabla \phi_m - \phi_m \nabla \phi_m^0 \right) dV = \oint_S \left(\phi_m^0 \frac{\partial \phi_m}{\partial n} - \phi_m \frac{\partial \phi_m^0}{\partial n} \right) dS = 0$$

where the unit vector $\underline{n}$ points out of the interior region V and the closed surface includes the plane of the interior enclosure surface, the cable surface, and the jump surface J, and the unit normal points out of the volume. Since the second term is single valued on the jump surface the two sides cancel. In addition, the second term also vanishes on the surface of the hole A, because the normal magnetic field of the auxiliary problem is zero on this surface. Finally, because the normal field in both problems vanishes on the cable and the conducting enclosure surfaces, we can write this as

$$\int_{J_+} \phi_m^0 \frac{\partial \phi_m}{\partial n} dS + \int_{J_-} \phi_m^0 \frac{\partial \phi_m}{\partial n} dS = - \int_A \phi_m^0 \frac{\partial \phi_m}{\partial n} dS$$

$$= \int_{J_+} \left[\left(\phi_m^0 \right)_{J_+} - \left(\phi_m^0 \right)_{J_-} \right] \frac{\partial \phi_m}{\partial n} dS$$

where we have used the reversal of the unit normal on the two jump surfaces along with continuity of the normal field (choosing $\underline{n}$ on the branch surface is chosen to point into the J_+ surface)

$$\left(\frac{\partial \phi_m}{\partial n} \right)_{J_+} = - \left(\frac{\partial \phi_m}{\partial n} \right)_{J_-}$$

The magnetic difference flux (versus the flux in the auxiliary problem) directed around the center conductor, emanating from J_+, is

$$\Phi = \mu_0 \int_{J_+} \frac{\partial \phi_m}{\partial n} dS$$

Noting that (where C is a path from J_+ to J_- around the cable)

$$I_0 = \oint_C \underline{H} \cdot \underline{d\ell} = - \oint_C \nabla \phi_m \cdot \underline{d\ell} = - \int_C \frac{\partial \phi_m}{\partial \ell} d\ell = - \left[\left(\phi_m^0 \right)_{J_-} - \left(\phi_m^0 \right)_{J_+} \right]$$

then yields

$$\Phi = -\mu_0 \int_A \frac{\phi_m^0}{I_0} \frac{\partial \phi_m}{\partial n} dS = -\mu_0 \int_A \frac{\phi_m^0}{I_0} \frac{\partial \phi_m^h}{\partial n} dS$$

We can replace the potential derivatives by the normal field in the hole (directed into the exterior half space)

$$\frac{\partial \phi_m^h}{\partial n} = -H_n \text{ on } A$$

If we apply Faraday's law on a contour C consisting of a small length $d\ell$ section of the jump surface J we find that the electric field integral gives the difference voltage dV along the line (time dependence $e^{-i\omega t}$ is used). At low frequencies we can write this as

$$\oint_C \underline{E} \cdot \underline{d\ell} = dV = i\omega \left(\Phi + L_0 d\ell I_0\right) = V_{eq} + i\omega \left(L_a + L_0 d\ell\right) I_0$$

where L_0 is the cable inductance per unit length of the line with the aperture shorted, L_a is a perturbation of the line inductance caused by the hole, and V_{eq} is an equivalent voltage source on the line at the hole; the inductance per unit length term is added here because the difference flux does not include it. The two other terms are separated by virtue of the fact there are two sources for the field in the aperture. One is the exterior short circuit field $\underline{H}^{sc}$ and the second is the interior current I_0. In this form no approximations of hole size or shape have been made other than the hole being small compared to the wavelength. So this could, in principle, be applied in cases where the following approximations do not hold, provided that the magnetic scalar potentials can be found or approximated in some more accurate manner. However, when we can proceed to the following approximate decomposition, the resulting formula can be applied to many different types of exterior drives, aperture types, and cables by simply switching the appropriate quantities, if they are know.

If the hole is small enough compared to other dimensions in the problem, we can approximate the auxiliary potential as

$$\frac{\phi_m^0}{I_0} \approx \frac{\phi_m^0}{I_0}\left(\underline{s}_A\right) - \frac{1}{I_0}\underline{H}^0\left(\underline{s}_A\right) \cdot \left(\underline{s} - \underline{s}_A\right)$$

where the vector on the surface of the aperture is $\underline{s}$ and $\underline{s}_A$ is the aperture center. The integration of the first term vanishes because there is no net magnetic flux through the hole and we can write

$$\Phi \approx -\mu_0 \frac{1}{I_0}\underline{H}^0\left(\underline{s}_A\right) \cdot \int_A \left(\underline{s} - \underline{s}_A\right) H_n dS$$

The magnetic dipole moment of the hole (responsible for coupling into the interior) is found from [13]

$$\underline{m}_a = -2\int_A \left(\underline{s} - \underline{s}_A\right) H_n dS = -2\underline{\alpha}_m \cdot \underline{H}^{sc}\left(\underline{s}_A\right)$$

where $\underline{\alpha}_m$ is the magnetic polarizability tensor of the hole and $\underline{H}^{sc}$ is the exterior short circuit magnetic field at the hole. Because there are two sources for the normal field we can write

$$\Phi \approx -\mu_0 \frac{1}{I_0}\underline{H}^0\left(\underline{s}_A\right) \cdot \underline{\alpha}_m \cdot \left[\underline{H}^{sc}\left(\underline{s}_A\right) - \underline{H}^0\left(\underline{s}_A\right)\right]$$

where the minus sign on the field from the interior source is introduced since the dipole moment for the hole changes sign in this case (the normal field would be pointed inward and need to be reversed). Thus the equivalent source voltage driven by the exterior field is

$$V_{eq} \approx -i\omega\mu_0 \frac{1}{I_0} \underline{H}^0 (\underline{s}_A) \cdot \underline{\alpha}_m \cdot \underline{H}^{sc} (\underline{s}_A)$$

and the the lumped inductance is

$$L_a \approx \mu_0 \frac{1}{I_0^2} \underline{H}^0 (\underline{s}_A) \cdot \underline{\alpha}_m \cdot \underline{H}^0 (\underline{s}_A)$$

The tensor polarizability $\underline{\alpha}_m$ only has components in the plane of the aperture, and for a circular aperture can be taken as a scalar.

In the magnetic coupling case we take the interior cable to be grounded to chassis on one end and terminated in a load (a high impedance measurement system) on the other end. The current I_0 is taken in the y direction along the cable, in the direction of the plus terminal of the lumped induced voltage source V_{eq}. In our case here we take the short circuit magnetic field to be in the x direction and thus the aperture induced dipole moment is related to the polarizability component in this direction through

$$m_x = -2\alpha_m H_x^{sc}$$

The tensor polarizability $\underline{\alpha}_e$ only has a normal component and can be taken as a scalar

$$p_z = 2\varepsilon_0 \alpha_e E_z^{sc}$$

and the voltage source in the time domain is

$$V_{eq} = -\frac{d\Phi_{eq}}{dt}$$

where the corresponding charge is

$$\Phi_{eq} = -\mu_0 \frac{1}{I_0} \underline{H}^0 (\underline{s}_A) \cdot \underline{\alpha}_m \cdot \underline{H}^{sc} (\underline{s}_A)$$

4.1.2 Magnetic Polarizability

For the circular aperture in a thin conducting plane the polarizability is [13]

$$\alpha_{m0} = \frac{4}{3} a^3$$

where a is the aperture radius. For small plane thickness from a variational calculation [14]

$$\alpha_m \approx \alpha_{m0} \left[1 - \frac{3\Delta}{2\pi a} \{ \ln (a/\Delta) + 1.88 \} - \frac{3\pi\Delta}{16a} \right]$$

However it is interesting that the barrier plane thickness $\Delta = 0.05$ inches cannot be ignored even though in our experiments we have a hole diameter of $2a = 0.5$ inches. Gluckstern [14] has shown that the first mode of the circular waveguide yields a polarizability

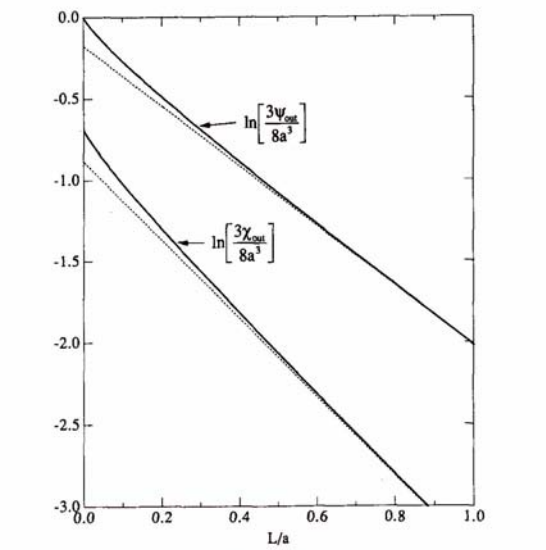

Fig. 5. "Outside" polarizability and susceptibility as a function of wall thickness. The dashed lines are the asymptotic limits for thick walls.

Figure 67. Comparison of exact solution and deep asymptotic formulas for magnetic ψ_{out} and electric χ_{out} polarizabilities for a circular hole in a thick conducting plane taken from [14].

$$\alpha_m \approx \alpha_{m0}\, 0.838\, e^{-1.841(\Delta/a)} \approx 0.580\alpha_{m0}$$

which is reasonably close to an exact solution for $\Delta/(2a) \geq 0.1$ [14], where $j'_{11} = 1.841$ is the first root of $J'_1(x) = 0$ [20]. Figure 67, taken from [14], shows a comparison of the exact solution and leading asymptotic forms of the magnetic $\psi_{out} = 2\alpha_m$ and electric $\chi_{out} = 2\alpha_e$ polarizabilities in a thick conducting plane (here $L = \Delta$). It is interesting that this small thickness makes such a reduction in polarizability.

In addition, for a thin plane, if the cable is a stripline of width comparable to or larger than the hole diameter and spacing from the hole, we can use the result of a circular hole with a backing conductor (approximately the stripline cable) to find an estimate for the reduced polarizability [13] shown in Figure 68.

We can write (α_e being the electric polarizability discussed below)

$$\alpha_{m0}/\alpha_m \approx 1 + (2/\pi)\sum_{n=1}^{\infty} F(nh/a) \approx 1.0722 \approx \alpha_{e0}/\alpha_e$$

where

$$F(x) = \arctan(1/x) + x - \left(x^3 + 3x/2\right)\ln\left(1 + 1/x^2\right)$$

with asymptotic form

$$F(x) \sim \frac{1}{12x^3}\left(1 - \frac{3}{5x^2}\right)$$

$$x^3 F(x) \sim 1/12$$

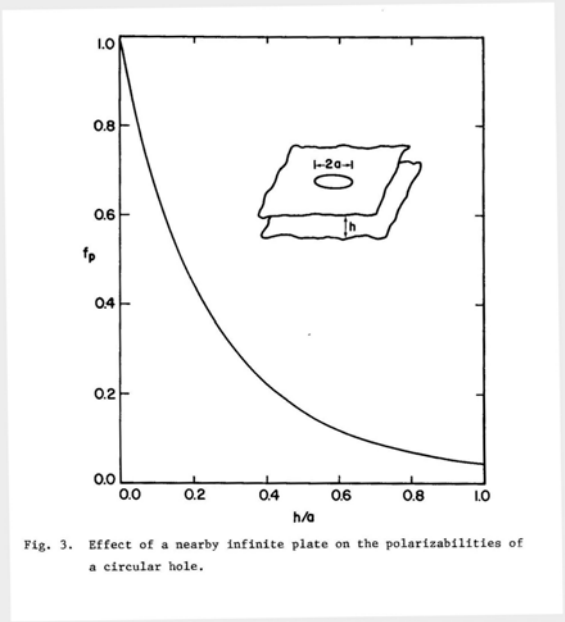

Fig. 3. Effect of a nearby infinite plate on the polarizabilities of a circular hole.

Figure 68. Figure from [13] showing change in polarizabilities of a circular hole because of proximity of interior ground plane.

Carrying out the summation for our case with $h = 0.2$ in and $a = 0.25$ in gives

$$F\left(h/a\right) = 0.08509190$$

$$F\left(2h/a\right) = 0.01652197$$

$$F\left(3h/a\right) = 0.005462843$$

$$F\left(4h/a\right) = 0.002402885$$

$$F\left(5h/a\right) = 0.001255136$$

$$F\left(6h/a\right) = 0.0007344289$$

and

$$1 + \left(2/\pi\right) \sum_{n=1}^{\infty} F\left(nh/a\right)$$

$$\approx 1 + \left(2/\pi\right) \left[\sum_{n=1}^{6} F\left(h/a\right) + \frac{1}{12} \left(\frac{a}{h}\right)^3 \left\{ \zeta\left(3\right) - 1 - \frac{1}{2^3} - \frac{1}{3^3} - \frac{1}{4^3} - \frac{1}{5^3} - \frac{1}{6^3} \right\} \right]$$

$$\approx 1 + \left(2/\pi\right) \left[0.1114692 + \frac{1}{12} \left(\frac{a}{h}\right)^3 \left\{ \zeta\left(3\right) - 1.190292 \right\} \right]$$

$$\approx 1.0722$$

where the zeta function of argument three is [20]

$$\zeta\left(3\right) = \sum_{n=1}^{\infty} n^{-3} = 1.20205690$$

or

$$\alpha_m / \alpha_{m0} \approx 0.933 \approx \alpha_e / \alpha_{e0}$$

Combining this with the waveguide decay gives an effective magnetic polarizability

$$\alpha_m^{eff} \approx 0.541 \alpha_{m0}$$

4.1.3 Effective Magnetic Field Drives

In our problem we are interested in direct current attachments to the conducting barrier near the hole.

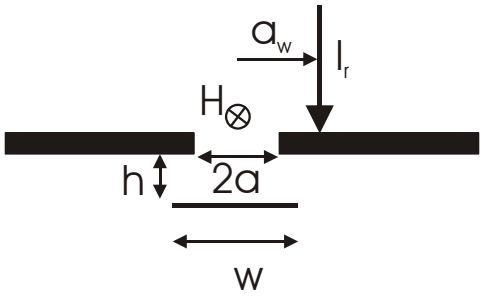

Figure 69. An idealized vertical current attached to the hole edge driving magnetic coupling to an interior cable. The cable has been rotated by ninety degrees from the orientation for maximal coupling simply to show the cross sectional characteristics in this two-dimensional drawing.

The short circuit field at the hole in these cases is not uniform. Nevertheless, by examining the penetrant magnetic fields through circular holes in a thin conducting plane with these current drives (in oblate spheroidal coordinates), it is possible to select effective values for the short circuit fields in the uniform case that produce the same penetrant dipole moments [15]. The cases examined in this report [15] were attempts at the extreme worst case and did not include some practical considerations needed to compare with experiments.

In the case where the current is injected perpendicular to the enclosure surface there was a spacing between the hole edge and the current attachment to the coupon. Figure 69 shows the current filament slightly displaced from the hole edge to account for the fact that the current carrying wire had a finite radius and insulation. Thus the attachment radius was (for $a = 0.25$ in)

$$a_w \approx 0.25 \text{ in} + 0.0625 \text{ in}$$

If we examine the appendix of the report [15], we see that the expansions of the short circuit potential on p. 54 can be extended to this case simply by replacing a by a_w. Then the ratio (a/a_w) will multiply the $m = 1$ term in the incident potential in the report on p. 55. Thus the scattered potential on p. 58 has a $m = 1$ term multiplied by (a/a_w). Therefore the dipole moment on p. 59 has the multiplier (a/a_w), which in our case was 0.8. Consequently the effective short circuit magnetic field from the filament can be taken as the short field at the hole center (here we take the current filament to be located at $y = -a_w$ with z positive in the direction of the half space containing the filament)

$$H^{sc}_{x(eff)}\left(\underline{s}_A\right) = \frac{I_r}{2\pi a_w}$$

This field, combined with the polarizability α_{m0} in a thin plane, then produces exactly the right dipole moment from this wire excitation [15]

$$m_x = -\frac{4a^2}{3\pi}\left(\frac{a}{a_w}\right) I_r$$

Because the discharge to the vicinity of the hole edge might have a tilt it is useful to bound the effect as shown in Figure 70 assuming a horizontal arrangement. The report [15] assumed that the filament was directly on the hole surface, but the experiment here required a slight displacement to account for the wire radius and insulation.

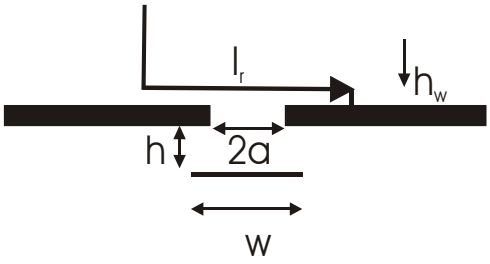

Figure 70. To capture the "worst case" tilt of the arc channel with respect to magnetic coupling we can consider the horizontal current filament drive shown in this figure. The cable has been rotated by ninety degrees from the orientation for maximal coupling simply to show the cross sectional characteristics in this two-dimensional drawing.

$$h_w \approx 0.0625 \text{ in}$$

To account for this displacement h_w in the calculations of [15] we take the short circuit potential for the displaced filament to be (in this reference we take the filament to be along the x axis at $z = h_w$ and $y = 0$, and hence the short circuit field on the surface is y directed)

$$\phi_m^{sc} = -\frac{I_r}{2\pi}\left[\arctan\left(\frac{y}{z-h_w}\right) - \arctan\left(\frac{y}{z+h_w}\right)\right]$$

The magnetic field is then

$$H_y^{sc} = -\frac{\partial \phi_m}{\partial y} = -\frac{I_r}{2\pi}\left[\frac{z-h_w}{y^2+(z-h_w)^2} - \frac{z+h_w}{y^2+(z+h_w)^2}\right]$$

$$H_z^{sc} = -\frac{\partial \phi_m}{\partial z} = -\frac{I_r}{2\pi}\left[\frac{y}{y^2+(z-h_w)^2} - \frac{y}{y^2+(z+h_w)^2}\right]$$

and on the surface $z = 0$

$$H_x^{sc} = \frac{I_r h_w/\pi}{y^2+h_w^2}$$

$$H_z^{sc}(x,y,0) = -\frac{I_r}{2\pi}\left[\frac{y}{y^2+h_w^2} - \frac{y}{y^2+h_w^2}\right] = 0$$

$$\phi_m^{sc}(x,y,0) = -\frac{I_r}{2\pi}\left[\arctan\left(\frac{y}{-h_w}\right) - \arctan\left(\frac{y}{+h_w}\right)\right]$$

Note that as $h_w \to 0$

$$\lim_{h_w\to 0}\frac{1}{\pi}\int_{-a}^{a} f(y)\frac{h_w}{y^2+h_w^2}dy = \lim_{h_w\to 0}\frac{1}{\pi}\int_{-a/h}^{a/h} f(yh)\frac{dy}{y^2+1} = f(0)\frac{1}{\pi}\int_{-\infty}^{\infty}\frac{dy}{1+y^2}$$

$$= f(0)$$

$$H_y^{sc} \to I_r \delta(y)$$

and

$$\phi_m^{sc} \to \frac{I_r}{2} \mathrm{sgn}(y) + c$$

where one half the first term is what was assumed for the incident potential in [15] p. 64. If we take

$$\arctan\left(\frac{y}{-h_w}\right) = -\arctan\left(\frac{y}{+h_w}\right)$$

then $c = 0$ and

$$\phi_m^{sc}(x, y, 0) = \frac{I_r}{\pi} \arctan\left(\frac{y}{h_w}\right)$$

and in addition

$$\phi_m^{i}(x, y, 0) = \frac{1}{2}\phi_m^{sc} = \frac{I_r}{2\pi} \arctan\left(\frac{y}{h_w}\right)$$

The solution in oblate spheroidal coordinates is

$$\phi_m(\zeta, \xi, \varphi) = \sum_{n=1}^{\infty} \sum_{m=1}^{n} B_{mn} Q_n^m(j\zeta) P_n^m(\xi) \sin(m\varphi)$$

Using

$$y = a\sqrt{1+\zeta^2}\sqrt{1-\xi^2}\sin\varphi$$

and applying the complementary (to the hole) disc boundary condition and matching gives

$$\phi_m(0, \xi, \varphi) = \phi_m^{i}(0, \xi, \varphi) \ , \ -1 < \xi < 1 \ , \ -\pi < \varphi < \pi$$

Orthogonality then yields [20]

$$B_{mn} Q_n^m(j0) \frac{2(n+m)!}{(2n+1)(n-m)!}\pi = \frac{I}{\pi} \int_{-1}^{1} P_n^m(\xi)\, d\xi \int_0^{\pi} \sin(m\varphi)\, d\varphi \arctan\left(\frac{a}{h_w}\sqrt{1-\xi^2}\sin\varphi\right)$$

For the dipole moment we only need the $n = m = 1$ term

$$P_1^1(\xi) = -\sqrt{1-\xi^2}$$

$$Q_1^1(j0) = \frac{\pi}{2}$$

$$B_{11} Q_1^1(j0) \frac{4}{3}\pi = -\frac{2}{\pi} I_r \int_0^1 \sqrt{1-\xi^2} d\xi \int_0^{\pi} \sin\varphi d\varphi \arctan\left(\frac{a}{h_w}\sqrt{1-\xi^2}\sin\varphi\right)$$

We carry the integration out exactly by first changing variables to $\rho = \sqrt{1-\xi^2}$

$$B_{11}Q_1^1(j0) = -\frac{3}{\pi^2}I_r\int_0^1\frac{d\rho}{\sqrt{1-\rho^2}}\int_0^{\pi/2}\rho\sin\varphi\rho d\varphi\arctan\left(\frac{a}{h_w}\rho\sin\varphi\right)$$

Next changing from polar coordinates (ρ,φ) to a Cartesian system (u,v) we find

$$B_{11}Q_1^1(j0) = -\frac{3}{\pi^2}I_r\int_0^1 u\arctan\left(\frac{a}{h_w}u\right)du\int_0^{\sqrt{1-u^2}}\frac{dv}{\sqrt{1-u^2-v^2}}$$

Carrying out the v integration

$$\int_0^{\sqrt{1-u^2}}\frac{dv}{\sqrt{1-u^2-v^2}} = \int_0^1\frac{d\nu}{\sqrt{1-\nu^2}} = \int_0^{\pi/2}d\theta = \pi/2$$

and thus

$$B_{11}Q_1^1(j0) = -\frac{3I_r}{2\pi}\int_0^1 u\arctan\left(\frac{a}{h_w}u\right)du = -\frac{3I}{2\pi}\left(\frac{h_w}{a}\right)^2\int_0^{a/h_w}u\arctan(u)\,du$$

$$= -\frac{3I}{2\pi}\left(\frac{h_w}{a}\right)^2\left[\frac{1}{2}\left(1+u^2\right)\arctan(u)-\frac{u}{2}\right]_0^{a/h_w} = -\frac{3I}{4\pi}\left[\left(1+h_w^2/a^2\right)\arctan(a/h_w)-\frac{h_w}{a}\right]$$

Therefore

$$B_{11}Q_1^1(j0)\,/\left(-I_r\frac{3}{8}\right) = \left(1+h_w^2/a^2\right)\frac{2}{\pi}\arctan(a/h_w)-\frac{2}{\pi}\frac{h_w}{a}$$

or

$$B_{11}Q_1^1(j0)\,/\left(-I_r\frac{3}{8}\right) = \left(1+h_w^2/a^2\right)\left\{1-\frac{2}{\pi}\arctan(h_w/a)\right\}-\frac{2}{\pi}\frac{h_w}{a}$$

Now if we expand the $\arctan(x)$ in a power series

$$B_{11}Q_1^1(j0)\,/\left(-I_r\frac{3}{8}\right) \sim \left(1+h_w^2/a^2\right)\left[1-\frac{2h_w}{\pi a}\left(1-\frac{1}{3}\frac{h_w^2}{a^2}\right)\right]-\frac{2h_w}{\pi a}$$

$$\sim 1-\frac{4h_w}{\pi a}+\left(\frac{h_w}{a}\right)^2-\frac{2}{\pi}\left(\frac{h_w}{a}\right)^3+\frac{2}{3\pi}\left(\frac{h_w}{a}\right)^3+\frac{2}{3\pi}\left(\frac{h_w}{a}\right)^5+\cdots,\ \frac{h_w}{a}\to 0$$

or alternatively

$$B_{11}Q_1^1(j0)\,/\left(-I_r\frac{3}{8}\right) \sim \left(1+h_w^2/a^2\right)\frac{2}{\pi}\frac{a}{h_w}\left(1-\frac{1}{3}\frac{a^2}{h_w^2}\right)-\frac{2}{\pi}\frac{h_w}{a}$$

$$\sim \frac{4}{3\pi}\frac{a}{h_w}\left(1-\frac{1}{2}\frac{a^2}{h_w^2}\right),\ \frac{a}{h_w}\to 0$$

Hence the ratio of the preceding exact result for $B_{11}Q_1^1(j0)\,/\left(-I_r\frac{3}{8}\right)$ to the leading term in the limit $a/h_w\to 0$ times the magnetic field $H_y^{sc}\sim I_r/(\pi h_w)$ in this limit provides the effective short circuit magnetic field $H_{y(eff)}^{sc}$ exciting the aperture. Changing the notation to a current filament along the $-y$ direction gives

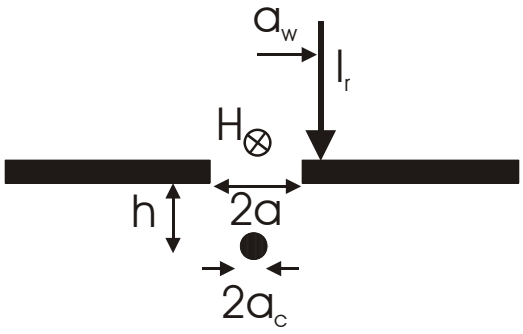

Figure 71. Magnetic coupling to a wire cable behind the hole. Note that the cable has been rotated by ninety degrees from the maximal coupling case for ease of illustration.

$$H^{sc}_{x(eff)}\left(\underline{s}_A\right) = \frac{3I_r}{2\pi a}\left[\left(1+h_w^2/a^2\right)\arctan\left(a/h_w\right) - h_w/a\right]$$

where again this produces the exact magnetic dipole moment for a horizontal line current excitation of the circular hole. In the limit $h_w << a$ this becomes [15]

$$H^{sc}_{x(eff)}\left(\underline{s}_A\right) \sim 3I_r/\left(4a\right)$$

and using

$$\alpha_{m0} = \frac{4}{3}a^3$$

gives

$$m_x = -2\alpha_{m0}H^{sc}_x = -2a^2 I_r$$

which agrees with the result on p. 65 of [15]. In the limit $h_w >> a$ this gives the obvious value from a line current imaged in the ground plane

$$H^{sc}_{x(eff)}\left(\underline{s}_A\right) \to \frac{2I_r}{2\pi h_w}$$

4.1.4 Wire Coupling

The final part of the coupling formula is the field at the hole (with the hole shorted) produced by a current on the cable or wire, as shown in Figure 71, normalized by that same current $H^0_x\left(\underline{s}_A\right)/I_0$. With the decomposition approach we can consider various types of cables (circular, stripline, etc.). Given a wire height h and wire radius a_c this is found to be the sum of the fields from the wire with current centroid at $-z = \sqrt{h^2 - a_c^2}$ and its image in the ground plane

$$H^0_x\left(\underline{s}_A\right)/I_0 = -1/\left(\pi\sqrt{h^2 - a_c^2}\right)$$

For $h >> a_c$

$$H^0_x\left(\underline{s}_A\right)/I_0 \sim -1/\left(\pi h\right)$$

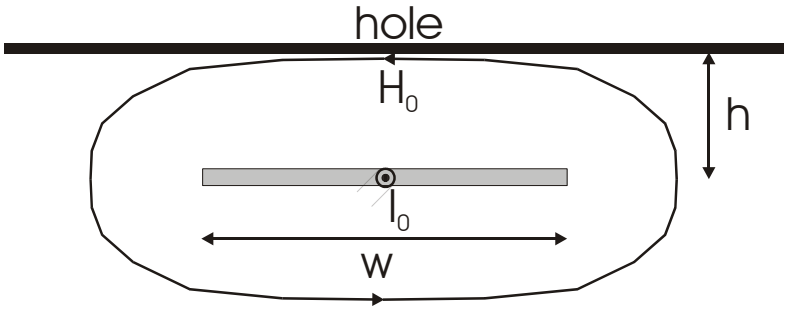

Figure 72. Magnetic field intensity at the hole due to current I_0 on the stripline with hole shorted. The positive x direction is taken to the left.

4.1.5 Stripline Coupling

We are also interested in a stripline cable as shown in Figure 72.

The case of a stripline of width w at an extremely small (by comparison to w) distance h below the hole gives

$$H_x^0\left(\underline{s}_A\right)/I_0 \sim -1/w$$

However it is important to address the case where the distance h is not so restricted to get a feel for the error in the preceding very rough approximation.

The problem of a stripline above a ground plane (or two strips) can be solved exactly by conformal mapping. In the conformal mapping solution we rotate the strip and its image by ninety degrees to $x = \pm h$, $|y| < w/2$ for convenience. The conformal transformation which maps two parallel strips with potentials $\pm U_0$ (at locations $x = \pm h$) of width w and separation $2h$ (one strip and a PEC symmetry plane at $x = 0$ and at zero potential) to two coplanar strips with inner edges at $\pm b$ and outer edges at $\pm d$ (the potentials on the coplanar strips are also $\pm U_0$) is [16]

$$z = x + iy = C_1 \int_0^{z_1} \left(z_1^2 - c^2\right) \frac{dz_1}{\sqrt{\left(z_1^2 - d^2\right)\left(z_1^2 - b^2\right)}}$$

where

$$\sqrt{\frac{K(k) - E(k)}{k^2 K(k)}} = \sin\lambda$$

$$\frac{\pi w/4}{h} = K(k)\, E(\lambda, k) - E(k)\, F(\lambda, k)$$

and

$$E(\lambda, k) = \int_0^{\lambda} d\theta \sqrt{1 - k^2 \sin^2\theta}$$

$$E(k) = E(\pi/2, k)$$

$$F(\lambda,k)=\int_0^{\lambda} d\theta/\sqrt{1-k^2\sin^2\theta}$$

$$K(k)=F(\pi/2,k)$$

is solved for k. The constants C_1, b, and c are found from

$$h/C_1=d\pi/\left[2K(k)\right]$$

$$d^2E(k)=c^2K(k)$$

$$\sqrt{\frac{d^2-c^2}{d^2-b^2}}=\sin\lambda$$

given that d is set arbitrarily (could be taken as unity). Note that the point between strips $z=0$ is mapped to the point between coplanar strips $z_1=0$. Next we note that Smythe [16] gives the transformation from a box with PECs at $W=\pm U_0$ and PMCs at $W=0,iV_1$ to the preceding coplanar strips

$$z_1=x_1+iy_1=b\ \mathrm{sn}\left(\frac{K_1W}{U_0},k_1\right)$$

$$W=C_2\int_0^{z_1}\frac{dz_1}{\sqrt{(z_1^2-b^2)(z_1^2-d^2)}}=-\frac{C_2}{d}\int_0^{z_1/b}\frac{dt}{\sqrt{(1-t^2)(1-k_1^2t^2)}}$$

$$=\frac{U_0}{K(k_1)}\mathrm{sn}^{-1}\left(\frac{z_1}{b},k_1\right)$$

where

$$k_1=b/d$$

and

$$C_2=-\frac{U_0d}{K(k_1)}$$

$$\mathrm{sn}^{-1}(y,k_1)=F(\arcsin y,k_1)=\int_0^{y}\frac{dt}{\sqrt{(1-t^2)(1-k_1^2t^2)}}$$

Note that the point $W=0$ maps to the point $z_1=0$. We can take the electric scalar potential to be

$$\phi^0=\mathrm{Re}\,(W)$$

$$\underline{E}^0=-\nabla\phi^0$$

The horizontal electric field is

$$E_x^0 = -\frac{\partial \phi^0}{\partial x} = -\operatorname{Re}\left(\frac{\partial W}{\partial x}\right) = -\operatorname{Re}\left(\frac{dW}{dz}\right) = -\operatorname{Re}\left(\frac{dW}{dz_1}\frac{dz_1}{dz}\right)$$

$$\frac{dW}{dz_1} = \frac{-U_0 d}{K(k_1)\sqrt{(z_1^2 - b^2)(z_1^2 - d^2)}}$$

$$\frac{dz}{dz_1} = \frac{2h}{\pi d} K(k) \frac{\left(z_1^2 - c^2\right)}{\sqrt{(z_1^2 - d^2)(z_1^2 - b^2)}}$$

or

$$E_x^0 = \operatorname{Re}\left[\frac{U_0 \pi d^2}{K(k_1)(z_1^2 - c^2) 2hK(k)}\right]$$

The value at the origin is

$$-hE_x^0(0,0)/U_0 = \frac{\pi d^2/\left(2c^2\right)}{K(k_1)K(k)}$$

or with $d = 1$ we have $b = k'$ and $E(k) = c^2 K(k)$

$$-hE_x^0(0,0)/U_0 = \frac{\pi/2}{K(k_1)E(k)} = \frac{\pi/2}{K(k')E(k)}$$

$$\sqrt{\frac{K(k) - E(k)}{k^2 K(k)}} = \sin\lambda$$

$$\frac{\pi w/4}{h} = \xi/2 = K(k)E(\lambda, k) - E(k)F(\lambda, k)$$

$$\sqrt{1 - k^2} = k'$$

Note that the capacitance per unit length is

$$C_0 = \varepsilon_0 \frac{K(k)}{K(k')}$$

It is interesting that an incredibly accurate approximation is [17]

$$\frac{K(k')}{K(k)} \approx \frac{1}{\pi} \ln\left(2\frac{1 + \sqrt{k'}}{1 - \sqrt{k'}}\right) \ , \ k' > 0.01$$

and thus the very accurate implicit form results

$$C_0 \approx \varepsilon_0 \frac{1}{\pi} \ln\left(2\frac{1 + \sqrt{k}}{1 - \sqrt{k}}\right) \ , \ k > 0.01$$

We would like to have the solutions for $\xi \geq 1$ or $k' \leq 0.5304 \rightarrow k \geq 0.8477$. Making use of the

expansions [20]

$$\frac{2}{\pi}K\left(k'\right) \sim 1 + k'^2/4 + \frac{9}{64}k'^4 + \cdots$$

$$E\left(k\right) = \frac{\pi}{2}F\left(-\frac{1}{2}, \frac{1}{2}; 1; k^2\right) \sim 1 + \left(k'^2/4\right)\left\{2\ln\left(4/k'\right) - 1\right\} + \cdots$$

if we take

$$\zeta = \ln\left(4/k'\right)$$

and consider the limit $k \to 1$, where

$$K\left(k\right) \sim \zeta + O\left(k'^2 \ln k'\right)$$

and

$$E\left(k\right) \sim 1 + O\left(k'^2 \ln k'\right)$$

with the asymptotic form

$$C_0 \sim \varepsilon_0 \frac{2}{\pi}\zeta$$

then we can write

$$\lambda \sim \frac{\pi}{2} - \sqrt{\zeta}$$

and

$$F\left(\lambda, k\right) \sim \ln\left[\frac{1 + \sqrt{1 - 1/\zeta}}{\sqrt{1/\zeta}}\right]$$

$$E\left(\lambda, k\right) \sim \sqrt{1 - 1/\zeta}$$

From the transcendental equation $\xi/2 = K\left(k\right)E\left(\lambda, k\right) - E\left(k\right)F\left(\lambda, k\right)$ we can then write

$$\xi \sim \zeta\sqrt{1 - 1/\zeta} - \ln\left[\frac{1 + \sqrt{1 - 1/\zeta}}{\sqrt{1/\zeta}}\right]$$

$$\sim \zeta - \frac{1}{2}\left\{\ln\left(4\zeta\right) + 1\right\} + \frac{1}{8\zeta}$$

Iteratively solving for 2ζ gives

$$2\zeta = 2\ln\left(4/k'\right) \sim \xi + 1 + \ln\left\{2\xi + 1 + 2\ln\left(2\xi + 4\right)\right\}$$

Thus an explicit approximation for the capacitance shown in Figure 73, with error shown in Figure 74, is

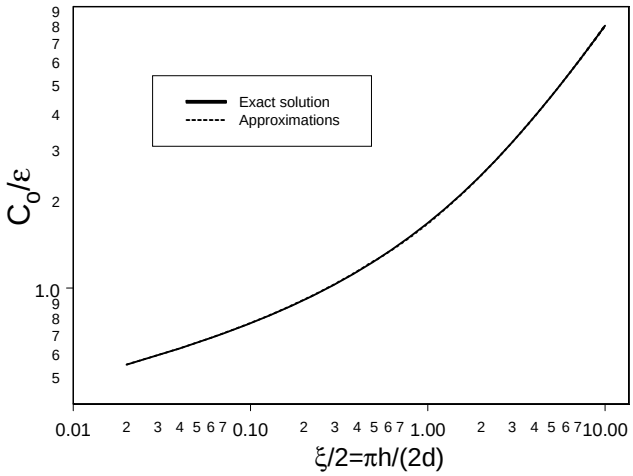

Figure 73. An explicit approximation for the capacitance per unit length versus the exact evaluation of the conformal mapping functions.

$$C_0 \approx \varepsilon_0 \frac{2}{\pi} \left[\xi + 1 + \ln \left\{ 2\xi + 1 + 2 \ln \left(2\xi + 4 \right) \right\} \right] \, , \, \xi \geq 1 \, , \, (0.5\% \text{ error})$$

$$C_0 \approx \varepsilon_0 \frac{2\pi}{\ln \left(4\pi / \xi \right)} \, , \, \xi \leq 1 \, , \, (0.5\% \text{ error})$$

where

$$\xi = \pi w / \left(2h \right)$$

The preceding field at the plane versus voltage is

$$-hE_x^0 \left(0, 0 \right) / U_0 = \frac{\pi / 2}{K \left(k' \right) E \left(k \right)} \sim \frac{1}{\left(1 + k'^2 / 4 \right) \left[1 - \left(k'^2 / 4 \right) \left\{ 2 \ln \left(4 / k' \right) - 1 \right\} \right]} \, , \, k' \to 0$$

The fit

$$-hE_x^0 \left(0, 0 \right) / U_0 \approx 1 - \frac{1}{4 \left(\xi^2 - 2 \ln \xi \right)} \, , \, \xi \geq 1$$

seems to work reasonably well as shown in Figure 75. The preceding quantity has been normalized so that it is the value of the origin electric field relative to that of the parallel plate value. This will be used in the electric coupling section below.

In the two-dimensional magnetic field problem we would take $A_{\tilde{z}}^0 = \text{Re} \left(W \right)$ and $\mu_0 \underline{H}^0 = \nabla \times \underline{A}^0 = -\underline{e}_z \times \nabla_t A_z^0$ versus $\phi^0 = \text{Re} \left(W \right)$ and $\underline{E}^0 = -\nabla_t \phi^0$ (with $\nabla_t = \underline{e}_x \frac{\partial}{\partial x} + \underline{e}_y \frac{\partial}{\partial y}$ the transverse gradient operator). To calculate the required magnetic field value we seek at the hole center, we need to change from the voltage normalization (the dual of which is the magnetic flux per unit length) to a total charge per unit length normalization (the dual of which is the total electric current).

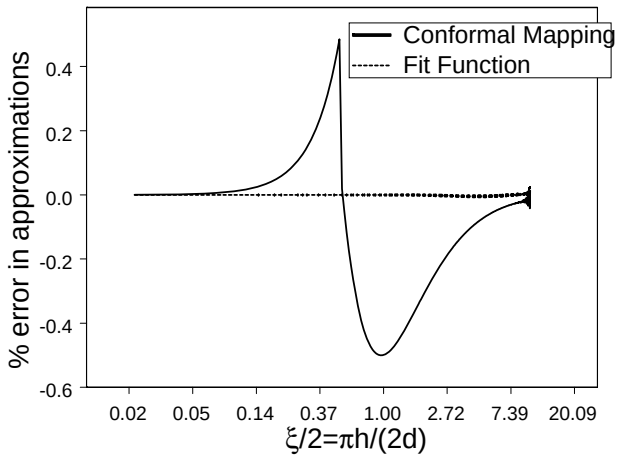

Figure 74. Relative error of explicit approximation for capacitance per unit length versus the exact conformal mapping solution.

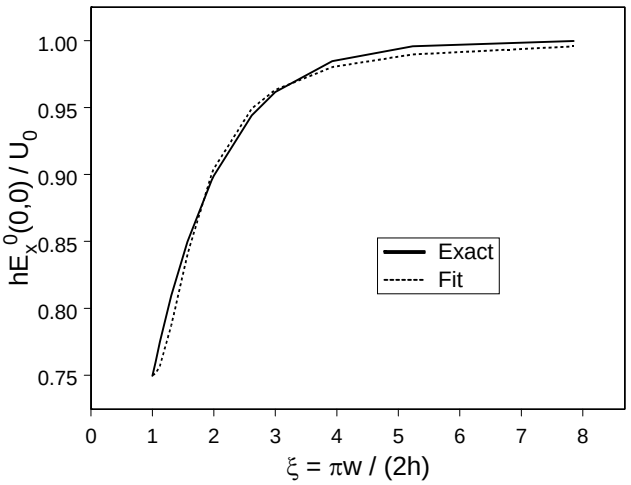

Figure 75. Comparison of field on symmetry plane at strip center from simple fit versus exact conformal mapping solution.

$$\int_{C_{strip}} \frac{\partial \phi^0}{\partial n} d\ell = q_0/\varepsilon_0$$

$$E_x^0(0,0) = -\frac{\partial \phi^0}{\partial x}(0,0)$$

$$\int_{C_{strip}} \frac{\partial A_z^0}{\partial n} d\ell = \mu_0 I_0$$

$$\mu_0 H_y^0(0,0) = -\frac{\partial A_z^0}{\partial x}(0,0)$$

From this we see that the results from the electrostatic problem can be used to obtain the desired quantity in the magnetostatic problem by means of

$$\varepsilon_0 E_x^0(0,0)/q_0 \rightarrow H_y^0(0,0)/I_0$$

We can use the capacitance per unit length to do this transformation to the charge per unit length. The ratio of the charge on the top of the strip (the uniform field part) to the total charge using the preceding capacitance fit is

$$\frac{\varepsilon_0 w/h}{C_0} = 2\frac{\varepsilon_0 \xi/\pi}{C_0} \approx \frac{\xi}{\xi + 1 + \ln\{2\xi + 1 + 2\ln(2\xi + 4)\}}, \; \xi \geq 1$$

$$\frac{\varepsilon_0 w/h}{C_0} = 2\frac{\varepsilon_0 \xi/\pi}{C_0} \approx \frac{\xi}{\pi^2}\ln(4\pi/\xi) \;\; , \;\; \xi \leq 1$$

Noting that the product of the capacitance per unit length and voltage is the charge per unit length $C_0 U_0 = q_0$ we can write

$$\left[-hE_x^0(0,0)/U_0\right]\left(\frac{\varepsilon_0 w/h}{C_0}\right) = -w\varepsilon_0 E_x^0(0,0)/q_0 \rightarrow -wH_y^0(0,0)/I_0$$

where the final quantity is what we seek. Thus, returning to the original coordinate system with $H_y^0 \rightarrow H_x^0$, gives

$$G \equiv \left[-wH_x^0(0,0)\right]/I_0 \approx \frac{\xi\left[1 - 1/\left\{4\left(\xi^2 - 2\ln\xi\right)\right\}\right]}{\xi + 1 + \ln\{2\xi + 1 + 2\ln(2\xi + 4)\}}, \; \xi \geq 1$$

In our case for $w = 0.5$ in and $h = 0.2$ in this gives

$$G \approx 0.517$$

It is somewhat surprising that the current carried by the strip is split nearly evenly between the two sides even though the height above the ground plane is not large.

Finally the voltage source induced on the interior stripline, due to indirect magnetic coupling, is

$$V_{eq} = -L_T \frac{dI_r}{dt} \approx -\frac{G}{w}\alpha_m^{eff}\mu_0 \frac{d}{dt} H_{x(eff)}^{sc}$$

and the transfer inductance is

$$L_T \approx \left[-H_x^0\left(0,0\right)/I_0\right]\alpha_m^{eff}\mu_0\left[H_{x(eff)}^{sc}/I_r\right] \approx \frac{G}{w}\alpha_m^{eff}\mu_0\left[H_{x(eff)}^{sc}/I_r\right]$$

$$\approx \frac{G}{2\pi a_w w}\alpha_m^{eff}\mu_0 \ , \ \text{vertical}$$

$$\approx \frac{G}{w}\alpha_m^{eff}\frac{3}{2\pi a}\left(h_w/a\right)\left[\left(a/h_w + h_w/a\right)\arctan\left(a/h_w\right) - 1\right]\mu_0 \ , \ \text{horizontal}$$

For the present example these give

$$L_T \approx 0.189 \text{ nH} \ , \ \text{vertical}$$

$$\approx 0.823 \text{ nH} \ , \ \text{horizontal}$$

The Velonex pulser has a maximum current rise rate of

$$\left(\frac{dI_r}{dt}\right)_{\max} \approx 0.83 \text{ kA}/\mu\text{s}$$

and thus the maximum open circuit voltage induced is

$$\left(V_{eq}\right)_{\max} = -L_T\left(\frac{dI_r}{dt}\right)_{\max} \approx -0.16 \text{ volts , vertical}$$

$$\approx -0.68 \text{ volts , horizontal}$$

which are reasonably close to the experimental levels below of -0.15 volts in the vertical and -0.66 volts in the horizontal.

Since we are interested in the largest voltage possible inside the metallic barrier due to a return stroke, we not only must maximize coupling, but also excite the aperture with a current having the fastest rise-rate representative of lightning. The rise-rate of the Velonex pulser is smaller than the one-percentile rise-rate of lightning. The one-percentile rise-rate (99 out of 100 return strokes have a rise-rate larger than this value) is [1]

$$\left(\frac{dI_r}{dt}\right)_{\max} \approx 400 \text{ kA}/\mu\text{s}$$

giving voltage levels due to magnetic coupling of

$$75 \text{ V} \leq \left(V_{eq}\right)_{\max} \leq 0.33 \text{ kV}$$

We also did an experiment with a wire having height $h \approx 0.3255$ in (and a wire diameter of $2a_c \approx 0.081$ in)

$$L_T \approx \frac{1}{2\pi^2 a_w\sqrt{h^2 - a_c^2}}\alpha_m^{eff}\mu_0 \approx 0.18 \text{ nH} \ , \ \text{vertical}$$

$$(V_{eq})_{\max} = -L_T \left(\frac{dI_r}{dt}\right)_{\max} \approx -0.15 \text{ volts , vertical}$$

compared to the measurement of 0.11 V (the sign here is dependent on which side of the hole with respect to the measurement system load the current injection takes place).

4.2 Electric Field Coupling

The electric field coupling problem to the interior cable is now formulated.

4.2.1 Reciprocity Formulation of Cable Current Source

The electric flux penetrating the hole induces an equivalent current source on the common mode (cable to enclosure) transmission line formed by the cable with respect to the chassis ground of the enclosure. We follow Latham's reciprocity approach [12] to determine the equivalent current source in terms of the exterior drive field, the hole properties, and the interior transmission line. Following the derivation in [12] we define an auxiliary electrostatic potential ϕ^0 without shield penetrations

$$\nabla^2 \phi^0 = 0 \tag{1}$$

with linear charge density q_0 per unit length on the cable conductor (and $-q_0$ on the inside surface of the enclosure for the return). We take the electric field to be the negative gradient of the potential

$$\underline{E}^0 = -\nabla \phi^0 \tag{2}$$

The boundary conditions are set to

$$\phi^0 = 0 \text{ on enclosure}$$

$$= V_0 = q_0/C_0 \text{ on cable conductor} \tag{3}$$

where C_0 is the capacitance per unit length of the cable with respect to the enclosure in the auxiliary problem. This capacitance per unit length will be discussed further later in this section.

The actual problem with the hole has electric potential ϕ^h satisfying Laplace's equation

$$\nabla^2 \phi^h = 0$$

with charge density q_0 on the center conductor. The boundary conditions are

$$\phi^h = 0 \text{ on enclosure}$$

$$= V_0 \text{ on cable conductor} \tag{4}$$

The difference potential can be defined

$$\phi = \phi^h - \phi^0$$

also satisfying

$$\nabla^2\phi = 0$$

Now we can write

$$\nabla \cdot \left(\phi^0 \nabla\phi - \phi\nabla\phi^0\right) = \phi^0\nabla^2\phi - \phi\nabla^2\phi^0 = 0$$

Integration over the interior volume V and using the divergence theorem (Green's theorem) gives

$$\int_V \nabla \cdot \left(\phi^0 \nabla\phi - \phi\nabla\phi^0\right) dV = \oint_S \left(\phi^0 \frac{\partial\phi}{\partial n} - \phi\frac{\partial\phi^0}{\partial n}\right) dS = 0$$

where the unit vector $\underline{n}$ points out of the interior region and the closed surface includes the plane of the interior enclosure surface and the cable surface S_{cab}. Using the boundary conditions we can write this as

$$\int_{S_{cab}} V_0 \frac{\partial\phi}{\partial n} dS = V_0 Q/\varepsilon_0 = \int_A \phi \frac{\partial\phi^0}{\partial n} dS$$

Now dividing by the potential V_0 and noting that the integral on the left side is the difference charge induced on the cable Q (versus the charge in the auxiliary problem) divided by the permittivity, we write

$$Q = \varepsilon_0 \int_A \phi \frac{1}{V_0}\frac{\partial\phi^0}{\partial n} dS = \varepsilon_0 \int_A \phi^h \frac{1}{V_0}\frac{\partial\phi^0}{\partial n} dS$$

Applying Ampere's law to the cable over length $d\ell$ (the contour C in this case has the form of two loops around the cable separated by this distance $d\ell$ and connected by two equal and opposite axial integration contours) gives

$$\oint_C \underline{H} \cdot \underline{d\ell} = dI = i\omega\left(Q + q_0 d\ell\right) = I_{eq} + i\omega\left(C_a + C_0 d\ell\right) V_0$$

where C_0 is the preceding cable capacitance per unit length of the line with the aperture shorted, C_a is a perturbation of the line capacitance caused by the hole, and I_{eq} is an equivalent current source on the line at the hole; the capacitance per unit length term is added here because the difference charge does not include it. The two other terms are separated by virtue of the fact there are two sources for the field in the aperture. One is the exterior short circuit field $\underline{E}^{sc}$ and the second is the interior voltage V_0. In this form no approximations of hole size or shape have been made other than the hole being small compared to the wavelength. So this could, in principle, be applied in cases where the following approximations do not hold, provided that the electric scalar potentials can be found or approximated in some more accurate manner. However, again when we can proceed to the following approximate decomposition, the resulting formula can be applied to many different types of exterior drives, aperture types, and cables by simply switching the appropriate quantities, if they are known.

If the hole is small enough compared to other dimensions in the problem, we can approximate the auxiliary potential in the aperture as a constant at the aperture center

$$-\underline{n}\frac{\partial\phi^0}{\partial n} \approx \underline{E}^0\left(\underline{s}_A\right)$$

where $\underline{E}^0\left(\underline{s}_A\right)$ is the interior field at the aperture center, driven by the charge per unit length q_0 on the cable with the aperture shorted (for a two dimensional field distribution with the unit vector $\underline{e}_y$ along the transmission line and $\underline{n} = \underline{e}_z$ pointing in the direction of the incident half space, duality gives $\varepsilon_0\underline{E}^0/q_0 = -\underline{e}_y \times \underline{H}^0/I_0$). Noting that $q_0 = C_0 V_0$ gives

$$Q \approx -\frac{1}{V_0}\varepsilon_0 \underline{n} \cdot \underline{E}^0(\underline{s}_A) \int_A \phi^h dS$$

The electric dipole moment of the hole (responsible for coupling into the interior) is found from [13]

$$\underline{p}_a = -2\varepsilon_0 \underline{n} \int_A \phi^h dS = 2\varepsilon_0 \underline{\alpha}_e \cdot \underline{E}^{sc}(\underline{s}_A)$$

where $\underline{\alpha}_e$ is the electric polarizability tensor of the hole and $\underline{E}^{sc}$ is the exterior short circuit electric field at the hole. Because there are two sources of the potential we can write

$$Q \approx \frac{\varepsilon_0}{V_0} \underline{E}^0(\underline{s}_A) \cdot \underline{\alpha}_e \cdot \left[\underline{E}^{sc}(\underline{s}_A) - \underline{E}^0(\underline{s}_A)\right]$$

where the minus sign on the field from the interior source is introduced since the dipole moment for the hole changes sign in this case (the normal in the dipole moment would be pointed inward and need to be reversed). Thus the equivalent source current driven by the exterior field is

$$I_{eq} \approx i\omega\varepsilon_0 \frac{1}{V_0} \underline{E}^0(\underline{s}_A) \cdot \underline{\alpha}_e \cdot \underline{E}^{sc}(\underline{s}_A)$$

and the the lumped capacitance is

$$C_a \approx -\varepsilon_0 \frac{1}{V_0^2} \underline{E}^0(\underline{s}_A) \cdot \underline{\alpha}_e \cdot \underline{E}^0(\underline{s}_A)$$

The tensor polarizability $\underline{\alpha}_e$ only has a normal component and can be taken as a scalar

$$p_z = 2\varepsilon_0 \alpha_e E_z^{sc}$$

and the current source in the time domain is

$$I_{eq} = \frac{dQ_{eq}}{dt}$$

where the corresponding charge is

$$Q_{eq} = -\frac{\varepsilon_0}{V_0} \underline{E}^0(\underline{s}_A) \cdot \underline{\alpha}_e \cdot \underline{E}^{sc}(\underline{s}_A)$$

In the electric coupling case we take the interior cable to be floating with respect to chassis on one end and terminated in a load (a low impedance measurement system) on the other end.

4.2.2 Electric Polarizability

For a circular hole the electric polarizability is half the magnetic

$$\alpha_{e0} = \frac{2}{3}a^3$$

However once again the plane thickness makes a difference [14]

$$\alpha_e \approx \alpha_{e0}\, 0.825 e^{-2.405(t/a)} \approx 0.510\alpha_{e0}$$

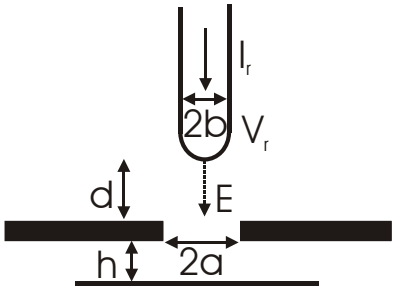

Figure 76. Electric field coupling to interior cable (or collector)

where $j_{01} = 2.405$ is the first root of $J_0(x) = 0$. Combining this with the correction for the proximity of the cable (or collector) (a backing ground plane)

$$\alpha_e^{eff} \approx 0.476\alpha_{e0}$$

4.2.3 Effective Electric Field Drive

In the experiment the exterior electric field was created by an electrode at potential V_r as shown in Figure 76. The short circuit field at the hole in these cases is not strictly uniform. Nevertheless, by examining the penetrant electric fields through circular holes in a thin conducting plane with these field drives (in oblate spheroidal coordinates), it is possible to select effective values for the short circuit fields in the uniform case that produce the same penetrant dipole moments [15].

There are several models for the field surrounding a rod electrode; a simple model, consisting of a line charge and a point charge, is shown in Figure 77 [21]. The potential above the ground plane from a semi-infinite line charge of strength q_r and a point source at the end of the line charge of strength Q_r is then

$$4\pi\varepsilon_0\phi^{sc}(\rho,z) = \int_{h'}^{R_1}\left[\frac{1}{\sqrt{\rho^2+(z-z')^2}} - \frac{1}{\sqrt{\rho^2+(z+z')^2}}\right] q(z')\,dz'$$

$$= q_r \ln\left[R_1 - z + \sqrt{\rho^2+(R_1-z)^2}\right] - q_r \ln\left[h' - z + \sqrt{\rho^2+(h'-z)^2}\right]$$

$$-q_r \ln\left[(R_1+z) + \sqrt{\rho^2+(R_1+z)^2}\right] + q_r \ln\left[h' + z + \sqrt{\rho^2+(h'+z)^2}\right]$$

$$+Q_r\left[\frac{1}{\sqrt{\rho^2+(h'-z)^2}} - \frac{1}{\sqrt{\rho^2+(h'+z)^2}}\right]$$

where

$$h' = d + b$$

and ρ and z are the usual cylindrical coordinates (with $z = 0$ on the top of the conducting plane). Taking the limit $R_1 \to \infty$ gives

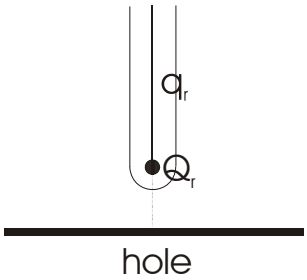

Figure 77. Simplified field model for rod plane geometry.

$$4\pi\varepsilon_0\phi^{sc}(\rho,z)=$$

$$q_r\left[\ln\left\{(h'+z)+\sqrt{\rho^2+(h'+z)^2}\right\}-\ln\left\{(h'-z)+\sqrt{\rho^2+(h'-z)^2}\right\}\right]$$

$$+Q_r\left[\frac{1}{\sqrt{\rho^2+(h'-z)^2}}-\frac{1}{\sqrt{\rho^2+(h'+z)^2}}\right] \tag{5}$$

If we match the average potential on the cylinder from h' to a large distance $h'+R_0=(R+1)\,h'$ (we used the value $R=10$, but the results are not too sensitive to the choice)

$$V_r=\langle\phi^{sc}\rangle=\frac{1}{R_0}\int_{h'}^{h'+R_0}\phi^{sc}dz$$

Using the identities

$$\int\ln\left(u+\sqrt{a^2+u^2}\right)du=u\ln\left(u+\sqrt{a^2+u^2}\right)-\int\frac{udu}{\sqrt{a^2+u^2}}$$

$$=u\ln\left(u+\sqrt{a^2+u^2}\right)-\sqrt{a^2+u^2}$$

$$\int\frac{1}{\sqrt{a^2+u^2}}du=\text{Arcsinh}\,(u/a)=\ln\left[u/a+\sqrt{(u/a)^2+1}\right]$$

$$=\ln\left(u+\sqrt{u^2+a^2}\right)-\ln a$$

we find

$$4\pi\varepsilon_0V_r=$$

$$q_r\frac{1}{R_0}\left[(2h'+R_0)\ln\left(2h'+R_0+\sqrt{a^2+(2h'+R_0)^2}\right)-(2h)\ln\left(2h'+\sqrt{a^2+(2h')^2}\right)\right.$$

$$\left.-\sqrt{a^2+(2h'+R_0)^2}+\sqrt{a^2+(2h')^2}\right]-q_0 2\ln a$$

$$+q_0\frac{1}{R_0}\left[R_0\ln\left(R_0+\sqrt{a^2+R_0^2}\right)-\sqrt{a^2+R_0^2}+a\right]$$

$$+Q_r\frac{1}{R_0}\left[\ln\left(R_0+\sqrt{R_0^2+a^2}\right)-\ln a\right]$$

$$-Q_0\frac{1}{R_0}\left[\ln\left\{2h'+R_0+\sqrt{(2h'+R_0)^2+a^2}\right\}-\ln\left\{2h'+\sqrt{(2h')^2+a^2}\right\}\right]$$

or for large $R>>1$

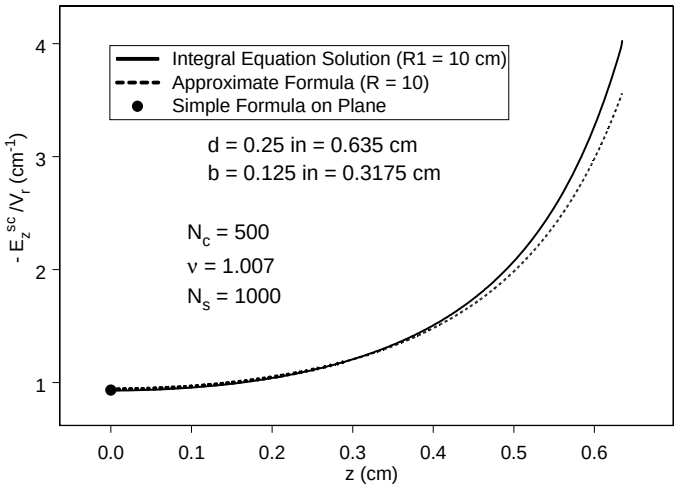

Figure 78. A comparison of the field on axis predicted by the formulas versus a numerical method of moments solution. Also shown is the value of the field on the plane from the simple formula.

$$4\pi\varepsilon_0 V_r \sim q_r \left[\Omega + 2\ln\left(R\right) - 2\right] \tag{6}$$

$$\Omega = 2\ln\left(2h'/b\right) \tag{7}$$

The reason why a finite average distance must be specified is that the true charge density has a slow decay along the length $O\left(1/\ln z\right)$ [18] rather than the constant being used here as an approximation. The other match condition is taken at the tip of the hemisphere $z = h' - b$, $\rho = 0$

$$4\pi\varepsilon_0\phi^{sc}\left(0,z\right) = q_r \ln\left(\frac{h'+z}{h'-z}\right) + Q_r\left(\frac{1}{h'-z} - \frac{1}{h'+z}\right)$$

or

$$4\pi\varepsilon_0 V_r \sim q_r \ln\left(2h'/b - 1\right) + Q_r \frac{1}{b}\left(1 - \frac{1}{2h'/b - 1}\right) \tag{8}$$

Note for $d = 2b = 0.25$ in we find $0.1616 \sim q_r/\left(4\pi\varepsilon_0 V_r\right)$ and $0.3083 \sim Q_r/\left(h' 4\pi\varepsilon_0 V_r\right)$. The field on axis at general z is then

$$-E_z^{sc}\left(0,z\right) \sim \frac{q_r}{4\pi\varepsilon_0}\left(\frac{1}{h'+z} + \frac{1}{h'-z}\right) + \frac{Q_r}{4\pi\varepsilon_0}\left[\frac{1}{\left(h'-z\right)^2} + \frac{1}{\left(h'+z\right)^2}\right] \tag{9}$$

A comparison of the values from these formulas with a numerical solution is shown in Figure 78, illustrating that near the plane $z = 0$ these are accurate.

The short circuit field on the plane directly below the rod can be simplified further as

$$-E_z^{sc}(0,0) \sim \frac{2V_r/h'}{\Omega_e}$$

where

$$\Omega_e = 2\ln(2h'/b) - 4b/h'$$

and the line charge density is approximately constant

$$q(z) \sim q_r = \frac{4\pi\varepsilon_0}{\Omega_e} V_r$$

This is shown as the dot in Figure 78. However, to be consistent with the drive field discussed in the magnetic field section, we instead choose the effective short circuit electric field so that it preserves the electric dipole moment of the penetration. This is done by again making use of oblate spheroidal coordinates to examine the penetration. In the useful equations report [15] we take the electrostatic potential to be the sum

$$\phi^{tot} = \phi^{sc} + \phi \ , \ z > 0$$

$$= \phi \ , \ z < 0$$

where the short circuit potential is ϕ^{sc}, $\underline{E}^{sc} = -\nabla\phi^{sc}$, and ϕ is the potential scattered by the hole. Continuity of the tangential electric field at the aperture, the fact that the total potential vanishes on the conducting plane, and the vanishing of the short circuit potential, means that

$$\phi \text{ continuous at } z = 0$$

$$\phi(\rho, z) = 0 \ , \ a < \rho < \infty$$

Continuity of the normal component of the electric field in the hole means that

$$-\frac{\partial\phi^{sc}}{\partial z}(\rho, +0) - \frac{\partial\phi}{\partial z}(\rho, +0) = -\frac{\partial\phi}{\partial z}(\rho, -0) \ , \ 0 < \rho < a$$

Noting that $-\partial\phi/\partial z$ is odd in z gives

$$\frac{1}{2}\frac{\partial\phi^{sc}}{\partial z}(\rho, +0) = -\frac{\partial\phi}{\partial z}(\rho, +0) \ , \ 0 < \rho < a$$

If we immerse a PMC disc of radius a in a potential field

$$\phi^i(\rho, z) = \frac{1}{2}\phi^{sc}(\rho, z)$$

we will find the same scattered potential in the upper half space $z > 0$ and negative the scattered potential of the hole problem in the lower half space $z < 0$ (the incident and scattered potentials in the disc problem are even in z).

The aperture potential then satisfies

$$\nabla^2\phi = 0$$

in the upper and lower half spaces. The boundary condition for the scattered potential is

$$-\frac{\partial\phi}{\partial z}(\rho, \pm 0) = \frac{\partial\phi^i}{\partial z}(\rho, \pm 0)$$

To obtain the aperture potential in the lower half space $z < 0$ we reverse the sign of the disc potential $\phi \to -\phi$.

We now use oblate spheroidal coordinates

$$\rho = a\sqrt{1+\zeta^2}\sqrt{1-\xi^2}\ , \quad -1 < \xi < 1\ ,\ 0 < \zeta < \infty$$

$$z = a\zeta\xi$$

The aperture potential is now expanded in oblate spheroidal coordinates

$$\phi = \sum_n A_n P_n(\xi) Q_n(j\zeta)$$

where the functions $P_n(j\zeta)$ are not included since this potential decays at infinity. Also the functions $Q_n(\xi)$ are not included since the potential must be finite at $\xi = \pm 1$. Now using orthogonality

$$\int_{-1}^{1} P_n(\xi) P_{n'}(\xi)\, d\xi = \frac{\delta_{nn'}}{n+1/2}$$

and the above boundary condition

$$-\frac{\partial\phi}{\partial z}(\rho, \pm 0) = \frac{\partial\phi^i}{\partial z}(\rho, \pm 0)$$

with

$$\frac{\partial\phi}{\partial z}(\rho, 0) \to \frac{1}{h_\zeta}\frac{\partial\phi}{\partial\zeta}(0,\xi) = \frac{1}{a}\sqrt{\frac{1+\zeta^2}{\xi^2+\zeta^2}}\frac{\partial\phi}{\partial\zeta}(0,\xi) = \frac{1}{a}\frac{1}{|\xi|}\frac{\partial\phi}{\partial\zeta}(0,\xi)$$

or

$$-\frac{1}{a}\frac{1}{|\xi|}\frac{\partial\phi}{\partial\zeta}(0,\xi) = \frac{\partial\phi^i}{\partial z}(\rho, \pm 0) = \pm\frac{1}{2}\frac{\partial\phi^{sc}}{\partial z}(\rho, 0)$$

gives

$$-\frac{1}{a}\sum_n A_n \int_{-1}^{1} P_n(\xi) P_{n'}(\xi)\, d\xi j Q_n'(j0) = \frac{1}{2}\int_{-1}^{1} P_{n'}(\xi)\frac{\partial\phi^{sc}}{\partial z}\left(\rho = a\sqrt{1-\xi^2}, 0\right)\xi d\xi$$

or

$$-A_n \frac{jQ_n'(j0)}{n+1/2} = \frac{a}{2}\int_{-1}^{1} P_n(\xi)\frac{\partial\phi^{sc}}{\partial z}\left(\rho = a\sqrt{1-\xi^2}, 0\right)\xi d\xi$$

$$jQ_n'(j0) = -j^{-1-n}\frac{\Gamma(1+n/2)}{\Gamma\left(\frac{n+1}{2}\right)}\sqrt{\pi}$$

The even coefficients vanish and the odd coefficients are

$$-A_n\frac{jQ_n'(j0)}{n+1/2} = a\int_0^1 P_n(\xi)\frac{\partial\phi^{sc}}{\partial z}\left(\rho = a\sqrt{1-\xi^2}, 0\right)\xi d\xi$$

Noting that the Legendre functions behave as

$$Q_n(j\zeta) \sim \frac{2n!}{(3/2)_n(2j\zeta)^{n+1}}\ ,\ \zeta\to\infty$$

we see that $n=1$ will be dominant away from the aperture. Thus in the hole problem ($\phi\to-\phi$) we have

$$\phi \sim -A_1P_1(\xi)Q_1(j\zeta) = -A_1\xi Q_1(j\zeta)$$

$$Q_1(j\zeta) = \zeta\,\mathrm{arccot}\,\zeta - 1$$

$$jQ_1'(j0) = \frac{\pi}{2}$$

where $\pi/2 > \mathrm{arccot}\,\zeta > 0$ for $0<\zeta<\infty$. Thus the $n=1$ term is

$$\phi \sim -A_1\xi(\zeta\,\mathrm{arccot}\,\zeta - 1)$$

Expanding for large ζ

$$\phi \sim \frac{A_1\xi}{3\zeta^2}$$

Using $r\sim a\zeta$ and $z = a\xi\zeta$ gives

$$\phi \sim \frac{A_1a^2z}{3r^3} = \frac{\underline{p}\cdot\underline{r}}{4\pi\varepsilon_0 r^3}$$

or

$$p_z = A_1\varepsilon_0 4\pi a^2/3$$

where

$$A_1 = \frac{3a}{\pi}\int_0^1 E_z^{sc}\left(\rho = a\sqrt{1-\xi^2}, 0\right)\xi^2 d\xi$$

If we transform to $\rho = a\sqrt{1-\xi^2}$ or $\xi = \sqrt{1-(\rho/a)^2}$

$$p_z = \varepsilon_0 A_1 4\pi a^2/3 = 4\varepsilon_0\int_0^a E_z^{sc}(\rho,0)\sqrt{a^2-\rho^2}\rho d\rho$$

$$= \frac{2}{\pi}\varepsilon_0 \int_0^a E_z^{sc}(\rho,0)\sqrt{a^2-\rho^2}2\pi\rho d\rho$$

If we replace the function of ρ by an effective value $E_{z(eff)}^{sc}$ and integrate we find

$$p_z = \frac{2}{\pi}\varepsilon_0 E_{z(eff)}^{sc}\int_0^a \sqrt{a^2-\rho^2}2\pi\rho d\rho = \frac{4}{3}a^3\varepsilon_0 E_{z(eff)}^{sc} = 2\alpha_e\varepsilon_0 E_{z(eff)}^{sc}$$

where again for a circular hole

$$\alpha_e = \frac{2}{3}a^3$$

Thus equating the effective value required to achieve the same dipole moment as the true field gives

$$2\alpha_e\varepsilon_0 E_{z(eff)}^{sc} = \frac{2}{\pi}\varepsilon_0 \int_0^a E_z^{sc}(\rho,0)\sqrt{a^2-\rho^2}2\pi\rho d\rho$$

$$E_{z(eff)}^{sc}/E_z^{sc}(0,0) = \frac{1}{\pi\alpha_e}\int_0^a \frac{E_z^{sc}(\rho,0)}{E_z^{sc}(0,0)}\sqrt{a^2-\rho^2}2\pi\rho d\rho$$

$$= \frac{2}{\alpha_e}\int_0^a \frac{E_z^{sc}(\rho,0)}{E_z^{sc}(0,0)}\sqrt{a^2-\rho^2}\rho d\rho$$

Numerical implementation can be carried out as

$$\rho_m = \left(\frac{m}{M}\right)a$$

$$\rho_{m-1/2} = \frac{1}{2}\left(\rho_m + \rho_{m-1}\right)$$

$$E_{z(eff)}^{sc}/E_z^{sc}(0,0) \approx \sum_{m=1}^{M}\frac{E_z^{sc}\left(\rho_{m-1/2},0\right)}{E_z^{sc}(0,0)}\frac{2}{\alpha_e}\int_{\rho_{m-1}}^{\rho_m}\sqrt{a^2-\rho^2}\rho d\rho$$

$$\approx \sum_{m=1}^{M}\frac{E_z^{sc}\left(\rho_{m-1/2},0\right)}{E_z^{sc}(0,0)}\frac{2/3}{\alpha_e}\left[\left(a^2-\rho_{m-1}^2\right)^{3/2}-\left(a^2-\rho_m^2\right)^{3/2}\right]$$

$$\approx \sum_{m=1}^{M}\frac{E_z^{sc}\left(\rho_{m-1/2},0\right)}{E_z^{sc}(0,0)}\left[\left(1-\rho_{m-1}^2/a^2\right)^{3/2}-\left(1-\rho_m^2/a^2\right)^{3/2}\right]$$

In the case of interest where $a = d = 0.25$ in and $b = 0.125$ in we find that $E_{z(eff)}^{sc}/E_z^{sc}(0,0) \approx 0.832$. In the case where $d = 0.25$ in, $b = 0.125$ in, and $2a = 0.69$ in we find $E_{z(eff)}^{sc}/E_z^{sc}(0,0) \approx 0.735$.

The potential from the point charge - line charge model is

$$4\pi\varepsilon_0\phi^{sc}(\rho,z) \sim$$

$$q_r\left[\ln\left\{(h'+z)+\sqrt{\rho^2+(h'+z)^2}\right\}-\ln\left\{(h'-z)+\sqrt{\rho^2+(h'-z)^2}\right\}\right]$$

$$+Q_r\left[\frac{1}{\sqrt{\rho^2+(h'-z)^2}}-\frac{1}{\sqrt{\rho^2+(h'+z)^2}}\right]$$

Thus the field is

$$-4\pi\varepsilon_0\frac{\partial\phi^{sc}}{\partial z}(\rho,z)=-4\pi\varepsilon_0E_z^{sc}(\rho,0)\sim$$

$$-q_r\left[\frac{1}{\sqrt{\rho^2+(h'+z)^2}}+\frac{1}{\sqrt{\rho^2+(h'-z)^2}}\right]$$

$$-Q_r\left[\frac{(h'-z)}{\left\{\rho^2+(h'-z)^2\right\}^{3/2}}+\frac{(h'+z)}{\left\{\rho^2+(h'+z)^2\right\}^{3/2}}\right]$$

and therefore on the ground plane

$$-2\pi\varepsilon_0E_z^{sc}(\rho,0)\sqrt{\rho^2+h'^2}\sim q_r+Q_rh'/\left(\rho^2+h'^2\right) \tag{10}$$

Inserting this into the dipole moment formula and letting $u=\rho^2$

$$p_z=-\frac{1}{\pi}\int_0^a\left[\frac{q_r}{\sqrt{\rho^2+h'^2}}+\frac{h'Q_r}{(\rho^2+h'^2)^{3/2}}\right]\sqrt{a^2-\rho^2}2\rho d\rho$$

$$=-\frac{1}{\pi}\int_0^{a^2}\left[\frac{q_r}{\sqrt{u+h'^2}}+\frac{h'Q_r}{(u+h'^2)^{3/2}}\right]\sqrt{a^2-u}du$$

Now taking $a^2-u=v^2$ and

$$r_0^2=a^2+h'^2 \tag{11}$$

$$p_z=-\frac{2}{\pi}\int_0^a\left[\frac{q_r}{\sqrt{r_0^2-v^2}}+\frac{h'Q_r}{(r_0^2-v^2)^{3/2}}\right]v^2dv$$

From [19]

$$\int\frac{x^2}{\sqrt{a+cx^2}}dx=\frac{x}{2c}\sqrt{a+cx^2}-\frac{a}{2c}\int\frac{dx}{\sqrt{a+cx^2}}$$

$$\int\frac{x^2}{(a+cx^2)^{3/2}}dx=-\frac{x}{c}/\sqrt{a+cx^2}+\frac{1}{c}\int\frac{dx}{\sqrt{a+cx^2}}$$

$$\int\frac{dx}{\sqrt{a+cx^2}}=\frac{1}{\sqrt{-c}}\arcsin\left(x\sqrt{-c/a}\right)$$

and thus

$$p_z = -\frac{2}{\pi} q_r \int_0^a \frac{v^2 dv}{\sqrt{r_0^2 - v^2}} - \frac{2}{\pi} h' Q_r \int_0^a \frac{v^2 dv}{\left(r_0^2 - v^2\right)^{3/2}}$$

$$= -\frac{2}{\pi} q_r \left[-\frac{v}{2}\sqrt{r_0^2 - v^2} + \frac{r_0^2}{2} \arcsin\left(v/r_0\right) \right]_0^a$$

$$-\frac{2}{\pi} h' Q_r \left[v/\sqrt{r_0^2 - v^2} - \arcsin\left(v/r_0\right) \right]_0^a$$

$$= -\frac{1}{\pi} q_r \left[-a\sqrt{r_0^2 - a^2} + r_0^2 \arcsin\left(a/r_0\right) \right] - \frac{2}{\pi} h' Q_r \left[a/\sqrt{r_0^2 - a^2} - \arcsin\left(a/r_0\right) \right]$$

$$= -\frac{1}{\pi} q_r \left[-ah' + r_0^2 \arcsin\left(a/r_0\right) \right] - \frac{2}{\pi} h' Q_r \left[a/h' - \arcsin\left(a/r_0\right) \right] \tag{12}$$

The electric dipole moment of the aperture is thus

$$p_z = \frac{2}{\pi} \varepsilon_0 \int_0^a E_z^{sc}\left(\rho, 0\right) \sqrt{a^2 - \rho^2} 2\pi\rho d\rho$$

$$= -q_r \left[\left(a^2 + h'^2\right) \arctan\left(a/h'\right) - ah' \right] / \pi + 2Q_r \left[h' \arctan\left(a/h'\right) - a \right] / \pi$$

and we can determine an effective value of the short circuit electric field, preserving the aperture dipole moment, by equating this to

$$p_z = 2\alpha_{e0} \varepsilon_0 E_{z(eff)}^{sc}$$

or

$$-\frac{4}{3} \pi a^3 \varepsilon_0 E_{z(eff)}^{sc} = q_r \left[-ah' + \left(a^2 + h'^2\right) \arctan\left(a/h'\right) \right] + 2Q_r \left[a - h' \arctan\left(a/h'\right) \right] \tag{13}$$

If we divide by the value on the plane at the center

$$-E_z^{sc}\left(0, 0\right) \approx \frac{q_r}{2\pi\varepsilon_0 h'} + \frac{Q_r/h'}{2\pi\varepsilon_0 h'}$$

we find the correction factor

$$E_{z(eff)}^{sc} / E_z^{sc}\left(0, 0\right) = \frac{h'}{2a^3/3} \frac{q_r \left[\left(a^2 + h'^2\right) \arctan\left(a/h'\right) - ah' \right] - 2Q_r \left[h' \arctan\left(a/h'\right) - a \right]}{q_r + Q_r/h'}$$

Thus in summary we have the effective short circuit field at the hole center

$$-\frac{1}{3} a E_{z(eff)}^{sc} / V_r = \left(\frac{q_r}{4\pi\varepsilon_0 V_r} \right) \left(h'/a\right) \left[\left(a/h' + h'/a\right) \arctan\left(a/h'\right) - 1 \right]$$

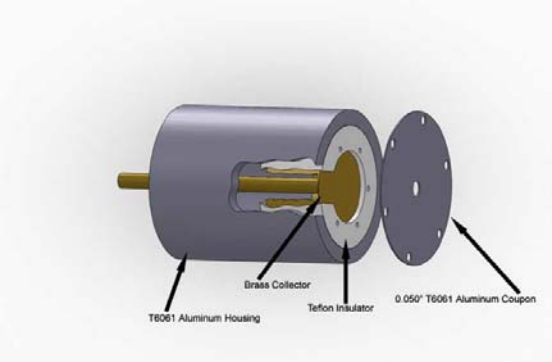

Figure 79. Experimental configuration for electric field indirect coupling.

$$+2\left(\frac{Q_r}{4\pi\varepsilon_0 V_r h'}\right)(h'/a)\left[1-(h'/a)\arctan\left(a/h'\right)\right]$$

where the normalized line charge density is

$$\frac{1}{\Omega+2\ln\left(R\right)-2}\sim\left(\frac{q_r}{4\pi\varepsilon_0 V_r}\right)\approx 0.1616$$

and where the normalized point charge value is

$$\frac{b}{h'}\left(\frac{2h'/b-1}{h'/b-1}\right)\left[1-\frac{\ln\left(2h'/b-1\right)}{\Omega+2\ln\left(R\right)-2}\right]\sim 2\left(\frac{Q_r}{4\pi\varepsilon_0 V_r h'}\right)\approx 0.6166$$

For the case here we find

$$-E^{sc}_{z(eff)}/V_r\approx 0.8294\ \mathrm{cm}^{-1}$$

4.2.4 Wire Coupling

In the case of a wire at a distance h below the hole

$$\underline{E}_0\left(\underline{s}_A\right)/V_0=\underline{e}_z/\left(\pi\sqrt{h^2-a_c^2}\right)\sim\underline{e}_z/\left(\pi h\right)$$

$$C_0=\frac{2\pi\varepsilon_0}{\mathrm{Arccosh}\left(h/a_c\right)}=\frac{2\pi\varepsilon_0}{\ln\left(h/a_c+\sqrt{h^2/a_c^2-1}\right)}\sim\frac{2\pi\varepsilon_0}{\ln\left(2h/a_c\right)}$$

where a_c is the radius of the wire.

4.2.5 Cable Coupling

In the case of the stripline cable we had above the fit with $-E^0_x\rightarrow E^0_z$

$$hE^0_z\left(0,0\right)/V_0\approx 1-\frac{1}{4\left(\xi^2-2\ln\xi\right)}\ ,\ \xi\geq 1$$

$$\xi=\pi w/\left(2h\right)$$

4.2.6 Collector Coupling

In the experiment we used a metallic collector of large dimensions, shown in Figure 79. For this geometry we use

$$E^0_z\left(\underline{s}_A\right)/V_0\approx 1/h$$

Thus we have

$$Q_{eq}\approx-\frac{\varepsilon_0}{h}\alpha_e^{eff}E^{sc}_{z(eff)}$$

and

$$I_{eq} = \frac{dQ_{eq}}{dt} = C_T \frac{dV_r}{dt} \approx -\frac{1}{h}\alpha_e^{eff}\varepsilon_0 \frac{d}{dt}E_{z(eff)}^{sc}$$

where

$$C_T \approx \left[E_z^0(0,0)/V_0\right]\alpha_e^{eff}\varepsilon_0\left[-E_{z(eff)}^{sc}/V_r\right] \approx -\frac{1}{h}\alpha_e^{eff}\varepsilon_0 E_{z(eff)}^{sc}/V_r \approx 0.01175 \text{ pF}$$

The PASD pulser has a maximum voltage rise rate of

$$\left(\frac{dV_r}{dt}\right)_{\max} \approx 3\frac{\text{kV}}{\text{ns}}$$

and thus the maximum short circuit current induced is

$$(I_{eq})_{\max} = C_T\left(\frac{dV_r}{dt}\right)_{\max} \approx 35.2 \text{ mA}$$

We actually measure the voltage on the brass collector with a 50 ohm measurement resistance (an optical data link) attached to it. The collector has a capacitance to the surrounding Faraday cage (coupon and housing shown in Figure 79), that was measured to be

$$C_c \approx 75.5 \text{ pF}$$

In addition there is a capacitance between leads to the measurement system estimated as $C_{lead} \approx 8$ pF. The time constant of the load is thus

$$\tau_{load} = (C_c + C_{lead})(50 \text{ ohms}) \approx 4.2 \text{ ns}$$

Since the PASD drive voltage rises rapidly to $V_r = 4.6$ kV in less than 2 ns (considerably less than the RC time constant), let us approximately ignore the 50 ohm load resistor and consider voltage division between the capacitors (we ignore C_T compared to the load capacitance)

$$V_c \approx \frac{C_T}{C_c + C_{lead}} V_r \approx 0.65 \text{ V}$$

which is very close to the experimental result 0.7 V as shown in Figure 86. When an experiment was done using a stripline rather than the collector, $C_T \approx 0.0115$ pF, the capacitance C_c drops to about $C_{cab} \approx 20$ pF and the calculated electric field coupled voltage increased to 1.9 V, which is close to the voltage that we measured of 2.2 V (not plotted).

The exterior electric field drive in a lightning environment is not as well characterized as the current time derivative. If we take the Sandia facility Marx voltage and double it at an open circuit, we expect a level near $V_r \approx 1.6$ MV (this level corresponds to a highly overvolted situation and will rapidly lead to breakdown of the gap which is being ignored here), an induced collector voltage of $V_c \approx 225$ V, and an induced cable voltage of 657 V.

4.3 Experiments

The results from the indirect coupling experiments are now discussed. The comparisons mentioned

Case	Drive	Model	Experiment
Mag (V) Strip	0.83 kA/μs	0.16 V	0.15 V
Mag (H) Strip	0.83 kA/μs	0.68 V	0.66 V
Mag (V) Wire	0.83 kA/μs	0.15 V	0.11 V
Elect Strip	4.6 kV (3 kV/ns)	0.65 V	0.7 V

Table 7. Comparison between indirect model and experiment

above are summarized in Table 7 (only the absolute values are listed).

4.3.1 Magnetic Coupling

The fixture for the magnetic coupling experiment is shown in Figure 80. The one half inch hole is shown with the shield cover removed so that the stripline cable can be easily seen. Figure 82 shows the Velonex pulser drive current and the voltage results for the vertical drive current case. Figure 83 shows the corresponding horizontal current drive.

The coupled voltage and Velonex pulser drive for the wire coupling experiment are shown in Figure 84.

4.3.2 Electric Coupling

The electric coupling experimental setup is shown in Figure 85. The PASD pulser output and coupled voltage are shown in Figure 86.

5 DIRECT HIGH VOLTAGE BREAKDOWN MECHANISM

This section considers direct charge and current coupling to the collector by means of the formation of an ionized path.

5.1 Threshold Levels

Here we apply ionization coefficients to determine threshold breakdown voltage levels [21]. Figure 87 illustrates an electron avalanche and charge growth in an electric field. This method uses the Townsend primary α and secondary γ ionization coefficients to develop the Townsend breakdown condition [23]

$$\int_C \alpha\left(E\right) ds = \ln\left(1 + 1/\gamma\right)$$

where the integration path C is the proposed discharge path. To transition to the streamer breakdown criterion [23]

$$\int_0^d \alpha ds = 17.7 + \ln\left(d/1 \text{ cm}\right)$$

we made use of the form [23]

$$\int_0^d \alpha ds - \mu d = \ln\left(1 + 1/\gamma_p\right)$$

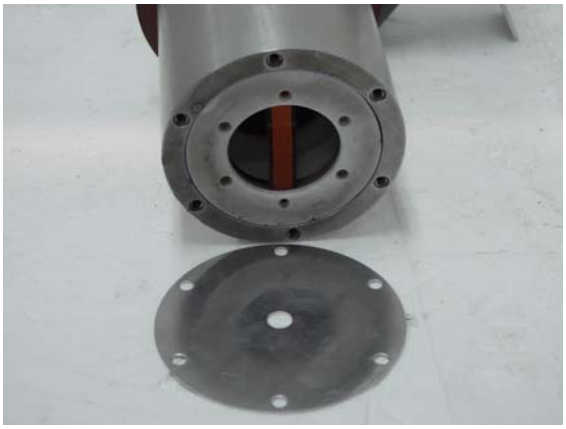

Figure 80. Fixture for magnetic indirect coupling experiment.

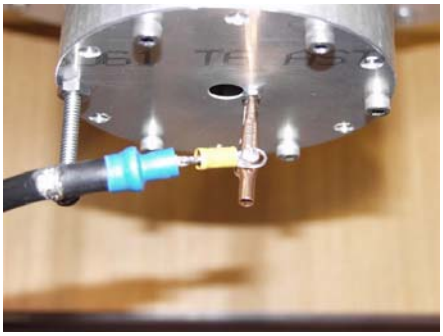

Figure 81. Vertical drive current in experiment.

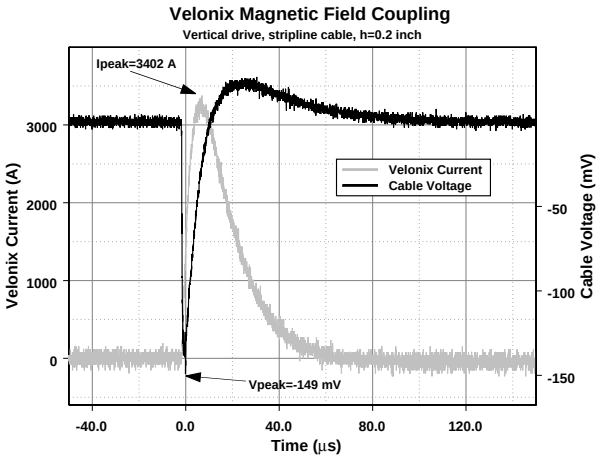

Figure 82. Magnetic coupling experiment with vertical current, using Velonex pulser.

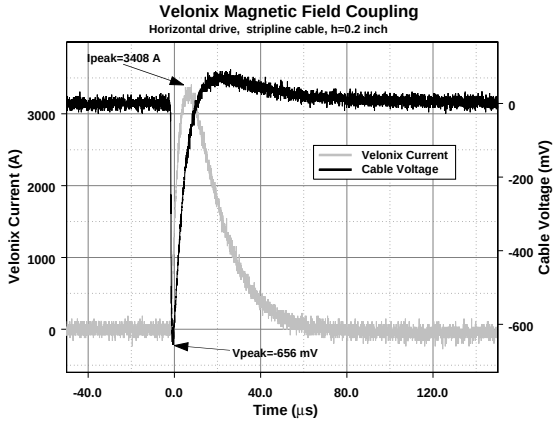

Figure 83. Magnetic coupling experiment with horizontal current, using Velonex pulser.

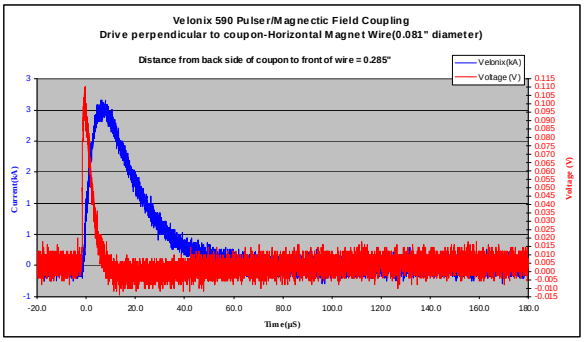

Figure 84. Velonex pulser drive and coupled wire voltage in vertical drive magnetic indirect coupling experiment.

Figure 85. Electric coupling experimental setup.

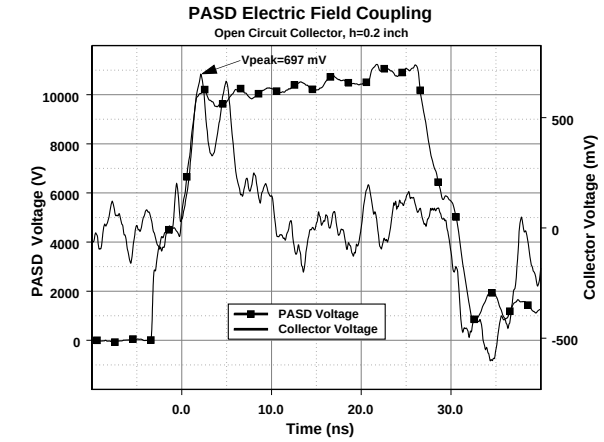

Figure 86. Electric coupled voltage experiment.

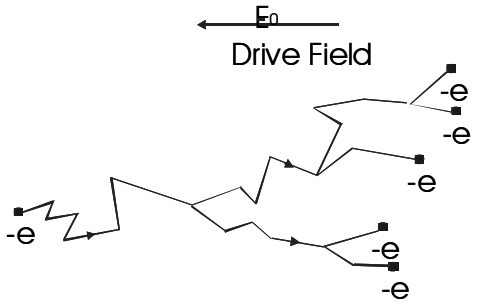

Figure 87. Electron avalanche and charge growth in an electric field.

which assumes that the secondary processes are limited to photon emission γ_p for a rapid breakdown of the gap. This form is motivated by photon absorption with coefficient μ in air, but we determined the parameters μ and γ_p by requiring the calculated breakdown voltage to be the same as that given by the Paschen curve in air [24]. Finally, to approximately differentiate between local corona breakdown and spark threshold we varied the electrode voltage so that the magnitude of the electric field along the path is always greater than the streamer sustaining field in air: $E_{\min} = 4.7$ kV/m [25]. Note that using this criterion to determine spark thresholds is somewhat empirical, and is based on comparisons with experimental data from various nonuniform field configurations..

5.2 Static Breakdown, No Residual Plasma

In this section we will examine the static breakdown characteristics between an electrode, which represents the second return stroke approaching the burnthrough hole, and a cable located behind the hole. By varying the locations of the electrode and the cable with respect to the hole and by varying the hole diameter, we hope to gain some understanding of the probability of breakdown to the cable versus the probability of breakdown to the hole edges. In all cases, the breakdown occurs in air. In this section, charged particles in the vicinity of the hole due to the burnthrough event are ignored.

5.2.1 Geometry

The geometry of interest is shown in Figure 88 (oblique view) and in Figure 89 (view of the x=0 plane). The electrode is initially centered and a distance d above the hole. The electrode is l_e long, has a radius of b and is capped by a hemisphere. A circular hole of radius a is cut in a square metal coupon, which is dimensioned 100 mm by 100 mm. Below the hole is a flat cable 10 mm wide and 100 mm long. Initially, the cable is centered and at a distance h below the hole. The entire geometry represents various pieces of metal, which are all modeled as perfect electrical conductors (PEC).

5.3 Calculation

In order to calculate the expected breakdown voltage between the pin electrode and the other two objects in the problem (the coupon and the cable) we follow the method outlined in [21]. The geometry is gridded as shown in Figure 90, using elements that have edge lengths of approximately 1 mm. The cable is colored yellow, the coupon green and the pin red. Initially we set the dimensions of the pin to be $l_e = 10$ mm and $b = 2$ mm. The boundary element, static code EIGER_S is used to calculate the charges on all three pieces of metal given a particular voltage configuration. The voltage on the pin was set to be negative compared to the voltage on both the coupon and the cable. We stipulate that the total charge for all three pieces of metal be zero so that all electric field lines terminate on the metal surfaces and none terminate at

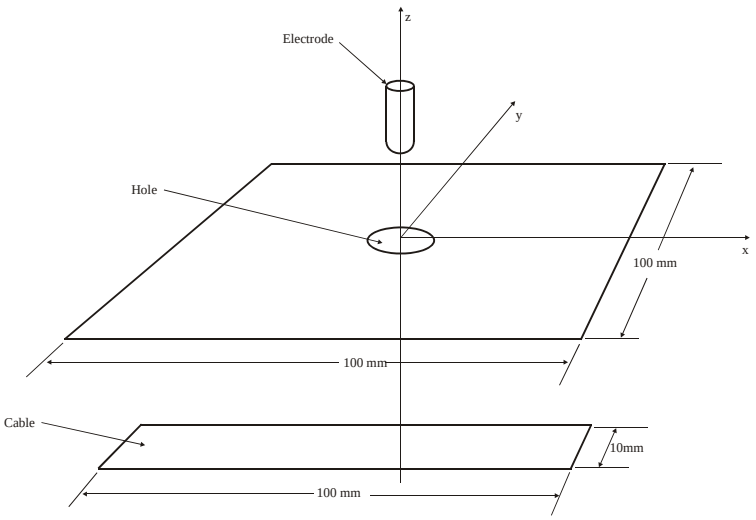

Figure 88. Oblique view of the geometry of interest.

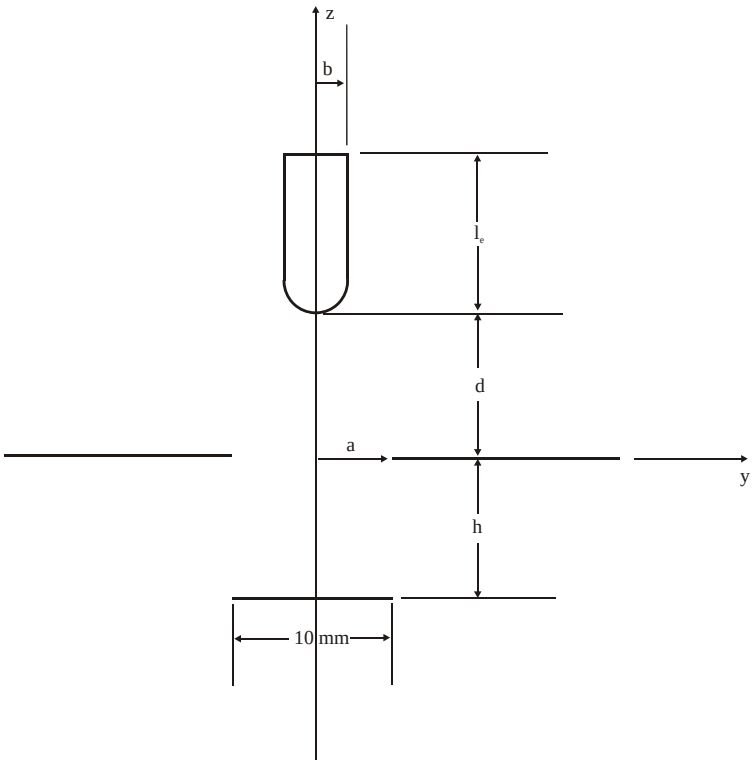

Figure 89. End view of cable, hole and electrode.

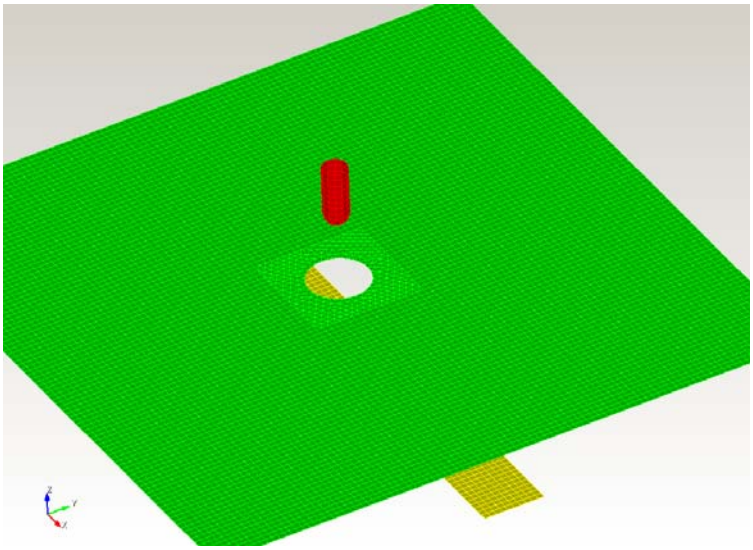

Figure 90. View of mesh.

infinity. We further require that the voltage difference from coupon to pin be 1 volt and that the voltage difference between cable and pin also be 1 volt (the coupon and the cable are at the same potential). After solving for the charge on all the surfaces, we post-process to calculate the field lines between the pin and the coupon or cable. The field line is the path that an electron would take starting from a point at or near the pin and allowed to drift under influence of the field. It is along these field lines that an avalanche will occur leading to streamer formation.

Figure 91 shows a scheme for designating the starting point of the avalanche in terms of a radius from the center of the hemisphere (r_{st}), an angle (θ_{st}) from the axis of the pin ($-\widehat{z}$) and an angle (ϕ_{st}) from the axis of the cable ($\widehat{x}$). Since the radius of the pin is 2 mm, we set $r_{st} = 2.01$ mm.

The breakdown characteristics of the gas depends on the first Townsend ionization coefficient (α) , which is, in turn, a function of the ratio of electric field over gas density. We assume that the measurements of α that we use in the code **Breakdown_alpha** were conducted at a pressure of 760 Torr and at 20^0 C (293^0 K), which yields a gas density $N = 2.504 \times 10^{25}$ gas particles/m^3 using the equation

$$N = \frac{P}{kT}$$

where P is the pressure in Pascals $\left(760 \text{ Torr} = 1.013 \times 10^5 \text{ Pa}\right)$, k is Boltzman's constant (1.38065×10^{-23} Joules/K^0), and T is the temperature in K^0. The breakdown calculations for this gas density represent the breakdown characteristics of a pre-drilled hole. Since burnthrough causes aluminum to vaporize, the boiling temperature of aluminum might give us some indication of the gas density in the vicinity of the burnthrough hole after it is formed. The boiling temperature of aluminum is 2519^0 C (2792^0 K). A pressure of 760 Torr and temperature of 2792^0 K yields a gas density of 2.628×10^{24} gas particles/m^3. **Breakdown_alpha** assumes a temperature of 20^0 C, so to achieve the 2.628×10^{24} particles/m^3 density we must scale the pressure to 79.8 Torr. Initially we will not account for the fact that α may change as the temperature rises, which is due in part to the fact that oxygen attachment decreases. In all the tables that follow we have results for pressures of 760 Torr and 79.8 Torr. We assume in this section that a particular gas density exists throughout the problem space. The more realistic case of the gas density varying in different regions – say the outside of the burnthrough hole is at higher temperature than the inside – will be taken up later.

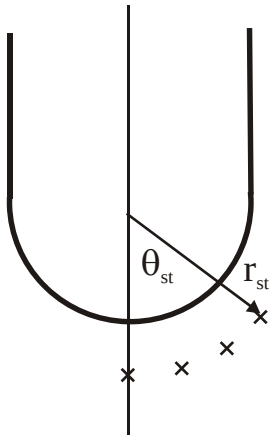

Figure 91. Starting point of avalanche near pin.

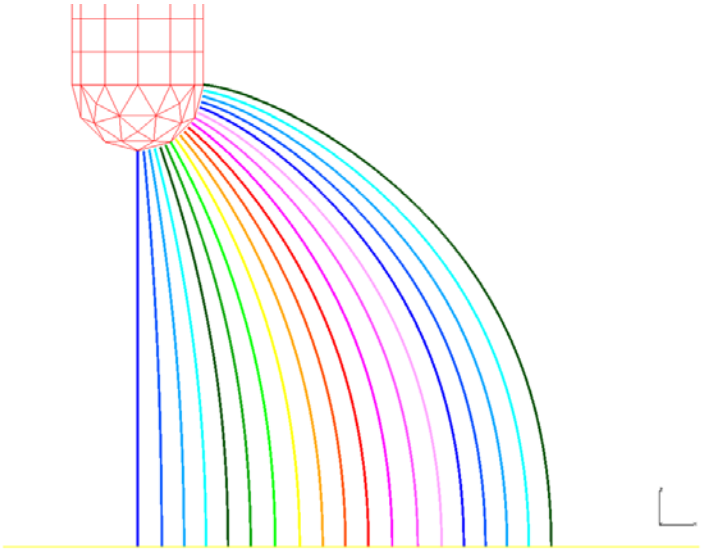

Figure 92. Breakdown paths along cable axis, pin at z = 6 mm, cable at z = -6 mm.

We begin by solving a series of problems that only involve the pin and the cable because we first want to determine how close the pin and cable need to be before breakdown occurs along at least some of the field lines and then introduce the effects of the coupon hole. We found that if the pin and cable are separated by 16 mm (or more), the field in the region between the pin and cable is too non-uniform to allow a spark to occur and only corona occurs. In other words, the voltage that causes enough growth of the avalanche to attain streamer threshold near the pin falls below the field required to sustain the streamer (4.7 kV/m at 760 Torr) in the vicinity of the cable. When we moved the pin and cable to be 14 mm apart, the field became uniform enough to allow a spark along a few field lines; those which started in the region of the pin from the tip where $\theta_{st} = 0^0$ to where θ_{st} was less than 20^0. Starting points further away $\left(\theta_{st} > 20^0\right)$ would again result in corona.

It appears that the sustaining field scales linearly with gas density. Using the technique described in [22] we found the sustaining field at 1 bar for three temperature: 20^0 C (room temperature), 660^0 C (melting temperature of aluminum) and 2519^0 C (boiling temperature of aluminum). We predicted sustaining fields of 3.5 kV/cm for 20^0 C (1.2 kV/cm lower than the accepted value), 1.3 kV/cm for 660^0 C (4.7 kV/cm scaled by 293/993 is 1.4 kV/cm) and 0.5 kV/cm for 2519^0 C (4.7 kV/cm scaled by 293/2792 is 0.5).

5.3.1 Pin 6mm above Coupon, Cable 6 mm below Coupon

We moved the pin and cable 12 mm apart, and found that if $\phi_{st} = 0^0$ breakdown would occur when $\theta_{st} < 70^0$. Figure 92 shows the breakdown paths between pin and cable for this case. The paths are calculated at 5^0 increments starting at $\theta_{st} = 0^0$ (Path 0, colored blue) and ending at $\theta_{st} = 90^0$ (Path 18, colored dark green). A detail of the paths near the pin is shown in Figure 93. Note that because the grid fits flat elements to a curved geometry, certain paths, i.e., Path 0 (colored dark blue), Path 6 (colored light green) or Path 12 (colored light pink) start in the vicinity of an edge.

Table 8 gives the predicted breakdown voltage for each path. The smallest breakdown voltage is associated with the straight-line path from pin to cable (Path 0). We expect that as the path length becomes longer, the breakdown voltage will increase. This is true in general, but Paths 6 and 12 deviate from this trend. The reason for this is, as noted previously, that these paths start in the vicinity of an

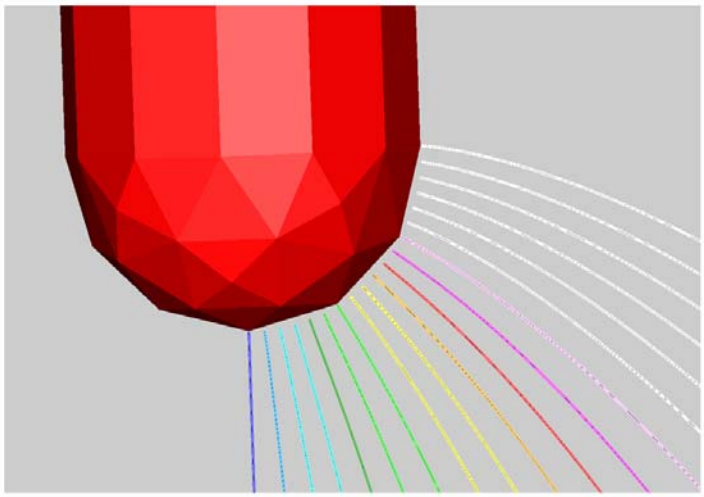

Figure 93. Detail of breakdown paths near pin.

Path	θ_{st}	BDV 760 Torr	BDV 79.8 Torr
0	0^0	16.4 kV	3.2 kV
2	10^0	17.2 kV	3.2 kV
4	20^0	17.3 kV	3.3 kV
6	30^0	16.6 kV	3.2 kV
8	40^0	17.7 kV	3.4 kV
10	50^0	18.1 kV	3.4 kV
12	60^0	18.0 kV	3.5 kV
14	70^0	19.7 kV	3.7 kV

Table 8. Breakdown voltages between pin and cable 12 mm apart, $\phi_{st} = 0^0$

edge caused by gridding and the field is artificially larger there. This larger field is enough to allow the integration of α along this path to achieve the conditions required for streamer threshold at a lower voltage. Figure 94 shows the field as a function of position along Path 0 with the voltage on the pin set to 16.37 kV. Note that the electric field falls off rapidly as a function of distance away from the pin, but it never falls below the field needed to sustain the streamer (the blue line). Figure 95 shows how the integral of α changes as a function of position along Path 0. Note that within 2 mm of the pin we have nearly achieved sufficient growth of the avalanche to reach a streamer. Since the field drops so rapidly as we travel away from the pin, the remainder of the path (~10 mm) is needed to actually achieve the growth required for breakdown.

Figure 96 shows the breakdown paths for $\phi_{st} = 90^0$. In this case, when θ_{st} is greater than 65^0, the breakdown path attaches to the back of the cable (the side opposite the pin). Prior to this occurring, however, at $\theta_{st} \geqq 45^0$, the field is too non-uniform to lead to breakdown and corona results. Table 9 gives the predicted breakdown voltage for the various paths when $\phi_{st} = 90^0$.

We next impose the green coupon with a hole of radius $a = 5$ mm midway between the pin and electrode. The coupon modifies the field lines as shown in Figures 97 and 100. The path along the pin axis (Path 0) proceeds from the pin through the hole and hits the cable as before. As θ_{st} increases, however, the path first passes through the hole, curves around and hits the side of the coupon on the opposite side of the pin (coupon back). As θ_{st} continues to increase, the field line exceeds the radius of the hole and hits the coupon on the same side as the pin (coupon front). The paths for $\phi_{st} = 0^0$ are shown in Figure 97 and their breakdown characteristics are summarized in Table 10 for gas pressures of 760 Torr and 79.8 Torr. Paths 0 through 4 pass through the hole and terminate on the cable. Paths 5 and 6 terminate on the back of the coupon and the remaining paths terminate on the front of the coupon. If we examine the field as a function of distance along Path 0, as shown in Figure 98, we note that in contrast to Figure 94, the field falls below the level needed to sustain the streamer shortly after the path enters the hole ($z = 0$ plane). Because of this, we conclude that breakdown along Path 0 takes the form of a corona. It is possible, to increase the voltage of the pin until the entire path is above the sustaining level. This occurs when the voltage is increased to 49.9 kV at 760 Torr or 5.2 kV at 79.8 Torr. Then breakdown will take the form of a spark. If corona occurs at the lowest breakdown level, parentheses will enclose the voltage in the tables that follow. The voltage inside the parentheses is the level needed to cause the breakdown to occur by spark. Figure 99 shows the fields along Path 7. In this case, the field along the entire path at the minimum breakdown voltage – 14.67 kV at 760 Torr – is greater than the sustaining voltage and breakdown will occur by spark.

The paths for $\phi_{st} = 90^0$ are shown in Figure 100 and summarized in Table 11. Paths 0 through 3 pass through the hole and terminate on the cable. Paths 4 through 6 terminate on the back of the coupon and the remaining paths terminate on the front of the coupon. Again, all of the paths that terminate on the cable will breakdown through corona rather than spark at the threshold voltage level. The pin voltage

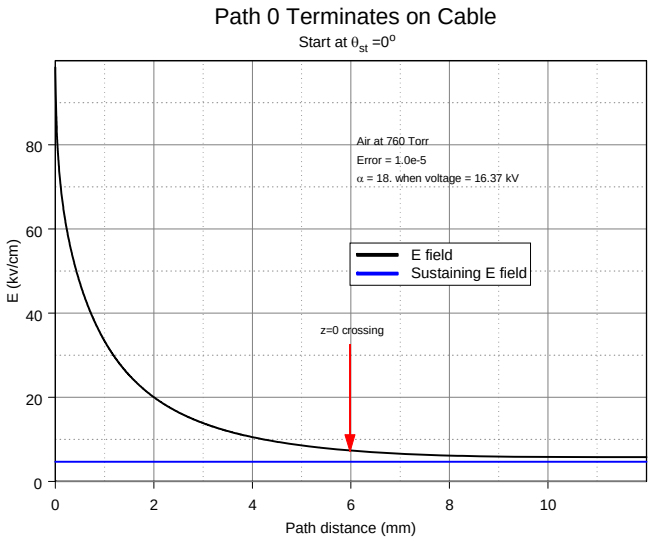

Figure 94. Field for path 0.

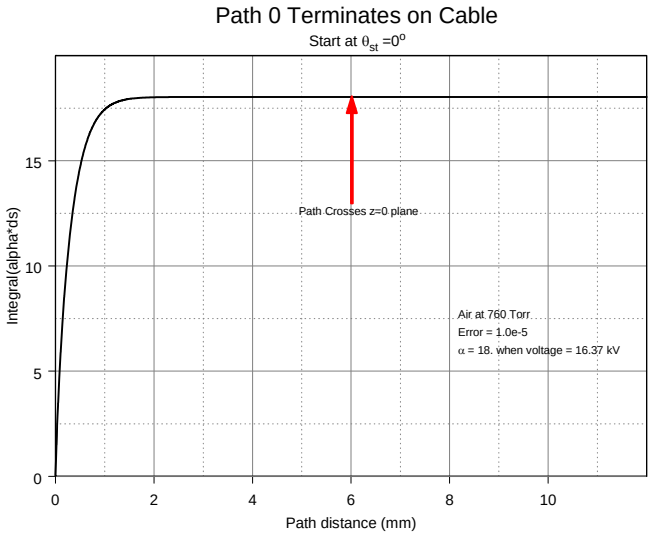

Figure 95. Integral of alpha along path 0.

Path	θ_{st}	BDV 760 Torr	BDV 79.8 Torr
0	0^0	16.4 kV	3.2 kV
2	10^0	17.3 kV	3.2 kV
4	20^0	17.5 kV	3.3 kV
6	30^0	17.1 kV	3.2 kV
8	40^0	16.9 kV	3.2 kV

Table 9. Breakdown voltages between pin and cable 12 mm apart, $\phi_{st} = 90^0$

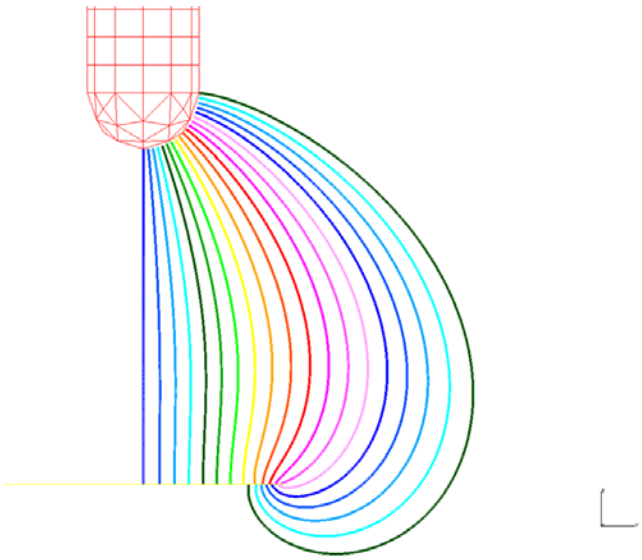

Figure 96. Breakdown paths perpendicular to cable axis, pin at z = 6 mm, cable at z = -6 mm.

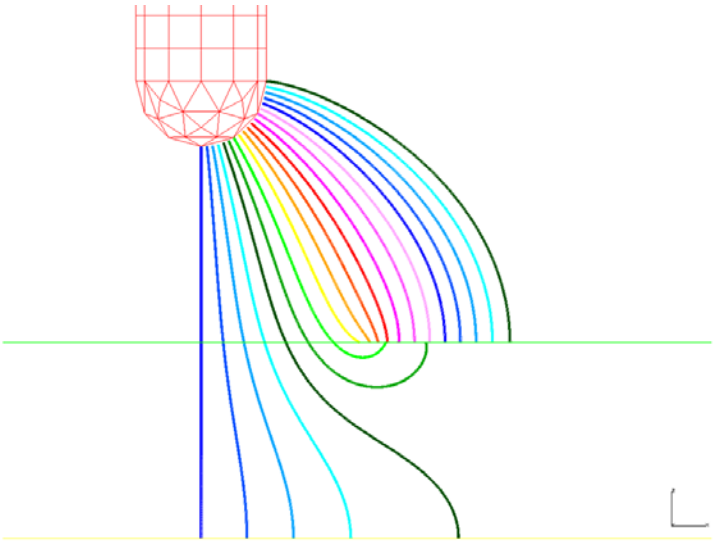

Figure 97. Paths through coupon hole along cable axis, pin at z = 6 mm, cable at z = -6 mm.

Path	θ_{st}	Path End	BDV 760 Torr	BDV 79.8 Torr
0	0^0	cable	(49.9 kV)	(5.2 kV)
1	5^0	cable	(53.0 kV)	(5.6 kV)
2	10^0	cable	(63.3 kV)	(6.6 kV)
3	15^0	cable	(97.5 kV)	(10.2 kV)
4	20^0	cable	(372.5 kV)	(39.1 kV)
5	25^0	coupon back	(114.1 kV)	(12.0 kV)
6	30^0	coupon back	(24.6 kV)	2.7 kV
7	35^0	coupon front	14.67 kV	2.7 kV
8	40^0	coupon front	15.1 kV	2.8 kV
9	45^0	coupon front	15.3 kV	2.8 kV
10	50^0	coupon front	15.4 kV	2.8 kV
14	70^0	coupon front	16.8 kV	3.1 kV
18	90^0	coupon front	17.5 kV	3.2 kV

Table 10. Breakdown voltage between pin (6 mm above coupon) and cable (6 mm below coupon) or between pin and coupon, $\phi_{st} = 0^0$

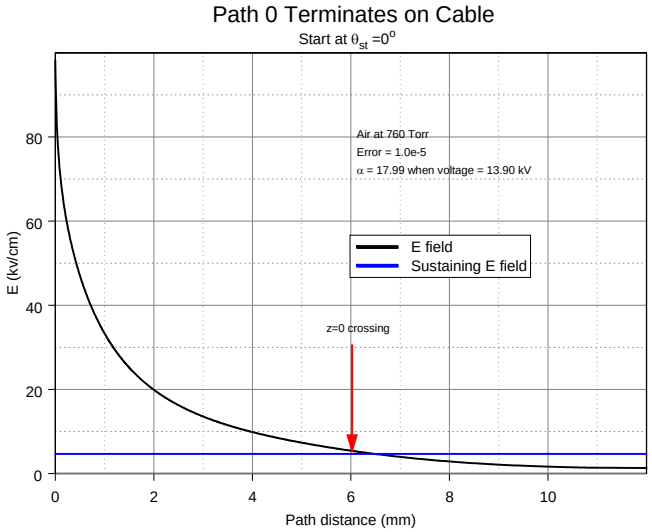

Figure 98. Field for path 0.

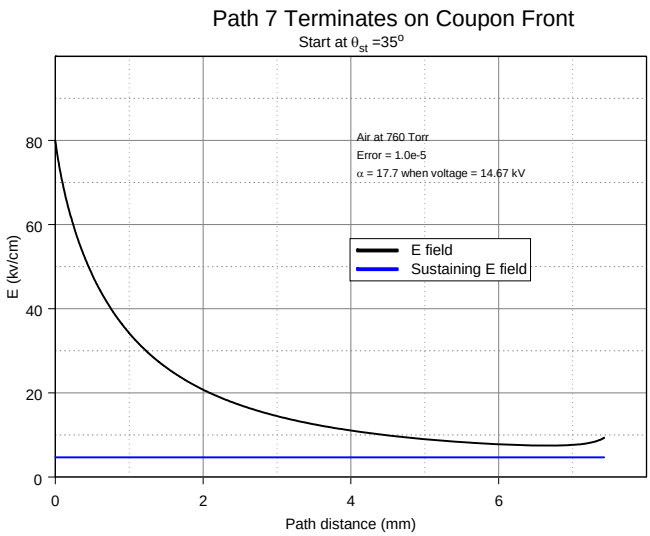

Figure 99. Field for path 7.

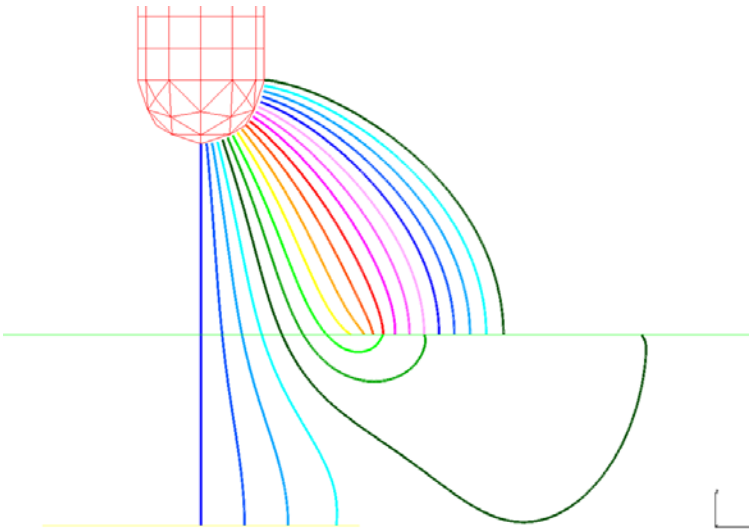

Figure 100. Paths through coupon hole perpendicular to cable axis, pin at z = 6 mm, cable at z = -6 mm.

must be increased to 49.9 kV to attain breakdown to the cable via spark.

From the results above we expect that if the coupon isn't present, that breakdown will occur between pin and cable at around 16.4 kV (Path 0). If we impose the coupon with the hole between the two, the field distribution changes. The coupon intercepts some of the paths, which restricts the paths that can transport electrons between pin and cable. Further, the coupon reduces the field surrounding the cable so that none of the paths that enter the hole will sustain a streamer at threshold. The paths that can sustain a streamer, all remain outside of the coupon and break down to the edge of the hole at around 14.5 kV (Path 7). If we increase the electrode voltage to 49.9 kV the entire Path 0 is above sustaining level and breakdown can occur to the cable. We need to assess the probability of breakdown along the single Path 0 just at breakdown threshold versus the many paths to the edge of the hole, which are at 3.4 times their breakdown threshold (49.9 kV/14.5 kV).

5.3.2 Pin 5 mm above Coupon, Cable 5 mm below Coupon

In this section we move the pin to 5 mm above the hole and the cable to 5 mm below the hole. Tables 12 and 13 show the breakdown voltages between pin and cable without the coupon for $\phi_{st} = 0^0$ and $\phi_{st} = 90^0$ respectively. We note that the lowest breakdown voltage is along Path 0 at 15.7 kV. The fields are more uniform than when the pin and cable were 12 mm apart and spark breakdown at threshold occurs over a wider range of θ_{st} . Tables 14 and 15 show the effect of placing a coupon with a 5 mm radius hole midway between the pin and cable. All paths that connect pin to cable corona at threshold. The lowest voltage that cause a spark breakdown pin to cable through the hole is 28.6 kV along Path 0. The threshold voltage that leads to spark breakdown occurs along Path 8 from pin to coupon front where $\phi_{st} = 90^0$ at 13.1 kV. Again there is a margin between the breakdown voltage from pin to cable versus the breakdown voltage from pin to hole edge but the margin isn't as large (28.6/13.1 = 2.2).

Path	θ_{st}	Path End	BDV 760 Torr	BDV 79.8 Torr
0	0^0	cable	(49.9 kV)	(5.2 kV)
1	5^0	cable	(52.8 kV)	(5.5 kV)
2	10^0	cable	(61.5 kV)	(6.5 kV)
3	15^0	cable	(83.2 kV)	(8.7 kV)
4	20^0	coupon back	(2170 kV)	(228.6 kV)
5	25^0	coupon back	(132.2 kV)	(13.9 kV)
6	30^0	coupon back	(26.4 kV)	(2.8 kV)
7	35^0	coupon front	14.5 kV	2.7 kV
8	40^0	coupon front	14.3 kV	2.7 kV
9	45^0	coupon front	14.2 kV	2.7 kV
10	50^0	coupon front	14.9 kV	2.8 kV
14	70^0	coupon front	17.0 kV	3.1 kV
18	90^0	coupon front	17.5 kV	3.2 kV

Table 11. Breakdown voltage between pin (6 mm above coupon) and cable (6 mm below coupon) or between pin and coupon, $\phi_{st} = 90^0$

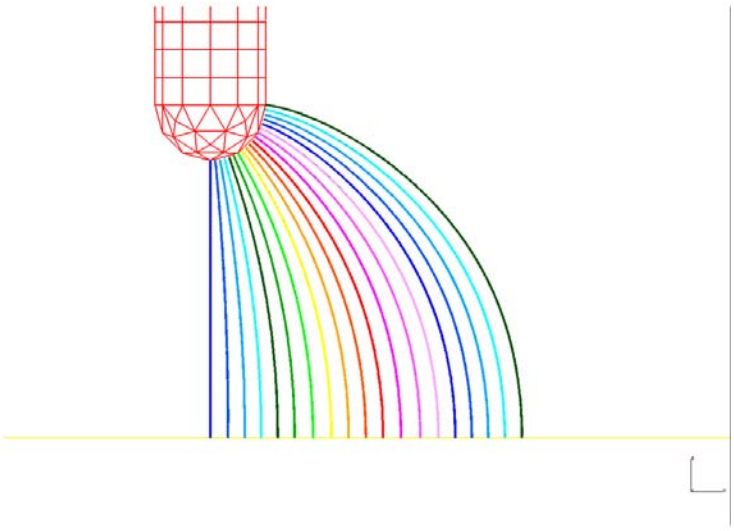

Figure 101. Breakdown paths along cable axis, pin at z = 5 mm, cable at z = -5 mm.

Path	θ_{st}	BDV 760 Torr	BDV 79.8 Torr
0	0^0	15.7 kV	3.0 kV
2	10^0	16.5 kV	3.1 kV
4	20^0	16.6 kV	3.1 kV
6	30^0	16.0 kV	3.1 kV
8	40^0	17.1 kV	3.2 kV
10	50^0	17.5 kV	3.3 kV
12	60^0	17.5 kV	3.3 kV
14	70^0	19.2 kV	3.6 kV
16	80^0	19.8 kV	3.7 kV
18	90^0	19.9 kV	3.7 kV

Table 12. Breakdown voltages between pin and cable 10 mm apart, $\phi_{st} = 0^0$

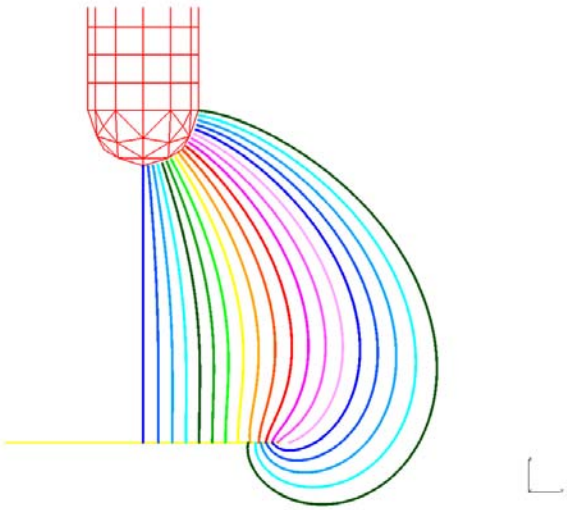

Figure 102. Breakdown paths perpendicular to cable axis, pin at z = 5 mm, cable at z = -5 mm.

Path	θ_{st}	BDV 760 Torr	BDV 79.8 Torr
0	0^0	15.7 kV	3.0 kV
2	10^0	16.6 kV	3.1 kV
4	20^0	16.8 kV	3.1 kV
6	30^0	16.5 kV	3.1 kV
8	40^0	16.3 kV	3.1 kV
10	50^0	17.0 kV	3.2 kV

Table 13. Breakdown voltages between pin and cable 10 mm apart, $\phi_{st} = 90^0$

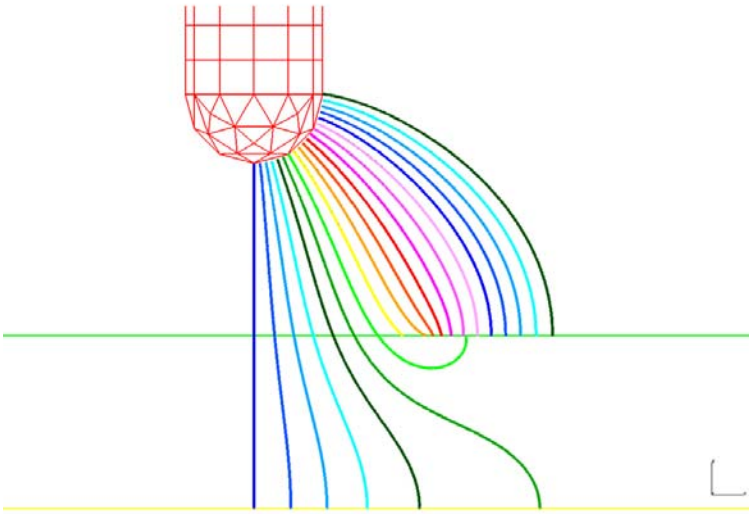

Figure 103. Paths through coupon hole along cable axis, pin at z = 5 mm, cable at z = -5 mm.

Path	θ_{st}	Path End	BDV 760 Torr	BDV 79.8 Torr
0	0^0	cable	(28.6 kV)	(3.0 kV)
1	5^0	cable	(30.2 kV)	(3.2 kV)
2	10^0	cable	(34.4 kV)	(3.6 kV)
3	15^0	cable	(43.3 kV)	(4.5 kV)
4	20^0	cable	(67.2 kV)	(7.1 kV)
5	25^0	cable	(463.6 kV)	(48.7 kV)
6	30^0	coupon back	(83.8 kV)	(8.8 kV)
7	35^0	coupon front	13.3 kV	2.6 kV
8	40^0	coupon front	13.8 kV	2.7 kV
9	45^0	coupon front	14.1 kV	2.7 kV
10	50^0	coupon front	14.2 kV	2.7 kV
14	70^0	coupon front	16.0 kV	3.0 kV
18	90^0	coupon front	17.1 kV	3.1 kV

Table 14. Breakdown voltage between pin (5 mm above coupon) and cable (5 mm below coupon) or between pin and coupon, $\phi_{st} = 0^0$

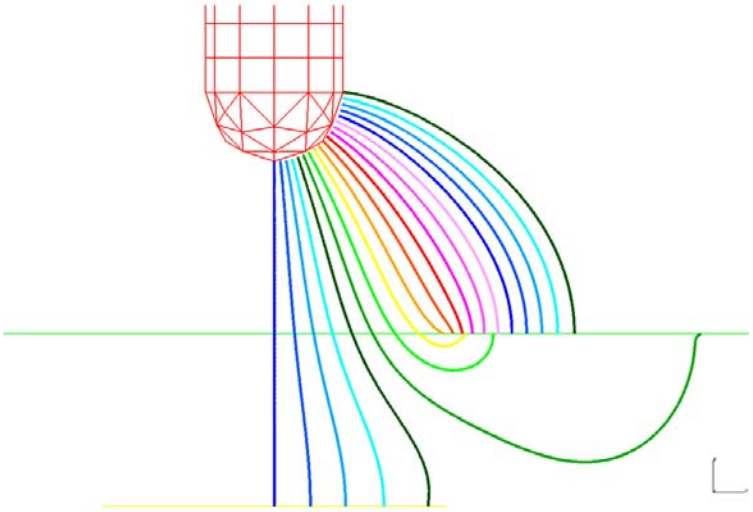

Figure 104. Paths through coupon hole perpendicular to cable axis, pin at z = 5 mm, cable at z = -5 mm.

Path	θ_{st}	Path End	BDV 760 Torr	BDV 79.8 Torr
0	0^0	cable	(28.6 kV)	(3.0 kV)
1	5^0	cable	(30.1 kV)	(3.2 kV)
2	10^0	cable	(34.0 kV)	(3.6 kV)
3	15^0	cable	(41.9 kV)	(4.4 kV)
4	20^0	cable	(57.4 kV)	(6.0 kV)
5	25^0	coupon back	(2390 kV)	(250.7 kV)
6	30^0	coupon back	(68.2 kV)	(7.2 kV)
7	35^0	coupon back	(20.2 kV)	2.6 kV
8	40^0	coupon front	13.1 kV	2.6 kV
9	45^0	coupon front	13.0 kV	2.6 kV
10	50^0	coupon front	13.7 kV	2.7 kV
14	70^0	coupon front	16.1 kV	3.0 kV
18	90^0	coupon front	17.1 kV	3.1 kV

Table 15. Breakdown voltage between pin (5 mm above coupon) and cable (5 mm below coupon) or between pin and coupon, $\phi_{st} = 90^0$

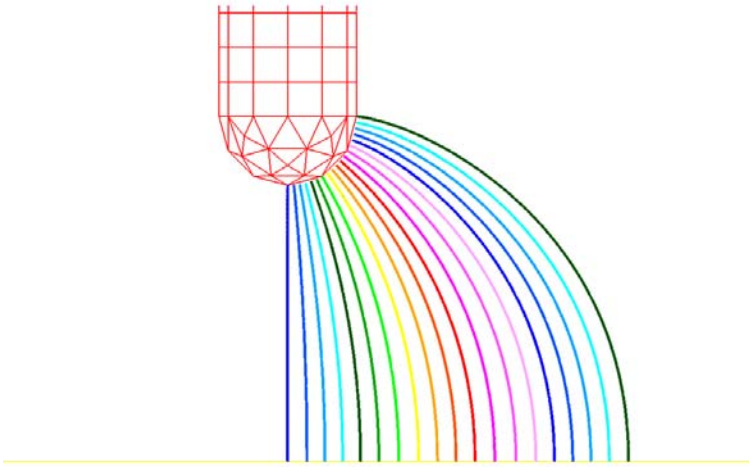

Figure 105. Breakdown paths along cable axis, pin at z = 4 mm, cable at z = -4 mm.

5.3.3 Pin 4 mm above Coupon, Cable 4 mm below Coupon

In this section we move the pin to 4 mm above the hole and the cable to 4 mm below the hole. Tables 16 and 17 show the breakdown voltages between pin and cable without the coupon for $\phi_{st} = 0^0$ and $\phi_{st} = 90^0$ respectively. We note that the lowest breakdown voltage is along Path 0 at 14.5 kV. The fields are more uniform than when the pin and cable were 10 mm apart and spark breakdown at threshold occurs over the entire range of θ_{st} being tested $\left(0^0 - 90^0\right)$ when $\phi_{st} = 0^0$ and the range $\left(0^0 - 70^0\right)$ when $\phi_{st} = 90^0$. Tables 18 and 19 show the effect of placing a coupon with a 5 mm radius hole midway between the pin and cable. All paths that connect pin to cable corona at threshold. The lowest voltage that cause a spark breakdown pin to cable through the hole is 15.6 kV along Path 0. The threshold voltage that leads to spark breakdown occurs along Path 8 from pin to coupon front where $\phi_{st} = 90^0$ at 12.4 kV. Again there is a margin between the breakdown voltage from pin to cable versus the breakdown voltage from pin to hole edge but the margin isn't as large (15.6/12.4 = 1.3).

5.3.4 Pin 2.5 mm above Coupon, Cable 2.5 mm below Coupon

In this set of simulations we will move the pin to 2.5 mm above the hole and the cable to 2.5 mm below the hole. Tables 20 and 21 show the breakdown voltages between pin and cable without the coupon for $\phi_{st} = 0^0$ and $\phi_{st} = 90^0$ respectively. We note that the lowest breakdown voltage is along Path 0 at 11.9 kV. The fields are even more uniform than when the pin and cable were 10 mm apart. Tables 22 and 23 show the effect of placing a coupon with a 5 mm radius hole midway between the pin and cable. Paths 0 through 7 are uniform enough that spark breakdown occurs at threshold. The lowest breakdown voltage is along Path 0 at 11.0 kV which is actually less than the breakdown predicted without the coupon. Breakdown to the coupon front occurs at 11.7 kV. The preferred breakdown path is along Path 0 to the cable. In this case the coupon is providing no protection to the cable.

Path	θ_{st}	BDV 760 Torr	BDV 79.8 Torr
0	0^0	14.5 kV	2.8 kV
2	10^0	15.2 kV	2.9 kV
4	20^0	15.3 kV	2.9 kV
6	30^0	16.0 kV	2.9 kV
8	40^0	14.9 kV	3.0 kV
10	50^0	16.6 kV	3.1 kV
12	60^0	16.7 kV	3.2 kV
14	70^0	18.4 kV	3.4 kV
16	80^0	19.0 kV	3.5 kV
18	90^0	19.2 kV	3.5 kV

Table 16. Breakdown voltages between pin and cable 8 mm apart, $\phi_{st} = 0^0$

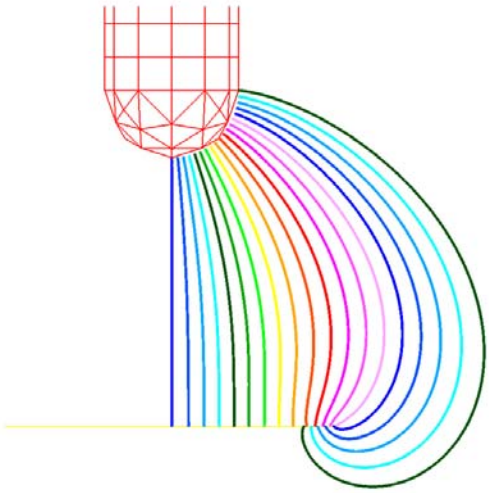

Figure 106. Breakdown paths perpendicular to cable axis, pin at z = 4 mm, cable at z = -4 mm.

Path	θ_{st}	BDV 760 Torr	BDV 79.8 Torr
0	0^0	14.5 kV	2.8 kV
2	10^0	15.4 kV	2.9 kV
4	20^0	15.6 kV	2.9 kV
6	30^0	15.4 kV	2.9 kV
8	40^0	15.3 kV	2.9 kV
10	50^0	16.2 kV	3.1 kV
12	60^0	17.5 kV	3.2 kV
14	70^0	18.7 kV	3.4 kV

Table 17. Breakdown voltages between pin and cable 8 mm apart, $\phi_{st} = 90^0$

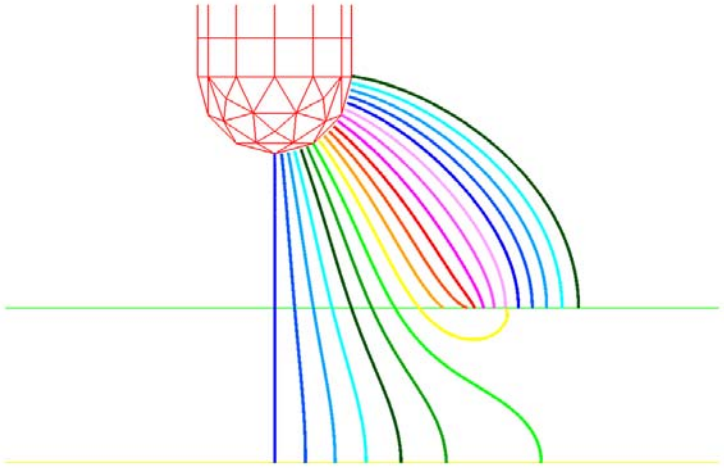

Figure 107. Paths through coupon hole along cable axis, pin at z = 4 mm, cable at z = -4 mm.

Path	θ_{st}	Path End	BDV 760 Torr	BDV 79.8 Torr
0	0^0	cable	(15.6 kV)	2.5 kV
1	5^0	cable	(15.8 kV)	2.5 kV
2	10^0	cable	(17.0 kV)	2.5 kV
3	15^0	cable	(19.5 kV)	2.6 kV
4	20^0	cable	(24.8 kV)	(2.6 kV)
5	25^0	cable	(37.3 kV)	(3.9 kV)
6	30^0	cable	(158 kV)	(16.6 kV)
7	35^0	coupon back	(39.0 kV)	(4.1 kV)
8	40^0	coupon front	13.1 kV	2.6 kV
9	45^0	coupon front	13.4 kV	2.6 kV
10	50^0	coupon front	13.5 kV	2.6 kV
14	70^0	coupon front	15.2 kV	2.9 kV
18	90^0	coupon front	16.3 kV	3.0 kV

Table 18. Breakdown voltage between pin (4 mm above coupon) and cable (4 mm below coupon) or between pin and coupon, $\phi_{st} = 0^0$

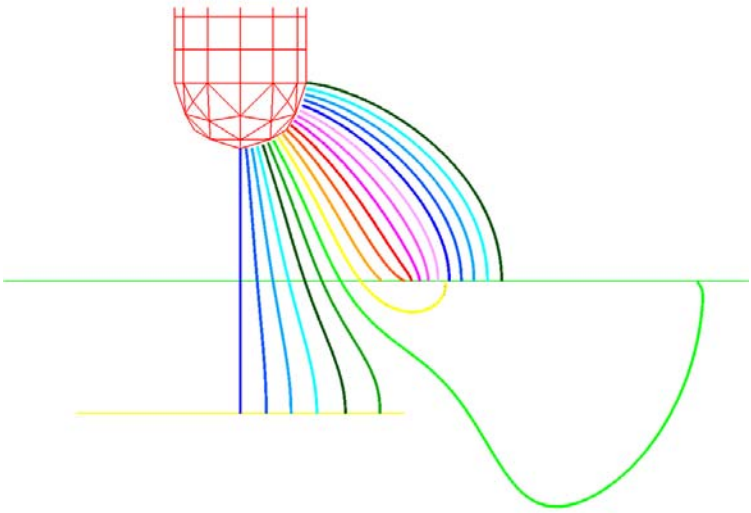

Figure 108. Paths through coupon hole perpendicular to cable axis, pin at z = 5 mm, cable at z = -4 mm.

Path	θ_{st}	Path End	BDV 760 Torr	BDV 79.8 Torr
0	0^0	cable	(15.6 kV)	2.5 kV
1	5^0	cable	(15.8 kV)	2.5 kV
2	10^0	cable	(16.9 kV)	2.5 kV
3	15^0	cable	(19.4 kV)	2.6 kV
4	20^0	cable	(24.2 kV)	2.6 kV
5	25^0	cable	(31.2 kV)	(3.3 kV)
6	30^0	coupon back	(4570 kV)	(48.0 kV)
7	35^0	coupon back	(72.5 kV)	(7.6 kV)
8	40^0	coupon front	12.4 kV	2.5 kV
9	45^0	coupon front	12.4 kV	2.5 kV
10	50^0	coupon front	13.1 kV	2.6 kV
14	70^0	coupon front	15.3 kV	2.9 kV
18	90^0	coupon front	16.3 kV	3.0 kV

Table 19. Breakdown voltage between pin (4 mm above coupon) and cable (4 mm below coupon) or between pin and coupon, $\phi_{st} = 90^0$

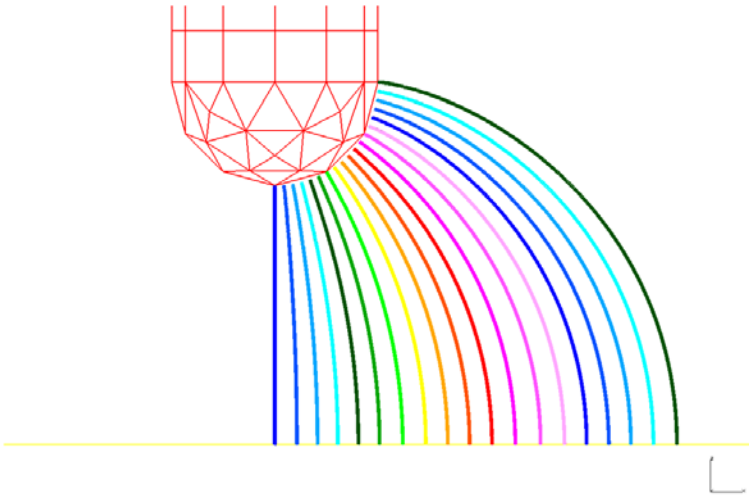

Figure 109. Breakdown paths along cable axis, pin at z = 2.5 mm, cable at z = -2.5 mm.

Path	θ_{st}	BDV 760 Torr	BDV 79.8 Torr
0	0^0	11.9 kV	2.4 kV
2	10^0	12.6 kV	2.5 kV
4	20^0	12.7 kV	2.5 kV
6	30^0	12.4 kV	2.5 kV
8	40^0	13.5 kV	2.6 kV
10	50^0	14.1 kV	2.7 kV
12	60^0	14.4 kV	2.8 kV
14	70^0	16.2 kV	3.0 kV
16	80^0	17.1 kV	3.1 kV
18	90^0	17.5 kV	3.2 kV

Table 20. Breakdown voltages between pin and cable 5 mm apart, $\phi_{st} = 0^0$

Path	θ_{st}	BDV 760 Torr	BDV 79.8 Torr
0	0^0	11.9 kV	2.4 kV
2	10^0	12.7 kV	2.5 kV
4	20^0	12.9 kV	2.5 kV
6	30^0	12.8 kV	2.5 kV
8	40^0	12.9 kV	2.6 kV
10	50^0	13.7 kV	2.7 kV
12	60^0	15.1 kV	2.9 kV
14	70^0	16.5 kV	3.1 kV
16	80^0	17.5 kV	3.2 kV
18	90^0	17.9 kV	3.3 kV

Table 21. Breakdown voltages between pin and cable 5 mm apart, $\phi_{st} = 90^0$

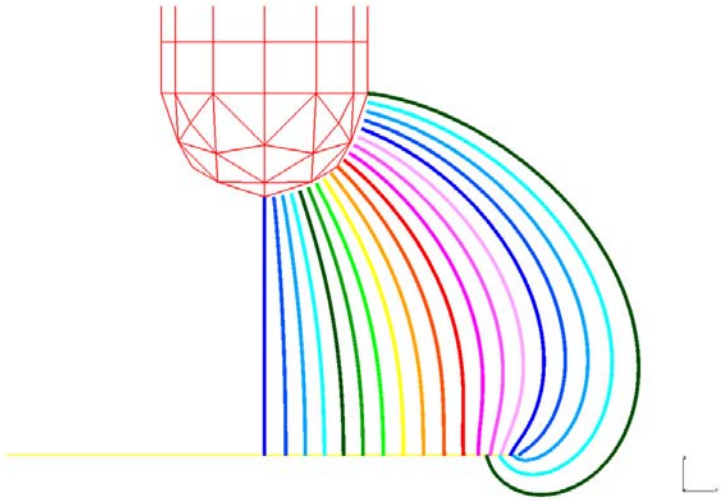

Figure 110. Breakdown paths perpendicular to cable axis, pin at z = 2.5 mm, cable at z = -2.5 mm.

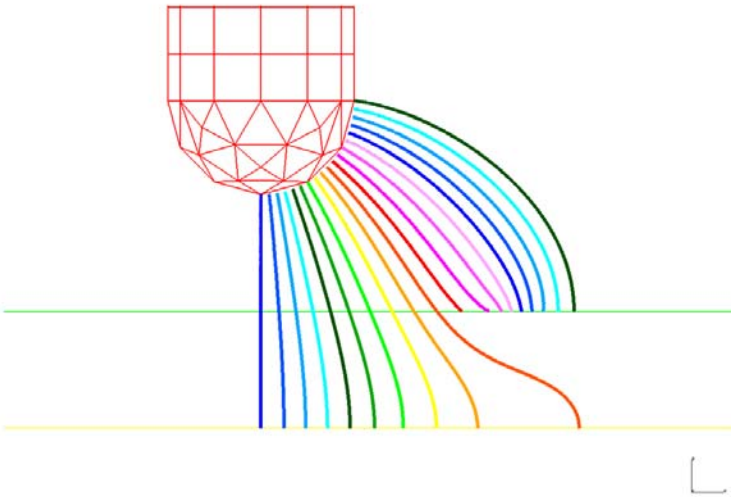

Figure 111. Paths through coupon hole along cable axis, pin at z = 2.5 mm, cable at z = -2.5 mm.

Path	θ_{st}	Path End	BDV 760 Torr	BDV 79.8 Torr
0	0^0	cable	11.0 kV	2.2 kV
1	5^0	cable	11.3 kV	2.3 kV
2	10^0	cable	11.6 kV	2.3 kV
3	15^0	cable	11.7 kV	2.3 kV
4	20^0	cable	11.7 kV	2.3 kV
5	25^0	cable	11.6 kV	2.3 kV
6	30^0	cable	11.3 kV	2.3 kV
7	35^0	cable	11.9 kV	2.4 kV
8	40^0	cable	(18.1) kV	2.4 kV
9	45^0	cable	(162) kV	(17.0 kV)
10	50^0	coupon front	12.1 kV	2.4 kV
14	70^0	coupon front	13.8 kV	2.6 kV
18	90^0	coupon front	14.9 kV	2.8 kV

Table 22. Breakdown voltage between pin (2.5 mm above coupon) and cable (2.5 mm below coupon) or between pin and coupon, $\phi_{st} = 0^0$

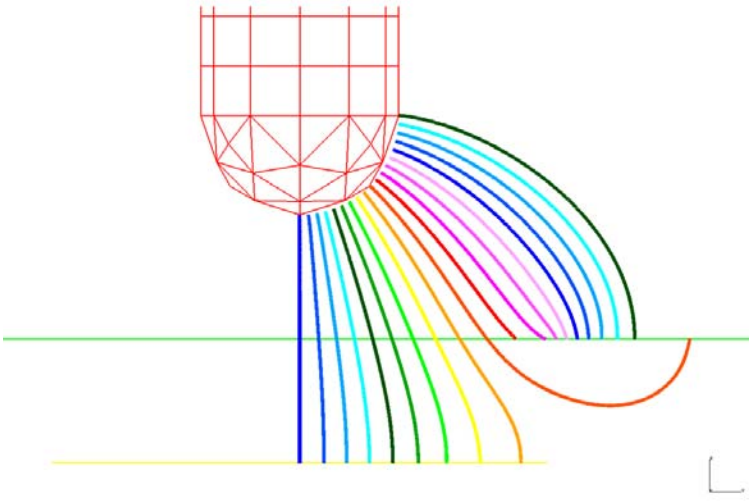

Figure 112. Paths through coupon hole perpendicular to cable axis, pin at z = 2.5 mm, cable at z = -2.5 mm.

Path	θ_{st}	Path End	BDV 760 Torr	BDV 79.8 Torr
0	0^0	cable	11.0 kV	2.2 kV
1	5^0	cable	11.4 kV	2.3 kV
2	10^0	cable	11.6 kV	2.3 kV
3	15^0	cable	11.8 kV	2.3 kV
4	20^0	cable	11.8 kV	2.3 kV
5	25^0	cable	11.8 kV	2.3 kV
6	30^0	cable	11.7 kV	2.3 kV
7	35^0	cable	11.7 kV	2.3 kV
8	40^0	cable	(15.6 kV)	2.3 kV
9	45^0	coupon back	(269 kV)	(28.2 kV)
10	50^0	coupon front	11.7 kV	2.4 kV
14	70^0	coupon front	13.9 kV	2.6 kV
18	90^0	coupon front	14.9 kV	2.8 kV

Table 23. Breakdown voltage between pin (2.5 mm above coupon) and cable (2.5 mm below coupon) or between pin and coupon, $\phi_{st} = 90^0$

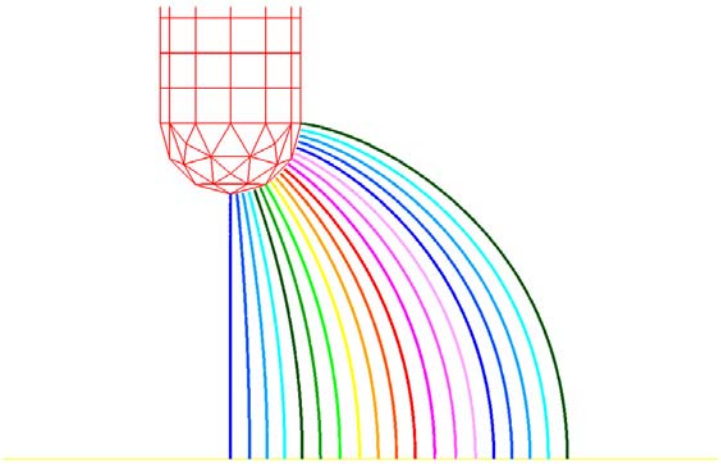

Figure 113. Breakdown paths along cable axis, pin at z = 2.5 mm, cable at z = -5.0 mm.

5.3.5 Pin 2.5 mm above Coupon, Cable 5 mm below Coupon

In the next set of simulations we will keep the pin at 2.5 mm above the hole and move the cable 5 mm away from the hole. Tables 24 and 25 show that without the coupon, the pin breaks down to the cable at the lowest value of 14.1 kV along Path 0. Tables 26 and 27 show that with the coupon in place, all of the paths from pin to cable breakdown at threshold via corona. If we increase the voltage between pin and cable to 14.8 kV, a spark breakdown will occur along Path 0. The breakdown along Path 10 ($\phi_{st} = 90^0$) occurs at 12.0 kV so Path 10 is over-volted by a factor of 1.2.

5.3.6 Pin 2.5 mm above Coupon, Cable 7.5 mm below Coupon

In the next set of simulations we will keep the pin at 2.5 mm above the hole and move the cable 7.5 mm away from the hole. We already have the results of pin and cable without the coupon, 10 mm apart : 15.7 kV along Path 0. Tables 28 and 29 show that with the coupon in place, all of the paths from pin to cable breakdown at threshold via corona. If we increase the voltage between pin and cable to 33.8 kV, a spark breakdown will occur along Path 0. The breakdown along Path 10 ($\phi_{st} = 90^0$) occurs at 12.0 kV so Path 10 is over-volted by a factor of 2.8.

5.3.7 Pin 5 mm above Coupon, Cable 2.5 mm below Coupon

In the next set of simulations we will put the pin at 5 mm above the hole and move the cable 2.5 mm away from the hole. We already have the results of pin and cable without the coupon, 7.5 mm apart : 14.1 kV along Path 0. Tables 30 and 31 show the effect of placing a coupon with a 5 mm radius hole between the pin and cable. Paths 0 through 3 are uniform enough that spark breakdown occurs at threshold. The lowest breakdown voltage is along Path 0 at 12.8 kV which is actually less than the breakdown predicted

Path	θ_{st}	BDV 760 Torr	BDV 79.8 Torr
0	0^0	14.1 kV	2.8 kV
2	10^0	14.8 kV	2.8 kV
4	20^0	15.0 kV	2.9 kV
6	30^0	14.5 kV	2.8 kV
8	40^0	15.7 kV	3.0 kV
10	50^0	16.3 kV	3.1 kV
12	60^0	16.5 kV	3.1 kV
14	70^0	18.2 kV	3.3 kV
16	80^0	18.8 kV	3.4 kV
18	90^0	19.0 kV	3.5 kV

Table 24. Breakdown voltages between pin and cable 7.5 mm apart, $\phi_{st} = 0^0$

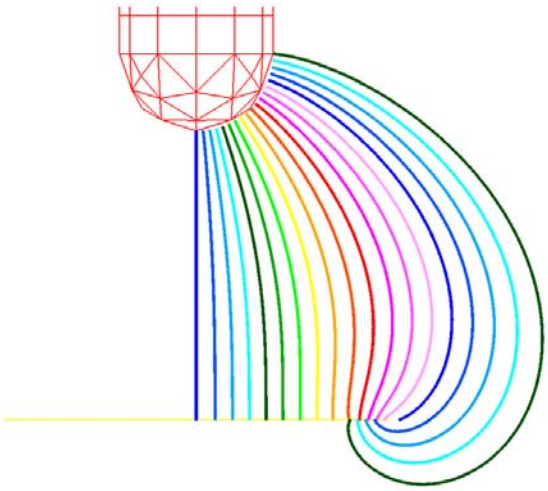

Figure 114. Breakdown paths perpendicular to cable axis, pin at z = 2.5 mm, cable at z = -5.0 mm.

Path	θ_{st}	BDV 760 Torr	BDV 79.8 Torr
0	0^0	14.1 kV	2.8 kV
2	10^0	15.0 kV	2.9 kV
4	20^0	15.2 kV	2.9 kV
6	30^0	15.1 kV	2.9 kV
8	40^0	15.0 kV	2.9 kV
10	50^0	15.8 kV	3.0 kV
12	60^0	17.3 kV	3.2 kV
14	70^0	18.5 kV	3.4 kV

Table 25. Breakdown voltages between pin and cable 7.5 mm apart, $\phi_{st} = 90^0$

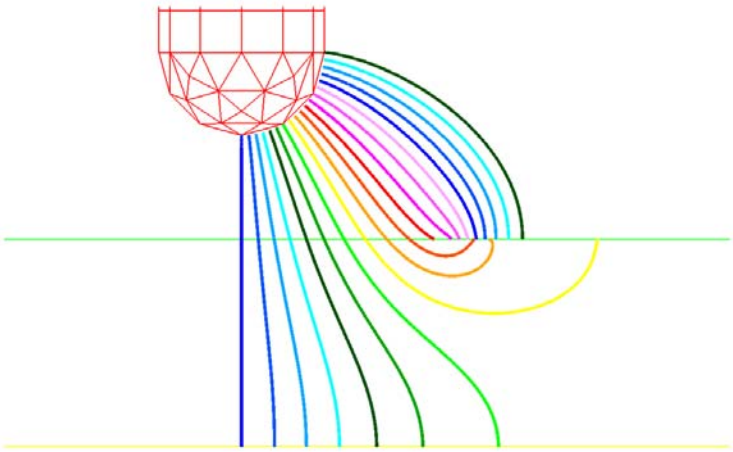

Figure 115. Paths through coupon hole along cable axis, pin at z = 2.5 mm, cable at z = -5.0 mm.

Path	θ_{st}	Path End	BDV 760 Torr	BDV 79.8 Torr
0	0^0	cable	(14.8 kV)	2.4 kV
1	5^0	cable	(15.0 kV)	2.4 kV
2	10^0	cable	(16.0 kV)	2.4 kV
3	15^0	cable	(18.4 kV)	2.4 kV
4	20^0	cable	(22.8 kV)	2.4 kV
5	25^0	cable	(32.1 kV)	(3.4 kV)
6	30^0	cable	(76.6 kV)	(8.0 kV)
7	35^0	coupon back	(219 kV)	(23.0 kV)
8	40^0	coupon back	(25.8 kV)	(2.7 kV)
9	45^0	coupon back	12.6 kV	2.5 kV
10	50^0	coupon front	12.4 kV	2.5 kV
14	70^0	coupon front	14.0 kV	2.7 kV
18	90^0	coupon front	15.0 kV	2.8 kV

Table 26. Breakdown voltage between pin (2.5 mm above coupon) and cable (5 mm below coupon) or between pin and coupon, $\phi_{st} = 0^0$

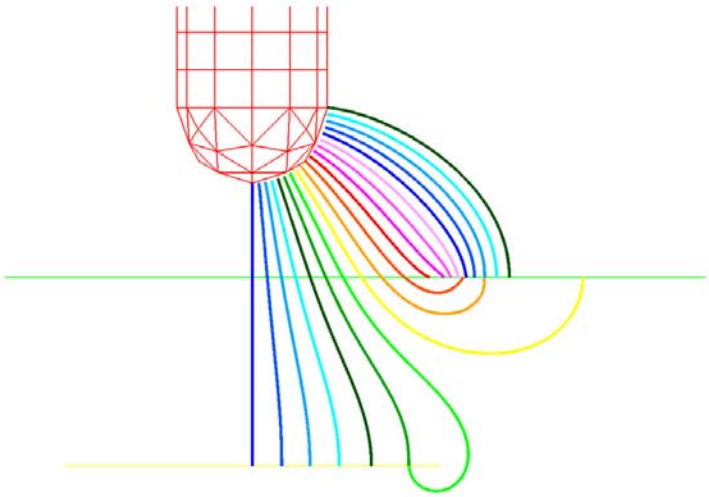

Figure 116. Paths through coupon hole perpendicular to cable axis, pin at z = 2.5 mm, cable at z = -5.0 mm.

Path	θ_{st}	Path End	BDV 760 Torr	BDV 79.8 Torr
0	0^0	cable	(14.8 kV)	2.4 kV
1	5^0	cable	(15.0 kV)	2.4 kV
2	10^0	cable	(16.0 kV)	2.4 kV
3	15^0	cable	(18.2 kV)	2.4 kV
4	20^0	cable	(22.1 kV)	2.4 kV
5	25^0	cable	(26.7 kV)	(2.8 kV)
6	30^0	cable	(221 kV)	(23.2 kV)
7	35^0	coupon back	(218 kV)	(22.9 kV)
8	40^0	coupon back	(43.0 kV)	(4.5 kV)
9	45^0	coupon back	(11.8 kV)	2.3 kV
10	50^0	coupon front	12.0 kV	2.4 kV
14	70^0	coupon front	14.0 kV	2.7 kV
18	90^0	coupon front	15.0 kV	2.8 kV

Table 27. Breakdown voltage between pin (2.5 mm above coupon) and cable (5 mm below coupon) or between pin and coupon, $\phi_{st} = 90^0$

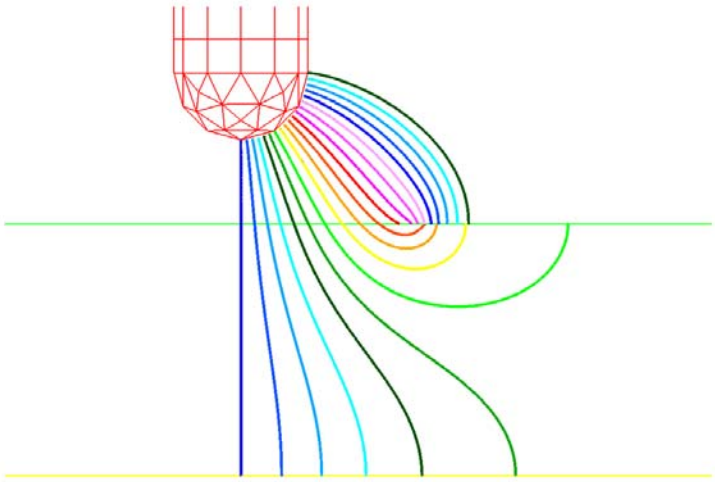

Figure 117. Paths through coupon hole along cable axis, pin at z = 2.5 mm, cable at z = -7.5 mm.

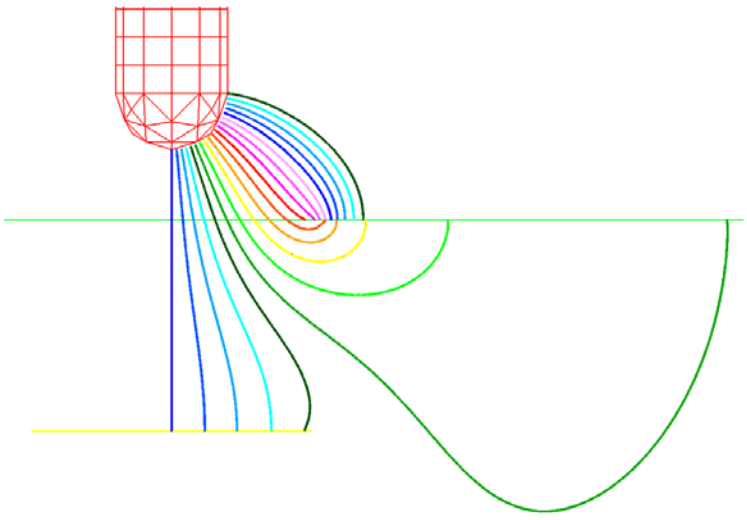

Figure 118. Paths through coupon hole perpendicular to cable axis, pin at z = 2.5 mm, cable at z = -7.5 mm.

Path	θ_{st}	Path End	BDV 760 Torr	BDV 79.8 Torr
0	0^0	cable	(33.8 kV)	(3.6 kV)
1	5^0	cable	(35.4 kV)	(3.7 kV)
2	10^0	cable	(39.7 kV)	(4.2 kV)
3	15^0	cable	(48.7 kV)	(5.1 kV)
4	20^0	cable	(75.0 kV)	(7.9 kV)
5	25^0	cable	(201 kV)	(21.1 kV)
6	30^0	coupon back	(256 kV)	(26.9 kV)
7	35^0	coupon back	(38.0 kV)	(4.0 kV)
8	40^0	coupon back	(13.8 kV)	2.5 kV
9	45^0	coupon back	12.6 kV	2.5 kV
10	50^0	coupon front	12.4 kV	2.5 kV
14	70^0	coupon front	14.0 kV	2.7 kV
18	90^0	coupon front	15.0 kV	2.8 kV

Table 28. Breakdown voltage between pin (2.5 mm above coupon) and cable (7.5 mm below coupon) or between pin and coupon, $\phi_{st} = 0^0$

without the coupon. Breakdown to the coupon front occurs at 13.0 kV. The preferred breakdown path is along Path 0 to the cable. In this case the coupon is providing no protection to the cable.

5.3.8 Pin 7.5 mm above Coupon, Cable 2.5 mm below Coupon

In the next set of simulations we will move the pin to 7.5 mm above the hole and keep the cable 2.5 mm away from the hole. We already have the results of pin and cable without the coupon, 10 mm apart : 15.7 kV along Path 0. Tables 32 and 33 show that with the coupon in place, all of the paths from pin to cable breakdown at threshold via corona. If we increase the voltage between pin and cable to 19.2 kV, a spark breakdown will occur along Path 0. The breakdown along Path 7 ($\phi_{st} = 90^0$) occurs at 14.6 kV so Path 7 is over-volted by a factor of 1.3.

5.3.9 Summary

Table 34 summarizes the breakdown results obtained so far. For 760 Torr, as long as the pin electrode and the cable are more than a hole radius away from the coupon, the pin to coupon gap is over-volted by more than a factor of two over the pin to cable gap. If the pin violates this criterion but the cable keeps its distance, the over-volting factor decreases but continues to provide some level of protection . If the cable violates the criterion, on the other hand and the pin keeps its distance, the protection is lost. At 79.8 Torr, the protection factor is cut roughly in half. At the high temperatures we must then rely on spatial variation of the temperature (hotter on the outside than on the inside) to maintain the level of protection.

5.4 Experimental Geometry

The geometry used to measure the breakdown levels is slightly different than the geometry analyzed above. In this section we analyze the breakdown levels of the experimental geometry shown in Figure 123 (oblique view) and in Figure 124 (side view). In this analysis the electrode has a pointed rather than a hemispherical end and the coupon has a thickness of 0.48 inches rather than being infinitesimally thin.

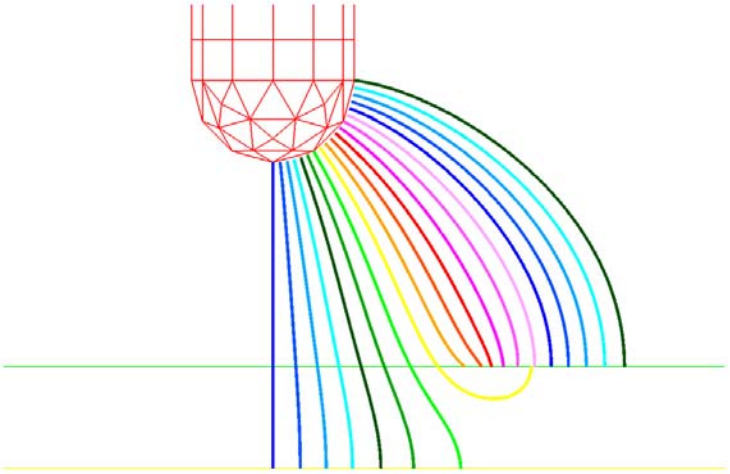

Figure 119. Paths through coupon hole along cable axis, pin at z = 5 mm, cable at z = -2.5 mm.

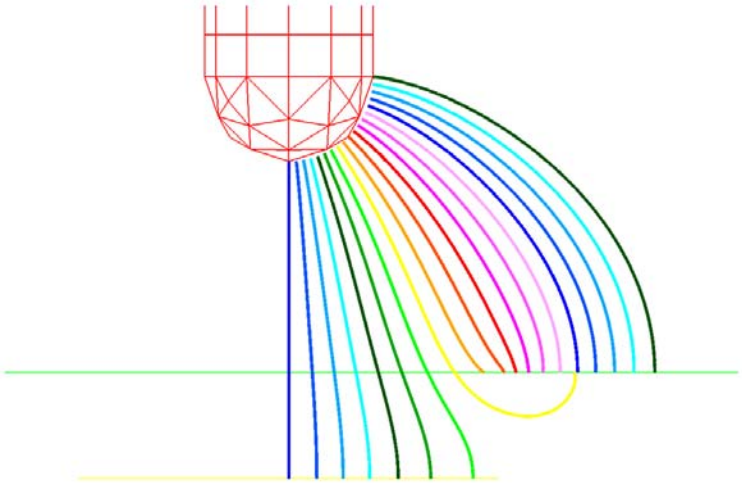

Figure 120. Paths through coupon hole perpendicular to cable axis, pin at z = 5 mm, cable at z = -2.5 mm.

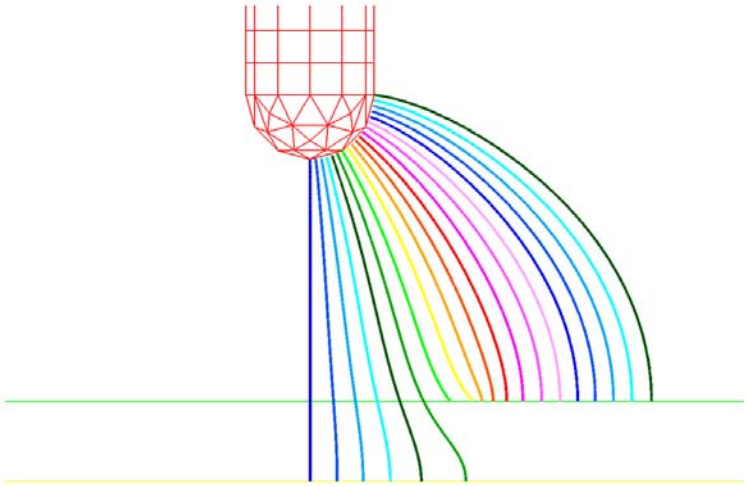

Figure 121. Paths through coupon hole along cable axis, pin at z = 7.5 mm, cable at z = -2.5 mm.

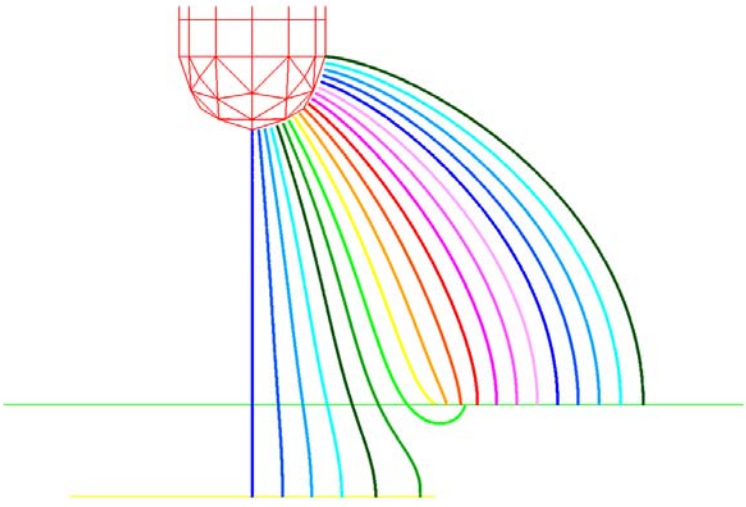

Figure 122. Paths through coupon hole perpendicular to cable axis, pin at z = 7.5 mm, cable at z = -2.5 mm.

Path	θ_{st}	Path End	BDV 760 Torr	BDV 79.8 Torr
0	0^0	cable	(33.8 kV)	(3.6 kV)
1	5^0	cable	(35.3 kV)	(3.7 kV)
2	10^0	cable	(39.0 kV)	(4.1 kV)
3	15^0	cable	(45.5 kV)	(4.8 kV)
4	20^0	cable	(67.1 kV)	(7.1 kV)
5	25^0	cable	(3600 kV)	(381.6 kV)
6	30^0	coupon back	(232 kV)	(24.4 kV)
7	35^0	coupon back	(45.3 kV)	(4.8 kV)
8	40^0	coupon back	(15.0 kV)	2.4 kV
9	45^0	coupon back	(11.7 kV)	2.4 kV
10	50^0	coupon front	12.0 kV	2.4 kV
14	70^0	coupon front	14.0 kV	2.7 kV
18	90^0	coupon front	15.0 kV	2.8 kV

Table 29. Breakdown voltage between pin (2.5 mm above coupon) and cable (7.5 mm below coupon) or between pin and coupon, $\phi_{st} = 90^0$

Rather than a cable underneath the hole we have a disk of metal representing the experimental collector. The dimensions have changed as well. The collector is a fixed distance 0.2 inches away from the back of the coupon. We examined two different diameter holes: 0.5 and 0.7 inches. The entire geometry is modeled as PEC. The mesh used is shown in Figure 125. We start the avalanches near the pin as we did before, but since the pin is pointed rather than rounded we need to designate the starting points of the paths differently. A way of defining the starting point is shown in Figure 126. The problem is now axisymmetric so we can confine our starting locations to the $y = 0$ plane. The starting points are defined as being on a line (seen as "x's" in Figure 126). The line is parallel to the surface of the pin and offset by a user-defined amount in the $-z$ direction. The distance along the line from axis to a particular starting point near the tip is described by the distance Δ_t; the distance along the line from the base of the tip to a point near the side of the pin is described by the distance Δ_s.

5.5 Results for 0.5 diameter hole

Figures 127 - 132 show the paths along which breakdown is predicted to occur for several cases of electrode tip position relative to the coupon barrier and interior collector. The breakdown is being predicted for air at 760 Torr. The hole diameter is 0.5 inches. At the collector or coupon end of the path in the figures, the predicted breakdown voltage is given in kV. The parentheses around the breakdown voltage indicates that corona will occur at a lower voltage and that we invoked the streamer sustaining field criterion to predict this spark voltage. In the middle of each path the path length is given in mm.

5.6 Results for 0.7 diameter hole

Figures 133 - 138 show the paths along which breakdown is predicted to occur for several cases of electrode tip position relative to the coupon barrier and interior collector. The breakdown is being predicted for air at 760 Torr. The hole diameter is 0.7 inches. At the collector or coupon end of the path in the figures, the predicted breakdown voltage is given in kV. The parentheses around the breakdown voltage indicates that corona will occur at a lower voltage and that we invoked the streamer sustaining field criterion to predict this spark voltage. In the middle of each path the path length is given in mm.

Path	θ_{st}	Anode Collision	BDV 760 Torr	BDV 79.8 Torr
0	0^0	cable	12.8 kV	2.5 kV
1	5^0	cable	13.2 kV	2.6 kV
2	10^0	cable	13.5 kV	2.6 kV
3	15^0	cable	13.6 kV	2.6 kV
4	20^0	cable	(14.5 kV)	2.6 kV
5	25^0	cable	(18.6 kV)	2.6 kV
6	30^0	cable	(32.1 kV)	(3.4 kV)
7	35^0	coupon back	(162 kV)	(17.0 kV)
8	40^0	coupon front	13.7 kV	2.7 kV
9	45^0	coupon front	14.0 kV	2.7 kV
10	50^0	coupon front	14.1 kV	2.7 kV
14	70^0	coupon front	15.9 kV	3.0 kV
18	90^0	coupon front	17.0 kV	3.1 kV

Table 30. Breakdown voltage between pin (5 mm above coupon) and cable (2.5 mm below coupon) or between pin and coupon, $\phi_{st} = 0^0$

Path	θ_{st}	Path End	BDV 760 Torr	BDV 79.8 Torr
0	0^0	cable	12.8 kV	2.5 kV
1	5^0	cable	13.2 kV	2.6 kV
2	10^0	cable	13.6 kV	2.6 kV
3	15^0	cable	13.7 kV	2.6 kV
4	20^0	cable	(14.3 kV)	2.6 kV
5	25^0	cable	(18.3 kV)	2.6 kV
6	30^0	cable	(26.9 kV)	(2.8 kV)
7	35^0	coupon back	(174 kV)	(18.3 kV)
8	40^0	coupon front	13.0 kV	2.6 kV
9	45^0	coupon front	13.0 kV	2.6 kV
10	50^0	coupon front	13.7 kV	2.7 kV
14	70^0	coupon front	16.1 kV	3.0 kV
18	90^0	coupon front	17.1 kV	3.1 kV

Table 31. Breakdown voltage between pin (5 mm above coupon) and cable (2.5 mm below coupon) or between pin and coupon, $\phi_{st} = 90^0$

Path	θ_{st}	Path End	BDV 760 Torr	BDV 79.8 Torr
0	0^0	cable	(19.2 kV)	2.7 kV
1	5^0	cable	(19.4 kV)	2.8 kV
2	10^0	cable	(20.6 kV)	2.8 kV
3	15^0	cable	(23.5 kV)	2.8 kV
4	20^0	cable	(30.4 kV)	(3.2 kV)
5	25^0	cable	(60.0 kV)	(6.3 kV)
6	30^0	coupon front	(14.3 kV)	2.8 kV
7	35^0	coupon front	14.8 kV	2.8 kV
8	40^0	coupon front	15.3 kV	2.9 kV
9	45^0	coupon front	15.6 kV	2.9 kV
10	50^0	coupon front	15.7 kV	3.0 kV
14	70^0	coupon front	17.3 kV	3.2 kV
18	90^0	coupon front	18.0 kV	3.3 kV

Table 32. Breakdown voltage between pin (7.5 mm above coupon) and cable (2.5 mm below coupon) or between pin and coupon, $\phi_{st} = 0^0$

Path	θ_{st}	Path End	BDV 760 Torr	BDV 79.8 Torr
0	0^0	cable	(19.2 kV)	2.7 kV
1	5^0	cable	(19.4 kV)	2.8 kV
2	10^0	cable	(20.6 kV)	2.8 kV
3	15^0	cable	(23.4 kV)	2.8 kV
4	20^0	cable	(29.9 kV)	(3.1 kV)
5	25^0	cable	(49.6 kV)	(5.2 kV)
6	30^0	coupon back	(56.5 kV)	(5.9 kV)
7	35^0	coupon front	14.6 kV	2.8 kV
8	40^0	coupon front	14.5 kV	2.8 kV
9	45^0	coupon front	14.4 kV	2.8 kV
10	50^0	coupon front	15.2 kV	2.9 kV
14	70^0	coupon front	17.5 kV	3.2 kV
18	90^0	coupon front	18.0 kV	3.3 kV

Table 33. Breakdown voltage between pin (7.5 mm above coupon) and cable (2.5 mm below coupon) or between pin and coupon, $\phi_{st} = 90^0$

Pin position (mm)	Cable Position (mm)	Protection Factor 760 Torr	Protection Factor 79.8 Torr
6	6	3.4	1.9
5	5	2.2	1.2
4	4	1.2	none
2.5	2.5	none	none
2.5	5	1.2	none
2.5	7.5	2.7	1.4
5	2.5	none	none
7.5	2.5	1.3	none

Table 34. Summary of protection

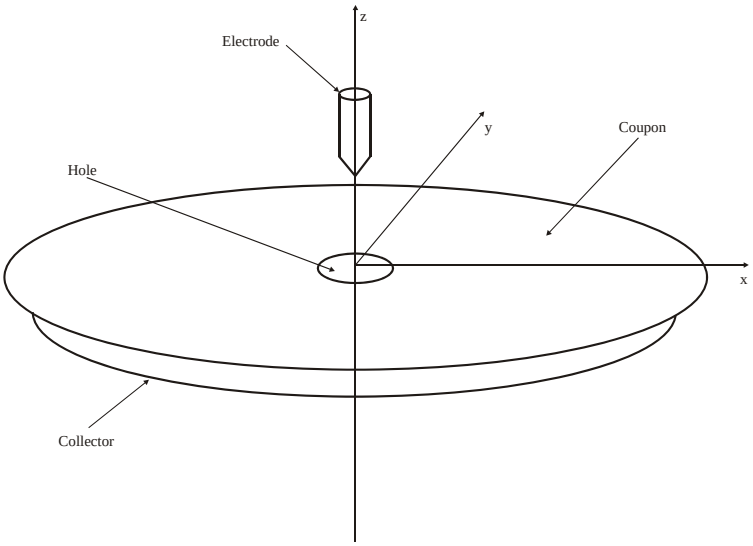

Figure 123. Oblique view of experimental geometry.

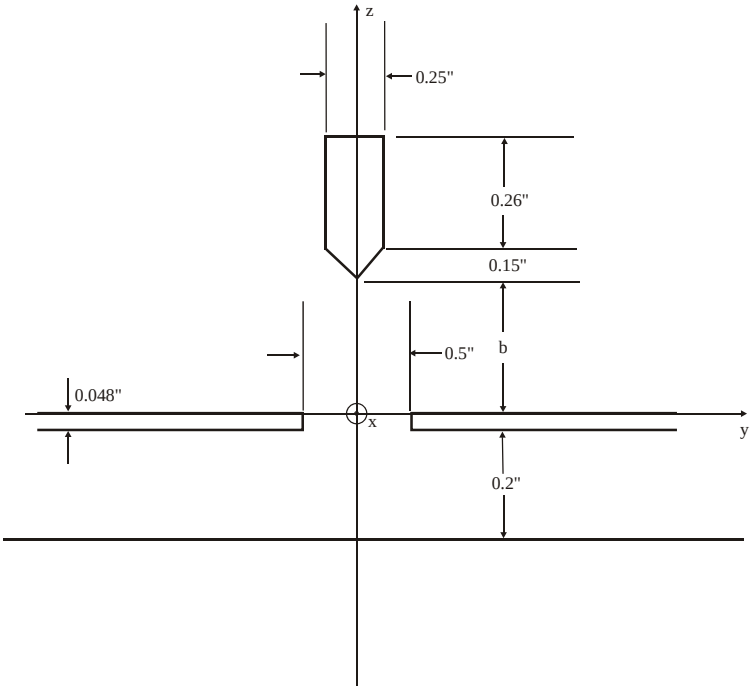

Figure 124. Side view of experimental geometry.

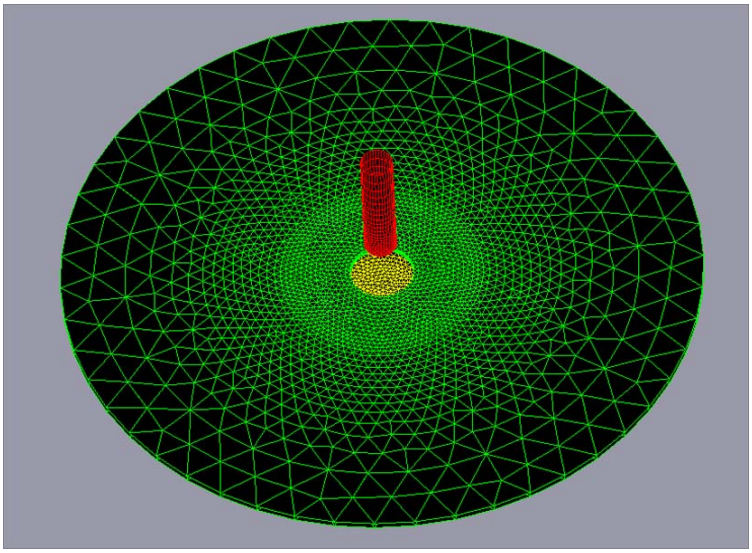

Figure 125. Mesh of experimental geometry.

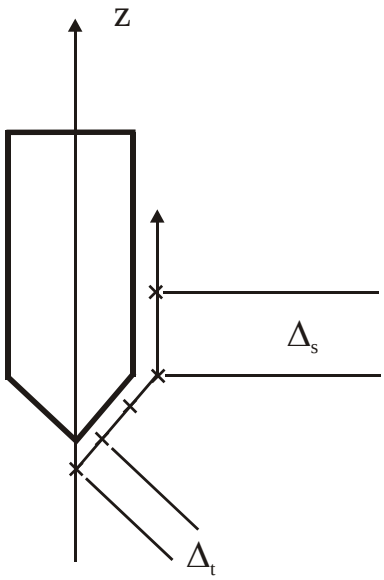

Figure 126. Starting point of avalanche near pin.

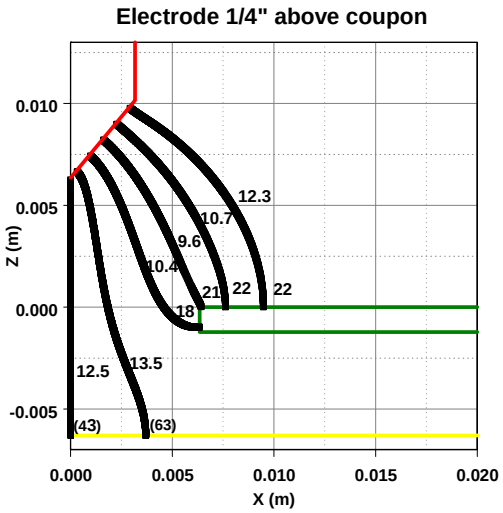

Figure 127. Pin 1/4" above coupon; 0.5" diameter hole.

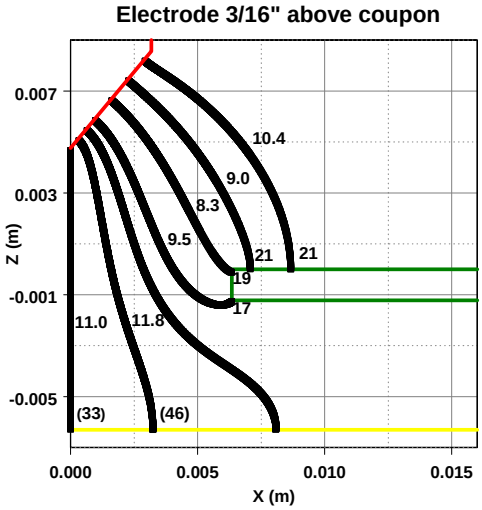

Figure 128. Pin 3/16" above coupon; 0.5" diameter hole.

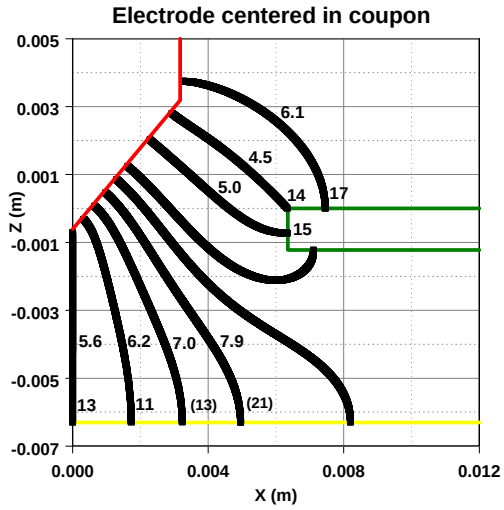

Figure 129. Pin centered in coupon hole; 0.5" diameter hole.

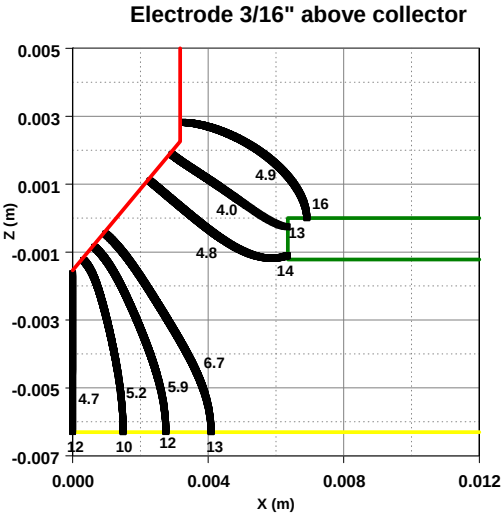

Figure 130. Pin 3/16" above collector; 0.5" diameter hole.

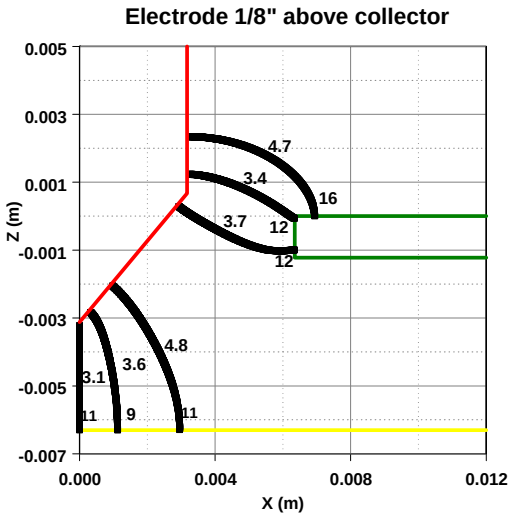

Figure 131. Pin 1/8" above collector; 0.5" diameter hole.

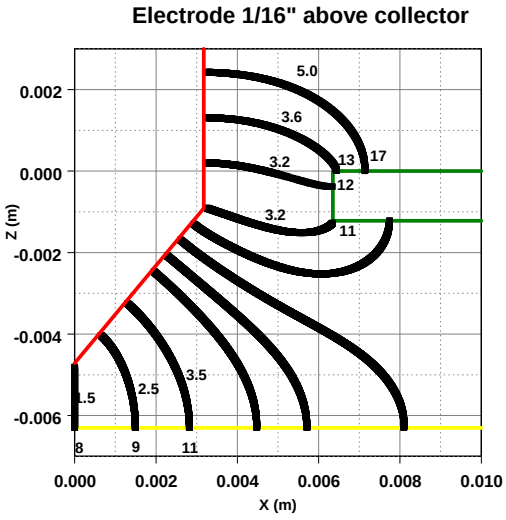

Figure 132. Pin 1/16" above collector; 0.5" diameter hole.

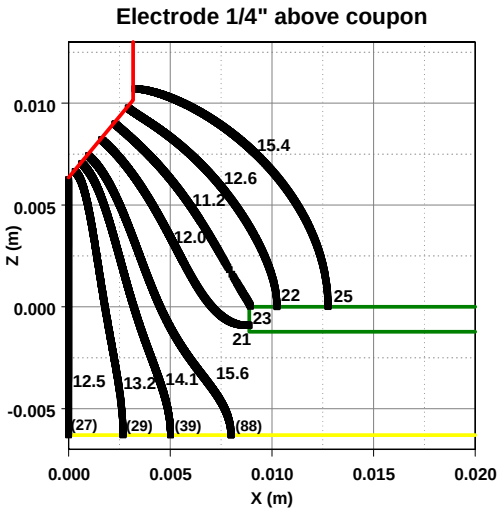

Figure 133. Pin 1/4" above coupon; 0.7" diameter hole.

5.7 Arc To Interior Collector

In order to experimentally examine the validity of the threshold calculations we are conducting experiments where the cathode is brought closer to a predrilled hole in order to induce a discharge to the collector itself. To think about the electrical transients in these experiments the simplified circuit model shown in Figure 139 can be considered. The collector to chassis capacitance is in the range

$$C_c \approx 20 - 75 \text{ pF}$$

depending on whether a strip cable or a piston collector is used. The twisted lead capacitance in parallel with this is

$$C_{lead} = 8 \text{ pF}$$

and thus the total is

$$C_{tot} = C_c + C_{lead} \approx 28 - 83 \text{ pF}$$

The transfer capacitance to the collector when the cathode is 0.25 inches above the plane is approximately

$$C \approx 0.0118 \text{ pF}$$

The lead inductance back to the ODL is estimated to be

$$L_{lead} \approx 70 \text{ nH}$$

The additional stripline inductance in series with this is estimated as

$$L_{strip} \approx 38 \text{ nH}$$

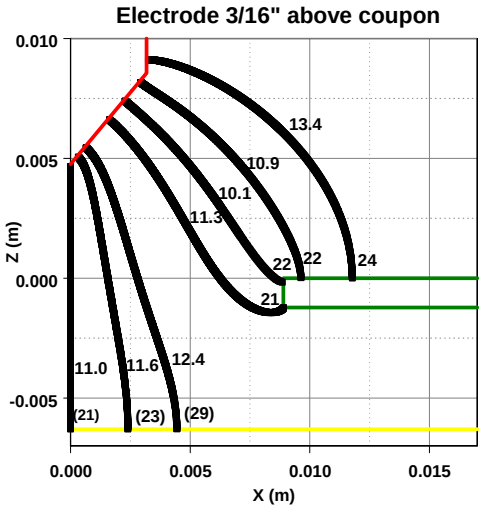

Figure 134. Pin 3/16" above coupon; 0.7" diameter hole.

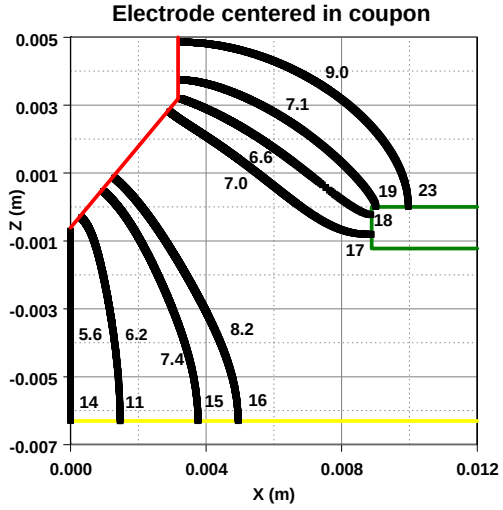

Figure 135. Pin centered in coupon hole; 0.7" diameter hole.

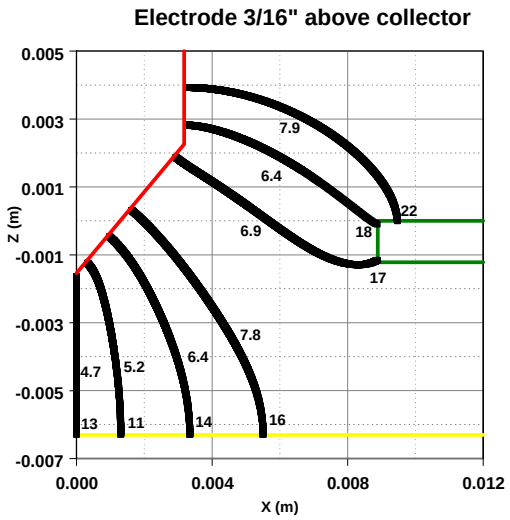

Figure 136. Pin 3/16" above coupon; 0.7" diameter hole.

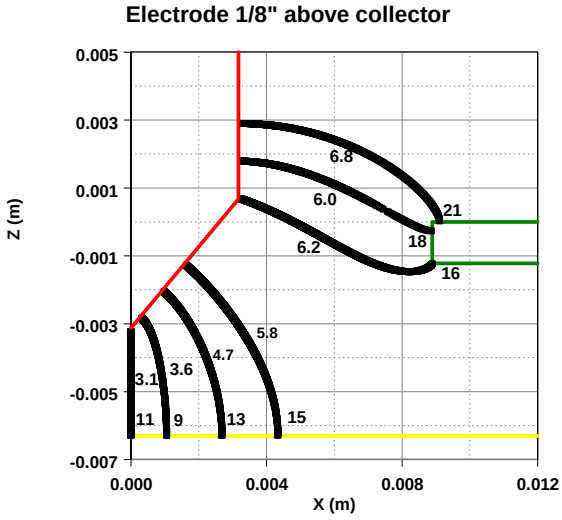

Figure 137. Pin 1/8" above coupon; 0.7" diameter hole.

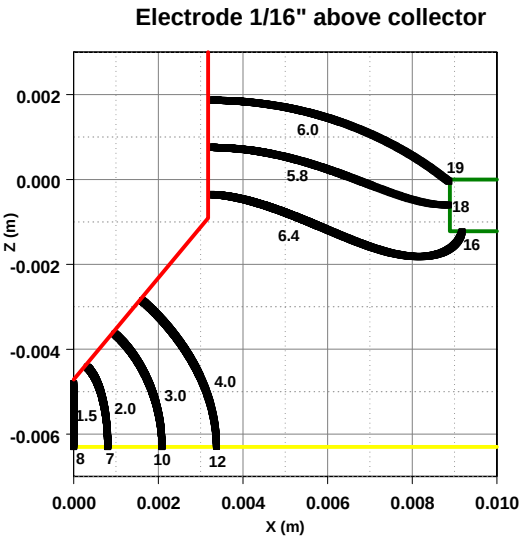

Figure 138. Pin 1/16" above coupon; 0.7" diameter hole.

and thus the total is

$$L_{tot} = L_{strip} + L_{lead} \approx 108 \text{ nH}$$

The measurement resistance can be taken as large as 1 Mohm (although shunt bypass capacitive reactances will need to be assessed for high values). Arc resistances are variable (and really consist of a transmission line or RLC ladder network). Proceeding from streamer phase to a hard arc these variable lumped arc resistances can drop from 100 Mohms to 1 ohm. The branch labeled with subscript c represents a path to the collector and the branch labeled with subscript cp represents a path to the coupon edge. As we push the cathode toward the hole we expect the voltage threshold for the discharge to develop will drop for the collector path until it becomes more favorable for the collector path to develop.

To capture a large portion of the voltage V_{oc} during the discharge process it is desirable to have $R_m > R_c$. However we also need the collector to charge which means that the voltage must be on long enough compared to the dime constant

$$\tau_c = \frac{R_c R_m}{R_c + R_m}(C_{tot} + C) \approx R_c C_{tot} < R_m C_{tot} \approx 28 - 83 \text{ ms}$$

This is a very long time compared to the pulser duration. Obviously if the discharge channel impedance R_c is comparable to the measurement impedance 1 Mohm, we will not see the discharge. Our hope is that as the channel resistance falls we achieve low enough values of discharge impedance that we can put this time constant in the discharge duration range. For the Velonex pulser the duration is a few microseconds $\tau_p \approx 3$ μs. This means that the channel impedance must fall to $36 - 107$ kohms. Thus this seems like a reasonable goal. If the channel resistance falls to more than an order of magnitude less in resistance of the measurement system we have a chance to charge up the collector setup and observe it.

Because the voltage on the Nanofast probe needs to be kept below 1 kV and the Velonex pulse puts out about 4 kV maximum, we may want to design R_m as a voltage divider circuit. It may be unwise to reduce the Velonex output below the approximate 4 kV level since we do want an arc to develop to the collector (and 4 kV will only breakdown a uniform field gap of just over 1 mm in length).

One question is about the observed indirect coupling that could be observed from the Velonex pulser (this is the coupling if we ignore R_c). Ignoring the inductance branch of the measurement circuit gives the range

$$V_m < \frac{C}{C + C_{tot}} V_{oc} \approx 0.8 - 2 \text{ V}$$

where we have used the value of C associated with the 0.25 inch cathode to coupon gap. Now if we reduce this gap we expect the capacitance C to increase. However, even a factor of ten increase results in reasonably small voltages, which should not lead to confusion with regard to the much larger direct coupling we are seeking.

During the lightning test there is a problem due to the charge time of the interior RC circuit. For a $R_m = 10$ kohm load and with an interior capacitance of $C_{tot} = 80$ pF the interior time constant is 0.8 μs. Also the interior resistance is high enough (10 kohm) that the conductive channel to the collector will take some time to establish and will have a relatively high impedance. If the establishment of the discharge path to chassis R_{cp} is very small due to a high level of overvoltage, then we may never see anything on the interior.

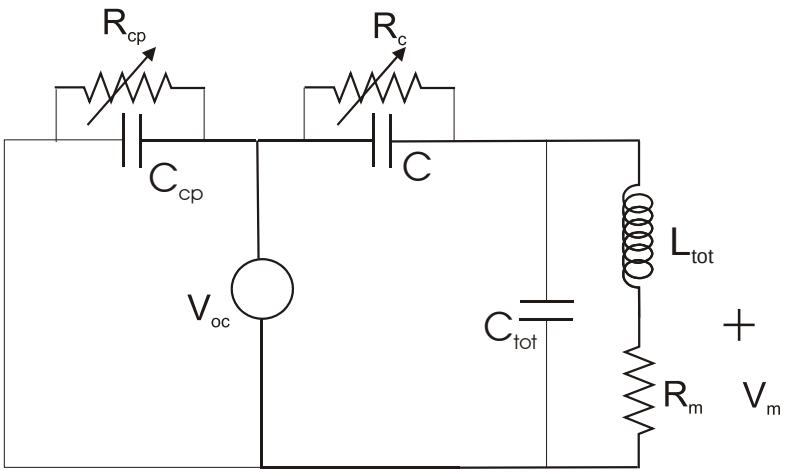

Figure 139. Circuit model of nonlinear breakdown process.

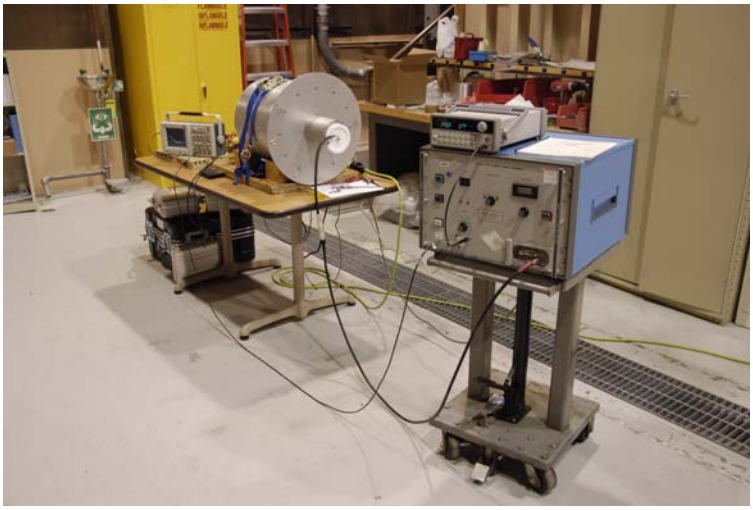

Figure 140. Velonex pulser in foreground with trigger unit on top. Measurement section in background.

5.8 Velonex Pulser Experiment

The Velonex pulser was used as a low level voltage source to gain insight on this measurement before going to the lightning simulator. The general setup is shown in Figure 140 with the Velonex pulser in the foreground and the measurement section in the background. Originally we used a 10 kohm to 1.3 ohm (CVR) resistive divider connected through attenuators to the Nanofast optical data link (ODL) (0.1 volts and 50 ohms) inside the small testing enclosure. Figure 141 shows the ODL in the foreground, the attenuator on the shelf inside the enclosure and the resistive divider at the end of the enclosure. The attenuator is electrically isolated from the enclosure by a rubber pad. Figure 142 shows a close-up of the resistive divider and Figure 143 shows the details of how the cable from the Velonex pulser is attached to the outside of the measurement section. Later we used a high voltage (40 kV), high impedance (100 Mohm), Tektronix probe, attached to a storage scope inside a larger screen box. With the Velonex pulser driving the setup at approximately 4 kV, we proved out both approaches as shown in Figure 144.

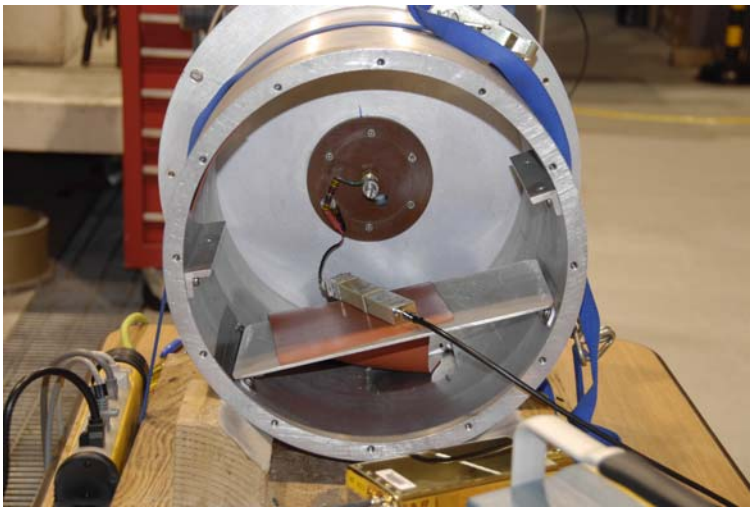

Figure 141. Inside view of the measurement section.

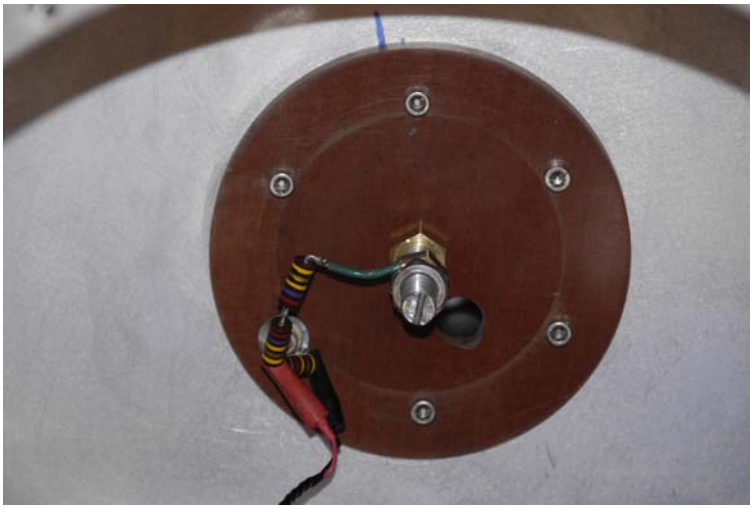

Figure 142. Detail of the CVR.

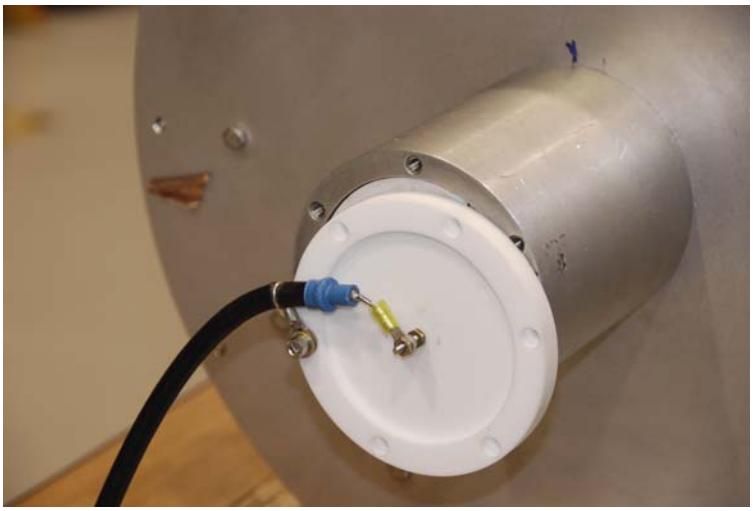

Figure 143. Outside of the measurement section showing details of the drive cable attachment from the Velonex pulser.

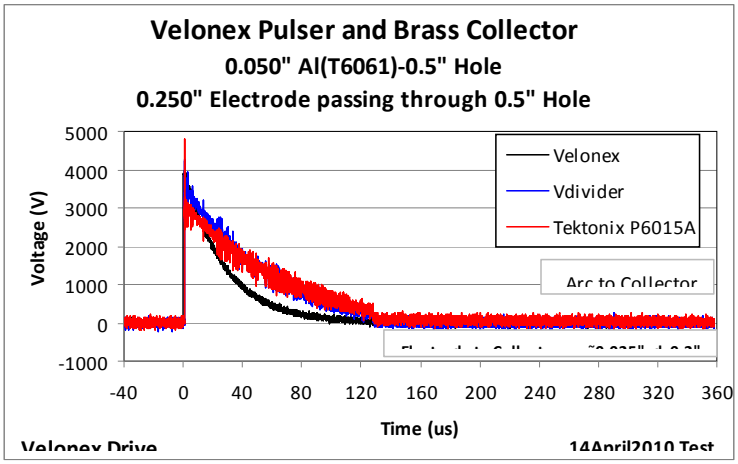

Figure 144. Voltage measurements from various sensors in the experiment.

It was also demonstrated that by varying the electrode-to-collector gap when the coupon had a 0.5 inch pre-drilled hole, we could obtain arcing at various levels along the Velonex pulser's rising voltage waveform. This is shown in Figures 145, 146, and 147 for gap spacings of $0.03, 0.025$ and 0.0 inches (touching) respectively.

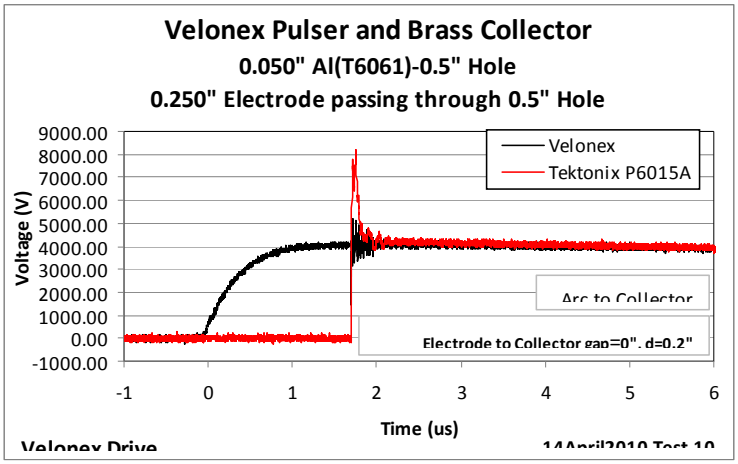

Figure 145. Breakdown to collector over a 0.03" gap.

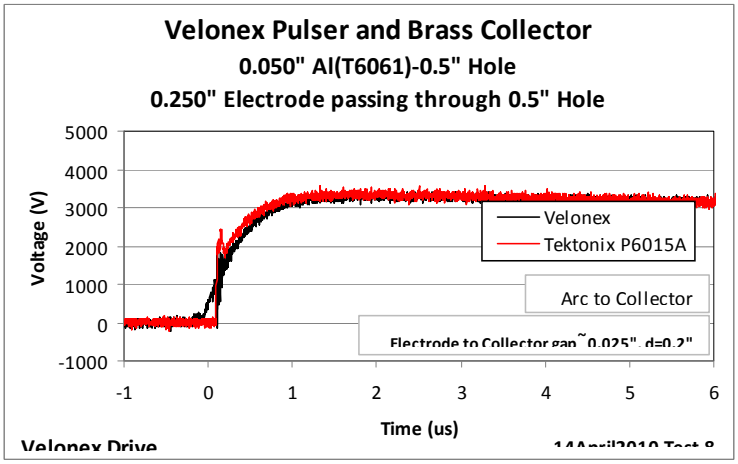

Figure 146. Breakdown to collector over a 0.01" gap.

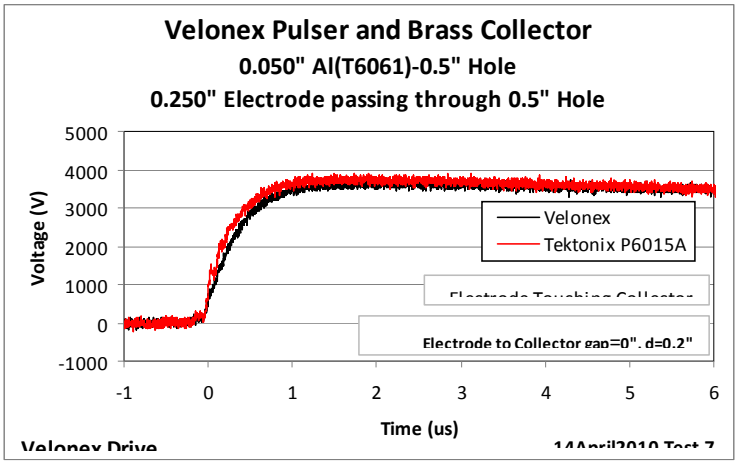

Figure 147. Breakdown to collector over a 0.01" gap.

5.9 Sandia Lightning Simulator Experiment

After gaining experience with the Velonex, which didn't have a large enough voltage to breakdown the gaps between the electrode and the coupon, the Sandia Lightning Simulator (SLS) was used. Figure 148 shows the electrode of the SLS and the pre-drilled 0.5 inch hole in the coupon. Figures 149 and 150 show close-ups of the electrode outside the hole and pushed into the hole respectively. In all measurement results shown, the high impedance, high voltage, Tektronix probe was used across a 10 kohm internal resistance to ground.

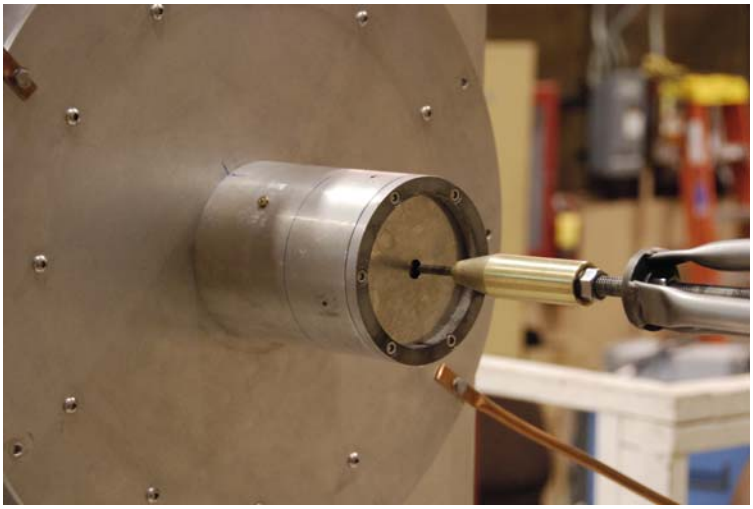

Figure 148. Electrode and coupon of the SLS experiment.

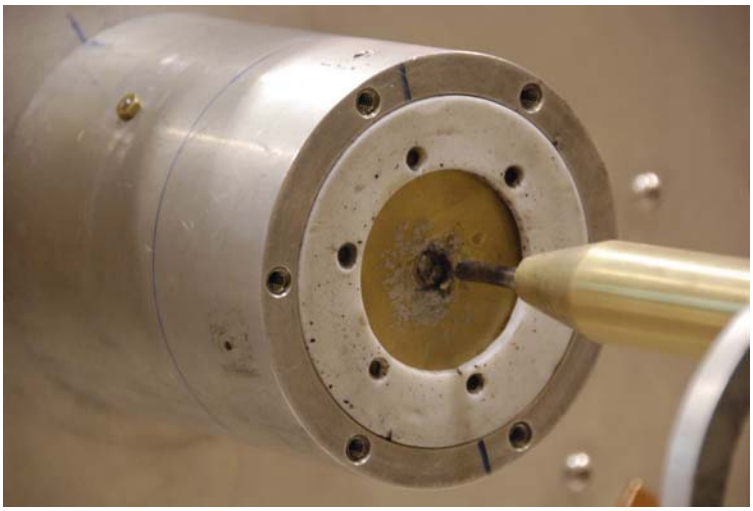

Figure 149. Closeup of electrode positioned outside the hole.

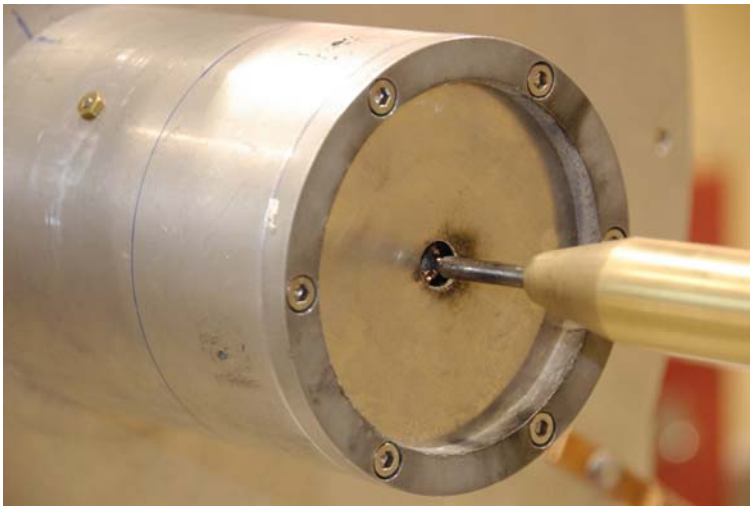

Figure 150. Closeup of electrode pushed into the hole.

When the electrode was pushed into the pre-drilled hole to distances between 3/16 and 1/8 inches from the collector we observed short (10 ns) high voltage (20 kV) pulses on the collector. This is shown in Figures 151 through 154. Which show results from gaps of 1/16 inches and 3/16 inches.

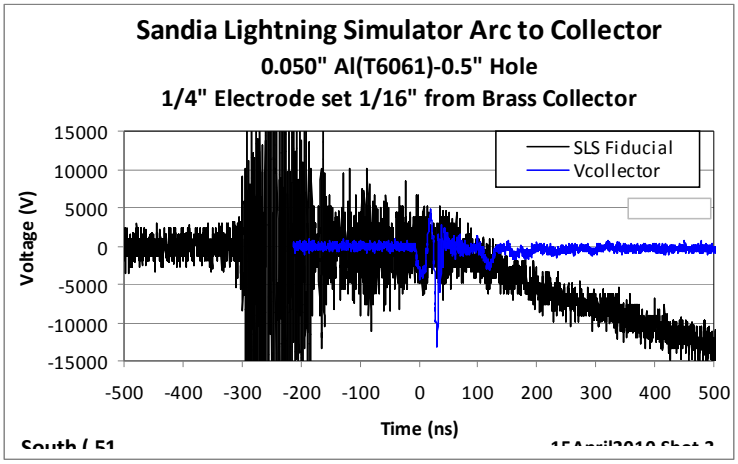

Figure 151. High voltage pulse (10 kV) on the collector from an electrode 1/16" away.

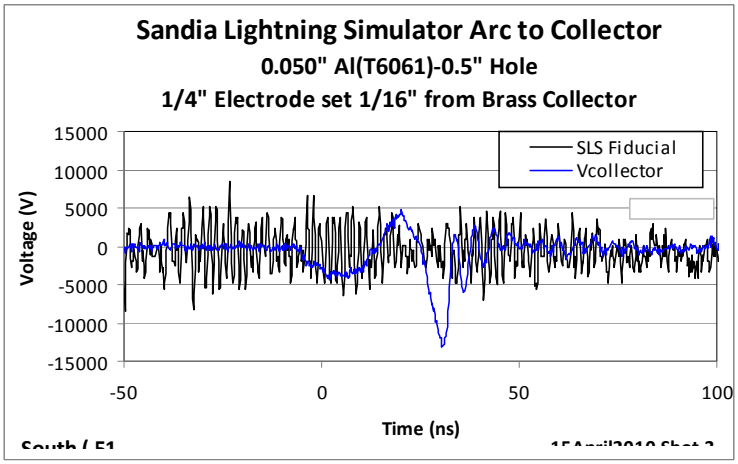

Figure 152. Detail of previous high voltage pulse.

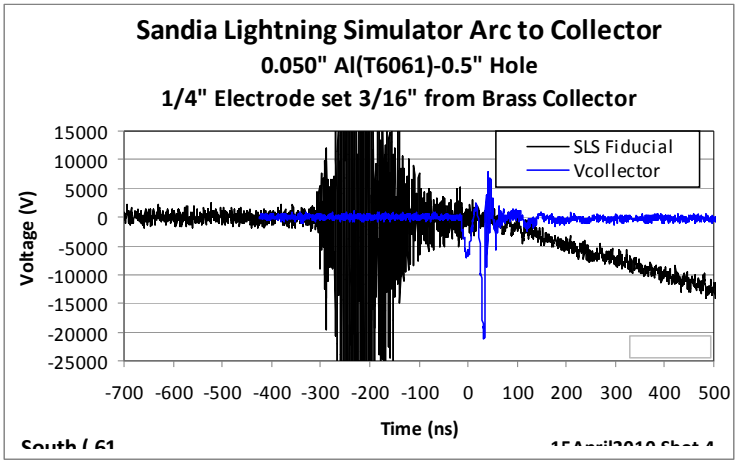

Figure 153. High voltage pulse (20 kV) on the collector from an electrode 3/16" away.

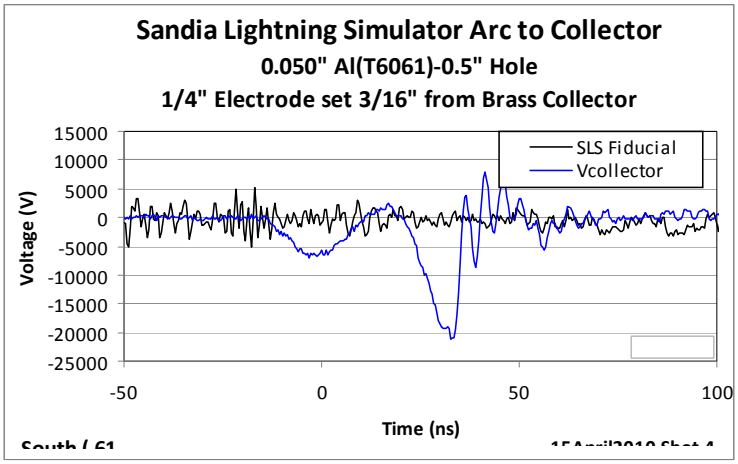

Figure 154. Detail of previous high voltage pulse.

5.9.1 Displacement Current Coupling

Because the responses observed in the lightning facility are so short in time before being quenched by a side flash to the coupon (and perhaps an internal flash to the coupon from the collector), it is important to ask if the responses could have been caused by displacement current coupling to the collector (indirect coupling).

These experiments used an existing collector with a 3/16 in erosion well at the electrode position (created during prior continuing current burnthrough tests). A simple estimate of this capacitance can be obtained by considering a spherical capacitor. The rod tip will be taken as a sphere of radius $r_i = 0.125$ in and the erosion well will be taken to have radius $r_o = 3/16$ in. The capacitance between these is found from

$$V = Q/C = \int_{r_i}^{r_o} E_r dr = \int_{r_i}^{r_o} \frac{Q}{4\pi\varepsilon_0 r^2} dr = \frac{Q}{4\pi\varepsilon_0}\left(\frac{1}{r_i} - \frac{1}{r_o}\right)$$

or

$$C = \frac{4\pi\varepsilon_0}{1/r_i - 1/r_o} \approx 1 \text{ pF}$$

We might have used a hemispherical calculation instead (0.5 pF), however the sphere should bound the extra capacitance of the rod side surface to the collector ground plane (limited by screening of the coupon).

This value forms a capacitive divider with the $C_c = 80$ pF collector to chassis capacitance. Now the 10 kohm resistor to chassis ground in parallel with the collector capacitance has a time constant $\tau = RC = (10 \text{ kohm})\,(80 \text{ pF}) = 800$ ns. This means that the capacitor is dominant for times on the order of 10s of nanoseconds. Hence the capacitive divider

$$V_c = V\frac{C}{C + C_c} \approx 0.0124V$$

would supply only small collector voltages. For example if we take the coupon side flash to be limited to $V_{cp} < 30$ kV/cm (1 cm) = 30 kV, we would observe less than 0.37 kV on the collector. It does not seem that indirect coupling can supply what we are observing in the experiment unless the electrode voltage

actually achieves much bigger levels $V = 20$ kV$/\,(0.0124) \approx 1600$ kV.

These results indicate that the SLS gaps are so overvolted that it is difficult to interpret the results. Basically, all gaps both to the coupon and to the collector break down and we can't determine which gap went first and at what level. We had to get this information from a lower voltage pulser that we could control the voltage level better. This is why we went to the PTX pulser which we will discuss in the next section. Prior to using the PTX pulser we attempted to get the breakdown information from a series of DC tests. Space charge distortion of the field prior to breakdown caused breakdown voltages that were approximately half of those predicted.

A second result doing this series of SLS tests was that we realized that the field arrived at the electrode prior to the current. This caused us to look earlier in time for results from indirect electrical coupling and lead to finding results that were missed when triggering off the current.

5.10 PTX Pulser Experiment

This subsection shows data from electrical breakdown experiments using a pulser with a rise time of about 100 ns and a maximum voltage under 50 kV. Again, we use a collector rather than a stripline to do the measurement. The plots show the pulser voltage waveform (black curve), the timing and behavior of the electric field (red curve), and the interior collector voltage as measured by a high impedance (100 Mohm) Tektronix probe (blue curve). The electric field probe is not calibrated since it was placed at the base of the aluminum housing rather than at the hole surface and is shown only to give timing information not actual E field levels. We actually scaled and shifted the red curve down in level to prevent it from obscuring the other curves. Note also that the time constant of the collector-probe load in this case is very large $\tau_{load} \approx 8.4$ ms; charge deposited on the collector thus takes a long time to dissipate to the surrounding Faraday cage if there were no other connection from collector to Faraday cage other than the Tektronix probe. One can use the initial collapse of the electric field probe (red curve) as an indicator of when a breakdown has occurred to the metallic barrier and the highest level reached by the voltage measurement (black curve) to determine the breakdown voltage.

For the case where the tip of the electrode is a distance of 3/16 in from the outside of the metallic barrier, shown in Figures 155 and 156, we suspect that the small voltage seen on the collector could be capacitive in nature. The transfer capacitance for this electrode height (from calculations using the hemispherical electrode model)

$$C_T \approx \varepsilon_0 \frac{2}{\Omega_e h h'} \alpha_e^{eff} \approx 0.022 \text{ pF}$$

$$\Omega_e = 2 \ln (2h'/b) - 4b/h'$$

$$h' = d + b$$

Voltage division using $V_r = 20$ kV then gives

$$V_c \approx \frac{C_T}{C_c + C_{lead}} V_r \approx 5.3 \text{ V}$$

We see about twice this level in Figure 155. The capacitance C_c is reduced somewhat by a cutout in the aluminum housing (to allow photography of the interior discharge), which would raise the calculated indirect level somewhat. The rapid fall in signal (in agreement with the exterior electric field (red curve)) also indicates that this might be indirect coupling. This result is in qualitative agreement with the threshold

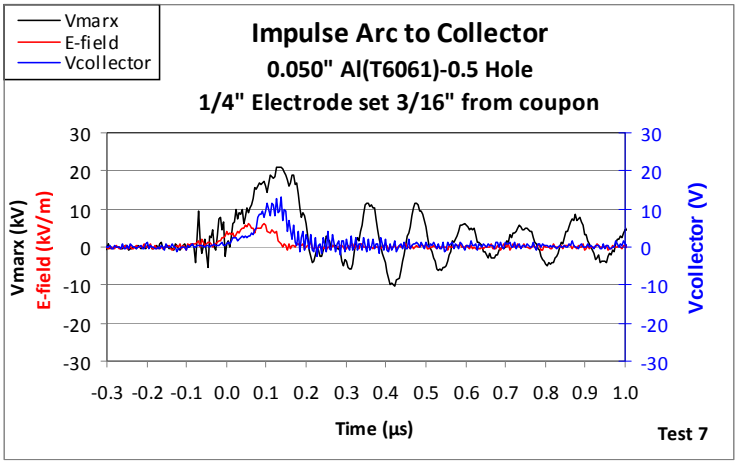

Figure 155. Voltage for the case where the electrode is exterior to the coupon barrier.

calculation results of Figure 155, where breakdown to the hole edge occurs at voltages $(17-21$ kV) lower than to the interior collector $(33-46$ kV) indicating that breakdown to the collector is unlikely. The measured breakdown voltage in Figure 155 (highest Marx voltage) is 20 kV.

Figures 157 and 158 show the case where the tip of the electrode is centered in the hole and midway through the thickness dimension of the metallic barrier. The measured results in Figure 157 indicate that we are transferring charge to the collector as evidenced by the large collector voltage (3.8 kV). In addition, the long discharge time indicates that the collector becomes isolated from the metallic barrier after the initial spark. The threshold calculations of Figure 157 indicate slightly smaller breakdown levels to the collector $(11-13$ kV) than to the metallic barrier $(15-17$ kV), which is less than the experimental levels: 20 kV to the collector (the Marx voltage when the collector voltage starts to rise) and greater than 20 kV to the metallic barrier (the highest Marx voltage).

Next the case where the electrode is slightly inside the barrier ($h = 0.2$ inches from collector to coupon surface) but still spaced 3/16 inches away from the collector is shown in Figures 159 and 160. The interior voltage is nearly the same as the preceding case. The threshold values are also similar in this case because of the peculiar geometry involving the 1/4 inch electrode and the 1/2 inch hole.

Finally, Figures 161 and 162 show the case where the electrode tip is inside the barrier and 1/16 in from the collector surface. Notice the higher level of voltage on the collector (8.3 kV). However also notice the rapid fall time of the interior voltage, indicating that we are likely observing a plasma connection to either the electrode or to the metallic barrier. An alternative explanation for these results involving indirect coupling with an increased transfer capacitance to the collector is unlikely since the collector-to-barrier capacitance will still be much larger than this transfer capacitance (and hence we would expect a much smaller collector voltage than electrode voltage). In this case the threshold calculations of Figure 161 indicate a larger breakdown voltage to the coupon hole edge $(11-17$ kV) than to the collector $(8-11$ kV). The experimental levels of $9-10$ kV to the collector (the Marx voltage where the collector voltage starts to rise) and $15-20$ kV breakdown to the metallic barrier hole edge (the highest Marx voltage) are in reasonable agreement with the calculations.

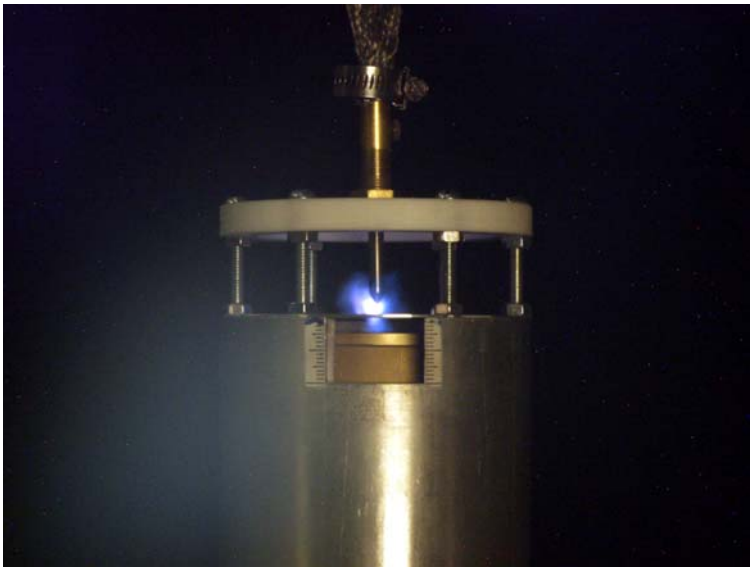

Figure 156. Picture of spark discharge in the case where the electrode is exterior to the coupon barrier.

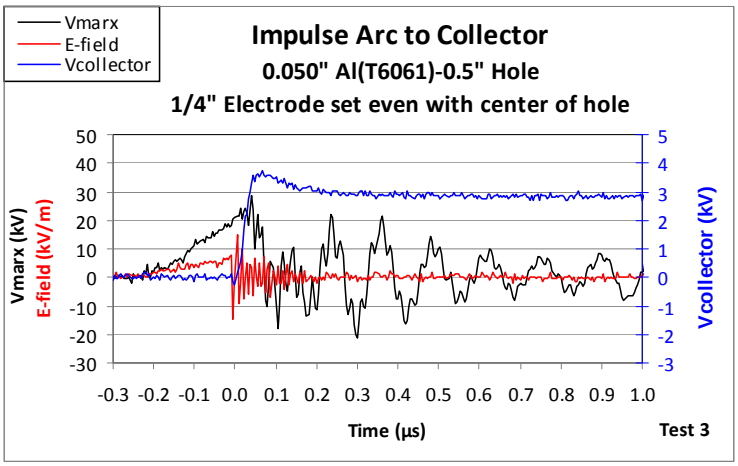

Figure 157. Voltage in the case where the electrode is even with the center of the coupon barrier.

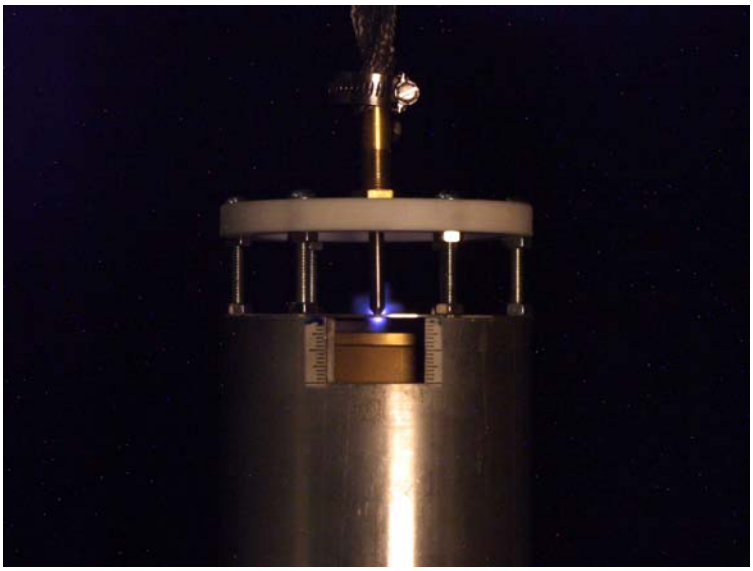

Figure 158. Picture of spark discharge in the case where the electrode is centered with respect to the coupon barrier.

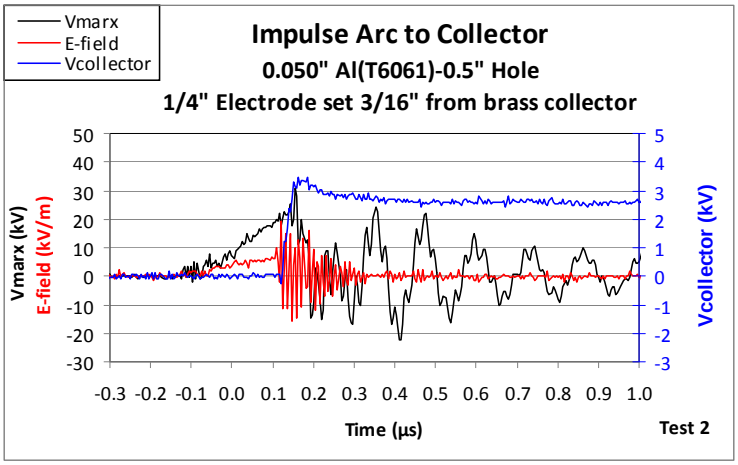

Figure 159. Voltage for the case where the electrode is interior to the barrier but nearer to the coupon than to the collector.

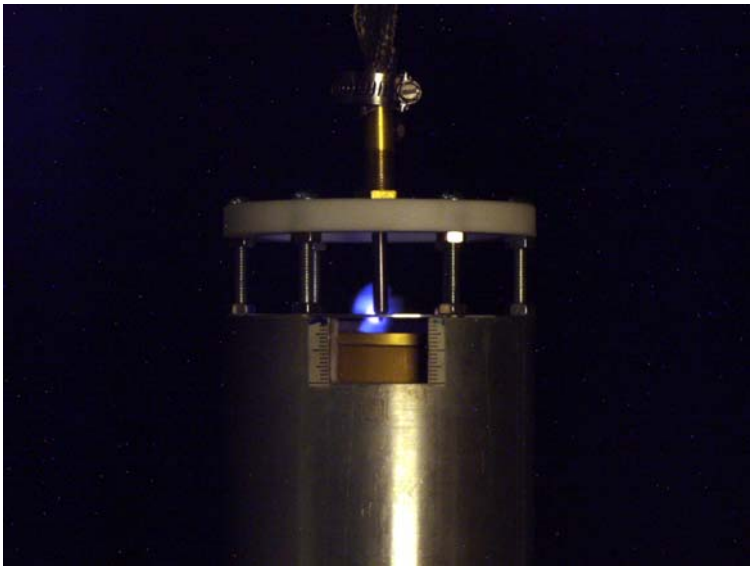

Figure 160. Picture of the case where the electrode is interior to the barrier.

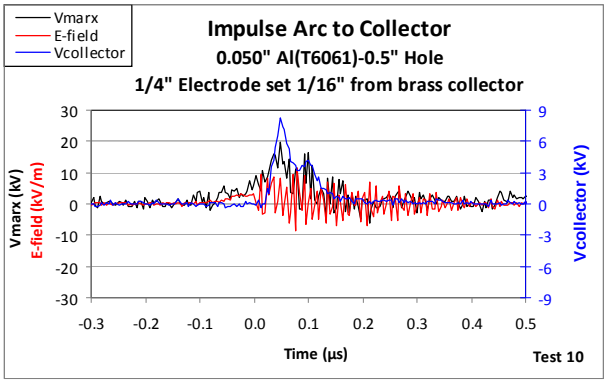

Figure 161. Voltage for case where electrode is near the collector.

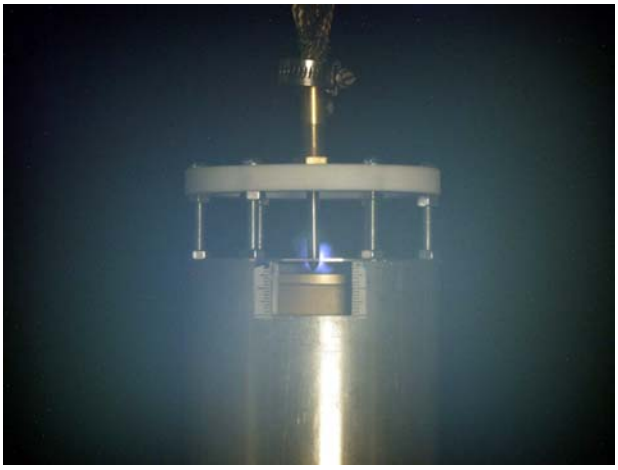

Figure 162. Picture for case where electrode is near the collector surface.

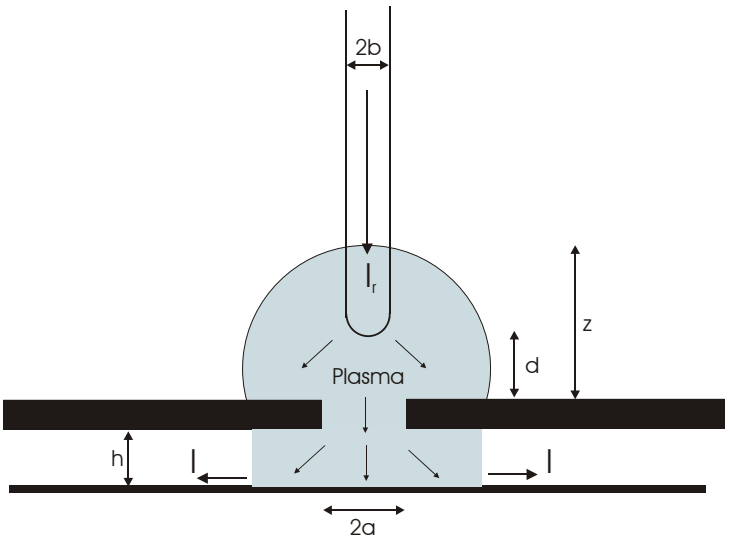

Figure 163. Illustration of plasma conduction to the enclosure and to an interior collector.

6 DIRECT PLASMA CONDUCTION MECHANISM

This section examines some of the properties of the ionized gas or plasma and considers direct conduction to the interior collector.

6.1 Baseline Resistive Coupling and Short Circuit Current

It is instructive first to ask what the previous indirect coupling models can tell us about conduction to the interior collector by means of a uniform plasma in the gas as illustrated in Figure 163. This is done by using the correspondence between the capacitance and conductance to determine the amount of current coupled to the interior versus that injected into the rod electrode. First we return to the capacitive problem to find the exterior rod-to-plane capacitance and then transition to the conductance.

The cumulative charge along the rod is the integral of the surface charge density σ_s over a surface $S(z)$ on the rod to distance z. Using the point charge and semi-infinite line charge model from the indirect coupling section we write this as

$$Q_r(z) = \int_{S(z)} \sigma_s dS \approx Q_r \left[2\pi b^2 + 2\pi \int_0^{\theta_0 = \arctan\left((z-h')/b\right)} b^2 \sin\theta d\theta \right] / \left(4\pi b^2\right) + \int_{h'}^{z} q_r(z)\, dz$$

where the normalized point charge value is ($\Omega = 2\ln(2h'/b)$ and $h' = d + b$)

$$\left(\frac{2h'/b - 1}{2h'/b - 2}\right)\left[1 - \frac{\ln(2h'/b - 1)}{\Omega + 2\ln(R) - 2}\right] \sim \frac{Q_r}{4\pi\varepsilon_0 V_r b}$$

The first integral on the right hand side accounts for the proportion of the point charge electric flux included on the cylindrical and hemispherical surfaces out to distance z from the ground plane. From the indirect coupling results we can write

$$-2\pi\varepsilon_0 b\frac{\partial\phi^{sc}}{\partial\rho}(b,z)\sim$$

$$\frac{q_r}{2}\left[-\frac{b^2/\sqrt{b^2+(h'+z)^2}}{(h'+z)+\sqrt{b^2+(h'+z)^2}}+\frac{b^2/\sqrt{b^2+(h'-z)^2}}{(h'-z)+\sqrt{b^2+(h'-z)^2}}\right]$$

$$+\frac{Q_r}{2}\left[\frac{b^2}{\left\{b^2+(h'-z)^2\right\}^{3/2}}-\frac{b^2}{\left\{b^2+(h'+z)^2\right\}^{3/2}}\right]$$

Using the identity

$$\int\frac{b^2}{\sqrt{b^2+u^2}+u}\frac{du}{\sqrt{b^2+u^2}}=\int\left(1-\frac{u}{\sqrt{b^2+u^2}}\right)du=u-\sqrt{b^2+u^2}$$

and only the charge in the physical space (not the image charge), we extend the integration to $-\infty$ to capture the flux on the hemispherical endcap

$$\frac{q_r}{2}\int_{-\infty}^{z}\frac{b^2/\sqrt{b^2+(h'-z)^2}}{(h'-z)+\sqrt{b^2+(h'-z)^2}}dz=\frac{q_r}{2}\int_{h'-z}^{\infty}\frac{b^2/\sqrt{b^2+u^2}}{u+\sqrt{b^2+u^2}}du$$

$$=\frac{q_r}{2}\left[-(h'-z)+\sqrt{b^2+(h'-z)^2}\right]=\frac{q_r}{2}\left[(z-h')+\sqrt{b^2+(z-h')^2}\right]$$

Thus for $z>h'$ we can write ($R=10$)

$$\frac{Q_r(z)}{4\pi\varepsilon_0 bV_r}\approx\frac{Q_r}{4\pi\varepsilon_0 V_r b}\left[1-\frac{1/2}{\sqrt{1+(z-h')^2/b^2}}\right]+\frac{\left\{(z-h')+\sqrt{b^2+(z-h')^2}\right\}/(2b)}{\Omega+2\ln(R)-2}$$

A comparison between this approximate expression and the numerical values of the rod charge are shown in Figure 164. The formula gives reasonably accurate answers for the accumulated charge along the cylinder. The numerical values are slightly larger than the analytical formula because the rod is truncated at 10 cm in the numerical simulation, and hence the charge is increased at the other end (the numerical values for larger values of z actually drop below the dashed curve if we extend the rod to $R_1=20$ cm). The reason why this capacitance (in the case of the extended rod beyond distance z) is of interest is because we intend to use it here to estimate the conductance of the rod-to-plane when a conductive plasma exists over a hemispherical region above the plane. Let us define the capacitance to a distance z by $C_r(z)V_r=Q_r(z)$. From the preceding indirect coupling calculations

$$C_T\approx\left[E_z^0(0,0)/V_0\right]\alpha_e^{eff}\varepsilon_0\left[-E_{z(eff)}^{sc}/V_r\right]\approx-\frac{1}{h}\alpha_e^{eff}\varepsilon_0 E_{z(eff)}^{sc}/V_r\approx 0.01175\text{ pF}$$

where the final value uses $2a\approx 0.5$ in, $t\approx 0.05$ in, $h\approx 0.2$ in, $d\approx 0.25$ in, and $2b\approx 0.25$ in.

Now if a plasma exists in the space about the rod electrode out to a hemispherical distance z, with conductivity σ we want to compute an estimate for the current splitting between the outer barrier and the interior collector. This uniform conductivity case is a first cut to model the highly overvolted very early time breakdown associated with the arrival of the return stroke. We can use the connection of the current

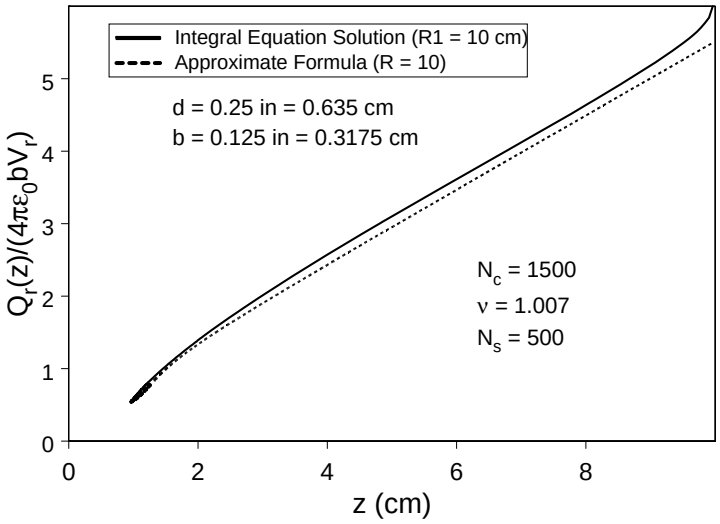

Figure 164. Comparison of cumulative charge along rod with hemispherical tip from point charge - line charge model versus numerical calculation.

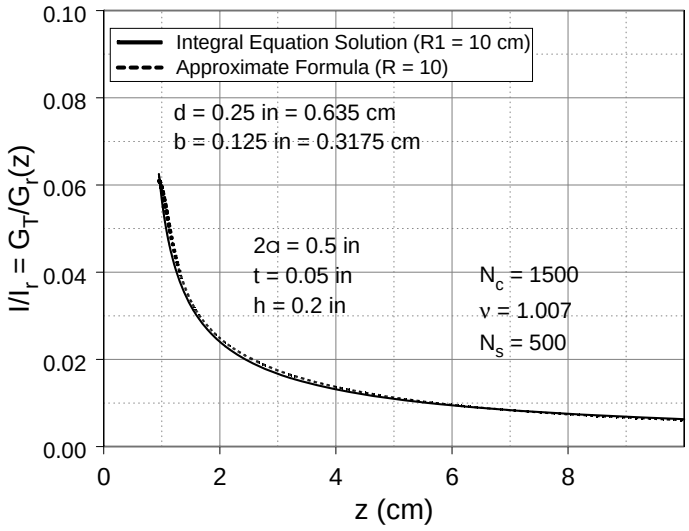

Figure 165. Conductive splitting of interior current versus drive current.

to conductance versus charge to capacitance and write

$$-i\omega\varepsilon_0 \to \sigma$$

$$-i\omega C \to G$$

$$-i\omega Q \to I$$

and thus

$$I_r = V_r G_r(z)$$

$$I = G_T V_r$$

or

$$I/I_r = G_T/G_r(z) = C_T/C_r(z)$$

which is shown in Figure 165.

In the experiment the second return stroke was taken to have a peak value of $I_r \approx 100$ kA and interior short circuit (0.005 ohm current viewing resistor) coupled currents of up to $I \approx 1$ kA were observed. This implies a ratio $I/I_r \approx 0.01$ which falls at a plasma radius of $z = 5$ cm. This is a relatively large ionization radius (Figure 166 shows the flash from the second return stroke in the burnthrough experiment) and variations in conductivity σ with radius would tend to reduce the required plasma radius for the same level of current splitting (this diversion might also be enhanced by virtue of the inductive voltage drop along the

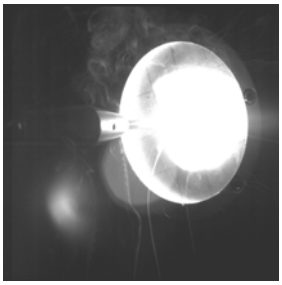

Figure 166. Flash from return second return stroke at electrode.

interior cabling perhaps driving current from the collector across the interior gap h back to the enclosure wall).

Note also that the coupled continuing current with a peak drive of $I_r \approx 500$ A was a major fraction (several hundred amperes in Schnetzer's original test as well as the recent measurement with the TTI ODL) and thus is quite different from the preceding uniform conductivity prediction. However, given the photographic evidence of a narrow plasma jet with enhanced conductivity connected directly to the interior collector as shown in Figure 167, as well as models in the literature for similar current jets in welding arcs, this is not surprising.

6.2 Impedance of Continuing Current Channels and Open Circuit Voltage

This subsection considers the impedance of observed continuing current channels between the collector and enclosure coupon in the case where the collector is attached to a high impedance measurement system. First it is instructive to consider the transmission line characteristic impedance of the lightning facility drive system to have an initial feel for what constitutes low or high impedances.

6.2.1 Biconical Transmission Line Results for SLS

The Sandia Lightning Facility (SLS) supplies an electromagnetic wave along a transmission system to the drive electrode. To get a feel for the early time impedance of the system we can apply a slender biconical transmission line model. A biconical region with fields (where R is the reflection coefficient at $r = 0$)

$$E_\theta r \sin\theta = \eta_0 H_0 \left(e^{ikr} + e^{-ikr} R\right)$$

$$H_\varphi r \sin\theta = H_0 \left(e^{ikr} - e^{-ikr} R\right)$$

$$\eta_0 = \sqrt{\mu_0/\varepsilon_0} \approx 120\pi \text{ ohms}$$

has current

$$I_0(r) = 2\pi H_\varphi r \sin\theta = 2\pi H_0 \left(e^{ikr} - e^{-ikr} R\right)$$

and voltage

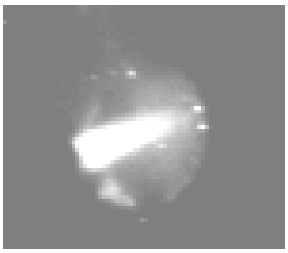

Figure 167. Plasma jet to interior collector during continuing current part of experiment with interior collector attached to the enclosure through a 0.005 ohm load (current measurement).

$$V_0(r) = \int_{\theta_0}^{\pi/2} rE_\theta d\theta = \eta_0 H_0 \left(e^{ikr} + e^{-ikr}R\right) \ln\left[\cot\left(\theta_0/2\right)\right]$$

The characteristic impedance of the biconical line is thus

$$Z_0 = \frac{\eta_0}{2\pi} \ln\left[\cot\left(\theta_0/2\right)\right]$$

Along the line with electrode radius b and distance z from the load we write $\theta_0 = \arctan\left(b/z\right) \sim b/z$, and for this slender limit

$$Z_0 \sim \frac{\eta_0}{2\pi} \ln\left(2z/b\right) \approx \ln\left(2z/b\right)\ 60 \text{ ohms}$$

The average over and electrode extending from $z = 0$ to $z = R_1$ is

$$\langle Z_0 \rangle \approx \frac{1}{R_1} \int_0^{R_1} \ln\left(2z/b\right) dz\ 60 \text{ ohms} \approx \left[\ln\left(2R_1/b\right) - 1\right]\ 60 \text{ ohms}$$

Now near the test object $b \approx 0.125$ in and further away this electrode size becomes larger. We see that for sizes comparable to the test object $R_1 = O\left(6 \text{ in}\right)$ and for propagation times $O\left(1 \text{ ns}\right)$ this characteristic impedance is in the range $\langle Z_0 \rangle = O\left(200 \text{ ohms}\right)$. Thus for load impedances Z_L much smaller than this range, the total early time voltage appearing at the load is much smaller than the forward traveling wave V_i

$$V_r = \left(1 + \frac{Z_L - \langle Z_0 \rangle}{Z_L + \langle Z_0 \rangle}\right) V_i \approx \left(2Z_L / \langle Z_0 \rangle\right) V_i << V_i,\ Z_L << \langle Z_0 \rangle$$

versus the case when the load impedance is much larger than $\langle Z_0 \rangle$

$$V_r \approx 2V_i,\ Z_L >> \langle Z_0 \rangle$$

In the first case the drive current will be

$$I_r \approx 2V_i / \langle Z_0 \rangle,\ Z_L << \langle Z_0 \rangle$$

These two cases are illustrated in Figure 168.

6.2.2 Welding literature

The welding literature can be used to estimate the dimension and temperature of continuing current discharges. Figure 169 from [11] shows a simulation of a free-burning arc in air with a current of 400 A. The diameter of the (10,000 K) contour at the axial midpoint is approximately 0.6 cm with area $A \approx 0.28$ cm^2.

6.2.3 Electrical Conductivity

The electrical conductivity of the plasma can be related to the temperature and density. Here we look at and compare three models for these values: two simple ones using the Born approximation and the WKB methods for estimating the Coulomb logarithm, and a more elaborate LMD model.

According to [31] the degree of ionization (ratio of electron number to atomic number can be estimated as

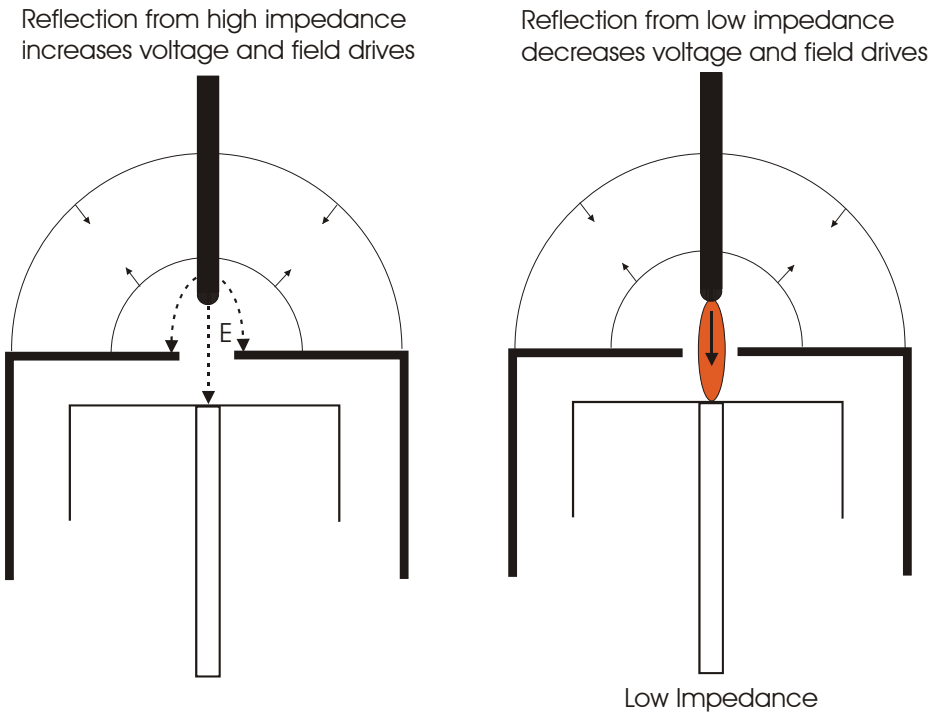

Figure 168. Reflection of an incident voltage wave from a rod-to-plane gap under open and near shorted conditions.

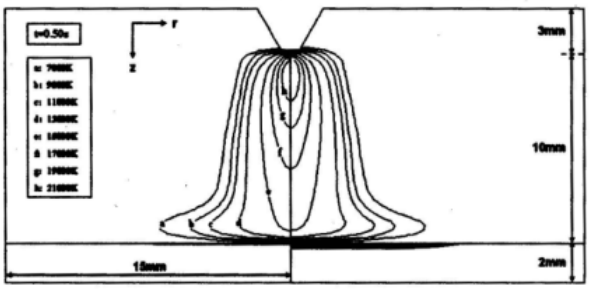

Figure 16. Plasma temperatures in the anode for an air-composite configuration at 400 A with (on the left) and without (on the right) consideration of the Joule effect in the material.

Figure 169. Simulation of a steady arc in air with a 400 A current taken from [11].

$$\alpha_e = n_e/n$$

$$\frac{\alpha^2}{1-\alpha} = 2\frac{u_1}{u_0}\frac{1}{n}\left(\frac{m_e k_B T}{2\pi\hbar^2}\right)^{3/2} e^{-I/(k_B T)}$$

where $m_e = 9.10953 \times 10^{-31}$ kg is the electron mass, $\hbar = 1.054589 \times 10^{-34}$ J-s is Planck's constant and $\varepsilon_0 = 8.854188 \times 10^{-12}$ F/m is the free space permittivity. Suppose we examine a temperature of $T = 11604.5$ K and use the ideal gas law to find the atomic density as $n \approx \left(2 \times 2.687 \times 10^{25}/\mathrm{m}^3\right)/40$. Now for an ionization energy $I \approx 15$ eV, a temperature $k_B T = 1$ eV, where electronic charge is $e = 1.602189 \times 10^{-19}$ C and Boltzmann's constant is $k_B = 1.38066 \times 10^{-23}$ J/C, and approximating $u_1/u_0 \to 1$, we find

$$\frac{\alpha_e^2}{1-\alpha_e} \approx 0.00137$$

or

$$\alpha_e \approx 0.037$$

At this level of ionization (3.7%) we use Spitzer's theory to infer the conductivity of the plasma. We set $n_e = Z n_i$ where $Z \approx 1$. The conductivity is then

$$\sigma = \frac{2\left(2k_B T\right)^{3/2}}{\pi^{3/2} Z e^2 m_e^{1/2} \ln\Lambda}\left(4\pi\varepsilon_0\right)^2$$

We first look at a model using the Born approximation [39]. The Debeye length is [39]

$$\lambda_D = \sqrt{\frac{\varepsilon_0 k_B T}{n_i e^2 Z\left(1+Z\right)}} \approx 23.6 \text{ nm} \tag{14}$$

The ion sphere radius is [39]

$$a = 1/\left(\frac{4}{3}\pi n_i\right)^{1/3} \approx 16.9 \text{ nm} \tag{15}$$

$$\lambda = \max\left(a, \lambda_D\right) \approx 23.6 \text{ nm} \tag{16}$$

The Coulomb logarithm is [39]

$$\ln\Lambda = \left(\ln\chi_1 - \frac{1}{2}\right) \approx 5.6 \tag{17}$$

where

$$\chi_1 = 2k_1\lambda = \frac{2m_e v_{e1}\lambda}{\hbar} \approx 452 \tag{18}$$

$$v_{e1} = \sqrt{7k_B T/m_e} \approx 1.11 \times 10^6 \text{ m/s} \tag{19}$$

The conductivity with the Born approximation is thus

Temperature (10^3 K)	Density (versus atmospheric)	Conductivity (10^3 S/m)
5	0.025	0.05
10	0.025	3.1
15	0.025	9.1
20	0.025	12
30	0.025	17
40	0.025	22
5	1	0.01
10	1	1.5
15	1	7.5

Table 35. LMD model air conductivities

$$\sigma \approx 5.9 \times 10^3 \text{ S/m}$$

Next we use the WKB method [40] to estimate the Coulomb logarithm as [41]

$$\ln \Lambda = \ln \chi_1 - \frac{1 - \cos(x) + x \sin(x)}{x^2} - \text{Cin}(x) + 1$$

$$= \ln \chi_1 - 1.64 \approx 4.5$$

where

$$\text{Cin}(x) = \int_0^x (1 - \cos u) \frac{du}{u}$$

$$x = \frac{m_e Z e^2}{\pi \varepsilon_0 k_1 \hbar^2} \approx 7.9$$

$$\text{Cin}(2.5\pi) \approx 2.5$$

The conductivity with the WKB method is then

$$\sigma \approx 7.3 \times 10^3 \text{ S/m}$$

Finally the LMD model is used [46], [38]. The conductivity for the same parameters as above is found to be $\sigma \approx 5.2 \times 10^3$ S/m. Table 35 shows values for the ranges of interest in the continuing current and return stroke discharges.

6.2.4 Column Impedance

During the course of burnthrough experiments we have observed plasma jet discharges to the interior collector during the continuing current phase of the drive. When the collector is grounded to the enclosure (for current measurements this is through a low impedance 0.005 ohm current viewing resistor) we have observed a single discharge to the collector as shown in Figure 167, but when the collector is floating with respect to chassis (for voltage measurements this connecting to chassis is through a many megaohm load) we have observed return discharges to the enclosure as shown in Figure 170. Figure 171 shows some possible current topologies under high impedance conditions. In the left figure multiple return arcs exist

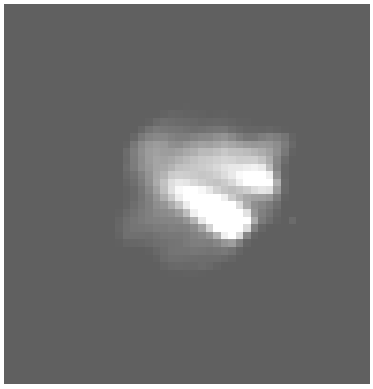

Figure 170. High speed photograph of continuing current and second return arc from collector to enclosure at hole edge under high impedance load conditions (voltage measurement).

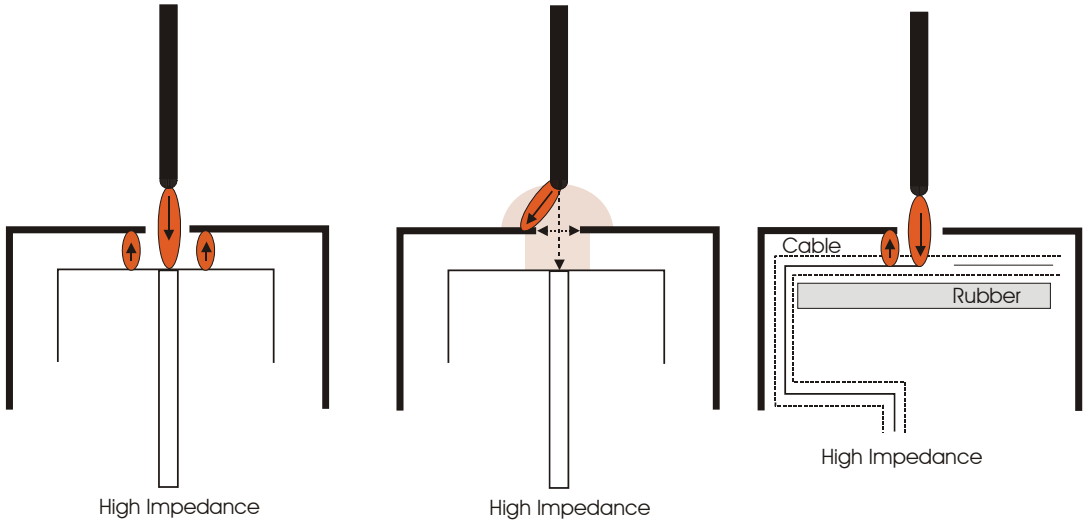

Figure 171. Topology of continuing current return to chassis in experiments with a high impedance load (voltage measurement).

from collector to enclosure, in the center figure the discharge has been diverted directly to the enclosure with some current flowing onto the collector, and on the right figure (with a cable collector) we have shown one return arc to the enclosure. Note that this topology describes one-to-one the coupling to a cable behind the hole as illustrated in Figure 172.

Now in the right of Figure 171, using information from the preceding two sections we estimate the return arc resistance as (we take $h \approx 0.2$ in ≈ 0.51 cm, $r_0 \approx 0.3$ cm, $A \approx 0.3$ cm^2 and $\sigma \approx 50$ S/cm)

$$R \approx \frac{h}{A\sigma} \approx 34 \text{ mohms}$$

The inductance of the column would be [42]

$$L \approx \frac{\mu_0 h}{2\pi} \left[\ln\left(2h/r_0\right) - 3/4\right] \approx 0.5 \text{ nH}$$

At very early times, when the incident voltage wave in the experiment impacts the rod tip, the low impedance load of the continuing current arc will result in a drive current

$$I_r \approx 2V_i / \langle Z_0 \rangle \approx 8 \text{ kA}$$

and thus an interior resistive voltage

$$V \approx 280 \text{ V}$$

The rise time of the current is expected to be of $O\left(10 \text{ ns}\right)$ and thus the inductive voltage $O\left(400 \text{ V}\right)$ is of the same order as the resistive component. These voltage levels are in the observed range during these experiments.

As the current rises we expect a channel expansion and heating to take place as depicted in Figure 173. If we use the Braginskii expansion model for the channel we can write

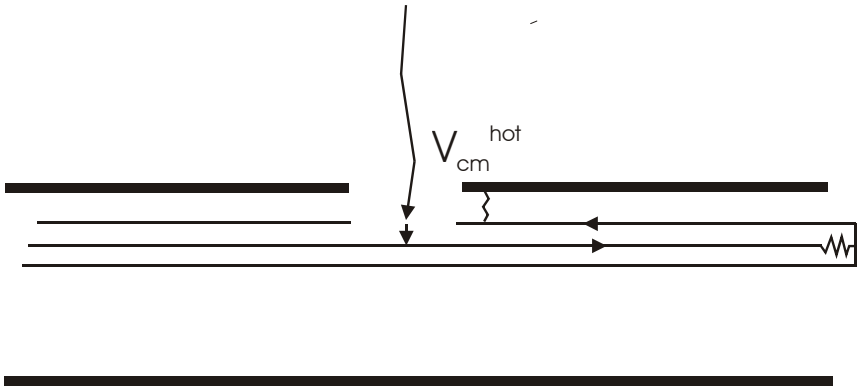

Figure 172. A cable coupling situation with discharge to interior conductor with return to chassis by means of second arc.

$$\frac{\xi}{K_p} p \frac{dA}{dt} = \xi \rho_0 \frac{1}{4\pi A} \left(\frac{dA}{dt} \right)^3 = \frac{I_r^2}{A\sigma}$$

$$p = K_p \rho_0 \frac{1}{4\pi A} \left(\frac{dA}{dt} \right)^2$$

and integration yields

$$A(t) = \pi a^2(t) = \left(\frac{4\pi}{\rho_0 \xi \sigma} \right)^{1/3} \int_0^t I_r^{2/3}(\tau)\, d\tau + A_0$$

where the undisturbed gas density is found from

$$p = n_m k T$$

$$n_m = \rho / m_m$$

If we take $T = 273.15$ K, $p = 101,325$ Pa, $k = 1.38066 \times 10^{-23}$ J/K, $n_m = 2.687 \times 10^{25}$ m^{-3} and average molecular mass

$$m_m = 2 \times (0.2 \times 16 + 0.8 \times 14) \times 1.674 \times 10^{-27} \text{ kg}$$

$$\rho_0 \approx 1.295 \times 10^{-3} \text{ g/cm}^3 = 1.295 \text{ kg/m}^3$$

the arc channel conductivity is taken as the fixed value (in the $2 - 4$ eV temperature range [30], [43]),

$$\sigma \approx 200 \text{ S/cm} = 2 \times 10^4 \text{ S/m}$$

and a constant dependent on gas properties, and somewhat on current rise rate, is taken as

$$\xi \approx 4.5$$

The resistance of the arc channel is then

$$R = \frac{h}{A\sigma} \tag{20}$$

The initial area constant A_0 is chosen as the continuing current area $A_0 \approx 0.3$ cm^2. If the return stroke current is taken as a ramp

$$I_r(t) = (t/\tau_r) I_r$$

we have

$$A(t) = \tau_r \left(\frac{4\pi I_r^2}{\rho_0 \xi \sigma} \right)^{1/3} \frac{3}{5} (t/\tau_r)^{5/3} + A_0$$

If we take $\tau_r = 1$ μs and $I_r = 100$ kA we find at $t = \tau_r$

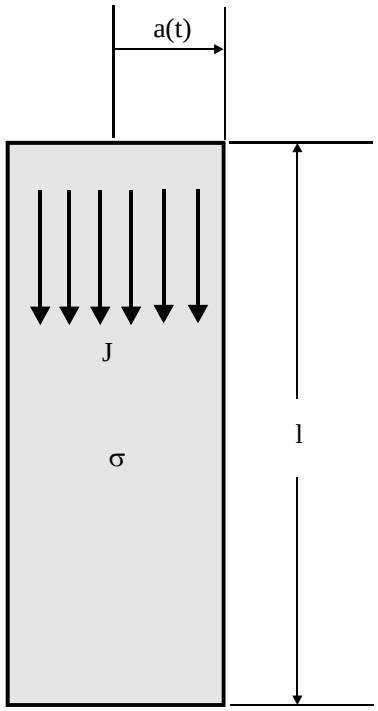

Figure 173. Channel expansion due to return stroke heating.

$$A\,(t) \approx 0.6 \text{ cm}^2 + A_0 \approx 0.9 \text{ cm}^2$$

and

$$R \approx 3 \text{ mohms}$$

Using $I_r = 100$ kA gives a resistive voltage

$$V_r \approx 300 \text{ V}$$

and the inductive voltage with the broader channel and slower current rise rate is smaller. Thus the full return stroke current expands and heats the channel so that the larger return stroke current does not lead to a larger voltage versus the early time level. Hence we would expect a very early time peak resulting from the continuing current channel resistance and inductance followed by a rapid reduction in inductive component and a slower decay in resistive voltage. This behavior is observed in the experimental waveform and the levels of Figure 174 are in the ballpark of what is observed. Of course multiple return arcs would reduce these predicted levels.

6.3 Direct Current Measurements of Plasma Distribution

In the previous subsections we either relied on assumptions, photographic evidence, simulations, or models for the plasma dimensions. This subsection outlines various concepts for measuring the evolution of the current distribution from the continuing current and second return stroke components on an electrode surface as a function of time. From video taken in the SLS we only know that when the second return stroke occurs there is a flash of light that saturates the camera film over one or two frames. It is difficult to determine the radial extent of the current carrying portion of the return stroke from this visual data.

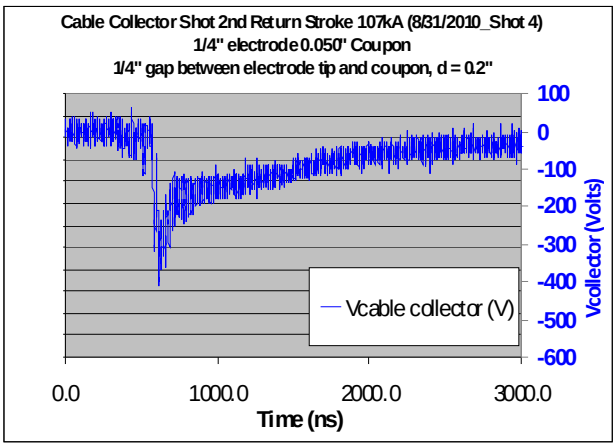

Figure 174. Coupled voltage to cable collector during two-return stroke/continuing current experiment.

Figure 175. Front of two "D" electrodes for measuring plasma radius.

Building an electrode to make this determination is difficult as well. The electrode must withstand the damage inflicted by the continuing current and then be able to distinguish between current flowing at various radii but not affect the extent of the current flow (due to it's impedance and the possibility of arcing or diversion of the discharge). We came up with three different designs, which we will discuss.

6.3.1 D design

This design was based on a papers by Olsen and Nestor who employed it to examine the extent of a steady argon arc driven by currents ranging from 200 to 800 amps [26], [27], [10]. They used water-cooled, thin copper electrodes to measure the amount of current on each side of the split between two "D" electrodes and from that data backed out the radius of the plasma. They were able to move the electrodes under the arc and the arc remained steady in extent and location while this was being done. To obtain the current distribution across the arc, the current has to straddle the split and not move. Our idea was to start the continuing current at a given location using a starter wire and assume that the return stroke occurred at the same location and that it didn't move while it was expanding. From this we would then be able to back out the current distribution as a function of time. The electrodes are shown in Figure 175. Instead of copper, we made our electrodes from stainless steel and we did not water cool the electrodes to keep the experiment simple. The back of the electrodes are shown in Figure 176 where we see that each "D" has two lugs to connect to. To minimize inductance of the measurement system, the current viewing resistors (CVRs) are connected directly to the lugs with side copper strips as shown in Figure 177.

Figure 178 shows the SLS electrode and damage to one of the "D" electrodes due to a return stroke current; note the evidence of arcing across the gap between the "D" electrodes. Damage to the electrodes from continuing current is clearly shown in Figures 179 and 180.

In order to cause the continuing current to attach to a specified location, we used a starter wire. Figures 181 through 183 show the continuing current flowing on the two "D" electrodes as the starter wire is moved toward the split between the two electrodes. When the starter wire is 9/16 inches away, all of the current flows on one of the electrodes. This is also the case when the starter wire is 3/8 inches away except that there is evidence that breakdown is occurring between the two electrodes at around 220 ms. When the starter wire is moved to 3/16 inches away, the current initially splits between the two electrodes, but then for some reason (either discharge column diameter, discharge movement, or possibly breakdown between

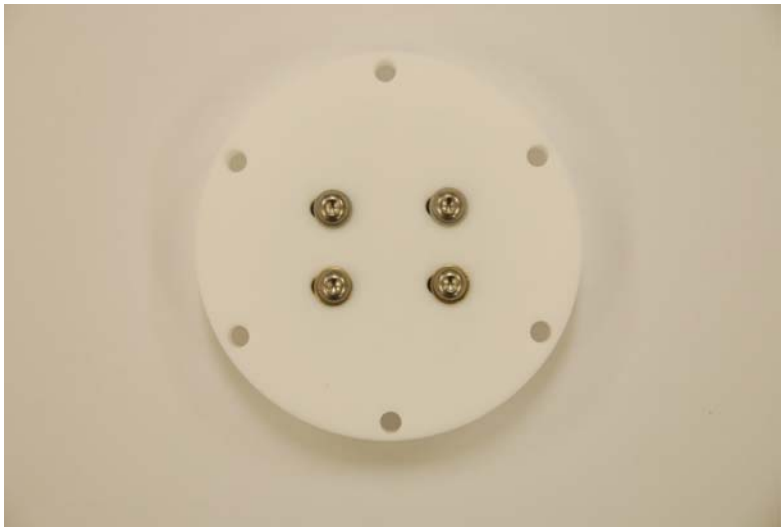

Figure 176. Back of "D" electrodes.

Figure 177. CVR's attached to back of "D" electrodes.

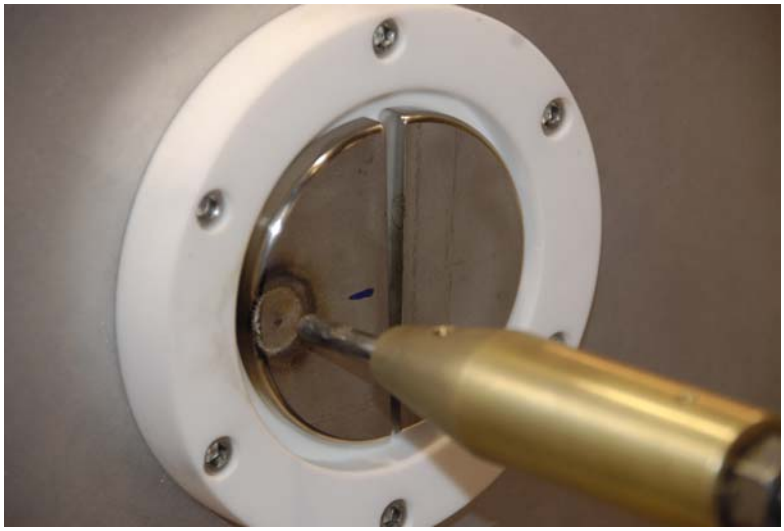

Figure 178. The electrode of the SLS and damage caused to the electrodes by the continuing current.

Figure 179. Damage to electrodes from continuing current.

Figure 180. Side view of electrode damage.

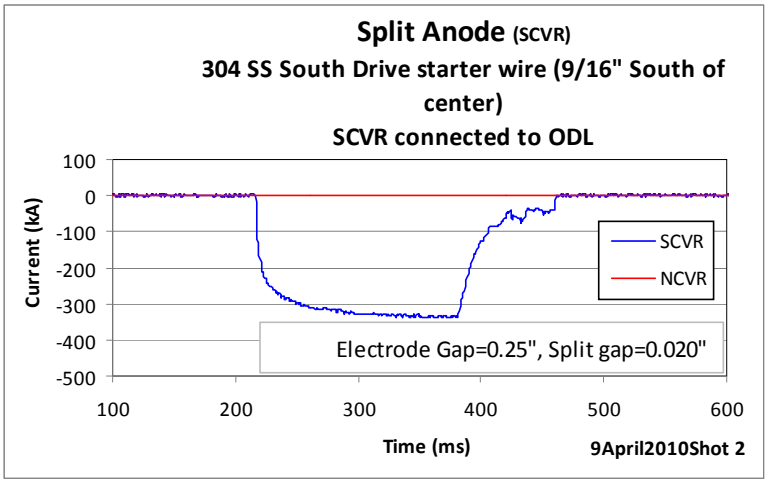

Figure 181. Current distribution for arc 9/16" offset from split.

"D" s) the current moves to one electrode; note that 3/16 inches is 0.475 cm, which is in the ballpark of the radius in Hsu's calculation shown in Figure 169 (note that there is a point anode rather than point cathode in this calculation).

The continuing current caused some damage, but the main problem with this measurement was that there was enough of a voltage difference between the two "Ds" that breakdown would occur between the two halves and actually in some cases would weld the two halves together. This problem caused us to abandon this method.

6.3.2 Ring Design

Figure 184 shows another concept for the device consisting of concentric rings of metal separated by insulators. The front and back view of the actual electrodes are shown in Figures 185 and 186. On the back, as shown in Figure 187, the rings are connected to chassis ground by CVRs so that the radial current profile can be sampled. There are issues with the inductance and resistance of the CVR circuits perturbing the current distribution, particularly for the return stroke profile. Inductance and resistance was reduced as much as possible by positioning the CVRs (these CVRs are smaller than in the case of the "D" electrodes because over the duration of the waveform only a portion of the return stroke current is expected to flow through each) close to the rings and using wide copper strips for connections as shown in Figure 188. Since each ring is instrumented individually and the CVRs to handle this size current are still physically large, there is competition for space in this measurement. The signals from the CVRs are brought outside the measurement box by optical data links (ODLs) which are shown in the measurement box in Figure 189.

Figure 190 shows the ring electrodes with the SLS electrode. These electrodes are not robust enough to handle the damage of the continuing current so their use was confined to measuring the expansion of the return stroke. There are questions about whether the rings with their separating insulation perturbs the current distribution. Because of physical space problems, we are limited to a maximum of four electrodes. Finally, even with all the care taken to minimize the CVRs inductance and resistance, there was still enough of a voltage difference to cause arcing between the CVRs as seen in Figure 191. Figure 192 shows the current on each ring as a function of time. The current starts in the center then moves to ring 3 and finally divides between ring 3 and 4. For some reason (possibly arcing) it doesn't seem to flow on ring 2 except at late time after 10 μs.

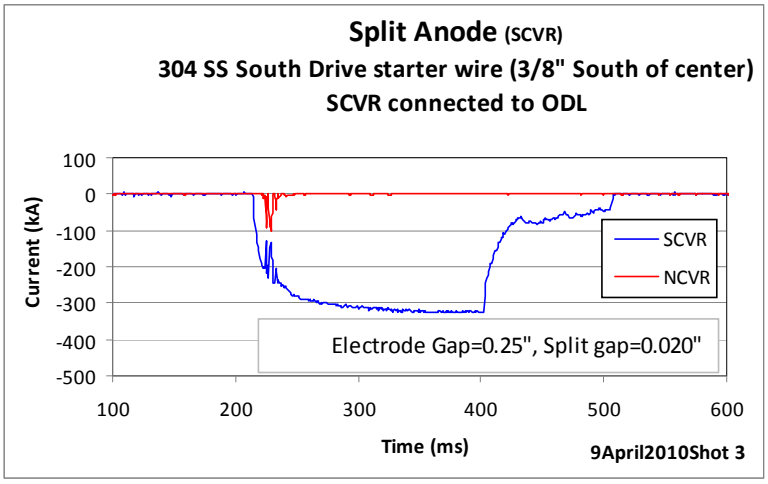

Figure 182. Current distribution for arc 3/8" offset from split.

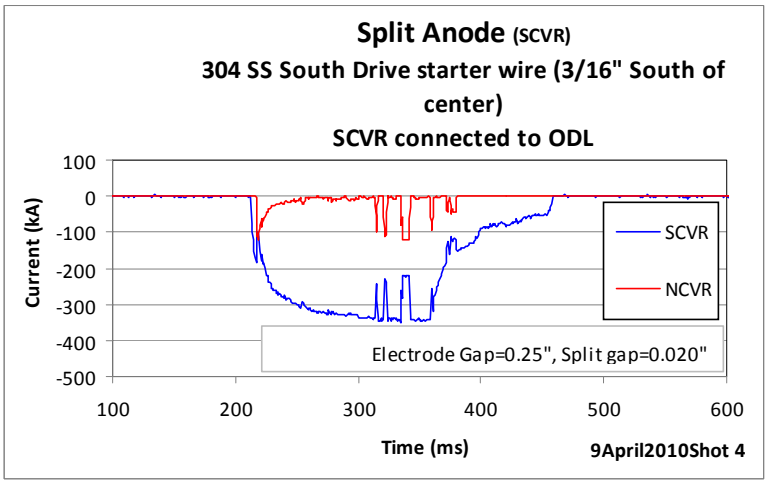

Figure 183. Current distribution for arc 3/16" offset from split.

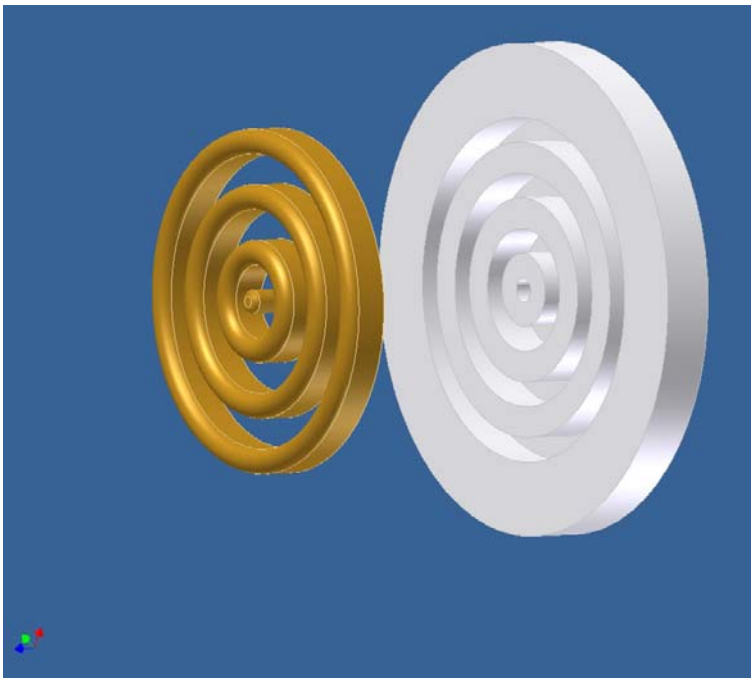

Figure 184. Schematic of brass rings placed inside a Teflon holder of the ring probe.

Figure 185. Front view of the ring electrodes. The radii of the ring centers are 1: 0 mm, 2: 4.75 mm, 3: 9.5 mm, 4: 14.3 mm.

Figure 186. Back view of the ring electrodes of the probe.

Figure 187. CVRs connected to each of the rings of the probe.

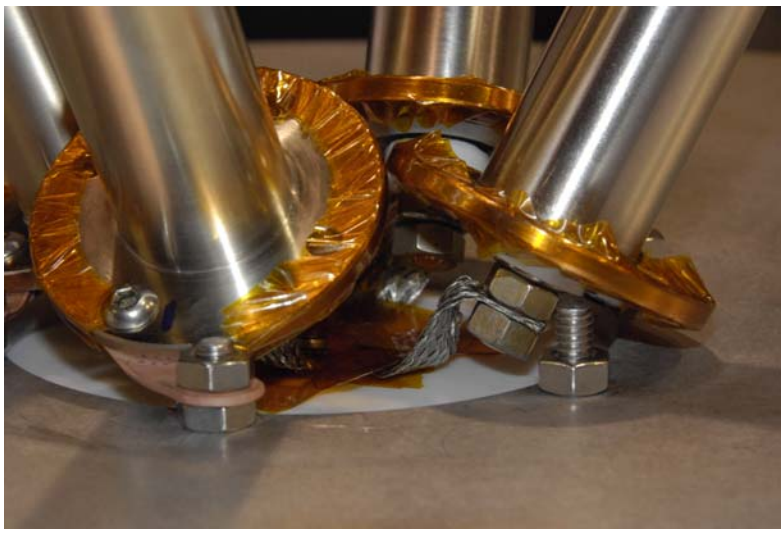

Figure 188. Detail of the method to minimize inductance of the CVRs.

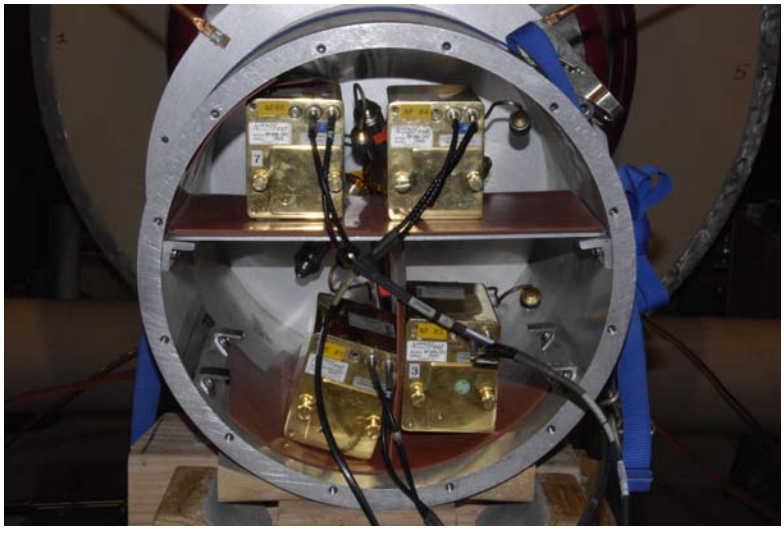

Figure 189. Layout of the 4 ODL's used in the measurement.

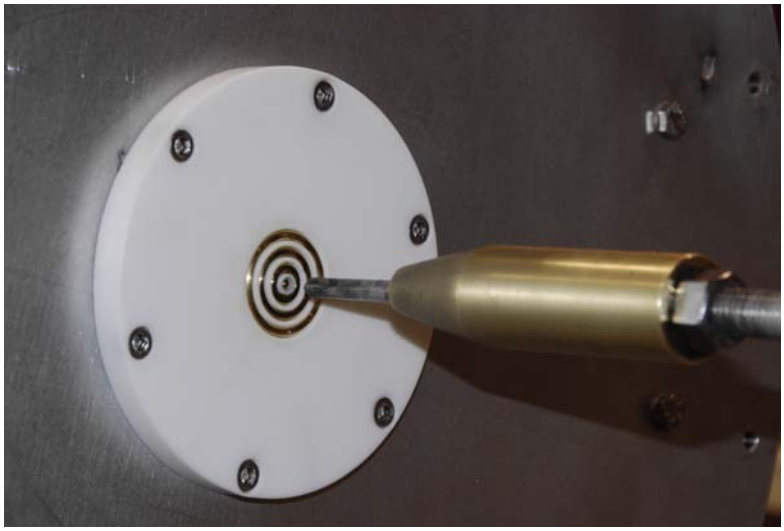

Figure 190. SLS electrode and the ring electrodes of the probe.

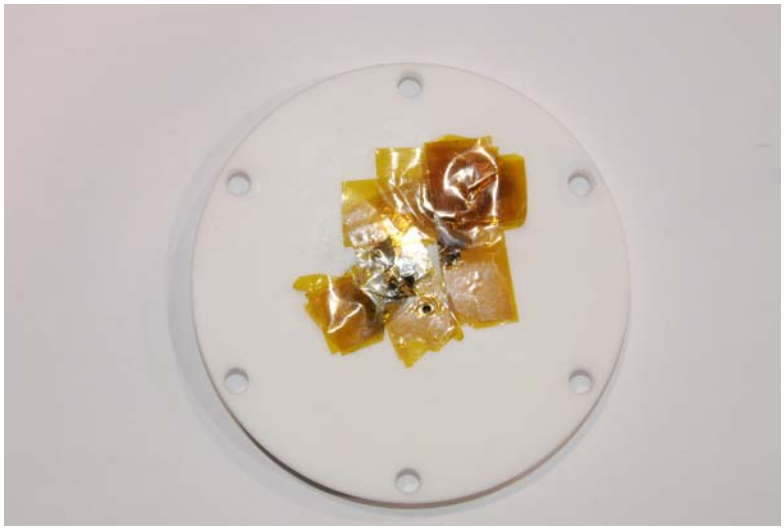

Figure 191. Evidence of arcing between the electrode rings of probe.

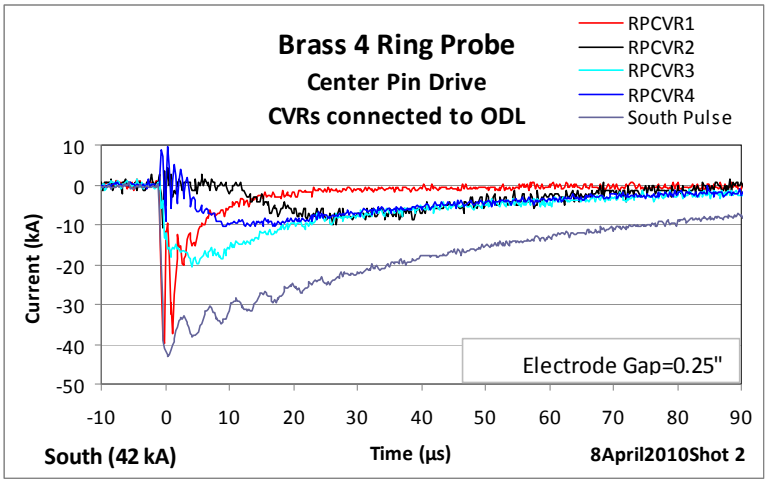

Figure 192. Current measured on each ring of probe.

6.3.3 Groove Probe

A third concept is to use the metal of the plane itself as a diagnostic for the current profile. A cross section is shown in Figure 193. The problem with this approach is that heating of the metal during the continuing current phase changes the properties and thus it was tried at first only with the return stroke (for which some change in properties due to impulse heating may also interfere with the interpretation).

If a radial volume current J_r is flowing outward in the rotationally symmetric fixture we can estimate the transfer voltage generated in the thin regions by using the effective surface current density K_r and the transfer impedance of the conductor layer. For simplicity here we look at the case where (in the real situation current is being injected over a range of r and the radial distribution of K_r is to be determined)

$$K_r = I/\left(2\pi r\right)$$

as

$$V \approx wK_r * Z_{pl}$$

where in the time domain the $*$ represents a convolution. The transfer impedance Z_{pl}, in the frequency domain is

$$Z_{pl}\left(\omega\right) = \frac{\left(1+i\right)\Delta/\delta}{\sin\left[\left(1+i\right)\Delta/\delta\right]}$$

where the skin depth is

$$\delta = \sqrt{2/\left(\omega\mu\sigma\right)}$$

In the case where the metal is sufficiently thin to make the current slowly varying compared to the diffusion time [44]

$$\tau = \mu\sigma\Delta^2/\pi^2$$

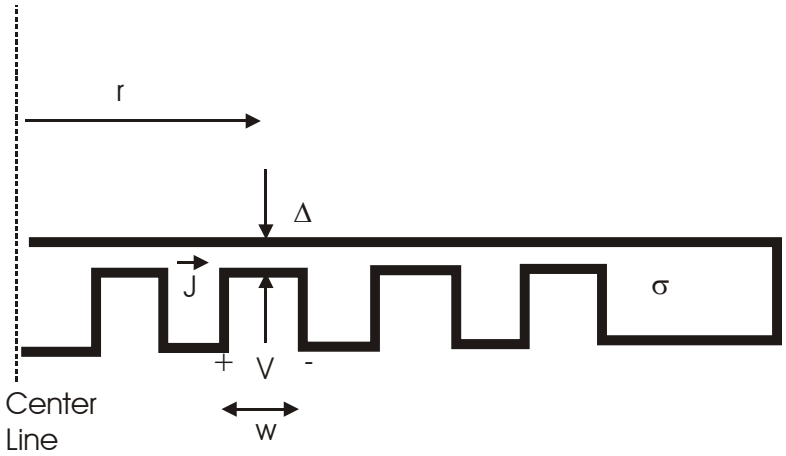

Figure 193. Cross section of the groove probe geometry.

this is approximately

$$V \approx K_r \frac{w}{\sigma \Delta}$$

If we use nonmagnetic stainless steel with $\sigma = 1.4 \times 10^6$ S/m and $\mu = \mu_0 = 4\pi \times 10^7$ H/m, and take $\Delta = 1$ mm (40 mils) we find that $\tau = 0.18$ μs. This is reasonably fast compared to return stroke rise times but the diffusion may still distort the results slightly (perhaps later we can back out the diffusion effects from the measurement for greater accuracy). Note that the time [13]

$$\tau_d = \mu \sigma \Delta^2$$

which is $\tau_d = 1.76$ μs is the time for which the diffusion effect can be ignored. Also the time [44]

$$\tau_s = \tau_c - \tau$$

where

$$\tau_c = \mu \sigma \Delta^2 / 6$$

which is $\tau_s = 0.115$ μs, is the time where we begin to see a response on the transfer impedance.

Now if we take $w \approx \Delta$ we find that for and outer radius $r = 1$ cm

$$V \approx \left(\frac{w}{2\pi \sigma \Delta r} \right) I \approx (11.37 \ \mu\text{ohm})\, I$$

If the voltage measurement accuracy is 10 millivolts then this indicates it is possible to measure variations in current of about 1 kA at the outer radius. This resolution would not be too bad for 100 kA return stroke currents, but we must make sure that any penetrant magnetic fields do not induce comparable voltages in the interior measurement loops.

Step Height Capacitance-Resistance Solution The capacitance per unit length of a junction between two heights s and s' of transmission line can be determined from conformal mapping [45]

$$C = \varepsilon_0 \left(\frac{\ell}{s} + \frac{\ell'}{s'} \right) + \frac{\varepsilon_0}{\pi} \left[\frac{1}{p} (1+p)^2 \ln(1+p) - \frac{1}{p} (1-p)^2 \ln(1-p) - 2\ln(4p) \right]$$

$$p = s/s' < 1$$

and $\ell >> s, \ell' >> s'$ are the distances from the height change out to which the capacitance per unit length is determined on either side of the junction. The first term is the uniform field component and the second term is the correction. Now by virtue of the two dimensional nature of this problem we want to use this to determine the correction to the conductance per unit length for current flow in the direction along the plates (this connection between different quantities is different than the three-dimensional connection between the capacitance and conductance used in the section below, because this capacitance step correction is for an electric field between the top and bottom electrodes, whereas we want a conductance for current flow from left to right between the electrodes). The original conformal mapping problem was set up with a potential difference between waveguide conductors

$$V = -\int_C \underline{E} \cdot \underline{d\ell} = \phi(\text{top}) - \phi(\text{bottom})$$

where

$$\underline{E} = -\nabla\phi$$

$$\phi = \mathrm{Im}\,(W)$$

and W is the complex potential in the problem [45]. Then the electric vector potential was take as

$$A_{ez} = -\varepsilon_0\,\mathrm{Re}\,(W)$$

$$\underline{D} = \varepsilon_0\underline{E} = -\nabla \times \underline{A}_e$$

and the charge per unit width on the top plate was evaluated using

$$Q = \int_S \underline{D}\cdot\underline{n}dS = -\oint_C \underline{A}_e\cdot\underline{d\ell} = A_{ez}\,(\text{left}) - A_{ez}\,(\text{right})$$

and thus

$$C = \frac{Q}{V} = \frac{A_{ez}\,(\text{left}) - A_{ez}\,(\text{right})}{\phi\,(\text{top}) - \phi\,(\text{bottom})} = -\varepsilon_0\frac{\mathrm{Re}\,(W\,(\text{left})) - \mathrm{Re}\,(W\,(\text{right}))}{\mathrm{Im}\,(W\,(\text{top})) - \mathrm{Im}\,(W\,(\text{bottom}))}$$

However we can also use the complex potential in the problem to evaluate the magnetic field by means of

$$A_z = \mathrm{Im}\,(W)$$

$$\underline{B} = \mu_0\underline{H} = \nabla \times \underline{A}$$

In this case the magnetic flux per unit width is the normalization

$$\Phi = \int_S \underline{B}\cdot\underline{n}dS = \oint_C \underline{A}\cdot\underline{d\ell} = A_z\,(\text{top}) - A_z\,(\text{bottom})$$

The magnetic potential drop in this case can be defined as

$$V_m = -\int_C \underline{H}\cdot\underline{d\ell} = \phi_m\,(\text{left}) - \phi_m\,(\text{right}) = \int_C K_z d\ell = I$$

where

$$\phi_m = -\frac{1}{\mu_0}\,\mathrm{Re}\,(W)$$

$$\underline{H} = -\nabla\phi_m$$

The inductance per unit width can then be written as

$$L = \frac{\Phi}{I} = \frac{\Phi}{V_m} = \frac{A_z\,(\text{top}) - A_z\,(\text{bottom})}{\phi_m\,(\text{left}) - \phi_m\,(\text{right})} = -\mu_0\frac{\mathrm{Im}\,(W\,(\text{top})) - \mathrm{Im}\,(W\,(\text{bottom}))}{\mathrm{Re}\,(W\,(\text{left})) - \mathrm{Re}\,(W\,(\text{right}))} = \mu_0\frac{\varepsilon_0}{C}$$

where the final relation follows from the preceding formula for the capacitance since the complex potential

is the same quantity. The conductance per unit width in the current flow problem has the same Neumann boundary conditions as in the inductance problem and thus we can write

$$G = \sigma \frac{L}{\mu_0} = \sigma \frac{\varepsilon_0}{C}$$

The resistance for each section of line is then

$$R = \frac{1}{\sigma} \frac{C}{\varepsilon_0}$$

To construct the total resistance at the step we divide this by the transverse width (for varying transverse width we need to integrate the sections of resistor in series) d_{ave}

$$R_{step} = \frac{R}{d_{ave}}$$

Using the preceding capacitance we thus find that the step resistance is

$$R_{step} \sigma d_{ave} = \left(\frac{\ell}{s} + \frac{\ell'}{s'} \right) + \frac{1}{\pi} \left[\frac{1}{p} (1+p)^2 \ln(1+p) - \frac{1}{p} (1-p)^2 \ln(1-p) - 2 \ln(4p) \right]$$

and therefore the radial voltage drop is

$$V = I R_{step}$$

and where d_{ave} is an average cross sectional dimension of the device at a certain radius. For the first uniform field term in this expression we want to allow the transverse width (the perimeter in this case) to vary with radius

$$d_{ave} = 2\pi r$$

and integrate over $r = \ell$. For the second term a choice for this dimension is

$$d_{ave} \approx 2\pi r_e$$

where r_e is the position of the step. Thus if we combine two steps in height with r_i being is the inner step radius and $r_o = r_i + w$ being the outer step radius with thickness $s = \Delta$ between them and distance $R' = h$ outside of the step, we can write in the planar case

$$R_{groove} \sigma d_{ave} = \frac{w}{s} + \frac{2h}{s'} + \frac{2}{\pi} \left[\frac{1}{p} (1+p)^2 \ln(1+p) - \frac{1}{p} (1-p)^2 \ln(1-p) - 2 \ln(4p) \right]$$

In an example where $s = 1$ mm, $s' = 4$ mm, $p = 1/4$, $w = 0.046$ in $= 1.1684$ mm, $2h = 3$ mm, $\sigma = 1.4 \times 10^6$ S/m, we obtained

$$R_{groove} \sigma d_{ave} = 1.1684 + 0.75 + 1.3$$

or

$$R_{groove} d_{ave} \approx 2.3 \ \mu\text{ohm} - \text{m}$$

A numerical simulation of this planar case gave 2.17 μohm-m, which is 6% below this value, but is still

reasonably close.

In the cylindrical case

$$R_{groove} = \frac{1}{2\pi s\sigma}\int_{r_i}^{r_o}\frac{dr}{r} + \frac{1}{2\pi s'\sigma}\left[\int_{r_i-h_i}^{r_i}\frac{dr}{r} + \int_{r_o}^{r_o+h_o}\frac{dr}{r}\right]$$

$$+\frac{1}{2\pi^2\sigma}\left(\frac{1}{r_i}+\frac{1}{r_o}\right)\left[\frac{1}{p}(1+p)^2\ln(1+p) - \frac{1}{p}(1-p)^2\ln(1-p) - 2\ln(4p)\right]$$

or

$$2\pi\sigma s R_{groove} = \ln(r_o/r_i) + p\ln\left(\frac{r_i}{r_o}\frac{r_o+h_o}{r_i-h_i}\right)$$

$$+\frac{s}{\pi}\left(\frac{1}{r_i}+\frac{1}{r_o}\right)\left[\frac{1}{p}(1+p)^2\ln(1+p) - \frac{1}{p}(1-p)^2\ln(1-p) - 2\ln(4p)\right]$$

Now taking $s = 1$ mm, $s' = 4$ mm, $p = 1/4$, $w = 0.046$ in $= 1.1684$ mm, $h_i + h_o = 2h = 3$ mm, $r_i = 3$ mm, $\sigma = 1.4 \times 10^6$ S/m, gives

$$R_{groove}\,(8.79646\text{ kS}) \approx 0.32892 + 0.25013 + 0.37258$$

or

$$R_{groove} \approx 0.108\text{ mohm}$$

A 3D simulation of this circular case gave 0.103 mohm, which is about 5% lower but is still reasonably close to the preceding formula. If we use a current of 100 kA we should expect a response of 10.8 volts.

Diffusion Effects From Thicker Regions The thicker region with thickness $s' = 4$ mm has a diffusion time of $\tau = \mu\sigma s'^2/\pi^2 = 2.85$ μs. Because the preceding static calculation indicates that these thicker regions, along with the junction corrections, contribute non-negligible resistances, it is of interest to inquire how much effect this diffusion has for the earlier times in the experiment. In this problem shown in Figure 194 the total surface current per unit width K_0 is specified and the volume current has no normal component on the free surfaces $J_n = 0$. We want to find the local voltage ΔV from one side of the step to the other.

The following canonical corner geometry shown in Figure 195 can be used to assess this issue when the skin depth δ is assumed to be larger than $s = \Delta = 1$ mm but smaller than $s' = 4$ mm.

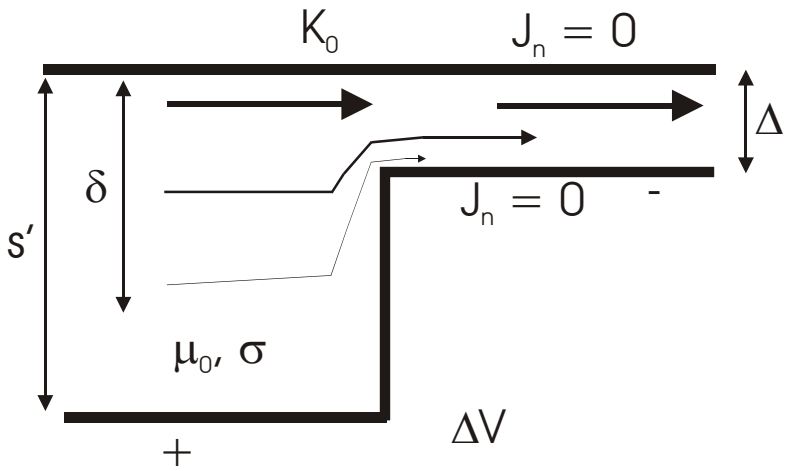

Figure 194. Single step in geometry of groove.

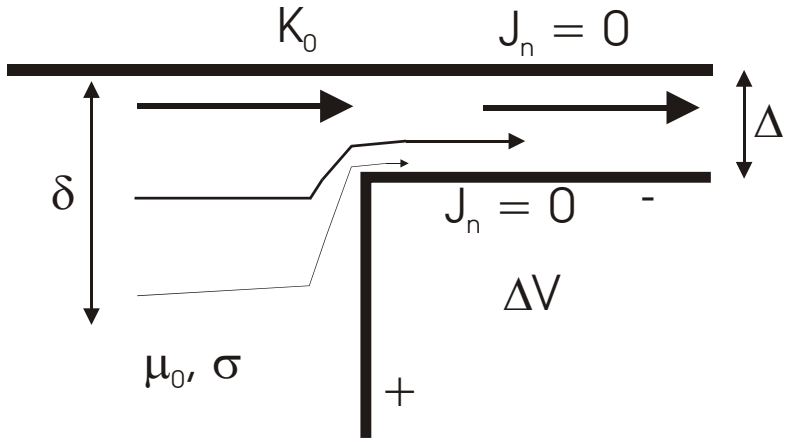

Figure 195. Single step in groove geometry with electrically thick dimension between grooves treated as half space.

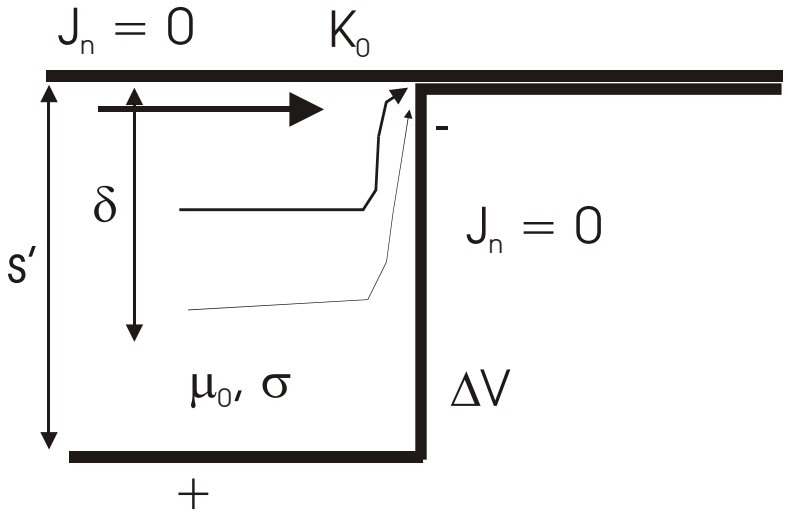

Figure 196. Single step in groove geometry with electrically thin dimension treated as a sink point.

We can alternatively simplify the problem by shrinking the thin $s = \Delta$ gap to a point current sink as shown in Figure 196. The voltage cannot be taken to the sink point but we can truncate the voltage calculation at an equivalent radius a_e from the sink point. This simplifies the problem because we can assume that the skin depth is larger then the right gap $s = \Delta = 1$ mm, which allows the equivalent radius a_e to be determined from static considerations alone.

If we also have the skin depth is smaller than the thicker region $s' = 4$ mm, we can eliminate this boundary as well as shown in Figure 197.

This final simplified picture of Figure 197 is now solved. The equations inside the conductor (for time dependence $e^{-i\omega t}$) are

$$\nabla \times \underline{E} = i\omega\mu_0 \underline{H}$$

$$\nabla \times \underline{H} = \sigma \underline{E}$$

The volume current density is

$$\underline{J} = \sigma \underline{E}$$

At the boundary we have

$$\underline{n} \cdot \underline{J} = 0$$

Thus eliminating the electric field gives

$$\nabla \times \nabla \times \underline{H} = \nabla (\nabla \cdot \underline{H}) - \nabla^2 \underline{H} = i\omega\mu_0\sigma \underline{H}$$

Because the magnetic induction

$$\underline{B} = \mu_0 \underline{H}$$

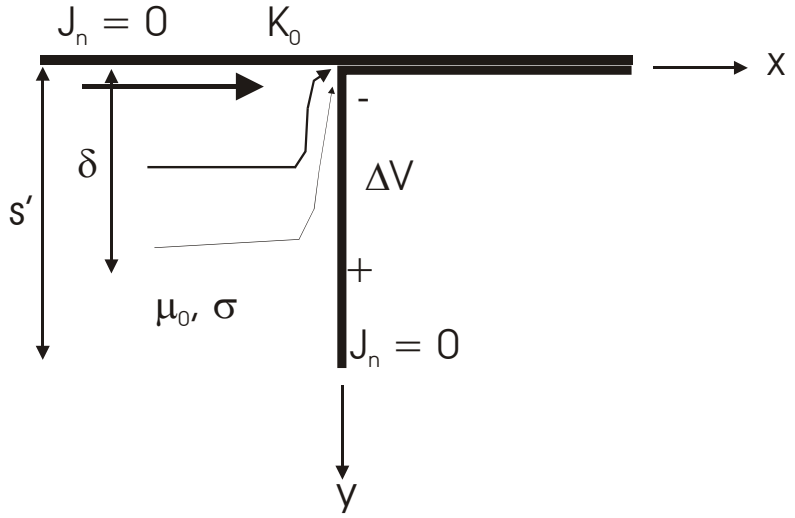

Figure 197. Single step in groove geometry with both half space and sink point approximations.

is solenoidal

$$\nabla \cdot \underline{B} = 0$$

we have

$$\left(\nabla^2 + \gamma^2\right) \underline{H} = 0$$

where

$$\gamma = \sqrt{i\omega\mu_0\sigma} = (1+i)/\delta$$

In this two dimensional geometry we can scalarize the problem in terms of the component of the magnetic field into the page H_z

$$\left(\nabla^2 + \gamma^2\right) H_z = 0$$

If we image the problem about $x = 0$ we double the sink current. In this two dimensional geometry the current sink is actually a semi-infinite current sheet above the conductor. Thus the magnetic field on the surface in the symmetrized problem is given by

$$H_z(x,0) = K_0 \mathrm{sgn}(x)$$

Applying the Fourier sine representation in x and taking the decaying solution as $y \to \infty$ gives

$$H_z(x,y) = \frac{2}{\pi}\int_0^\infty A(u)\, e^{i\sqrt{\gamma^2-u^2}y} \sin(ux)\, du$$

From the sine integral function

$$\mathrm{Si}(x/\varepsilon) = \int_0^{x/\varepsilon} \sin(u)\frac{du}{u} = \int_0^{1/\varepsilon} \sin(ux)\frac{du}{u}$$

and its known limit ($\varepsilon \to 0$)

$$\mathrm{Si}(\infty) = \pi/2$$

we see that $A(u) = K_0/u$. Thus the solution to the problem is

$$H_z(x,y) = K_0\frac{2}{\pi}\int_0^\infty e^{i\sqrt{\gamma^2-u^2}y} \sin(ux)\frac{du}{u}$$

This should satisfy the boundary conditions

$$J_x(0,y) = \sigma E_x(0,y) = \frac{\partial H_z}{\partial y}(0,y) = 0\ ,\ y > 0$$

$$J_y(x,0) = \sigma E_y(x,0) = -\frac{\partial H_z}{\partial x}(x,0) = 0\ ,\ x \neq 0$$

by symmetry. Note that the second condition is obviously true since $H_z(x,0) = K_0\ \mathrm{sgn}(x)$. The first condition is also true by virtue of the sine transform (convergence is assured by the presence of the exponential for $y > 0$).

Now we need to find the voltage ΔV. We integrate the surface electric field $-E_y(0,y)$ from the equivalent radius a_e to ∞.

$$\Delta V = -\int_{a_e}^{\infty} E_y(0,y)\,dy = \int_{a_e}^{\infty} K_0 \frac{2}{\pi\sigma} \int_0^{\infty} e^{i\sqrt{\gamma^2-u^2}y} du dy = K_0 \frac{i2}{\pi\sigma} \int_0^{\infty} \frac{e^{i\sqrt{\gamma^2-u^2}a_e}}{\sqrt{\gamma^2-u^2}} du$$

The branch points of the integrand are at $u = \pm\gamma$ and the real axis path is below the branch point at $u = \gamma$. Let us rotate the path of integration to $-i\infty$

$$\Delta V = K_0 \frac{i2}{\pi\sigma} \int_0^{-i\infty} \frac{e^{i\sqrt{\gamma^2-u^2}a_e}}{\sqrt{\gamma^2-u^2}} du = K_0 \frac{2}{\pi\sigma} \int_0^{\infty} \frac{e^{i\sqrt{\gamma^2+u^2}a_e}}{\sqrt{\gamma^2+u^2}} du$$

Now if we let

$$u = \gamma \sinh v$$

$$\Delta V = K_0 \frac{2}{\pi\sigma} \int_0^{\infty} e^{i\gamma a_e \cosh v} dv = K_0 \frac{2}{\pi\sigma} K_0(-i\gamma a_e) = K_0 \frac{i}{\sigma} H_0^{(1)}(\gamma a_e)$$

Because we assume that $a_e/\delta << 1$ we can expand the Hankel function as

$$\Delta V \sim K_0 \frac{i}{\sigma}\left[1 + i\frac{2}{\pi}\left\{\ln(\gamma a_e/2) + \gamma'\right\}\right] = (K_0/\sigma)\left[\frac{i}{2} + \frac{2}{\pi}\ln\left(\frac{\delta\sqrt{2}}{a_e e^{\gamma'}}\right)\right]$$

where $\gamma' \approx 0.5772$ is Euler's constant. If we consider the lightning waveform as a falling exponential

$$I(t) = I_0 e^{-\alpha t} = I_0 \frac{1}{2\pi i} \int_{c-i\infty}^{c+i\infty} \frac{e^{st}}{s+\alpha} ds$$

As an approximation we could consider averaging the frequency in the above expression $s = -i\omega$

$$\ln(\gamma a_e/2) = \ln\left(\sqrt{-s\mu_0\sigma}a_e/2\right) = i\frac{\pi}{2} + \ln\left(\sqrt{s\mu_0\sigma}a_e/2\right)$$

$$\langle \ln(s) \rangle = \frac{1}{2\pi i} \int_{c-i\infty}^{c+i\infty} \frac{\ln(s)\, e^{st}}{s+\alpha} ds \Big/ \frac{1}{2\pi i} \int_{c-i\infty}^{c+i\infty} \frac{e^{st}}{s+\alpha} ds$$

If we take the limit of a step function $\alpha \to 0$ the integral is easy

$$\langle \ln(s) \rangle = \frac{1}{2\pi i} \int_{c-i\infty}^{c+i\infty} \ln(s)\, e^{st} \frac{ds}{s} = -\gamma' - \ln(t)$$

and thus

$$\Delta V \sim K_0 \frac{i}{\sigma}\left[i\frac{2}{\pi}\left\{\ln\left(\sqrt{\mu_0\sigma}a_e/2\right) + \frac{1}{2}\ln(s) + \gamma'\right\}\right]$$

or using the average

$$\Delta V \sim -\left(K_0/\sigma\right)\frac{2}{\pi}\left\{\ln\left(\sqrt{\mu_0\sigma}a_e/2\right)+\frac{1}{2}\left\langle\ln\left(s\right)\right\rangle+\gamma'\right\}$$

$$\sim -\left(K_0/\sigma\right)\frac{2}{\pi}\left\{\ln\left(\sqrt{\mu_0\sigma}a_e/2\right)-\frac{1}{2}\ln\left(t\right)+\gamma'/2\right\}$$

$$\sim -\left(K_0/\sigma\right)\frac{2}{\pi}\ln\left(\sqrt{e^{\gamma'}\mu_0\sigma/t}a_e/2\right)$$

Going to cylindrical geometry the current per unit length is replace by

$$K_0 = I_0/\left(2\pi r\right)$$

where r is the radius of the step.

$$2\pi\sigma s R_{diff} \sim -s\left(\frac{1}{r_i}+\frac{1}{r_o}\right)\frac{2}{\pi}\ln\left(\sqrt{e^{\gamma'}\mu_0\sigma/t}a_e/2\right)$$

How should we select a_e? In the report [45] we have

$$Q_R = -A_{ez}\left(z=iR_2\right)+A_{ez}\left(-R+is\right)$$

where we take $R >> s$ and $s << R_2 << s'$.

$$z=\frac{s'}{\pi}\int_{-1}^{z_1}\sqrt{\frac{z_1+p^2}{z_1+1}}\frac{dz_1}{z_1}+is'$$

$$p = s/s'$$

$$A_{ez} = -V\frac{\varepsilon_0}{\pi}\ln\left|z_1\right|$$

The point $z_1=-p^2$ maps to $z=is$. The point $z_1=-1$ maps to $z=is'$. The point $z=-R+is$ maps to $z_1=-\varepsilon_1$ where

$$\ln\left(1/\varepsilon_1\right)\sim\frac{\pi}{s}R+\frac{1}{p}\ln\left(\frac{1+p}{1-p}\right)+\ln\left(\frac{1-p^2}{4p^2}\right)$$

The point $z=iR_2$ maps to the point $z_1=-d_1$ with $(p^2<d_1<1)$

$$iR_2=\frac{s'}{\pi}\int_{-1}^{-d_1}\sqrt{\frac{z_1+p^2}{z_1+1}}\frac{dz_1}{z_1}+is'$$

We note that if $p^2\to 0$ we want $1>d_1>>p^2$ and thus

$$R_2/s' = 1-\frac{1}{\pi}\int_{d_1}^{1}\sqrt{\frac{z_1-p^2}{1-z_1}}\frac{dz_1}{z_1}$$

Substituting

$$\frac{z_1 - p^2}{1 - z_1} = u^2$$

$$z_1 = \frac{u^2 + p^2}{u^2 + 1}$$

$$dz_1 = 2\frac{1 - p^2}{(u^2 + 1)^2} u du$$

$$\sqrt{\frac{d_1 - p^2}{1 - d_1}} = u_1$$

gives

$$R_2/s' - 1 = \frac{2}{\pi} \int_{u_1}^{\infty} \left(\frac{p^2}{u^2 + p^2} - \frac{1}{u^2 + 1} \right) du$$

$$= \frac{2}{\pi} p \int_{u_1/p}^{\infty} \frac{du}{u^2 + 1} - \frac{2}{\pi} \int_{u_1}^{\infty} \frac{du}{u^2 + 1}$$

$$= \frac{2}{\pi} p \left[\frac{\pi}{2} - \arctan\left(u_1/p\right) \right] - \frac{2}{\pi} \left[\frac{\pi}{2} - \arctan\left(u_1\right) \right]$$

$$= \frac{2}{\pi} p \arctan\left(p/u_1\right) - \frac{2}{\pi} \arctan\left(1/u_1\right)$$

or

$$R_2/s' = \frac{2}{\pi} p \arctan\left(p/u_1\right) + \frac{2}{\pi} \arctan\left(u_1\right)$$

Now we want $R_2 << s'$. This means that we expect $u_1 << 1$ or $d_1 << 1 - d_1$ or $p^2 << d_1 << 1/2$ and thus $u_1 \sim \sqrt{d_1}$ and $p/u_1 = \sqrt{p^2/d_1} << 1$. Then

$$R_2/s' \sim \frac{2}{\pi} p^2/d_1 + \frac{2}{\pi} \sqrt{d_1} \sim \frac{2}{\pi} \sqrt{d_1}$$

Thus

$$Q_R/V = \frac{\varepsilon_0}{\pi} \ln\left|z_1\left(z = iR_2\right)\right| - \frac{\varepsilon_0}{\pi} \ln\left|z_1\left(z = -R + is\right)\right|$$

$$= \frac{\varepsilon_0}{\pi} \ln\left|d_1\right| - \frac{\varepsilon_0}{\pi} \ln\left|\varepsilon_1\right|$$

$$= \frac{2\varepsilon_0}{\pi} \ln\left|\frac{\pi R_2}{2s'}\right| + \frac{\varepsilon_0}{\pi} \left[\frac{\pi}{s} R + \frac{2}{p} \ln\left(1 + p\right) - 2\ln\left(2p\right) \right]$$

$$\sim \frac{2\varepsilon_0}{\pi} \ln\left|\frac{\pi R_2}{2s'}\right| + \varepsilon_0 R/s + \frac{2\varepsilon_0}{\pi} \left[1 - \ln\left(2p\right)\right]$$

$$\sim \frac{2\varepsilon_0}{\pi} \ln\left(\frac{\pi R_2 e}{4s}\right) + \varepsilon_0 R/s$$

The final term is the uniform field contribution to the capacitance in the gap s with length from the junction R. The first term is the cylindrical field contribution to the capacitance with outer radius R_2 and inner radius

$$a_e = \frac{4s}{\pi e} \approx \frac{s}{2.1349}$$

Thus we find

$$2\pi\sigma s R^{(2)}_{groove} \approx \ln\left(r_o/r_i\right) + s\left(\frac{1}{r_i} + \frac{1}{r_o}\right)\frac{2}{\pi}\ln\left\{\sqrt{\frac{4t}{e^{\gamma'}\mu_0\sigma}}/\left(\frac{4s}{\pi e}\right)\right\}$$

For $r_i = 5.4991$ mm and $r_o = 6.6929$ mm with $s = 1$ mm and $t = 1$ μs, we find

$$\sqrt{\frac{4t}{e^{\gamma'}\mu_0\sigma}} \approx 1.13 \text{ mm}$$

$$a_e = \frac{4s}{\pi e} \approx 0.468 \text{ mm}$$

$$2\pi\sigma s R^{(2)}_{groove} \approx 0.19646 + 0.18569 = 0.38215$$

$$R^{(2)}_{groove} \approx 43.44 \ \mu\text{ohm}$$

If we use $t = 2$ μs we find

$$\sqrt{\frac{4t}{e^{\gamma'}\mu_0\sigma}} \approx 1.60 \text{ mm}$$

$$a_e = \frac{4s}{\pi e} \approx 0.468 \text{ mm}$$

$$2\pi\sigma s R^{(2)}_{groove} \approx 0.19646 + 0.25878 = 0.455239$$

$$R^{(2)}_{groove} \approx 51.75 \ \mu\text{ohm}$$

These magnitudes are somewhat smaller than the value from static analysis for groove 2 in Table 36 , but we are finding the side wall term to be equal in magnitude to the thin groove region (the precise selection of the value of ω or s is of some question here, but the preceding averaging procedure seems reasonable).

If we consider the lightning waveform as a rising exponential

$$I(t) = I_0\left(1 - e^{-\beta t}\right) = I_0 \frac{1}{2\pi i}\int_{c-i\infty}^{c+i\infty}\left(\frac{1}{s} - \frac{1}{s+\beta}\right)e^{st}ds$$

As an approximation we could consider averaging the frequency in the above expression $s = -i\omega$

$$\ln\left(\gamma a_e/2\right)=\ln\left(\sqrt{-s\mu_0\sigma}a_e/2\right)=i\frac{\pi}{2}+\ln\left(\sqrt{s\mu_0\sigma}a_e/2\right)$$

$$\left\langle \ln\left(s\right)\right\rangle =\left[\frac{1}{2\pi i}\int_{c-i\infty}^{c+i\infty}\ln\left(s\right)e^{st}\frac{ds}{s}-\frac{1}{2\pi i}\int_{c-i\infty}^{c+i\infty}\frac{\ln\left(s\right)e^{st}}{s+\beta}ds\right]/\left[1-\frac{1}{2\pi i}\int_{c-i\infty}^{c+i\infty}\frac{e^{st}}{s+\beta}ds\right]$$

$$=\left[-\gamma'-\ln\left(t\right)-\frac{1}{2\pi i}\int_{c-i\infty}^{c+i\infty}\frac{\ln\left(s\right)e^{st}}{s+\beta}ds\right]/\left(1-e^{-\beta t}\right)$$

$$\frac{1}{2\pi i}\int_{c-i\infty}^{c+i\infty}\frac{\ln\left(s\right)e^{st}}{s+\beta}ds=\lim_{\nu\to0}\frac{\partial}{\partial\nu}\left[\frac{1}{2\pi i}\int_{c-i\infty}^{c+i\infty}\frac{s^{\nu}e^{st}}{s+\beta}ds\right]$$

Carrying out the integration (near the pole we let $s=\beta e^{\pm i\pi}+\varepsilon e^{i\theta}$)

$$\frac{1}{2\pi i}\int_{c-i\infty}^{c+i\infty}\frac{\ln\left(s\right)e^{st}}{s+\beta}ds=\frac{1}{2\pi i}\int_{-\beta+\varepsilon}^{0}\left[\ln\left(\beta\right)-i\pi\right]e^{st}\frac{ds}{s+\beta}+\frac{1}{2\pi i}\int_{0}^{-\beta+\varepsilon}\left[\ln\left(\beta\right)+i\pi\right]e^{st}\frac{ds}{s+\beta}$$

$$+\frac{1}{2\pi i}\int_{-\infty}^{-\beta-\varepsilon}\left[\ln\left(\beta\right)-i\pi\right]e^{st}\frac{ds}{s+\beta}+\frac{1}{2\pi i}\int_{-\beta-\varepsilon}^{-\infty}\left[\ln\left(\beta\right)+i\pi\right]e^{st}\frac{ds}{s+\beta}$$

$$+\frac{1}{2\pi i}\int_{-\pi}^{0}\frac{\left[\ln\left(\beta\right)-i\pi\right]e^{-\beta t}}{\varepsilon e^{i\theta}}i\varepsilon e^{i\theta}d\theta+\frac{1}{2\pi i}\int_{0}^{\pi}\frac{\left[\ln\left(\beta\right)+i\pi\right]e^{-\beta t}}{\varepsilon e^{i\theta}}i\varepsilon e^{i\theta}d\theta$$

$$=-P\int_{-\infty}^{0}e^{st}\frac{ds}{s+\beta}+\ln\left(\beta\right)e^{-\beta t}=P\int_{0}^{\infty}e^{-st}\frac{ds}{s-\beta}+\ln\left(\beta\right)e^{-\beta t}$$

$$=e^{-\beta t}P\int_{-\beta t}^{\infty}e^{-s}\frac{ds}{s}+\ln\left(\beta\right)e^{-\beta t}=e^{-\beta t}\left\{-\operatorname{Ei}\left(\beta t\right)+\ln\left(\beta\right)\right\}$$

or

$$\left\langle \ln\left(s\right)\right\rangle =\left[-\gamma'-\ln\left(t\right)-e^{-\beta t}\left\{-\operatorname{Ei}\left(\beta t\right)+\ln\left(\beta\right)\right\}\right]/\left(1-e^{-\beta t}\right)$$

Now if we have reached the current peak then $\beta t>>1$ and this goes to the step result

$$\left\langle \ln\left(s\right)\right\rangle =-\gamma'-\ln\left(t\right)$$

From these results we can also carry out the double exponential waveform

$$\left\langle \ln\left(s\right)\right\rangle =\left[\frac{1}{2\pi i}\int_{c-i\infty}^{c+i\infty}\frac{\ln\left(s\right)e^{st}}{s+\alpha}ds-\frac{1}{2\pi i}\int_{c-i\infty}^{c+i\infty}\frac{\ln\left(s\right)e^{st}}{s+\beta}ds\right]/\left[\frac{1}{2\pi i}\int_{c-i\infty}^{c+i\infty}\frac{e^{st}}{s+\alpha}ds-\frac{1}{2\pi i}\int_{c-i\infty}^{c+i\infty}\frac{e^{st}}{s+\beta}ds\right]$$

$$\left[e^{-\alpha t}\left\{-\operatorname{Ei}\left(\alpha t\right)+\ln\left(\alpha\right)\right\}-e^{-\beta t}\left\{-\operatorname{Ei}\left(\beta t\right)+\ln\left(\beta\right)\right\}\right]/\left(e^{-\alpha t}-e^{-\beta t}\right)$$

$$2\pi\sigma sR_{groove}^{(2)}\sim\ln\left(r_o/r_i\right)-s\left(\frac{1}{r_i}+\frac{1}{r_0}\right)\frac{2}{\pi}\left\{\ln\left(\sqrt{\mu_0\sigma}a_e/2\right)+\frac{1}{2}\left\langle \ln\left(s\right)\right\rangle +\gamma'\right\}$$

The double exponential waveform has a peak at time t_p

$$\alpha t_p = \frac{\ln(\beta/\alpha)}{\beta/\alpha - 1}$$

with value I_p

$$I_p/I_0 = (\beta/\alpha - 1)(\beta/\alpha)^{-(\beta/\alpha)/(\beta/\alpha - 1)}$$

Now taking the value of α to be approximately given by the fall time t_f to half maximum value

$$\alpha \approx \ln(2)/t_f$$

gives

$$t_p/t_f \approx \frac{\ln(\beta/\alpha)/\ln(2)}{\beta/\alpha - 1}$$

If we take $t_p = 2$ μs and $t_f = 50$ μs we find

$$\beta/\alpha \approx 190$$

$$I_p/I_0 \approx 0.9675$$

Thus if $I_p = 50$ kA we need $I_0 = 51.68$ kA. Thus at the peak time $t = t_p$

$$\alpha t_p \approx 0.027726$$

$$\mathrm{Ei}(\alpha t_p) \approx -2.980254$$

$$\beta t_p \approx 5.268$$

$$\mathrm{Ei}(\beta t_p) \approx 46.47$$

$$\langle \ln(s) \rangle = \left[e^{-\alpha t} \left\{ -\mathrm{Ei}(\alpha t) + \ln(\alpha) \right\} - e^{-\beta t} \left\{ -\mathrm{Ei}(\beta t) + \ln(\beta) \right\} \right] / \left(e^{-\alpha t} - e^{-\beta t} \right) \approx 12.75$$

$$2\pi\sigma s R^{(2)}_{groove} \sim \ln(r_o/r_i) - s\left(\frac{1}{r_i} + \frac{1}{r_0}\right)\frac{2}{\pi}\left\{ \ln\left(\sqrt{\mu_0\sigma}\, a_e/2\right) + \frac{1}{2}\langle \ln(s) \rangle + \gamma' \right\}$$

$$\approx 0.19646 + 0.237 \approx 0.433$$

$$R^{(2)}_{groove} \approx 49.3 \ \mu\mathrm{ohm}$$

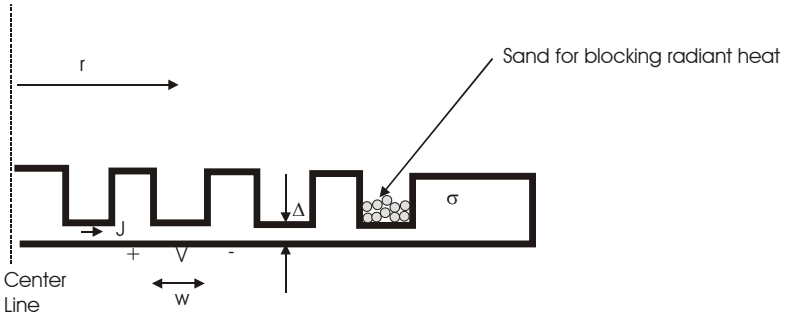

Figure 198. Inverted groove probe with protection against radiant heat at groove base.

Inverted Design Note that we might also be concerned about surface heating and consequent changes in electrical conductivity. This could pose problems in interpretation of the measurement. One concept for avoiding this effect is shown on the figure. We invert the groove probe so that the discharge occurs to the teeth and the measurement is made on the smooth side. Sand could be added to partially block radiant heating of the bottom groove surface.

Thicker Interior Concept Both the groove probe and the inverted groove probe (no sand was tried) suffer from melting issues of the thinner regions at the end of the continuing current phase of the strike even when water cooling was tried. Other materials can also be considered (copper was used before in the split probes [10]). The thermal diffusivity is

$$\alpha_T = \kappa / \left(\rho_M C_p \right)$$

where for stainless steel the mass density is $\rho_M \approx 7800$ kg/m^3, the thermal conductivity is $\kappa_T \approx 15 - 20$ W/(m-K), and the specific heat is $C_p \approx 520$ J/(kg-K) [34]. The thermal time constant for a layer of thickness $\Delta = 1$ mm is then

$$\tau_T = O\left[\Delta^2 / \left(8 \alpha_T \right) \right] \approx O\left(25 \text{ ms} \right)$$

For copper $\rho_M \approx 8933$ kg/m^3, $\kappa_T \approx 400$ W/(m-K), $C_p \approx 400$ J/(kg-K) [34] and thus for a $\Delta = 1$ mm thick layer

$$\tau_T = O\left(1.1 \text{ ms} \right)$$

Even using water cooling and the higher thermal conductivities associated with copper, and shorter duration (30 ms) and smaller amplitude (250 A) continuing currents, these issues were shown to destroy the 1 mm thick coupons (simulating the probe grooves) when the second return stroke hit. Thus we never achieved measurements of the transition from continuing current to return stroke. Another concept for getting around this problem is shown in Figure 199. In this case we give up on measuring the continuing current plasma radius (created by the continuing current generator) and attempt to handle the heat generated during this initial startup phase of the discharge with a thick probe center. The subsequent transition to the return stroke now is expected to quickly expand the plasma column over the grooves for which we can measure the voltages.

Probe Geometry The back of the actual groove probe (the side facing away from the SLS electrode) is shown in Figure 200, while the front side is shown in Figure 201. Wires that connect the groove centers to the voltage waveform recorder are shown in Figure 202. The groove probe is mounted to a measurement box that shields the equipment from the fields produced by the SLS and the voltage waveform recorder is

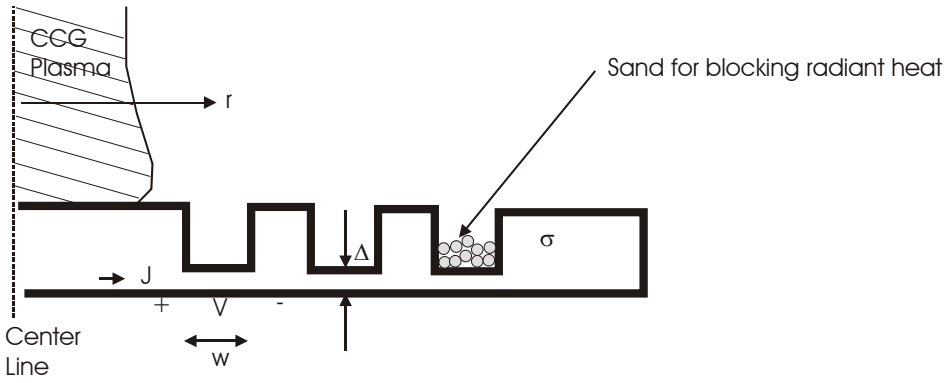

Figure 199. Inverted groove probe concept with solid metal center to handle continuing current (CCG) heating and outer grooves to observe the subsequent return stroke expansion.

Figure 200. Back side of groove probe.

placed inside the box as shown in Figure 203. The outside of the measurement box with the groove probe in its side and the SLS electrode is shown in Figure 204. Voltage waveforms as recorded by the waveform recorder are shown in Figure 205. Figure 206 shows the minor damage to the groove probe caused by a return stroke.

Figure 201. Front side of groove probe.

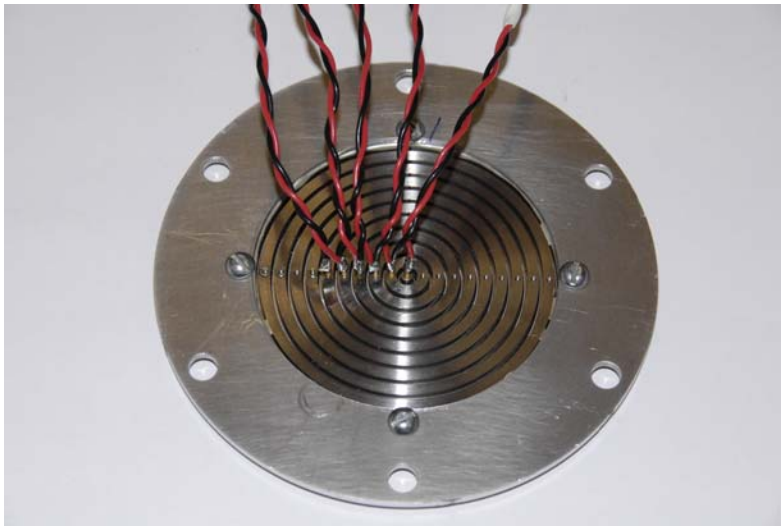

Figure 202. Back side of groove probe wired for voltage measurements.

Figure 203. Inside of measurement box showing voltage waveform recording equipment.

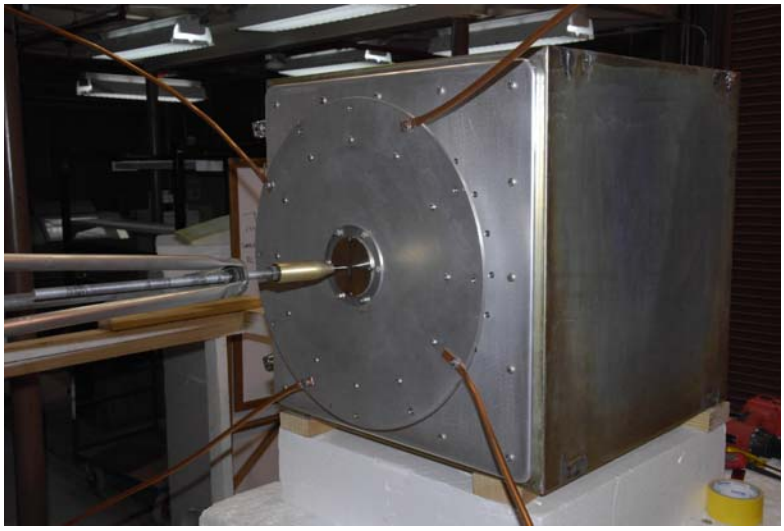

Figure 204. View of SLS electrode, groove probe and the measuement box.

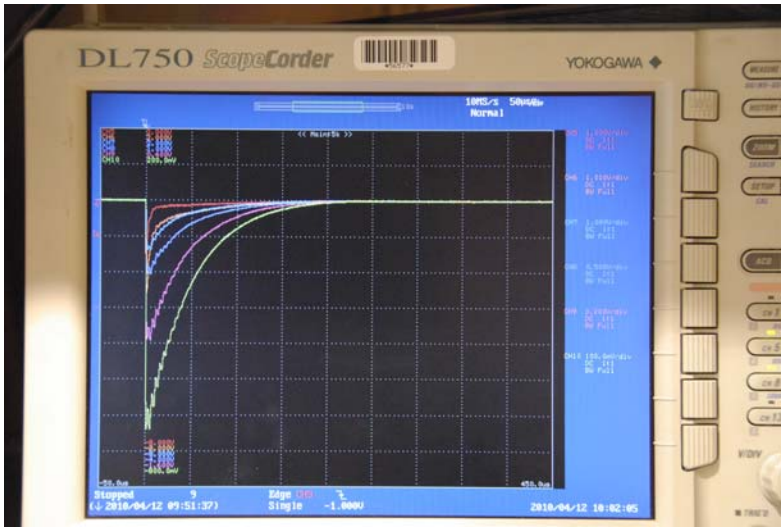

Figure 205. Recorded voltage waveforms from between the grooves

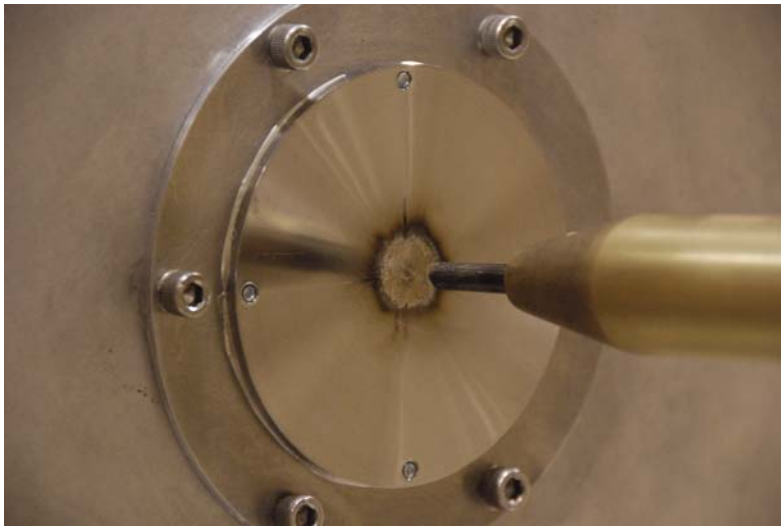

Figure 206. Minor damage to the groove probe caused by the return stroke.

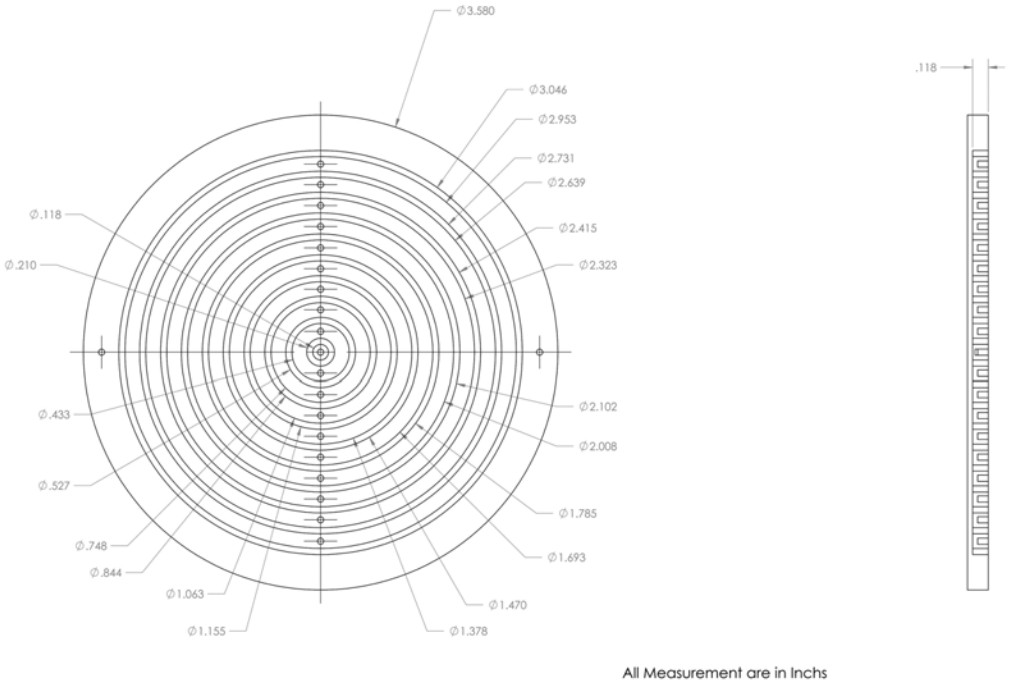

Figure 207. Dimensions of groove probe.

The Table 36 shows the r_i and r_o values for each groove taken from Figure 207. Now taking $s = 1$ mm, $s' = 4$ mm, $p = 1/4$, $w^{(n)} = r_o^{(n)} - r_i^{(n)}$, $2h_i^{(n)} = r_i^{(n)} + r_o^{(n-1)}$, $2h_o^{(n)} = r_i^{(n+1)} + r_o^{(n)}$, $h_i^{(1)} = r_i^{(1)} - s'/e^{\gamma'}$ (this value comes about from the effective radius for transfer resistance of a layer with a point drive on the input side $s'/e^{\gamma'}$, however since it gives a value greater than r_i^1 it means that the region of thickness s comes into the picture as well, and complicates the problem to the point that we do not have a canonical value, nevertheless use of this value basically cancels the second term in the expression below meaning that the resistance comes from the junction effects and the w region alone), $\gamma' \approx 0.5772$, $\sigma = 1.4 \times 10^6$ S/m, $\Delta V^{(n)} = IR^{(n)}$, $I^{(n)} = 50$ kA, gives

$$R/\left(0.1136821 \text{ mohm}\right) = \ln\left(r_o/r_i\right) + \frac{1}{4}\ln\left(\frac{r_i}{r_o}\frac{r_o + h_o}{r_i - h_i}\right) + \left(\frac{1}{r_i} + \frac{1}{r_o}\right) 0.6500 \text{ mm}$$

Braginskii Model We now summarize the Braginskii model for the late time spark expansion [30]. A side view of this geometry is shown in Figure 208. Current density $J_z\left(t\right)$ flows through the channel as indicated by the arrows. The channel radius is given by $a\left(t\right)$, which increases with respect to time. The electrical conductivity of the channel is given by σ. The length of the channel between the two electrodes is ℓ. A top view of the channel is shown in Figure 209. The arrows around the perimeter of the channel indicate that the channel is expanding.

The assumptions in this model are that the current flowing through a fixed conductivity gas expands the channel at supersonic velocity driving a cylindrical shock wave. It is thus the expansion of the channel that reduces the resistance of the arc in this model. The channel radius $a\left(t\right)$ is obtained as

n	r_i (mm)	r_o (mm)	w (mm)	h_i (mm)	h_o (mm)	R (μohm)	ΔV (volts)
1	1.4986	2.667	1.1684	−0.7473	1.41605	143.146	7.157
2	5.4991	6.6929	1.1938	1.41605	1.40335	60.683	3.034
3	9.4996	10.7188	1.2192	1.40335	1.39065	36.409	1.820
4	13.5001	14.6685	1.1684	1.39065	1.41605	28.015	1.401
5	17.5006	18.669	1.1684	1.41605	1.41605	20.003	1.000
6	21.5011	22.6695	1.1684	1.41605	1.41605	16.370	0.819
7	25.5016	26.6954	1.1938	1.41605	1.40335	13.946	0.697
8	29.5021	30.6705	1.1684	1.40335	1.42240	12.003	0.600
9	33.5153	34.6837	1.1684	1.42240	1.40970	10.595	0.530
10	37.5031	38.6842	1.1811	1.40970			

Table 36. Analytic ring resistance

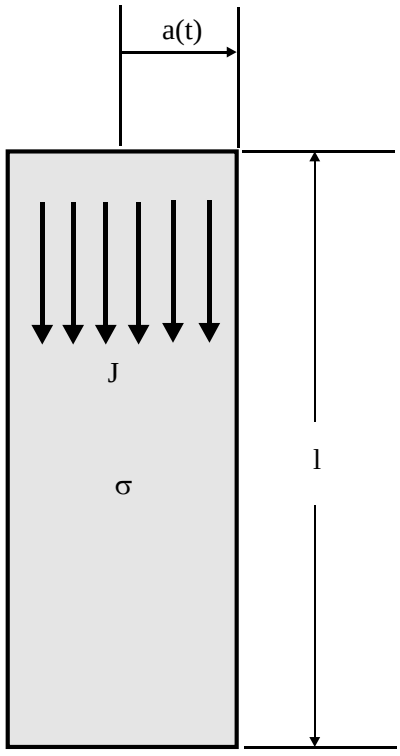

Figure 208. Side view of arc channel.

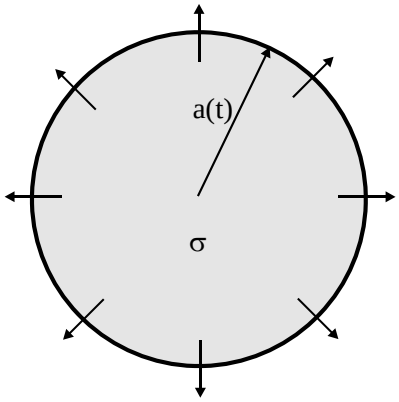

Figure 209. Top view of the arc channel.

$$a^2(t) = \left(\frac{4}{\pi^2 \rho_0 \xi \sigma}\right)^{1/3} \int_0^t I^{2/3}(\tau)\, d\tau$$

where the undisturbed gas density is found from

$$p = n_m k T$$

$$n_m = \rho / m_m$$

If we take $T = 273.15$ K, $p = 101,325$ Pa, $k = 1.38066 \times 10^{-23}$ J/K, $n_m = 2.687 \times 10^{25}$ m^{-3} and average molecular mass

$$m_m = 2 \times (0.2 \times 16 + 0.8 \times 14) \times 1.674 \times 10^{-27} \text{ kg}$$

$$\rho_0 \approx 1.295 \times 10^{-3} \text{ g/cm}^3 = 1.295 \text{ kg/m}^3$$

In this simple arc channel model the channel conductivity is taken as a fixed value [41] (the value taken here is a factor of two larger than that discussed above, but the density and temperature in the channel may not be the same as the preceding case since we are not considering an initial steady current here, nevertheless there is uncertainty about this value)

$$\sigma \approx 400 \text{ S/cm} = 4 \times 10^4 \text{ S/m}$$

and a constant dependent on gas properties, and somewhat on current rise rate, is taken as

$$\xi \approx 4.5$$

The resistance of the arc channel is then

$$R = \frac{\ell}{\pi a^2 \sigma} \tag{21}$$

For the exponential fall waveform

$$I(t) = I_0 e^{-\alpha t}$$

where for a fall time to half maximum of τ_f

$$\alpha = \ln(2/\tau_f)$$

$$a^2(t) = \left(\frac{4 I_0^2}{\pi^2 \rho_0 \xi \sigma}\right)^{1/3} \frac{3}{2\alpha} \left[1 - e^{-2\alpha t/3}\right] \rightarrow \left(\frac{4 I_0^2}{\pi^2 \rho_0 \xi \sigma}\right)^{1/3} \frac{3}{2\alpha}$$

Taking $I_0 = 50$ kA and $\tau_f = 50$ μs

$$a(\infty) = \left(\frac{2 I_0}{\pi \sqrt{\rho_0 \xi \sigma}}\right)^{1/3} \sqrt{\frac{3\tau_f}{2 \ln 2}} \approx 42.02 \text{ mm}$$

Using $t = 5$ μs

$$a(t) = \left(\frac{2I_0}{\pi\sqrt{\rho_0 \xi \sigma}}\right)^{1/3} \sqrt{\frac{3\tau_f}{2\ln 2}\left[1 - 2^{-2t/(3\tau_f)}\right]} \approx \left(\frac{2I_0}{\pi\sqrt{\rho_0 \xi \sigma}}\right)^{1/3} \sqrt{t} \approx 8.93 \text{ mm}$$

and at $t = 10$ μs $a(t) = 12.49$ mm. Note that at $t = 50$ μs $a(t) = 25.6$ mm. Also note that at 1 μs (this is really like 2 μs if the rise time is about a microsecond) we find $a(t) \approx 4.0$ mm and thus it is not surprising that the voltage of the first groove does not reach the full predicted voltage and that it begins to fall after a short time. It is also not surprising that the second groove begins to fall after a few microseconds, but does achieve the peak level.

Note that shot number two has a rise time of about 1 μs and a fall time of about 45 μs with a peak amplitude of about 40 kA. If we fit this with a decaying exponential with a step at time zero we can approximate the rise time by shifting the start time to 0.5 μs.

Taking $I_0 = 40$ kA and $\tau_f = 45$ μs

$$a(\infty) = \left(\frac{2I_0}{\pi\sqrt{\rho_0 \xi \sigma}}\right)^{1/3} \sqrt{\frac{3\tau_f}{2\ln 2}} \approx 20.46 \text{ mm}$$

At time $t = 0$ we begin at $a(t) = 0$ (we would add 0.5 μs for the rise time). Using $t = 1$ μs (we would add 0.5 μs for the rise time)

$$a(t) = \left(\frac{2I_0}{\pi\sqrt{\rho_0 \xi \sigma}}\right)^{1/3} \sqrt{\frac{3\tau_f}{2\ln 2}\left[1 - 2^{-2t/(3\tau_f)}\right]} \approx \left(\frac{2I_0}{\pi\sqrt{\rho_0 \xi \sigma}}\right)^{1/3} \sqrt{t} \approx 2.07 \text{ mm}$$

Using $t = 4$ μs (we would add 0.5 μs for the rise time)

$$a(t) = \left(\frac{2I_0}{\pi\sqrt{\rho_0 \xi \sigma}}\right)^{1/3} \sqrt{\frac{3\tau_f}{2\ln 2}\left[1 - 2^{-2t/(3\tau_f)}\right]} \approx \left(\frac{2I_0}{\pi\sqrt{\rho_0 \xi \sigma}}\right)^{1/3} \sqrt{t} \approx 4.1 \text{ mm} = r_i^{(2)} - h_i^{(2)}$$

Using $t = 9$ μs (we would add 0.5 μs for the rise time)

$$a(t) = \left(\frac{2I_0}{\pi\sqrt{\rho_0 \xi \sigma}}\right)^{1/3} \sqrt{\frac{3\tau_f}{2\ln 2}\left[1 - 2^{-2t/(3\tau_f)}\right]} \approx \left(\frac{2I_0}{\pi\sqrt{\rho_0 \xi \sigma}}\right)^{1/3} \sqrt{t} \approx 6.08 \text{ mm}$$

Using $t = 16$ μs (we would add 0.5 μs for the rise time)

$$a(t) = \left(\frac{2I_0}{\pi\sqrt{\rho_0 \xi \sigma}}\right)^{1/3} \sqrt{\frac{3\tau_f}{2\ln 2}\left[1 - 2^{-2t/(3\tau_f)}\right]} \approx 8.0 \text{ mm} = r_i^{(3)} - h_i^{(3)}$$

Using $t = 42$ μs (we would add 0.5 μs for the rise time)

$$a(t) = \left(\frac{2I_0}{\pi\sqrt{\rho_0 \xi \sigma}}\right)^{1/3} \sqrt{\frac{3\tau_f}{2\ln 2}\left[1 - 2^{-2t/(3\tau_f)}\right]} \approx 12.1 \text{ mm} = r_i^{(4)} - h_i^{(4)}$$

Using $t = 93.5$ μs (we would add 0.5 μs for the rise time)

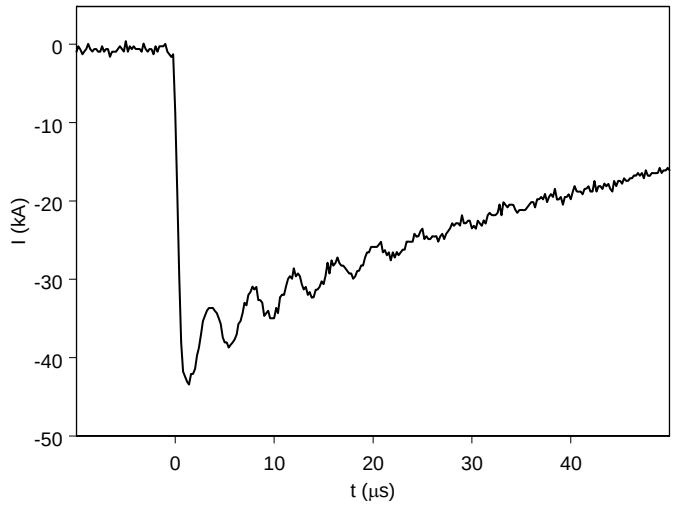

Figure 210. Drive current for Shot 2.

$$a\left(t\right)=\left(\frac{2I_0}{\pi\sqrt{\rho_0\xi\sigma}}\right)^{1/3}\sqrt{\frac{3\tau_f}{2\ln 2}\left[1-2^{-2t/(3\tau_f)}\right]}\approx 16.1\text{ mm}=r_i^{(5)}-h_i^{(5)}$$

The data from shot number two is shown in the following two figures

We next have attempted to sync the data by shifting the voltage data by

$$t-49.5\ \mu\text{s}\rightarrow t'$$

and have windowed the data from the current pulse start at $t'=0$ to $t=50$ μs. In addition we have scaled the voltage data by the current and by the average groove perimeter $2\pi\left\langle r\right\rangle=\pi\left(r_i+r_0\right)$, or by the current density K_0.

From this scaling we wanted to see a flat characteristic to the distant grooves and a fall-off in the closer grooved data. This is what we see on the figure. We have placed open circles at the beginning of the fall-off characteristics. In addition we have lined up the Braginskii expansion radius (adding one half microsecond to a step function excitation with 40 kA peak and 45 μs fall to half maximum) with the inner pickoff radius $r_i-h_i=\left\langle r\right\rangle-w/2-h_i$. The thinking here is that as the channel radius reaches this point the voltage of this particular groove region will begin to fall. Note that the Braginskii model is for an arc in gas rather than a discharge to a surface. To check this assumption we ran an ALEGRA simulation on a channel next to a surface and it agreed with the Braginskii model near the surface [29].

Another approach to scaling these results is to fit the current injection for each groove by the ratio of areas function

$$I^{(n)}/I_0\approx\left(\pi\left\langle r_n\right\rangle^2\right)/A\left(t\right)\ ,\ I^{(n)}/I_0<1$$

where $\tau_f=45$ μs

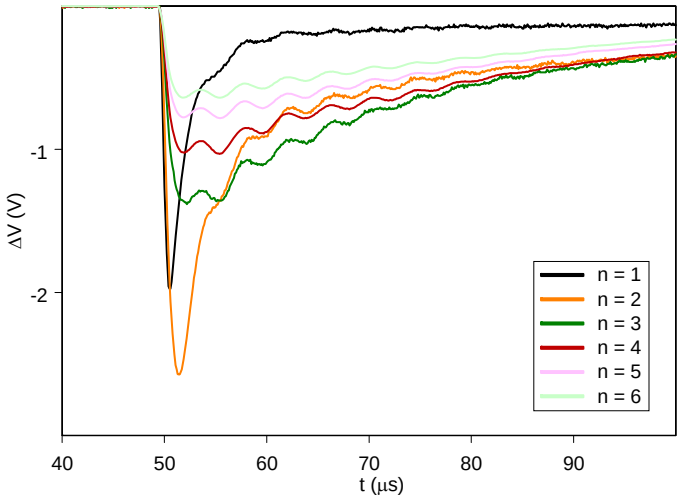

Figure 211. Measured voltage differences on grooves for Shot 2.

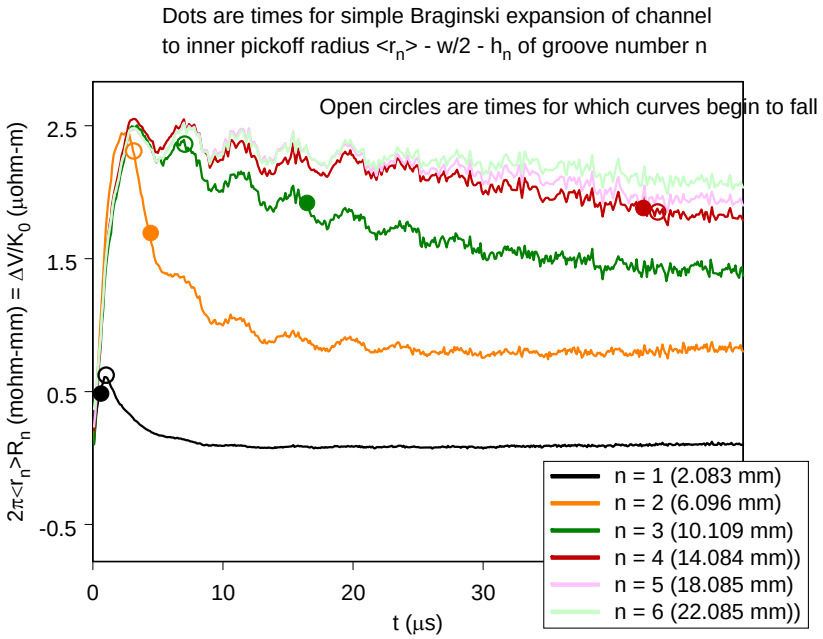

Figure 212. Difference voltages with surface current density scaled out (equal to groove perimeter times groove resistance). The beginning of the fall of the scaled data (open dots) indicates when the current column passes the groove radius. The current column radius prediction from a free space Braginskii hydrodynamic expansion model is shown as the solid dots.

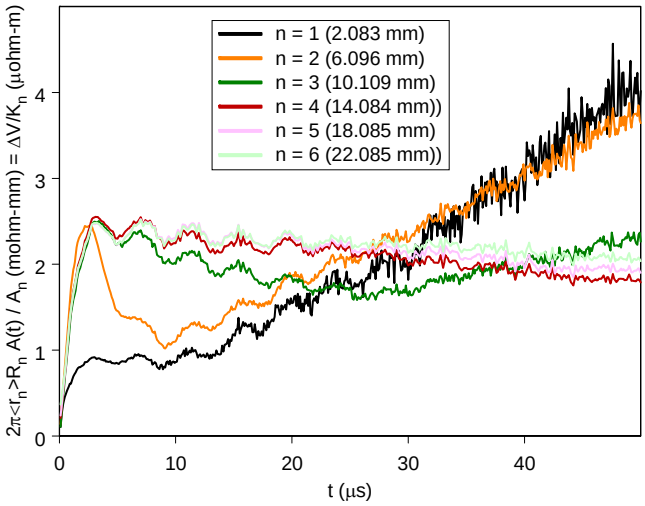

Figure 213. Manipulation of voltage differences by use of expanding area of discharge predicted by Braginskii model.

$$A(t) = \pi a^2(t) = A_\infty \left[1 - 2^{-2t/(3\tau_f)}\right]$$

and the constant A_∞ might be adjusted in value (in the Braginskii model)

$$A_\infty = \pi \left(\frac{2I_0}{\pi\sqrt{\rho_0 \xi \sigma}}\right)^{2/3} \frac{3\tau_f}{2\ln 2} \approx 20.5 \text{ mm}$$

We see from Figure 213 that the Braginskii front is expanding too slowly at early time (and hence does not boost the smaller rings sufficiently in this region because the front does not cross the center line of each early enough, although a continuous transition function based on the numerical cylinder model would do better than this center-groove step turn-on model) and too rapidly at late time (this boosts the smaller rings by virtue of the fact that the current density on these rings is becoming too small at late time in this model). In addition the droop observed in the distant rings (in both this figure and the preceding figure) seems like it is indicative of an expanding front thickness with time (rather than the sharp Braginskii front). An expanding front would allow some current beyond these rings at the later times, which when corrected would slightly boost these values.

The fact that we are measuring surface current rather than the current in the volume, in addition, to the fact that the electrode gap is only 0.25 in = 5 mm apart (a 2D spreading effect for large distances) are probably the drivers for these discrepancies.

Numerical Simulations In this sub-section we will describe the numerical methods used to determine the resistance between various points on the groove probe and how we used this information to interpret the measured results. The numerical simulations were done using the static, boundary element code **EIGER_S,** which solves for the potential and the normal gradient of the potential on a surface. We used **EIGER_S** to solve for the capacitance between two points on the probe and then used the analogy between capacitance and conductance to calculate the resistance between these two points.

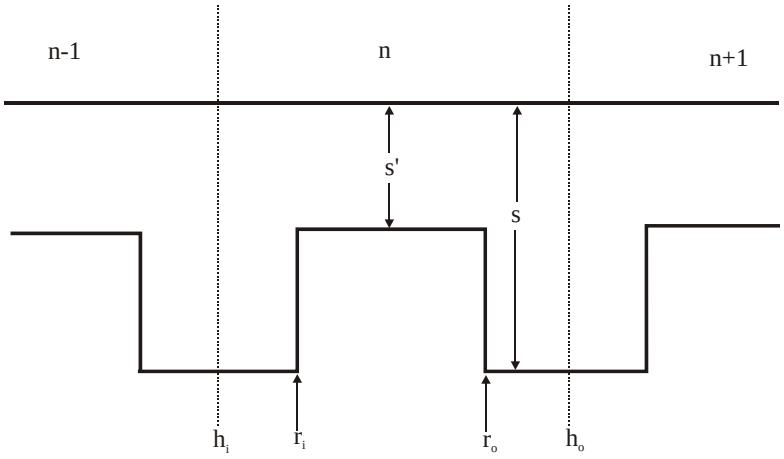

Figure 214. Cross section of groove n in the groove probe.

If we look at the cross-section of a portion of the groove probe we have the geometry shown in Figure 214. This cross-section is spun around the $\widehat{z}$ axis to form the groove probe. Shown is the region from pickoff point to pickoff point on either side of one groove.

Let us begin by calculating the resistance across a single groove from the ring-like surface formed by h_i to the ring-like surface formed by h_o. This can be done by solving for the capacitance of the cross-section shown in Figure 215. On the inner (h_i) and outer (h_o) surface we place a PEC boundary. On the inner PEC boundary (red) we set the potential to 1 volt and on the outer PEC boundary (yellow) we set the potential to be 0 volts. To confine the electric displacement $\overrightarrow{D}$ within the structure (the analog is that the electric current density J is confined within the conducting structure) we make all surfaces connecting the inner and outer surfaces – the green surfaces – to be PMC. The normal component of $\overrightarrow{D}$ is zero on a PMC surface. Since the problem is rotationally symmetric, we don't have to rotate the cross section 360^0 and grid the entire structure, rather, we can rotate the cross section a few degrees, place PMC surfaces on the exposed sides preventing the D field from crossing those surfaces, find the conductance of that structure and add the conductances in parallel to obtain the conductance of the entire 360^0. Initially, when we were calculating the conductance of single rings we gridded 45^0 sectors, but as we included more rings in the problem we went to 5^0 sectors to reduce the number of unknowns. The total conductance calculated was independent of the sector size chosen. We also didn't have to use the charge-balancing procedure. Perhaps because of the fact that the region was entirely enclosed by either PEC or PMC surfaces, the charge on all PEC surfaces added to zero implying that no electric flux went to a surface at infinity. The mesh is shown in Figure 216. Note that the colors of the mesh match the colors in Figure 215.

It is known that capacitance and conductance are analogous quantities so that conductance between two conductors (G) is related to the capacitance between two conductors (C) by

$$G = C\frac{\sigma}{\varepsilon}$$

where σ is the conductivity of the actual material between the two electrodes and ε is the assumed permittivity of the material in the problem that we solve [28]. In solving for the capacitance between the red and yellow electrode, we assume that the permittivity is that of free-space $\left(\varepsilon_0 = 8.854 \times 10^{-12}\ \mathrm{F/m}\right)$. The σ is that of stainless steel, $\sigma_{ss} = 1.4 \times 10^6\ (\Omega - \mathrm{m})^{-1}$ We assumed that the conductance did not vary spatially. We solve for the capacitance by

$$C = \frac{Q}{V}$$

where Q is the charge on one of the electrodes and V is the voltage difference between the two electrodes

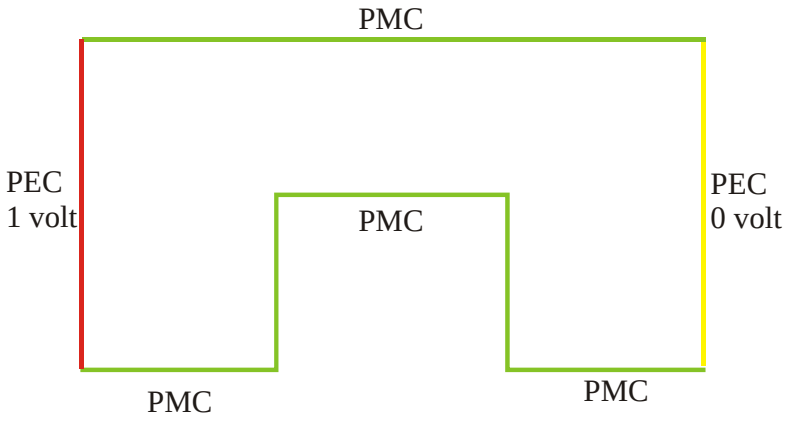

Figure 215. Cross section of ring with boundary conditions.

Figure 216. Mesh for single ring of groove probe.

(1 Volt in this case). The quantity that **EIGER_S** solves for on a PEC is $\partial\phi/\partial n$ at the center of each element where ϕ is the potential and n is the surface normal. This quantity is the normal electric field $\left(-\partial\phi/\partial n = \widehat{n}\cdot\overrightarrow{E}\right)$on the PEC electrode. Basic electromagnetics says

$$\begin{aligned} Q &= \int\limits_{electrode} \rho_s ds \\ &= \int\limits_{electrode} \left(\widehat{n}\cdot\overrightarrow{D}\right) ds \\ &= \int\limits_{electrode} \varepsilon\left(\widehat{n}\cdot\overrightarrow{E}\right) ds \\ &\approx -\varepsilon\sum_i \frac{\partial\phi_i}{\partial n}\Delta s_i \end{aligned}$$

where ρ_s is the charge density on the electrode, the integral is over a single electrode, the summation is over all elements on the electrode and Δs_i is the area of the ι^{th} element. The summation results are printed for each electrode by **EIGER_S** in the file ***.chg**. Once we obtain G of the gridded sector we get the total conductance between rings by adding the conductance of the sectors in parallel. Say we gridded a 45^0 sector then 8 of these sectors would make up the entire electrode ring and

$$G_{tot} = 8G$$

Finally, the resistance between the red and yellow electrodes is

$$R = \frac{1}{G_{tot}}$$

Finding the resistance between a top electrode and a point on the bottom is slightly more complicated and is discussed next. Consider the cross-section shown in Figure 217 where we want to find the resistance between the red disk on the top of the electrode and the point labeled $P1$ at the bottom of the electrode. We grid a 45^0 sector of the geometry as shown in Figure 216. To calculate the capacitance we use the calculated Q on the red electrode as before, but the voltage in the denominator is that between the red electrode (1 Volt) and the potential at the position $P1$. The quantity that EIGER_S solves for on a PMC surface is the electric potential ϕ at nodes, which are at the corners of elements. It is convenient when generating the grid to position a node at the position of interest. If the potential at the position of interest is ϕ_1 then

$$C = \frac{Q}{\phi_1}$$

The remainder of the calculation proceeds as before.

6.3.4 Results

If the radius of the red electrode in Figure 215 is assumed to be 400μm and we are interested in the transfer resistance between the red electrode and the point $P1$ (on axis but at the bottom of the electrode) we find that the charge on the red electrode is $1.756\times10^{-4}\varepsilon_0$ coulombs. The potential at $P1$ is 0.2529 V. The transfer capacitance between $P1$ and the outer electrode (at zero potential) of the 45^0 sector is then

$$\begin{aligned} C &= \frac{1.762\times10^{-4}\varepsilon_0}{0.2529} \\ &= 6.967\times10^{-4}\varepsilon_0 \end{aligned}$$

Using the analogy with $\sigma = 1.4\times10^6$ S/m, $G = 975.4$ S and accounting for the 8 sectors that make up the

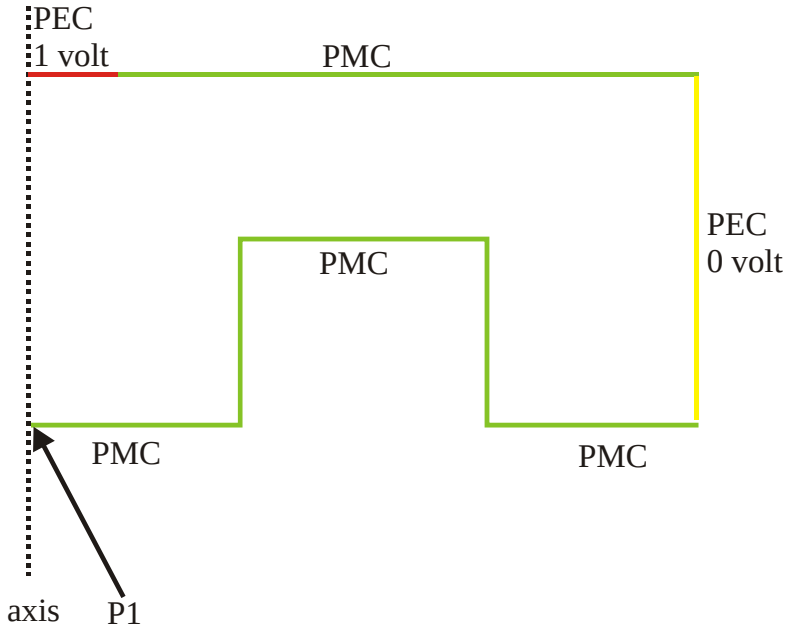

Figure 217. Cross section including the center axis of groove probe.

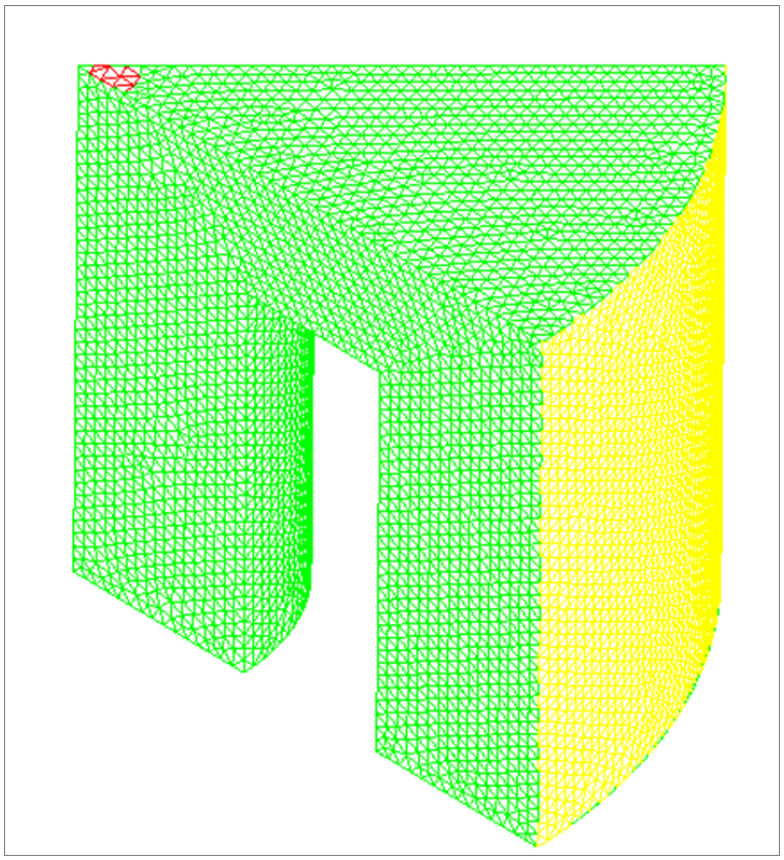

Figure 218. Mesh for center sector of groove probe.

n	Sector Angle	Element Size (μm)	Number of Elements	Charge/ε_0	V (Volts)	G (S)	G_{tot} (S)	R_{num} (μohm)	$R_{analytic}$ (μohm)
1	45^0	100	13.9 K	1.762×10^{-4}	0.2529	972	7803	128	143.15
2	45^0	100	24.8 K	1.558×10^{-3}	1.0	2181.	17440	57.3	60.68
2	10^0	100	9.9 K	3.462×10^{-4}	1.0	484.7	17450	57.3	60.68
3	10^0	100	12.6 K	5.808×10^{-4}	1.0	813.1	29270	34.2	36.41
4	10^0	100	15.4 K	8.261×10^{-4}	1.0	1156.5	4163.5	24.0	28.015
5	10^0	100	18.3 K	1.059×10^{-3}	1.0	1482.0	53351	18.7	20.003
5	2^0	100	4.6 K	2.127×10^{-4}	1.0	297.8	53600	18.7	20.003
5	2^0	200	1.1 K	2.130×10^{-4}	1.0	298.1	53663	18.6	20.003
6	2^0	100	4.9 K	2.599×10^{-4}	1.0	363.8	65482	15.3	16.370
7	2^0	200	1.4 K	3.053×10^{-4}	1.0	427.4	76936	13.0	13.946
8	2^0	100	5.8 K	3.533×10^{-4}	1.0	494.6	89019	11.2	12.003
9	2^0	100	6.3 K	3.995×10^{-4}	1.0	559.3	100673	9.9	10.595

Table 37. Comparison of numerical and analytic ring resistance

entire electrode

$$\begin{aligned} G_{tot} &= 8G \\ &= 7803.2 \text{ S} \end{aligned}$$

and $R = 128$ μohm. Calculations for this center section and each of the rings are given in Table 37 (the first entry is a transfer resistance but all other entries are radial ring-to-ring resistances just like in the preceding analysis).

Except for the center section (11% relative error), the numerical resistance results are close to ($< 7\%$ relative error), but slightly below the analytical results.

Our next step to interpret the experimental data for the groove probe, namely determine the current distribution on the top of the probe given measured voltage information on the rings on the bottom of the probe Figure 219 shows the cross section of the groove probe that we simulated. We calculated the resistance between the red electrode and the center of each of the rings out to the sixth ring using the method discussed in the previous subsection. The red electrode, set at 1 volt, represents a uniform disk of current flowing into the probe. To ensure uniformity of current, we tied all the elements on the red electrode to a single unknown and all the elements on the yellow electrode to another single unknown. We didn't do this in the previous section; each PEC element had an unknown associated with it, so the current could vary somewhat as a function of position on the electrode (the original PEC electrode would generate larger currents at the outer edge). The groove probe was meshed out to the mid-point of ring 7 (28098.75 μm). The current exits the probe at the yellow electrode (set at 0 volts). To determine the distribution of the current flowing into the probe as a function of time, we calculated the six ring resistances for red electrodes having six different radii. The radii chosen were at the center of rings 1 - 5 and half-way out the center cylinder, i.e., $r_0 = 749$ μm, $r_1 = 4083$ μm, $r_2 = 8096$ μm, $r_3 = 12109$ μm, $r_4 = 16085$ μm and $r_5 = 20085$ μm.

Figure 220 shows a mesh of a 5^0 sector of the cross-section. The red electrode shown is the r_1 case. The green surfaces are PMC. The mesh was constructed so that the potential at the center of each ring did not have to be interpolated.

Accounting for the fact that it takes 72 of the 5^0 sectors to make up the 360^0 probe, the resistance

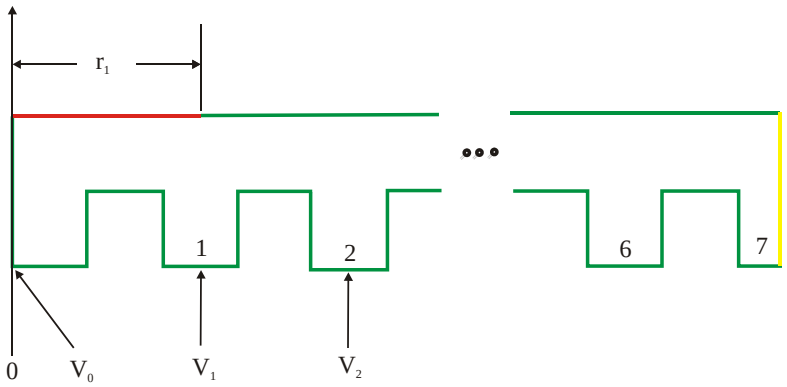

Figure 219. Cross section of simulated 7 ring groove probe.

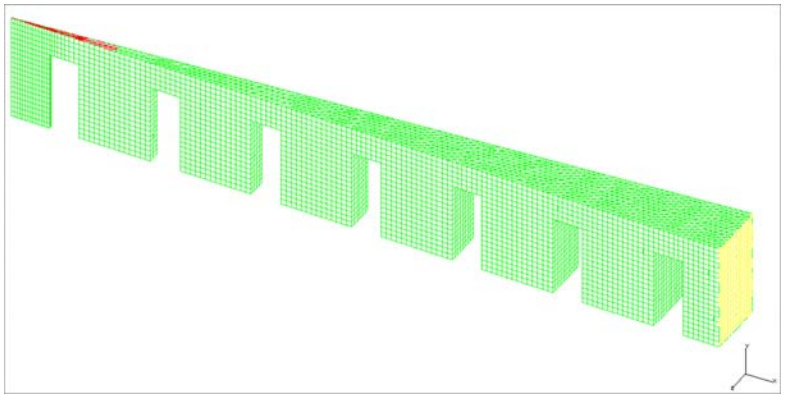

Figure 220. Mesh for $r_1 = 4083$ μm and 5^0 sector of groove probe.

n	V_n (Volt)	R_n (μohm)	ΔR_n (μohm)
0	0.6386	163.41	$---$
1	0.3580	290.33	126.92
2	0.2312	347.66	57.33
3	0.1560	381.67	34.01
4	0.1035	405.41	23.74
5	0.06268	423.86	18.45
6	0.02927	238.97	15.11

Table 38. Ring resistances for r_0 excitation

between the red electrode and the center of ring n is given by

$$R_n = \frac{(1.0 - V_n)\,\varepsilon_0}{72Q\sigma}$$

and difference

$$\Delta R_n = \frac{(V_n - V_{n-1})\,\varepsilon_0}{72Q\sigma}$$

Note that the center of the 0^{th} ring is defined to be the axis of the probe. V_n is the potential calculated at the center of ring n and σ is 1.4×10^6 $(\Omega - m)^{-1}$. As the disk radius becomes larger, voltages that are greater than 1 volt occur in the region below the red electrode (this could be partly due to the fact uniform current density produces a varying potential on the electrode with an average of unity). We note these voltages but set the calculated resistance to zero when this occurs.

If the red electrode has a radius r_0, $Q = 2.1938 \times 10^{-5}\varepsilon_0$ and the resistances between rings are shown in Table 38. If the red electrode has a radius r_1, $Q = 5.6288 \times 10^{-5}\varepsilon_0$ and the resistances between rings are shown in Table 39. If the red electrode has a radius r_2, $Q = 8.8552 \times 10^{-5}\varepsilon_0$ and the resistances between rings are shown in Table 40. If the red electrode has a radius r_3, $Q = 1.2847 \times 10^{-4}\varepsilon_0$ and the resistances between rings are shown in Table 41. If the red electrode has a radius r_4, $Q = 1.8545 \times 10^{-4}\varepsilon_0$ and the resistances between rings are shown in Table 42. If the red electrode has a radius r_5, $Q = 2.8203 \times 10^{-4}\varepsilon_0$ and the resistances between rings are shown in Table 43.

In the experiment a return-stroke current, which is shown in Figure 210 flows into the top of the probe. As the current flows across the grooves, the resistance of the probe causes a voltage drop between the rings. Voltage was measured as a function of time between the centers of six consecutive rings of the probe. These voltages can be expressed in terms of the already-defined voltages in Figure 219 as

$$\begin{aligned} \Delta V_1 &= V_1 - V_0 \\ \Delta V_2 &= V_2 - V_1 \\ \Delta V_3 &= V_3 - V_2 \\ \Delta V_4 &= V_4 - V_3 \\ \Delta V_5 &= V_5 - V_4 \\ \Delta V_6 &= V_6 - V_5 \end{aligned} \tag{22}$$

These voltages were plotted previously in Figure 211. To obtain the distribution of current on the top of the groove probe, we solve the following matrix equation for $[I]$

$$[\Delta R]\,[I] = [\Delta V] \tag{23}$$

where $[\Delta R]$ is a 6×6 matrix whose columns consist of the last column (labeled ΔR) of each of the above tables from $n = 1, ..., 6$. Column 1 of the matrix is from the r_0 table, column 2 from the r_1 table, and so forth. $[\Delta V]$ is a 6×1 vector, whose elements are ΔV_n as defined in Equation (22) at a given time. $[I]$ is a

n	V_n (Volt)	R_n (μohm)	ΔR_n (μohm)
0	1.0566	0.00	$---$
1	0.8792	21.29	21.29
2	0.5751	74.89	53.60
3	0.3885	107.78	32.89
4	0.2851	130.77	22.99
5	0.1565	148.67	17.90
6	0.07312	163.36	14.69

Table 39. Ring resistances for r_1 excitation

n	V_n (Volt)	R_n (μohm)	ΔR_n (μohm)
0	1.1115	0.00	$---$
1	1.0267	0.00	0.00
2	0.8867	12.69	12.69
3	0.5985	44.98	32.29
4	0.3973	67.53	22.55
5	0.2409	85.04	17.51
6	0.1126	99.41	14.37

Table 40. Ring resistances for r_2 excitation

n	V_n (Volt)	R_n (μohm)	ΔR_n (μohm)
0	1.1449	0.00	$---$
1	1.0457	0.00	0.00
2	1.0142	0.00	0.00
3	0.8732	9.79	9.79
4	0.5739	32.91	23.12
5	0.3469	50.43	17.52
6	0.1620	64.71	14.28

Table 41. Ring resistances for r_3 excitation

n	V_n (Volt)	R_n (μohm)	ΔR_n (μohm)
0	1.1831	0.00	$---$
1	1.0563	0.00	0.00
2	1.0375	0.00	0.00
3	1.0052	0.00	0.00
4	0.8469	8.19	8.19
5	0.5029	26.59	18.32
6	0.2336	41.00	14.41

Table 42. Ring resistances for r_4 excitation

n	V_n (Volt)	R_n (μohm)	ΔR_n (μohm)
0	1.2435	0.00	$---$
1	1.0718	0.00	0.00
2	1.0536	0.00	0.00
3	1.0369	0.00	0.00
4	0.9972	0.10	0.10
5	0.7967	7.15	7.05
6	0.3593	22.54	15.49

Table 43. Ring resistances for r_5 excitation

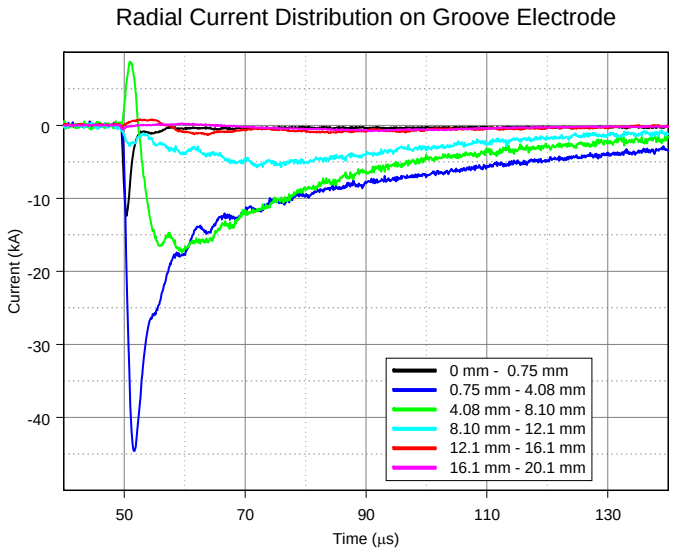

Figure 221. Current at various radii on groove probe.

6×1 vector whose elements, when solved, are the weighting of each current disk: $r_0, ..., r_6$. Since the disks overlap one another, in order to get the current flowing through the various annuluses, we first convert to current density by dividing each current by the disk area. We then add the current densities that contribute to each annulus and multiply the area of the annulus to convert back to current. In general,

$$I_i = \pi \left(r_i^2 - r_{i-1}^2\right) \sum_{n=i+1}^{6} \frac{I_n}{\pi r_n^2} \quad \text{for } r_{i-1} < r < r_i$$

A plot of I as a function of time is shown in Figure 221. The figure indicates that in the first half a microsecond the current is confined to the radius less than 4.08 mm (black and blue lines). Then the current stops flowing in the center disk and flows principally in the first annulus (blue line) until 10 μs after the start of the risetime., where it flows equally in the first and second annulus (blue and green line). Some current flows in the third annulus between 8.10 mm and 12.1 mm (the light cyan curve). The current doesn't seem to flow significantly in regions with radii larger than 12.1 mm (red and magenta curves). If the calculated current is added it compares well with the drive current as shown in Figure 222. The drive current was shifted 50.7 μs later in time to make the comparison. Note that the Braginskii predictions for the current column radius reaching the center of each groove shown in Figure 212 (note that the color coding is different in this previous figure) agree reasonably well with the rise of each current band in this data.

Another configuration that is used experimentally is the groove probe turned upside-down so that the return stroke attaches to the grooved side of the probe and the voltages are measured on the smooth side. This is shown in cross-section in Figure 223. Again we are simulating a portion of the full probe out to a point half-way across the seventh ring. We are calculating the resistance between the red electrode, placed on one of the rings on its top and at points aligned with the midpoints of six of the grooves. The red electrode, set at one volt, is put across each of the inner six rings. Figure 223 shows the red electrode at the 0^{th} ring position. The yellow electrode, set to 0 volt, is at the outer diameter of the simulation. Figure 224 shows the mesh applied to a 5^0 sector. In this case the red electrode is at the first ring position.

If the red electrode on the 0 ring , $Q = 1.601 \times 10^{-5} \varepsilon_0$ and the resistances between rings are shown in

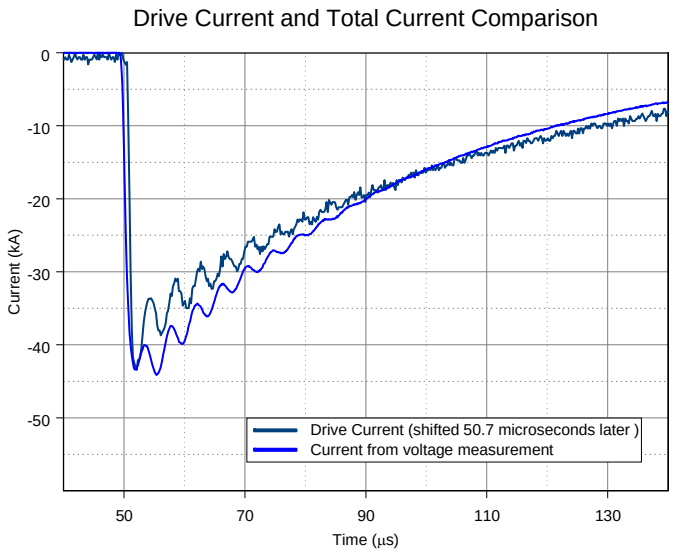

Figure 222. Comparison of calculated current and drive current.

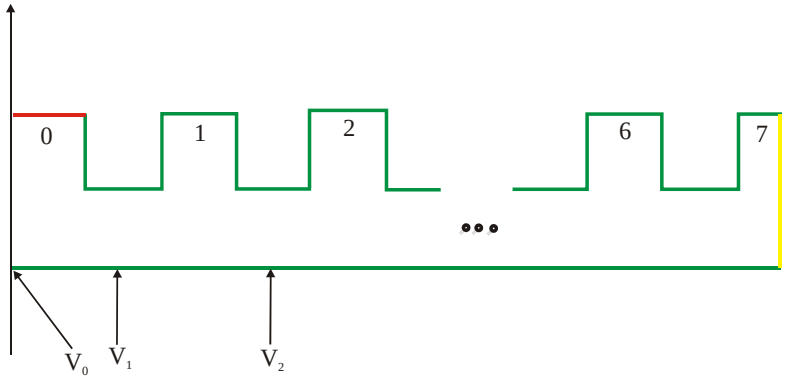

Figure 223. Inverted groove probe cross-section.

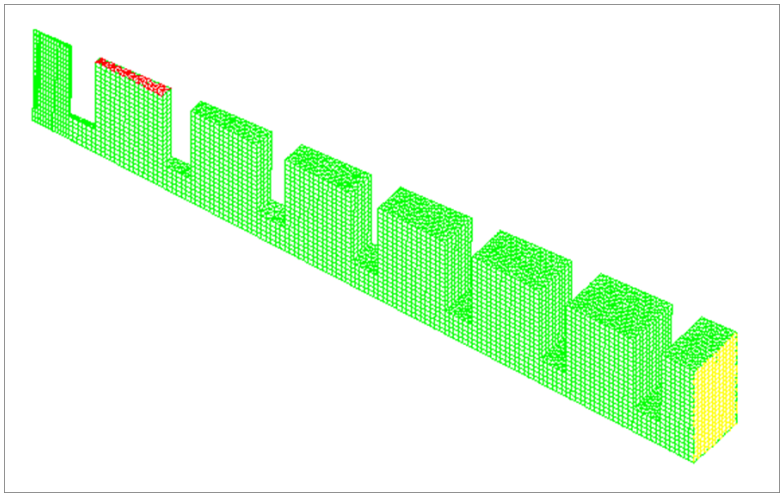

Figure 224. Mesh for first ring and 5^0 sector.

n	V_n (Volt)	R_n (μohm)	ΔR_n (μohm)
0	0.47200	326.03	$---$
1	0.35872	395.98	70.0
2	0.20846	488.76	92.8
3	0.13848	531.97	43.2
4	0.093068	560.01	28.0
5	0.059368	580.82	20.8
6	0.032522	597.40	16.6

Table 44. Inverted ring resistances for r_0 excitation

Table 44. If the red electrode on the 1 ring , $Q = 5.331 \times 10^{-5}\varepsilon_0$ and the resistances between rings are shown in Table 45. If the red electrode on the 2 ring, $Q = 8.493 \times 10^{-5}\varepsilon_0$ and the resistances between rings are shown in Table 46. If the red electrode on the 3 ring, $Q = 1.2579 \times 10^{-4}\varepsilon_0$ and the resistances between rings are shown in Table 47. If the red electrode on the 4 ring, $Q = 1.8750 \times 10^{-4}\varepsilon_0$ and the resistances between rings are shown in Table 48. If the red electrode on the 5 ring, $Q = 2.9885 \times 10^{-4}\varepsilon_0$ and the resistances between rings are shown in Table 49.

The measured voltage between the grooves is shown in Figure 225. Again we fill and solve Equation (23) and obtain the results for current in Figure 226. This current is wrong in that it predicts a huge, almost oscillating current from groove to groove. It is reminiscent of results from an ill-conditioned matrix system. We tried to find what was wrong with this solution but all of our efforts were fruitless and we had to move on (the problem is left to future work).

7 OBSERVATIONS

We have collected some of the general observations from the previous burnthrough experiments and analyses in Figure 227. Note that we have observed very large voltage levels (>20kV) through predrilled holes with cathodes protruding inside the barrier (and several kVs when even with the barrier), but not in burnthrough experiments in this project.

8 CONCLUSIONS

Using the original experiments of 1994 as a starting point, this new project was directed understanding the coupling mechanisms leading to electrical penetration of a metallic barrier when lightning burnthrough occurs. These mechanisms included indirect magnetic and electric field coupling, direct discharge attachment to the interior, and direct plasma conduction to the interior. We thus considered coupling to interior cables and metallic collectors by means of burnthrough of a metallic barrier using a combination of high level experiments in the Sandia Lightning Simulator and smaller laboratory scale experiments using a variety of pulsers. The experimental setup was similar to that used in the original experiments and involved burnthrough of a 0.05 inch thick aluminum barrier. High speed photography was used to understand what was taking place during the burnthrough event; these images were correlated in time with the electrical responses. Predrilled holes were also subjected to return strokes and other lower level drives in an effort to isolate certain penetration mechanisms.

More severe levels of continuing current charge transfer were used than in the original experiments. This resulted in higher levels of interior short circuit current and open circuit voltage as well as shorter current rise times and rise rates. Photography indicated that penetrant holes opened up prior to the second

n	V_n (Volt)	R_n (μohm)	ΔR_n (μohm)
0	0.86598	24.94	$---$
1	0.86401	25.31	0.0
2	0.69225	57.27	32.0
3	0.46004	100.48	43.2
4	0.30915	128.56	28.1
5	0.19720	149.40	20.8
6	0.10802	165.99	16.6

Table 45. Inverted ring resistances for r_1 excitation

n	V_n (Volt)	R_n (μohm)	ΔR_n (μohm)
0	0.89254	12.55	$---$
1	0.89059	12.78	0.0
2	0.88932	12.93	0.0
3	0.73373	31.10	18.2
4	0.49319	59.20	28.1
5	0.31457	80.07	20.9
6	0.17231	96.69	16.6

Table 46. Inverted ring resistances for r_2 excitation

n	V_n (Volt)	R_n (μohm)	ΔR_n (μohm)
0	0.89083	8.61	$---$
1	0.88864	8.78	0.0
2	0.88731	8.89	0.0
3	0.88830	8.81	0.0
4	0.73182	21.15	12.3
5	0.46688	42.04	20.9
6	0.25571	58.70	16.7

Table 47. Inverted ring resistances for r_3 excitation

n	V_n (Volt)	R_n (μohm)	ΔR_n (μohm)
0	0.87740	6.49	$---$
1	0.87509	6.61	0.0
2	0.87357	6.69	0.0
3	0.87460	6.64	0.0
4	0.87733	6.49	0.0
5	0.69741	16.01	9.9
6	0.38208	32.70	16.7

Table 48. Inverted ring resistances for r_4 excitation

n	V_n (Volt)	R_n (μohm)	ΔR_n (μohm)
0	0.84106	5.28	$---$
1	0.83787	5.38	0.0
2	0.83630	5.43	0.0
3	0.83716	5.41	0.0
4	0.84000	5.31	0.0
5	0.84380	5.19	0.0
6	0.6103	12.94	7.8

Table 49. Inverted ring resistances for r_5 excitation

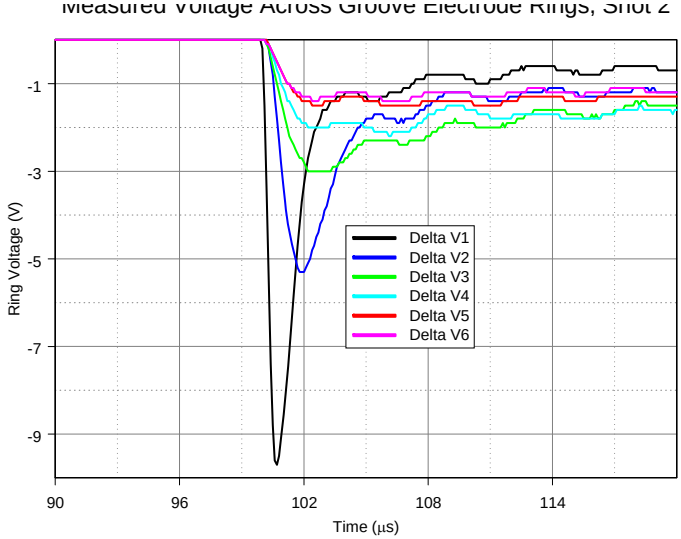

Figure 225. Measured voltage between the flipped or inverted groove probe.

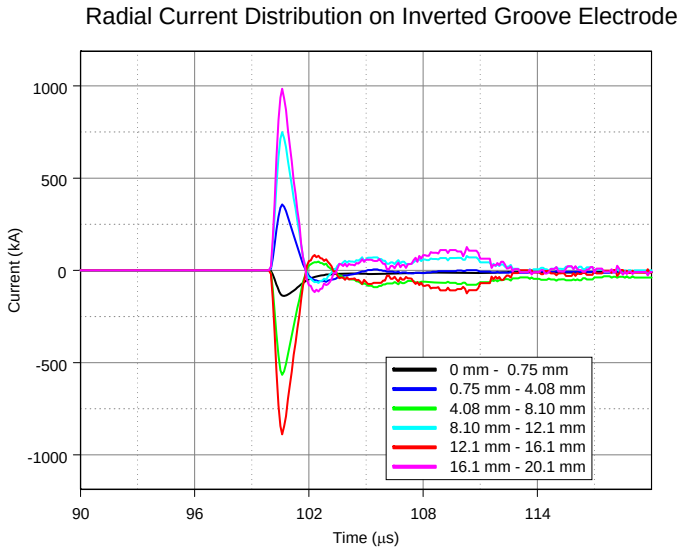

Figure 226. Current on the flipped or inverted groove probe.

- Extreme continuing current duration
  - Less than one inch diameter hole in fifty mil aluminum
  - One kiloampere penetrant current level with submicrosecond rise time
- Multiple return strokes
  - Enlarge hole size by less than factor of two
- Early time voltage penetration
  - Less than one kilovolt penetrant voltage level with less than ten nanosecond rise time
- Discharge paths and thresholds of single return stroke
  - For typical electrode offset (> 0.25 in) discharge path to barrier hole edge instead of interior collector or cable
- Indirect coupling levels from model
  - Magnetic levels for extreme lightning (scaled to extreme lightning) less than one kilovolt
  - Electric levels for extreme lightning (scaled to simulator open circuit drive) less than one kilovolt
- Continuing current plasma under open circuit load
  - Less than one kilovolt penetrant voltage due to continuing current arc resistance

Figure 227. Some observations from the burnthrough experiments and analyses associated with this project.

return stroke when more severe durations of continuing current were used during the interstroke interval. The effects of multiple return strokes were explored by initiating the continuing current with a thin starter wire (which quickly vaporizes) and reserving the two return strokes (the limit of the Sandia Lightning Simulator) for later in the burnthrough event. Interior open circuit voltages were never observed to be greater than one kilovolt in any burnthrough experiment (levels in the tens of kilovolts were observed when predrilled holes were used with rod electrodes protruding through the barrier) and short circuit currents only slightly exceeded one kiloampere.

Simple models of indirect (magnetic and electric) coupling to the interior conductor were compared and found to be in reasonable agreement with low level experiments when the injecting electrode was driven below ionization thresholds. Interestingly it was found that barrier thickness was an important parameter to include even when it was one tenth of the hole diameter. The indirect magnetic field coupling levels, when extrapolated to extreme lightning, result in interior open circuit voltage levels in the several hundred volt range.

Breakdown threshold calculations were made using ionization coefficients and numerical models for the field through the barrier hole from a rod-to-plane drive configuration (the experimental setup). These were compared to experimental measurements of interior voltages when the electrode was driven above breakdown levels. It was found that the threshold calculations could be correlated with the experiments as far as determining the path of the discharge. Exterior electrode tip positions led to small (ten volts) indirect interior voltage levels. Interior voltage levels of several kilovolts were reached as the electrode came into alignment with the barrier surface. Interior voltage levels of just under 10 kV were reached when the electrode protruded into the interior.

Approximate models were also constructed to examine penetrant current levels and interior voltages resulting from plasma conduction to the interior collector. These predictions were in the ballpark of the high level measurements of open circuit voltage and short circuit current.

9 REFERENCES

[1] R. J. Fisher and M. A. Umann, “Recommended baseline direct-strike lightning environment for stockpile-to-target sequences”, Sandia National Laboratories Report, SAND89-0192, May 1989.

[2] M. J. Kofoid, “Lightning discharge heating of aircraft skins”, Journal of Aircraft, vol. 7, no. 1, Jan.-Feb. 1970, pp. 21-26.

[3] P. F. Little, A. W. Hanson, J. A. Dobbing, “Arcs on metal sheets in simulated lightning discharges”, I.E.E.E. Conference, Seattle, 1977.

[4] A. Kern, “Time dependent temperature distribution in metal sheets caused by direct lightning strikes”, Sixth International Symposium on High Voltage Engineering, New Orleans, Louisiana, 28 Aug. - 1 Sept., 1989, pp. 1-4.

[5] A. Kern, “Simulation and measurement of melting effects on metal sheets caused by direct lightning strikes”, ICOCSE, Cocoa Beach, 1990, pp. 51-1 - 51-10.

[6] Dowden and P. Kapadia, “Plasma arc welding: a mathematical model of the arc,” J. Phys. D: Appl. Phys. Vol. 27, pp. 902-910, 1994.

[7] W. Zischank, S. Drumm, R. J. Fisher, G. H. Schnetzer, and M. E. Morris, "Reliable Simulation of Metal Surface Penetration by Lightning Continuing Currents, Conference 1995.

[8] G. H. Schnetzer, R. J. Fisher and M. A. Dinallo, “Measured responses of internal enclosures and cables due to burnthrough penetration of weapon cases by lightning”, Sandia National Laboratories Report, SAND94-0312, UC-706, August 1994.

[9] N. Cianos and E. T. Pierce, “A Ground-Lightning Environment for Engineering Usage,” TS-3141/7723,

Menlo Park: Stanford Research Institute, Aug. 1972.

[10] O. H. Nestor, "Heat Intensity and Current Density Distributions at the Anode of High Current, Inert Gas Arcs," Journal of Applied Physics, Vol. 33, No. 5, May 1962.

[11] K. C. Hsu, K. Etemadi and E. Pfender, "Study of the free-burning high-intensity arc", Journal of Applied Physics, vol. 54, no. 3, March 1983, pp. 1293-1301.

[12] R. W. Latham, "Small Holes in Cable Shields," AFWL Interaction Note 118, Sept. 1972.

[13] K. S. H. Lee (editor), **EMP Interaction: Principles, Techniques, and Reference Data**, Washington: Hemisphere Pub. Corp., 1986, pp. 187, 479-485, 559-570.

[14] R. L. Gluckstern and J. A. Diamond, "Penetration of Fields Through a Circular Hole in a Wall of Finite Thickness," IEEE Transactions on Microwave Theory and Techniques, Vol. 39, No. 2, pp. 274-279, Feb. 1991.

[15] R. E. Jorgenson and L. K. Warne, "Useful Equations for Calculating the Induced Voltage Inside a Faraday Cage that has been Struck by Lightning," Sandia National Laboratories Report, SAND2001-2950, Sept. 2001.

[16] W. R. Smythe, **Static and Dynamic Electricity**, New York: Hemisphere Pub. Corp., 1989, pp. 100-102.

[17] W. Hilberg, "From Approximations to Exact Relations for Characteristic Impedances," IEEE Trans. on Microwave Theory and Tech., Vol. MTT-17, No. 5, May 1969, pp. 259-265.

[18] L. K. Warne and K. C. Chen, "Effective Impedance of Bolt Loads on Narrow Slot Apertures Having Depth," Journal of Electromagnetic Waves and Applications, Vol. 6, No. 7, pp. 891-910, 1992.

[19] I. S. Gradshteyn and I. M. Ryzhik, **Table of Integrals, Series, and Products**, New York: Academic Press, 1965, p. 86.

[20] M. Abramowitz and I. A. Stegun (editors), **Handbook of Mathematical Functions**, New York: Dover, 1970, pp. 332-339, 409, 411, 556-565, 589-594, 807, 811.

[21] L. K. Warne, R. E. Jorgenson, and S. D. Nicolaysen, "Ionization Coefficient Approach to Modeling Breakdown in Nonuniform Geometries," Sandia National Laboratories Report, SAND2003-4078, Nov. 2003.

[22] L. K. Warne, R. E. Jorgenson and J. M Lehr, "Surface Interactions Involved in Flashover with High Density Electronegative Gases", Sandia National Laboratories Report, SAND2010-0268, January 2010.

[23] E. Nasser, **Fundamentals of Gaseous Ionization and Plasma Electronics**, New York: Wiley-Interscience, 1971.

[24] J. M. Meek and J. D. Craggs (Ed.), **Electrical Breakdown of Gases**, New York: John Wiley and Sons, 1978, p. 542.

[25] Y. P. Raizer, **Gas Discharge Physics**, Berlin: Springer, 1991, p. 355.

[26] H. N. Olsen, "Thermal and Electrical Properties of an Argon Plasma", The Physics of Fluids, Vol. 2, No. 6, Nov.-Dec. 1959, pp. 614-623.

[27] O. H. Nestor and H. N. Olsen, "Numerical Methods For Reducing Line And Surface Probe Data," SIAM Review, Vol 2, No. 3, July 1960, pp. 200-207.

[28] C. T. A. Johnk, **Engineering Electromagnetic Fields and Waves**, Wiley & Sons, New York, 1975, pp. 245-249.

[29] J. H. Niederhaus, private conversation.

[30] S. I. Braginskii, "Theory of the development of a spark channel, Sov. Physics - JEPT, vol. 34(7), pp. 1068-1074, Dec. 1958.

[31] Ya. B. Zel'dovich and Yu P. Raizer, **Physics of Shock Waves and High-Temperature Hydrodynamic Phenomena**, Vol. 1 and 2, New York: Academic Press, 1966, p. 195.

[32] T. A. Haill, K. R. Cochrane, C. J. Garasi, T. A. Mehlhorn, A. C. Robinson, and R. M. Summers,

"ALEGRA-MHD: Version 4.6," Sandia National Laboratories Report, SAND2004-5997, December 2004.

[33] W. Benenson, J. W. Harris, H. Stocker, H. Lutz (editors), **Handbook of Physics**, New York: Springer-Verlag, Inc., 2002, p. 1072.

[34] G. W. C. Kaye and T. H. Laby, **Tables of Physical and Chemical Constants**, New York: John Wiley & Sons, 1986.

[35] E. U. Condon and H. Odishaw (editors), **Handbook of Physics**, New York: McGraw-Hill Book Co., p. 7-35.

[36] I. S. Grigoriev and E. Z. Meilikhov (editors), **Handbook of Physical Quantities**, New York: CRC Press, pp. 519-520.

[37] L. D. Landau and E. M. Lifshitz, **Statistical Physics**, Oxford: Pergamon Press, 1958, pp. 225-228.

[38] Y. T. Lee and R. M. More, "An electron conductivity model for dense plasmas," Physics of Fluids, Vol. 27, No. 5, pp. 1273-1286, May 1984.

[39] W. Stygar, G. A. Gerdin, and D. L. Fehl, "Analytic electrical-conductivity tensor of a nondegenerate Lorentz plasma," Physical Review E. Vol. 66, pp. 046417/1-15, 2002.

[40] T. G. Newton, **Scattering Theory of Waves and Particles**, New York: Springer-Verlag, 1982, Chapter 18.

[41] L. K. Warne, R. E. Jorgenson, A. C. Day, and T. G. Olson, "Arc Models," Sandia National Laboratories Report, SAND2008-3648P, Sept. 15, 2010.

[42] F. W. Grover, **Inductance Calculations**, New York: Dover Pub., Inc., 1962, p. 35.

[43] T. H. Martin, J. F. Seamen, D. O. Jobe, "Energy Losses in Switches," Pulsed Power Conference, 1993.

[44] W. A. Johnson, L. K. Warne, and K. C. Chen, "Linear Diffusion and Internal Voltages in Conducting Enclosures Subjected to a Direct Lightning Strike," Electromagnetics, Vol 15, pp. 189-207, 1995.

[45] L. K. Warne, R. D. Moyer, T. E. Koontz, and M. E. Morris, "A Radial Transmission Line Material Measurement Apparatus," Sandia National Laboratories Report, SAND92-2788, May 1993.

[46] M. P. Desjarlais, "Practical Improvements to the Lee-More Conductivity Model Near the Metal-Insulator Transition," Contrib. Plasma Phys., Vol. 41, No. 2-3, 2001, pp. 267-270.

10 APPENDICES

Appendices giving details on each of the five experimental rounds are now listed along with a list of equipment used.

Summary of

Round 1 Testing

for LDRD

"Field and Charge Penetration by Lightning Burnthrough"

Authors: Leonard Martinez, SNL Department 1653
Larry Warne, SNL Department 1653
Roy Jorgenson, SNL Department 1653

Measurements by: Leonard Martinez, SNL Department 1653
Ed Bystrom, SNL Department 1535

Test Support: John Jojola, SNL Department 1653
Sandra Montoya, K-Tech Corporation

Revision: Rev 0.

Date: September 2009

Experimental Plan (First Round)

Abstract: This first round of experiments has three primary goals. The first is to demonstrate that we can repeat the essential voltage and current measurements conducted by Schnetzer [1] in the early 1990s. The second is to provide correlated high speed photographic records of the exterior plasma behavior and extent for both the return stroke and continuing current phases of the flash. The third is to conduct some additional shots directed at covering any missing characteristics, in the spirit of severe lightning, that might impact our understanding of the results and possibly redirect the concurrent and future modeling efforts.

The plan follows with extra shots and the photographic efforts separately called out.

0. Noise Shots

Conduct 50 kA return stroke shots with solid coupon in place to check integrity of Faraday cage. Repeat with bronze wool shorting collector to coupon to assess diffusion coupling to measurement loop. These should be repeated eventually for voltage measurement setup.

Conduct 50 kA return stroke shots with predrilled coupon (0.5 inch hole) in place. Check response with and without cable to Nanofast interrupted (before capacitance C_s on p. 9 of Schnetzer's report) to make sure the signal is that delivered by the cable (and not propagated around the break). This should be repeated eventually for voltage measurement setup.

Notes: Isolate Nanofast from chassis ground. Isolate CVT from collector cable. Use 0.005Ω CVR

Noise Shots- Current (See Appendix A)

Date	Shot #	SLS Current	d	Description
3/25/2009	9	48 kA	0.2	0.050" T6061 Al coupon, 1/4" Tungsten Electrode, 1/4" Electrode Gap. CVR, CVT and cables connected to Nanofasts. Collector Current (noise floor ~3 A)
3/25/2009	10	54 kA	0.2	0.050" T6061 Al coupon, 1/4" Tungsten Electrode, 1/4" Electrode Gap. Cables connected to Nanofasts (no CVR or CVT in Circuit). Collector Current (noise floor ~3 A)
3/25/2009	11	47 kA	0.2	0.050" T6061 Al coupon with 0.5" hole in center, 1/4" Tungsten Electrode, 1/4" Electrode Gap. Cables connected to Nanofasts (no CVR or CVT in Circuit). Collector Current (noise floor ~3 A)
3/25/2009	12	54 kA	0.2	0.050" T6061 Al coupon with 0.5" hole in center, 1/4" Tungsten Electrode, 1/4" Electrode Gap. CVR, CVT and cables connected to Nanofasts. Collector Current (700 A)
3/27/2009	4	46 kA	0.2	0.050" T6061 Al coupon. Bronze wool between coupon and brass collector, 1/4" Tungsten Electrode, 1/4" Electrode Gap, Nanofasts with cables connected to CVR and CVT. Collector Current (7 A)
3/27/2009	5	56 kA	0.2	0.050" T6061 Al coupon. #6-32 set screw between coupon and brass collector, 1/4" Tungsten Electrode, 1/4" Electrode Gap, Nanofasts with cables connected to CVR and CVT. Collector Current (40 A)
4/8/2009	3	52 kA	0.2	0.050" T6061 Al coupon with 0.125" hole in center, 1/4" Tungsten Electrode, 1/4" Electrode Gap. CVR, CVT and cables connected to Nanofasts. Collector Current (20 A)

Noise Shots- Voltage (See Appendix B)

Date	Shot #	SLS Current	d	Description
5/11/2009	3	50 kA	0.2	0.050" T6061 Al, 1/4" Tungsten Electrode, 1/4" Electrode Gap, Nanofast with cable connected to V50kΩ. Collector Voltage (noise floor 0.9 V)
5/11/2009	2	53 kA	0.2	0.050" T6061 Al, 1/4" Tungsten Electrode, 1/4" Electrode Gap, Nanofast with cable not connected to V50kΩ. Collector Voltage (noise floor ~0.3 V)
5/11/2009	1	49 kA	0.2	0.050" T6061 Al w/0.5" hole in center, 1/4" Tungsten Electrode, 1/4" Electrode Gap, Nanofast with cable not connected to V50kohm. Collector Voltage (noise floor ~0.3 V)
4/15/2009	8	54 kA	0.2	0.050" T6061 Al coupon with 0.5" hole in center, 1/4" Tungsten Electrode, 1/4" Electrode Gap. V50kΩ and cable connected to Nanofast. Collector Voltage (45 V)
4/17/2009	1	59 kA	0.2	0.050" T6061 Al coupon, bronze wool between coupon and brass collector,1/4" Tungsten Electrode, 1/4" Electrode Gap, V50kΩ and cable connected to Nanofast. Collector Voltage (0.8 V)
4/17/2009	2	55 kA	0.2	0.050" T6061 Al coupon, #6-32 set screw between coupon and brass collector,1/4" Tungsten Electrode, 1/4" Electrode Gap, V50kΩ and cable connected to Nanofast. Collector Voltage (1.8 V)
4/16/2009	1	61 kA	0.2	0.050" T6061 Al coupon with 0.125" hole in center, 1/4" Tungsten Electrode, 1/4" Electrode Gap. V50kΩ and cable connected to Nanofast. Collector Voltage (9 V)

1. Predrilled Hole - Disk Collector

Begin with 0.5 inch predrilled hole in 6061 alloy aluminum coupon.

Conduct 8 shots with 100 kA return strokes only. These shots relate to Table 5-1 of Schnetzer's report [1] (there a 0.125 inch hole was used).

Four shots will measure short circuit current using CVT and CVR (0.005Ω) sensors. Two of these use a spacing of 0.2 inches between the collector surface and the back surface of the coupon. Two use a spacing of 0.8 inches from the collector to the back surface of the coupon. Four shots will measure open circuit voltage by a technique similar to that described in Schnetzer's report. Two of these use a collector to coupon spacing of 0.2 inches and two use a spacing of 0.8 inches.

If these shots show currents significantly larger than 300 A or voltages larger than 100 V we will repeat measurements with 0.125 inch predrilled hole in coupon.

These shots will consume 1 or 2 coupons.

Note: We may want to increase the electrode spacing on these shots with the 0.5 inch holes to check the proximity and plasma jet effects.

Current Shots (See Appendix C)

Date	Shot #	SLS Current	d	Description
7/27/2009	2	112 kA	0.2	0.050" T6061 Al w/0.5" hole in center, 1/4" Tungsten Electrode, 1/4" Electrode Gap, Nanofasts with cables connected to CVR and CVT. Collector Current (600 A)
7/27/2009	3	113 kA	0.2	0.050" T6061 Al w/0.5" hole in center, 1/4" Tungsten Electrode, 1/4" Electrode Gap, Nanofasts with cables connected to CVR and CVT. Collector Current (600 A)
7/27/2009	4	105 kA	0.8	0.050" T6061 Al w/0.5" hole in center, 1/4" Tungsten Electrode, 1/4" Electrode Gap, Nanofasts with cables connected to CVR and CVT. Collector Current (700 A)
7/28/2009	2	111 kA	0.8	0.050" T6061 Al w/0.5" hole in center, 1/4" Tungsten Electrode, 1/4" Electrode Gap, Nanofasts with cables connected to CVR and CVT. Collector Current (700 A)
7/28/2009	3	107 kA	0.2	0.050" T6061 Al w/0.125" hole in center, 1/4" Tungsten Electrode, 1/4" Electrode Gap, Nanofasts with cables connected to CVR and CVT. Collector Current (100 A)

Voltage Shots (See Appendix D)

Date	Shot #	Current	d	Description
4/16/2009	2	119 kA	0.2	0.050" T6061 Al w/0.125" hole in center, 1/4" Tungsten Electrode, 1/4" Electrode Gap, V50kΩ and cable connected to Nanofast. Collector Voltage (13 V)
4/16/2009	6	108 kA	0.2	0.050" T6061 Al w/0.125" hole in center, 1/4" Tungsten Electrode, 1/4" Electrode Gap, V50kΩ and cable connected to Nanofast. Collector Voltage (14 V)
4/16/2009	5	105 kA	0.2	0.050" T6061 Al w/0.5" hole in center, 1/4" Tungsten Electrode, 1/4" Electrode Gap, V50kΩ and cable connected to Nanofast. Collector Voltage (80 V)
4/16/2009	7	103 kA	0.8	0.050" T6061 Al coupon with 0.5" hole in center, 1/4" Tungsten Electrode, 1/4" Electrode Gap. V50kΩ and cable connected to Nanofast. Collector Voltage (42 V)
4/16/2009	8	103 kA	0.8	0.050" T6061 Al coupon with 0.5" hole in center, 1/4" Tungsten Electrode, 1/4" Electrode Gap. V50kΩ and cable connected to Nanofast. Collector Voltage (42 V)
4/16/2009	9	95 kA	0.8	0.050" T6061 Al w/0.125" hole in center, 1/4" Tungsten Electrode, 1/4" Electrode Gap, V50kΩ and cable connected to Nanofast. Collector Voltage (8 V)

2. First Return Stroke and Continuing Current – Disk Collector
These four shots will use a 50 kA return stroke followed by a 500 A peak continuing current with a duration of approximately 2 seconds. The distance from the collector to the back surface of the coupon will be 0.2 inches. These shots relate to Tables 5-2 and 6-1 of Schnetzer's report [1].
Two shots will measure short circuit current using CVT and CVR (0.005Ω) sensors. Two shots will measure open circuit voltage.

These shots will consume 4 coupons.

Current Shots (See Appendix E)

Date	Shot #	SLS Current	d	Description
7/28/2009	5	53kA 538A	0.2	0.050" T6061 Al, no hole in center, 1/4" Tungsten Electrode, 1/4" Electrode Gap, Cables connected to CVR (TTI ODL). Collector Current (210A)
7/28/2009	6	51kA 532A	0.2	0.050" T6061 Al, no hole in center, 1/4" Tungsten Electrode, 1/4" Electrode Gap, Cables connected to CVR (TTI ODL). Collector Current (80A)

Voltage Shots (See Appendix F)

Date	Shot #	SLS Current	d	Description
2/12/2010	5	54kA 397A	0.2	0.050" T6061 Al, no hole in center, 1/4" Tungsten Electrode, 1/4" Electrode Gap, V5kΩ and cable connected to (TTI ODL). Collector Voltage (5V)
2/12/2010	6	55kA 387A	0.2	0.050" T6061 Al, no hole in center, 1/4" Tungsten Electrode, 1/4" Electrode Gap, V5kΩ and cable connected to (TTI ODL). Collector Voltage (10V)
2/12/2010	7	53kA 350A	0.2	0.050" T6061 Al, no hole in center, 1/4" Tungsten Electrode, 1/4" Electrode Gap, V5kΩ and cable connected to (TTI ODL). Collector Voltage (7V)

3. First Return Stroke, Continuing Current, Second Return Stroke – Disk Collector
These eight shots will consist of a 50 kA first return stroke for triggering the arc, a 500 A peak continuing current with 2 second duration, and a 100 kA second return stroke occurring at 100 ms after the first return stroke. These shots relate to Tables 5-3 and 6-1 in Schnetzer's report [1].
Four shots will measure short circuit current using CVT and CVR (0.005Ω) sensors. Two of these use a spacing of 0.2 inches between the collector surface and the back surface of the coupon. Two use a spacing of 0.8 inches from the collector to the back surface of the coupon. Four shots will measure open circuit voltage by a technique similar to that described in Schnetzer's report. Two of these will use a collector to coupon spacing of 0.2 inches and two use a spacing of 0.8 inches. **No voltage or current tests conducted for the above section.**

These 8 shots will consume 8 coupons.

In addition to these shots four more shots will be conducted with a 500 ms spacing between first and second return strokes. The purpose is to capture second return stroke coupling to the collector with extreme continuing current lightning burnthrough parameters [2] (the hole continually enlarges with time due to the continuing current). Two of these shots will measure short circuit current. One shot will use a collector to coupon spacing of 0.2 inches and one shot will use a collector to coupon spacing of 0.8 inches. The other two shots will measure open circuit voltage. Again one shot will use a collector to coupon spacing of 0.2 inches and one shot will use a collector to coupon spacing of 0.8 inches. **No open circuit voltage shots conducted.**

These four extra shots will consume another 4 coupons.

Current Shots (See Appendix G)

Date	Shot #	SLS Current	d	Description
4/6/2009	10 100ms	56kA 494A 88kA	0.2	0.050" T6061 Al coupon, 1/4" Tungsten Electrode, 1/4" Electrode Gap. CVR, CVT and cables connected to Nanofasts. Collector Current (86 A_438 A Clipped) Video
4/30/2009	5 100ms	46kA 398A 68kA	0.2	0.050" T6061 Al coupon, 1/4" Tungsten Electrode, 1/4" Electrode Gap. CVR, CVT and cables connected to Nanofasts. Collector Current (25 A)
4/6/2009	12 500ms	54kA 449A 113kA	0.2	0.050" T6061 Al coupon, 1/4" Tungsten Electrode, 1/4" Electrode Gap. CVR, CVT and cables connected to Nanofasts.. Collector Current (538 A) Video
4/6/2009	14 500ms	54kA 455A 71kA	0.8	0.050" T6061 Al coupon, 1/4" Tungsten Electrode, 1/4" Electrode Gap. CVR, CVT and cables connected to Nanofasts. Collector Current (286 A) Video
4/8/2009	2 100ms	55kA 463A 71kA	0.8	0.050" T6061 Al coupon, 1/4" Tungsten Electrode, 1/4" Electrode Gap. CVR, CVT and cables connected to Nanofasts.. Collector Current (101 A)

Visual recording will be carried out during this particular test sequence. This will consist of high speed photography (20 kframes/s) with two views of the exterior surface. We are after three things in these measurements. First, to correlate hole creation and plasma behavior and extent with electrical measurements. Second, to have a record of plasma spatial extent during the continuing current or free burning arc phase. Third, to capture plasma spatial extent of the return stroke phase. These three goals will require different exposure levels, the return stroke being the brightest (2-6 eV?), the free burning continuing arc being the next brightest (1-2 eV?), and the hot metallic hole surface being the dimmest (0.1 - 0.3 eV). Because of this different exposures on different shots will likely be required.

4. First Return Stroke and Continuing Current – Cable Collector

These four shots will use a 50 kA first return stroke followed by a 500 A peak continuing current with 2 second duration. These four shots will use a stripline cable below the coupon as a collector. The distance from the coupon back surface to the cable will nominally be 0.2 inches. The cable will rest on an insulating pad on top of the preceding disk collector. These shots relate to Table 7-1 of Schnetzer's report [1]. These shots will focus on common mode current and thus all conductors of the stripline will be connected in parallel at the measurement end. Two shots will measure short circuit current CVR (0.005Ω) and two shots will measure open circuit voltage. **No current shots conducted**

These four shots will consume 4 coupons and 4 cable samples.

Voltage Shots (See Appendix H)

Date	Shot #	SLS Current	d	Description
3/4/2010	4	56kA No CCG	0.2	0.050" T6061 Al, 1/4" Tungsten Electrode, 1/4" Electrode Gap, V5kΩ and cable connected to TTI(ODL). Cable collector not connected to ODL (NOISE SHOT) Collector Voltage (<1V)
3/4/2010	3	42 kA 361A	0.2	0.050" T6061 Al, 1/4" Tungsten Electrode, 1/4" Electrode Gap, V5kΩ and cable connected to TTI(ODL). Collector Voltage (22V clipped)
3/4/2010	5	32 kA 347A	0.2	0.050" T6061 Al, 1/4" Tungsten Electrode, 1/4" Electrode Gap, V5kΩ and cable connected to Nanofast. Collector Voltage (40V)

5. First Return Stroke, Continuing Current, Second Return Stroke – Cable Collector
These four shots will use a 50 kA first return stroke, a 500 A peak continuing current with 2 second duration, and a 100 kA second return stroke following the first stroke by 100 ms. The distance from the coupon to the cable will be 0.2 inches. These shots are not repeats of work in the Schnetzer report [1], but are included to provide cable data for the full lighting threat waveform. **No shots conducted for this task.**

Two shots will measure short circuit current and two shots will measure open circuit voltage.

These four shots will consume 4 coupons and 4 cable samples.

We also intend to add two extra shots with alternative cable samples provided by Kim Merewether. These are intended to see if there are any differences due to cable type. These two extra shots will use the same parameters as the preceding. One will measure short circuit current and one will measure open circuit voltage. **No shots conducted for this task.**

These extra two shots will consume 2 coupons and 2 alternative cable samples.

6. Indirect coupling-Magnetic and Electric Field
The purpose of these shots is to develop an understanding of magnetic and electric field coupling with a ½" predrilled hole with low level current and voltage sources. Both stripline cable (Velonex only) and brass collectors will be used. A commercially available Velonex model 590 will be used for the magnetic field tests and an SNL developed Pulse Arrested Spark Discharge PASD pulser with integral voltage probe will be used for the electric field tests. Distance between Back of pre-drilled coupon and brass collector or strip cable (without brass collector) is 0.2" (d=0.2"). 300MHz and 1GHz bandwidth Nanofast fiber optic links will be used to measure the collector voltages for the Velonex and PASD tests respectively.

Velonex/Magnetic Field Tests (See Appendix I)

Test #	Test Date	Coupling Mechanism	Type of Noise Shot	Velonex drive relative to coupon	Cable Orientation
1	7/31/2009	Inductive Noise shot	Both clip leads on barrel	Perpendicular to coupon, **I=3402 A**	Vertical **Vcable=2.6mV**
2	7/31/2009	Inductive Noise shot	Both clip leads on barrel	Parallel to coupon (Horizontal), **I=3354 A**	Vertical **Vcable=2.6mV**
3	7/31/2009	Inductive	Both clip leads on	1/4" full radius brass electrode,	Vertical

		Noise shot	barrel	1/4" from coupon, **V=3890 V**	**Vcable=3.0mV**
4	7/31/2009	Inductive Noise shot	Both clip leads on barrel	Perpendicular to coupon, **I=3422 A**	Horizontal **Vcable=2.5mV**
5	7/31/2009	Inductive Noise shot	Both clip leads on barrel	Parallel to coupon (Horizontal), **I=3424 A**	Horizontal **Vcable=2.5mV**
6	7/31/2009	Inductive Noise shot	Both clip leads on barrel	1/4" full radius brass electrode, 1/4" from coupon, **V=3873 V**	Horizontal **Vcable=2.8mV**
7	7/31/2009	Inductive	Test Shot	1/4" full radius brass electrode, 1/4" from coupon, **V=3810 V**	Horizontal **Vcable=2.7mV**
8	7/31/2009	Inductive	Test Shot	Parallel to coupon (Horizontal), **I=3437 A**	Horizontal **Vcable=105mV**
9	7/31/2009	Inductive	Test Shot	Perpendicular to coupon, **I=3372 A**	Horizontal **Vcable=67mV**
10	7/31/2009	Inductive	Test Shot	Perpendicular to coupon, **I=3342 A**	Vertical **Vcable=149mV**
11	7/31/2009	Inductive	Test Shot	Parallel to coupon (Horizontal), **I=3408 A**	Vertical **Vcable=656mV**
12	7/31/2009	Inductive	Test Shot	1/4" full radius brass electrode, 1/4" from coupon, **V=3868 V**	Vertical **Vcable=2.5mV**

PASD Electric Field Tests (See Appendix J)

Test #	**Test date**	**Coupling Mechanism**	**Type of Shot**	**PASD drive relative to coupon**	**Cable orientation**
Cal	8/11/2009	PASD Calibration Shot	PASD Calibration	PASD Calibration Shot **VPASD=2190 V**	**Vprobe=2190 V**
1	8/11/2009	Capacitive	Both clip leads on barrel (Collector/Noise)	1/4" full radius brass electrode, 1/4" from coupon, **VPASD=4056 V**	Horizontal **Vcollect=53 mV**
2	8/11/2009	Capacitive	Collector Shot	1/4" full radius brass electrode, 1/4" from coupon, **VPASD=4390 V**	Horizontal **Vcollect=358 mV**
3	8/11/2009	Capacitive	Both clip leads on barrel (Cable/Noise)	1/4" full radius brass electrode, 1/4" from coupon, **VPASD=9222 V**	Horizontal **Vcable=88 mV**
4	8/11/2009	Capacitive	Cable Shot	1/4" full radius brass electrode, 1/4" from coupon, **VPASD=9054 V**	Horizontal **Vcable=1316 mV**
2	9/3/2009	PASD Calibration Shot	PASD Calibration	PASD Calibration Shot **VPASD=2650 V**	**Vprobe=2650 V**
3	9/3/2009	Capacitive	Both clip leads on barrel (Cable/Noise)	1/4" full radius brass electrode, 1/4" from coupon **VPASD=8000 V**	Horizontal **Vcable=80 mV**
1	9/3/2009	Capacitive	Cable Test Shot	1/4" full radius brass electrode, 1/4" from coupon **VPASD=10000 V**	Horizontal **Vcable=2.2 V**
4	9/3/2009	Capacitive	Both clip leads on barrel (Collector/Noise)	1/4" full radius brass electrode, 1/4" from coupon **VPASD=10000 V**	Brass Collector **Vcollect=86 mV**
5	9/3/2009	Capacitive	Collector Test Shot	1/4" full radius brass electrode, 1/4" from coupon **VPASD=10500 V**	Brass Collector **Vcollect=645 mV**

References:

[1] G. H. Schnetzer, R. J. Fisher, and M. A. Dinallo, “Measured Responses of Internal Enclosures and Cables Due To Burnthrough Penetration of Weapon Cases by Lightning,” SAND94-0312, August 1994.

[2] R. J. Fisher and M. A. Uman, “Recommended Baseline Direct-Strike Lightning Environment for Stockpile-to-Target Sequences,” SAND 89-0192, May 1989.

Task 0: Noise Shots-Current

Description:

Solid 0.050" 6061 Al, 1/4" Tungsten Electrode, 1/4" Electrode Gap, Nanofasts with cables connected to CVR and CVT

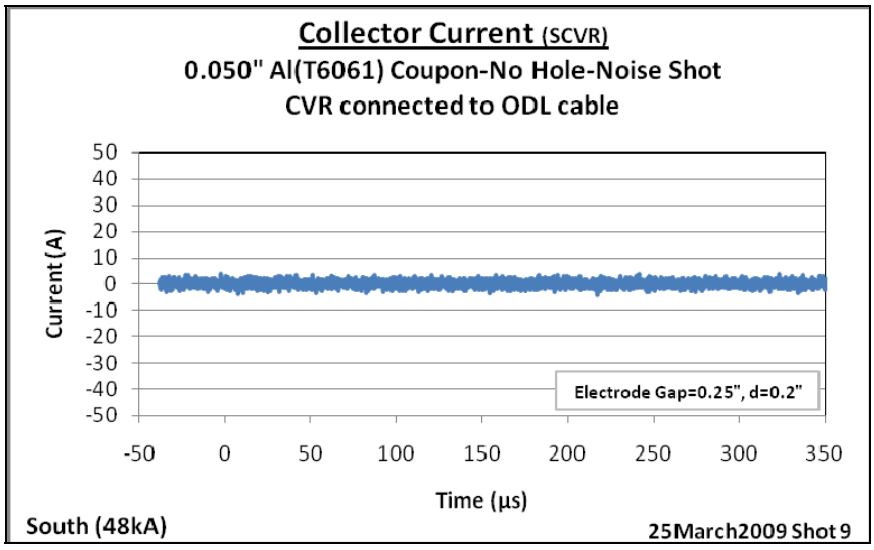

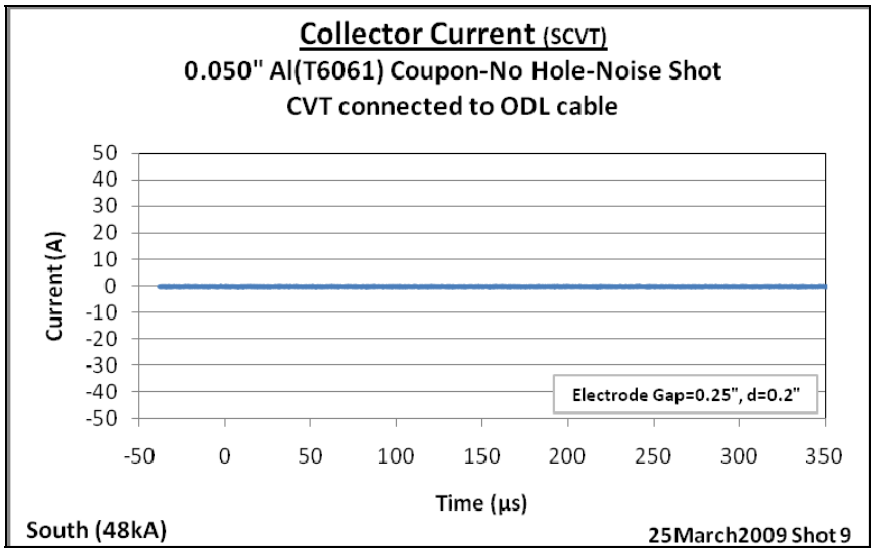

Task 0: Noise Shots-Current

Description:

Solid 0.050" 6061 Al, 1/4" Tungsten Electrode, 1/4" Electrode Gap, Nanofasts with cables connected. CVR and CVT not connected

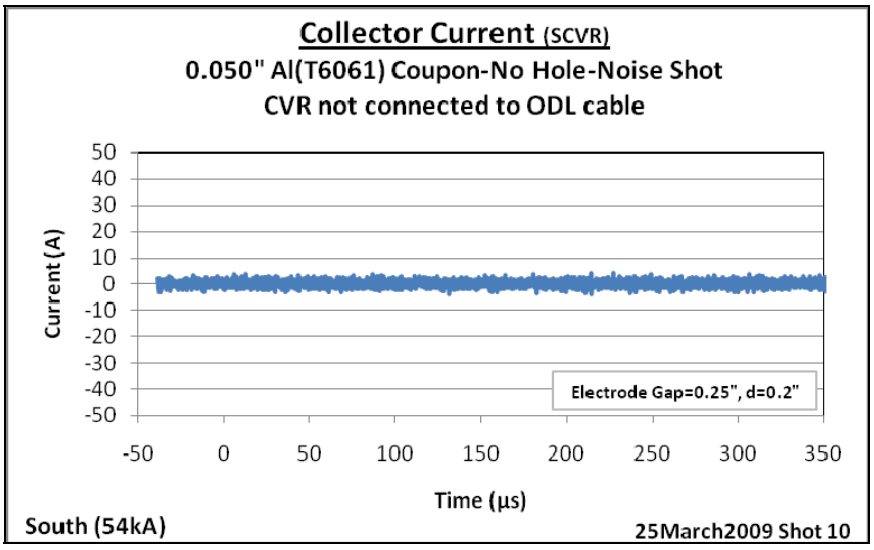

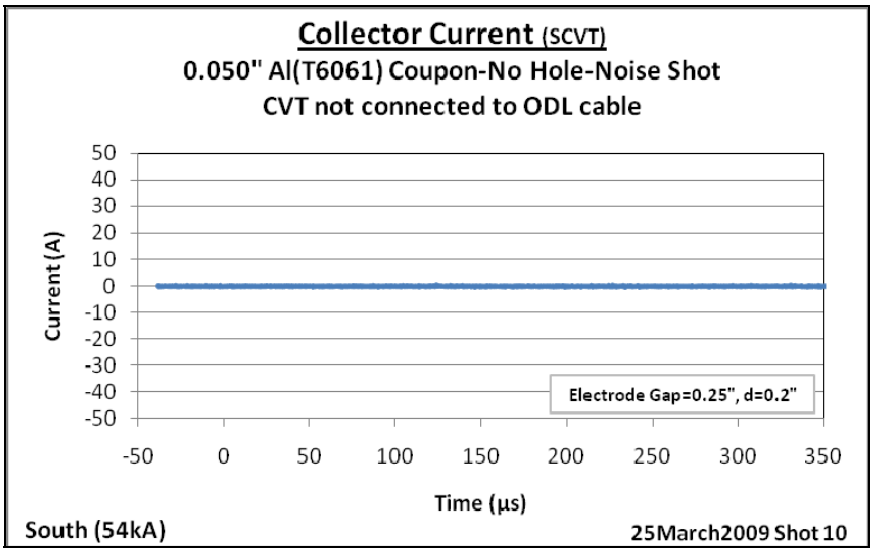

Task 0: Noise Shots-Current

Description:

0.050" 6061 Al w/0.5" hole in center, 1/4" Tungsten Electrode, 1/4" Electrode Gap, Nanofasts with cables connected. No CVR and CVT

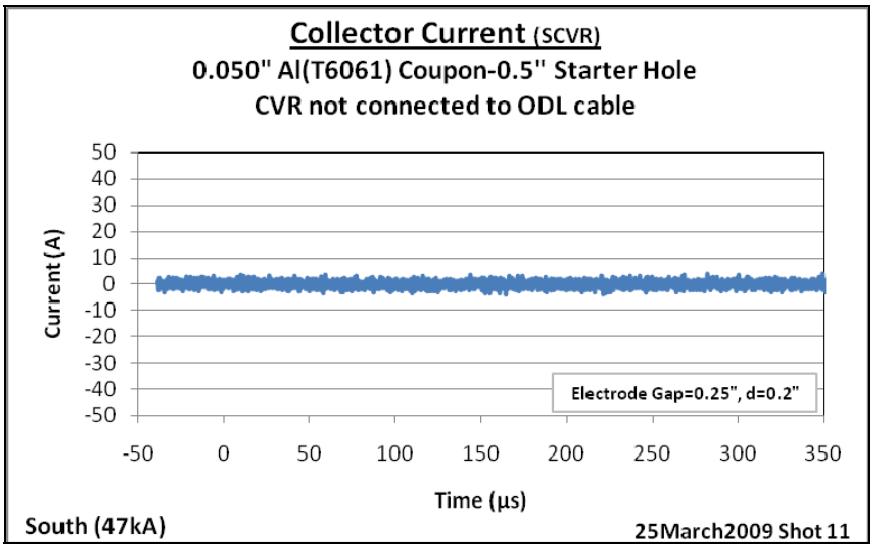

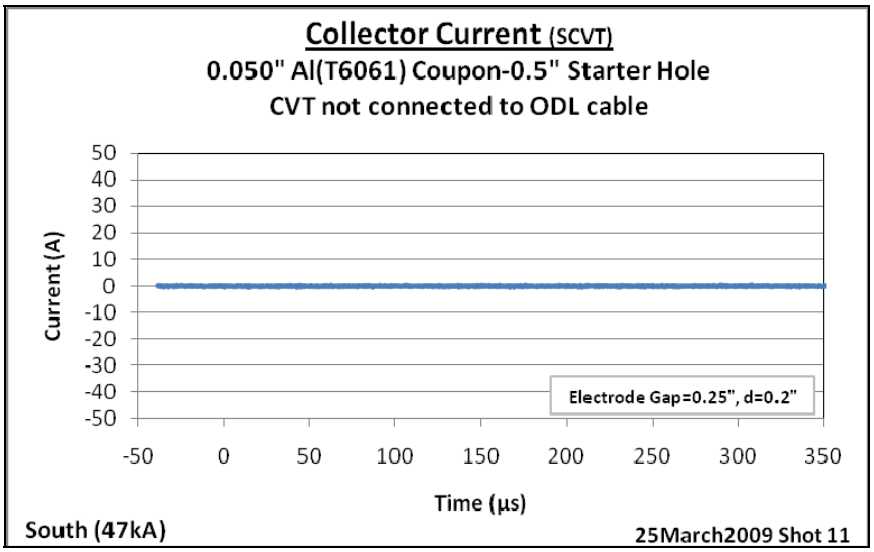

Task 0: Noise Shots-Current

Description:

0.050" 6061 Al w/0.5" hole in center, 1/4" Tungsten Electrode, 1/4" Electrode Gap, Nanofasts with cables connected to CVR and CVT

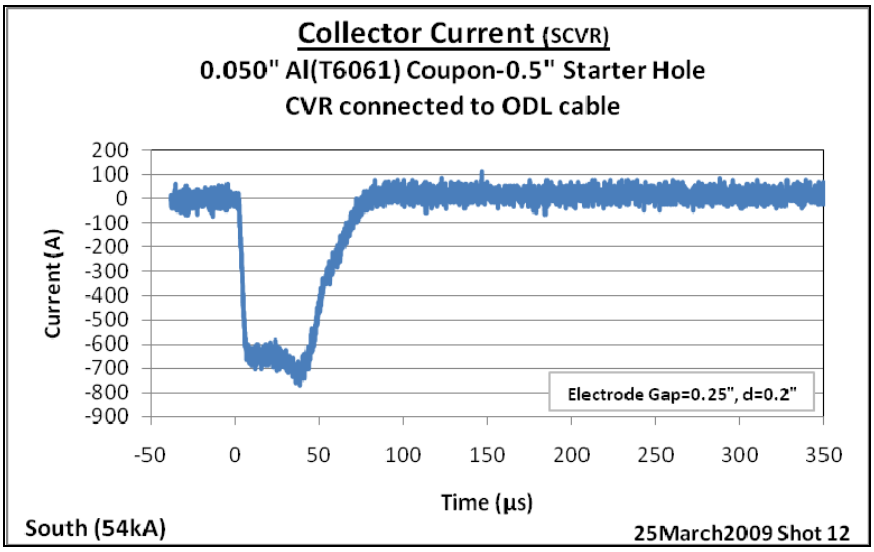

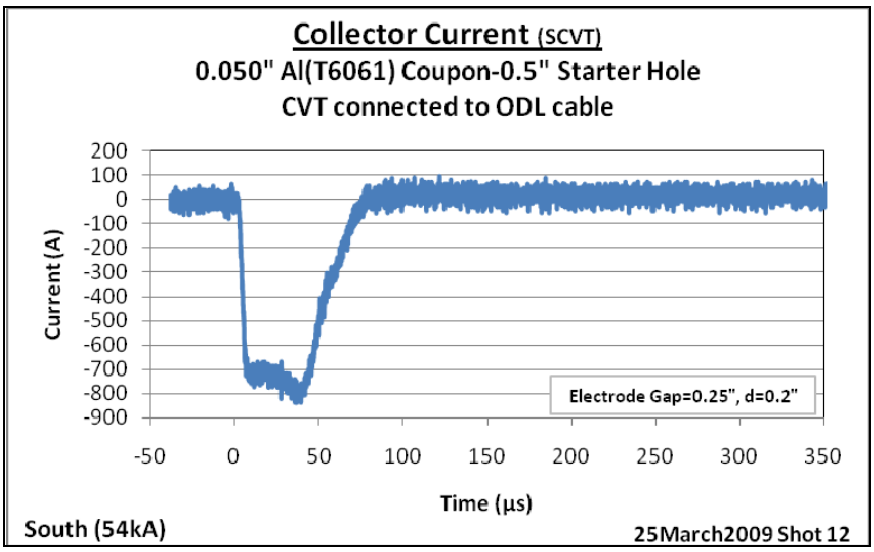

Task 0: Noise Shots-Current

Description:

0.050" 6061 Al w/bronze wool between coupon and brass collector, 1/4" Tungsten Electrode, 1/4" Electrode Gap, Nanofasts with cables connected to CVR and CVT

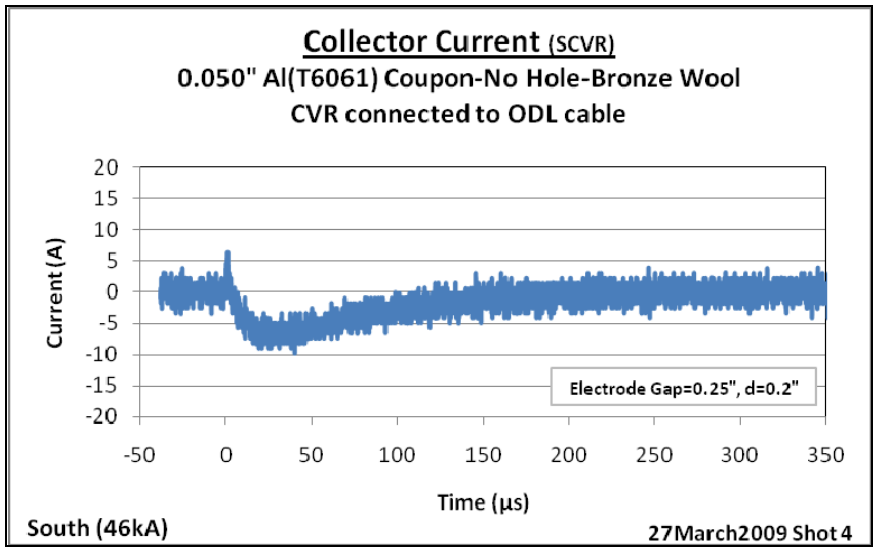

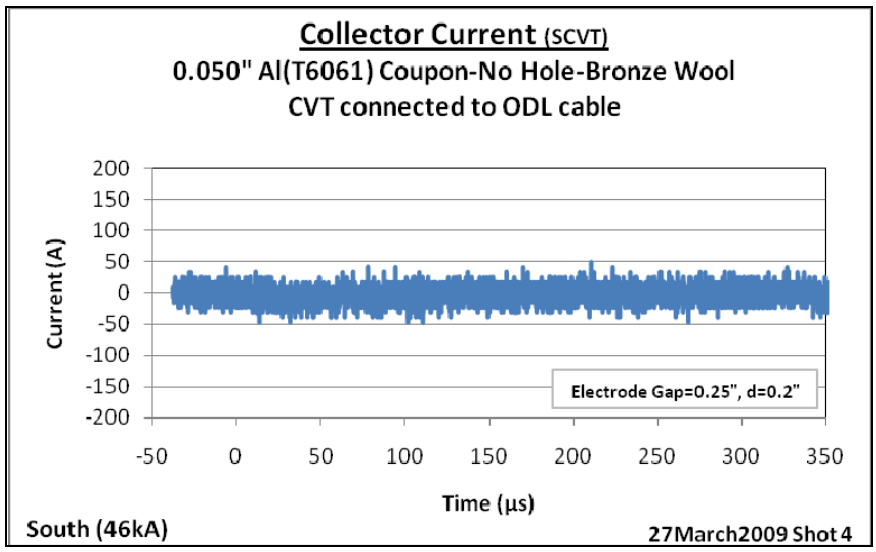

Task 0: Noise Shots-Current

Description:

0.050" 6061 Al w/#6-32 set screw between coupon and brass collector, 1/4" Tungsten Electrode, 1/4" Electrode Gap, Nanofasts with cables connected to CVR and CVT

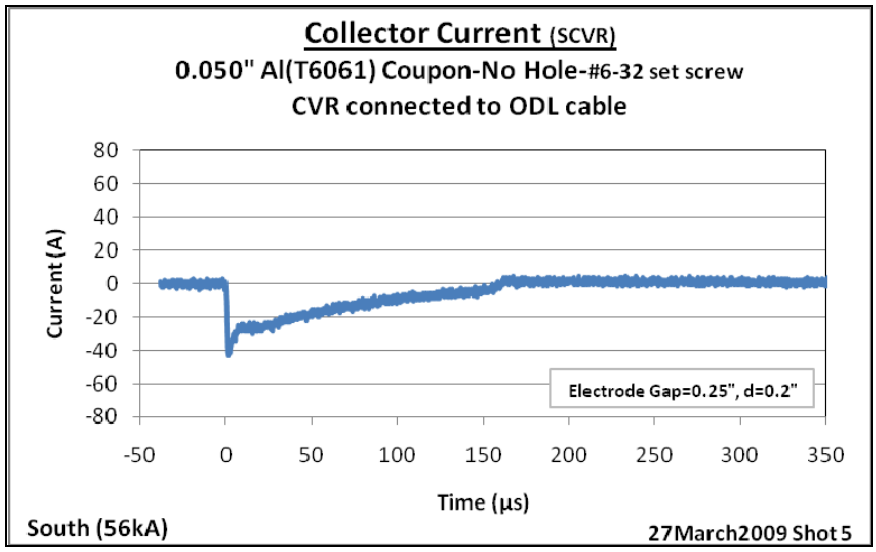

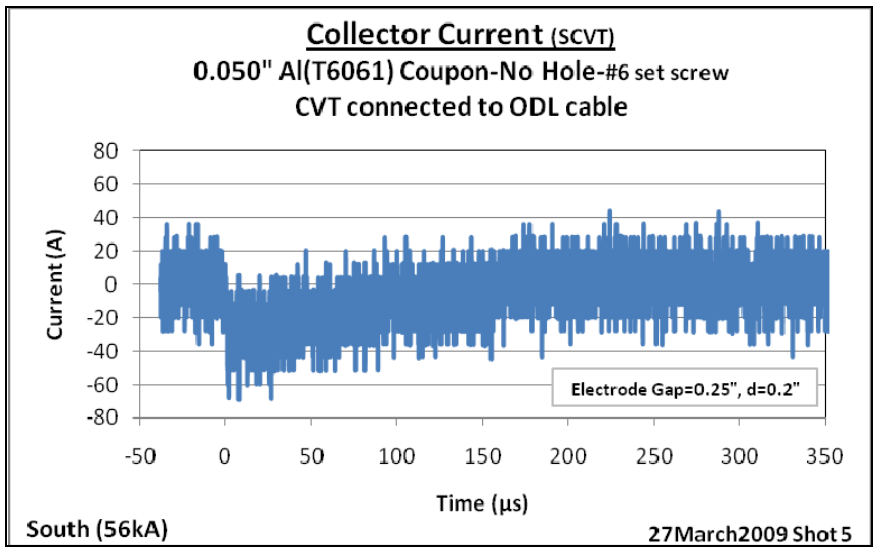

Task 0: Noise Shots-Current

Description:

0.050" Aluminum Coupon (No grid) 1/8" hole in center of coupon, 1/4" Tungsten Electrode, 1/4" Electrode Gap, Nanofasts with cables connected to CVR and CVT. (0.2" between Coupon and collector)

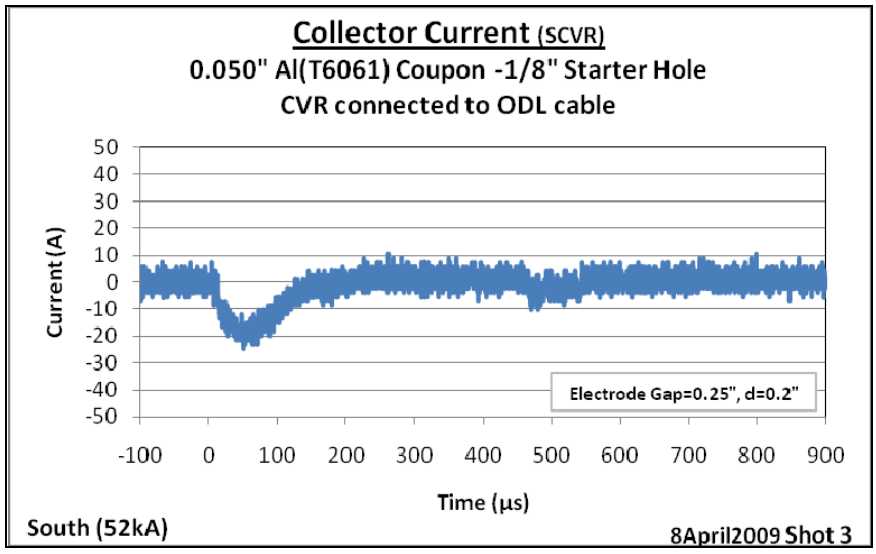

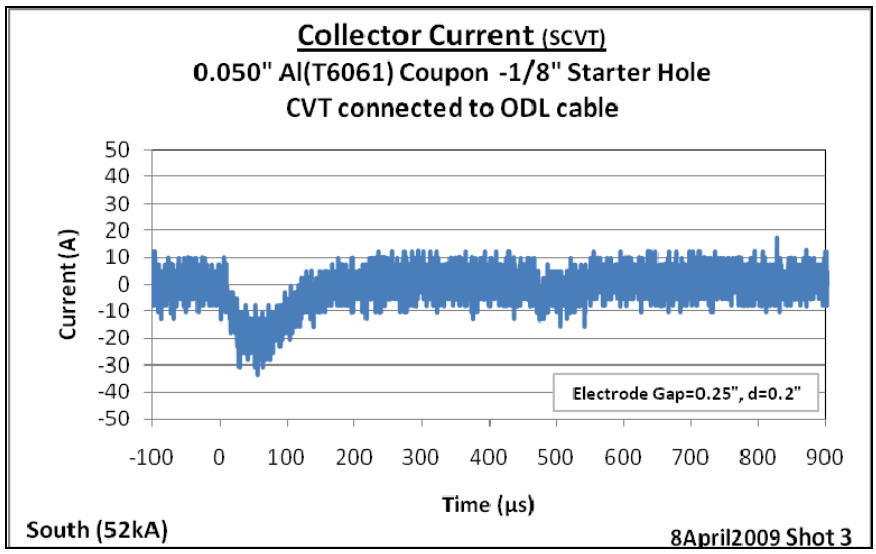

Task 0: Noise Shots-Voltage

Description:

0.050" T6061 Al , 1/4" Tungsten Electrode, 1/4" Electrode Gap, Nanofast with cable connected to V50kohm. (0.2" between Coupon and collector)

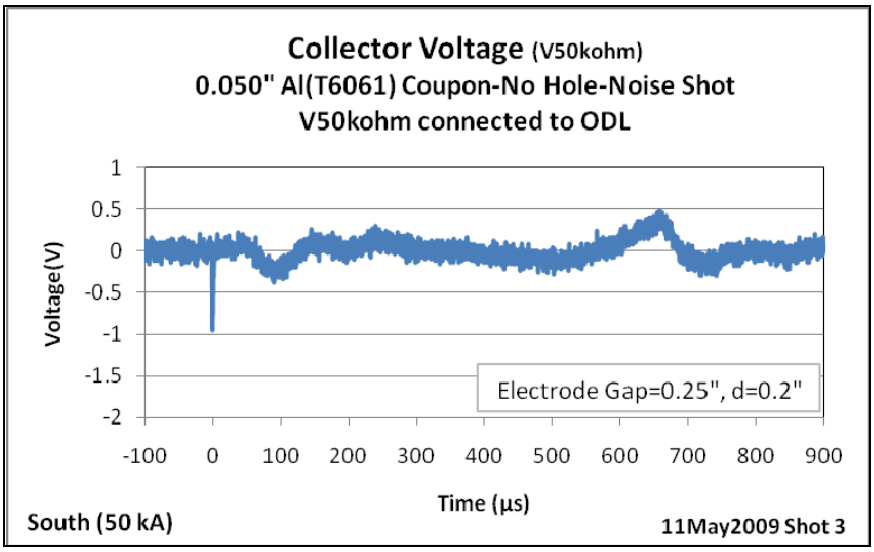

Description:

Noise-0.050" T6061 Al w/0.5" hole in center, 1/4" Tungsten Electrode, 1/4" Electrode Gap, Nanofast with cable not connected to V50kohm. (0.2" between Coupon and collector)

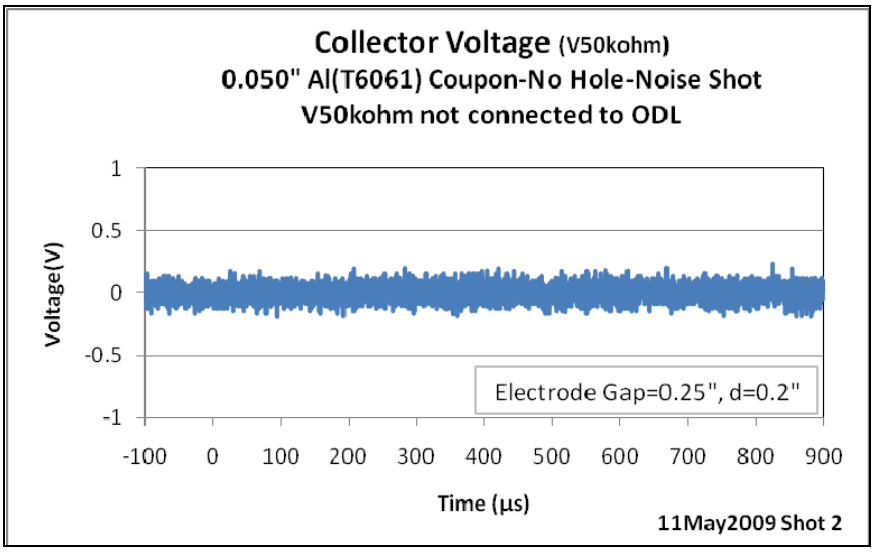

Task 0: Noise Shots-Voltage

Description:

Noise-0.050" T6061 Al w/0.5" hole in center, 1/4" Tungsten Electrode, 1/4" Electrode Gap, Nanofast with cable not connected to V50kohm. (0.2" between Coupon and collector)

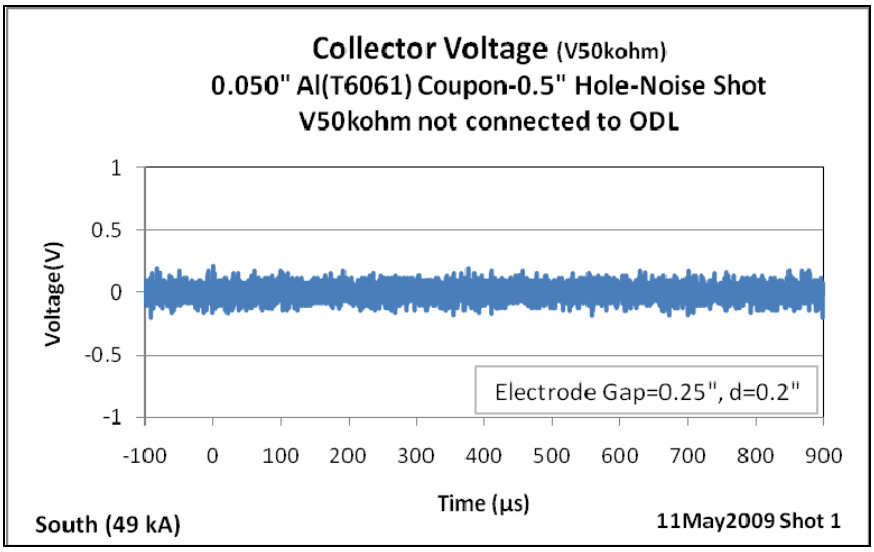

Description:

Noise-0.050" T6061 Al w/0.5" hole in center, 1/4" Tungsten Electrode, 1/4" Electrode Gap, Nanofast with cable connected. to V50kohm

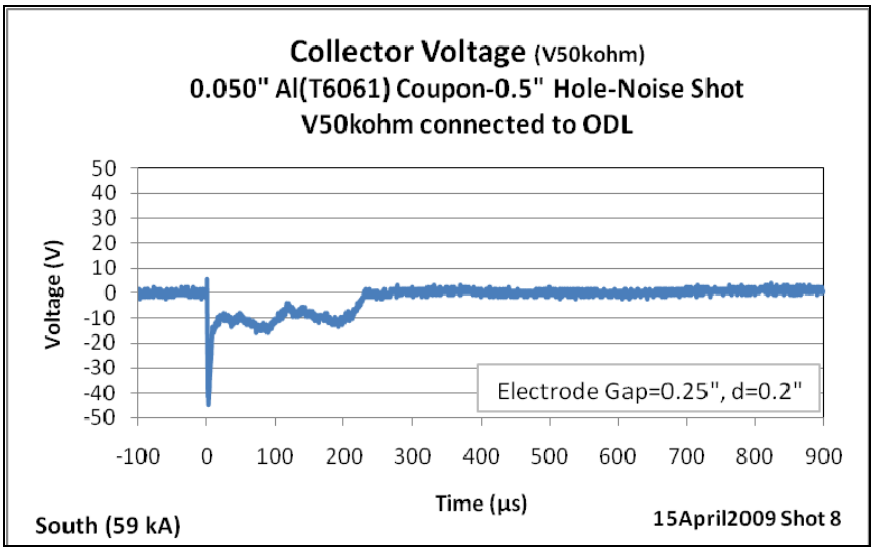

Task 0: Noise Shots-Voltage

Description:

Solid 0.050" T6061 Al, Bronze wool between coupon and brass collector, 1/4" Tungsten Electrode, 1/4" Electrode Gap, Nanofast with cable connected to V50kohm (0.2" between Coupon and collector)

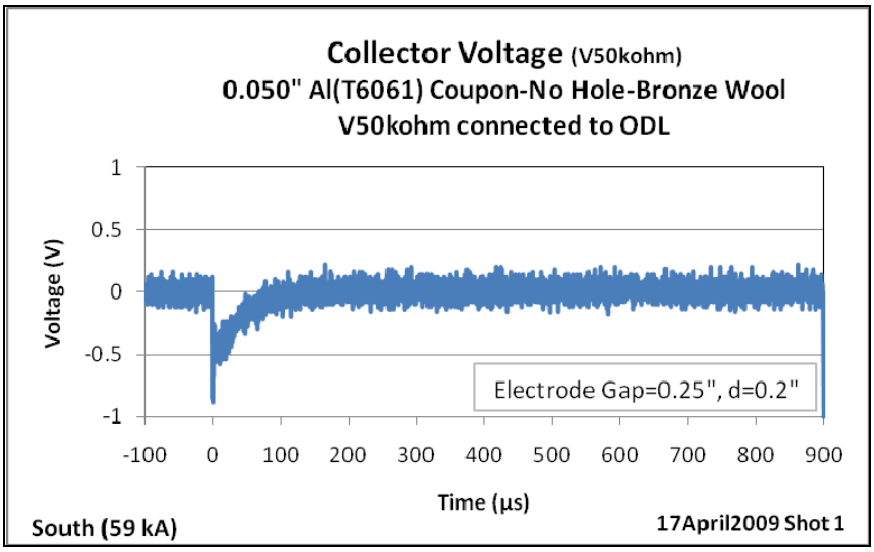

Description:

Solid 0.050" T6061 Al, #6-32 set screw between coupon and brass collector,1/4" Tungsten Electrode, 1/4" Electrode Gap, Nanofast with cable connected to V50kohm (0.2" between Coupon and collector)

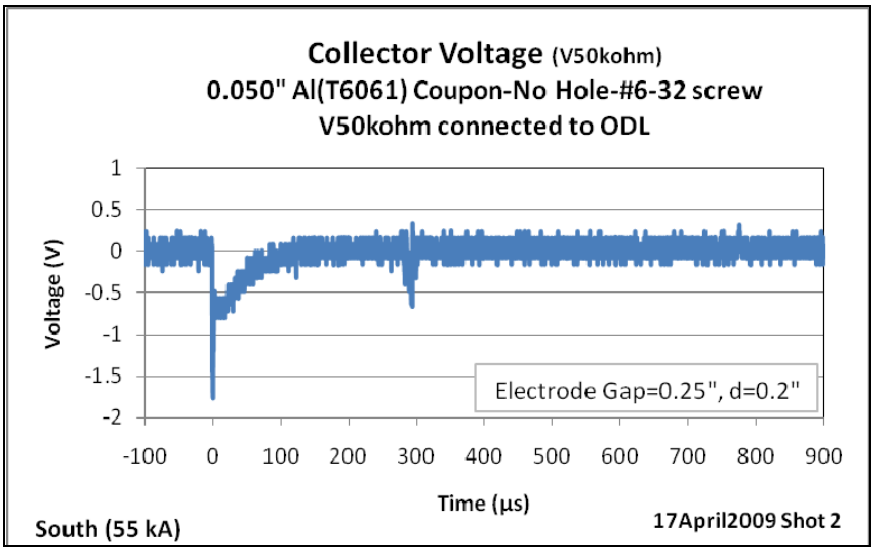

Task 0: Noise Shots-Voltage

Description:

Noise-0.050" T6061 Al w/0.125" hole in center, 1/4" Tungsten Electrode, 1/4" Electrode Gap, Nanofast with cable connected to V50kohm

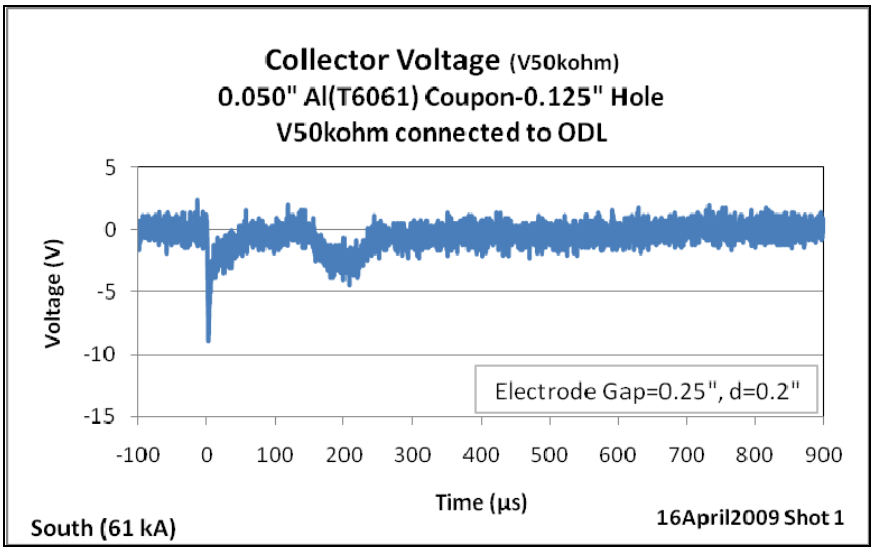

Task 1: Predrilled Hole-Disc collector- Current

Description:

0.050" Thick 6061 Al w/0.5" hole in center, 1/4" Tungsten Electrode, 1/4" Electrode Gap, Nanofasts with cables connected to CVR and CVT

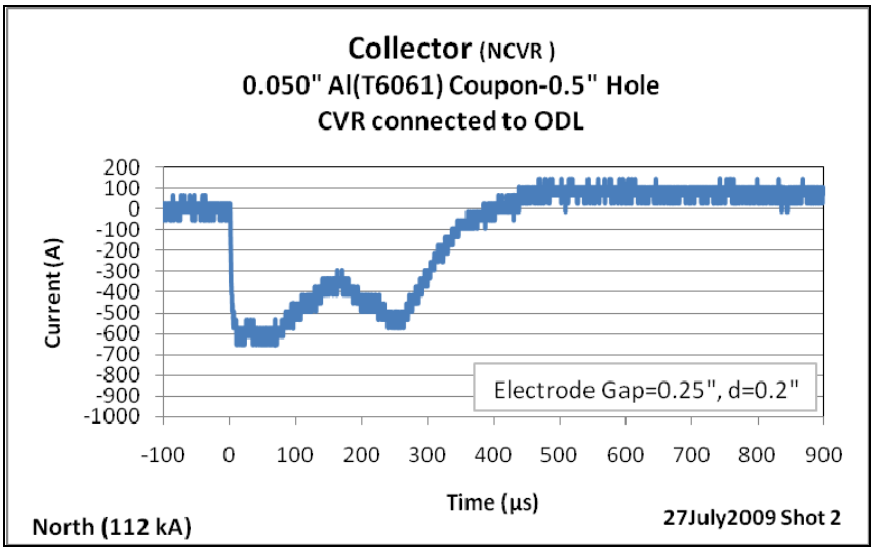

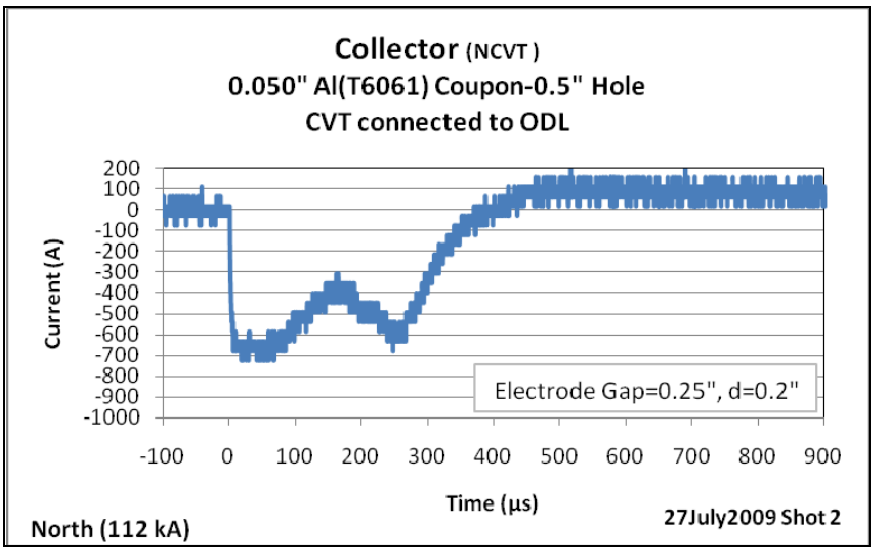

Task 1: Predrilled Hole-Disc collector- Current

Description:

0.050" Thick 6061 Al w/0.5" hole in center, 1/4" Tungsten Electrode, 1/4" Electrode Gap, Nanofasts with cables connected to CVR and CVT

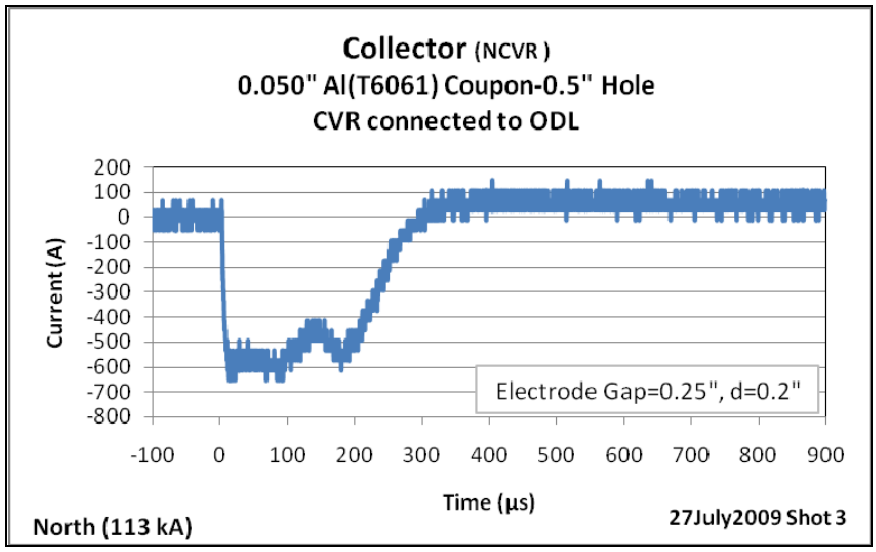

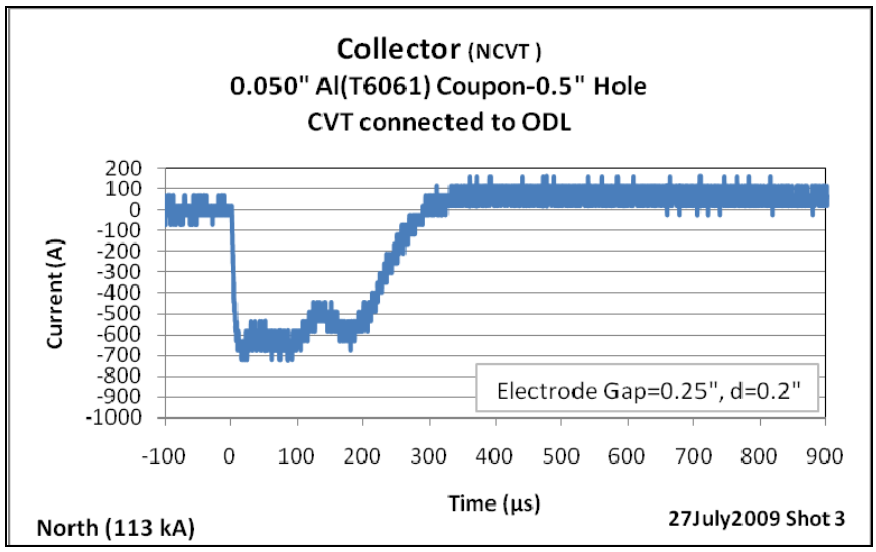

Task 1: Predrilled Hole-Disc collector- Current

Description:

0.050" Thick 6061 Al w/0.5" hole in center, 1/4" Tungsten Electrode, 1/4" Electrode Gap, Nanofasts with cables connected to CVR and CVT

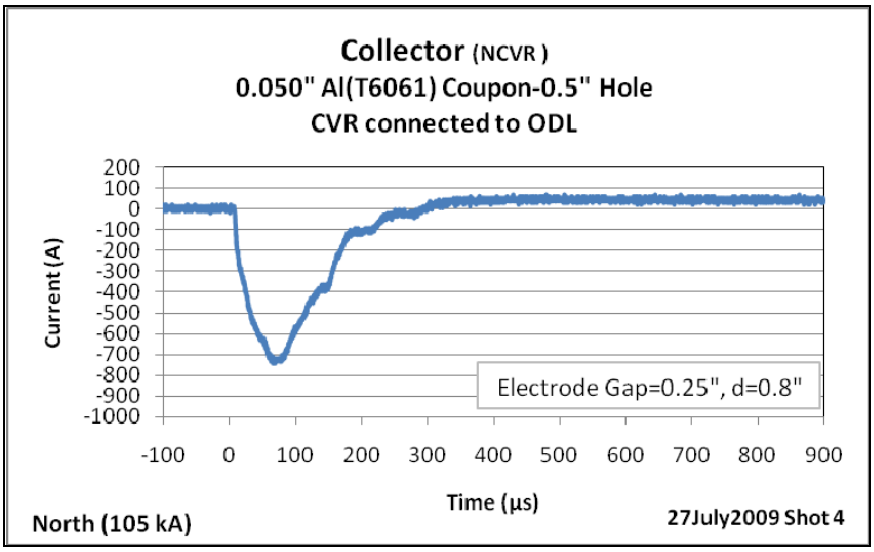

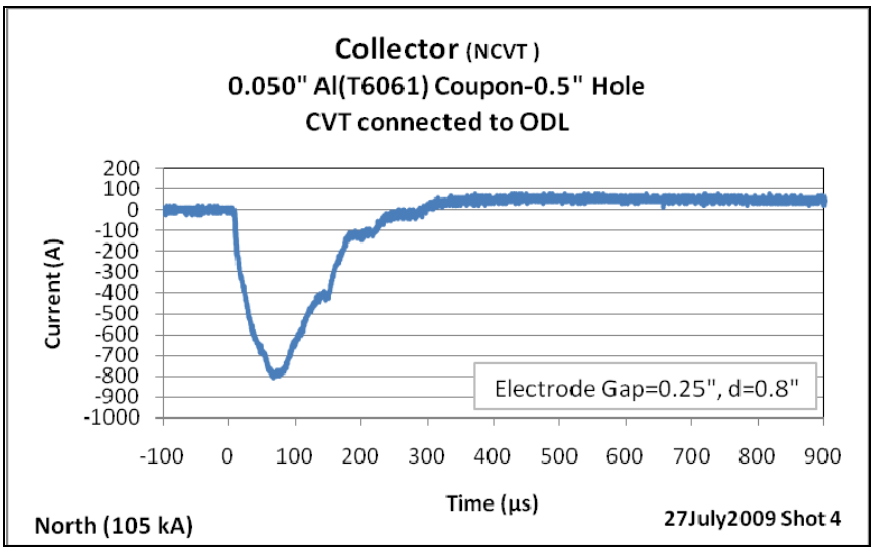

Task 1: Predrilled Hole-Disc collector- Current

Description:

0.050" Thick 6061 Al w/0.5" hole in center, 1/4" Tungsten Electrode, 1/4" Electrode Gap, Nanofasts with cables connected to CVR and CVT

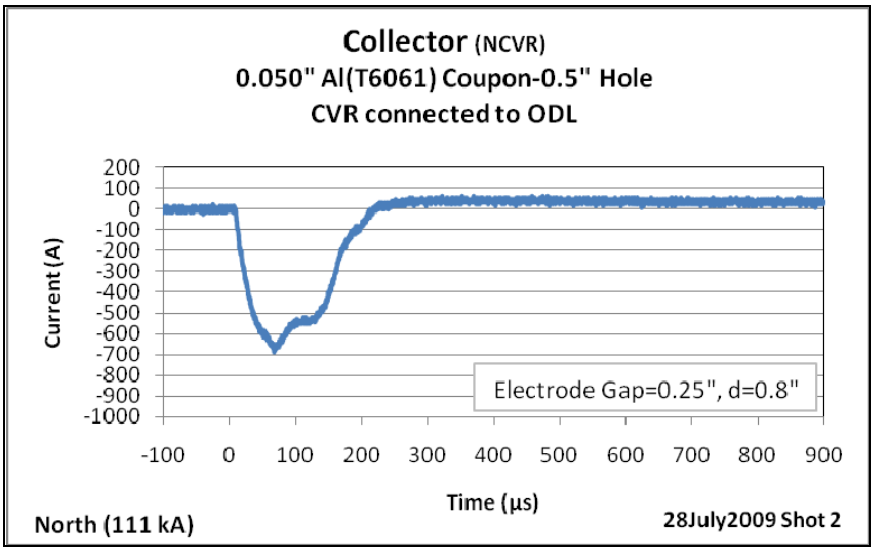

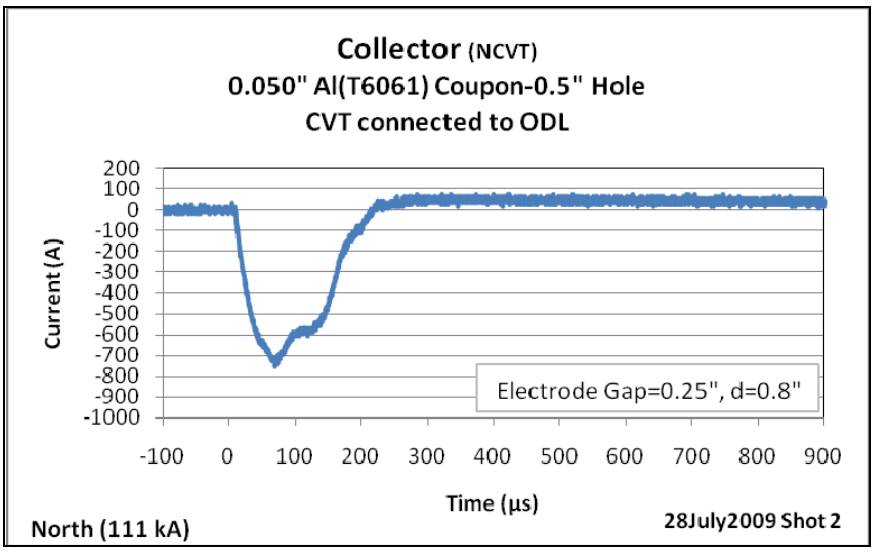

Task 1: Predrilled Hole-Disc collector- Current

Description:

0.050" Thick 6061 Al w/0.125" hole in center, 1/4" Tungsten Electrode, 1/4" Electrode Gap, Nanofasts with cables connected to CVR and CVT

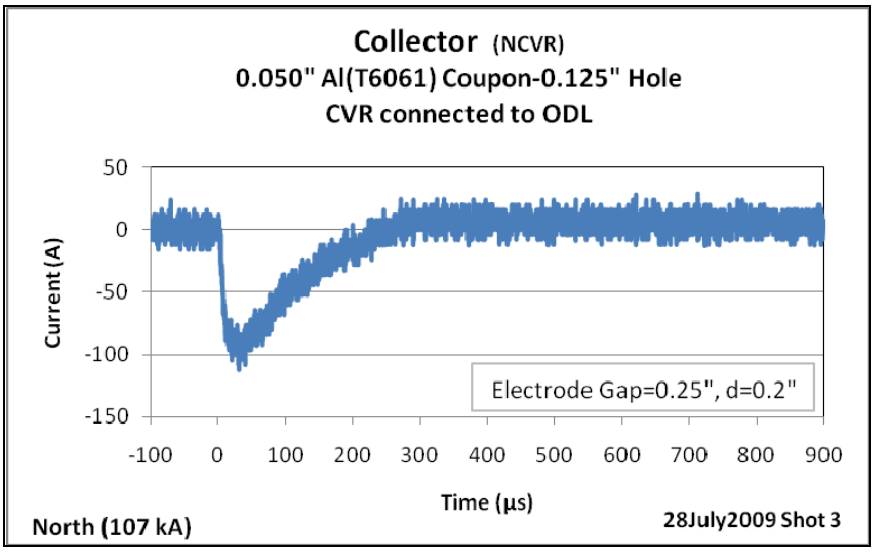

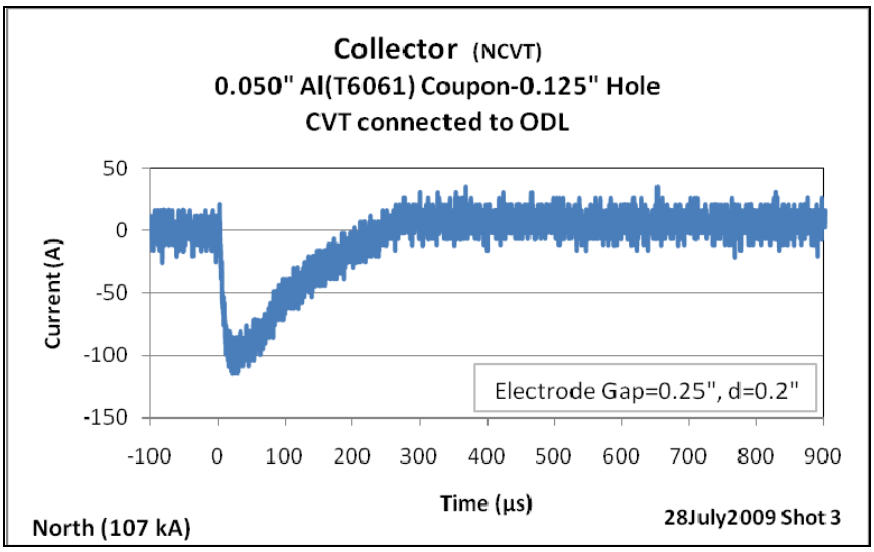

Task 1: Predrilled Hole-Disc collector- Voltage

Description:

Noise-0.050" T6061 Al w/0.125" hole in center, 1/4" Tungsten Electrode, 1/4" Electrode Gap, Nanofast with cable connected to V50kohm

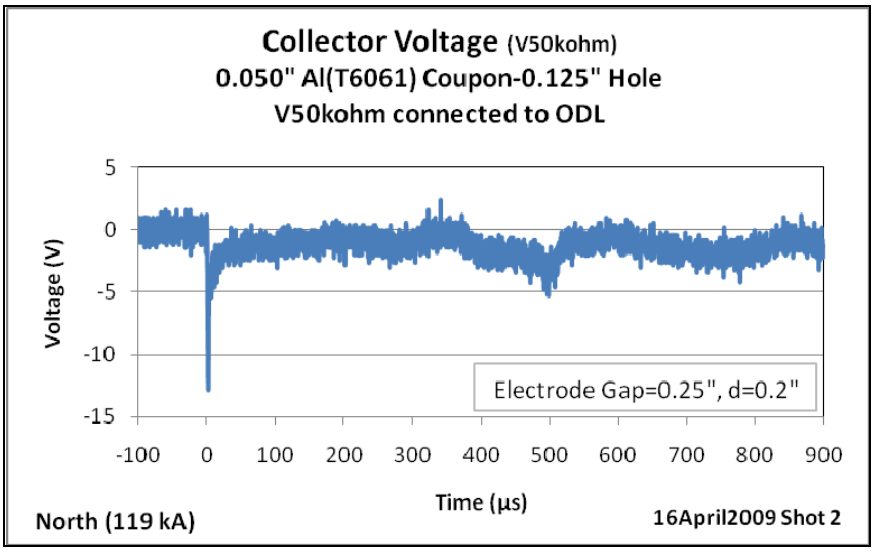

Description:

Noise-0.050" T6061 Al w/0.125" hole in center, 1/4" Tungsten Electrode, 1/4" Electrode Gap, Nanofast with cable connected to V50kohm

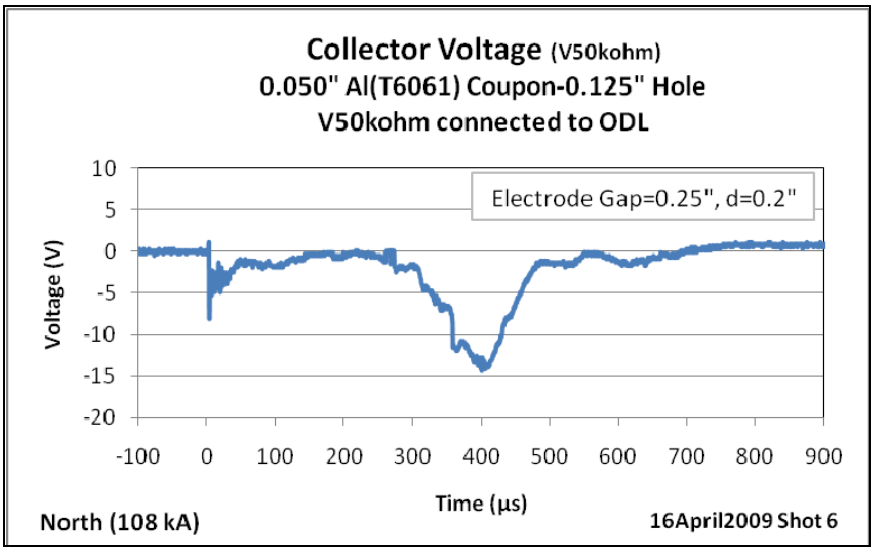

Task 1: Predrilled Hole-Disc collector- Voltage

Description:

Noise-0.050" T6061 Al w/0.5" hole in center, 1/4" Tungsten Electrode, 1/4" Electrode Gap, Nanofast with cable connected to V50kohm

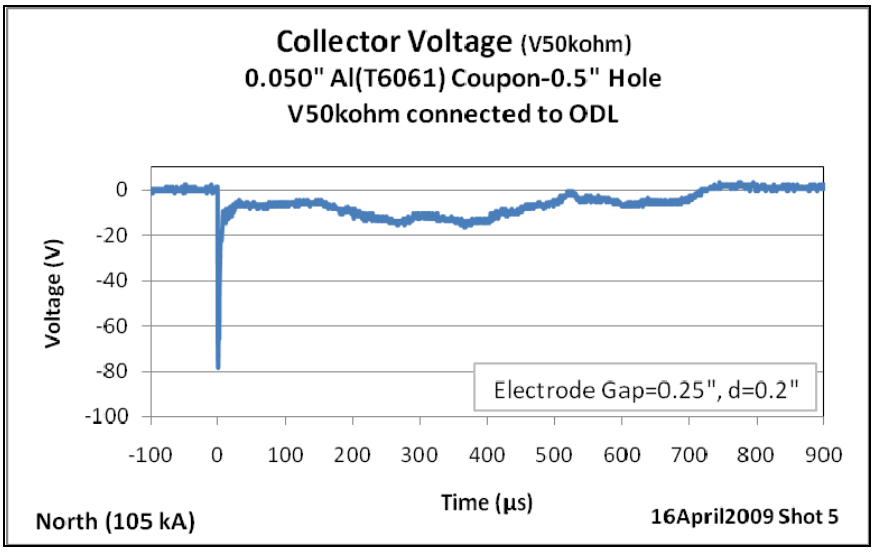

Description:

Noise-0.050" T6061 Al w/0.5" hole in center, 1/4" Tungsten Electrode, 1/4" Electrode Gap, Nanofast with cable connected to V50kohm

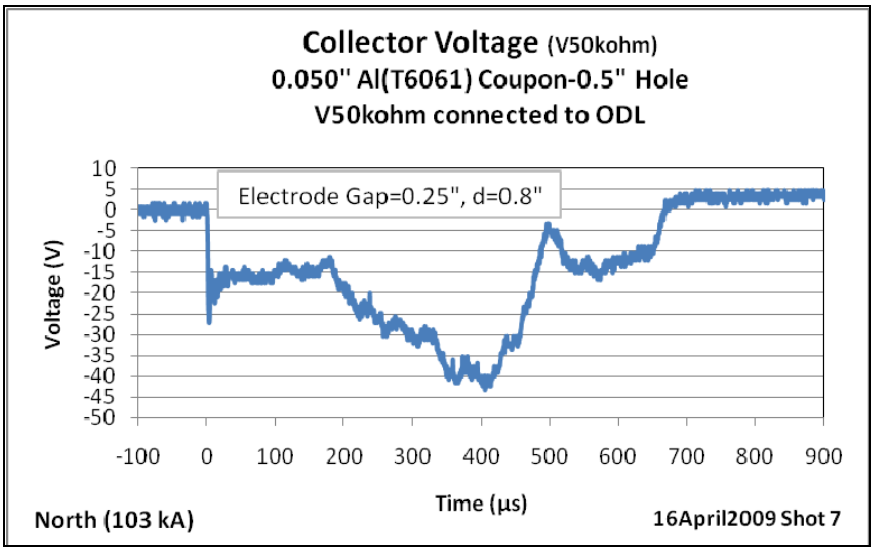

Task 1: Predrilled Hole-Disc collector- Voltage

Description:

Noise-0.050" T6061 Al w/0.5" hole in center, 1/4" Tungsten Electrode, 1/4" Electrode Gap, Nanofast with cable connected to V50kohm

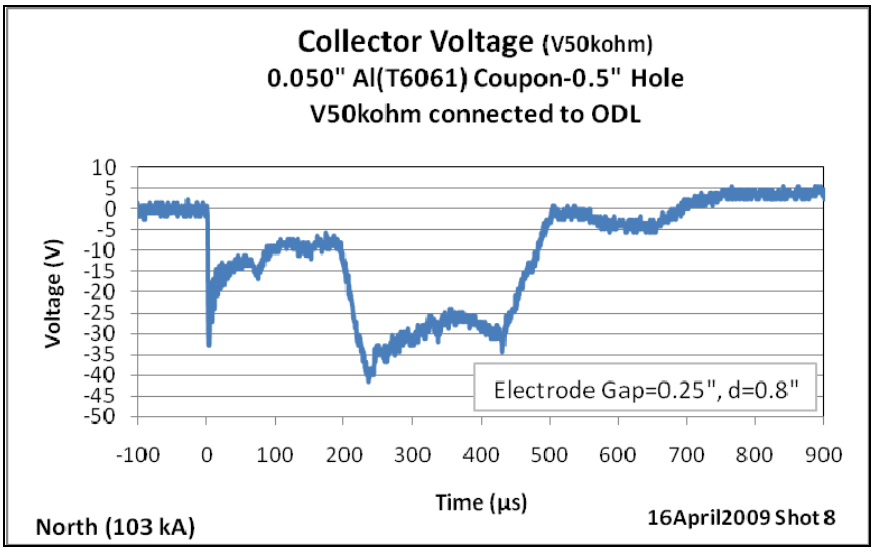

Description:

Noise-0.050" T6061 Al w/0.125" hole in center, 1/4" Tungsten Electrode, 1/4" Electrode Gap, Nanofast with cable connected to V50kohm

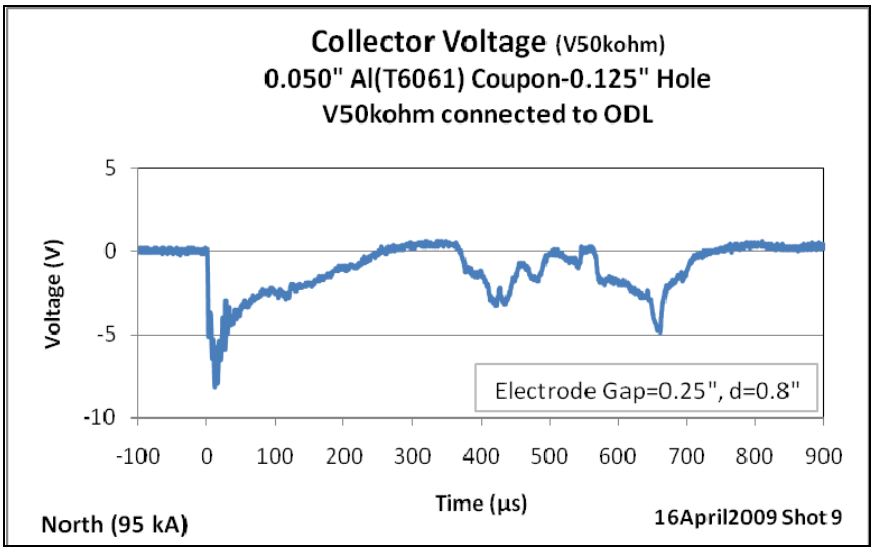

2. First Return Stroke and Continuing Current – Disk Collector-Current

Description:

0.050" T6061 Al, no hole in center, 1/4" Tungsten Electrode, 1/4" Electrode Gap, Cables connected to CVR (TTI ODL).

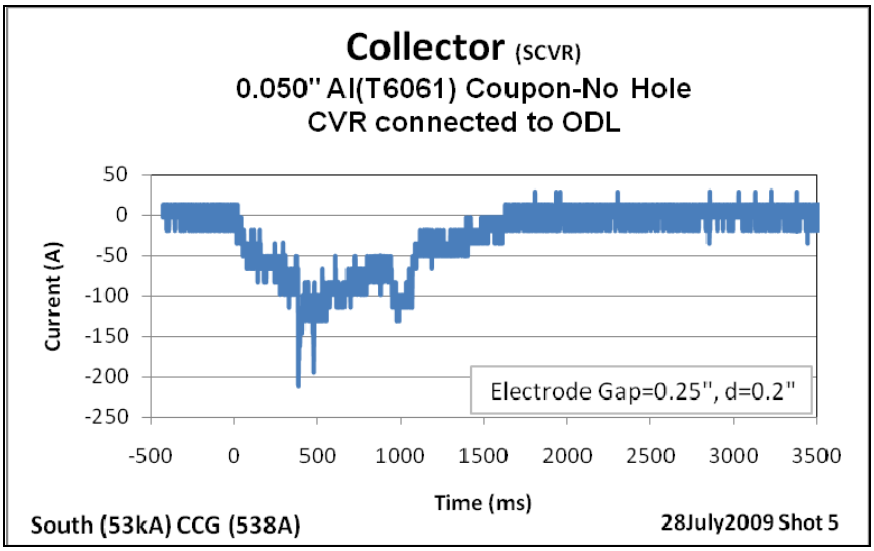

Description:

0.050" T6061 Al, no hole in center, 1/4" Tungsten Electrode, 1/4" Electrode Gap, Cables connected to CVR (TTI ODL).

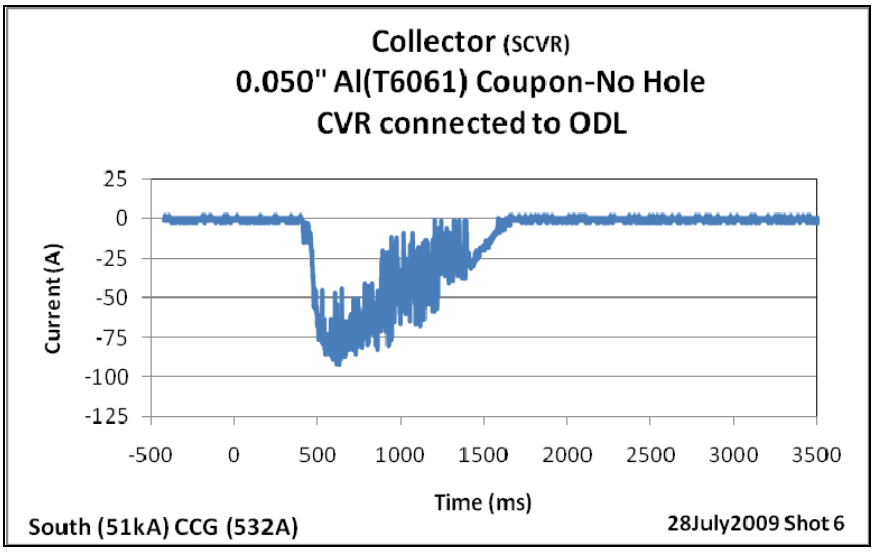

2. First Return Stroke and Continuing Current – Disk Collector-Voltage

Description:

0.050" T6061 Al, no hole in center, 1/4" Tungsten Electrode, 1/4" Electrode Gap, V5kΩ and cable connected to (TTI ODL).

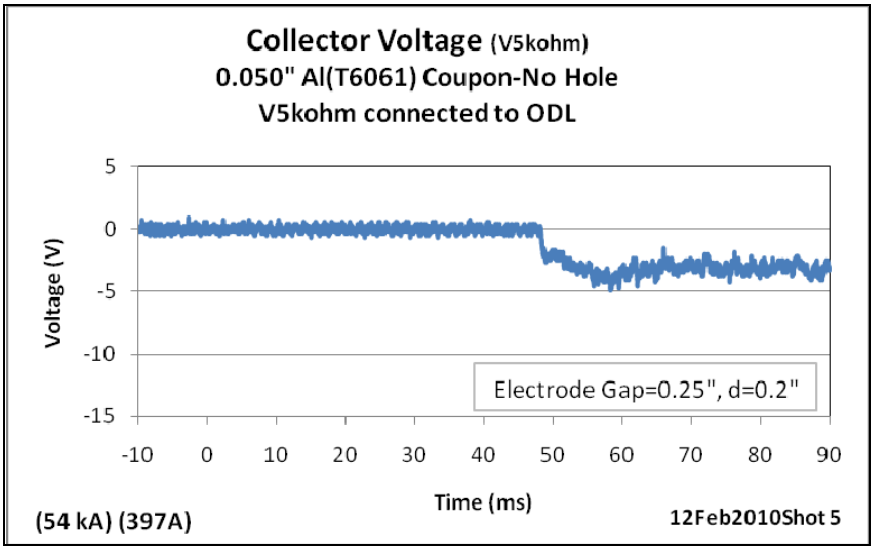

Description:

0.050" T6061 Al, no hole in center, 1/4" Tungsten Electrode, 1/4" Electrode Gap, V5kΩ and cable connected to (TTI ODL).

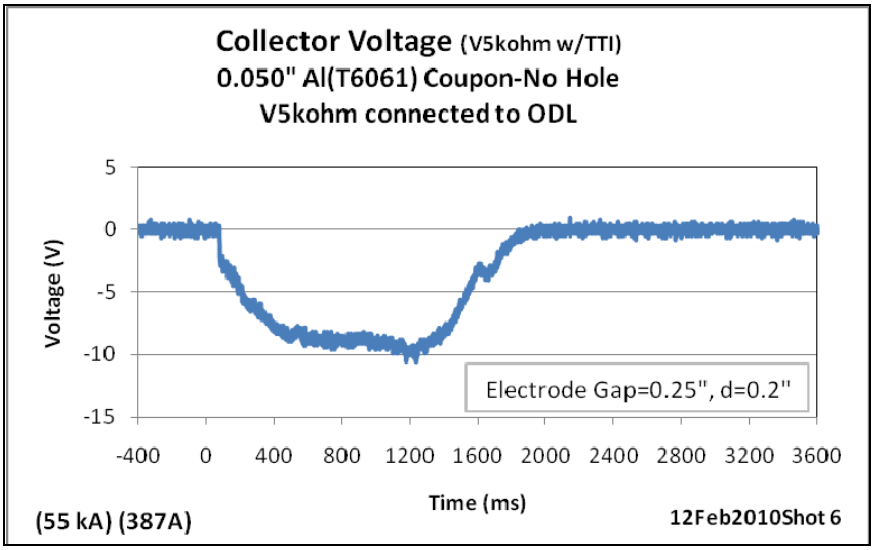

2. First Return Stroke and Continuing Current – Disk Collector-Voltage

Description:

0.050" T6061 Al, no hole in center, 1/4" Tungsten Electrode, 1/4" Electrode Gap, V5kΩ and cable connected to (TTI ODL).

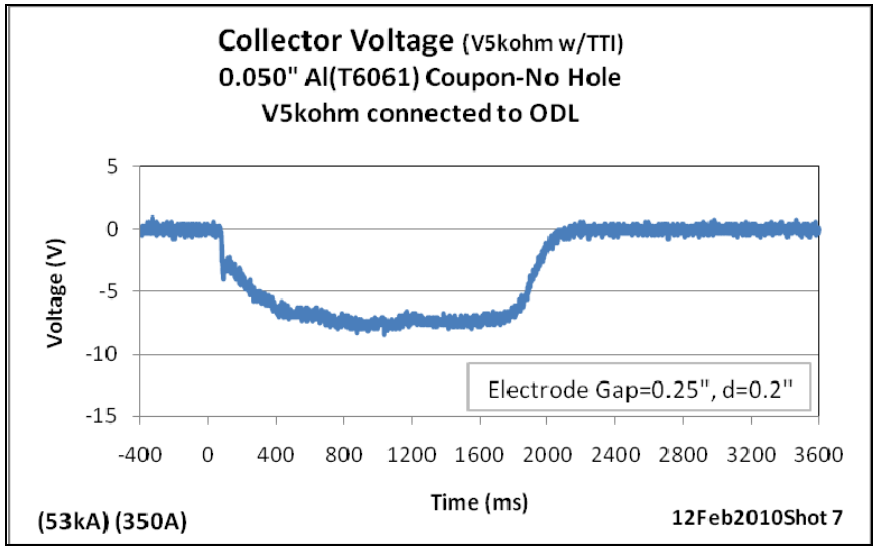

Task 3 First Return Stroke, Continuing Current, Second Return Stroke – Disk Collector - Current

Description:

Double Pulse Photometric Current Shot
0.050" Aluminum Coupon (1"grid), 1/4" Tungsten Electrode, 1/4" Electrode Gap, Nanofasts with cables connected to CVR & CVT. 100ms inter-pulse period. (0.2" between Coupon and collector)

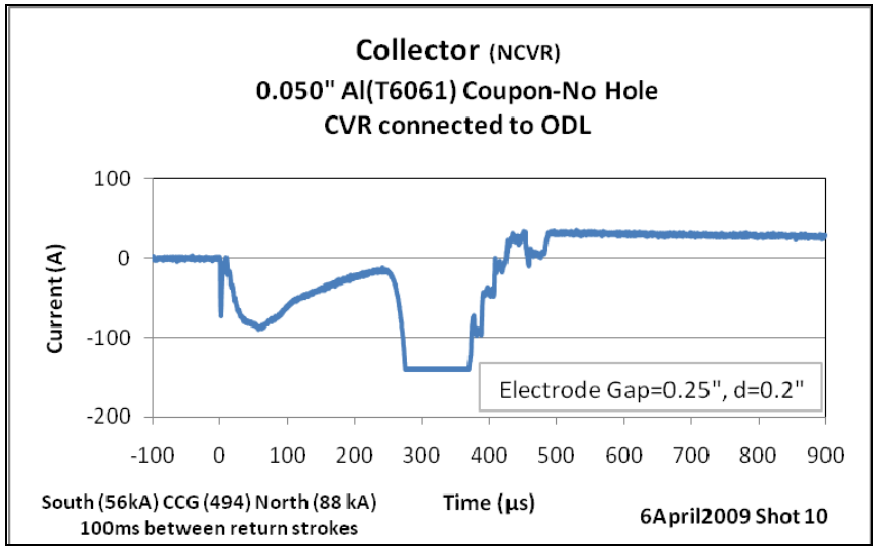

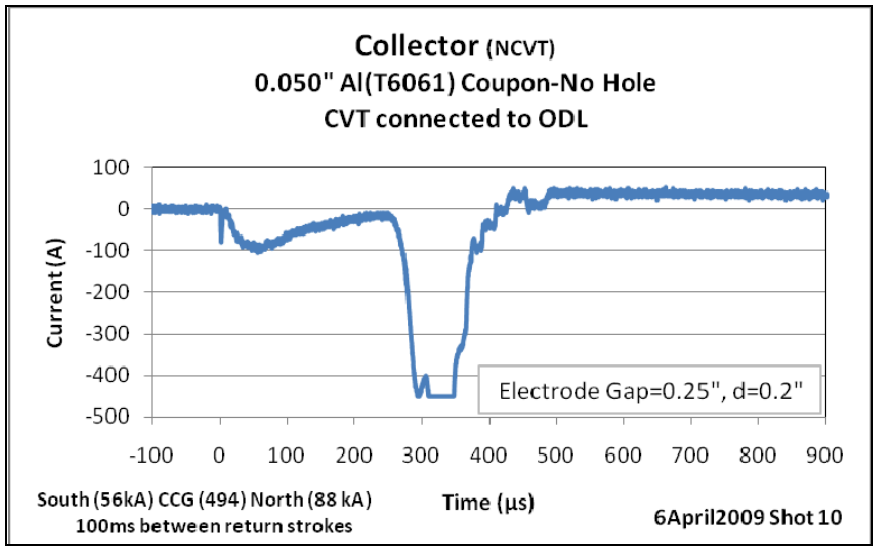

Task 3: First Return Stroke, Continuing Current, Second Return Stroke – Disk Collector - Current

Description:

Double Pulse Photometric Current Shot
0.050" Aluminum Coupon (1"grid), 1/4" Tungsten Electrode, 1/4" Electrode Gap, Nanofasts with cables connected to CVR & CVT. 100ms inter-pulse period. (0.2" between Coupon and collector)

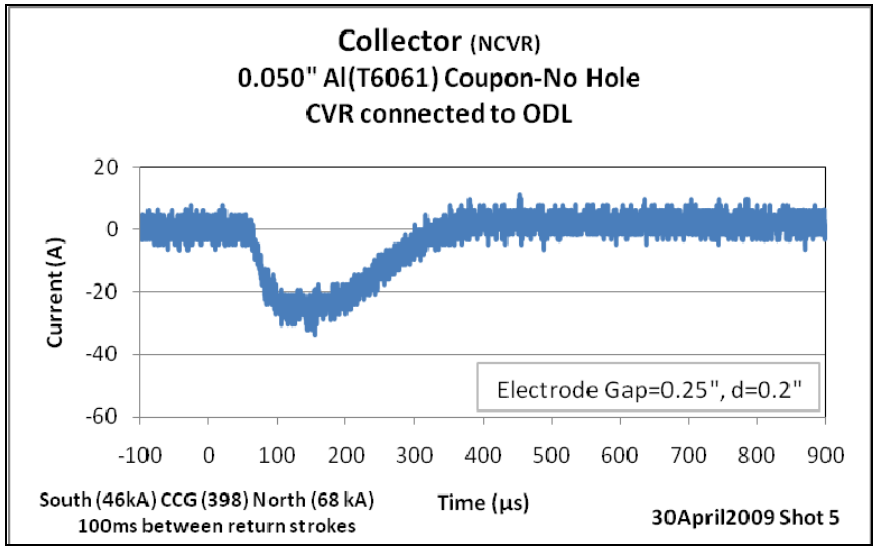

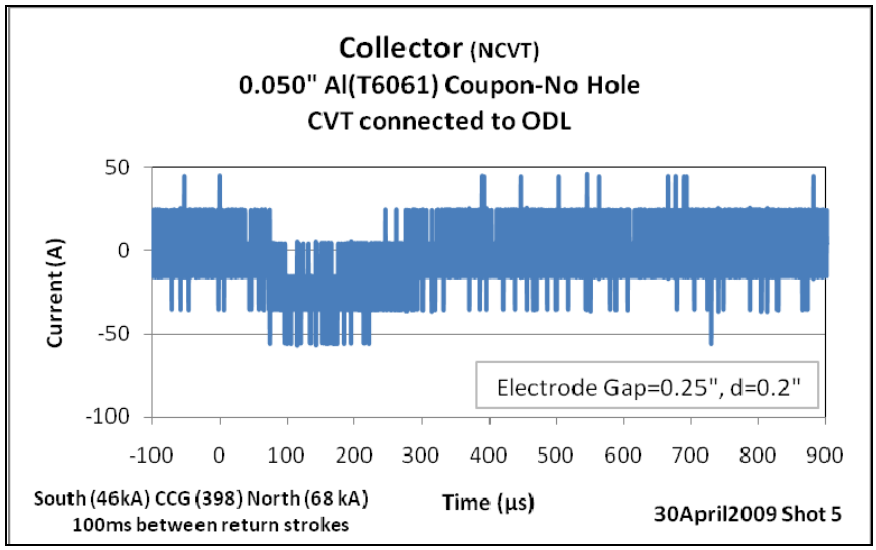

Task 3: First Return Stroke, Continuing Current, Second Return Stroke – Disk Collector - Current

Description:

Double Pulse Photometric Current Shot
0.050" Aluminum Coupon (1"grid), 1/4" Tungsten Electrode, 1/4" Electrode Gap, Nanofasts with cables connected to CVR & CVT. 500ms inter-pulse period. (0.2" between Coupon and collector)

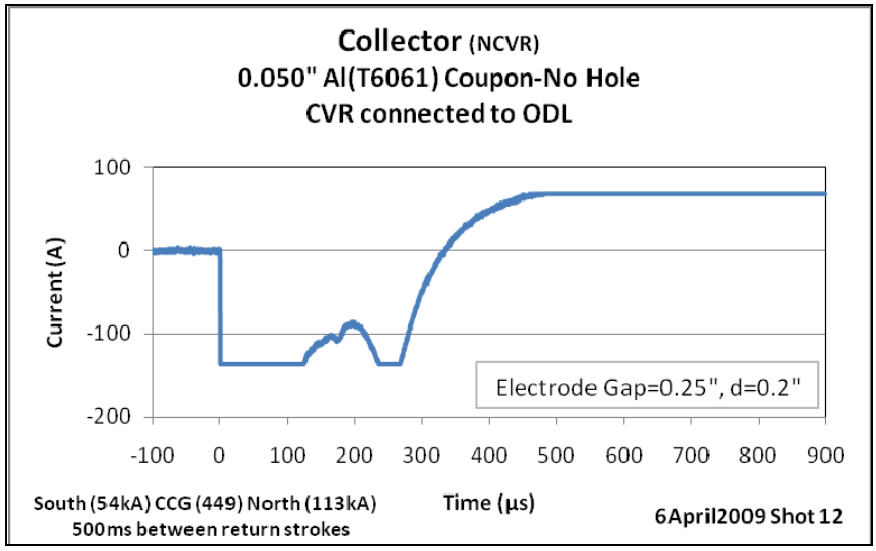

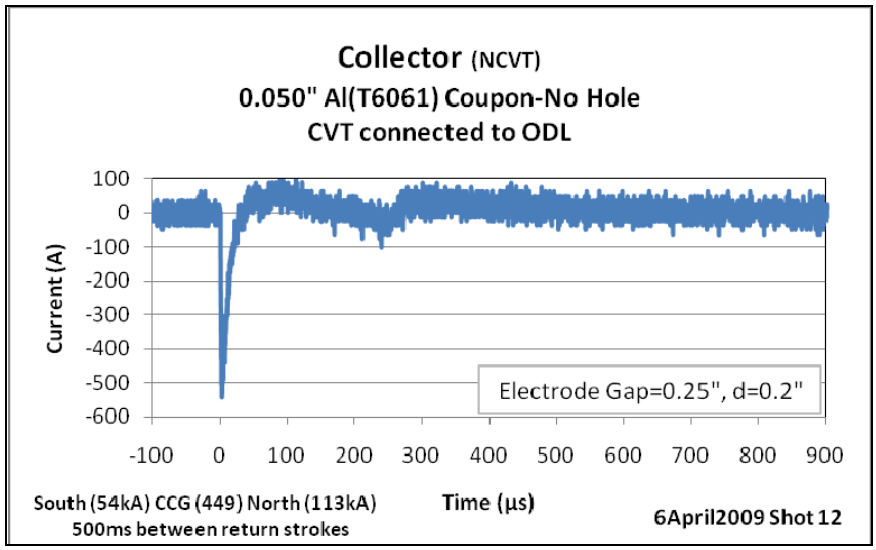

Task 3: First Return Stroke, Continuing Current, Second Return Stroke – Disk Collector - Current

Description:

Double Pulse Photometric Current Shot
0.050" Aluminum Coupon (1"grid), 1/4" Tungsten Electrode, 1/4" Electrode Gap, Nanofasts with cables connected to CVR & CVT. 500ms inter-pulse period. (0.8" between Coupon and collector)

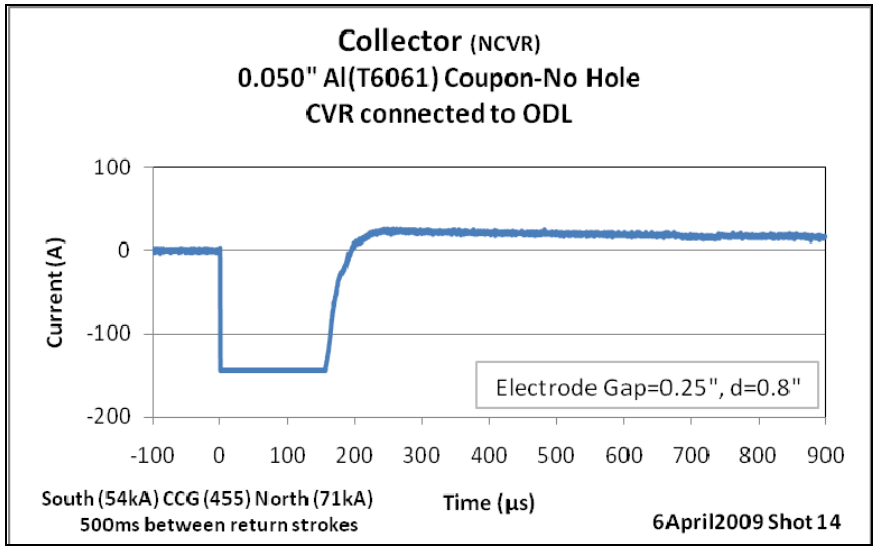

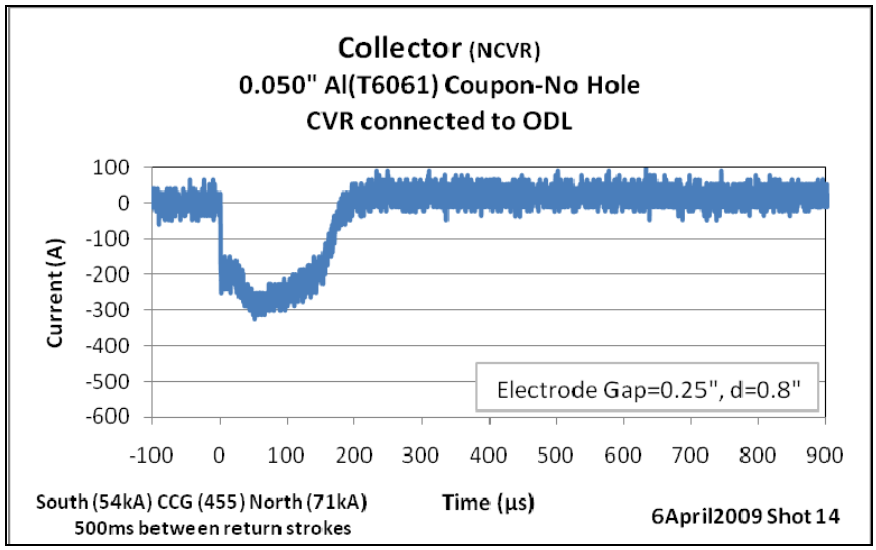

Task 3: First Return Stroke, Continuing Current, Second Return Stroke – Disk Collector - Current

Description:

Double Pulse Photometric Current Shot
0.050" Aluminum Coupon (1"grid), 1/4" Tungsten Electrode, 1/4" Electrode Gap, Nanofasts with cables connected to CVR & CVT. 100ms inter-pulse period. (0.8" between Coupon and collector)

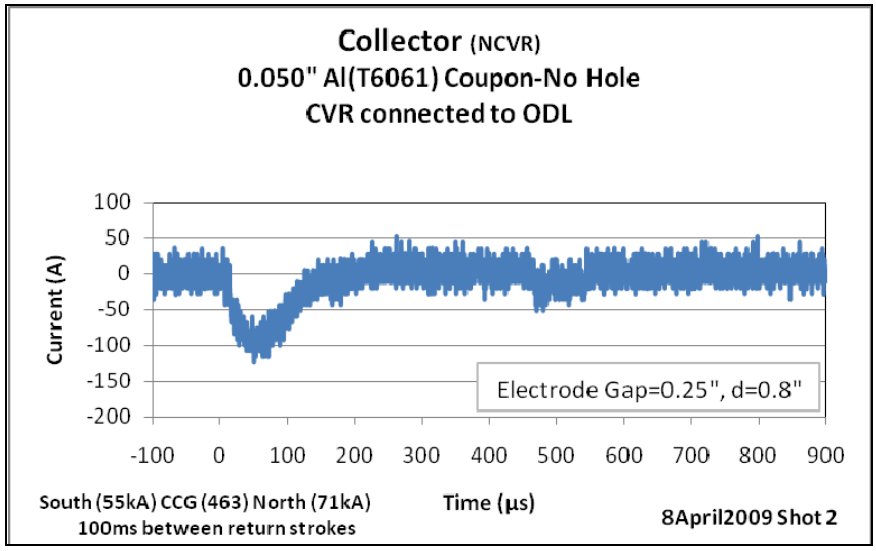

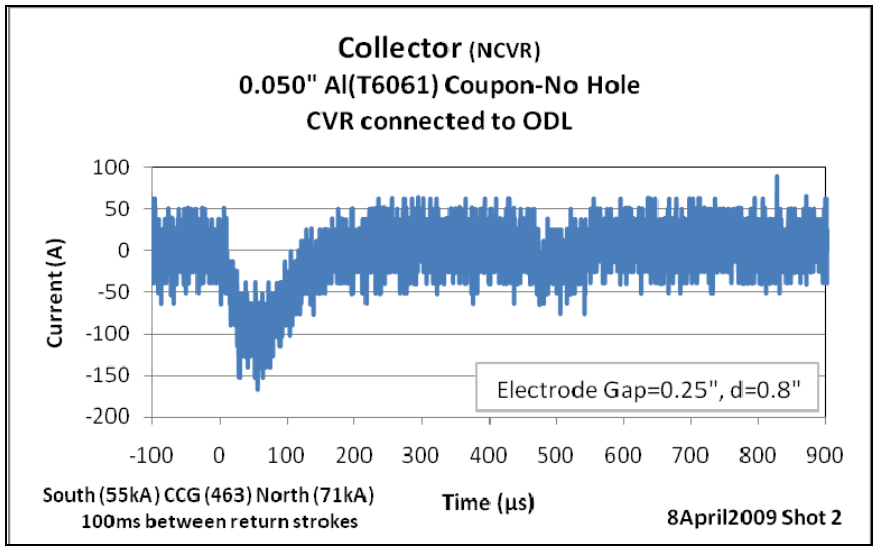

4. First Return Stroke and Continuing Current – Cable Collector-Voltage

Description:

0.050" T6061 Al, 1/4" Tungsten Electrode, 1/4" Electrode Gap, V5kΩ and cable connected to TTI(ODL). Cable collector not connected to ODL (NOISE SHOT)

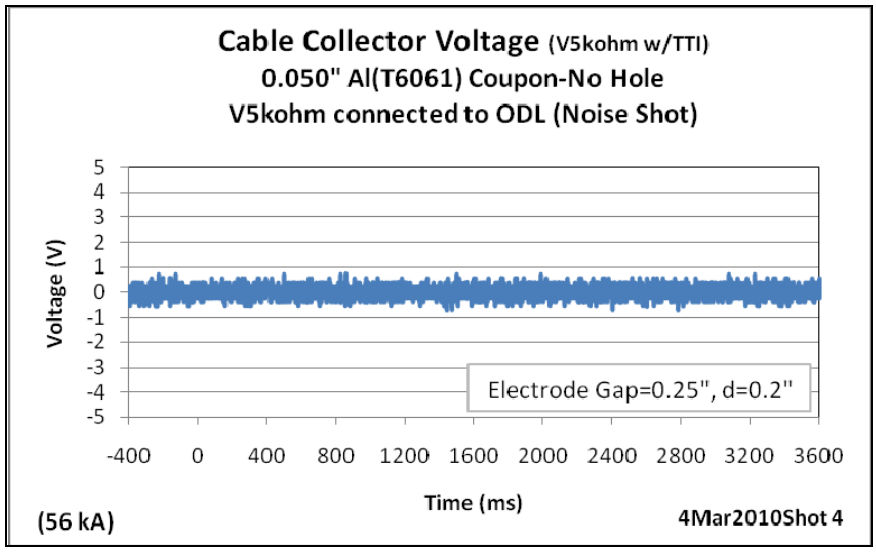

Description:

0.050" T6061 Al, 1/4" Tungsten Electrode, 1/4" Electrode Gap, V5kΩ and cable connected to TTI(ODL)

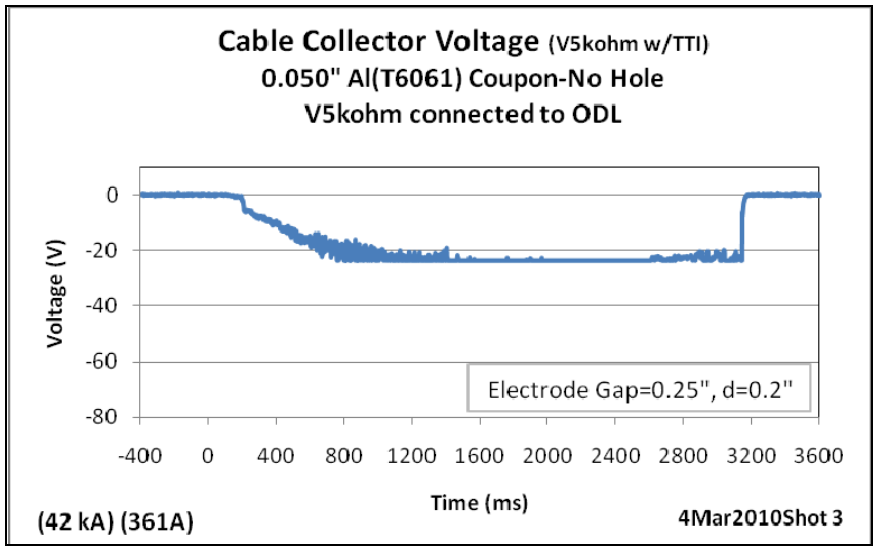

4. First Return Stroke and Continuing Current – Cable Collector-Voltage

Description:

0.050" T6061 Al, 1/4" Tungsten Electrode, 1/4" Electrode Gap, V5kΩ and cable connected to TTI(ODL)

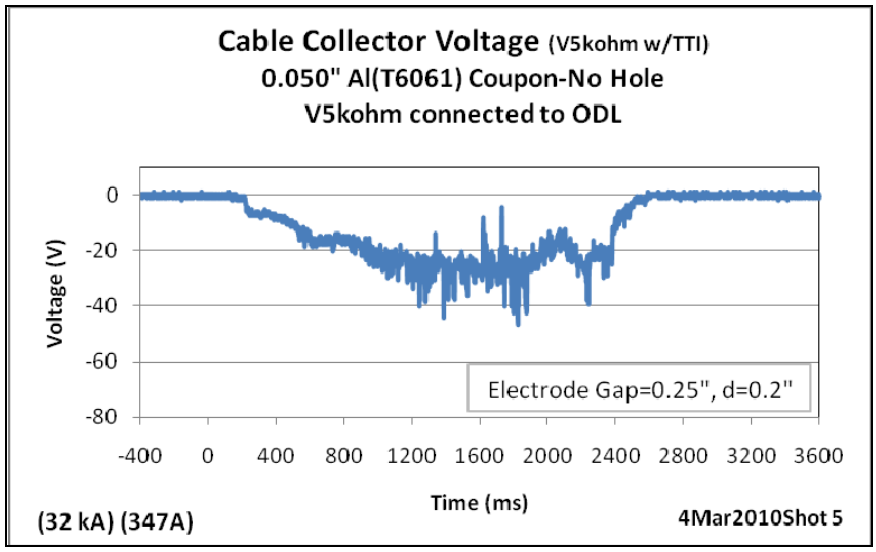

6. Indirect coupling-Magnetic and Electric Field

The purpose of these shots is to develop an understanding of magnetic and electric field coupling with a ½" predrilled hole with low level current and voltage sources. Both stripline cable and brass collectors will be used. A commercially available Velonex model 590 will be used for the magnetic field tests and an SNL developed Pulse Arrested Spark Discharge PASD pulser with integral voltage probe will be used for the electric field tests. Distance between Back of pre-drilled coupon and brass collector or strip cable (without brass collector) is 0.2" (d=0.2"). 300MHz and 1GHz bandwidth Nanofast fiber optic links will be used to measure the collector voltages for the Velonex and PASD tests respectively.

Velonex 590 Noise Shots

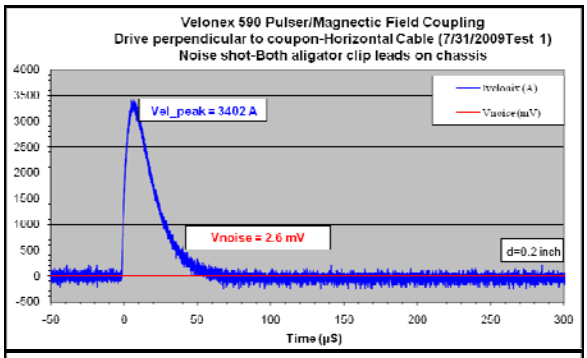

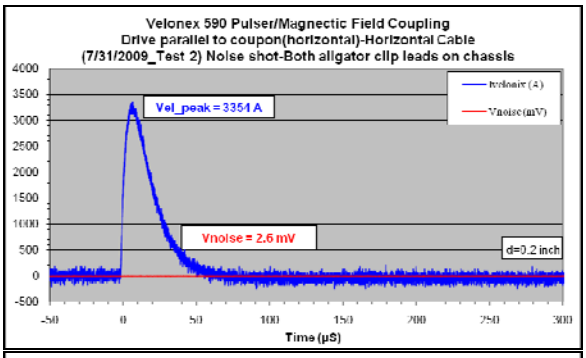

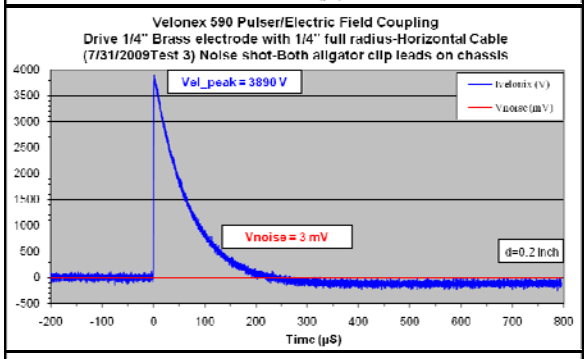

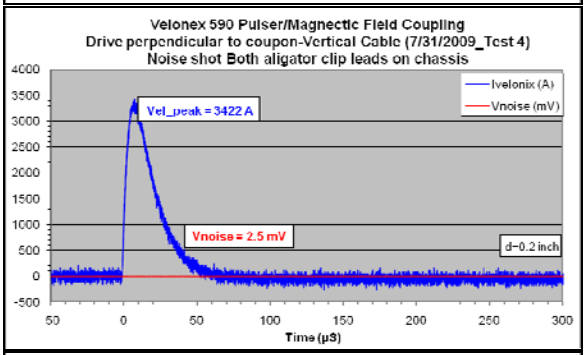

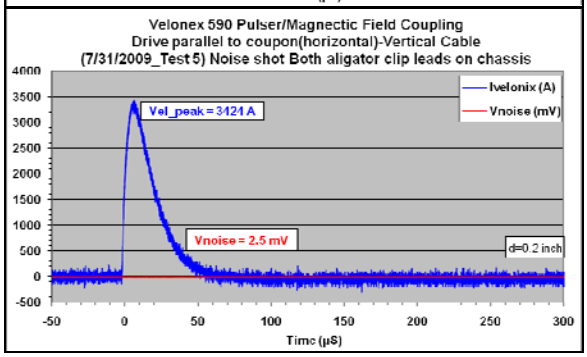

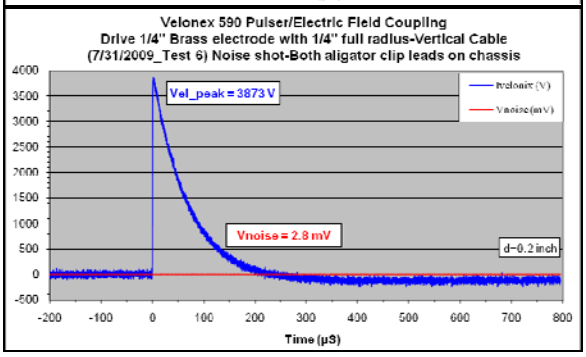

6. Indirect coupling-Magnetic and Electric Field

The purpose of these shots is to develop an understanding of magnetic and electric field coupling with a ½" predrilled hole with low level current and voltage sources. Both stripline cable and brass collectors will be used. A commercially available Velonex model 590 will be used for the magnetic field tests and an SNL developed Pulse Arrested Spark Discharge PASD pulser with integral voltage probe will be used for the electric field tests. Distance between Back of pre-drilled coupon and brass collector or strip cable (without brass collector) is 0.2" (d=0.2"). 300MHz and 1GHz bandwidth Nanofast fiber optic links will be used to measure the collector voltages for the Velonex and PASD tests respectively.

Velonex 590 Test Shots

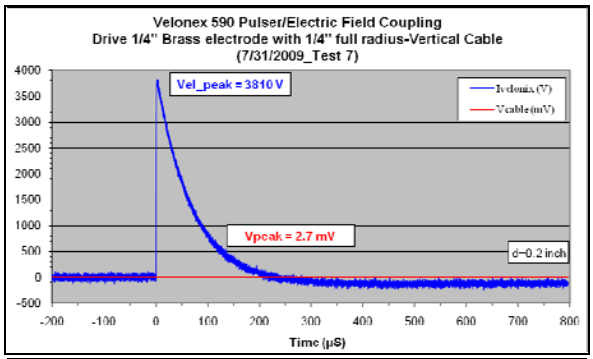

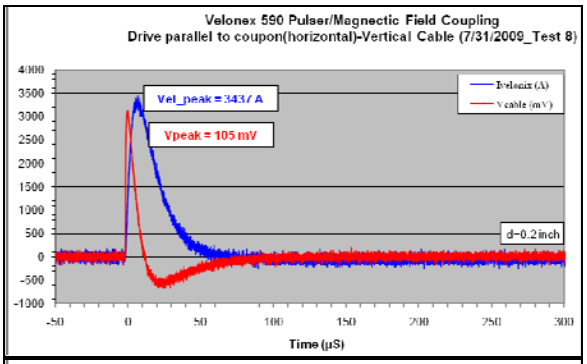

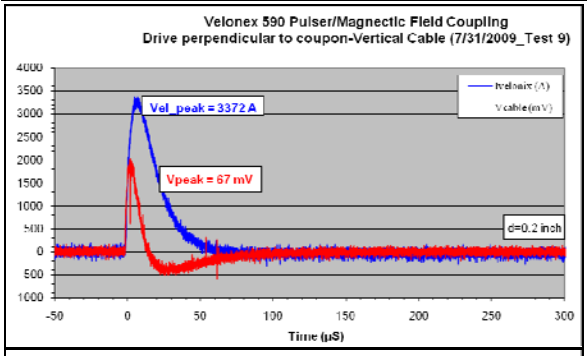

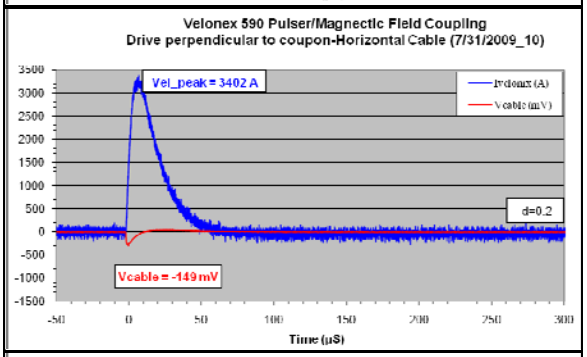

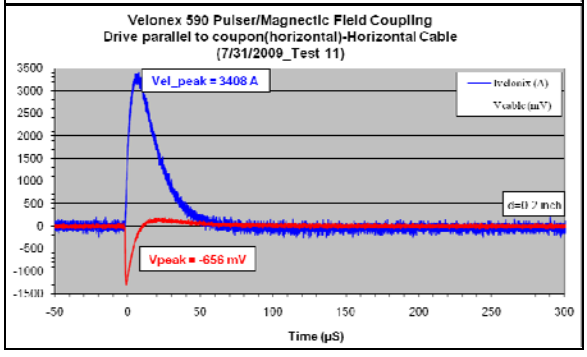

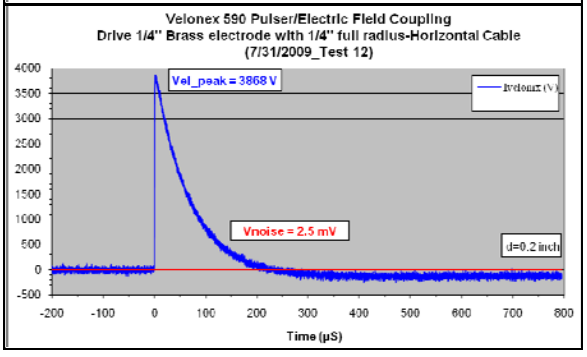

6. Indirect coupling-Magnetic and Electric Field

The purpose of these shots is to develop an understanding of magnetic and electric field coupling with a ½" predrilled hole with low level current and voltage sources. Both stripline cable and brass collectors will be used. A commercially available Velonex model 590 will be used for the magnetic field tests and an SNL developed Pulse Arrested Spark Discharge PASD pulser with integral voltage probe will be used for the electric field tests. Distance between Back of pre-drilled coupon and brass collector or strip cable (without brass collector) is 0.2" (d=0.2"). 300MHz and 1GHz bandwidth Nanofast fiber optic links will be used to measure the collector voltages for the Velonex and PASD tests respectively. **PASD Shots**

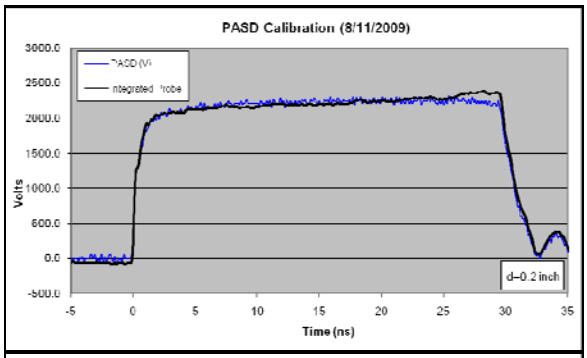

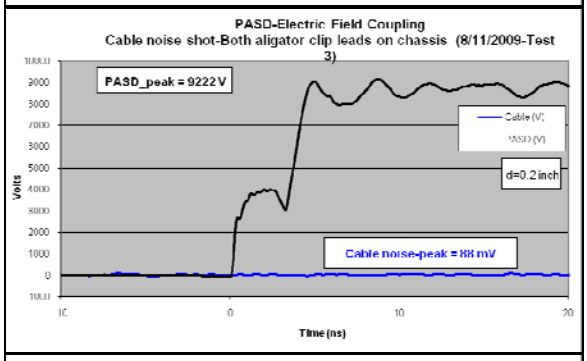

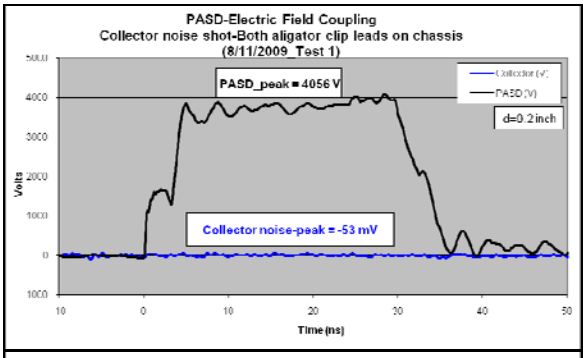

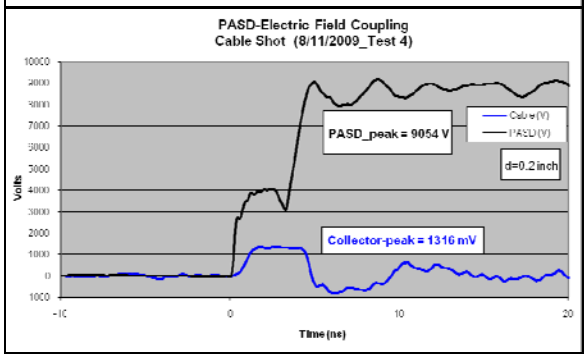

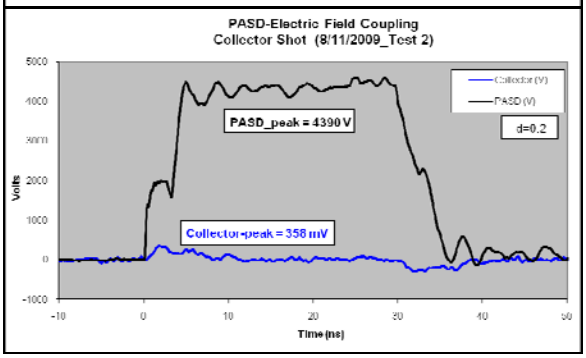

6. Indirect coupling-Magnetic and Electric Field

The purpose of these shots is to develop an understanding of magnetic and electric field coupling with a ½" predrilled hole with low level current and voltage sources. Both stripline cable and brass collectors will be used. A commercially available Velonex model 590 will be used for the magnetic field tests and an SNL developed Pulse Arrested Spark Discharge PASD pulser with integral voltage probe will be used for the electric field tests. Distance between Back of pre-drilled coupon and brass collector or strip cable (without brass collector) is 0.2" (d=0.2"). 300MHz and 1GHz bandwidth Nanofast fiber optic links will be used to measure the collector voltages for the Velonex and PASD tests respectively. **PASD Shots**

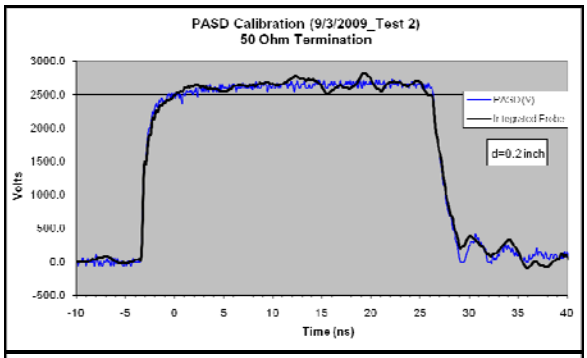

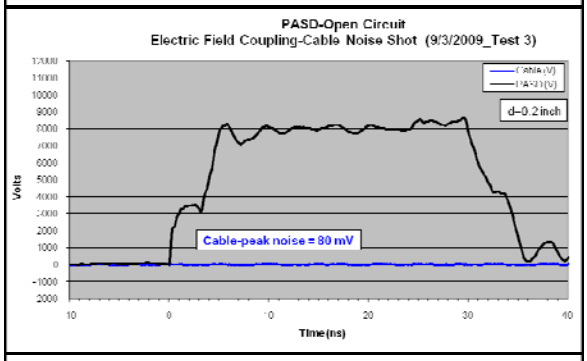

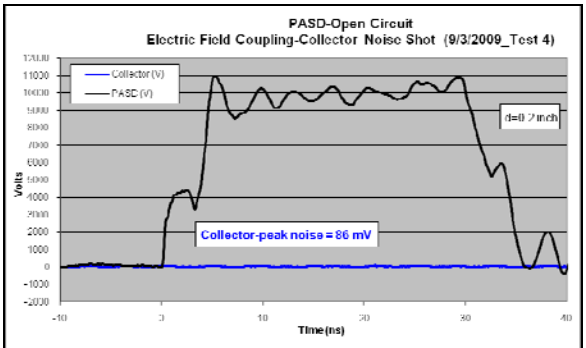

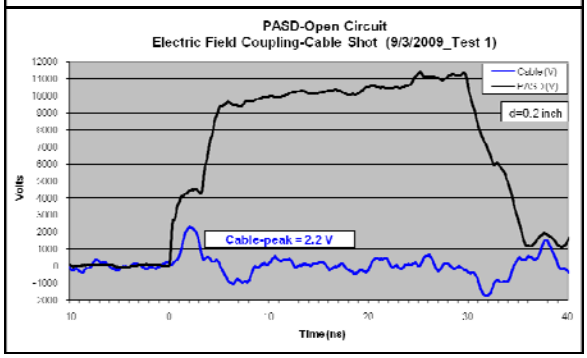

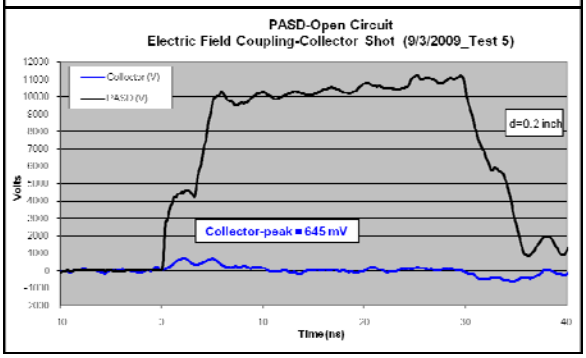

Summary of

Round 2 Testing

for LDRD

"Field and Charge Penetration by Lightning Burnthrough"

Authors: Leonard Martinez, SNL Department 1653
Larry Warne, SNL Department 1653
Roy Jorgenson, SNL Department 1653

Measurements by: Leonard Martinez, SNL Department 1653
Ed Bystrom, SNL Department 1535

Test Support: John Jojola, SNL Department 1653
Sandra Montoya, K-Tech Corporation

Revision: Rev 0.

Date: September 2009

Experimental Plan (Second Round)

Abstract: This second round of experiments has five primary goals. The first is to repeat the double return stroke coupling experiments carried out in the first round but with the interior cable shorted to chassis at one end (this forms the nonlinear analog of the magnetic indirect coupling shots). The second is to gather interior photographic evidence for the timing of the initial barrier penetration by the continuing current, as well as information on the spatial extent of the interior plasma. The third is to examine near worst case hole size and coupling by initiating the continuing current arc with a starter wire (which rapidly vaporizes), allowing the twin return strokes from the Sandia lightning simulator to enlarge the hole dimensions, and mimic a severe lightning flash. The fourth is to lay the groundwork for examining arc attachment probabilities to the interior collector (or cable) by examining breakdown paths when the source electrode is moved closer to a predrilled coupon.. The fifth goal is to demonstrate the late time coupling observed in the original 1990s tests by exploiting an alternative optical data link (ODL), with frequency responses to DC (these were not captured in round one because the high frequency ODL used there was directed at the time regime around the return stroke and did not have the DC response to look at the entire burnthrough record).

The plan follows with extra shots and the photographic efforts separately called out.

0. Noise Shots

There are a couple of new issues to address in the noise shots. First we will have a slot cut in the Faraday cage which can result in field penetration and coupling to the interior cabling and ODL. Second, we plan to do a few experiments with the ODL having DC response (TTI ODL). We need to check for late time diffusion voltages (some of which could have been filtered in prior experiments. In addition, the TTI ODL is unshielded.

Conduct 50 kA return stroke shots with solid coupon in place to check coupling levels from the slot in the Faraday cage. Repeat with bronze wool shorting collector to coupon to assess diffusion coupling to measurement loop. These should be repeated eventually for voltage measurement setup.

The TTI measurements for late time penetration may require the complete Faraday cage setup, depending on the what the noise shots show.

Conduct 50 kA return stroke shots with predrilled coupon (0.5 inch hole) in place. Check response with and without cable to Nanofast interrupted (before capacitance C_s on p. 9 of Schnetzer's report) to make sure the signal is that delivered by the cable (and not propagated around the break). This should be repeated eventually for voltage measurement setup.

Notes: Isolate Nanofast from chassis ground. Isolate CVT from collector cable.

Noise Shots- Current (See Appendix A)

Date	Shot #	SLS Current	d	Description
9/8/2009	2	58kA	0.2	0.050" T6061 Al, no hole in center, 1/4" Tungsten Electrode, 1/4" Electrode Gap, Nanofasts with cables connected to CVR and CVT Respectively. (0.2" between Coupon and collector) 1" x 1.5" slot in barrel near coupon. **Collector Current (3A)**
9/8/2009	4	53kA	0.2	0.050" T6061 Al, with 0.5" hole in center, 1/4" Tungsten Electrode, 1/4" Electrode Gap, Nanofasts with cables connected to CVR and CVT Respectively. (0.2" between Coupon and collector) 1" x 1.5" slot in barrel near coupon. **Collector Current (500A)**
9/8/2009	5	47kA	0.2	0.050" T6061 Al, with 0.5" hole in center, 1/4" Tungsten Electrode, 1/4" Electrode Gap, Nanofasts with cables disconnected from CVR and CVT Respectively. (0.2" between Coupon and collector) 1" x 1.5" slot in barrel near coupon. **Collector Current (50mA)**
9/9/2009	9	38kA	0.2	Solid 0.050" T6061 Al, Bronze wool between coupon and brass collector, 1/4" Tungsten Electrode, 1/4" Electrode Gap, Nanofasts with cables connected to CVR and CVT 1" x 1.5" slot in barrel near coupon. **Collector Current (20A)**

Noise Shots- Voltage (See Appendix B)

Date	Shot #	SLS Current	d	Description
9/9/2009	2	55kA	0.2	0.050" T6061 Al, no hole in center, 1/4" Tungsten Electrode, 1/4" Electrode Gap, Nanofast with cable disconnected from V50k Ω. (0.2" between Coupon and collector) 1" x 1.5" slot in barrel near coupon. **Collector Voltage (0.25V)**
9/9/2009	3	48kA	0.2	0.050" T6061 Al, no hole in center, 1/4" Tungsten Electrode, 1/4" Electrode Gap, Nanofast with cable connected to V50kΩ. (0.2" between Coupon and collector) 1" x 1.5" slot in barrel near coupon. **Collector Voltage (3.5V)**
9/9/2009	4	57kA	0.2	0.050" T6061 Al, no hole in center, 1/4" Tungsten Electrode, 1/4" Electrode Gap, Nanofast with cable connected to V50kΩ. (0.2" between Coupon and collector) 1" x 1.5" slot in barrel near coupon Repeat of Shot 3. **Collector Voltage (4V)**
9/9/2009	5	36kA	0.2	0.050" T6061 Al, with 0.5" hole in center, 1/4" Tungsten Electrode, 1/4" Electrode Gap, Nanofast with cable connected to V50kΩ. (0.2" between Coupon and collector) 1" x 1.5" slot in barrel near coupon. **Collector Voltage (30V)**
9/9/2009	6	49kA	0.2	0.050" T6061 Al, with 0.5" hole in center, 1/4" Tungsten Electrode, 1/4" Electrode Gap, Nanofast with cable disconnected from V50kΩ. (0.2" between Coupon and collector) 1" x 1.5" slot in barrel near coupon. **Collector Voltage (0.25V)**

9/9/2009	7	44kA	0.2	Solid 0.050" T6061 Al, Bronze wool between coupon and brass collector, 1/4" Tungsten Electrode, 1/4" Electrode Gap, Nanofast with cable connected to V50kΩ (0.2" between Coupon and collector) 1" x 1.5" slot in barrel near coupon. **Collector Voltage (3.6V)**
9/9/2009	8	47kA	0.2	Solid 0.050" T6061 Al, Bronze wool between coupon and brass collector, 1/4" Tungsten Electrode, 1/4" Electrode Gap, Nanofast with cable connected to V50kΩ (0.2" between Coupon and collector) 1" x 1.5" slot in barrel near coupon Repeat of Shot 7. **Collector Voltage (5.4V)**

1. First Return Stroke, Continuing Current, Second Return Stroke – Cable Collector – Visible High Speed Photograph of Exterior Side of Coupon

These four shots will use a 50 kA return stroke followed by a 500 A peak continuing current with a duration of approximately 2 seconds. A second return stroke with a peak of 100 kA will be fired 100 ms from the first return stroke on two of the shots and at 500 ms from the first return stroke on the other two. The distance from the strip cable to the back surface of the coupon will be 0.2 inches. These shots will measure open circuit voltage on the strip cable with the other end of the cable shorted to chassis at the side wall of the instrumentation barrel. We will use the barrel without the slot on these shots since only exterior photography will be carried out. The interior collector must be replaced by an insulator for holding the cable in place to correspond to the indirect measurements. **No tests were conducted for this task.**

The purpose of these four shots is to record cable voltage when the other end of the cable is shorted to chassis as a companion of nonlinear coupling shots to be compared to the linear indirect coupling measurements done on a lab setup.

Visual recording will be carried out during this particular test sequence. This will consist of high speed photography (20 kframes/s) with two views of the coupon surface.

These four shots will consume 4 coupons.

2. First Return Stroke, Continuing Current, Second Return Stroke – Disk Collector – Visible High Speed Photograph of Interior Side of Coupon

These eight shots will use a 50 kA return stroke followed by a 500 A peak continuing current with a duration of approximately 2 seconds. A second return stroke with a peak of 100 kA will be fired 100 ms from the first return stroke on four of the shots and at 500 ms from the first return stroke on the other four. The distance from the collector to the back surface of the coupon will be 0.2 inches for two shots and 0.8 inches for two shots. These shots will measure open circuit voltage. Noise shots will indicate whether voltage measurements are possible with the slot present. If pickup is large we may have to switch to current measurements.
High speed photograph will be carried out with images from the front of the coupon where the lightning current is incident as well as on the interior of the coupon. These may only be possible with the 0.8 inch spacing. The purpose of the interior photography is to clearly establish the timing of the first coupon puncture by looking for interior visible light (of course some light may result from coupon heating).

Visual recording will be carried out during this particular test sequence. This will consist of high speed photography (20 kframes/s) with two views of the coupon surface. We are after three things in these measurements. First, to correlate hole creation and plasma behavior and extent with electrical measurements. Second, to have a record of plasma spatial extent during the continuing current or free burning arc phase. Third, to capture plasma spatial extent of the return stroke phase. These three goals will require different exposure levels, the return stroke being the brightest (2-6 eV?), the free burning continuing arc being the next brightest (1-2 eV?), and the hot metallic hole surface being the dimmest (0.1 - 0.3 eV). Because of this different exposures on different shots will likely be required.

These eight shots will consume 8 coupons.

Voltage Shots (See Appendix C)

Date	Shot #	SLS Current	d	Description
9/10/2009	4	S(55kA) CCG(479A) 100ms N(102kA)	0.8	0.050" T6061 Al, no hole in center, 1/4" Tungsten Electrode, 1/4" Electrode Gap, Nanofast with V50k Ω. (0.8" between Coupon and collector) 1" x 1.5" slot in barrel near coupon. **Collector Voltage (35V) Photometric Data**
9/11/2009	1	S(58 kA) CCG(471A) 100ms N(107kA)	0.8	0.050" T6061 Al, no hole in center, 1/4" Tungsten Electrode, 1/4" Electrode Gap, Nanofast with V50k Ω. (0.8" between Coupon and collector) 1" x 1.5" slot in barrel near coupon. **Collector Voltage (10V) Photometric Data**
9/11/2009	2	S(46 kA) CCG(438A) 500ms N(109kA)	0.8	0.050" T6061 Al, no hole in center, 1/4" Tungsten Electrode, 1/4" Electrode Gap, Nanofast with V50k Ω. (0.8" between Coupon and collector) 1" x 1.5" slot in barrel near coupon. **Collector Voltage (28V) Photometric Data**
9/11/2009	3	S(33 kA) CCG(475A) 500ms N(106 kA)	0.8	0.050" T6061 Al, no hole in center, 1/4" Tungsten Electrode, 1/4" Electrode Gap, Nanofast with V50k Ω. (0.8" between Coupon and collector) 1" x 1.5" slot in barrel near coupon. **Collector Voltage (25V) Photometric Data**
9/14/2009	1	S (40 kA) CCG(463A) 500ms N(71 kA)	0.2	0.050" T6061 Al, no hole in center, 1/4" Tungsten Electrode, 1/4" Electrode Gap, Nanofast with V50k Ω. (0.2" between Coupon and collector) 1" x 1.5" slot in barrel near coupon. **Collector Voltage (20V) Photometric Data**
9/14/2009	2	S (51 kA) CCG(495A) 500ms N(78 kA)	0.2	0.050" T6061 Al, no hole in center, 1/4" Tungsten Electrode, 1/4" Electrode Gap, Nanofast with V50k Ω. (0.2" between Coupon and collector) 1" x 1.5" slot in barrel near coupon. **Collector Voltage (38V) Photometric Data**

9/14/2009	3	S(51kA) CCG(467A) 100ms N(86 kA)	0.2	0.050" T6061 Al, no hole in center, 1/4" Tungsten Electrode, 1/4" Electrode Gap, Nanofast with V50k Ω. (0.2" between Coupon and collector) 1" x 1.5" slot in barrel near coupon. **Collector Voltage (50V) Photometric Data**
9/14/2009	4	S(41 kA) CCG(496A) 100ms N(76 kA)	0.2	0.050" T6061 Al, no hole in center, 1/4" Tungsten Electrode, 1/4" Electrode Gap, Nanofast with V50k Ω. (0.2" between Coupon and collector) 1" x 1.5" slot in barrel near coupon. **Collector Voltage (8V) Photometric Data**

3. First Return Stroke, Continuing Current, Second Return Stroke – No Collector – Axial (Normal Angle) Visible Interior Photography

These four shots will consist of a 50 kA first return stroke for triggering the arc, a 500 A peak continuing current with 2 second duration, and a 100 kA second return stroke occurring at either 100 ms after the first return stroke (two shots) or 500 ms after the first return stroke (two shots). There will be no electrical measurements. High speed photography will be used from both the exterior and interior sides of the coupons. The purpose is to get a high angle view of the coupon interior with the collector and all other instrumentation removed to clear up any confusion about the grazing angle images on the preceding shots. Photometric shots only, No electrical data collected.

Photometric Shots

Date	Shot #	SLS Current	d	Description
9/17/2009	7	S(61kA) CCG(467A) 100ms N(90kA)	0.8	0.050" T6061 Al, No Hole in center, 1/4" Tungsten Electrode, 1/4" Electrode Gap, (0.2" between Coupon and collector) Solid barrel. 100ms interpulse spacing. **Photometric Data**
9/17/2009	8	S(48kA) CCG(524A) 500ms N(114kA)	0.8	0.050" T6061 Al, No Hole in center, 1/4" Tungsten Electrode, 1/4" Electrode Gap, (0.2" between Coupon and collector) Solid barrel. 500ms interpulse spacing. **Photometric Data**

These 4 shots will consume 4 coupons.

In addition to these shots two more may be carried out with the starter wire arrangement discussed next. **No starter wire shots conducted.**

These two extra shots will consume another 2 coupons.

4. Starter Wire, Continuing Current, First Return Stroke, Continuing Current, Second Return Stroke – Disc Collector – High Speed Photography

These eight shots will use a thin starter wire to initiate the continuing current, a 500 A peak continuing current with 2 second duration, a 50 kA first return stroke 400 ms following the fusing of the starter wire, and a 100 kA second return stroke following the first stroke by 100 ms. The distance from the coupon to the collector will be 0.2 inches for two shots and 0.8 inches for two shots. The attempt here is to provide the worst-case hole size within natural lightning

statistical parameters at the time of the second return stoke. We are attempting to first melt and perforate the coupon, blow a bigger hole in it with the first return stroke, and couple voltage and current in with the second return stroke. Natural lightning may have several return strokes, but by providing near worst case continuing current duration and amplitude, followed by a large return stroke, and an extreme return stroke, we hope to capture near maximum penetrant levels. Four shots will measure short circuit current and four shots will measure open circuit voltage.

These eight shots will consume 8 coupons.

Current Shots (See Appendix D)

Date	Shot #	SLS Current	d	Description
9/16/2009	4	Starter 400ms S(56kA) CCG(530A) 100ms N(101kA)	0.8	0.050" T6061 Al, no hole in center, 1/4" Tungsten Electrode, 1/4" Electrode Gap, Nanofast with 5mΩ CVR. Starter wire CCG for 400ms Spulse CCG for 100ms Npulse (0.8" between Coupon and collector) 1" x 1.5" slot in barrel near coupon. **Collector Current (S350A, N110A) Photometric Data**
9/16/2009	5	Starter 400ms S(55 kA) CCG(506A) 100ms N(99kA)	0.8	0.050" T6061 Al, no hole in center, 1/4" Tungsten Electrode, 1/4" Electrode Gap, Nanofast with 5mΩ CVR. Starter wire CCG for 400ms Spulse CCG for 100ms Npulse (0.8" between Coupon and collector) 1" x 1.5" slot in barrel near coupon. **Collector Current (S200A, N1150A) Photometric Data**
9/17/2009	1	Starter 400ms S(58 kA) CCG(522A) 100ms N(109kA)	0.2	0.050" T6061 Al, no hole in center, 1/4" Tungsten Electrode, 1/4" Electrode Gap, Nanofast with 5mΩ CVR. Starter wire CCG for 400ms Spulse CCG for 100ms Npulse (0.2" between Coupon and collector) Solid barrel **Collector Current (S300A, N1100) Photometric Data**
9/17/2009	2	Starter 400ms S(50 kA) CCG(514A) 100ms N(109 kA)	0.2	0.050" T6061 Al, no hole in center, 1/4" Tungsten Electrode, 1/4" Electrode Gap, Nanofast with 5mΩ CVR. Starter wire CCG for 400ms Spulse CCG for 100ms Npulse (0.2" between Coupon and collector) Solid barrel **Collector Current (S300A, N1150) Photometric Data**

Voltage Shots (See Appendix E)

Date	Shot #	SLS Current	d	Description
9/16/2009	2	Starter 400ms S(36kA) CCG(477A) 100ms N(106kA)	0.8	0.050" T6061 Al, no hole in center, 1/4" Tungsten Electrode, 1/4" Electrode Gap, Nanofast with V50k Ω. Starter wire CCG for 400ms Spulse CCG for 100ms Npulse (0.8" between Coupon and collector) 1" x 1.5" slot in barrel near coupon. **Collector Voltage (S5V, N15V) Photometric Data**

9/16/2009	3	Starter 400ms S(59 kA) CCG(486A) 100ms N(99kA)	0.8	0.050" T6061 Al, no hole in center, 1/4" Tungsten Electrode, 1/4" Electrode Gap, Nanofast with V50k Ω. Starter wire CCG for 400ms Spulse CCG for 100ms Npulse (0.8" between Coupon and collector) 1" x 1.5" slot in barrel near coupon. **Collector Voltage (S13V, N38V) Photometric Data**
9/17/2009	3	Starter 400ms S(55 kA) CCG(502A) 100ms N(108kA)	0.2	0.050" T6061 Al, no hole in center, 1/4" Tungsten Electrode, 1/4" Electrode Gap, Nanofast with V50k Ω. Starter wire CCG for 400ms Spulse CCG for 100ms Npulse (0.2" between Coupon and collector) Solid barrel **Collector Voltage (S13V, N36V) Photometric Data**
9/17/2009	4	Starter 400ms S(56 kA) CCG(551A) 100ms N(91 kA)	0.2	0.050" T6061 Al, no hole in center, 1/4" Tungsten Electrode, 1/4" Electrode Gap, Nanofast with V50k Ω. Starter wire CCG for 400ms Spulse CCG for 100ms Npulse (0.2" between Coupon and collector) Solid barrel **Collector Voltage (S19V N85) Photometric Data**

High speed photography will be needed on these shots to document hole size chronology and timing of the strokes. If the normal incidence photography proves valuable on the preceding series we will conduct two extra shots with this angle of photography and the instrumentation removed from the interior. **Two extra shots with instrumentation removed were not conducted.**

These extra shots will consume an additional 2 coupons.

We may add two additional shots with a cable present. The cable spacing will be 0.2 inches. One shot will have the cable floating and one shot will have the cable shorted to chassis on one end. **No floating cable tests were conducted.**

These additional shots will consume 2 coupons and 2 cables.

5. Predrilled Hole - Disk Collector – Closer Spaced Electrode – Precursor to Collector Attachment Experiments

Use 0.5 inch predrilled hole in 6061 alloy aluminum coupon. Conduct 6 shots with 50 kA return strokes only. These shots will look at open circuit voltage in this series. The first two will be at 0.25 inch electrode spacing. These will be compared to previous predrilled hole levels (10 V - 50 V). The next two shots will use 0.125 inch electrode spacing. Depending on the increases in the levels observed we will or will not proceed to 0.0625 inch spacing.

Voltage Shots (See Appendix E)

Date	Shot #	SLS Current	d	Description
9/18/2009	1	S(31kA)	0.2	0.050" T6061 Al, with 0.5" hole in center, 1/4" Tungsten Electrode, 1/4" Electrode Gap, Nanofast with cable connected to V50kΩ. (0.2" between Coupon and collector) **Collector Voltage (50V)**

9/182009	2	S(53kA)	0.2	0.050" T6061 Al, with 0.5" hole in center, 1/4" Tungsten Electrode, 1/4" Electrode Gap, Nanofast with cable connected to V50kΩ. (0.2" between Coupon and collector) **Collector Voltage (52V)**
9/18/2009	3	S(60kA)	0.2	0.050" T6061 Al, with 0.5" hole in center, 1/4" Tungsten Electrode, 1/8 Electrode Gap, Nanofast with cable connected to V50kΩ. (0.2" between Coupon and collector) **Collector Voltage (69V)**
9/18/2009	4	S(60kA)	0.2	0.050" T6061 Al, with 0.5" hole in center, 1/4" Tungsten Electrode, 1/16" Electrode Gap, Nanofast with cable connected to V50kΩ. (0.2" between Coupon and collector) **Collector Voltage (90V)**
9/18/2009	5	S(52kA)	0.2	0.050" T6061 Al, with 0.5" hole in center, 1/4" Tungsten Electrode, 1/16" Electrode Gap, Nanofast with cable connected to V50kΩ. (0.2" between Coupon and collector) **Collector Voltage (91V)**

In FY10 we plan to continue this experiment until we achieve arc attachment to the collector. This will require either the use of a sacrificial ODL (older, possibly expendable, units we have in hand need some refurbishment for use) or some form of protection on the newer nanofast ODL. The purpose of these shots is to experimentally test the arcing threshold predictions for collector attachment versus attachment to the chassis (coupon). This type of information is important in establishing how probable interior arc attachments are.

These shots will consume 1 or 2 coupons.

6. First Return Stroke and Continuing Current – Disc Collector – Late Time Voltage and Current

These four shots will use a 50 kA first return stroke followed by a 500 A peak continuing current with 2 second duration. These four shots will use a disc collector below the coupon. The distance from the coupon back surface to the cable will nominally be 0.2 inches on two shots and 0.8 inches on two shots. Two shots will measure short circuit current and two shots will measure open circuit voltage. The TTI ODL will be used to capture late time penetrations which were filtered out in round one experiments.

Current Shots (See Appendix G)

Date	Shot #	SLS Current	d	Description
2/17/2010	5	S(53kA) CCG (400A)	0.8	0.050" T6061 Al, no hole in center, 1/4" Tungsten Electrode, 1/4" Electrode Gap, TTI F/O with 5mΩ CVR. (0.8" between Coupon and collector) **Collector Current (25A)**
2/17/2010	6	S(61 kA) CCG (386A)	0.8	0.050" T6061 Al, no hole in center, 1/4" Tungsten Electrode, 1/4" Electrode Gap, TTI F/O with 5mΩ CVR. (0.8" between Coupon and collector) **Collector Current (43A)**

Voltage Shots (See Appendix H)

Date	Shot #	SLS Current	d	Description
2/23/2010	5	S(27 kA) CCG (375A)	0.8	0.050" T6061 Al, no hole in center, 1/4" Tungsten Electrode, 1/4" Electrode Gap, TTI F/O with 5kΩ Resistor. (0.8" between Coupon and collector) **Collector Voltage (10V)**
2/23/2010	7	S(55kA) CCG (363A)	0.8	0.050" T6061 Al, no hole in center, 1/4" Tungsten Electrode, 1/4" Electrode Gap, TTI F/O with 50kΩ Resistor. (0.8" between Coupon and collector) **Collector Voltage (35V)**
2/26/2010	7	S(45 kA) CCG (379A)	0.8	0.050" T6061 Al, no hole in center, 1/4" Tungsten Electrode, 1/4" Electrode Gap, TTI F/O with 50kΩ Resistor. (0.8" between Coupon and collector) **Collector Voltage (15V)**
3/3/2010	3	S(58 kA) CCG (351A)	0.8	0.050" T6061 Al, no hole in center, 1/4" Tungsten Electrode, 1/4" Electrode Gap, NF Hi-Z probe. (0.8" between Coupon and collector) **Collector Voltage (20V)**
2/26/2010	5	S(51 kA) CCG (375A)	0.2	0.050" T6061 Al, no hole in center, 1/4" Tungsten Electrode, 1/4" Electrode Gap, TTI F/O with 50kΩ Resistor. (0.2" between Coupon and collector) **Collector Voltage (10V)**
2/26/2010	6	S(59 kA) CCG (388A)	0.2	0.050" T6061 Al, no hole in center, 1/4" Tungsten Electrode, 1/4" Electrode Gap, TTI F/O with 50kΩ Resistor. (0.2" between Coupon and collector) **Collector Voltage (10V)**

Battery life (one hour) is a critical issue with these ODLs.

These four shots will consume 4 coupons and 4 cable samples.

References:

[1] G. H. Schnetzer, R. J. Fisher, and M. A. Dinallo, "Measured Responses of Internal Enclosures and Cables Due To Burnthrough Penetration of Weapon Cases by Lightning," SAND94-0312, August 1994.

[2] R. J. Fisher and M. A. Uman, "Recommended Baseline Direct-Strike Lightning Environment for Stockpile-to-Target Sequences," SAND 89-0192, May 1989.

[3] L. K. Warne, L. E. Martinez, and R. E. Jorgenson, "Experimental Plan (First Round)," Internal Sandia Memorandum, March 27, 2009.

Task 0: Noise Shots-Current

Description:
Solid 0.050" 6061 Al, 1/4" Tungsten Electrode, 1/4" Electrode Gap, Nanofast with cable connected to 5mΩ CVR. Distance from back of coupon to collector is 0.2”
1" x 1.5" slot in barrel near coupon

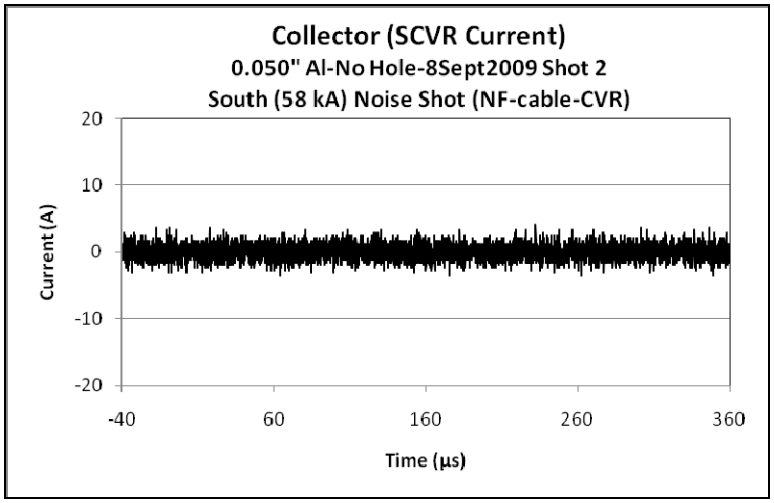

Description:
0.050" 6061 Al with 0.5” hole, 1/4" Tungsten Electrode, 1/4" Electrode Gap, Nanofast with cable connected to 5mΩ CVR. Distance from back of coupon to collector is 0.2”
1" x 1.5" slot in barrel near coupon

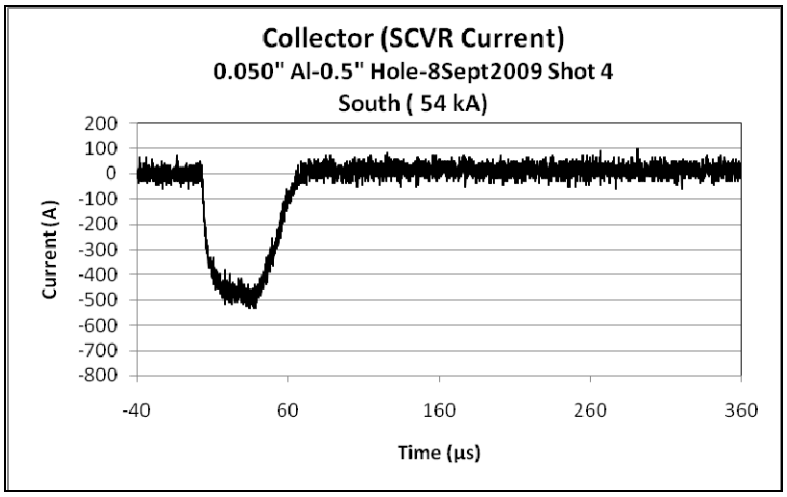

Task 0: Noise Shots-Current

Description:
0.050" 6061 Al with 0.5" hole, 1/4" Tungsten Electrode, 1/4" Electrode Gap, Nanofast with cable disconnected to 5mΩ CVR. Distance from back of coupon to collector is 0.2"
1" x 1.5" slot in barrel near coupon

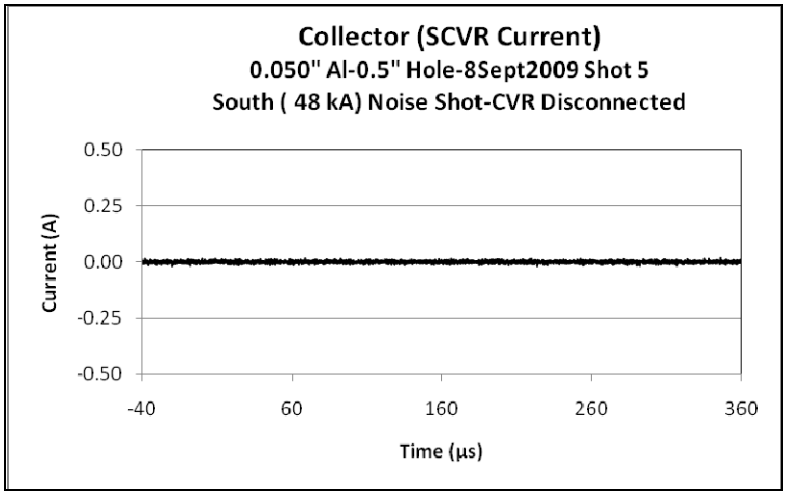

Description:
Solid 0.050" T6061 Al, Bronze wool between coupon and brass collector, 1/4" Tungsten Electrode, 1/4" Electrode Gap, Nanofasts with cables connected to 5mΩ CVR. Distance from back of coupon to collector is 0.2"
1" x 1.5" slot in barrel near coupon

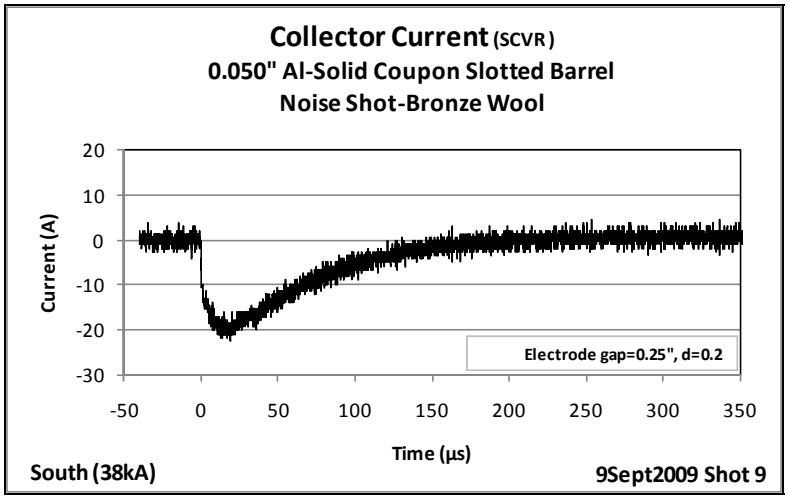

Task 0: Noise Shots-Voltage

Description:
Solid 0.050" 6061 Al, 1/4" Tungsten Electrode, 1/4" Electrode Gap, Nanofast with cable disconnected from V50k probe. Distance from back of coupon to collector is 0.2"
1" x 1.5" slot in barrel near coupon

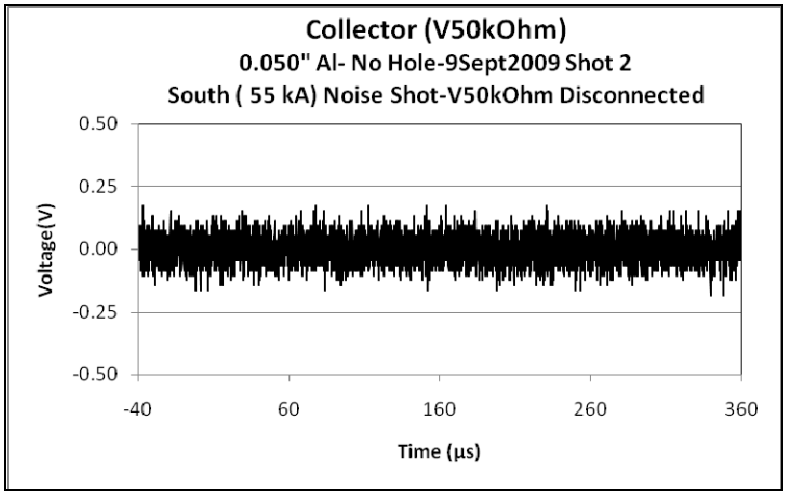

Description:
Solid 0.050" 6061 Al, 1/4" Tungsten Electrode, 1/4" Electrode Gap, Nanofast with cable connected to V50k probe. Distance from back of coupon to collector is 0.2"
1" x 1.5" slot in barrel near coupon

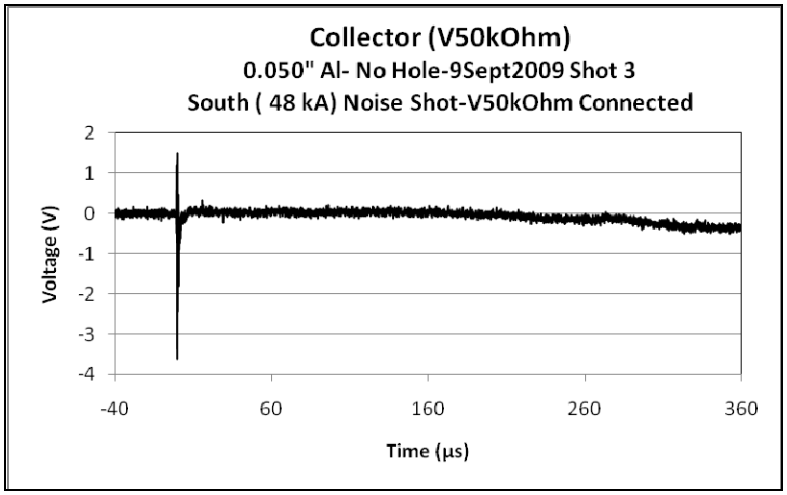

Task 0: Noise Shots-Voltage

Description:
Solid 0.050" 6061 Al, 1/4" Tungsten Electrode, 1/4" Electrode Gap, Nanofast with cable connected to V50k probe. Distance from back of coupon to collector is 0.2”
1" x 1.5" slot in barrel near coupon

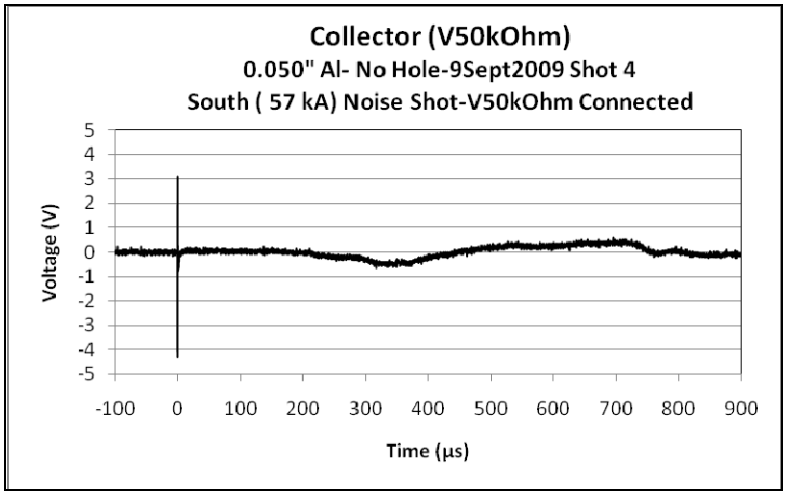

Description:
0.050" 6061 Al with 0.5” hole, 1/4" Tungsten Electrode, 1/4" Electrode Gap, Nanofast with cable connected to V50k probe. Distance from back of coupon to collector is 0.2”
1" x 1.5" slot in barrel near coupon

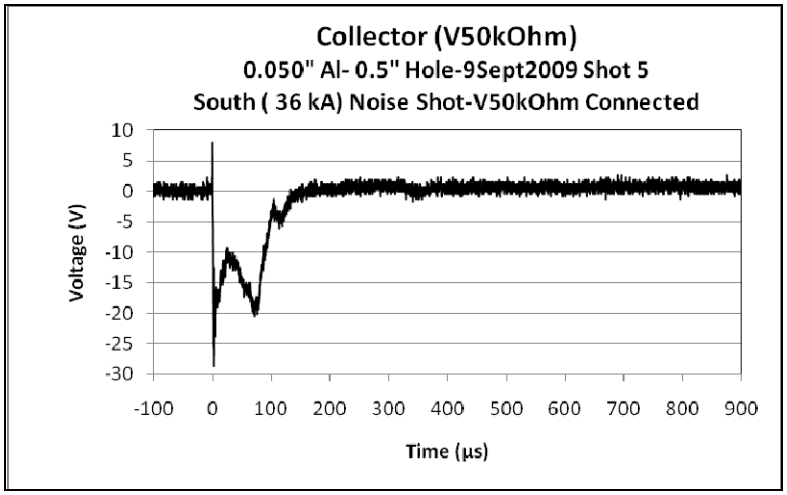

Task 0: Noise Shots-Voltage

Description:
0.050" 6061 Al with 0.5” hole, 1/4" Tungsten Electrode, 1/4" Electrode Gap, Nanofast with cable disconnected from V50k probe. Distance from back of coupon to collector is 0.2”
1" x 1.5" slot in barrel near coupon

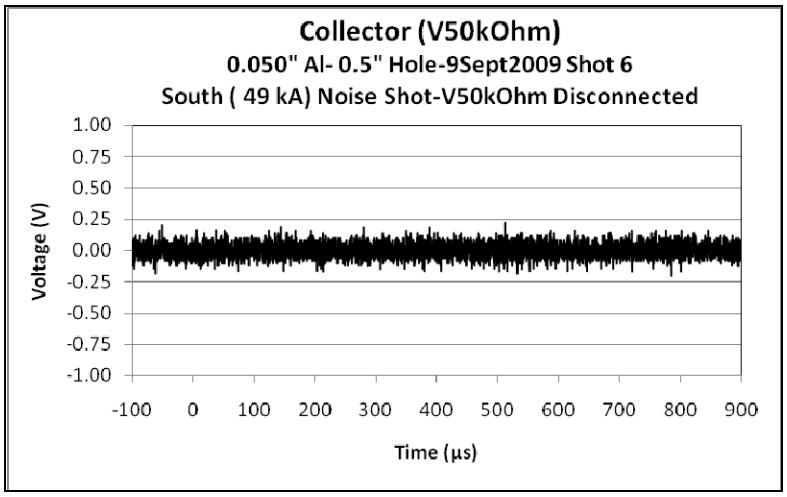

Description:
0.050" 6061 Al with 0.5” hole, 1/4" Tungsten Electrode, 1/4" Electrode Gap, Nanofast with cable connected to V50k probe. Distance from back of coupon to collector is 0.2” Bronze wool between coupon and collector
1" x 1.5" slot in barrel near coupon

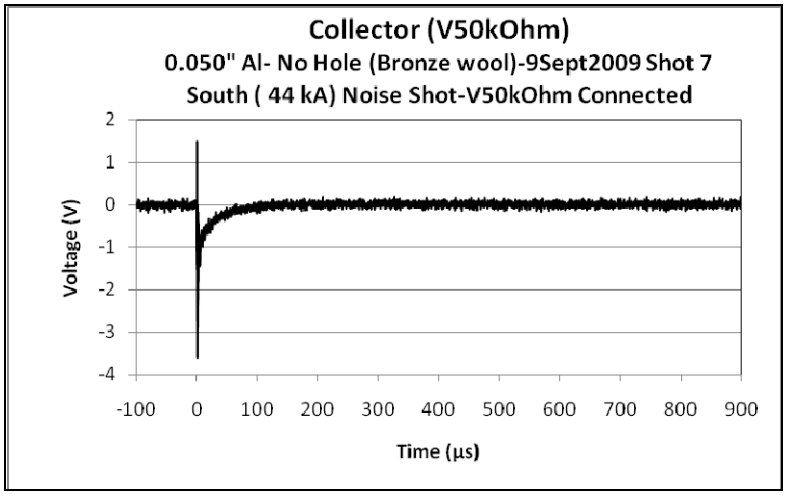

Task 0: Noise Shots-Voltage

Description:
0.050" 6061 Al with 0.5" hole, 1/4" Tungsten Electrode, 1/4" Electrode Gap, Nanofast with cable connected to V50k probe. Distance from back of coupon to collector is 0.2" Bronze wool between coupon and collector
1" x 1.5" slot in barrel near coupon

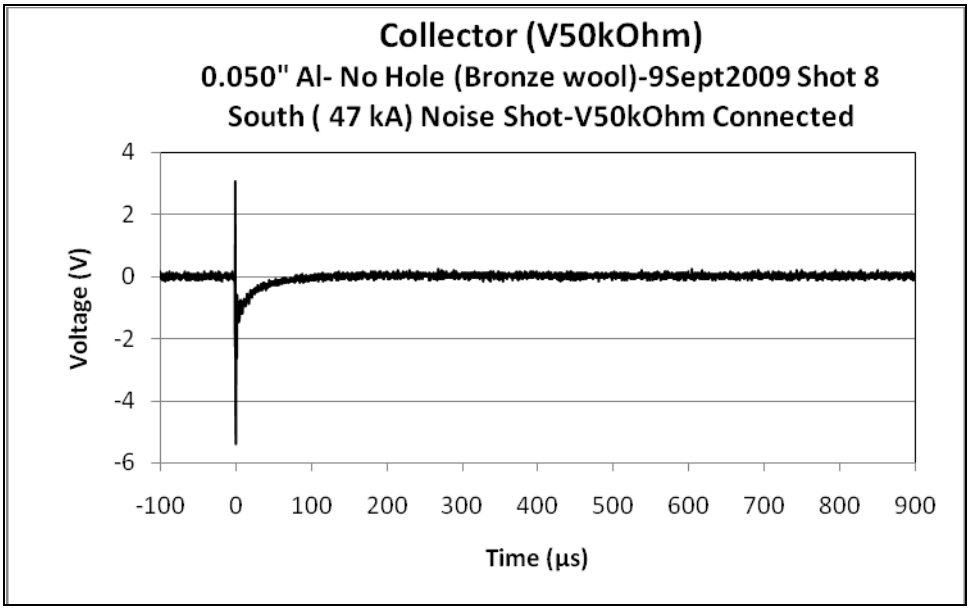

Task 2: First Return Stroke, Continuing Current, Second Return Stroke – Disk Collector – Visible High Speed Photograph of Interior Side of Coupon

Description:
Solid 0.050" 6061 Al, 1/4" Tungsten Electrode, 1/4" Electrode Gap, Nanofast with cable connected to V50k probe. Distance from back of coupon to collector is 0.8", 100ms interpulse 1" x 1.5" slot in barrel near coupon

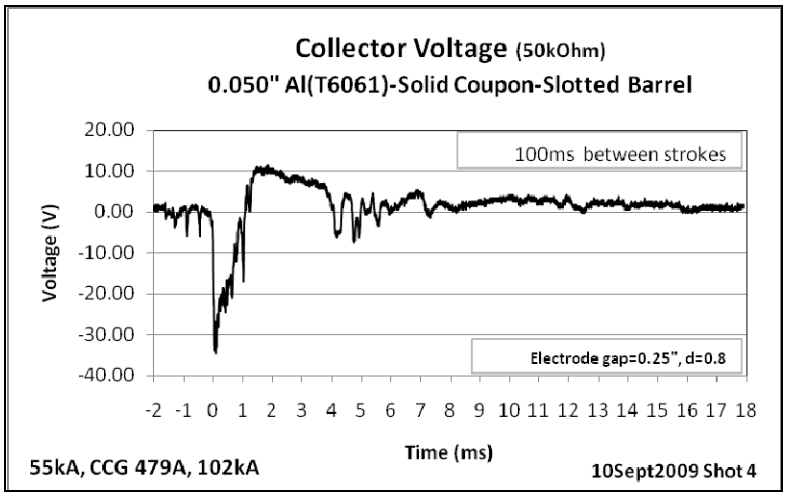

Description:
Solid 0.050" 6061 Al, 1/4" Tungsten Electrode, 1/4" Electrode Gap, Nanofast with cable connected to V50k probe. Distance from back of coupon to collector is 0.8", 100ms interpulse 1" x 1.5" slot in barrel near coupon

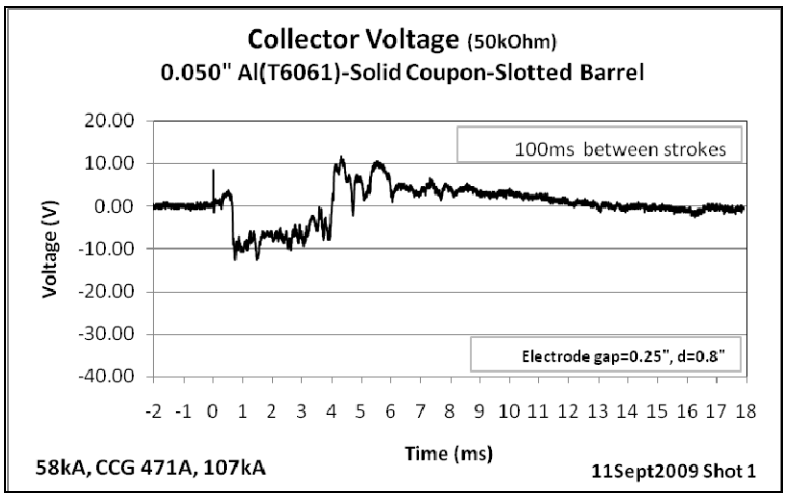

Task 2: First Return Stroke, Continuing Current, Second Return Stroke – Disk Collector – Visible High Speed Photograph of Interior Side of Coupon

Description:
Solid 0.050" 6061 Al, 1/4" Tungsten Electrode, 1/4" Electrode Gap, Nanofast with cable connected to V50k probe. Distance from back of coupon to collector is 0.8", 500ms interpulse 1" x 1.5" slot in barrel near coupon

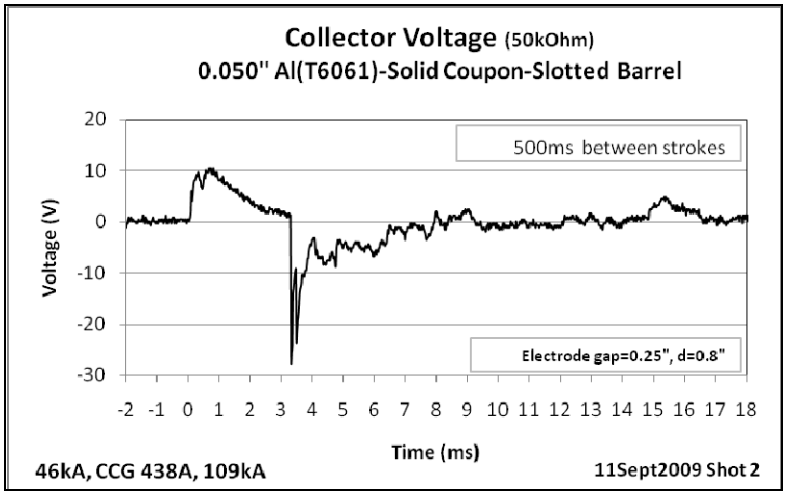

Description:
Solid 0.050" 6061 Al, 1/4" Tungsten Electrode, 1/4" Electrode Gap, Nanofast with cable connected to V50k probe. Distance from back of coupon to collector is 0.8", 500ms interpulse 1" x 1.5" slot in barrel near coupon

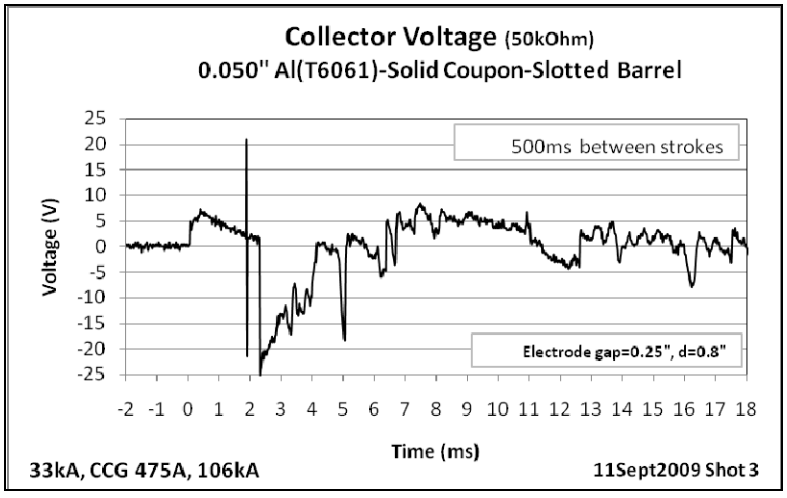

Task 2: First Return Stroke, Continuing Current, Second Return Stroke – Disk Collector – Visible High Speed Photograph of Interior Side of Coupon

Description:
Solid 0.050" 6061 Al, 1/4" Tungsten Electrode, 1/4" Electrode Gap, Nanofast with cable connected to V50k probe. Distance from back of coupon to collector is 0.2", 500ms interpulse 1" x 1.5" slot in barrel near coupon

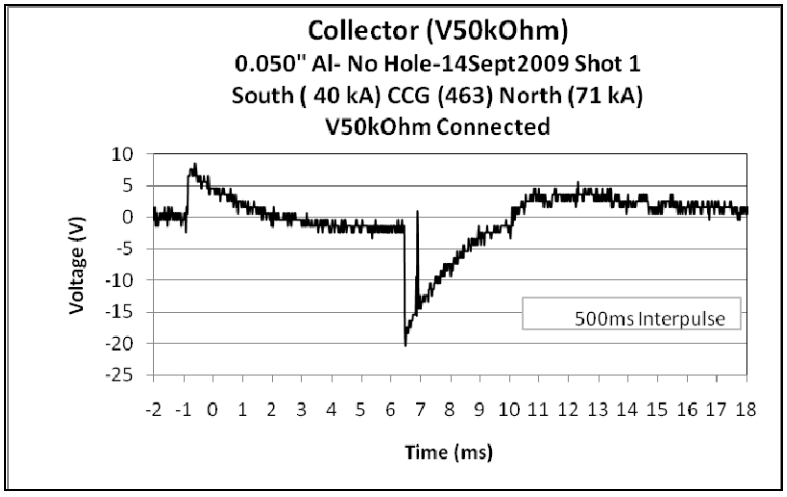

Description:
Solid 0.050" 6061 Al, 1/4" Tungsten Electrode, 1/4" Electrode Gap, Nanofast with cable connected to V50k probe. Distance from back of coupon to collector is 0.2", 500ms interpulse 1" x 1.5" slot in barrel near coupon

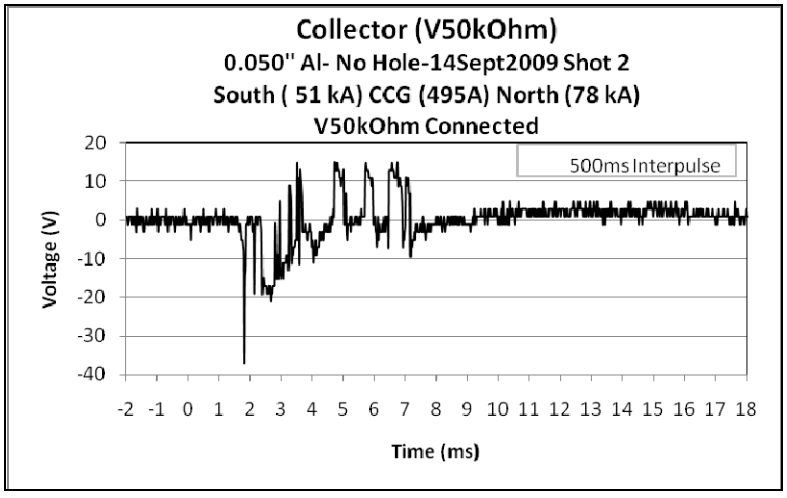

Task 2: First Return Stroke, Continuing Current, Second Return Stroke – Disk Collector – Visible High Speed Photograph of Interior Side of Coupon

Description:
Solid 0.050" 6061 Al, 1/4" Tungsten Electrode, 1/4" Electrode Gap, Nanofast with cable connected to V50k probe. Distance from back of coupon to collector is 0.2", 100ms interpulse 1" x 1.5" slot in barrel near coupon

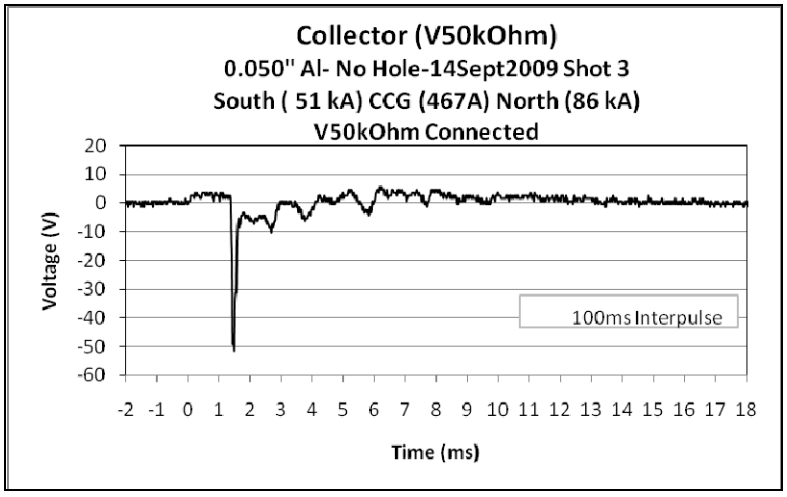

Description:
Solid 0.050" 6061 Al, 1/4" Tungsten Electrode, 1/4" Electrode Gap, Nanofast with cable connected to V50k probe. Distance from back of coupon to collector is 0.2", 100ms interpulse 1" x 1.5" slot in barrel near coupon

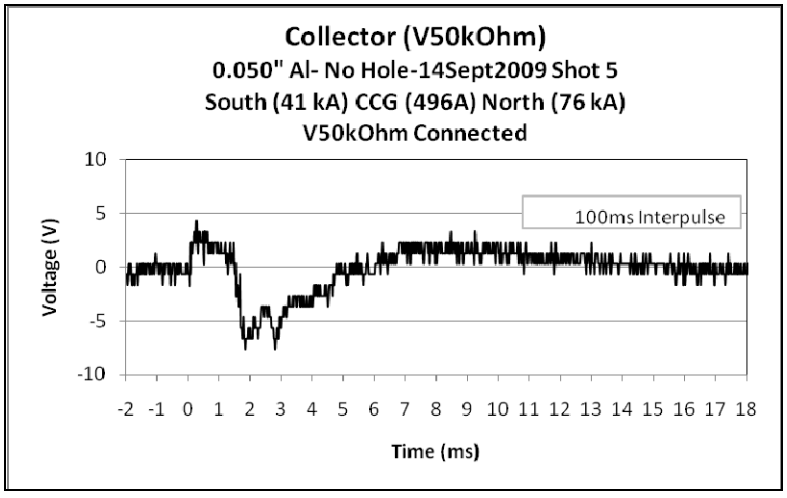

Task 4: Starter Wire, Continuing Current, First Return Stroke, Continuing Current, Second Return Stroke – Disc Collector – High Speed Photography

Description: Long time scale-current
Solid 0.050" 6061 Al, 1/4" Tungsten Electrode, 1/4" Electrode Gap, Nanofast with 5mΩ CVR. Starter wire CCG for 400ms Spulse CCG for 100ms Npulse. Distance from back of coupon to collector is 0.8", 1" x 1.5" slot in barrel near coupon.

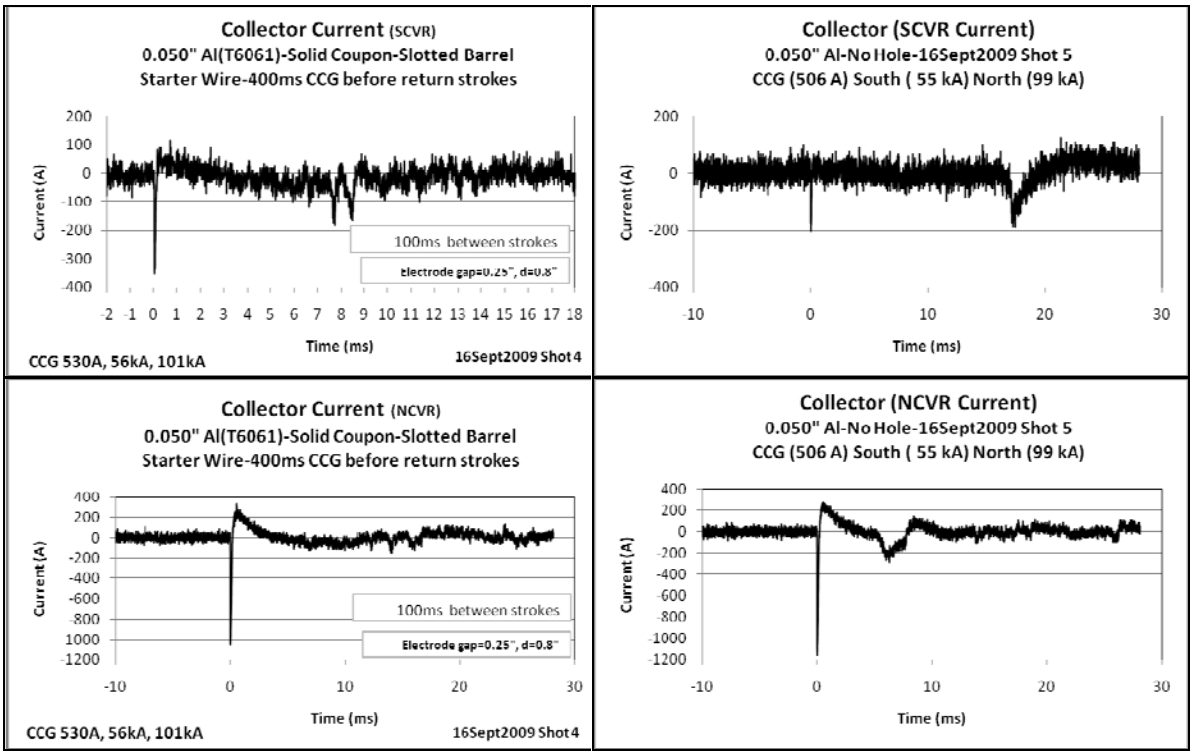

Task 4: Starter Wire, Continuing Current, First Return Stroke, Continuing Current, Second Return Stroke – Disc Collector – High Speed Photography

Description: Long time scale-current
Solid 0.050" 6061 Al, 1/4" Tungsten Electrode, 1/4" Electrode Gap, Nanofast with 5mΩ CVR. Starter wire CCG for 400ms Spulse CCG for 100ms Npulse. Distance from back of coupon to collector is 0.2", Solid barrel

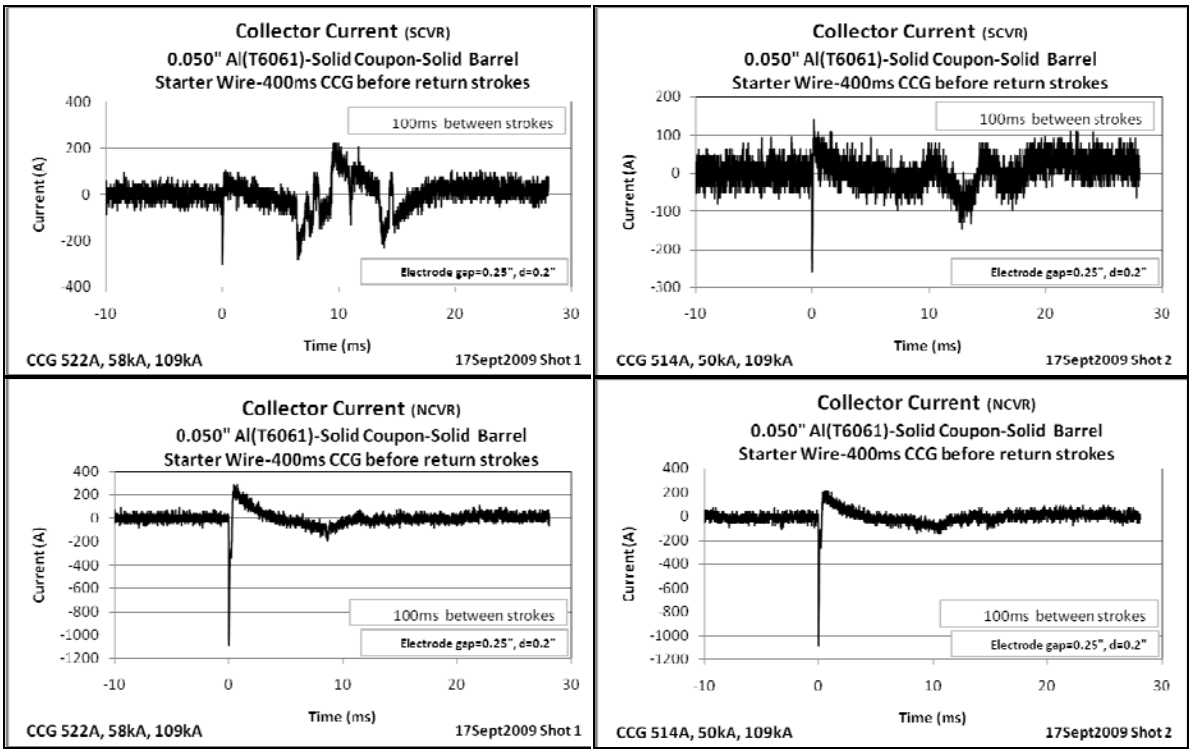

Description: Short time scale-current for Shot 2 above

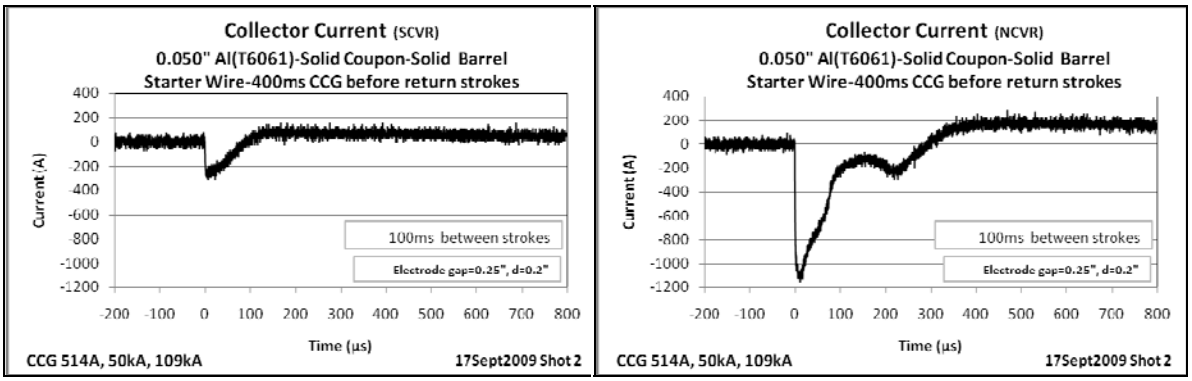

Task 4: Starter Wire, Continuing Current, First Return Stroke, Continuing Current, Second Return Stroke – Disc Collector – High Speed Photography

Description: Long time scale-voltage
Solid 0.050" 6061 Al, 1/4" Tungsten Electrode, 1/4" Electrode Gap, Nanofast with 50kΩ resistor. Starter wire CCG for 400ms Spulse CCG for 100ms Npulse. Distance from back of coupon to collector is 0.8", 1" x 1.5" slot in barrel near coupon.

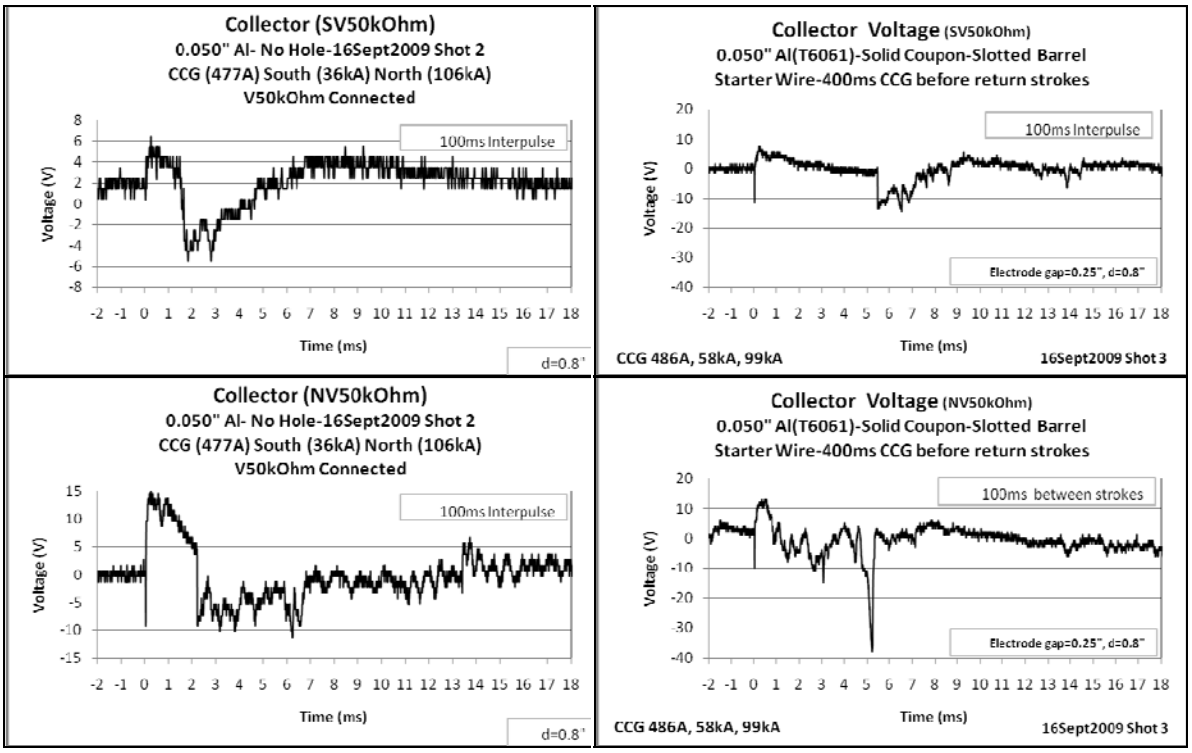

Task 4: Starter Wire, Continuing Current, First Return Stroke, Continuing Current, Second Return Stroke – Disc Collector – High Speed Photography

Description: Long time scale-voltage
Solid 0.050" 6061 Al, 1/4" Tungsten Electrode, 1/4" Electrode Gap, Nanofast with 50kΩ resistor. Starter wire CCG for 400ms Spulse CCG for 100ms Npulse. Distance from back of coupon to collector is 0.2", 1" x 1.5" solid barrel

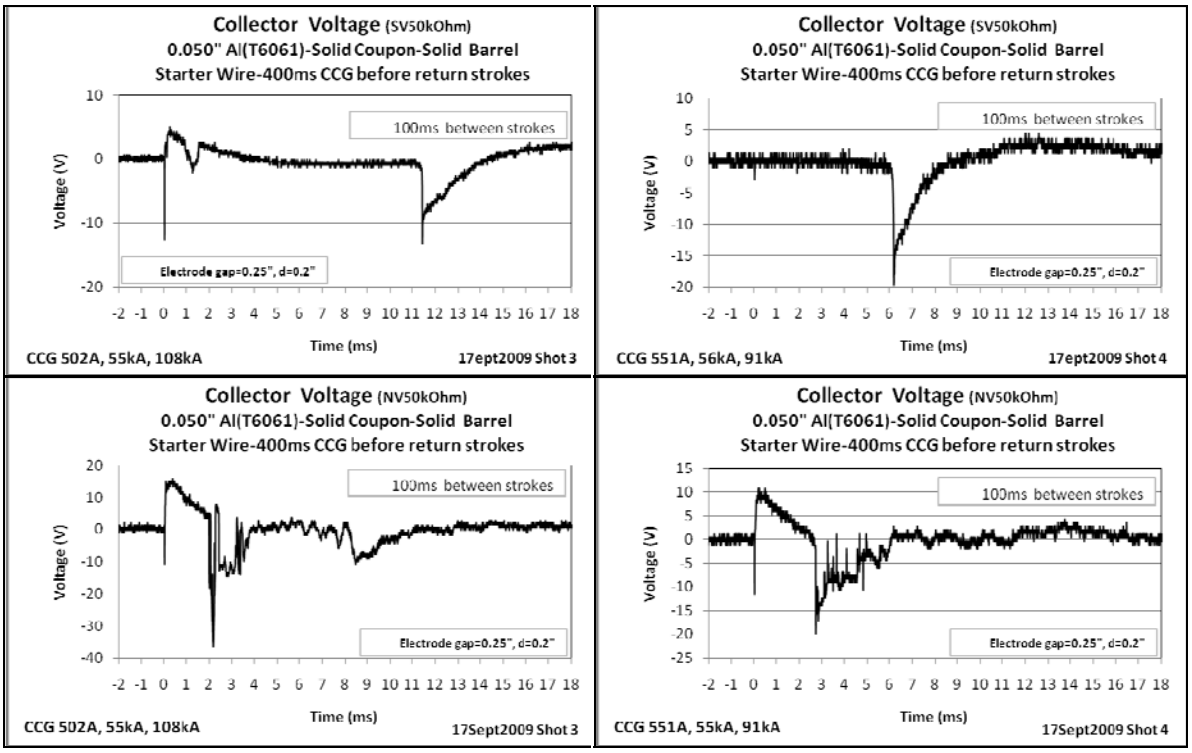

Description: Short time scale-voltage for Shot 4 above

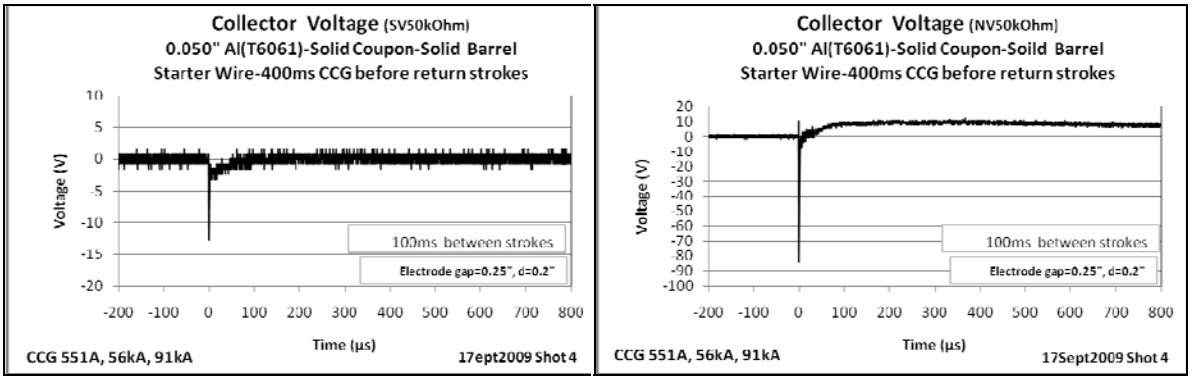

5. Predrilled Hole - Disk Collector – Closer Spaced Electrode – Precursor to Collector Attachment Experiments

Description:
0.050" T6061 Al, with 0.5" hole in center, 1/4" Tungsten Electrode, 1/4" Electrode Gap, Nanofast with cable connected to V50kΩ. (0.2" between Coupon and collector)

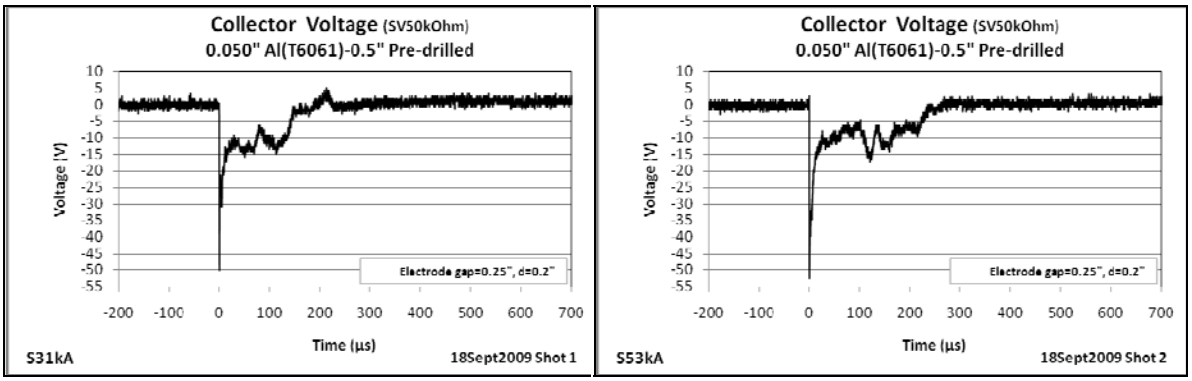

Description:
0.050" T6061 Al, with 0.5" hole in center, 1/4" Tungsten Electrode, 1/8" Electrode Gap, Nanofast with cable connected to V50kΩ. (0.2" between Coupon and collector)

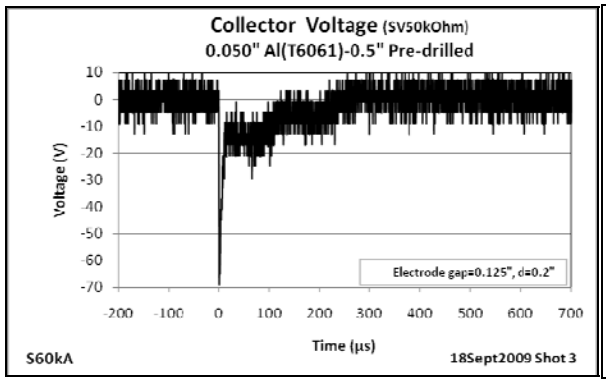

No Data

Description:
0.050" T6061 Al, with 0.5" hole in center, 1/4" Tungsten Electrode, 1/8" Electrode Gap, Nanofast with cable connected to V50kΩ. (0.2" between Coupon and collector)

5. Predrilled Hole - Disk Collector – Closer Spaced Electrode – Precursor to Collector Attachment Experiments

Description:
0.050" T6061 Al, with 0.5" hole in center, 1/4" Tungsten Electrode, 1/16" Electrode Gap, Nanofast with cable connected to V50kΩ. (0.2" between Coupon and collector)

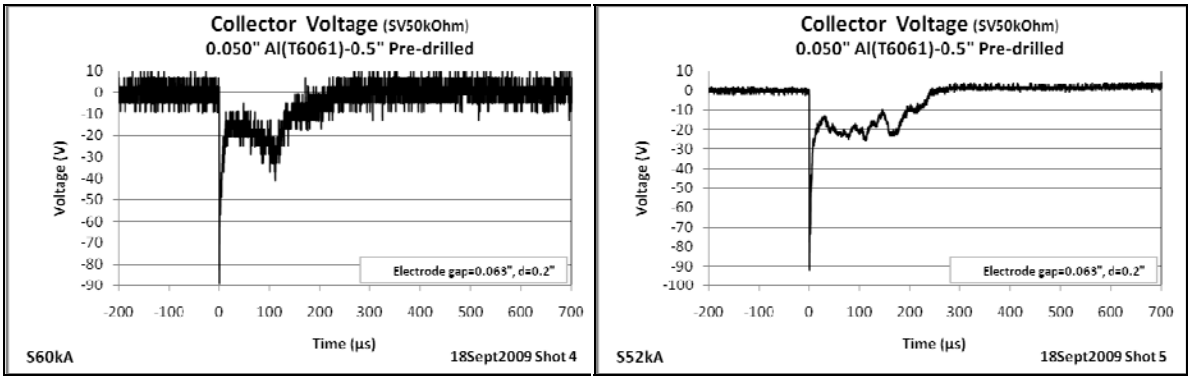

6. First Return Stroke and Continuing Current – Disc Collector – Late Current

Description:
0.050" T6061 Al, no hole in center, 1/4" Tungsten Electrode, 1/4" Electrode Gap, TTI F/O with 5mΩ CVR. (0.8" between Coupon and collector)

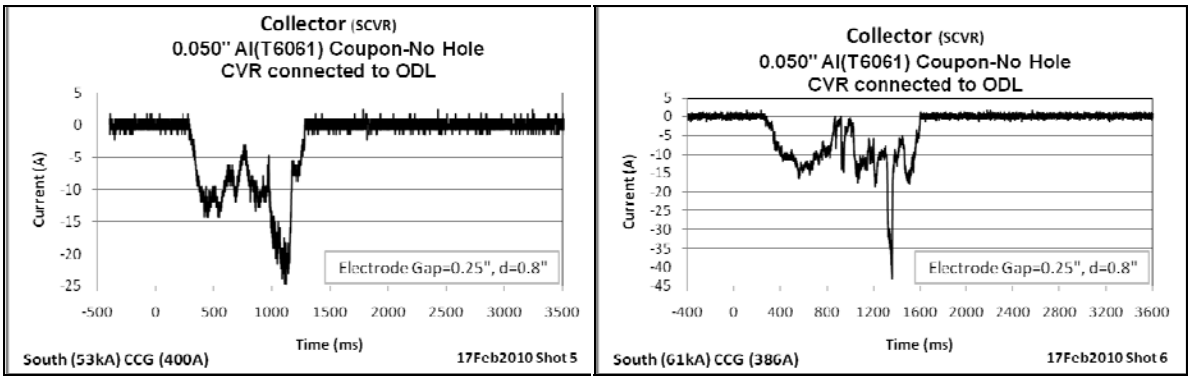

6. First Return Stroke and Continuing Current – Disc Collector – Late Time Voltage

Description:
0.050" T6061 Al, no hole in center, 1/4" Tungsten Electrode, 1/4" Electrode Gap
(0.8" between Coupon and collector)

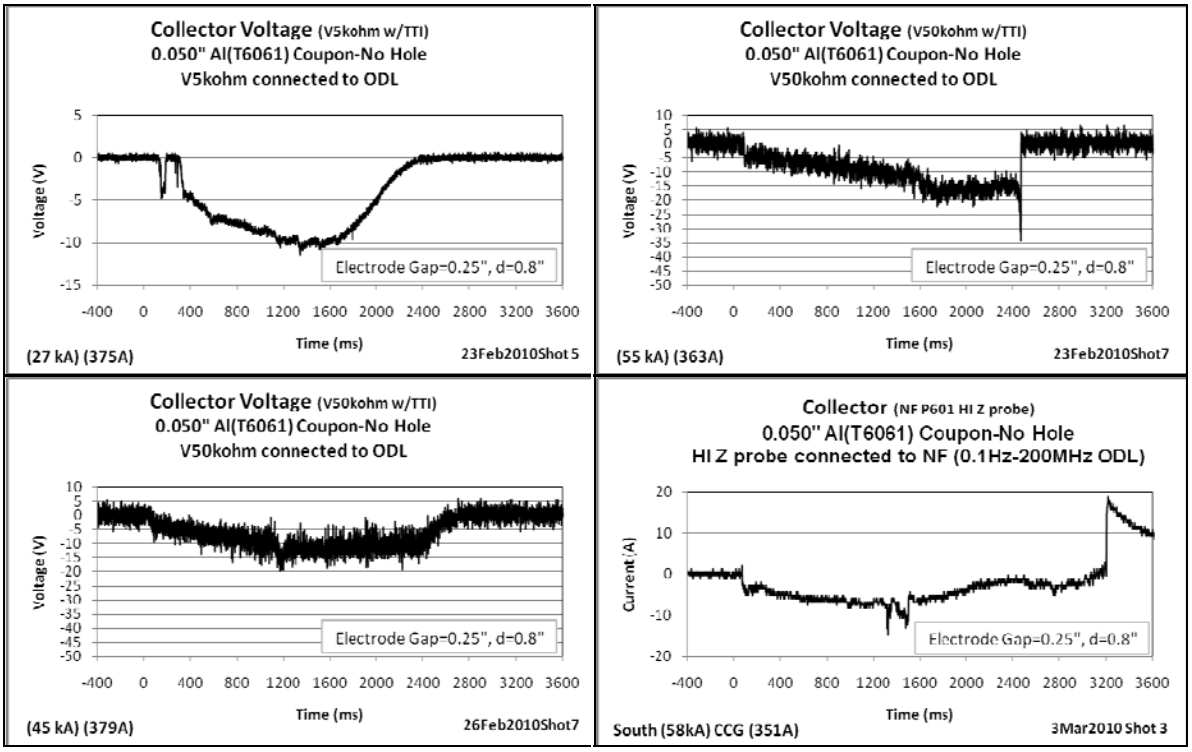

6. First Return Stroke and Continuing Current – Disc Collector – Late Time Voltage

Description:
0.050" T6061 Al, no hole in center, 1/4" Tungsten Electrode, 1/4" Electrode Gap, TTI F/O with V50kΩ. (0.2" between Coupon and collector)

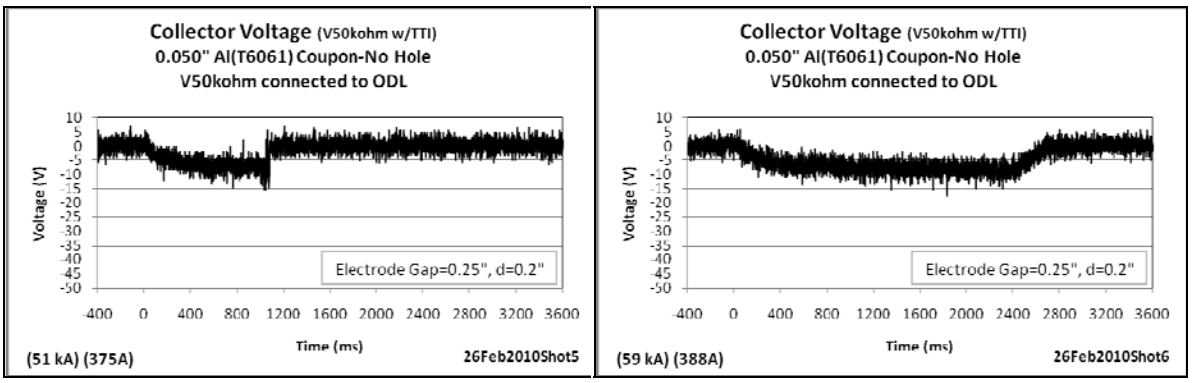

Summary of

Round 3 Testing

for LDRD

"Field and Charge Penetration by Lightning Burnthrough"

Authors: Leonard Martinez, SNL Department 1653
Larry Warne, SNL Department 1653
Roy Jorgenson, SNL Department 1653

Measurements by: Leonard Martinez, SNL Department 1653
Ed Bystrom, SNL Department 1535

Test Support: John Jojola, SNL Department 1653
Sandra Montoya, K-Tech Corporation

Revision: Rev 2.

Date: October 2010

Experimental Plan (Third Round)

Abstract: This third round of experiments has five primary goals plus planning for round four experiments later in the year. The first is to understand the plasma extent and current distribution in the continuing current arc and in the return stroke. In particular we want to understand what happens to the radial plasma and current distribution when a continuing current arc is established and then transitions into a return stroke. This information will help to establish the reasons for why the observed voltages on interior collectors do not rise to high levels during this sequence of events. (We do not know whether interior collector impedances play any role in diverting the return stroke to chassis ground at the edge of the coupon. This issue may be addressed further in round four). The second goal is to demonstrate the voltage that can be induced in indirect coupling to a round wire rather than the strips investigated in preceding experiments. The third goal is to examine the nonlinear burnthrough coupling to the differential mode in a multi-conductor stripline. It is of interest here to establish any further shielding to be gained versus the common mode coupling. The fourth goal is to "test to arc attachment," demonstrating that under certain conditions a discharge can be established to the interior collector. The idea here is to use a predrilled hole and show that as the injection electrode is brought closer to the electrode we eventually establish a discharge path to the collector. This data can be compared to arcing threshold calculations, which have been performed on cables behind holes. The fifth goal is to examine the effect of interior insulation on barrier hole size. As part of this fifth goal interior cables resting on insulating layers will be measured as well. The final goal is to perform planning for the round four experiments, which will include an attempt at spectral measurements in the discharge that have the potential of providing volumetric resolution rather than the surface profile alone.

The plan follows with extra shots and the photographic efforts separately called out.

0. Noise Shots

We anticipate that some noise shots may be required for the current profile measurements to assess magnetic (or electric) coupling to the measurement circuitry. Because the differential mode coupling measurements are new we also anticipate noise shots being required. On the "test to failure" experiment we will need to have an idea of how the ODL will respond to large input signals to know what to expect on the test. **Noise shots conducted in Rounds 1 & 2 were used as baseline configurations for all tests in Round 3. No differential mode coupling tests were conducted; therefore no differential mode noise shots were needed.**

1. Radial Current Distribution Measurements – Starter Wire and Continuing – Visible High Speed Photograph of Exterior Side of Coupon

This task will require near DC response and hence the use of TTI optical data links.

A. SPLIT ANODE PROBE

A technique used in the welding literature is to purposely move the arc discharge over a split anode while monitoring the two split anode currents. An inversion technique is then applied to back out the radial current profile. The arc movement is induced either by

mechanical movement of the cathode electrode or by application of magnetic fields. The detail of how this movement might be carried out here still needs to be worked out. One idea is to use a set of fixed normal displacement positions of the cathode electrode with respect to the cut between "D" shaped electrodes. This approach seems the most promising for the short term and also offers the possibility of gathering data on the return stroke current distribution. The "D" electrodes are designed large enough (~ 3 inch diameter) to collect all the current in the arc.

The experiments will begin with cathode positions near the center of the split anode probe to see if near equal current splitting occurs. Next cathode positions will attempt to see if nearly all current can be displaced to each individual half of the split anode. These experiments will initially use the same one quarter inch electrode spacing used by Schnetzer and our previous experiments (although in round four we may go to large electrode spacing to ascertain the behavior of the arc root).

South and North Currents (See Appendix B)

Date	Shot #	CCG Current	d Split	Description
4/6/2010	3	477A	0.020"	304 SS Split Anode Probe 0.020" between halves. 1/4" tungsten electrode positioned 1 ¼" left of vertical on South electrode. Cu tape starter wire (1/16" wide by 0.003" thick) connecting tungsten electrode to South SS electrode. Photometric data **Collector Current (S 341A, N 0A)**
4/6/2010	4	471A	0.020"	304 SS Split Anode Probe 0.020" between halves. 1/4" tungsten electrode positioned ½" left of vertical on South electrode. Cu tape starter wire (1/16" wide by 0.003" thick) connecting tungsten electrode to South SS electrode. Photometric data **Collector Current (S 341A, N 0A)**
4/6/2010	5	463A	0.010"	304 SS Split Anode Probe 0.010" between halves. 1/4" tungsten electrode positioned ½" left of vertical on South electrode. Cu tape starter wire (1/16" wide by 0.003" thick) connecting tungsten electrode to South SS electrode. Photometric data. **Collector Current (S 333A, N 0A)**
4/6/2010	6	514A	0.005"	304 SS Split Anode Probe 0.005" between halves. 1/4" tungsten electrode positioned ½" left of vertical on South electrode. Cu tape starter wire (1/16" wide by 0.003" thick) connecting tungsten electrode to South SS electrode. Photometric data **Collector Current (S 212A, N 157A)**
4/9/2010	1	486A	0.020"	304 SS Split Anode Probe 0.020" between halves. 1/4" tungsten electrode positioned ¾" left of vertical on South electrode. Cu tape starter wire (1/16" wide by 0.003" thick) connecting tungsten electrode to South SS electrode. CCG fused with NLS-30 fuse. Photometric data **Collector Current (S 330A, N 0A)**

4/9/2010	2	461A	0.020”	304 SS Split Anode Probe 0.020" between halves. 1/4" tungsten electrode positioned 9/16" left of vertical on South electrode. Cu tape starter wire (1/16" wide by 0.003" thick) connecting tungsten electrode to South SS electrode. CCG fused with NLS-30 fuse. Photometric data **Collector Current (S 330A, N 0A)**
4/9/2010	3	453A	0.020”	304 SS Split Anode Probe 0.020" between halves. 1/4" tungsten electrode positioned 3/8" left of vertical on South electrode. Cu tape starter wire (1/16" wide by 0.003" thick) connecting tungsten electrode to South SS electrode. CCG fused with NLS-30 fuse. Photometric data **Collector Current (S 282A, N 100A)**
4/9/2010	4	486A	0.020”	304 SS Split Anode Probe 0.020" between halves. 1/4" tungsten electrode positioned 3/16" left of vertical on South electrode. Cu tape starter wire (1/16" wide by 0.003" thick) connecting tungsten electrode to South SS electrode. CCG fused with NLS-30 fuse. Photometric data **Collector Current (S 350A, N 123A)**

B. CVR RING PROBE

The ring probe consists of four separate circular rings resting in an insulating support. The rings are tied to chassis through CVRs so that the current injected in each ring can be backed out of the measurements. These shots will use a starter wire and a 500 A continuing current. The objective is to estimate the arc radial current distribution and thereby gain insight on the extent of the arc plasma. Results will be compared to welding literature data (although currents of 200 A are typical). TTI DC ODLs would be required here for the late time response expected with the continuing current. **No tests were conducted for this task.**

Visual recording will be carried out during this particular test sequence. This will consist of high speed photography (20 kframes/s) with two views of the coupon surface. This recording will help correlate any arc wander with the measurements.
These shots will consume coupons and possibly ring probe metallic elements. It is hoped that the split anode can be polished and restored after shots.

2. Radial Current Distribution Measurements – Single Return Stroke – Visible High Speed Photograph of Exterior Side of Coupon

In this experiment a 50-100 kA return stroke will be used. The objective is to measure the radial current distribution during the return stoke.

A. SPLIT ANODE PROBE

As discussed in the preceding task, fixed electrode displacement positions may allow this technique to be used for the faster return stoke.

South and North Currents (See Appendix C)

Date	Shot #	SLS Current	d Split	Description
4/5/2010	2	52kA	0.010”	304 SS Split Anode Probe 0.010" between halves. 1/4" tungsten electrode positioned 1 ¼” left of vertical on South electrode. Arcing at 0.010" gap. CVR grounds were loose! Photometric data. **Collector Current (S 32kA, N 30A)**
4/5/2010	4	42kA	0.050”	304 SS Split Anode Probe 0.050" between halves. 1/4" tungsten electrode positioned 1 ¼” left of vertical on South electrode. Photometric data. **Collector Current (S 27kA, N 22A)**

B. METAL RING PROBE (Grooved SS Probe)

A metal ring probe is being designed to provide small voltages from the return stroke current that can be monitored. The probe consists of a thick stainless steel coupon with circular rings milled out to a thickness of approximately 1 mm. The groove width would also be of order of 1 mm to allow sufficient radial resolution, with spacing between rings of 2-3 mm. Current flowing through the thinner metallic regions induces a voltage on the interior side, which can be monitored. A document exists discussing the design issues (including diffusion time constants). This technique may suffer problems when exposed to the continuing current due to metallic heating (changing the resistance of the groove regions) but should be applicable to the return stroke. A twelve channel data recorder is available for measuring the array of voltages here.

Voltages (See Appendix D)

Date	Shot #	SLS Current	Description
4/12/2010	2	30kA	304 SS Grooved Probe. Photometric data. P1 is center **(P1=1.9V, P2=2.6V, P3=1.4V, P4=1.0V, P5=0.75V, P6=0.6V)**
4/12/2010	3	57kA	304 SS Grooved Probe. Photometric data. P1 is center **(P1=2.3V, P2=3.2V, P3=1.75V, P4=1.4V, P5=1.0V, P6=0.75V)**
4/12/2010	4	42kA	304 SS Grooved Probe. Photometric data. P1 is center **(P1=2.7V, P2=2.4V, P3=1.3V, P4=0.9V, P5=0.75V, P6=0V)**

C. CVR RING PROBE (Brass concentric rings)

Inductance issues in the wiring to the CVRs will need to be addressed. Also the effect of the CVR impedances on the current distribution is unknown.

Currents (See Appendix E)

Date	Shot #	SLS Current	Description
4/8/2010	2	42kA	304 SS Grooved Probe. Photometric data. P1 is center (Center Pin=40kA, Ring 1=20kA, Ring 2=10kA, Ring 3=10kA

Visual recording will be carried out during this particular test sequence in hope of gaining insight on the discharge path and distribution. This will consist of high speed photography (20 kframes/s) with two views of the coupon surface.

3. Radial Current Distribution Measurements – Starter Wire Continuing Current and Single Return Stroke – Visible High Speed Photograph of Exterior Side of Coupon

The purpose of these final shots is to investigate the current profile transition between continuing current with amplitude of 500 A and a subsequent return stroke with an amplitude of 100 kA. The continuing current interval in this case can be shortened to prevent damage to the probe, but long enough to eliminate the starter wire and set up the plasma. We are thinking of a time interval of 50 – 100 ms, although the continuing current will do damage after the measurement window (unless fusing can mitigate the long continuing current interval). The measurement focus is on the transition and return stroke time interval. **No tests were conducted for this task.**

Visual recording will be carried out during this particular test sequence. This will consist of high speed photography (20 kframes/s) with two views of the coupon surface.

A. SPLIT ANODE PROBE

As discussed in the preceding task, fixed electrode displacement positions may allow this technique to be used for the faster return stoke as well as the continuing current. Therefore this technique may be the most robust to use with both continuing current and return stroke currents present (the thicker metal allowed would make damage from the continuing current minimal and CVR sensors can be used which will not change calibration with metal surface temperatures as might happen with the metallic ring probe design). **No tests were conducted for this task.**

B. METAL RING PROBE

This will be the same as the preceding except using the metal ring probe discussed in the preceding test. The difficulty with this probe is metallic heating during the continuing current interval resulting in changes to probe sensitivity. Also late time continuing current could melt the sensor regions and cause large internal voltages and damage (say to the data recorder). **No tests were conducted for this task.**

C. CVR RING PROBE

This is the same as discussed in previous experiments. **No tests were conducted for this task.**

4. Indirect Coupling Experiment for Circular Wire – Velonix Pulser – Wire Cable Collector

These experiments are the same as the indirect magnetic coupling experiments performed previously on strips except that we will be using a circular wire. A predrilled coupon with a 0.5 inch hole will be used. One end of the interior wire will terminate on chassis ground and the voltage at the other end will be measured. We anticipate using a 0.08 inch diameter conductor with an insulating jacket. A standoff distance of 0.2 inches from the plane will be used.

Current (See Appendix F)

Date	Shot #	Velonex Current	d	Description
5/20/2010	1	4245A	0.260”	Drive perpendicular to coupon-Horizontal Magnet Wire (0.043" diameter). Distance from back side of coupon to front of wire = 0.260" **Cable Voltage (0.210V)**
5/20/2010	2	2545A	0.285”	Drive perpendicular to coupon-Horizontal Magnet Wire (0.081" diameter). Distance from back side of coupon to front of wire = 0.285" **Cable Voltage (0.110V)**
5/20/2010	3	4159A	0.260”	Drive perpendicular to coupon-Vertical Magnet Wire (0.043" diameter). Distance from back side of coupon to front of wire = 0.260" **Cable Voltage (0.032V)**
5/20/2010	4	2555A	0.285”	Drive perpendicular to coupon-Vertical Magnet Wire (0.081" diameter). Distance from back side of coupon to front of wire = 0.285" **Cable Voltage (0.012V)**

These experiments are planned for the last week in March.

5. Test to Arc Attachment

The plan here is to use a predrilled hole of 0.5 inch diameter and move the injecting electrode in toward the hole until an arc from the return stroke (50-100 kA) attaches to the collector. The interest is in measuring the largest interior voltage that can be attained. The smallest interior collector spacing of 0.2 inches will be used. This will be compared to arc threshold calculations to establish confidence in such predictions. It will also confirm the severity of the drive if conditions are allowed to develop to such an extreme geometrical configuration.

Velonex Pulser-Voltage (See Appendix G)

Date	Shot #	Velonex Voltage	d	Coll. gap	Description
4/14/2010	7	3.8kV	0.2”	0.000”	0.050" T6061 Al, with 0.5" hole in center, 1/4" Tungsten Electrode, 9540Ω between collector and ground, Tektronix HV Probe **Touching collector**
4/14/2010	3	3.1kV	0.2”	0.025”	0.050" T6061 Al, with 0.5" hole in center, 1/4" Tungsten Electrode, 9540Ω between collector and ground, Tektronix HV Probe **Touching collector**
4/14/2010	6	3.4kV	0.2”	0.025”	0.050" T6061 Al, with 0.5" hole in center, 1/4" Tungsten Electrode, 9540Ω between collector and ground, Tektronix HV Probe **Touching collector**
4/14/2010	8	3.4kV	0.2”	0.025”	0.050" T6061 Al, with 0.5" hole in center, 1/4" Tungsten Electrode, 9540Ω between collector and ground, Tektronix HV Probe **Touching collector**

4/14/2010	9	4.0kV	0.2”	0.030”	0.050" T6061 Al, with 0.5" hole in center, 1/4" Tungsten Electrode, 9540Ω between collector and ground, Tektronix HV Probe **Touching collector**

SLS-Voltage (See Appendix H)

Date	Shot #	SLS Current	d	Description
4/20/2010	8	41kA	0.2”	0.050" T6061 Al, with 0.5" hole in center, 1/4" Tungsten Electrode 1” Electrode to coupon gap, 9351Ω between collector and ground, Tektronix HV Probe **Vcollector=20V**
4/20/2010	2	61kA	0.2”	0.050" T6061 Al, with 0.5" hole in center, 1/4" Tungsten Electrode 1/4” Electrode to coupon gap, 9351Ω between collector and ground, Tektronix HV Probe **Vcollector=60V**
4/20/2010	3	57kA	0.2”	0.050" T6061 Al, with 0.5" hole in center, 1/4" Tungsten Electrode 0” (Centered) Electrode to coupon, 9351Ω between collector and ground, Tektronix HV Probe **Vcollector=350V**
4/20/2010	4	60kA	0.2”	0.050" T6061 Al, with 0.5" hole in center, 1/4" Tungsten Electrode 3/16” Electrode to collector gap, 9351Ω between collector and ground, Tektronix HV Probe **Vcollector=1,344V**
4/15/2010	5	61kA	0.2”	0.050" T6061 Al, with 0.5" hole in center, 1/4" Tungsten Electrode 3/16” Electrode to collector gap 9351Ω between collector and ground, Tektronix HV Probe **Vcollector=20,000V**
4/20/2010	5	36kA	0.2”	0.050" T6061 Al, with 0.5" hole in center, 1/4" Tungsten Electrode 3/16” Electrode to collector gap 9351Ω between collector and ground, Tektronix HV Probe **Vcollector=2,800V**
4/20/2010	6	60kA	0.2”	0.050" T6061 Al, with 0.5" hole in center, 1/4" Tungsten Electrode 1/8” Electrode to collector gap 9351Ω between collector and ground, Tektronix HV Probe **Vcollector=12,670**
4/20/2010	7	52kA	0.2”	0.050" T6061 Al, with 0.5" hole in center, 1/4" Tungsten Electrode 1/16” Electrode to collector gap 9351Ω between collector and ground, Tektronix HV Probe **Vcollector=20,000V**
4/15/2010	3	51kA	0.2”	0.050" T6061 Al, with 0.5" hole in center, 1/4" Tungsten Electrode 1/16” Electrode to collector gap 9351Ω between collector and ground, Tektronix HV Probe **Vcollector=13,000V**

We anticipate using the Nanofast high impedance probe for this experiment. However time constant issues need to be examined further to make sure we do not filter out early time voltage spikes (occurring before a side flash to the coupon edge). These issues have to do with the early time discharge impedance, collector capacitance (which could be

reduced by using a strip cable), and the measurement impedance (larger the better so that it does not compete with the discharge impedance).

A second issue in this experiment is collector to coupon standoff voltages. We need to examine further how big this is and whether insulation extending to, and slightly interior to, the coupon edges might be another useful experiment to achieve largest interior voltages.

This experiment is planned for last week of March or first week in April.

6. Interior Insulation Effects and Cable

This set of experiments will measure coupling to a strip cable placed on an insulating layer as well as documenting the change in coupon damage resulting from the change in interior collecting structure from that of a large metallic collector to a cable and to an insulating layer. **No tests were conducted for this task.**

We anticipate an experiment with a strip cable collector on an insulating layer as well as an experiment with an insulating layer alone.

A spacing of 0.2 inches will be used and photography is required to pick out hole size and discharge path (coupon edge versus cable collector).

7. Planning for Round Four

During the round three experiments some planning for round four will be done. In particular, the possibility of using a plasma diverter (to eliminate the plasma jet from the cathode) and of making spectral measurements will be explored. The issue of internal impedance (inductive reactance) diverting the path of a return stroke attachment from the collector to the coupon rim will also be examined further and future experiments planned to minimize this effect. Also arc root current distribution for larger electrode spacing is of interest to relate results to longer lightning discharges. In addition the possibility of polarity changes will be discussed (anode electrode?). **No tests were conducted for this task.**

References:

[1] G. H. Schnetzer, R. J. Fisher, and M. A. Dinallo, "Measured Responses of Internal Enclosures and Cables Due To Burnthrough Penetration of Weapon Cases by Lightning," SAND94-0312, August 1994.

[2] R. J. Fisher and M. A. Uman, "Recommended Baseline Direct-Strike Lightning Environment for Stockpile-to-Target Sequences," SAND 89-0192, May 1989.

[3] L. K. Warne, L. E. Martinez, and R. E. Jorgenson, "Experimental Plan (First Round)," Internal Sandia Memorandum, March 27, 2009.

[4] L. K. Warne, L. E. Martinez, and R. E. Jorgenson, "Experimental Plan (Interim Low Level)," Internal Sandia Memorandum, June, 2009.

[5] L. K. Warne, L. E. Martinez, and R. E. Jorgenson, "Experimental Plan (Second Round)," Internal Sandia Memorandum, September 8, 2009.

1. Radial Current Distribution Measurements – Starter Wire and Continuing – Visible High Speed Photograph of Exterior Side of Coupon-Split Anode Probe

Description:
304 SS Split Anode Probe 0.020" between halves. 1/4" tungsten electrode positioned on South electrode (left of vertical). Cu tape starter wire (1/16" wide by 0.003" thick) connecting tungsten electrode to South SS electrode. Photometric data

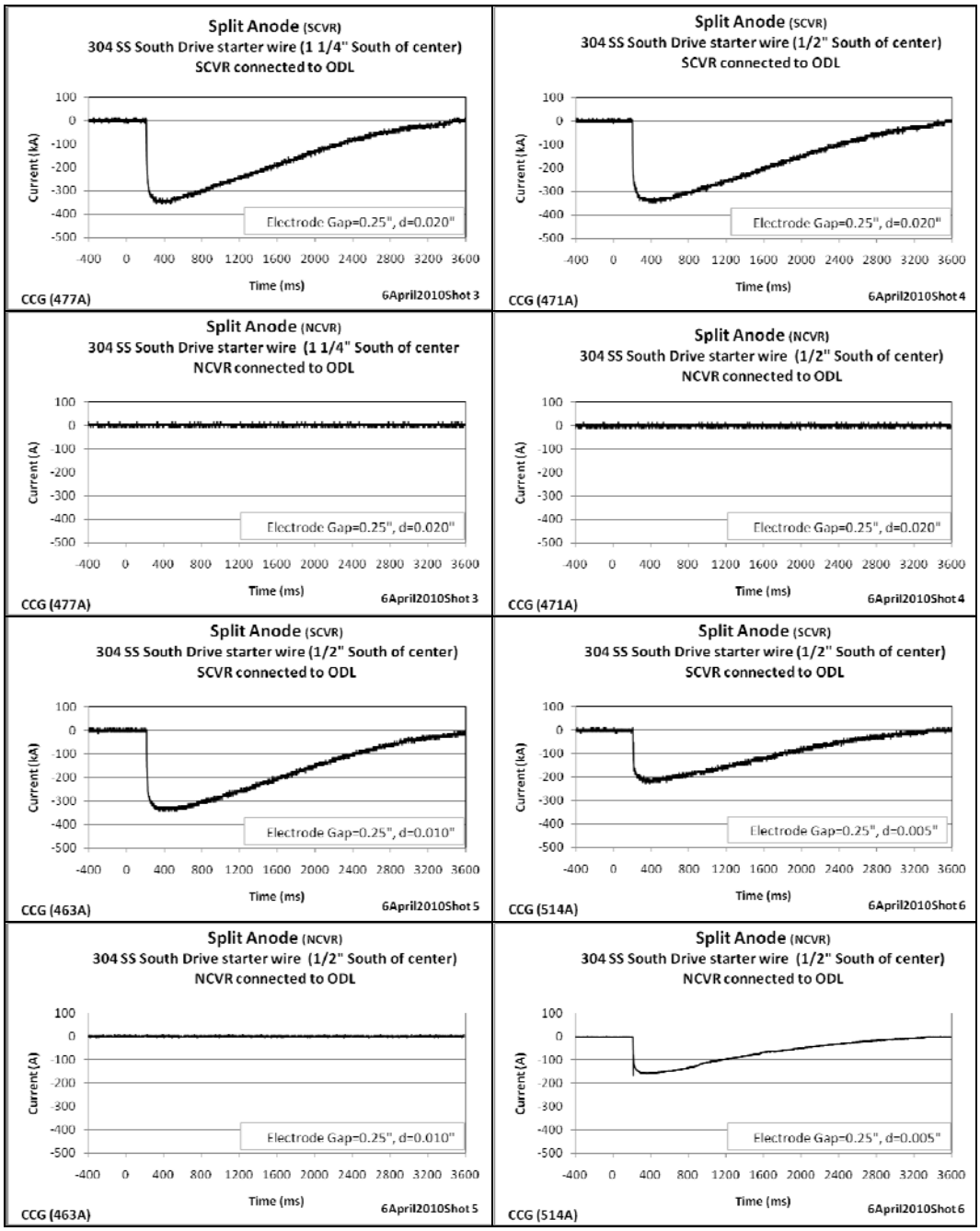

1. Radial Current Distribution Measurements – Starter Wire and Continuing – Visible High Speed Photograph of Exterior Side of Coupon-Split Anode Probe

Description:
304 SS Split Anode Probe 0.020" between halves. 1/4" tungsten electrode positioned on South electrode (left of vertical). Cu tape starter wire (1/16" wide by 0.003" thick) connecting tungsten electrode to South SS electrode. Photometric data. CCG fused with Littlefuse model NLS 30.

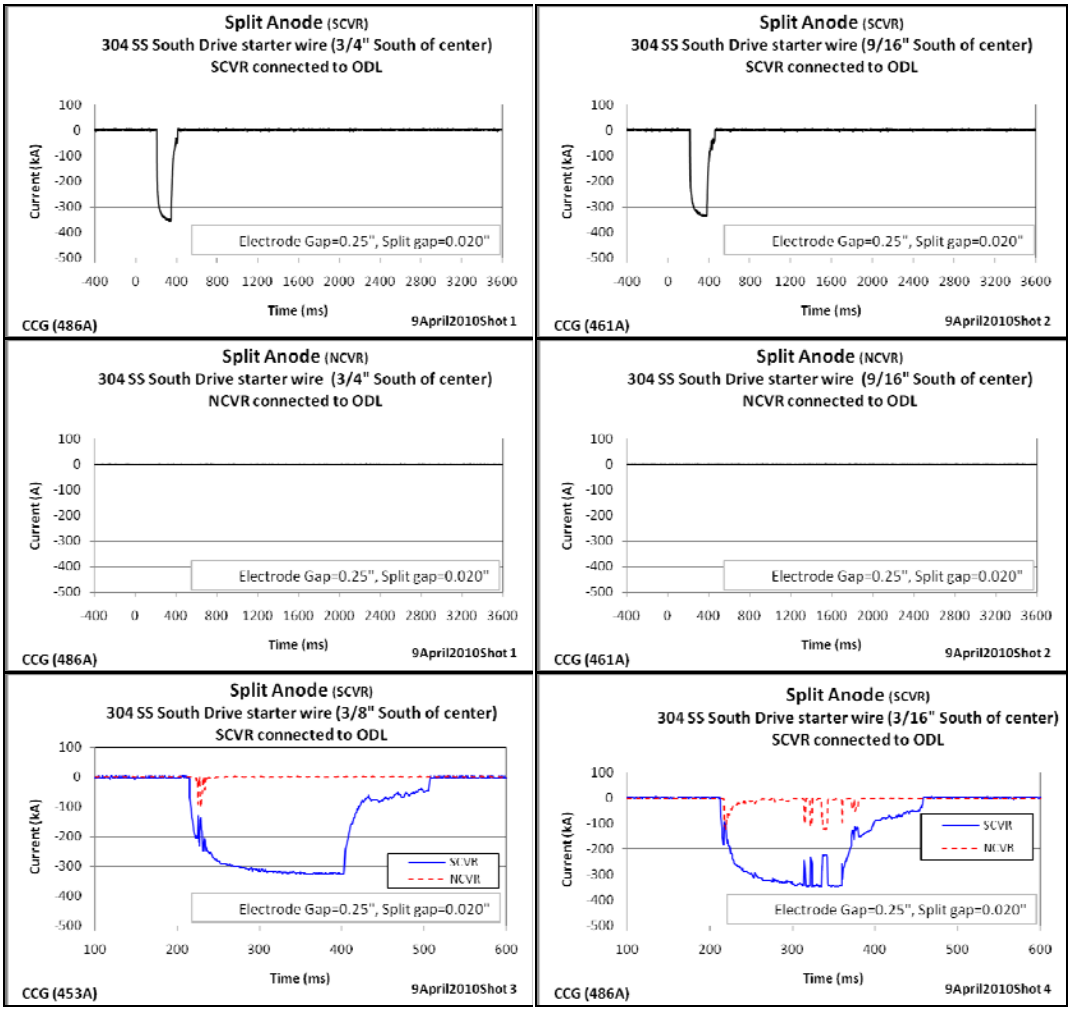

2. Radial Current Distribution Measurements – Single Return Stroke – Visible High Speed Photograph of Exterior Side of Coupon

In this experiment a 50-100 kA return stroke will be used. The objective is to measure the radial current distribution during the return stoke.

Description: Split Anode
304 SS Split Anode Probe 0.010" and 0.050" between halves. 1/4" tungsten electrode positioned 1 ¼" left of vertical on South electrode

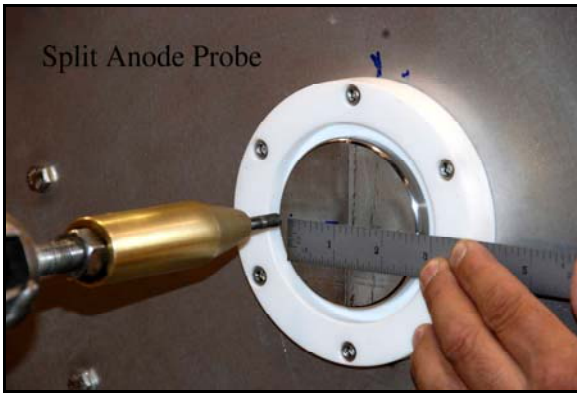

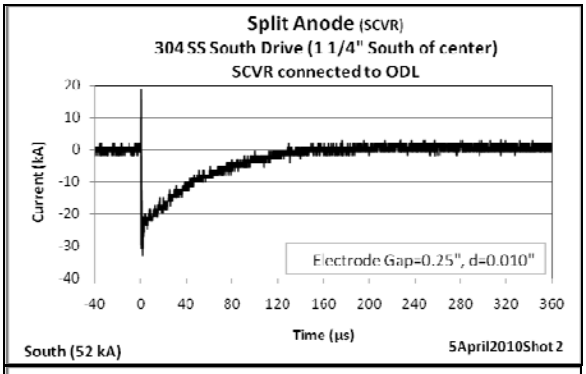

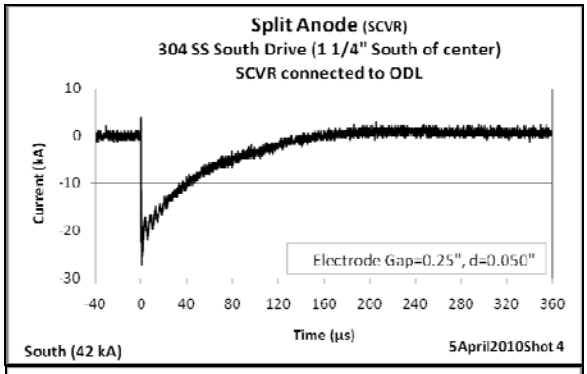

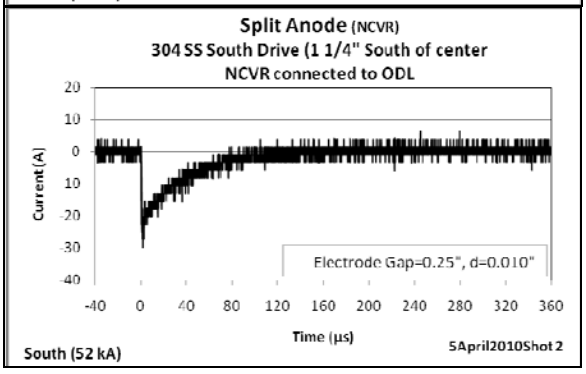

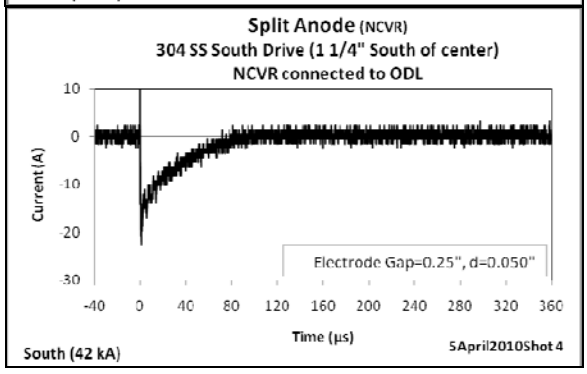

2. Radial Current Distribution Measurements – Single Return Stroke – Visible High Speed Photograph of Exterior Side of Coupon

In this experiment a 50-100 kA return stroke will be used. The objective is to measure the radial current distribution during the return stoke.

Description: Metal Ring Probe
304 SS Grooved Probe.

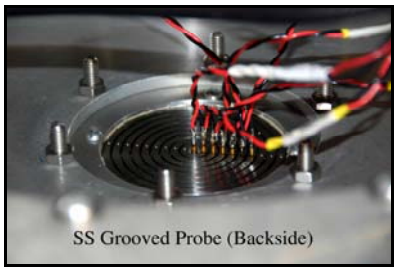

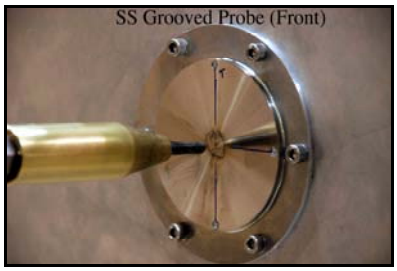

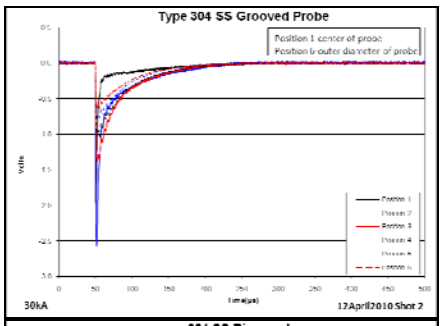

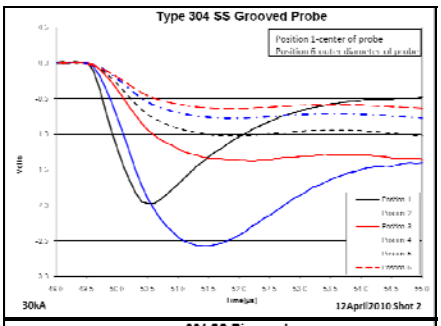

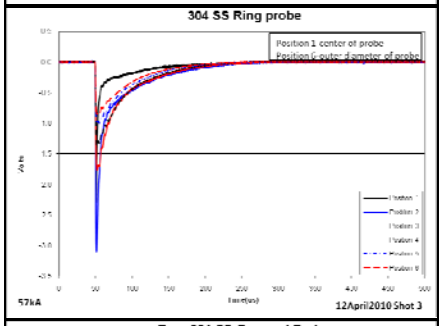

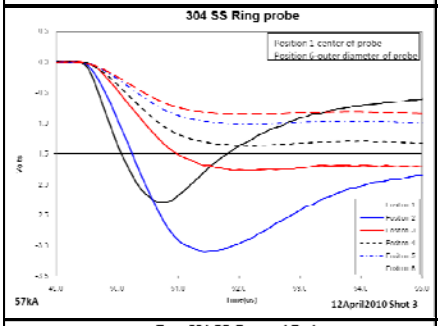

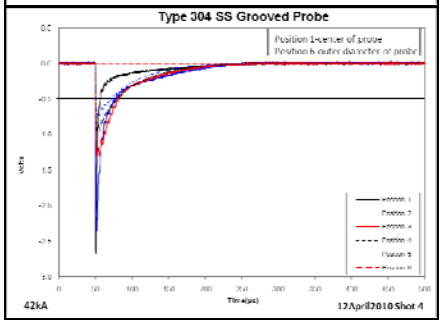

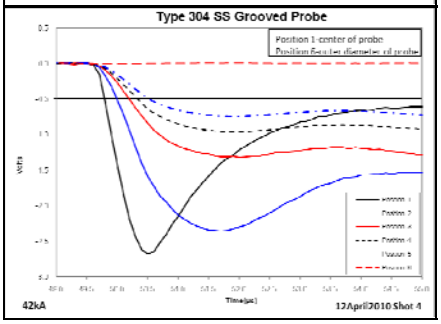

2. Radial Current Distribution Measurements – Single Return Stroke – Visible High Speed Photograph of Exterior Side of Coupon

In this experiment a 50-100 kA return stroke will be used. The objective is to measure the radial current distribution during the return stoke.

Description: CVR Ring Probe
Brass Concentric Rings

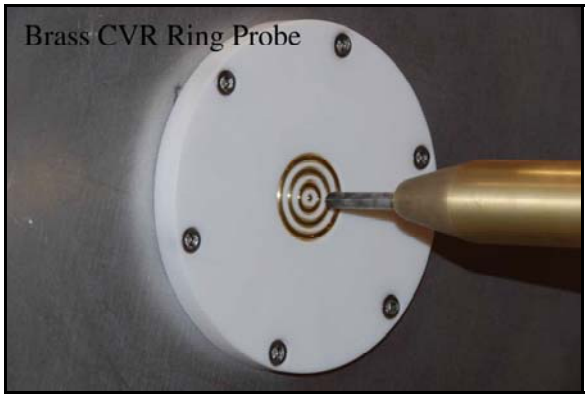

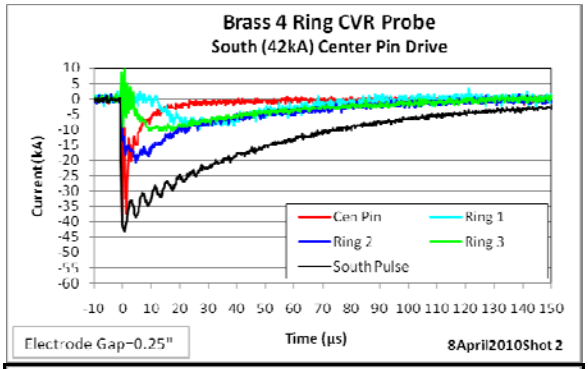

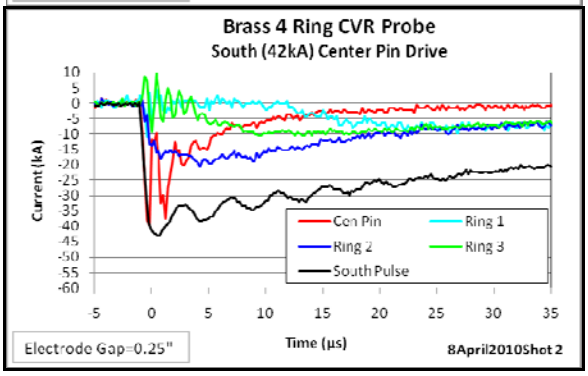

4. Indirect Coupling Experiment for Circular Wire – Velonex Pulser – Wire Cable Collector

Description: Drive perpendicular to coupon-Horizontal and Vertical Magnet Wire orientations (0.043" and 0.081" diameters). **Velonex Pulser**

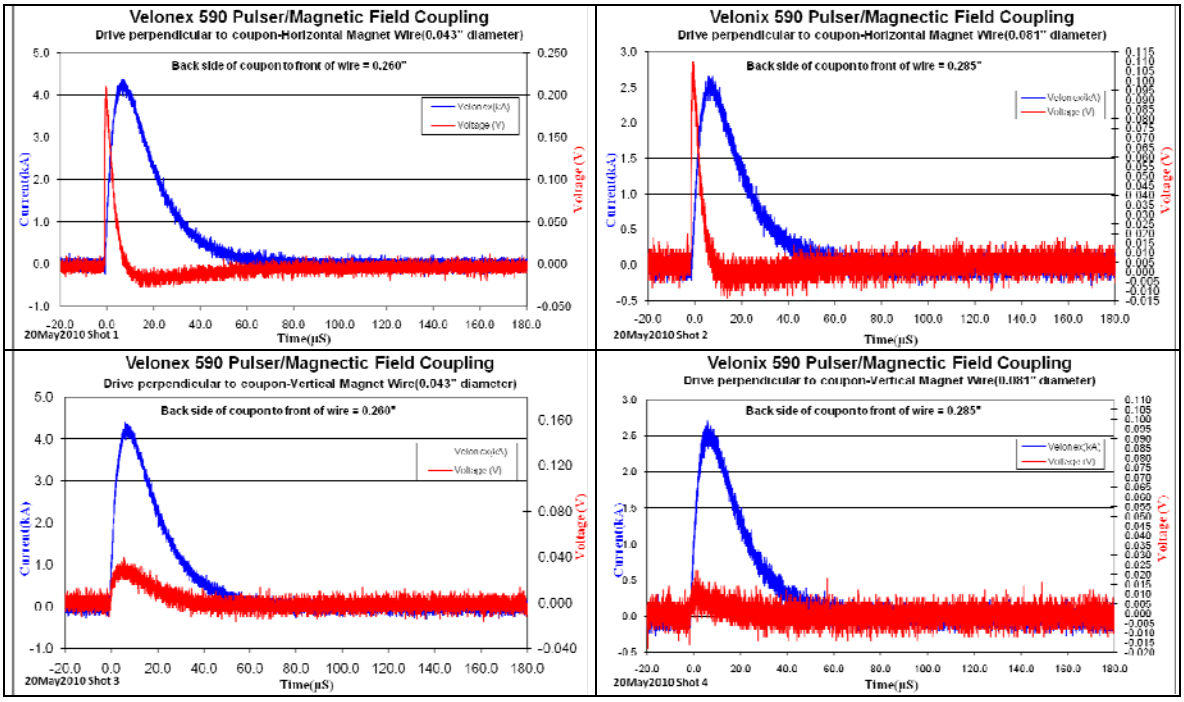

5. Test to Arc Attachment

The plan here is to use a predrilled hole of 0.5 inch diameter and move the injecting electrode in toward the hole until an arc from the return stroke (50-100 kA) attaches to the collector.

Description: 0.050" T6061 Al, with 0.5" hole in center, 1/4" Tungsten Electrode, 9540Ω between collector and ground, Tektronix HV Probe. 0", 0.025", and 0.030" gap between electrode and brass collector. **Velonex Pulser**

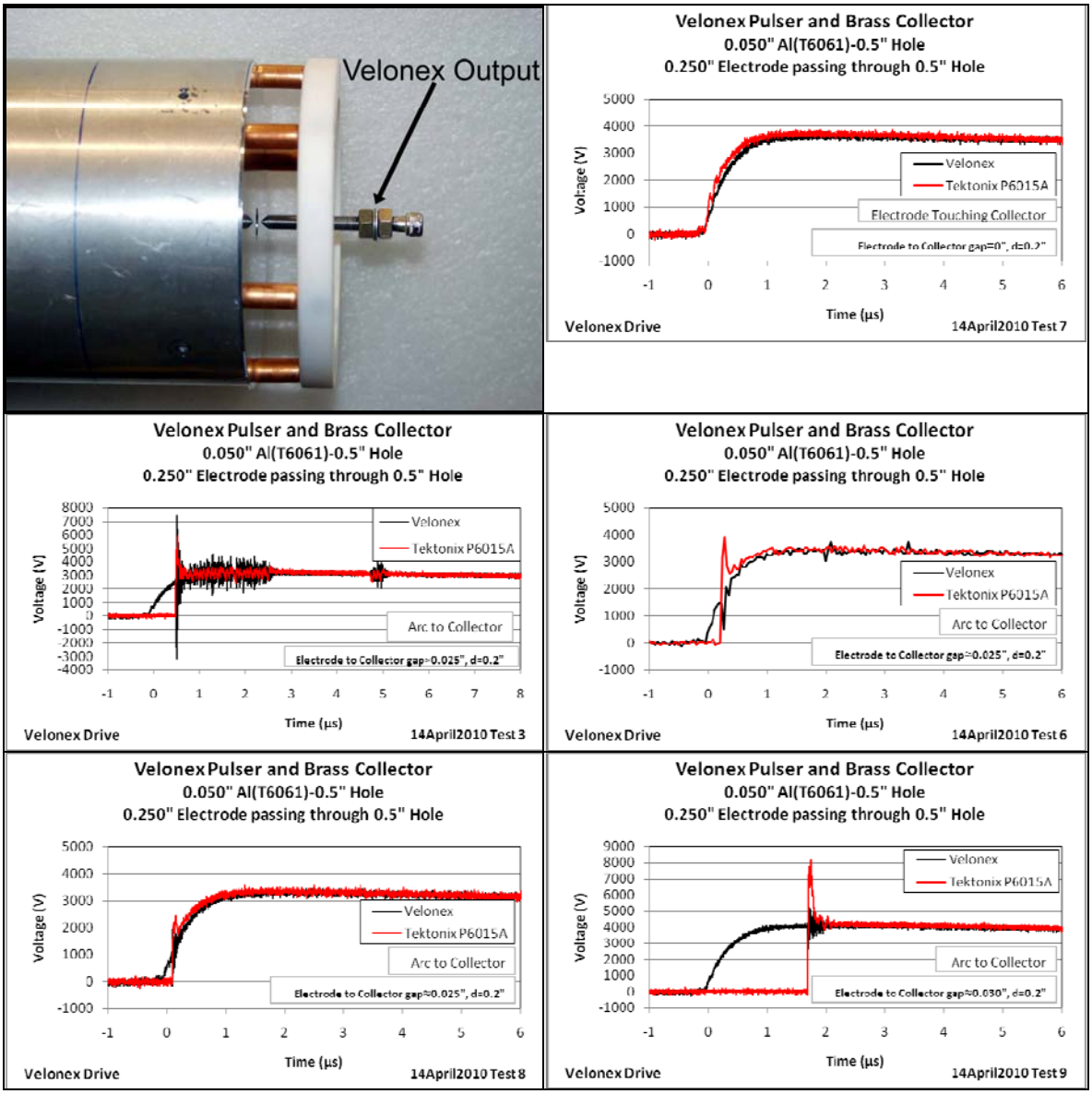

5. Test to Arc Attachment

The plan here is to use a predrilled hole of 0.5 inch diameter and move the injecting electrode in toward the hole until an arc from the return stroke (50-100 kA) attaches to the collector. Tektronix HV probe

Description: 0.050" T6061 Al, with 0.5" hole in center, 1/4" Tungsten Electrode, 9351Ω between collector and ground, Tektronix HV Probe **Sandia Lightning Simulator**

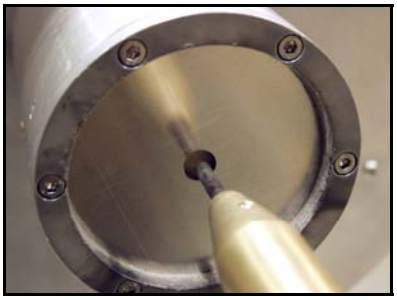

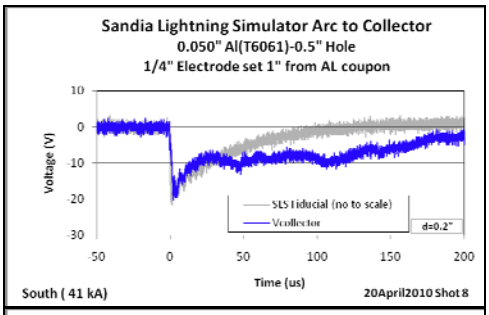

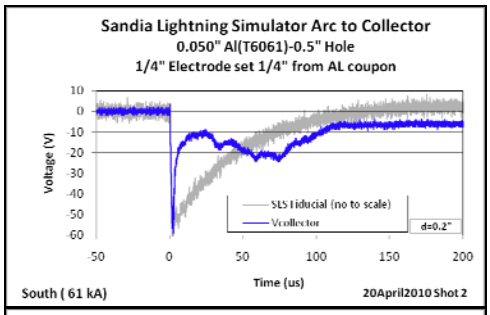

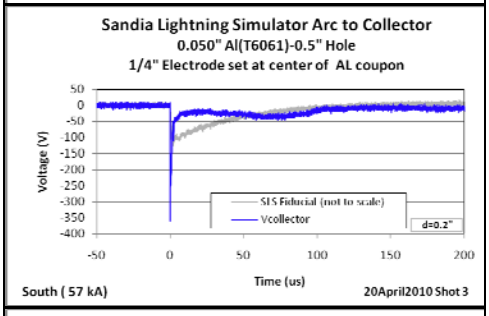

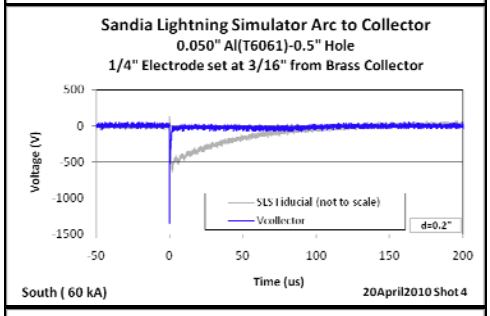

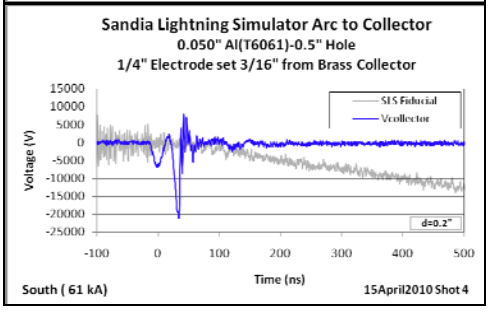

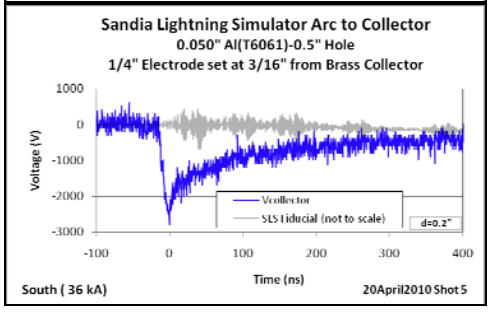

5. Test to Arc Attachment

The plan here is to use a predrilled hole of 0.5 inch diameter and move the injecting electrode in toward the hole until an arc from the return stroke (50-100 kA) attaches to the collector. Tektronix HV probe

Description: 0.050" T6061 Al, with 0.5" hole in center, 1/4" Tungsten Electrode, 9351Ω between collector and ground, Tektronix HV Probe **Sandia Lightning Simulator**

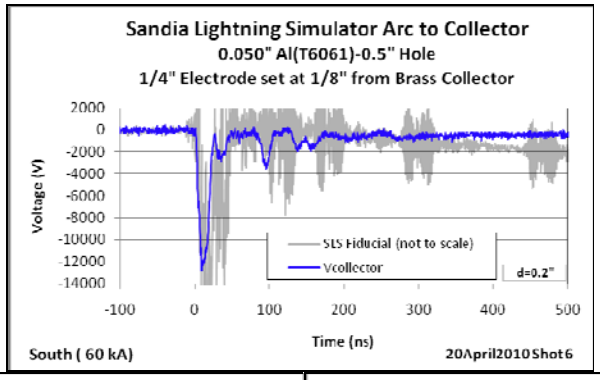

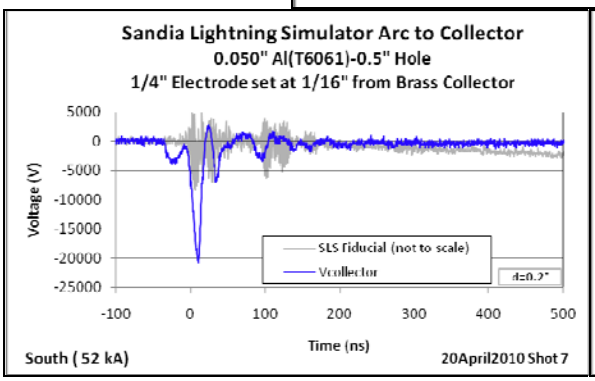

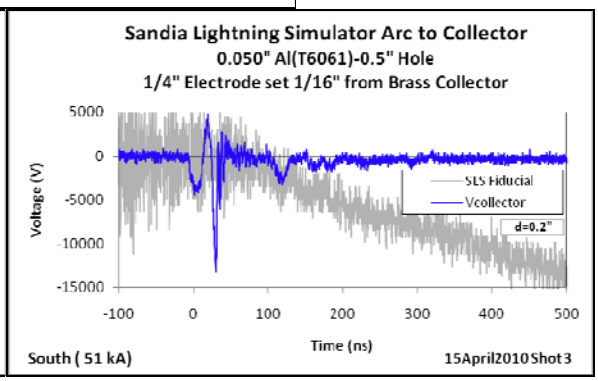

Summary of

Round 4 Testing

for LDRD

"Field and Charge Penetration by Lightning Burnthrough"

Authors: Leonard Martinez, SNL Department 1653
Larry Warne, SNL Department 1653
Roy Jorgenson, SNL Department 1653

Measurements by: Leonard Martinez, SNL Department 1653
Ed Bystrom, SNL Department 1535

Test Support: John Jojola, SNL Department 1653
Sandra Montoya, K-Tech Corporation

Revision: Rev 1.

Date: September 2010

Experimental Plan (Fourth Round)

Abstract: This fourth round of experiments has three primary goals. The first goal is to "test to arc attachment" during the standard burnthrough sequence, either ruling out or demonstrating that under certain conditions a discharge can be established to the interior collector. (We do not know yet whether interior collector impedances play any role in diverting the return stroke to chassis ground at the edge of the coupon.) The idea here is repeat the original two-return-stroke plus continuing-current-burnthrough and voltage-coupling experiment, but examine the early time region to see if any interior voltage pulses (resulting from a discharge path to the collector) were missed during the second return stroke Marx bank voltage-erection time-interval. These data (along with predrilled hole discharge data, discussed below) can be compared to arcing threshold calculations, which have been performed on cables behind holes. We also plan to measure the Sandia Lightning simulator incident electric field (or voltage) waveform to calibrate the drive for the test to arc attachment experiment. The second goal is to understand what happens to the radial plasma and current distribution when a continuing current arc is established and then transitions into a return stroke. This measurement will make use of water cooled probes. The information gathered will help to establish the reasons for why the observed voltages on interior collectors have not in the past risen to high levels during this sequence of events. In addition, we also plan to use the inverted current distribution (groove) probe arrangement to see if heating of the outer surface of the probe played any role in the groove probe voltage levels, from a single return stroke measured in round three. The third goal is to examine the effect of interior insulation on barrier hole size. Finally we intend to explore further the possibility of doing spectral measurements in FY11 and some other planning as well. These spectral measurements have the potential of providing volumetric resolution rather than the surface profile alone.

The plan follows with extra shots and the photographic efforts separately called out.

0. Noise Shots

The noise shots on the "test to arc attachment" experiments with the predrilled hole could involve the same setup but with a solid coupon. The noise shots on the SLS burnthrough and "test to arc attachment" experiment could involve a return stroke without continuing current (and a solid coupon).

Incident Electric Field Noise Shots- Voltage (See Appendix A)

Date	Shot #	SLS Current	d	Description
8/19/2010	3	56kA	0.45"	0.050" T6061 Al, no hole in center, 1/4" Tungsten Electrode, 1" Electrode Gap, Tektronix P6015 HV probe (0.45" between Coupon and collector) **Vcollector=1V**
8/25/2010	7	60kA	0.2"	0.050" T6061 Al, no hole in center, 1/4" Tungsten Electrode, 1" Electrode Gap, Tektronix P6015 HV probe (0.2" between Coupon and collector) **Vcollector=2V**

1. Calibration of Voltage Wave from Lightning Simulator

The plan here is to measure the electric field (probably with a monopole probe mounted in a ground plane at the test object plane) during the early time associated with the Marx bank voltage erection. This measurement is important to calibrate the discharge to collector experiments, since this voltage wave determines the incident field in those experiments. If a monopole probe is used, we can locate it on the ground plane, but off center from the cathode rod of the simulator. This will allow us to measure the field with both open (before arcing, with a one or two inch gap) and short circuit conditions. For the predrilled hole experiments the load looks like an open circuit, whereas for the established arc during the continuing current burnthrough event, the load may look more like a short circuit. The time focus here is prior to current rise, during the Marx voltage erection process.

Incident Electric Field Shots- Volts/meter (See Appendix B)

Date	Shot #	SLS Current	d	Description
8/19/2010	3	56kA	0.45”	0.050" T6061 Al, no hole in center, 1/4" Tungsten Electrode, 1" Electrode Gap, Tektronix P6015 HV probe (0.45" between Coupon and collector) **Electric Field=400kV/m**
8/25/2010	7	60kA	0.2”	0.050" T6061 Al, no hole in center, 1/4" Tungsten Electrode, 1" Electrode Gap, Tektronix P6015 HV probe (0.2" between Coupon and collector) **Electric Field=422kV/m**

2. Test to Arc Attachment

The plan here is to repeat the original two-return stroke plus continuing current experiments conducted at the beginning of the project, but examine the early time regime during Marx bank voltage erection to see if any discharge paths form to the interior collector during the transition from continuing current to second return stroke.

The one quarter inch spacing from cathode electrode to collector will be used. The first return stroke to initiate the arc will be about 50 kA. The continuing current will have a level of 500 A. The interstroke interval will be taken as 500 ms, so that a clear burnthrough hole exists and a plasma jet can be established to the collector electrode, before the second return stroke. If evidence of large voltage discharges to the collector is found, it would be of interest to examine the 100 ms interstroke interval used in the original tests on this problem. **No tests with 100ms interstroke interval were conducted.** The second return stroke should be nominally 100 kA. The interest is in measuring the largest interior voltage that can be attained, focusing on the very early time associated with the Marx voltage erection associated with the second return stroke. The smallest interior collector spacing from coupon of 0.2 inches will be used. The data will be compared to arc threshold calculations. This data will also give more confidence that nothing has been missed at early time. We anticipate using the Tektronix high

impedance, high voltage, probe for this experiment (with a range up to 50 kV), and the digital strip chart recorder inside the large shield box.

There is an issue with collector to chassis grounding in this experiment. We anticipate one measurement with the collector floating (actually there will be a very high impedance connection through the Tektronix probe). But the establishment of a plasma jet connection to the collector either may not be possible in this floating case or it might lead to a jet to the collector and another series jet from collector to coupon to establish the current return (and we have observed this phenomenon in side view interior photography). Consequently it makes sense to add a case where a lower impedance connection to chassis (in parallel to the Tektronix probe) is also present. This could have the form of a low value resistance (to allow a voltage measurement) or it could take the form of a known inductance (for example, a length of wire). This latter connection would provide a low impedance path to ground for the continuing current to establish the plasma jet to the collector, but it would isolate the collector for the faster subsequent return stoke. It also would mimic a grounded cable situation. With a return stroke current derivative of order 100 kA/microsecond an inductance of 100 nH would provide 10 kV. For example, the inductance could be generated by a 0.2 inch diameter rod (inside a 4 inch diameter case) with a length greater than 6 inches. The resistance should be kept to less than 0.1 ohms. This still results in 25 kW of power being delivered by a 500 A continuing current (we do not want wire fusing).

Voltage (See Appendix C)

Date	Shot #	SLS Current	d	Description
8/30/2010	5	S (34kA) CCG(496A) N(83kA)	0.2”	Solid 0.050" T6061 Al, 1/4" Tungsten Electrode, 1/4" Electrode Gap, Tektronix P6015 HV probe. 500ms between pulses **Vcollector=120V Clipped**
8/30/2010	6	S (54 kA) CCG(471A) N (99 kA)	0.2”	Solid 0.050" T6061 Al, 1/4" Tungsten Electrode, 1/4" Electrode Gap, Tektronix P6015 HV probe. 500ms between pulses **Vcollector=120V**
8/31/2010	2	S (58 kA) CCG(500A) N (98 kA)	0.2”	Solid 0.050" T6061 Al, 1/4" Tungsten Electrode, 1/4" Electrode Gap, collector inductive setup LS=132nH,Lp=146nH, R=27.3mOhm Parameters measured with Agilent 4263B LCR Meter @100kHz, Tektronix P6015 HV probe. 500ms between pulses **Vcollector=20V**

If large discharge voltages are observed on the collector it would be desirable to increase the cathode to collector spacing to one inch to see if the effect is reduced. **No large discharge voltages were observed, so collector spacing was not increased.**

A second issue in this experiment is collector to coupon standoff voltages. We need to examine further how big this is and whether insulation extending to, and slightly interior to, the coupon edges might be another useful experiment to achieve largest interior voltages.

Visual recording will be carried out during this particular test sequence in hope of gaining insight on the discharge path. This will consist of high speed photography (20 kframes/s) with two views of the coupon surface

3. Predrilled Hole Discharge Penetration

In this set of experiments we plan to repeat the Velonex predrilled hole "discharge to collector" experiments but using higher voltage equipment. We will use a 0.5 inch hole in the coupon. The collector spacing will initially be 0.2 inches from the coupon, but we may back this off to 0.4 inches and 0.8 inches depending on what we find in the experiment. First we plan to use a slow ramp source with a range from 0-200 kV and initial cathode spacing to coupon of 0.25 inches. The cathode spacing will be varied to generate an array of data. First the cathode spacing will be reduced until a discharge is formed to the collector. Next the spacing will be increased and the indirect coupling levels will be noted. If a discharge appears at 0.25 inches, the spacing will be increased until only indirect levels appear.

Velonex Voltage Tests (See Appendix D)

Date	Test #	Velonex (V)	d	Description
8/16/2010	1	3326	0.2"	1/4" electrode, 0.020" gap from electrode tip to solid 0.050" T6061 Al. coupon. NOISE SHOT Tektronix P6015 HV probe **Vcollector=2V noise**
8/16/2010	2	4696	0.2"	1/4" electrode, T6061 Al. coupon with 0.5" hole in center. Electrode center of hole. No gap from electrode tip to Aluminum coupon. Tektronix P6015 HV probe **Vcollector=4.6V**
8/16/2010	3	5031	0.2"	1/4" electrode, T6061 Al. coupon with 0.5" hole in center. Electrode through and center of hole. 3/16" gap from electrode tip to internal brass collector. Tektronix P6015 HV probe **Vcollector=7.1V**
8/16/2010	4	4686	0.2"	1/4" electrode, T6061 Al. coupon with 0.5" hole in center. Electrode through and center of hole. 1/8" gap from electrode tip to internal brass collector. Tektronix P6015 HV probe **Vcollector=11.1V**
8/16/2010	5	4844	0.2"	1/4" electrode, T6061 Al. coupon with 0.5" hole in center. Electrode through and center of hole. 1/16" gap from electrode tip to internal brass collector. Tektronix P6015 HV probe **Vcollector=15.8V**
8/16/2010	6	4911	0.2"	1/4" electrode, T6061 Al. coupon with 0.5" hole in center. Electrode through and center of hole. 0.017" gap from electrode tip to internal brass collector. Tektronix P6015 HV probe **Vcollector=4930V**

DC Voltage Tests (See Appendix E)

Date	Test #	kVDC	d	Description
7/22/2010	1	8.2	0.2”	1/4" electrode, 1/4" gap from electrode tip to solid 0.050" T6061 Al. coupon. Still Photo-open shutter. Tektronix P6015 HV probe **Vcollector=0V**
7/22/2010	2	7.8	0.2”	1/4" electrode, 1/4" gap from electrode tip to 0.050" T6061 Al. coupon with 0.5" hole in center. Still Photo-open shutter. Tektronix P6015 HV probe **Vcollector=125V**
7/22/2010	3	7.8	0.2”	1/4" electrode, T6061 Al. coupon with 0.5" hole in center. Electrode center of hole. No gap from electrode tip to Aluminum coupon. Still Photo-open shutter. Tektronix P6015 HV probe **Vcollector=1.44kV**
7/22/2010	4	6.8	0.2”	1/4" electrode, T6061 Al. coupon with 0.5" hole in center. Electrode through and center of hole. 3/16" gap from electrode tip to internal brass collector. Still Photo-open shutter. Tektronix P6015 HV probe **Vcollector=6.4kV**
7/22/2010	5	7.6	0.2”	1/4" electrode, T6061 Al. coupon with 0.5" hole in center. Electrode through and center of hole. 3/16" gap from electrode tip to internal brass collector. Still Photo-open shutter. Tektronix P6015 HV probe **Vcollector=7.0kV**
8/3/2010	6	5.8	0.2”	1/4" electrode, T6061 Al. coupon with 0.5" hole in center. Electrode through and center of hole. 1/8" gap from electrode tip to internal brass collector. Still Photo-open shutter. Tektronix P6015 HV probe **Vcollector=5.8kV**
8/3/2010	7	6.2	0.2”	1/4" electrode, T6061 Al. coupon with 0.5" hole in center. Electrode through and center of hole. 1/8" gap from electrode tip to internal brass collector. Still Photo-open shutter. Tektronix P6015 HV probe **Vcollector=6.2kV**
8/3/2010	8	5.2	0.2”	1/4" electrode, T6061 Al. coupon with 0.5" hole in center. Electrode through and center of hole. 1/16" gap (0.066") from electrode tip to internal brass collector. Still Photo-open shutter. Tektronix P6015 HV probe **Vcollector=5.2kV**
8/3/2010	9	4.9	0.2”	1/4" electrode, T6061 Al. coupon with 0.5" hole in center. Electrode through and center of hole. 1/16" gap (0.066") from electrode tip to internal brass collector. Still Photo-open shutter. Tektronix P6015 HV probe **Vcollector=4.9kV**
8/3/2010	10	6.4	0.2”	1/4" electrode, T6061 Al. coupon with 0.5" hole in center. Electrode center of hole. No gap from electrode tip to Aluminum coupon. Still Photo-open shutter. Tektronix P6015 HV probe **Vcollector=940V**

8/3/2010	11	8.7	0.2”	1/4" electrode, 1/4" gap from electrode tip to 0.050" T6061 Al. coupon with 0.5" hole in center. Still Photo-open shutter. Audible and visual corona at 10 kV. Tektronix P6015 HV probe **Vcollector=100V**
8/3/2010	12	10.2	0.2”	1/4" electrode, 1/4" gap from electrode tip to 0.050" T6061 Al. coupon with 0.5" hole in center. Still Photo-open shutter. Audible and visual corona at 9 kV. Tektronix P6015 HV probe **Vcollector=150V**
8/4/2010	13	11.6	0.2”	1/4" electrode, 1/2" gap from electrode tip to 0.050" T6061 Al. coupon with 0.5" hole in center. Still Photo-open shutter. Tektronix P6015 HV probe **Vcollector=300V**
8/4/2010	14	NA	0.2”	1/4" electrode, 1/2" gap from electrode tip to 0.050" T6061 Al. coupon with 0.5" hole in center. Still Photo-open shutter. Tektronix P6015 HV probe **Vcollector= NO DATA**
8/4/2010	15	17.7	0.2”	1/4" electrode, 3/4" gap from electrode tip to 0.050" T6061 Al. coupon with 0.5" hole in center. Still Photo-open shutter. Tektronix P6015 HV probe **Vcollector=150V**
8/4/2010	16	17.2	0.2”	1/4" electrode, 3/4" gap from electrode tip to 0.050" T6061 Al. coupon with 0.5" hole in center. Still Photo-open shutter. Tektronix P6015 HV probe **Vcollector=170V**
8/4/2010	17	16.1	0.2”	1/4" electrode, 3/4" gap from electrode tip to 0.050" T6061 Al. coupon with 0.5" hole in center. VIDEO RECORDING #1. Tektronix P6015 HV probe **Vcollector=150V**
8/5/2010	18	5.9	0.2”	1/4" electrode, T6061 Al. coupon with 0.5" hole in center. Electrode through and center of hole. 3/16" gap from electrode tip to internal brass collector. VIDEO RECORDING #3. Tektronix P6015 HV probe **Vcollector=5.9kV**

After this array of data is recorded a set of pulsed discharge experiments will be conducted using the Pantex pulser. This pulser has a minimum level is 130-150 kV and a maximum of 450 kV. The cathode rod spacing will be selected after a review of the slow voltage drive data. **The Pantex pulser was modified to produce a 0-60kV pulse for these tests.**

Pantex Voltage Tests (See Appendix F)

Date	Test #	kVDC	d	Description
9/24/2010	22	30	0.2”	1/4" electrode, 1/4" gap from electrode tip to solid 0.050" T6061 Al. coupon. Still Photo-open shutter. Tektronix P6015 HV probe **Vcollector=1.5V**
9/23/2010	11	20	0.2”	1/4" electrode, T6061 Al. coupon with 1/2" hole. 1/16" gap from electrode tip to Brass collector. Still Photo-open shutter. Brass collector is 0.2" away from back side of Al. coupon. Tektronix P6015 HV probe **Vcollector=7kV**

9/23/2010	12	20	0.2”	1/4" electrode, T6061 Al. coupon with 1/2" hole. 1/16" gap from electrode tip to Brass collector. Still Photo-open shutter. Brass collector is 0.2" away from back side of Al. coupon. Tektronix P6015 HV probe **Vcollector=7kV**
9/23/2010	13	15	0.2”	1/4" electrode, T6061 Al. coupon with 1/2" hole. 1/8" gap from electrode tip to Brass collector. Still Photo-open shutter. Brass collector is 0.2" away from back side of Al. coupon. Tektronix P6015 HV probe **Vcollector=3.3kV**
9/23/2010	14	17	0.2”	1/4" electrode, T6061 Al. coupon with 1/2" hole. 1/8" gap from electrode tip to Brass collector. Still Photo-open shutter. Brass collector is 0.2" away from back side of Al. coupon. Tektronix P6015 HV probe **Vcollector=4.7kV**
9/23/2010	15	25	0.2”	1/4" electrode, T6061 Al. coupon with 1/2" hole. 3/16" gap from electrode tip to Brass collector. Still Photo-open shutter. Brass collector is 0.2" away from back side of Al. coupon. Tektronix P6015 HV probe **Vcollector=3.4kV**
9/23/2010	16	15	0.2”	1/4" electrode, T6061 Al. coupon with 1/2" hole. 3/16" gap from electrode tip to Brass collector. Still Photo-open shutter. Brass collector is 0.2" away from back side of Al. coupon. Tektronix P6015 HV probe **Vcollector=2.2kV**
9/23/2010	17	21	0.2”	1/4" electrode, T6061 Al. coupon with 0.5" hole in center. Electrode center of hole. No gap from electrode tip to Aluminum coupon. Still Photo-open shutter. Brass collector is 0.2" away from back side of Al. coupon. Tektronix P6015 HV probe **Vcollector=2.5kV**
9/23/2010	18	25	0.2”	1/4" electrode, T6061 Al. coupon with 0.5" hole in center. Electrode center of hole. No gap from electrode tip to Aluminum coupon. Still Photo-open shutter. Brass collector is 0.2" away from back side of Al. coupon. Tektronix P6015 HV probe **Vcollector=3.5kV**
9/24/2010	19	27	0.2”	1/4" electrode, T6061 Al. coupon with 0.5" hole in center. 3/16" gap from electrode tip to Aluminum coupon. Still Photo-open shutter. Brass collector is 0.2" away from back side of Al. coupon. Tektronix P6015 HV probe **Vcollector=16V**
9/24/2010	20	22	0.2”	1/4" electrode, T6061 Al. coupon with 0.5" hole in center. 3/16" gap from electrode tip to Aluminum coupon. Still Photo-open shutter. Brass collector is 0.2" away from back side of Al. coupon. Tektronix P6015 HV probe **Vcollector=15V**

Electric field probe data will be taken to calibrate the incident voltage wave? **Due to the test configuration e-field data was only used as a fiducial to identify incoming pulse.**

Several open shutter photos will be taken for publication purposes.

One additional shot at the Sandia Lightning Simulator with a ½" pre-drilled hole with the ¼" electrode placed 1/16" from brass collector. High speed photography will be used on this shot.

SLS Arc to Failure Voltage (See Appendix G)

Date	Shot #	SLS Current (kA)	d	Description
8/27/2010	2	42	0.2"	0.050" T6061 Al coupon with 0.5" hole in center, 1/4" Tungsten Electrode, 1/16" gap from electrode tip to Brass Collector. High speed photography. Tektronix P6015 HV probe **Vcollector=5kV**

4. Radial Current Distribution Measurements – Single Return Stroke – Visible High Speed Photograph of Exterior Side of Coupon

In this experiment a 50-100 kA return stroke will be used. The objective is to measure the radial current distribution during the return stoke.

Visual recording will be carried out during this particular test sequence in hope of gaining insight on the discharge path and distribution. This will consist of high speed photography (20 kframes/s) with two views of the coupon surface.

B. INVERTED METAL RING PROBE

An inverted metal ring probe is being fabricated to check whether surface flash heating, and consequent changes in electrical conductivity, could have had an effect in round three experiments with the original groove probe. This probe consists of a thick stainless steel coupon with circular rings milled out to a thickness of approximately 1 mm. The groove width is also of order of 1 mm to allow sufficient radial resolution, with spacing between rings of 2-3 mm. Current flowing through the thinner metallic regions induces a voltage on the interior side, which can be monitored. A document exists discussing the design issues (including diffusion time constants). We intend to attach to the center region with the grooves facing the return stroke. The idea here is to use the thinner stainless steel regions as low inductance current viewing resistors (hopefully displaced away from the hot arc plasma).

Voltage (See Appendix H)

Date	Shot #	SLS Current (kA)	Description
9/2/2010	4	112	1/4" Tungsten Electrode, 1/4" Gap to SS Inverted Grooved Probe, Yokogawa (6 Channel),

There is a concern about radiant heating reaching the bottoms of the grooves and raising the temperature of the thin stainless steel region at the base. It is thought that a possible fix for this is to pour ceramic beads into the grooves to block the photons from reaching the base; however this will require that the probe be arranged in a horizontal position to contain the beads.

A twelve channel data recorder is available for measuring the array of voltages here.

5. Radial Current Distribution Measurements – Starter Wire/Return Stroke Continuing Current and Second Return Stroke – Visible High Speed Photograph of Exterior Side of Coupon

Tests conducted with double pulse (no starter wire)

The purpose of these shots is to investigate the current profile transition between continuing current with amplitude of 500 A and a subsequent return stroke with an amplitude of 100 kA. The continuing current interval in this case can be shortened to prevent damage to the probe, but long enough to (eliminate the starter wire and) set up the plasma. We are thinking of a time interval of 50 – 100 ms, although the continuing current may do damage after the measurement window (unless fusing can mitigate the long continuing current interval). The measurement focus is on the transition and return stroke time interval.

Visual recording will be carried out during this particular test sequence. This will consist of high speed photography (20 kframes/s) with two views of the coupon surface.

A. WATER COOLED METAL GROOVE PROBE

A cooling attachment has been designed to establish a flow of de-ionized water into the groove region and inhibit melting of the probe during the continuing current phase of this transition experiment. The cooling will also help mitigate heating of the thin stainless steel groove regions but may not prevent the outer surface from being raised in temperature. Consequently the inverted probe will also be used to check this effect. **No tests conducted.**

B. WATER COOLED INVERTED METAL GROOVE PROBE

This will be the same inverted groove probe as described in the preceding section except it will include a water cooling attachment. These results will be compared to the preceding setup to see if flash heating of the thin groove regions changed the results.

Voltage (See Appendix I)

Date	Shot #	SLS Currents	Description
9/7/2010	7	S53kA CCG(443A) N18kA	0.050" T6061 Al coupon, 1/4" Tungsten Electrode, 1/4" Gap between electrode and coupon, the water cooled groove probe inverted(the groove side faces electrode) (0.2"between Coupon and brass collector)NLS-30 fuse in series with CCG Simulator malfunction only 18kA ringing waveform on output. Probe wall breached by current. Yokogawa (6 Channel)

C. WATER COOLED CVR RING PROBE
The plan here was to examine if it made any sense to replace the rings with hollow tubes having an attachment to a water inlet and outlet. This would be an addition to the grooved probes. **No tests were conducted.**

6. Interior Insulation Effects and Cable Coupling
This set of experiments will measure coupling to a strip cable placed on an insulating layer as well as documenting the change in coupon damage resulting from the change in interior collecting structure from that of a large metallic collector to a cable and to an insulating layer. **Interpulse period for these tests was 500ms.**

We anticipate an experiment with a strip cable collector on an insulating layer as well as an experiment with an insulating layer alone. **A test without an insulating layer was used instead of an insulating layer alone.**

Strip Cable Voltage Tests (See Appendix J)

Date	Shot #	SLS Currents	d	Description
8/31/2010	3	S48kA CCG(459A) N100kA)	0.2”	0.050" T6061 Al coupon, 1/4" Tungsten Electrode, 1/4" Gap between electrode and coupon. Cable collector: 0.5" x 0.0025" thick copper sheet between 0.7" x 0.003" thick Kapton sheets set on 1/16" thick x 3 1/2" diameter rubber gasket. Cable and rubber gasket covering brass collector. V5K probe (LOOSE SMA CONNECTOR?) Vcollector= 700V
8/31/2010	4	S54kA) CCG(467A) N107kA)	0.2”	0.050" T6061 Al coupon, 1/4" Tungsten Electrode, 1/4" Gap between electrode and coupon. Cable collector: 0.5" x 0.0025" thick copper sheet between 0.7" x 0.003" thick Kapton sheets set on 1/16" thick x 3 1/2" diameter rubber gasket. Cable and rubber gasket covering brass collector. V5K probe Vcollector= 400V
9/1/2010	1	S46kA) CCG(486A) N96kA)	0.2”	0.050" T6061 Al coupon, 1/4" Tungsten Electrode, 1/4" Gap between electrode and coupon. Cable collector: 0.5" x 0.0025" thick copper sheet between 0.7" x 0.003" thick Kapton sheets set on 1/16" thick x 3 1/2" diameter rubber gasket. Cable and rubber gasket covering brass collector. V5K probe Vcollector= 400V
9/1/2010	3	S48kA CCG (450-500A*) North 99kA	0.2”	0.050" T6061 Al coupon, 1/4" Tungsten Electrode, 1/4" Gap between electrode and coupon No CCG acquired* No cable collector or Rubber gasket covering brass collector. Vcollector= 100V

A spacing of 0.2 inches will be used and photography is required to pick out hole size and discharge path (coupon edge versus cable collector).

7. Planning for FY11

During the round four experiments some planning for FY11 will be done. In particular, the possibility of using a plasma diverter (to eliminate the plasma jet from the cathode) and of making spectral measurements will be explored. The issue of internal impedance (inductive reactance) diverting the path of a return stroke attachment from the collector to the coupon rim will also be examined further and future experiments planned to minimize this effect. Also arc root current distribution for larger electrode spacing is of interest to relate results to longer lightning discharges. In addition the possibility of polarity changes will be discussed (anode electrode?). **No Tests were conducted for this task.**

References:

[1] G. H. Schnetzer, R. J. Fisher, and M. A. Dinallo, "Measured Responses of Internal Enclosures and Cables Due To Burnthrough Penetration of Weapon Cases by Lightning," SAND94-0312, August 1994.

[2] R. J. Fisher and M. A. Uman, "Recommended Baseline Direct-Strike Lightning Environment for Stockpile-to-Target Sequences," SAND 89-0192, May 1989.

[3] L. K. Warne, L. E. Martinez, R. E. Jorgenson, and K. O. Merewether, "Experimental Plan (First Round)," Internal Sandia Memorandum, March 27, 2009.

[4] L. K. Warne, L. E. Martinez, R. E. Jorgenson, and K. O. Merewether, "Experimental Plan (Interim Low Level)," Internal Sandia Memorandum, June, 2009.

[5] L. K. Warne, L. E. Martinez, R. E. Jorgenson, and K. O. Merewether, "Experimental Plan (Second Round)," Internal Sandia Memorandum, September 8, 2009.

[6] L. K. Warne, L. E. Martinez, R. E. Jorgenson, and K. O. Merewether, "Experimental Plan (Third Round)," Internal Sandia Memorandum, March 15, 2010.

0. Noise Shots

The noise shots on the "test to arc attachment" experiments with the predrilled hole could involve the same setup but with a solid coupon. The noise shots on the SLS burnthrough and "test to arc attachment" experiment could involve a return stroke without continuing current (and a solid coupon).

Description: 0.050" T6061 Al, no hole in center, 1/4" Tungsten Electrode, 1" Electrode Gap, Tektronix P6015 HV probe (0.45" between Coupon and collector)

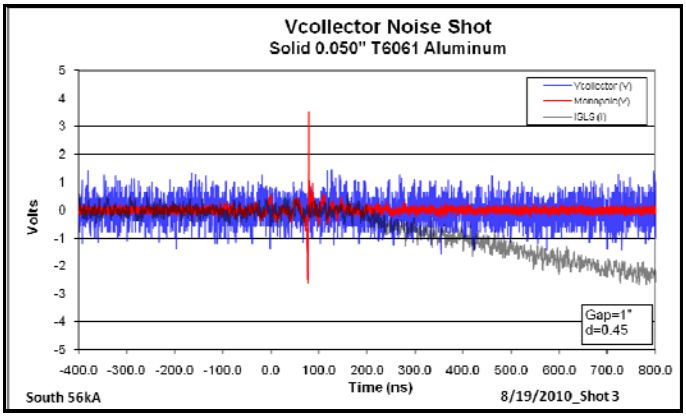

Description: 0.050" T6061 Al, no hole in center, 1/4" Tungsten Electrode, 1" Electrode Gap, Tektronix P6015 HV probe (0.2" between Coupon and collector)

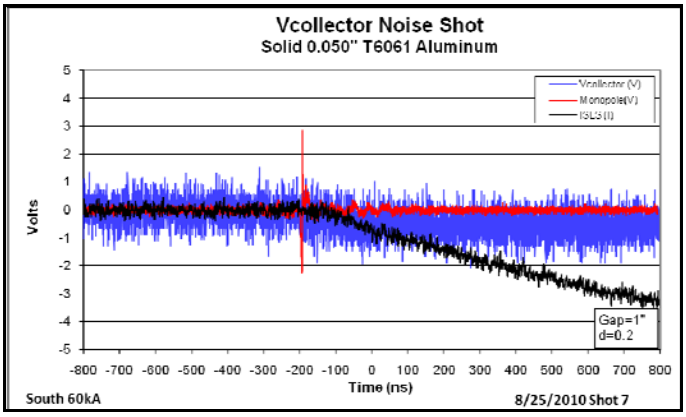

1. Calibration of Voltage Wave From Lightning Simulator

This measurement is important to calibrate the discharge to collector experiments, since this voltage wave determines the incident field in those experiments.

Description: 0.050" T6061 Al, no hole in center, 1/4" Tungsten Electrode, 1" Electrode Gap, Tektronix P6015 HV probe (0.45" between Coupon and collector)

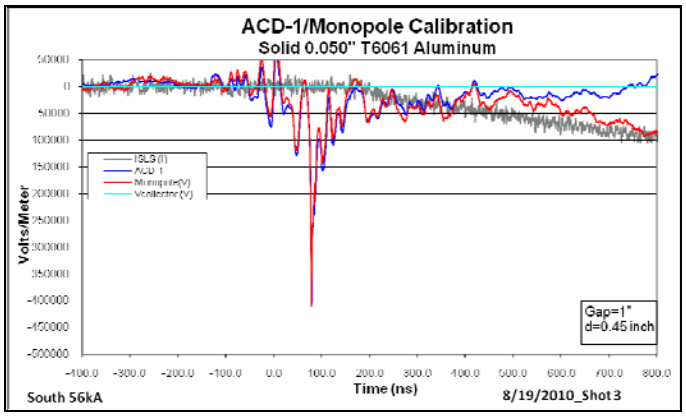

Description: 0.050" T6061 Al, no hole in center, 1/4" Tungsten Electrode, 1" Electrode Gap, Tektronix P6015 HV probe (0.2" between Coupon and collector)

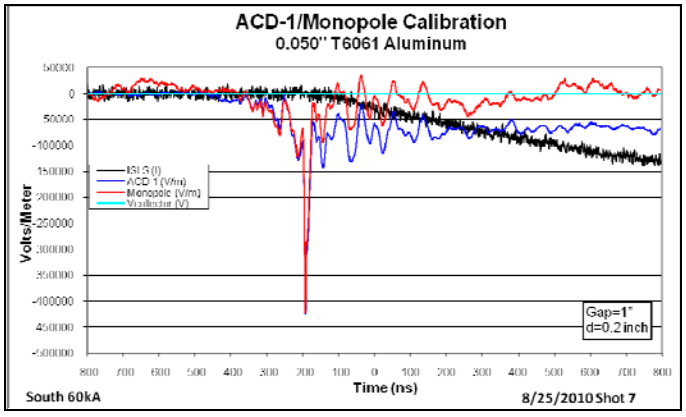

2. Test to Arc Attachment

The plan here is to repeat the original two-return stroke plus continuing current experiments conducted at the beginning of the project, but examine the early time regime during Marx bank voltage erection to see if any discharge paths form to the interior collector during the transition from continuing current to second return stroke.

Description: Solid 0.050" T6061 Al, 1/4" Tungsten Electrode, 1/4" Electrode Gap, Tektronix P6015 HV probe. 500ms between pulses. **Hole sizes after 500ms of CCG.**

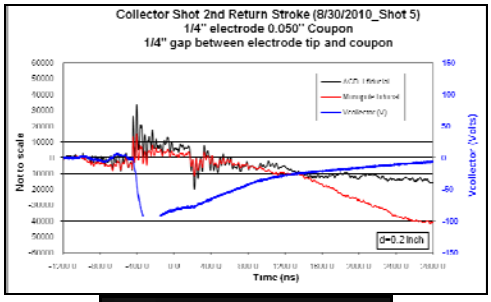

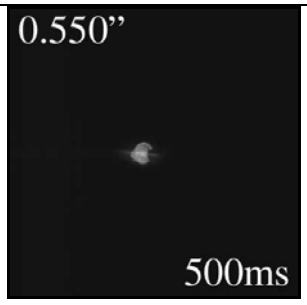

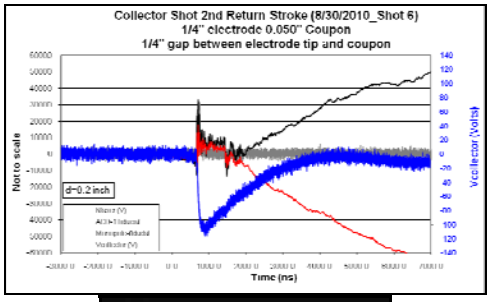

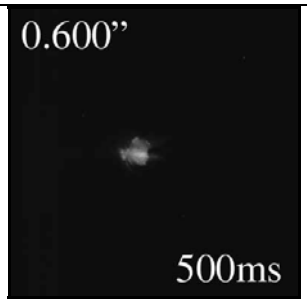

Description: Solid 0.050" T6061 Al, 1/4" Tungsten Electrode, 1/4" Electrode Gap, collector inductive setup LS=132nH,Lp=146nH, R=27.3mOhm Parameters measured with Agilent 4263B LCR Meter @100kHz, Tektronix P6015 HV probe. 500ms between pulses

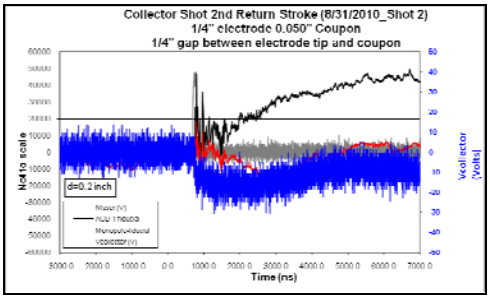

3. Predrilled Hole Discharge Penetration

In this set of experiments we plan to repeat the Velonex predrilled hole "discharge to collector" experiments but using higher voltage equipment. Velonex arc to collector Tektronix P6015 HV probe

Description: **Shot 1**: 1/4" electrode, 0.020" gap from electrode tip to solid 0.050" T6061 Al. coupon. NOISE SHOT

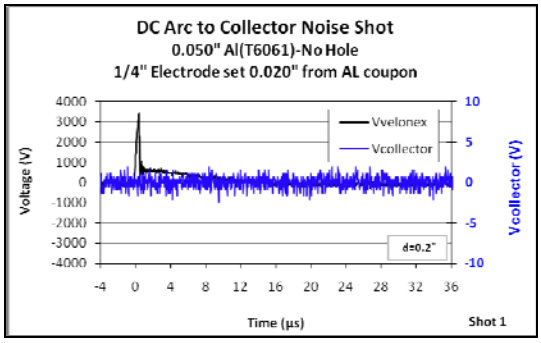

Description: **Shot 2**: 1/4" electrode, T6061 Al. coupon with 0.5" hole in center. Electrode center of hole. No gap from electrode tip to Aluminum coupon.

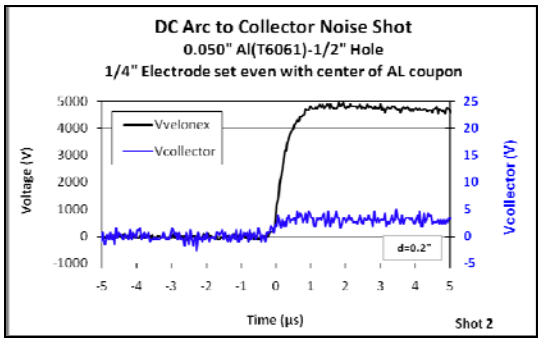

Description: **Shot 3**: 1/4" electrode, T6061 Al. coupon with 0.5" hole in center. Electrode through, and center of hole. 3/16" gap from electrode tip to internal brass collector.

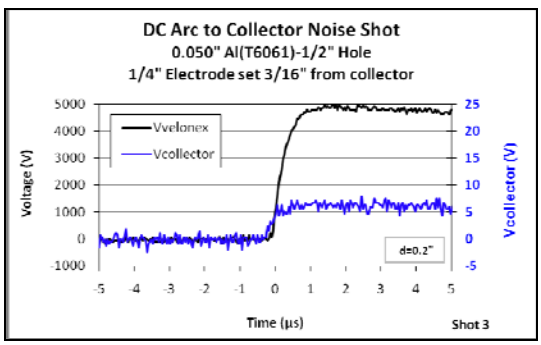

3. Predrilled Hole Discharge Penetration

In this set of experiments we plan to repeat the Velonex predrilled hole "discharge to collector" experiments but using higher voltage equipment. Velonex arc to collector Tektronix P6015 HV probe

Description: **Shot 4**: 1/4" electrode, T6061 Al. coupon with 0.5" hole in center. Electrode through, and center of hole. 1/8" gap from electrode tip to internal brass collector.

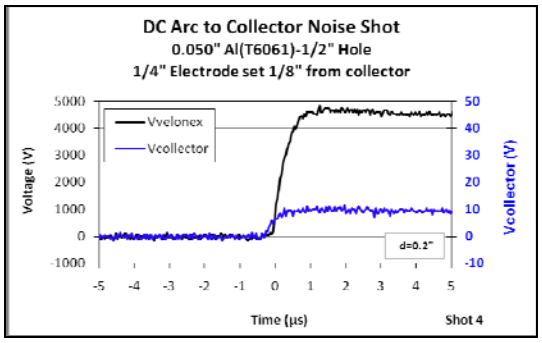

Description: **Shot 5**: 1/4" electrode, T6061 Al. coupon with 0.5" hole in center. Electrode through, and center of hole. 1/16" gap from electrode tip to internal brass collector.

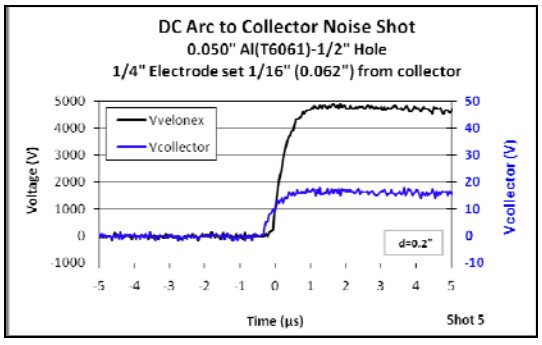

Description: **Shot 6**: 1/4" electrode, T6061 Al. coupon with 0.5" hole in center. Electrode through, and center of hole. 0.017" gap from electrode tip to internal brass collector.

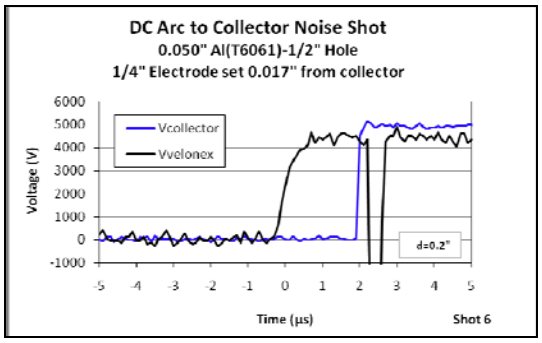

3. Predrilled Hole Discharge Penetration- DC ramp tests

In this set of experiments we plan to use a slow ramp source with a range from 0-200 kV Tektronix P6015 HV probe

Description: **Test 1:** 1/4" electrode, 1/4" gap from electrode tip to solid 0.050" T6061 Al. coupon. Still Photo-open shutter

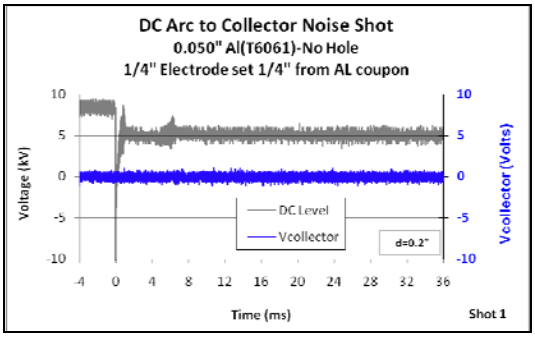

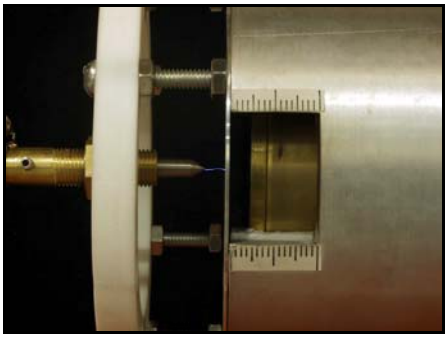

Description: **Test 2:** 1/4" electrode, 1/4" gap from electrode tip to 0.050" T6061 Al. coupon with 0.5" hole in center. Still Photo-open shutter

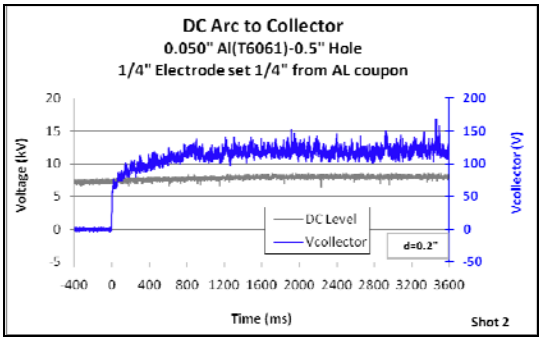

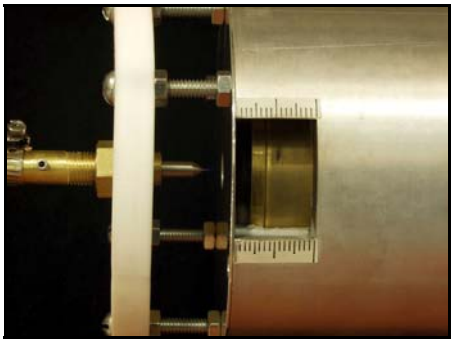

Description: **Test 3:** 1/4" electrode, T6061 Al. coupon with 0.5" hole in center. Electrode center of hole. No gap from electrode tip to Aluminum coupon. Still Photo-open shutter

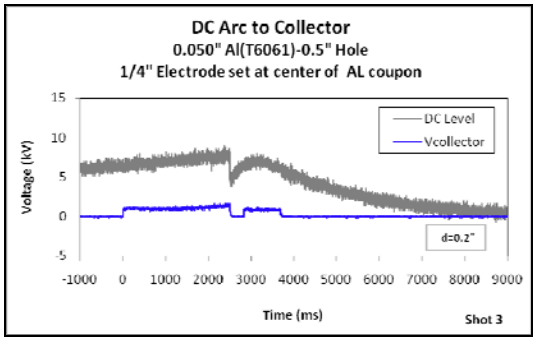

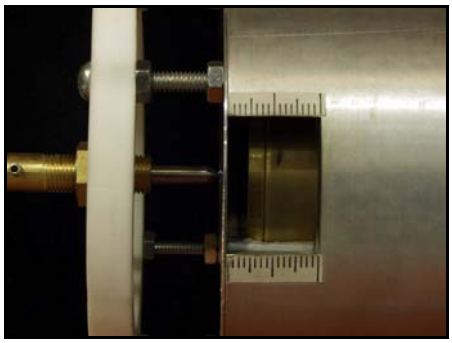

3. Predrilled Hole Discharge Penetration- DC ramp tests

In this set of experiments we plan to use a slow ramp source with a range from 0-200 kV Tektronix P6015 HV probe

Description: **Test 4:** 1/4" electrode, T6061 Al. coupon with 0.5" hole in center. Electrode through, and center of hole. 3/16" gap from electrode tip to internal brass collector. Still Photo-open shutter

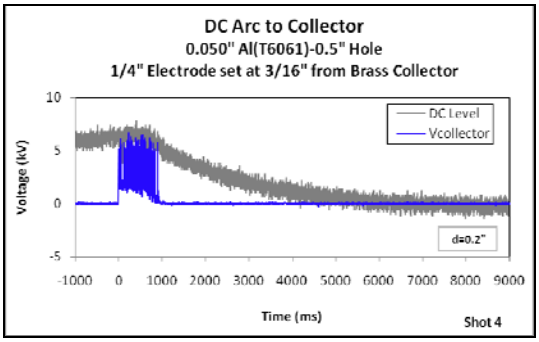

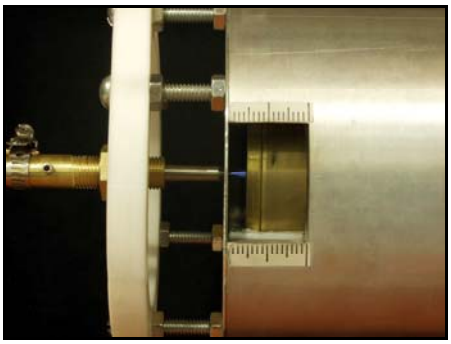

Description: **Test 5:** 1/4" electrode, T6061 Al. coupon with 0.5" hole in center. Electrode through, and center of hole. 3/16" gap from electrode tip to internal brass collector. Still Photo-open shutter

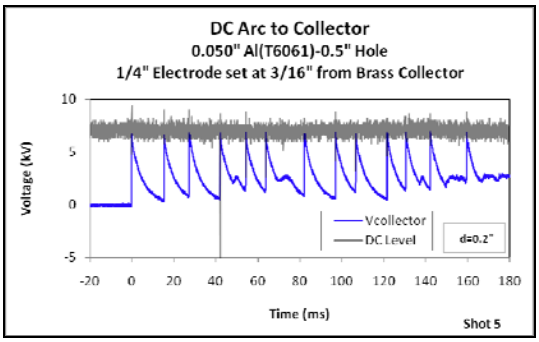

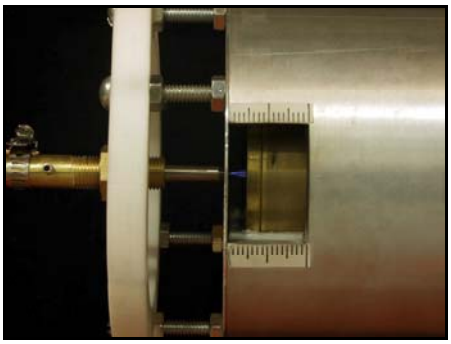

Description: **Test 6:** 1/4" electrode, T6061 Al. coupon with 0.5" hole in center. Electrode through, and center of hole. 3/16" gap from electrode tip to internal brass collector. Still Photo-open shutter

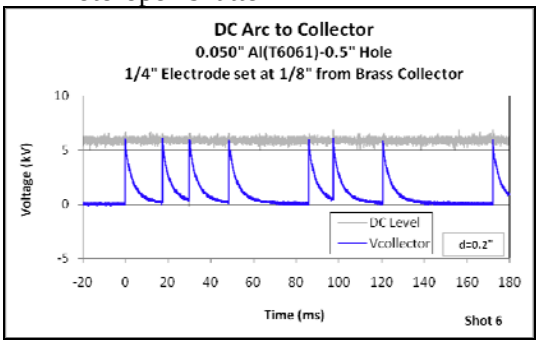

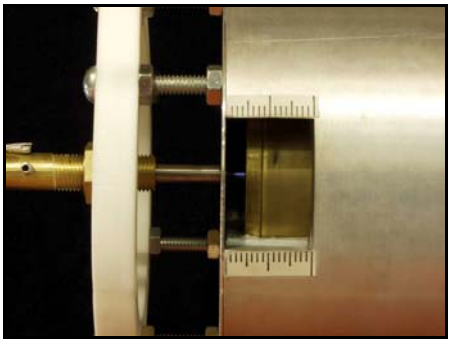

3. Predrilled Hole Discharge Penetration- DC ramp tests

In this set of experiments we plan to use a slow ramp source with a range from 0-200 kV Tektronix P6015 HV probe

Description: **Test 7:** 1/4" electrode, T6061 Al. coupon with 0.5" hole in center. Electrode through, and center of hole. 1/8" gap from electrode tip to internal brass collector. Still Photo-open shutter

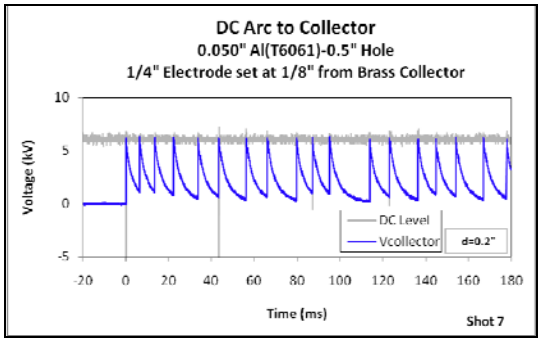

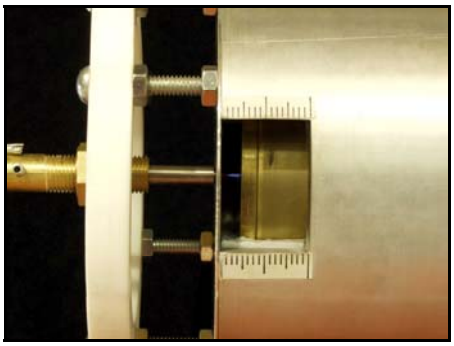

Description: **Test 8:** 1/4" electrode, T6061 Al. coupon with 0.5" hole in center. Electrode through, and center of hole. 1/16" gap (0.066") from electrode tip to internal brass collector. Still Photo-open shutter

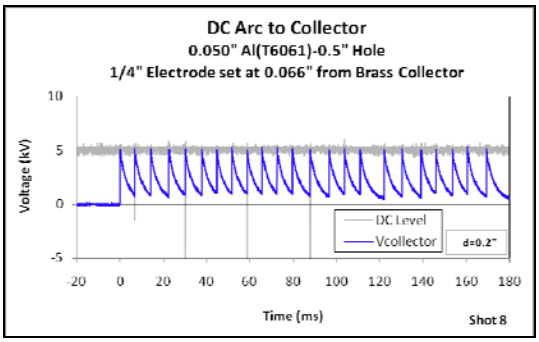

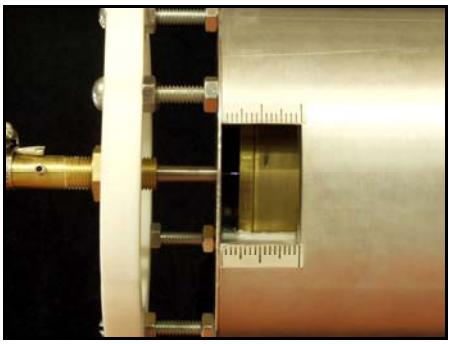

Description: **Test 9:** 1/4" electrode, T6061 Al. coupon with 0.5" hole in center. Electrode through, and center of hole. 1/16" gap (0.066") from electrode tip to internal brass collector. Still Photo-open shutter

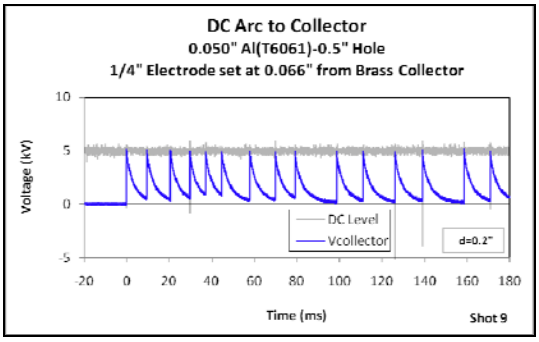

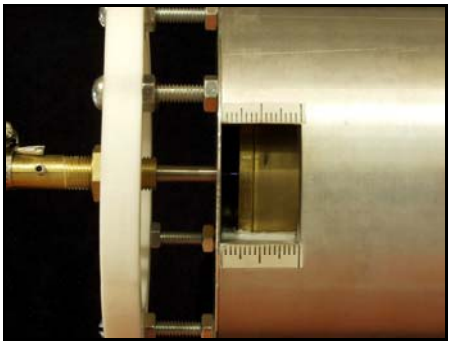

3. Predrilled Hole Discharge Penetration- DC ramp tests

In this set of experiments we plan to use a slow ramp source with a range from 0-200 kV Tektronix P6015 HV probe

Description: **Test 10:** 1/4" electrode, T6061 Al. coupon with 0.5" hole in center. Electrode center of hole. No gap from electrode tip to Aluminum coupon. Still Photo-open shutter

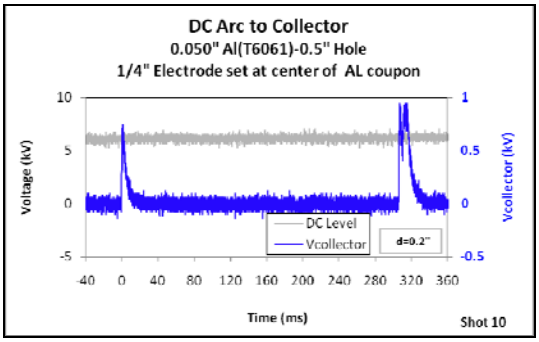

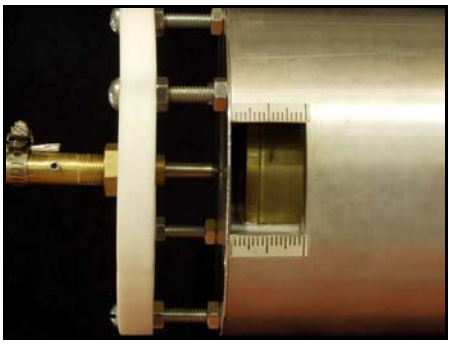

Description: **Test 11:** 1/4" electrode, 1/4" gap from electrode tip to 0.050" T6061 Al. coupon with 0.5" hole in center. Still Photo-open shutter. Audible and visual corona at 10 kV

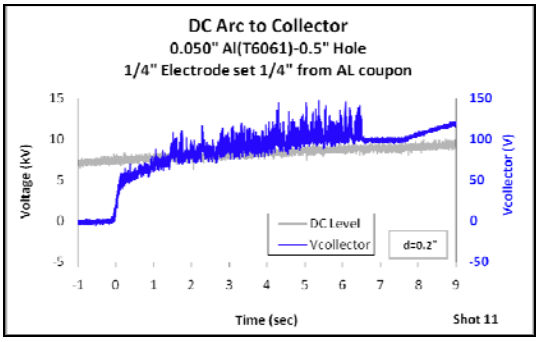

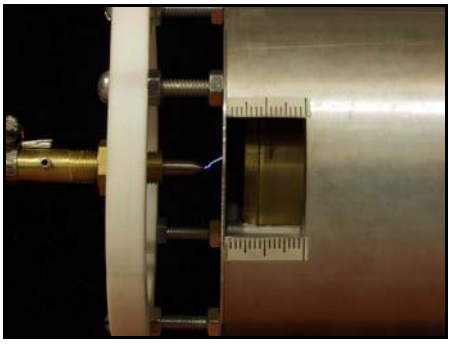

Description: **Test 12:** 1/4" electrode, 1/4" gap from electrode tip to 0.050" T6061 Al. coupon with 0.5" hole in center. Still Photo-open shutter. Audible and visual corona at 9 kV

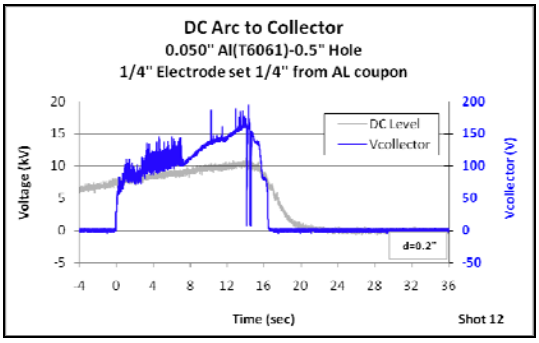

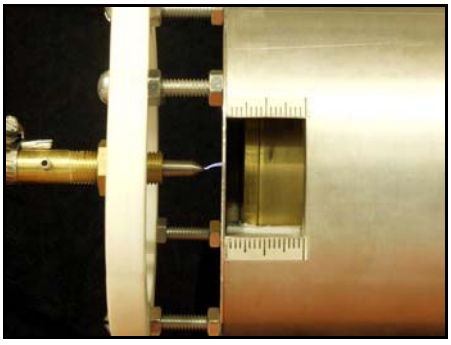

3. Predrilled Hole Discharge Penetration- DC ramp tests

In this set of experiments we plan to use a slow ramp source with a range from 0-200 kV Tektronix P6015 HV probe

Description: **Test 13:** 1/4" electrode, 1/2" gap from electrode tip to 0.050" T6061 Al. coupon with 0.5" hole in center. Still Photo-open shutter

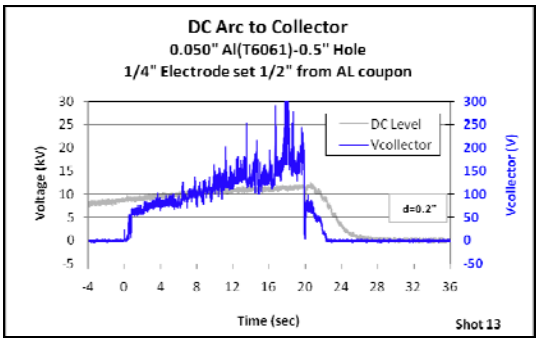

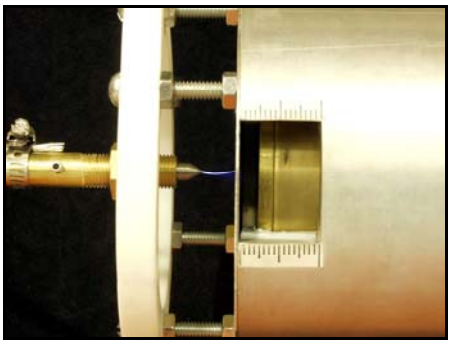

Description: **Test 14:** 1/4" electrode, 1/2" gap from electrode tip to 0.050" T6061 Al. coupon with 0.5" hole in center. Still Photo-open shutter

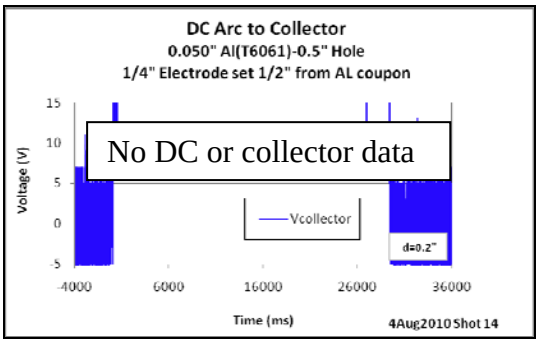

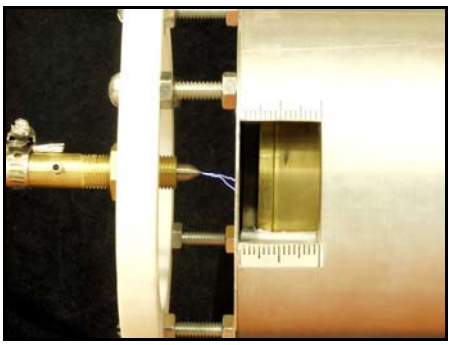

Description: **Test 15:** 1/4" electrode, 3/4" gap from electrode tip to 0.050" T6061 Al. coupon with 0.5" hole in center. Still Photo-open shutter

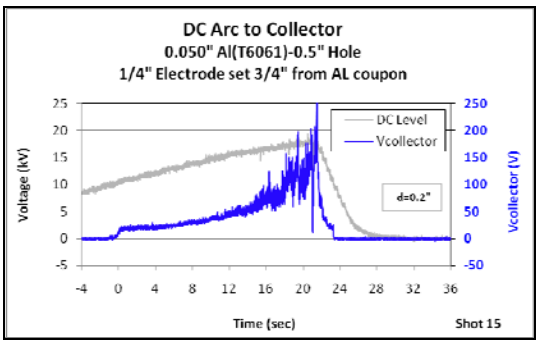

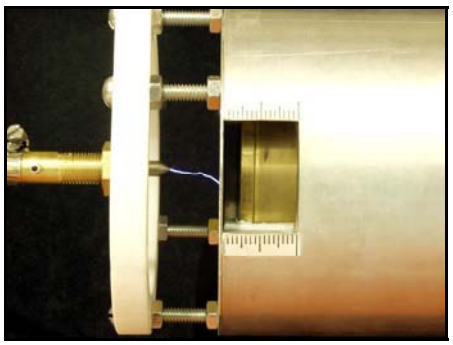

3. Predrilled Hole Discharge Penetration- DC ramp tests

In this set of experiments we plan to use a slow ramp source with a range from 0-200 kV Tektronix P6015 HV probe

Description: **Test 16:** 1/4" electrode, 3/4" gap from electrode tip to 0.050" T6061 Al. coupon with 0.5" hole in center. Still Photo-open shutter

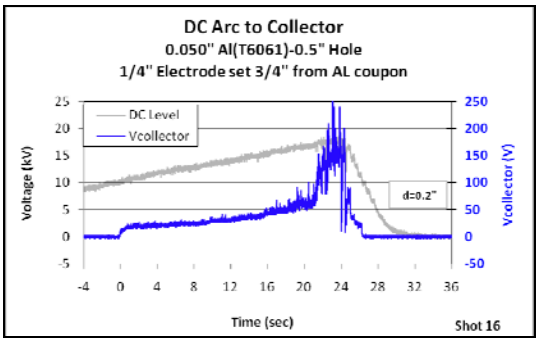

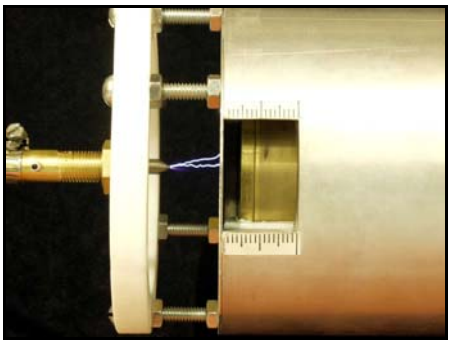

Description: **Test 17:** 1/4" electrode, 3/4" gap from electrode tip to 0.050" T6061 Al. coupon with 0.5" hole in center. VIDEO RECORDING #1

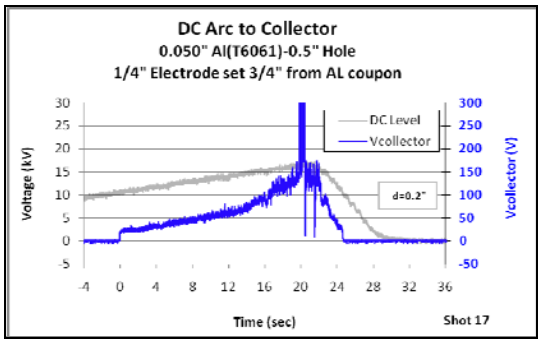

Description: **Test 18:** 1/4" electrode, T6061 Al. coupon with 0.5" hole in center. Electrode through, and center of hole. 3/16" gap from electrode tip to internal brass collector. VIDEO RECORDING #3

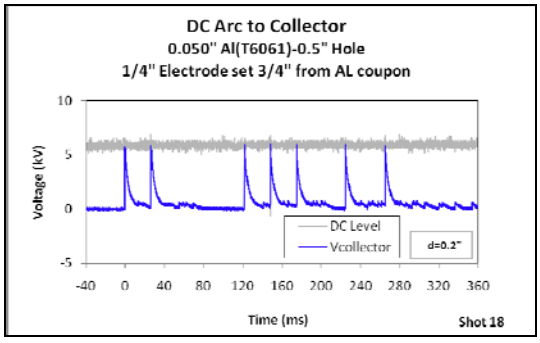

3. Predrilled Hole Discharge Penetration- Pantex Pulser

In this set of experiments we will use the Pantex impulse test bed.

Description: **Test 22:** 1/4" electrode, T6061 solid Al. coupon with no hole. 3/16" gap from electrode tip to Aluminum coupon. Still Photo-open shutter. Brass collector is 0.2" away from back side of Al. coupon. NOISE SHOT

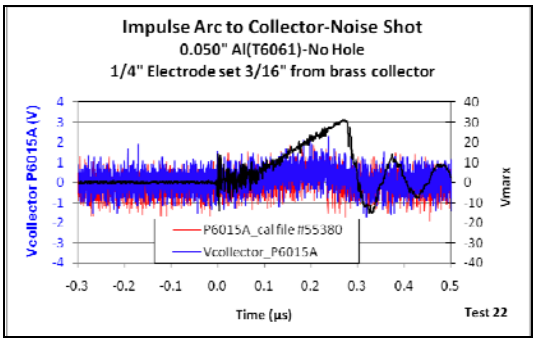

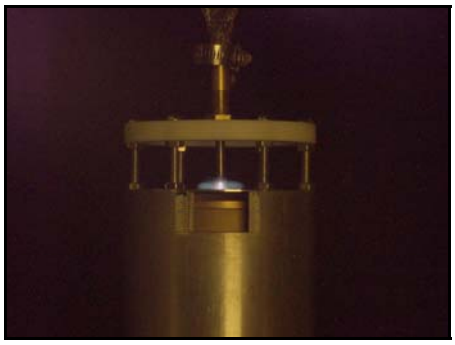

Description: **Test 11:** 1/4" electrode, T6061 Al. coupon with 1/2" hole. 1/16" gap from electrode tip to Brass collector. Still Photo-open shutter. Brass collector is 0.2" away from back side of Al. coupon.

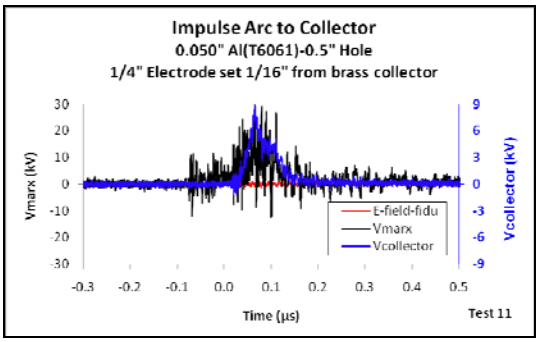

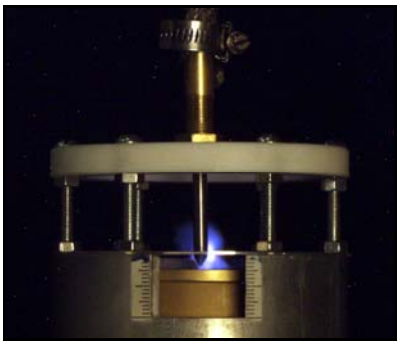

Description: **Test 12:** 1/4" electrode, T6061 Al. coupon with 1/2" hole. 1/16" gap from electrode tip to Brass collector. Still Photo-open shutter. Brass collector is 0.2" away from back side of Al. coupon.

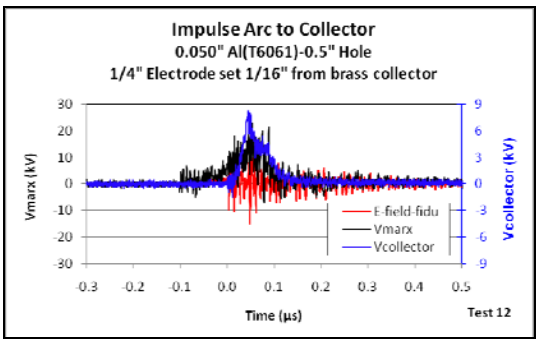

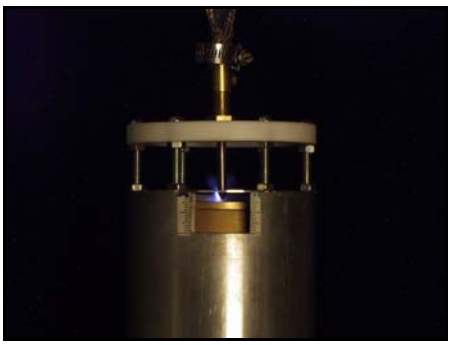

3. Predrilled Hole Discharge Penetration- Pantex Pulser

In this set of experiments we will use the Pantex impulse test bed.

Description: **Test 13:** 1/4" electrode, T6061 Al. coupon with 1/2" hole. 1/8" gap from electrode tip to Brass collector. Still Photo-open shutter. Brass collector is 0.2" away from back side of Al. coupon.

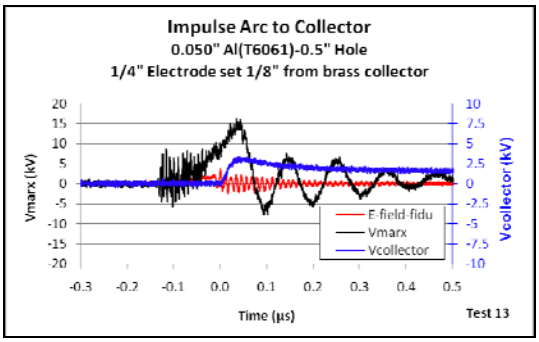

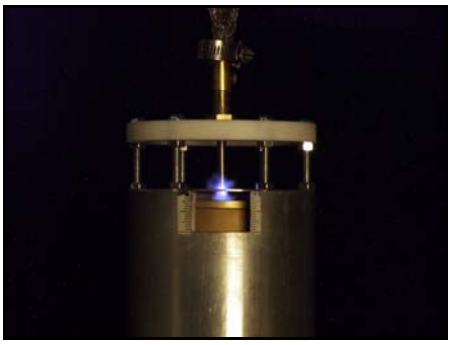

Description: **Test 14:** 1/4" electrode, T6061 Al. coupon with 1/2" hole. 1/8" gap from electrode tip to Brass collector. Still Photo-open shutter. Brass collector is 0.2" away from back side of Al. coupon.

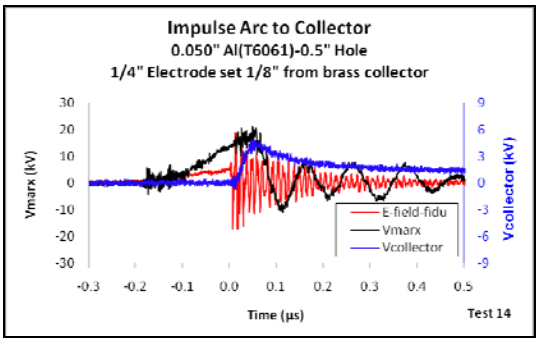

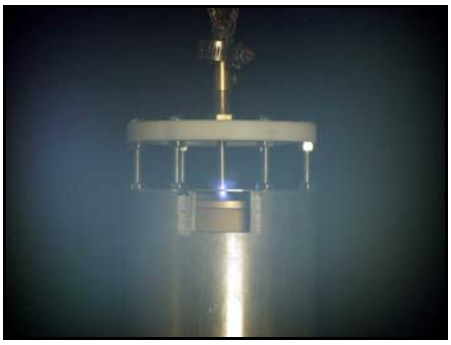

Description: **Test 15:** 1/4" electrode, T6061 Al. coupon with 1/2" hole. 3/16" gap from electrode tip to Brass collector. Still Photo-open shutter. Brass collector is 0.2" away from back side of Al. coupon.

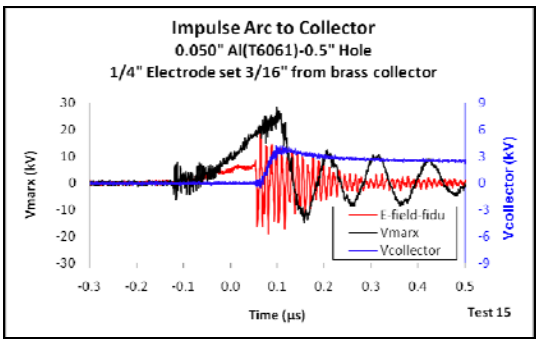

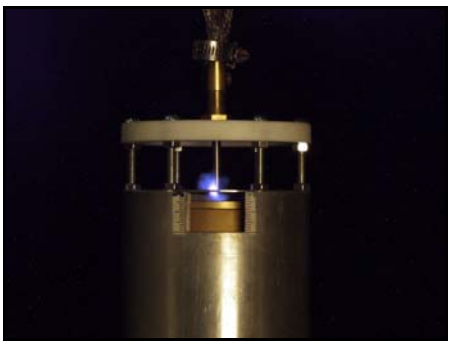

3. Predrilled Hole Discharge Penetration- Pantex Pulser

In this set of experiments we will use the Pantex impulse test bed.

Description: **Test 16:** 1/4" electrode, T6061 Al. coupon with 1/2" hole. 3/16" gap from electrode tip to Brass collector. Still Photo-open shutter. Brass collector is 0.2" away from back side of Al. coupon.

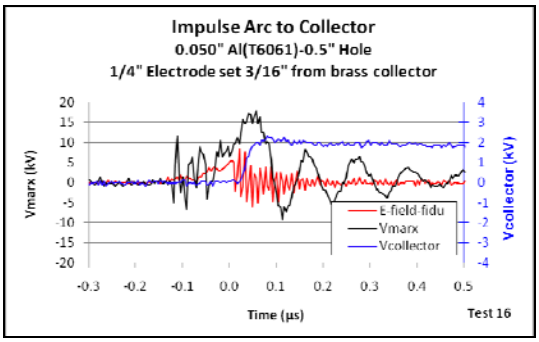

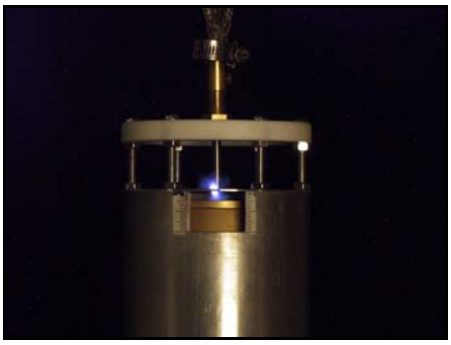

Description: **Test 17:** 1/4" electrode, T6061 Al. coupon with 0.5" hole in center. Electrode center of hole. No gap from electrode tip to Aluminum coupon. Still Photo-open shutter. Brass collector is 0.2" away from back side of Al. coupon.

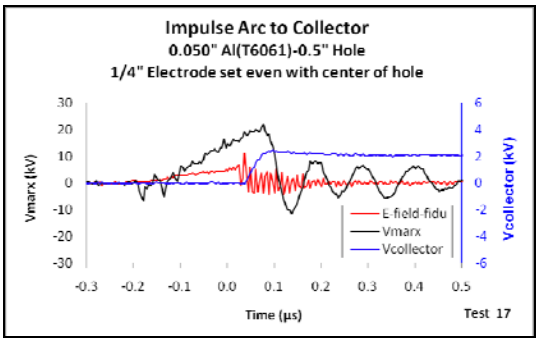

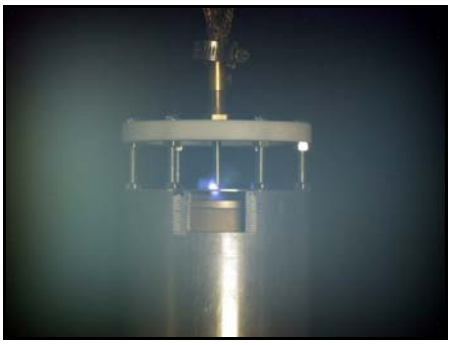

Description: **Test 18:** 1/4" electrode, T6061 Al. coupon with 0.5" hole in center. Electrode center of hole. No gap from electrode tip to Aluminum coupon. Still Photo-open shutter. Brass collector is 0.2" away from back side of Al. coupon.

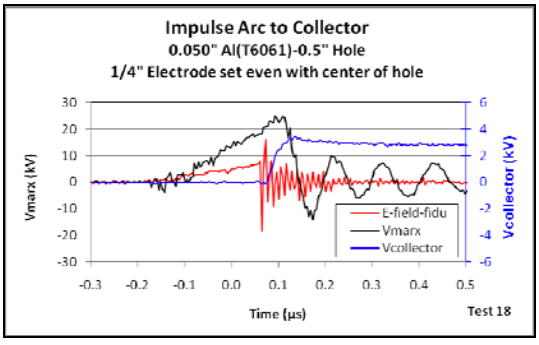

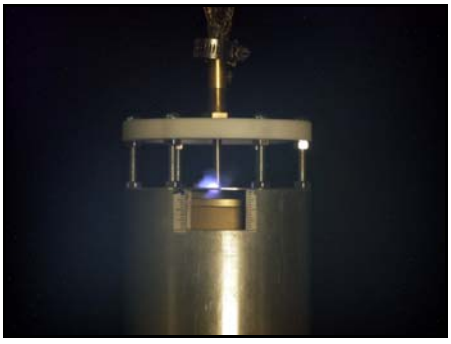

3. Predrilled Hole Discharge Penetration- Pantex Pulser
In this set of experiments we will use the Pantex impulse test bed.

Description: **Test 19:** 1/4" electrode, T6061 Al. coupon with 0.5" hole in center. 3/16" gap from electrode tip to Aluminum coupon. Still Photo-open shutter. Brass collector is 0.2" away from back side of Al. coupon.

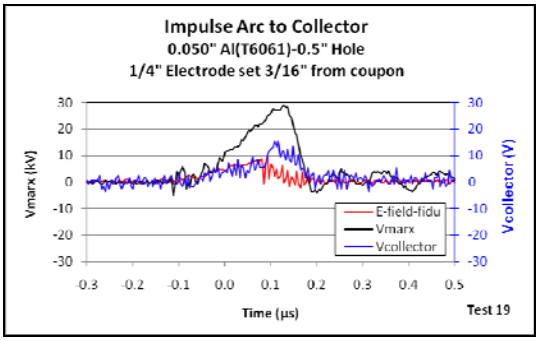

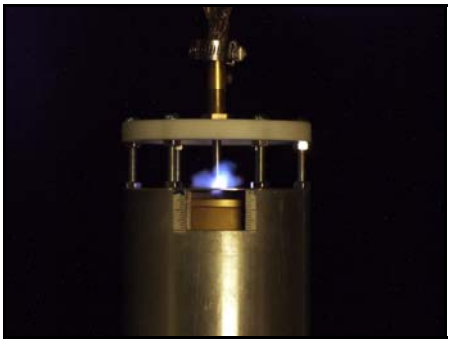

Description: **Test 20:** 1/4" electrode, T6061 Al. coupon with 0.5" hole in center. 3/16" gap from electrode tip to Aluminum coupon. Still Photo-open shutter. Brass collector is 0.2" away from back side of Al. coupon.

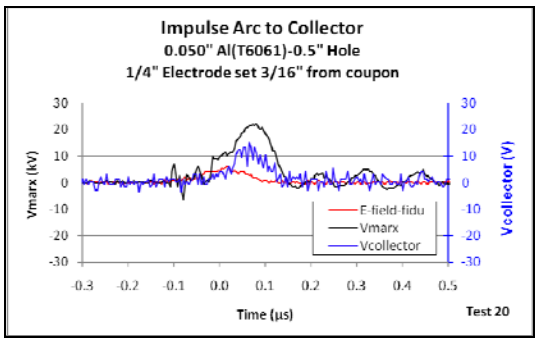

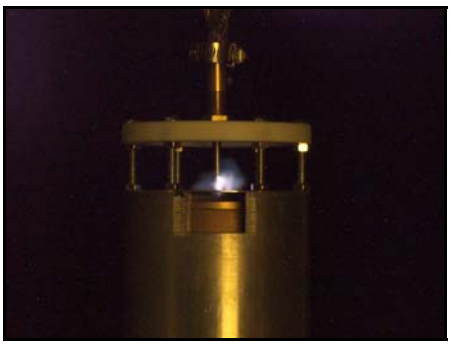

3. Predrilled Hole Discharge Penetration- Sandia Lightning Simulator
In this set of experiments we will use the Sandia Lightning Simulator.

Description: 0.050" T6061 Al coupon with 0.5" hole in center, 1/4" Tungsten Electrode, 1/16" gap from electrode tip to Brass Collector. High speed photography. Tektronix P6015 HV probe

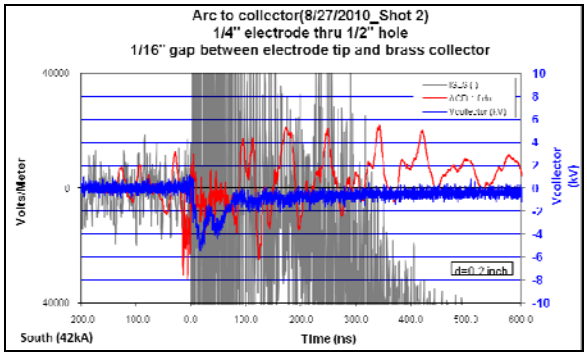

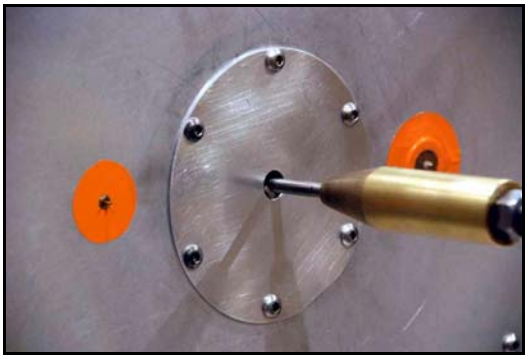

4. Radial Current Distribution Measurements – Single Return Stroke – Visible High Speed Photograph of Exterior Side of Coupon

In this experiment a 50-100 kA return stroke will be used. The objective is to measure the radial current distribution during the return stoke.

Description: 1/4" Tungsten Electrode, 1/4" Gap to SS Inverted Grooved Probe from Round 3, Yokogawa (6 Channel)

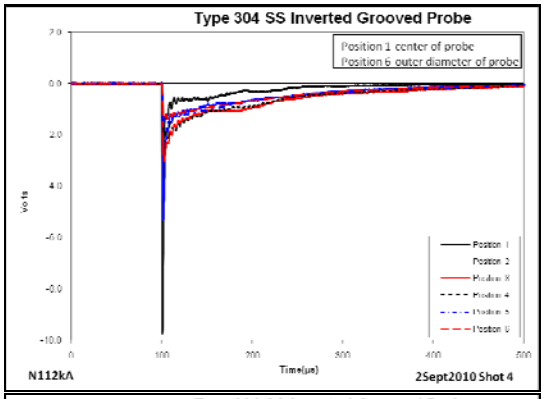

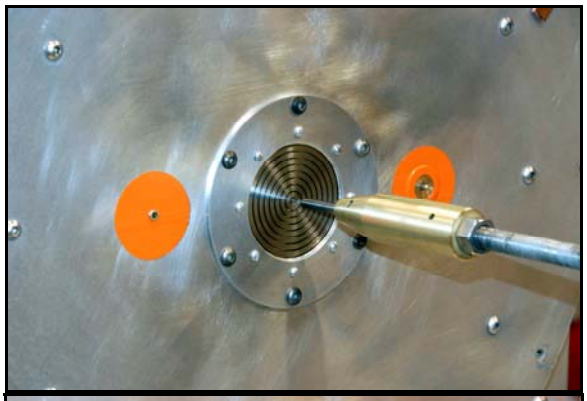

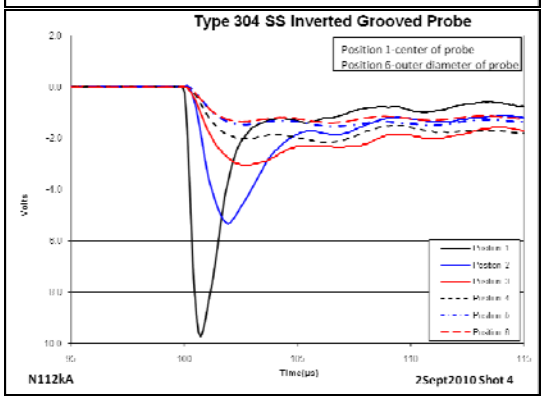

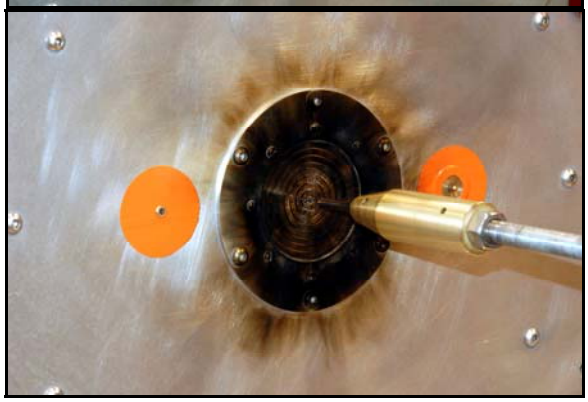

5. Radial Current Distribution Measurements – Starter Wire/Return Stroke Continuing Current and Second Return Stroke – Visible High Speed Photograph of Exterior Side of Coupon

This will be the same inverted groove probe as described in the preceding section except it will include a water cooling attachment.

Description: 0.050" T6061 Al coupon, 1/4" Tungsten Electrode, 1/4" Gap between electrode and coupon, the water cooled groove probe inverted(the groove side faces electrode) (0.2"between Coupon and brass collector)NLS-30 fuse in series with CCG Simulator malfunction only 18kA ringing waveform on output. Probe wall breached by current. Yokogawa (6 Channel)

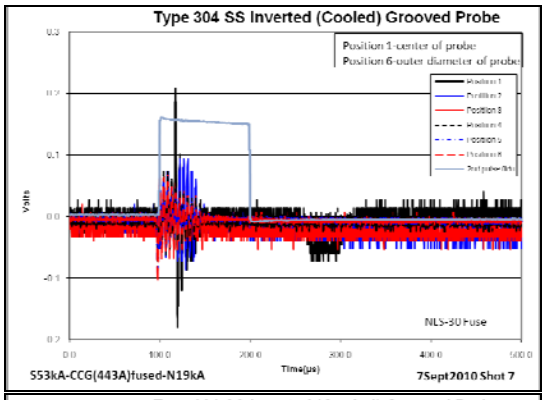

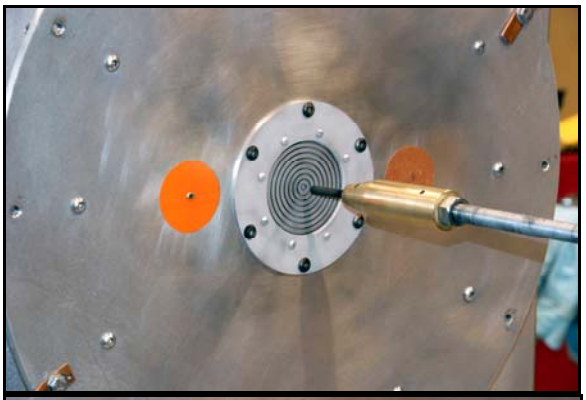

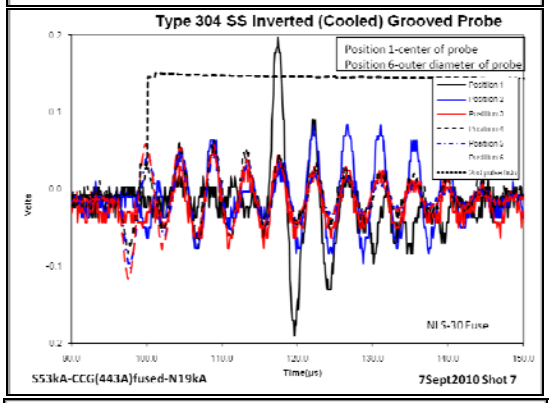

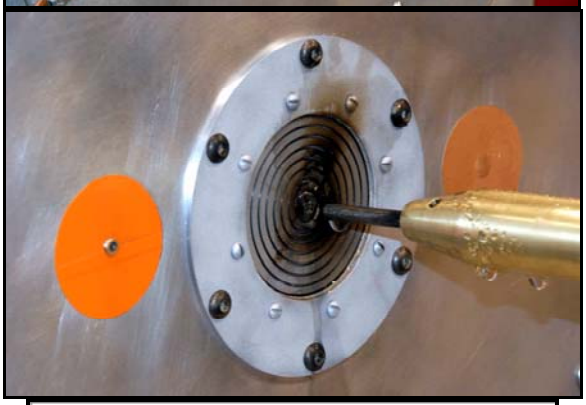

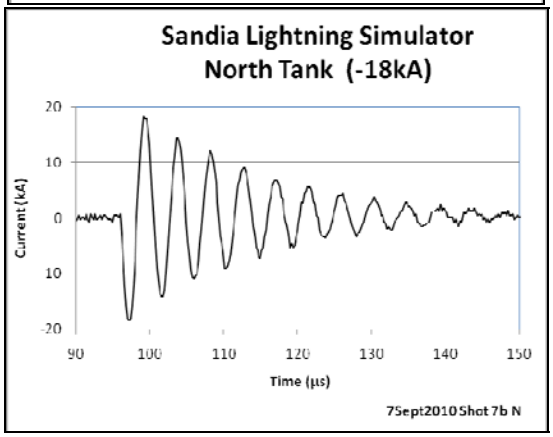

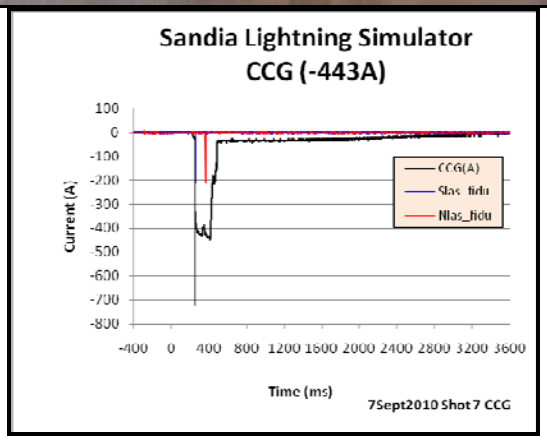

6. Interior Insulation Effects and Cable Coupling

This set of experiments will measure coupling to a strip cable placed on an insulating layer

Description: 0.050" T6061 Al coupon, 1/4" Tungsten Electrode, 1/4" Gap between electrode and coupon. Cable collector: 0.5" x 0.0025" thick copper sheet between 0.7" x 0.003" thick Kapton sheets set on 1/16" thick x 3 1/2" diameter rubber gasket. Cable and rubber gasket covering brass collector, V5K probe (LOOSE SMA CONNECTOR?) **Hole size after 500ms of CCG.**

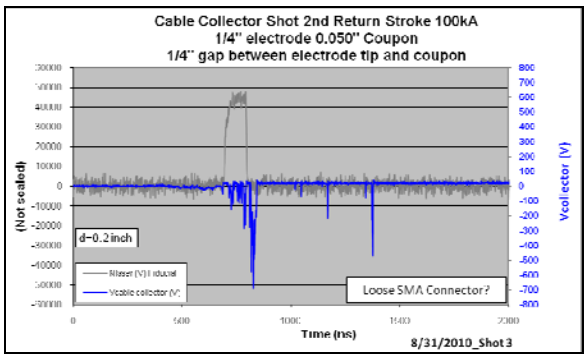

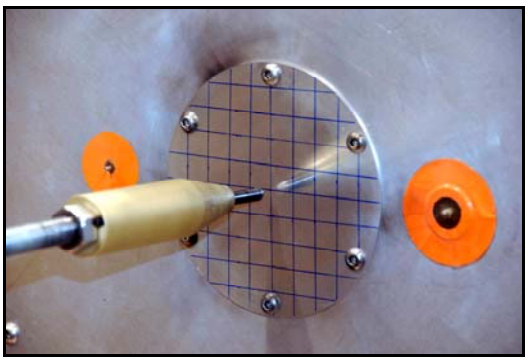

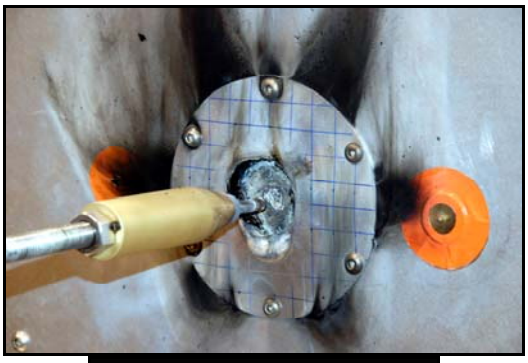

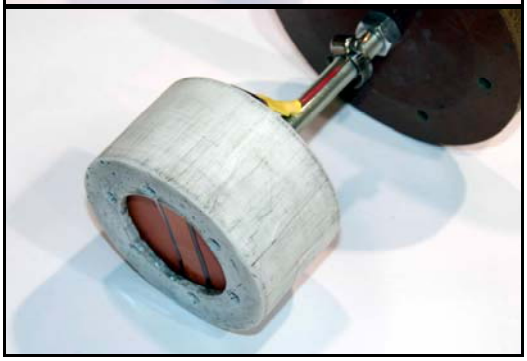

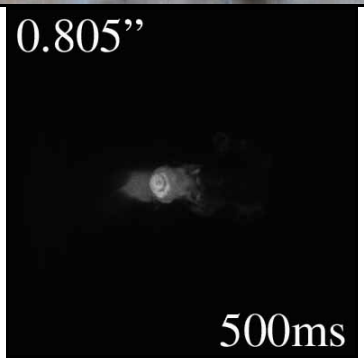

6. Interior Insulation Effects and Cable Coupling

This set of experiments will measure coupling to a strip cable placed on an insulating layer

Description: 0.050" T6061 Al coupon, 1/4" Tungsten Electrode, 1/4" Gap between electrode and coupon. Cable collector: 0.5" x 0.0025" thick copper sheet between 0.7" x 0.003" thick Kapton sheets set on 1/16" thick x 3 1/2" diameter rubber gasket. Cable and rubber gasket covering brass collector, V5K probe, **Hole size after 500ms of CCG.**

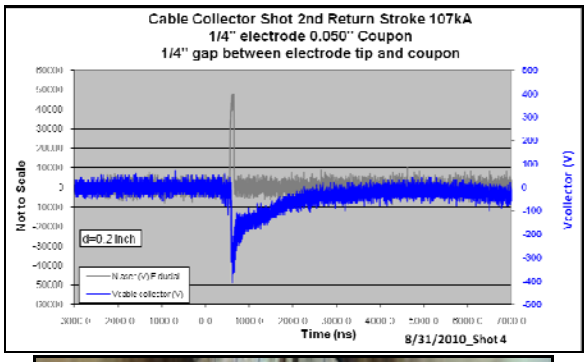

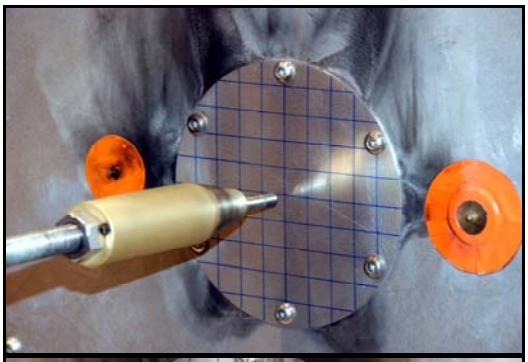

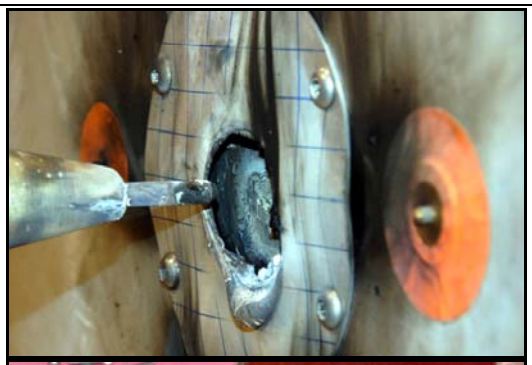

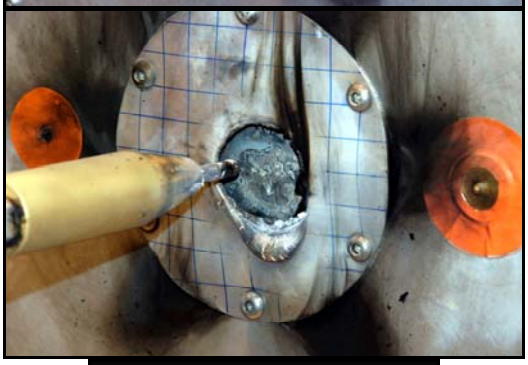

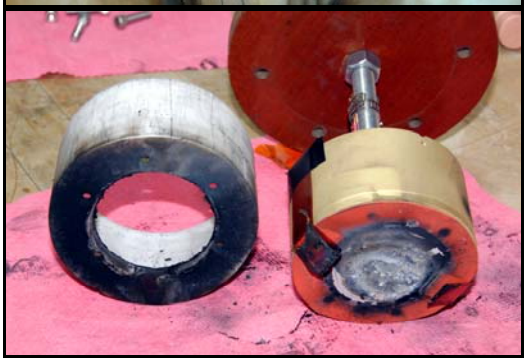

6. Interior Insulation Effects and Cable Coupling

This set of experiments will measure coupling to a strip cable placed on an insulating layer

Description: 0.050" T6061 Al coupon, 1/4" Tungsten Electrode, 1/4" Gap between electrode and coupon. Cable collector: 0.5" x 0.0025" thick copper sheet between 0.7" x 0.003" thick Kapton sheets set on 1/16" thick x 3 1/2" diameter rubber gasket. Cable and rubber gasket covering brass collector, V5K probe, **Hole size after 500ms of CCG.**

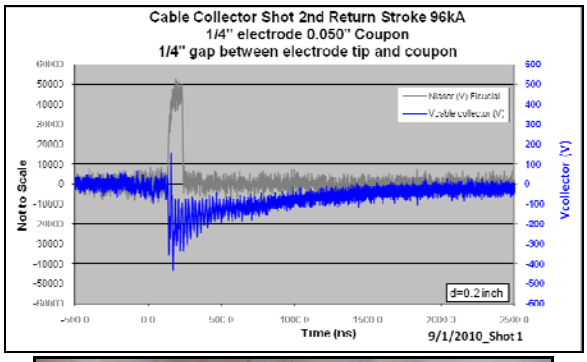

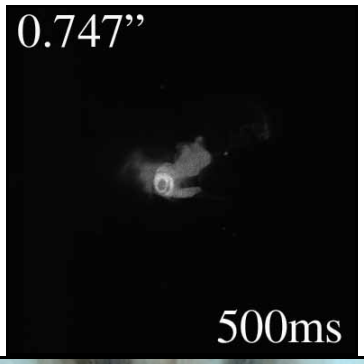

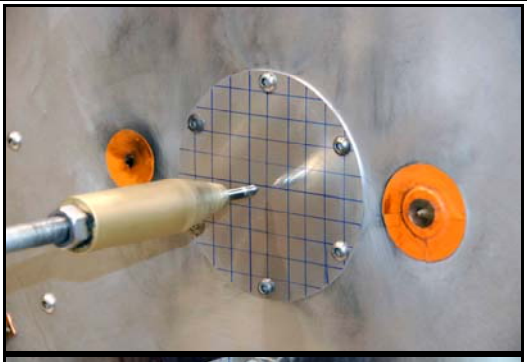

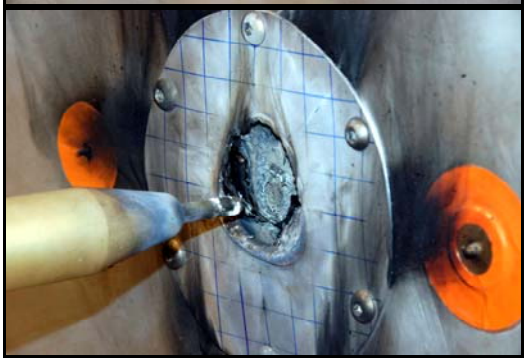

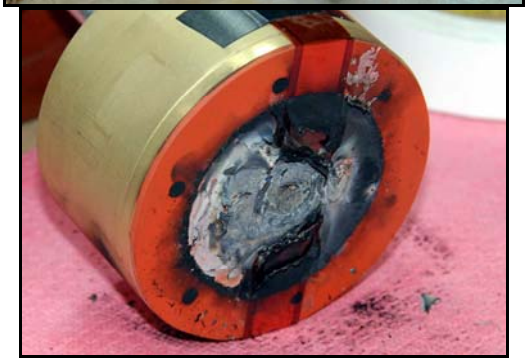

6. Interior Insulation Effects and Cable Coupling

This set of experiments will use no insulating layer to cover the brass collector.

Description: 0.050" T6061 Al coupon, 1/4" Tungsten Electrode, 1/4" Gap between electrode and coupon, No CCG acquired, No cable collector or Rubber gasket covering brass collector**. Hole size after 500ms of CCG.**

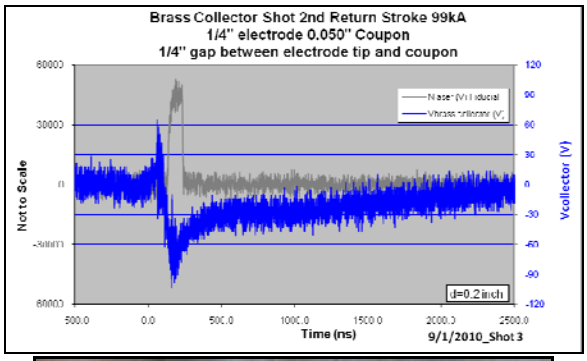

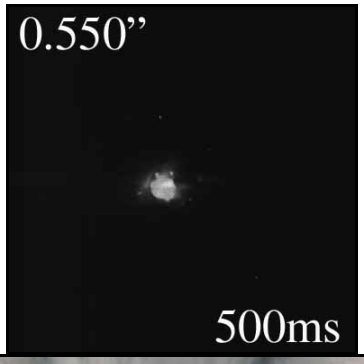

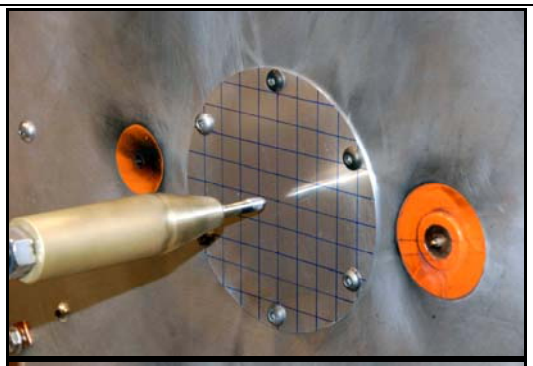

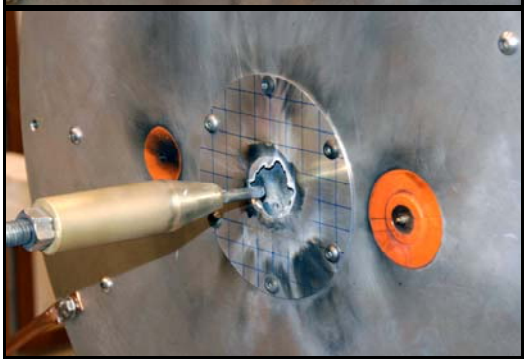

Summary of

Round 5 Testing

for LDRD

"Field and Charge Penetration by Lightning Burnthrough"

Authors: Leonard Martinez, SNL Department 1653
Larry Warne, SNL Department 1653
Roy Jorgenson, SNL Department 1653

Measurements by: Leonard Martinez, SNL Department 1653
Ed Bystrom, SNL Department 1535

Test Support: John Jojola, SNL Department 1653
Sandra Montoya, K-Tech Corporation

Revision: Rev 0.

Date: September 2011

Experimental Plan (Fifth Round)

Abstract: This fifth round of experiments has two primary goals and a secondary goal. The first and most important primary goal is to carry out experiments directed at pinning down the largest open circuit early time penetrant voltage. We have observed that early time recording is essential to capturing this coupling and that the cable versus the piston collector seems to give the largest levels. We plan to exercise variations in the hole size in starter wire double return stroke/continuing current experiments using the Sandia SLS and compare with indirect and direct predictions of coupled voltage to get more insight on this issue.

The second primary goal is to assess the dynamic source impedance to the cable by conducting experiments with different load impedances in the measurement system.

The third (secondary) goal is to collect data on a larger spacing between the electrode and the coupon. This data may include early time voltage, current and load impedance.

Because the cable experiments resulted in higher voltages it seems preferable to use the cable where available.

Because the Tektronix high impedance – high voltage probe seems like the cleanest open circuit voltage measurement setup we prefer to go this route on these experiments. However in the first experiment we must check to see if we obtain the same results as previously observed with the 5 kohm setup (400-700 V) with a 500 ms CCG current duration between return strokes.

The second experiment is directed at the time evolution of the source impedance, and will use lower impedance measurement loads.

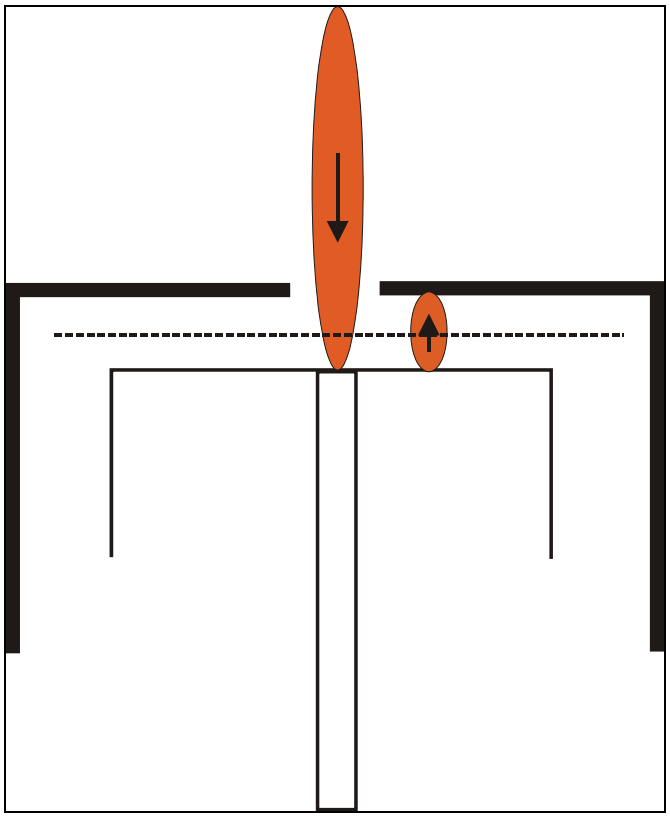

Arc return to case

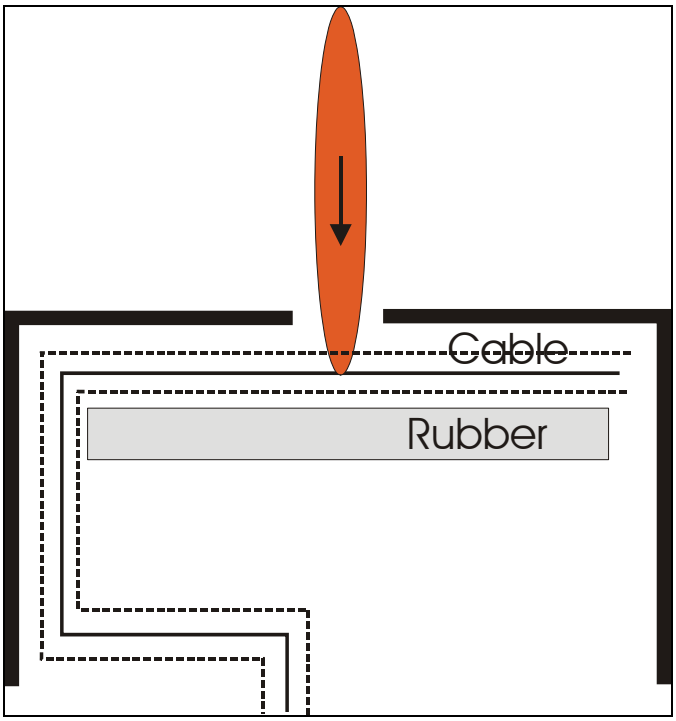

Stripline cable with rubber insulator

0. Noise Shots and incident electric field measurement

Noise shots for Tektronix P6015A HV probe and incident electric field measurement.

Noise Shot/Incident E-field (See Appendix A)

Date	Shot #	SLS Currents	d	Description
5/24/2011	8	S56kA	0.45”	0.050" T6061 Al coupon w/ 0.5" Hole, 1/4" Tungsten Electrode, 1" Gap (Open Circuit) between electrode and coupon (0.45" between Coupon and brass collector), Calibration of SNL 4.3mm Monopole (scale factor = 2 x AD10 scale factor) with Prodyn AD-10 E-field probe. Incident **E-field = 488kV/meter** Tektronix P6015 noise shot (**Vcollector=5V**)

1. Double return stroke with starter wire

The plan here is to repeat the original two-return stroke plus continuing current experiments but initiate the discharge with a starter wire. We expect about 400 ms to the first return stroke of 50 kA and 500 ms to the second return stroke (after the beginning of the continuing current) of 100 kA. We expect this to achieve hole sizes similar to the first item above but with a more defendable extreme lightning waveform. Tektronix high impedance load should be used. The spacing to the cable or piston collector will be 0.2 inches. Two shots on the cable and two shots on the piston collector should be done. **Tests conducted with 500ms (simulator timing error) of CCG before 1st return stroke and 100ms between 1st and 2nd return strokes.**

Voltage (See Appendix B)

Date	Shot #	SLS Currents	d	Description
8/4/2011	4	CCG (416A) S50kA N140kA	0.2”	Cu Starter wire (0.008" dia.) First return stroke 500ms from start of CCG, second return stroke 100ms later. 0.050" T6061 Al coupon, 1/4" Tungsten Electrode, 1/4" Gap between electrode and coupon (0.2" between Coupon and Piston Collector) Tektronix P6015 HV probe **Vcollector (1st)= 60V, Vcollector (2nd)=230V**
8/4/2011	5	CCG (404A) S48kA N134kA	0.2”	Cu Starter wire (0.008" dia.) First return stroke 500ms from start of CCG, second return stroke 100ms later. 0.050" T6061 Al coupon, 1/4" Tungsten Electrode, 1/4" Gap between electrode and coupon (0.2" between Coupon and Piston Collector) Tektronix P6015 HV probe **Vcollector (1st)= 50V , Vcollector (2nd)= 225V**
8/10/2011	2	CCG (391A) S54kA N110kA	0.2”	Cu Starter wire (0.008" dia.) First return stroke 500ms from start of CCG, second return stroke 100ms later. 0.050" T6061 Al coupon, 1/4" Tungsten Electrode, 1/4" Gap between electrode and coupon (0.2" between Coupon and Cable Collector) Tektronix P6015 HV probe **Vcollector (1st)= 100V, Vcollector (2nd)= 650V**

8/10/2011	3	CCG (400A) S47kA N97kA	0.2”	Cu Starter wire (0.008" dia.) First return stroke 500ms from start of CCG, second return stroke 100ms later. 0.050" T6061 Al coupon, 1/4" Tungsten Electrode, 1/4" Gap between electrode and coupon (0.2" between Coupon and Cable Collector) Tektronix P6015 HV probe **Vcollector (1st)= 98V, Vcollector (2nd)= 217V**

Next to capture very extreme charge transfer levels (350 C) the CCG interval to the first return stroke of 50 kA will be extended to 600-700 ms, with 100 ms additional time to the second return stroke of 100 kA. A piston collector with 0.2 inch spacing will be used. **Interval extended to 900ms to achieve 350 coulombs of charge transfer before 1st return stroke.**

Voltage (See Appendix C)

Date	Shot #	SLS Currents	d	Description
8/12/2011	2	CCG (391A) S46kA N136kA	0.2”	Cu Starter wire (0.008" dia.) First return stroke 900ms from start of CCG, second return stroke 100ms later. 0.050" T6061 Al coupon, 1/4" Tungsten Electrode, 1/4" Gap between electrode and coupon (0.2" between Coupon and Piston Collector) Tektronix P6015 HV probe **Vcollector (1st)= 60V, Vcollector (2nd)=230V**
8/24/2011	7	CCG (440A) S47kA N109kA	0.2”	Cu Starter wire (0.008" dia.) First return stroke 900ms from start of CCG, second return stroke 100ms later. 0.050" T6061 Al coupon, 1/4" Tungsten Electrode, 1/4" Gap between electrode and coupon (0.2" between Coupon and Piston Collector) Tektronix P6015 HV probe **Vcollector (1st)= 50V , Vcollector (2nd)= 225V**
8/25/2011	2	CCG (471A) S47kA N107kA	0.2”	Cu Starter wire (0.008" dia.) First return stroke 900ms from start of CCG, second return stroke 100ms later. 0.050" T6061 Al coupon, 1/4" Tungsten Electrode, 1/4" Gap between electrode and coupon (0.2" between Coupon and Piston Collector) Tektronix P6015 HV probe **Vcollector (1st)= 50V , Vcollector (2nd)= 225V**

Finally using the starter wire, the original CCG durations of 400 ms and an additional 100 ms the return strokes will be increased to 100 kA and 200 kA. A piston collector with 0.2 inch spacing will be used. **No Tests Were Conducted**

2. Dynamic source impedance experiment

The plan here is to vary the source impedance in the measurement system from a short circuit (0.005 ohm CVR), to a nominal load (0.5-1 ohm CVR), to an open circuit (Tektronix probe). The purpose is to assess the load effect on the source impedance fall in time. This will use 50 kA return stroke, 500 ms CCG current, and 100 kA return stroke. The collector spacing will be 0.2 inches. **No 0.5-1 ohm Tests Were Conducted**

Voltage (See Appendix D)

Date	Shot #	SLS Currents	d	Description
8/26/2011	2	CCG (445A) S49kA N77kA	0.2”	First return stroke, 500ms CCG, second return stroke. 0.050" T6061 Al coupon, 1/4" Tungsten Electrode, 1/4" Gap between electrode and coupon (0.2" between Coupon and Piston Collector) Tektronix P6015 HV probe **Vcollector (2^{nd})=71V**
8/26/2011	3	CCG (441A) S47kA N102kA	0.2”	First return stroke, 500ms CCG, second return stroke. 0.050" T6061 Al coupon, 1/4" Tungsten Electrode, 1/4" Gap between electrode and coupon (0.2" between Coupon and Piston Collector) Tektronix P6015 HV probe **Vcollector (2^{nd})=90V**
9/13/2011	3	CCG (443A) S47kA N73kA	0.2”	First return stroke, 500ms CCG, second return stroke. **0.060"** T6061 Al coupon, 1/4" Tungsten Electrode, 1/4" Gap between electrode and coupon (0.2" between Coupon and Piston Collector) 5mΩ CVR **Vcollector (2^{nd})=0.5V**
9/13/2011	4	CCG (432A) S49kA N112kA	0.2”	First return stroke, 500ms CCG, second return stroke. 0.050" T6061 Al coupon, 1/4" Tungsten Electrode, 1/4" Gap between electrode and coupon (0.2" between Coupon and Piston Collector) 5mΩ CVR **Vcollector (2^{nd})=1.3V**

A final set of shots will use 0.8 inch spacing and the slotted fixture with interior photography. Both 0.5-1 ohm loads and open and short circuit measurements will be conducted. **No Tests Were Conducted**

3. Cable connection removed from piston

The plan here is to repeat the original two-return stroke plus continuing current experiments with 500 ms duration but remove the connection of the cable to the piston and leave the piston floating. Tektronix high impedance load. It will be good to see how large the open circuit voltage becomes. Two shots with 0.2 inch cable spacing will be done.

Voltage (See Appendix E)

Date	Shot #	SLS Currents	d	Description
8/26/2011	4	CCG (441A) S52kA N93kA	0.2”	First return stroke, 500ms CCG, second return stroke. 0.050" T6061 Al coupon, 1/4" Tungsten Electrode, 1/4" Gap between electrode and coupon (0.2" between Coupon and isolated cable collector) Tektronix P6015 HV probe **Vcollector (2^{nd})= 156V**
8/26/2011	5	CCG (440A) S58kA N93kA	0.2”	First return stroke, 500ms CCG, second return stroke. 0.050" T6061 Al coupon, 1/4" Tungsten Electrode, 1/4" Gap between electrode and coupon (0.2" between Coupon and isolated cable collector) Tektronix P6015 HV probe **Vcollector (2^{nd})= 176V**

4. Bigger hole size The plan here is to repeat the original two-return stroke plus continuing current experiments with a longer fictitious (700 ms?) duration between return strokes to mimic the larger hole size of test 2, and associated with the cable experiments. Tektronix high impedance load. **No Tests Were Conducted**

5. Smaller hole size
The plan here is to repeat the original two-return stroke plus continuing current experiments with a shorter (300 ms) duration between return strokes to achieve a smaller hole size in the cable experiments. Tektronix high impedance load. Repeat 500 ms spacing first to see if we obtain the same voltage levels as observed with the 5 kohm load (400-700 volts). **No Tests Were Conducted**

6. Larger discharge gap
The plan here is to increase the discharge gap to one inch and measure the discharge radial development. One inch cathode spacing will also be used to examine effect of plasma jet. These will involve the usual double return stroke 50 kA and 100 kA levels with 500 ms CCG current in between. The piston collector will be used with 0.2 inch spacing. Both short circuit current and open circuit voltage will be measured.

Voltage (See Appendix F)

Date	Shot #	SLS Currents	d	Description
9/7/2011	5	CCG (396A) S31kA N52kA	0.2”	First return stroke, 500ms CCG, second return stroke. 0.050" T6061 Al coupon, 1/4" Tungsten Electrode, 1" Gap between electrode and coupon (0.2" between Coupon and Piston Collector) Tektronix P6015 HV probe **Vcollector (2^{nd})=73V**
9/12/2011	3	CCG (416A) S46kA N82kA	0.2”	First return stroke, 500ms CCG, second return stroke. 0.050" T6061 Al coupon, 1/4" Tungsten Electrode, 1" Gap between electrode and coupon (0.2" between Coupon and Piston Collector) Tektronix P6015 HV probe **Vcollector (2^{nd})=72V**
9/12/2011	4	CCG (432A) S46kA N81kA	0.2”	First return stroke, 500ms CCG, second return stroke. 0.050" T6061 Al coupon, 1/4" Tungsten Electrode, 1" Gap between electrode and coupon (0.2" between Coupon and Piston Collector) 5mΩ CVR **Vcollector (2^{nd})=3.3V**
9/13/2011	2	CCG (412A) S40kA N94kA	0.2”	First return stroke, 500ms CCG, second return stroke. 0.050" T6061 Al coupon, 1/4" Tungsten Electrode, 1" Gap between electrode and coupon (0.2" between Coupon and Piston Collector) 5mΩ CVR **Vcollector (2^{nd})=2.4V**

7. Differential mode cable experiment The plan here is to examine differential mode voltage in bi and tri-foil striplines. Open circuit voltage measurements will be made with 0.2 inch spacing to the cable. Double return stroke 50 kA and 100 kA levels with 500 ms CCG current will be used. **No Tests Were Conducted**

8. Insulation investigation

The plan here is to measure the coupled voltage when a layer of Kapton insulation is added to the top of the piston collector. The spacing of 0.2 inches will be used (0.8 inch spacing would only be considered if unusually high levels are recorded with this spacing on number 2 above). Kapton insulation will be added to the top of the piston leaving a 0.5 inch hole at the burnthrough location. Double return stroke 50 kA and 100 kA levels with 500 ms CCG current will be used. **No Tests Were Conducted**

9. Predrilled hole experiments (PTX or SLS?) performed at SLS

The plan here is to repeat the predrilled hole experiments using the SLS with early time recording. In addition some shots with maximum hole dimensions (0.7 in) will be conducted with either the PTX pulser and/or the SLS. Another goal of this experiment is to see if attached electrons surrounding the continuing current plasma play a role in the uniform ioinization taking place when the return stroke voltage wave hits. With the predrilled hole these should not be present. Finally, it would be useful to vary the load impedance of the measurement system on the collector. High impedance voltage measurements (megaohms), low impedance current measurements (<<1 ohm), and one ohm loads would be of interest to track the development of the discharge channel. Variations in the cathode distance to the coupon will be necessary (0.25 in, 0 in, 1 in) are good candidates. **Only 100MΩ loads were used in these tests.**

0.5" Pre-drilled Voltage (See Appendix G)

Date	Shot #	SLS Current (kA)	d	Description
5/25/2011	2	50	0.2"	0.050" T6061 Al coupon w/ 0.5" Hole, 1/4" Tungsten Electrode, 1" Gap (Open Circuit) between electrode and coupon (0.2" between Coupon and brass collector) Tektronix P6015 HV probe **Vcollector=30V**
5/25/2011	3	56	0.2"	0.050" T6061 Al coupon w/ 0.5" Hole, 1/4" Tungsten Electrode, 1" Gap (Open Circuit) between electrode and coupon (0.2" between Coupon and brass collector) Tektronix P6015 HV probe **Vcollector=40V**
5/25/2011	4	57	0.2"	0.050" T6061 Al coupon w/ 0.5" Hole, 1/4" Tungsten Electrode, 1/4" Gap (Open Circuit) between electrode and coupon (0.2" between Coupon and brass collector) Tektronix P6015 HV probe **Vcollector=55V**
5/25/2011	5	56	0.2"	0.050" T6061 Al coupon w/ 0.5" Hole, 1/4" Tungsten Electrode, 1/4" Gap (Open Circuit) between electrode and coupon (0.2" between Coupon and brass collector) Tektronix P6015 HV probe **Vcollector=60V**
5/25/2011	7	54	0.2"	0.050" T6061 Al coupon w/ 0.5" Hole, 1/4" Tungsten Electrode, 0" Gap (Open Circuit) between electrode and coupon (0.2" between Coupon and brass collector) Tektronix P6015 HV probe **Vcollector=1,075V**
5/25/2011	8	51	0.2"	0.050" T6061 Al coupon w/ 0.5" Hole, 1/4" Tungsten Electrode, 0" Gap (Open Circuit) between electrode and coupon (0.2" between Coupon and brass collector) Tektronix P6015 HV probe **Vcollector=635V**

5/25/2011	10	50	0.2”	0.050" T6061 Al coupon w/ 0.5" Hole, 1/4" Tungsten Electrode, 0.125" Gap (Open Circuit) between electrode and brass collector (0.2" between Coupon and brass collector) Tektronix P6015 HV probe **Vcollector=4,125V**
5/25/2011	11	56	0.2”	0.050" T6061 Al coupon w/ 0.5" Hole, 1/4" Tungsten Electrode, 0.125" Gap (Open Circuit) between electrode and brass collector (0.2" between Coupon and brass collector) Tektronix P6015 HV probe **Vcollector=2,900V**
5/25/2011	12	58	0.2”	0.050" T6061 Al coupon w/ 0.5" Hole, 1/4" Tungsten Electrode, 0.125" Gap (Open Circuit) between electrode and brass collector (0.2" between Coupon and brass collector) Tektronix P6015 HV probe **Vcollector=5,600V**
5/25/2011	13	54	0.2”	0.050" T6061 Al coupon w/ 0.5" Hole, 1/4" Tungsten Electrode, 0.0625" Gap (Open Circuit) between electrode and brass collector (0.2" between Coupon and brass collector) Tektronix P6015 HV probe **Vcollector=11,270V**
5/25/2011	14	56	0.2”	0.050" T6061 Al coupon w/ 0.5" Hole, 1/4" Tungsten Electrode, 0.0625" Gap (Open Circuit) between electrode and brass collector (0.2" between Coupon and brass collector) Tektronix P6015 HV probe **Vcollector=10,835V**

0.7” Pre-drilled Voltage (See Appendix H)

Date	Shot #	SLS Current (kA)	d	Description
6/1/2011	2	48	0.2”	0.050" T6061 Al coupon w/ 0.7" Hole, 1/4" Tungsten Electrode, 1" Gap (Open Circuit) between electrode and coupon (0.2" between Coupon and brass collector) Tektronix P6015 HV probe **Vcollector=33V**
6/1/2011	3	44	0.2”	0.050" T6061 Al coupon w/ 0.7" Hole, 1/4" Tungsten Electrode, 1" Gap (Open Circuit) between electrode and coupon (0.2" between Coupon and brass collector) Tektronix P6015 HV probe **Vcollector=41V**
6/1/2011	4	52	0.2”	0.050" T6061 Al coupon w/ 0.7" Hole, 1/4" Tungsten Electrode, 1/4" Gap (Open Circuit) between electrode and coupon (0.2" between Coupon and brass collector) Tektronix P6015 HV probe **Vcollector=555V**
6/1/2011	5	48	0.2”	0.050" T6061 Al coupon w/ 0.7" Hole, 1/4" Tungsten Electrode, 1/4" Gap (Open Circuit) between electrode and coupon (0.2" between Coupon and brass collector) Tektronix P6015 HV probe **Vcollector=912V**
6/2/2011	2	53	0.2”	0.050" T6061 Al coupon w/ 0.7" Hole, 1/4" Tungsten Electrode, 0" Gap (Open Circuit) between electrode and coupon (0.2" between Coupon and brass collector) Tektronix P6015 HV probe **Vcollector=18,362V**

6/2/2011	3	49	0.2”	0.050" T6061 Al coupon w/ 0.7" Hole, 1/4" Tungsten Electrode, 0" Gap (Open Circuit) between electrode and coupon (0.2" between Coupon and brass collector) Tektronix P6015 HV probe **Vcollector=17,118V**
6/2/2011	4	59	0.2”	0.050" T6061 Al coupon w/ 0.7" Hole, 1/4" Tungsten Electrode, 0.125" Gap (Open Circuit) between electrode and brass collector (0.2" between Coupon and brass collector) Tektronix P6015 HV probe **Vcollector=12,666V**
6/2/2011	5	48	0.2”	0.050" T6061 Al coupon w/ 0.7" Hole, 1/4" Tungsten Electrode, 0.125" Gap (Open Circuit) between electrode and brass collector (0.2" between Coupon and brass collector) Tektronix P6015 HV probe **Vcollector=10,230V**
6/2/2011	6	52	0.2”	0.050" T6061 Al coupon w/ 0.7" Hole, 1/4" Tungsten Electrode, 0.0625" Gap (Open Circuit) between electrode and brass collector (0.2" between Coupon and brass collector) Tektronix P6015 HV probe **Vcollector=20,000V**
6/2/2011	7	48	0.2”	0.050" T6061 Al coupon w/ 0.7" Hole, 1/4" Tungsten Electrode, 0.0625" Gap (Open Circuit) between electrode and brass collector (0.2" between Coupon and brass collector) Tektronix P6015 HV probe **Vcollector=7,203V**

10. Cable sticking out of hole The plan here is to epoxy the cable to the rubber insulator to prevent distortion during the experiment? **No Tests Were Conducted**

11. Outer radius current probe experiment

The idea here is to construct another current probe with a thick interior region and grooves only at the outer radii. The goal is to have the CCG current terminate on the inner thicker region (without measurement) and to see if the transition into the return stoke rapidly expands the current column to the out grooves. **Tests were conducted to evaluate burnthrough of 0.040” copper and stainless steel coupons at variety of currents and durations. These tests were conducted with starter wires and commercial fuses to limit current durations. Thicker coupons were not evaluated to determine minimum thickness required to burnthrough of proposed current probe.**

Outer radius current probe evaluation (See Appendix I)

Date	Shot #	CCG Current (A)	Description
2/25/2011	2	283A (90ms)	Water cooled copper coupon test. 0.040" thick x 5" dia copper disc. 1/4" tungsten electrode with 1/4" gap between electrode tip and copper coupon. 1/16" wide copper tape starter wire. Littelfuse Class K5 NLS-20 fuse. Post shot inspection revealed that the fuse had blown, Fuse Time=90ms **Small pin hole in copper plate (water shooting out)**

2/28/2011	2	175A (160ms)	Water cooled copper coupon test. 0.040" thick x 5" dia. copper disc. 1/4" tungsten electrode with 1/4" gap between electrode tip and copper coupon. 1/16" wide copper tape starter wire. Bussman NOS-15 fuse. Post shot inspection revealed that the fuse had blown, Fuse Time= 160 ms. **No hole in copper plate**
2/28/2011	3	161A (215ms)	Water cooled coupon test. 0.040" thick x 5"x5" Stainless Steel plate. 1/4" tungsten electrode with 1/4" gap between electrode tip and SS coupon. 1/16" wide copper tape starter wire. Bussman NOS-15 fuse. Post shot inspection revealed that the fuse had blown, Fuse Time=215ms **Small pin hole in SS plate (water shooting out)**
3/23/2011	3	126A (400ms)	Non cooled coupon test. No cooling fixture used.0.040" thick x 5" dia. copper disc. 1/4" tungsten electrode with 1/4" gap between electrode tip and Cu coupon. 1/16" wide copper tape starter wire (Cu tape adhesive side on Tungsten, Cu tape at coupon-copper side to coupon taped on with Kapton tape. Bussman NOS-15 fuse. Post shot inspection revealed that the fuse had blown, Fuse Time=400ms. A small (0.100" diameter) copper bubble formed on the back side of the copper coupon. **No visible puncture**
3/23/2011	5	216A (28ms)	Non cooled coupon test. No cooling fixture used.0.040" thick x 5" dia. copper disc. 1/4" tungsten electrode with 1/4" gap between electrode tip and Cu coupon. 1/16" wide copper tape starter wire. (Cu tape adhesive side on Tungsten, Cu tape at coupon-copper side to coupon taped on with Kapton tape. Littelfuse Class K5 NLS-15. Post shot inspection revealed that the fuse had blown, Fuse Time=28ms **No visible puncture**

12. Outer radius voltage probe experiment

The idea here is to do the same thing as in the previous setup but instead of measuring the current distribution by means of the groove CVRs we intend to have a series of holes in the barrier with small plates behind each for which a high impedance measurement will be made to record the early time voltage. **No Tests Were Conducted**

References:

[1] G. H. Schnetzer, R. J. Fisher, and M. A. Dinallo, "Measured Responses of Internal Enclosures and Cables Due To Burnthrough Penetration of Weapon Cases by Lightning," SAND94-0312, August 1994.

[2] R. J. Fisher and M. A. Uman, "Recommended Baseline Direct-Strike Lightning Environment for Stockpile-to-Target Sequences," SAND 89-0192, May 1989.

[3] L. K. Warne, L. E. Martinez, R. E. Jorgenson, and K. O. Merewether, "Experimental Plan (First Round)," Internal Sandia Memorandum, March 27, 2009.

[4] L. K. Warne, L. E. Martinez, R. E. Jorgenson, and K. O. Merewether, "Experimental Plan (Interim Low Level)," Internal Sandia Memorandum, June, 2009.

[5] L. K. Warne, L. E. Martinez, R. E. Jorgenson, and K. O. Merewether, "Experimental Plan (Second Round)," Internal Sandia Memorandum, September 8, 2009.

[6] L. K. Warne, L. E. Martinez, R. E. Jorgenson, and K. O. Merewether, "Experimental Plan (Third Round)," Internal Sandia Memorandum, March 15, 2010.

[7] L. K. Warne, L. E. Martinez, R. E. Jorgenson, and K. O. Merewether, "Experimental Plan (Fourth Round)," Internal Sandia Memorandum, August 15, 2010.

Additional Comments In Round Five Planning:
This fifth round of experiments has two primary goals. The first and most important goal is to carry out experiments directed at understanding why the round four cable coupling experiment resulted in much larger interior voltages than previously observed. In particular, several differences between the previous "piston" collector and the cable collector that may be relevant to this issue have been identified. The next two figures show the piston topology and the cable topology. So far five issues have been identified.

1. Bigger hole size. We know that the hole existing at the end of the burnthrough experiment was larger in the cable setup versus the piston setup (50% bigger?). At the time of the second return stroke (500 ms after continuing current initiation) we may be able to identify from the movies how much bigger. Is the short duration voltage spike in the cable setup a consequence of direct or indirect coupling? Can a calculation supply evidence for one or the other? Should we try more predrilled hole tests in the SLS with bigger holes based on the movie results for the cable? Is forced erosion the reason for the hole size difference (or is there some other reason)?

2. Insulation and suppression of clamping. We have observed in previous burnthrough experiments with the piston collector a return discharge between the collector and the chassis (coupon). Is this plasma connection responsible for clamping the voltage between the collector and chassis to low levels (50 V)? Would an insulation layer (Kapton) between the piston and the coupon mimic the effect of the cable insulation and give evidence for this being a contributor to the large voltages in the cable experiments?

3. Smaller capacitance. We know that the piston collector to chassis capacitance (85 pF) is considerably larger than the cable to chassis capacitance (15 pF). Could the change in time constant resulting from this difference have filtered out the early time voltage spike?

4. Cable sticking out of hole. We know that the cable burns through at the attachment point. Is there any force present that could cause the cable end to protrude through the hole at the time of the second return stroke? The resulting increase in antenna effective height could be a large contributor to the coupling.

5. Smaller inductance. We know that the routing of the cable with respect to the can wall reduces the inductance somewhat in the cable experiment versus the piston experiment. Could the increased inductance in the piston have lead to a filtering effect?

0. Noise Shots and incident electric field measurement

Noise shots for Tektronix P6015A HV probe and incident electric field measurement

Description: 0.050" T6061 Al coupon w/ 0.5" Hole, 1/4" Tungsten Electrode, 1" Gap (Open Circuit) between electrode and coupon (0.45" between Coupon and brass collector), Calibration of SNL 4.3mm Monopole (scale factor = 2 x AD10 scale factor) with Prodyn AD-10 E-field probe.

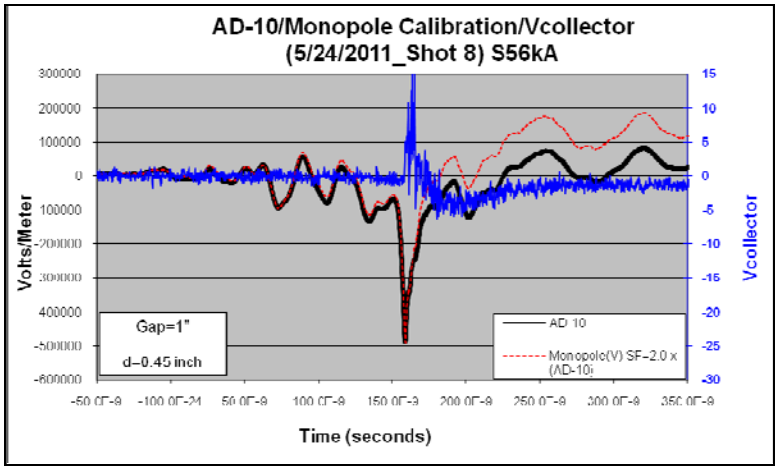

1. Double return stroke with starter wire-Piston collector

The plan here is to repeat the original two-return stroke plus continuing current experiments but initiate the discharge with a starter wire.

Description: Cu Starter wire (0.008" dia.) First return stroke 500ms from start of CCG, second return stroke 100ms later. 0.050" T6061 Al coupon, 1/4" Tungsten Electrode, 1/4" Gap between electrode and coupon (0.2" between Coupon and Piston Collector) Tektronix P6015 HV probe

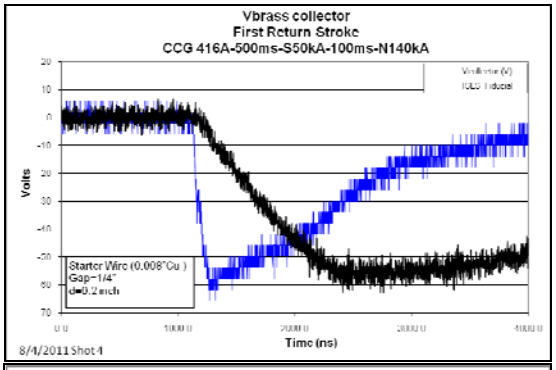

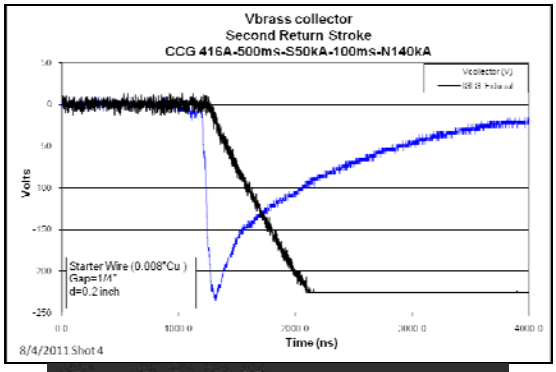

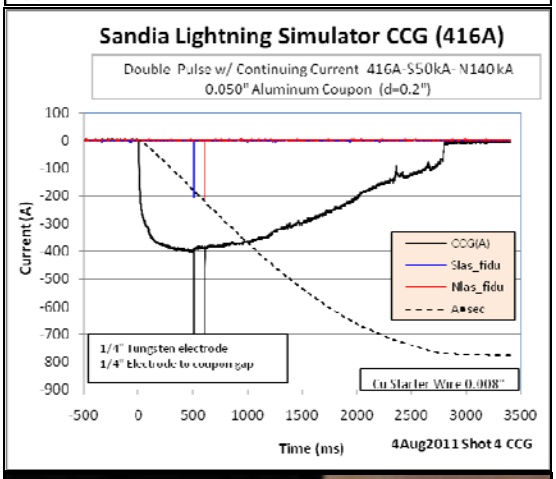

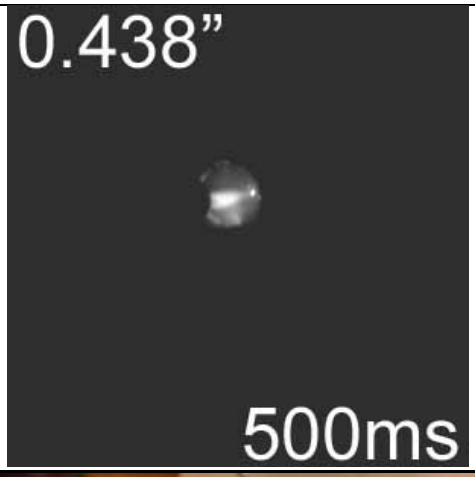

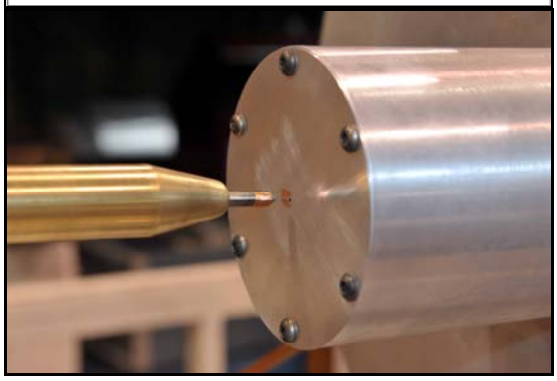

1. Double return stroke with starter wire-Piston collector

The plan here is to repeat the original two-return stroke plus continuing current experiments but initiate the discharge with a starter wire.

Description: Cu Starter wire (0.008" dia.) First return stroke 500ms from start of CCG, second return stroke 100ms later. 0.050" T6061 Al coupon, 1/4" Tungsten Electrode, 1/4" Gap between electrode and coupon (0.2" between Coupon and Piston Collector) Tektronix P6015 HV probe

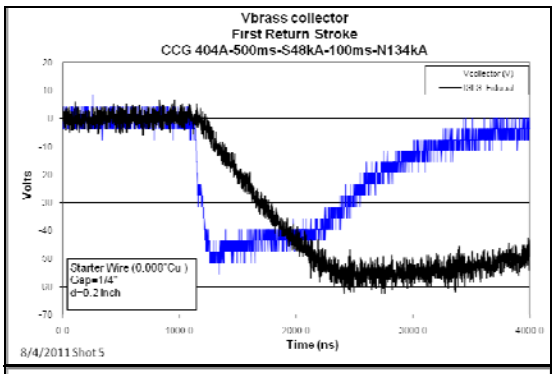

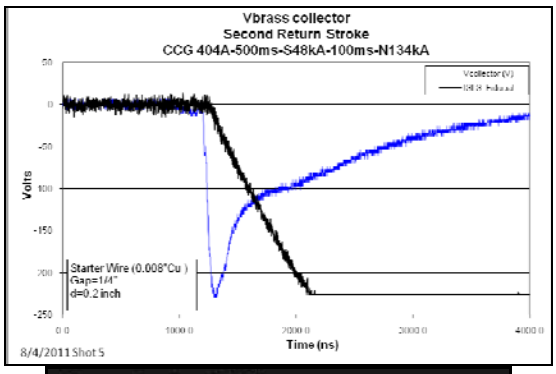

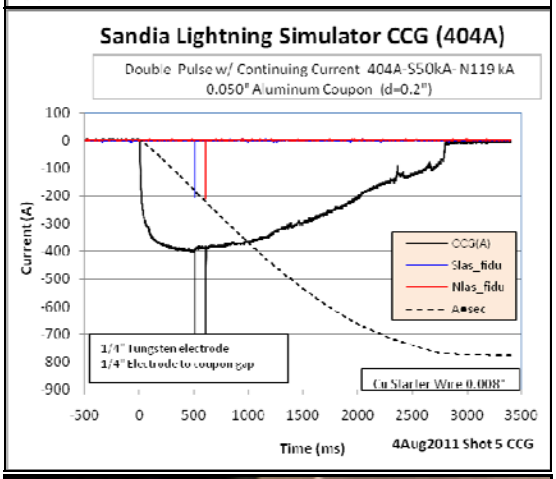

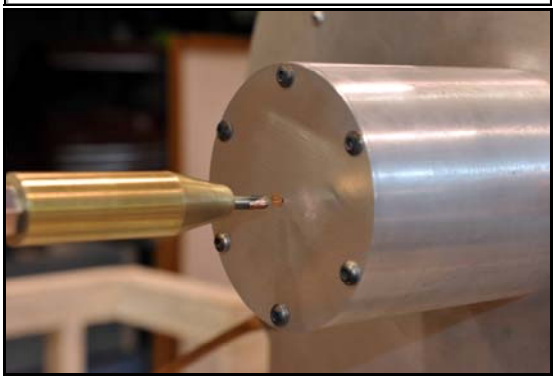

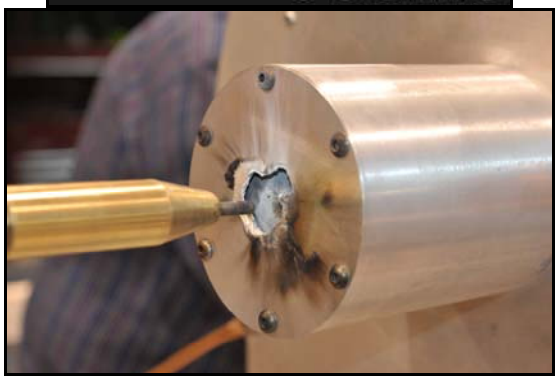

1. Double return stroke with starter wire-Cable collector

The plan here is to repeat the original two-return stroke plus continuing current experiments but initiate the discharge with a starter wire.

Description: Cu Starter wire (0.008" dia.) First return stroke 500ms from start of CCG, second return stroke 100ms later. 0.050" T6061 Al coupon, 1/4" Tungsten Electrode, 1/4" Gap between electrode and coupon (0.2" between Coupon and Cable Collector) Tektronix P6015 HV probe

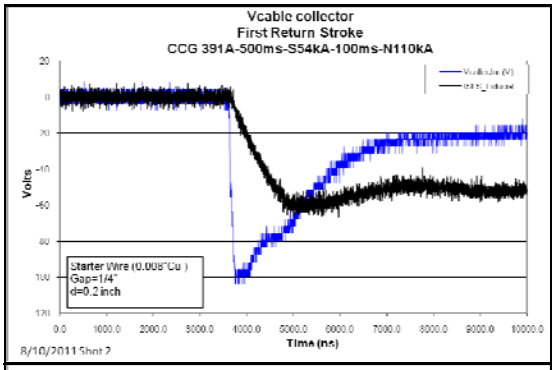

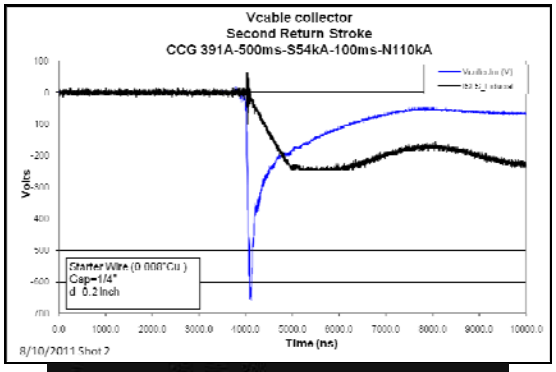

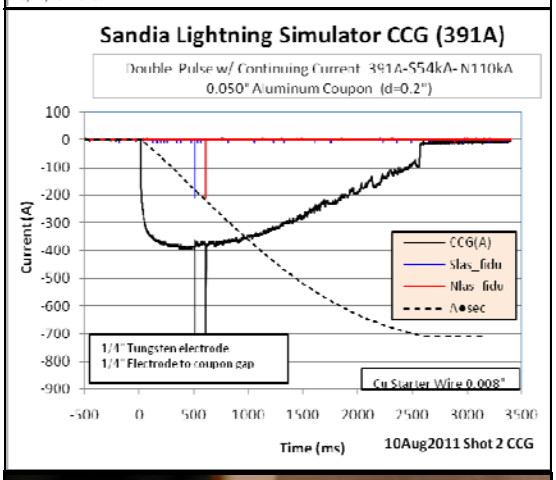

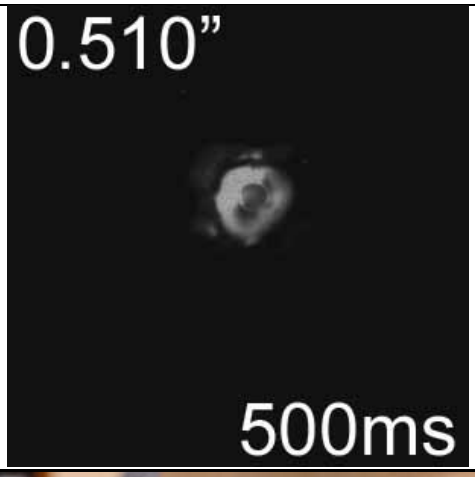

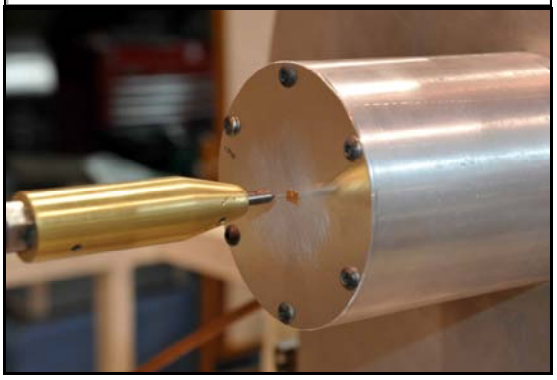

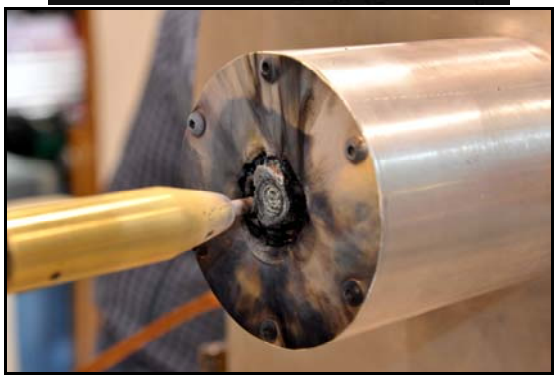

1. Double return stroke with starter wire-Cable collector

The plan here is to repeat the original two-return stroke plus continuing current experiments but initiate the discharge with a starter wire.

Description: Cu Starter wire (0.008" dia.) First return stroke 500ms from start of CCG, second return stroke 100ms later. 0.050" T6061 Al coupon, 1/4" Tungsten Electrode, 1/4" Gap between electrode and coupon (0.2" between Coupon and Cable Collector) Tektronix P6015 HV probe

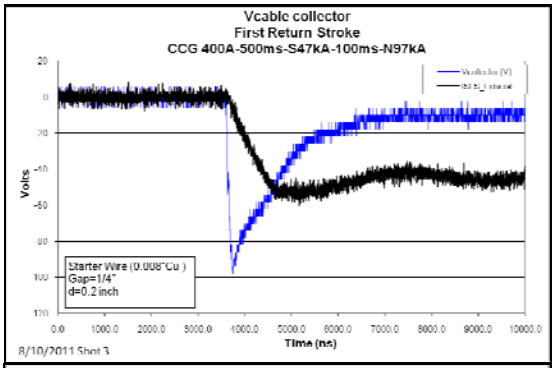

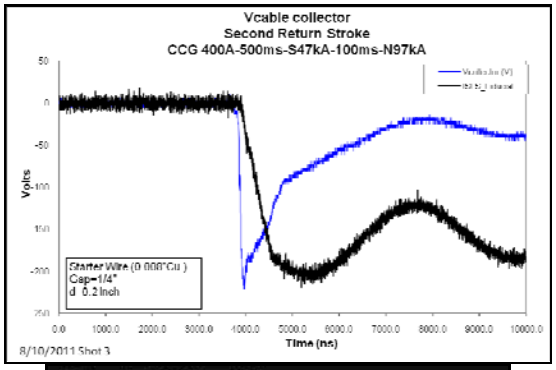

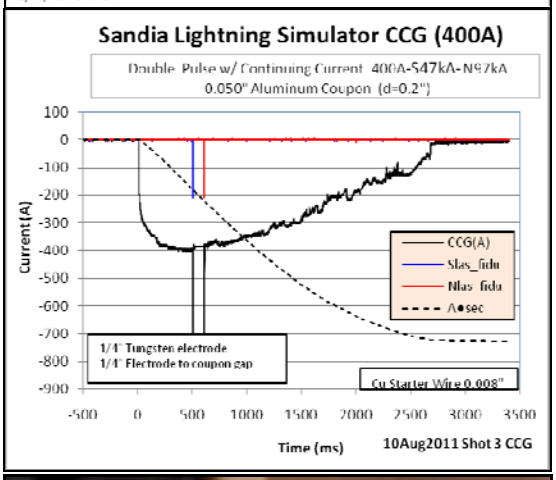

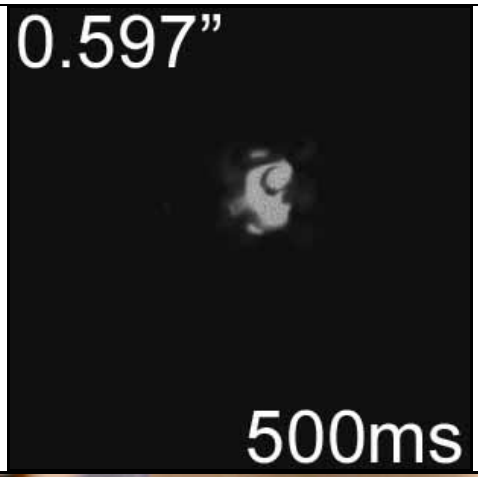

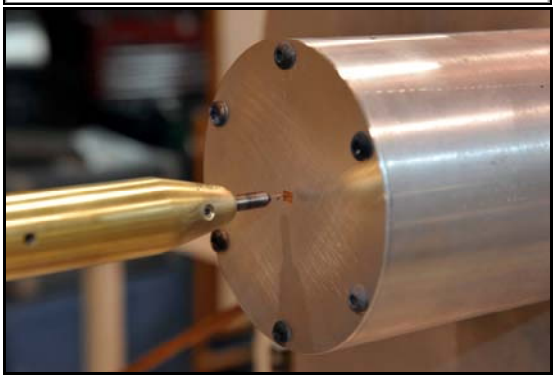

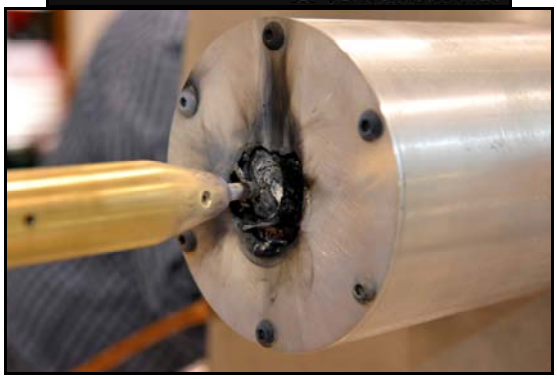

1. Double return stroke with starter wire-Piston collector

The plan here is to repeat the original two-return stroke plus continuing current experiments but initiate the discharge with a starter wire.

Description: Cu Starter wire (0.008" dia.) First return stroke 900ms from start of CCG, second return stroke 100ms later. 0.050" T6061 Al coupon, 1/4" Tungsten Electrode, 1/4" Gap between electrode and coupon (0.2" between Coupon and Piston Collector) Tektronix P6015 HV probe

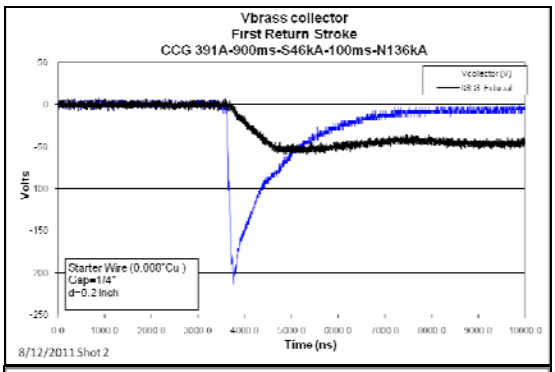

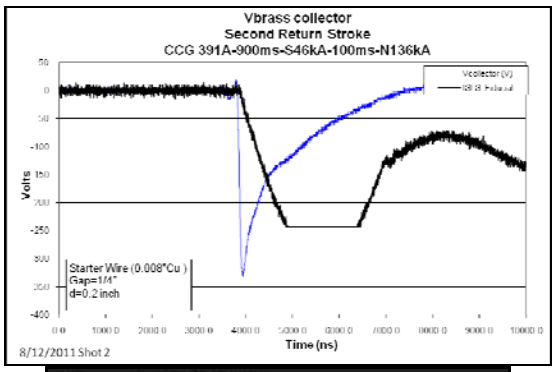

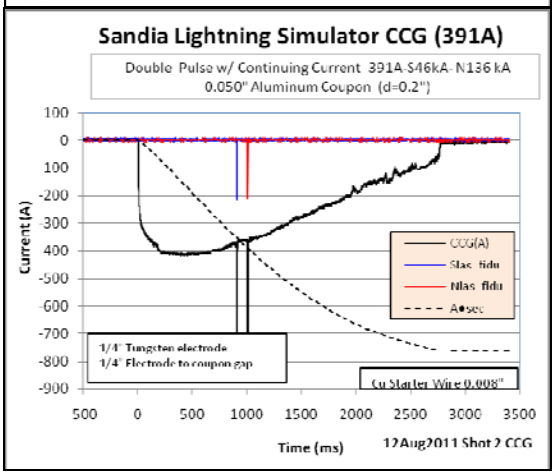

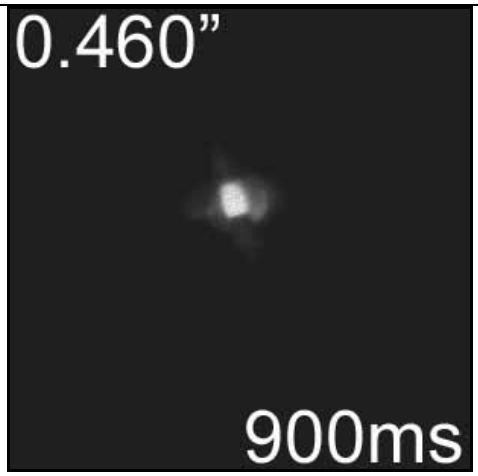

1. Double return stroke with starter wire-Piston collector

The plan here is to repeat the original two-return stroke plus continuing current experiments but initiate the discharge with a starter wire.

Description: Cu Starter wire (0.008" dia.) First return stroke 900ms from start of CCG, second return stroke 100ms later. 0.050" T6061 Al coupon, 1/4" Tungsten Electrode, 1/4" Gap between electrode and coupon (0.2" between Coupon and Piston Collector) Tektronix P6015 HV probe

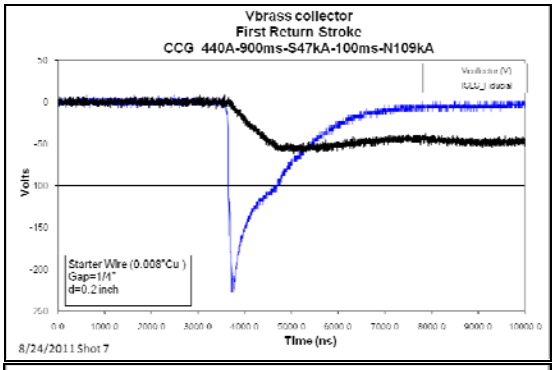

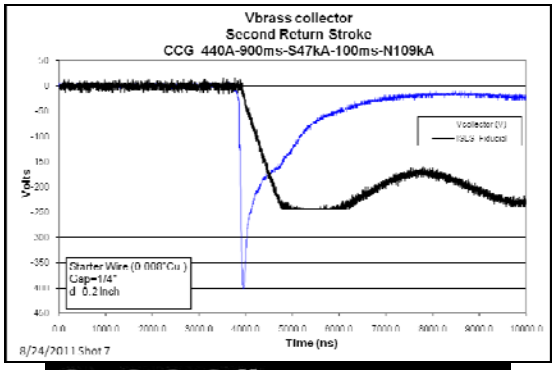

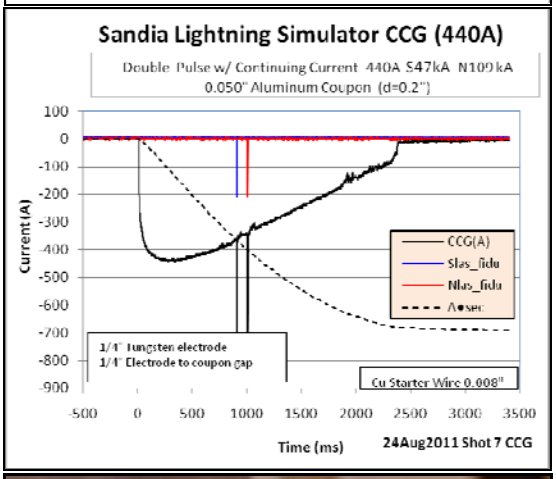

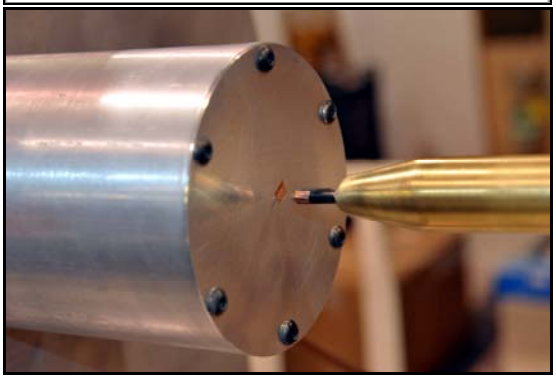

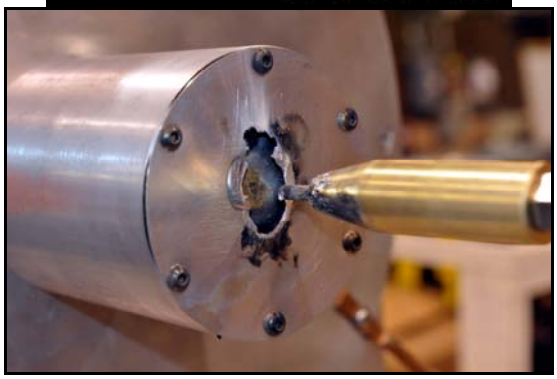

1. Double return stroke with starter wire-Piston collector

The plan here is to repeat the original two-return stroke plus continuing current experiments but initiate the discharge with a starter wire.

Description: Cu Starter wire (0.008" dia.) First return stroke 900ms from start of CCG, second return stroke 100ms later. 0.050" T6061 Al coupon, 1/4" Tungsten Electrode, 1/4" Gap between electrode and coupon (0.2" between Coupon and Piston Collector) Tektronix P6015 HV probe

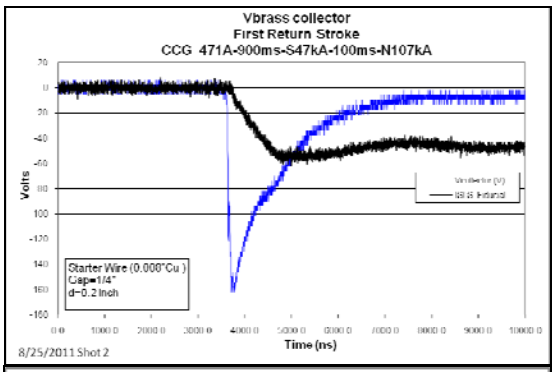

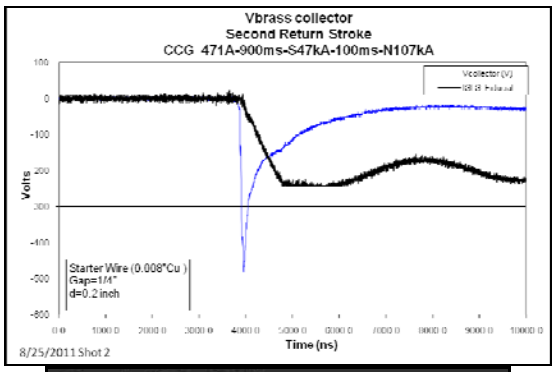

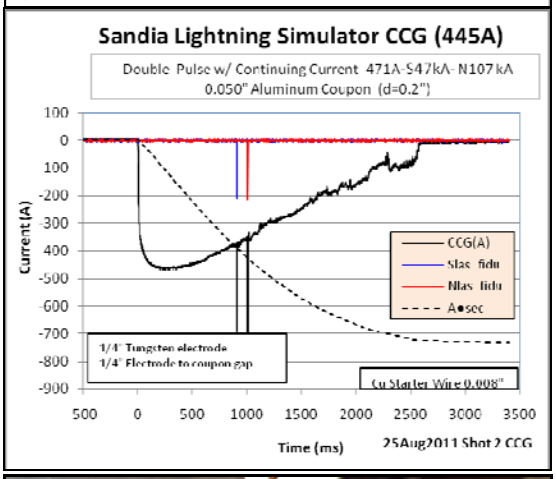

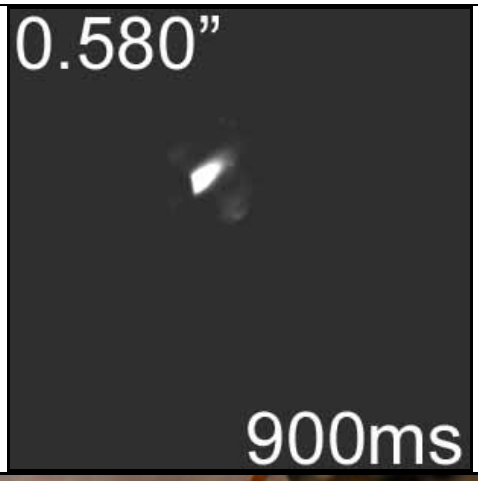

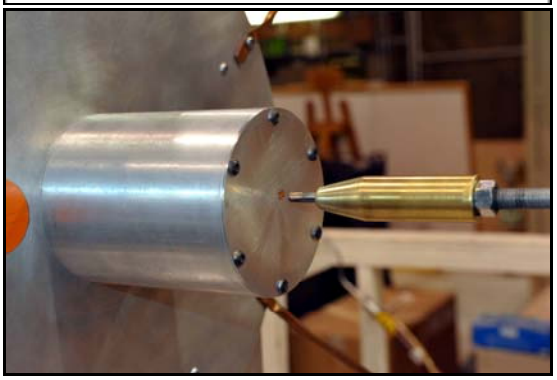

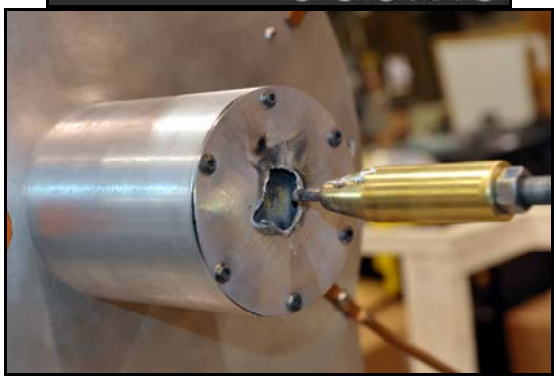

2. Dynamic source impedance experiment-Tektronix 100MΩ probe
The plan here is to vary the source impedance in the measurement system from a short circuit (0.005 ohm CVR), to a nominal load (0.5-1 ohm CVR), to an open circuit (Tektronix probe).

Description: First return stroke, 500ms CCG, second return stroke. 0.050" T6061 Al coupon, 1/4" Tungsten Electrode, 1/4" Gap between electrode and coupon (0.2" between Coupon and Piston Collector) Tektronix P6015 HV probe

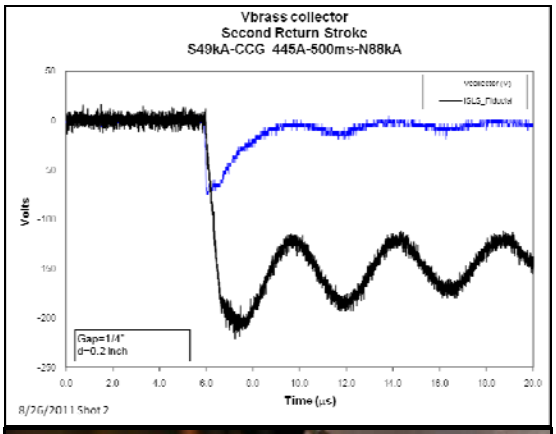

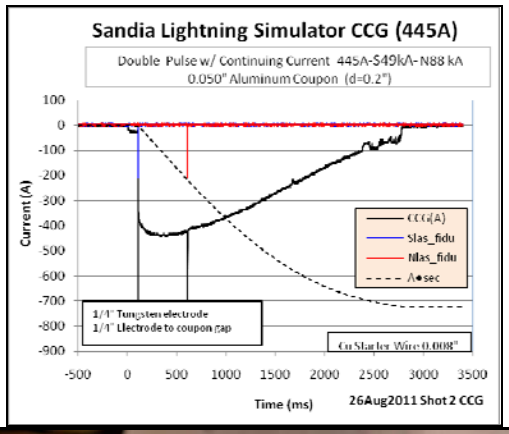

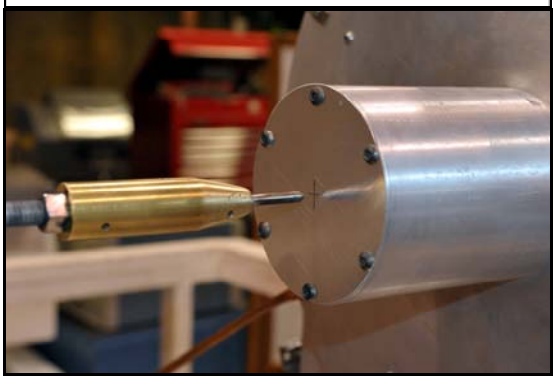

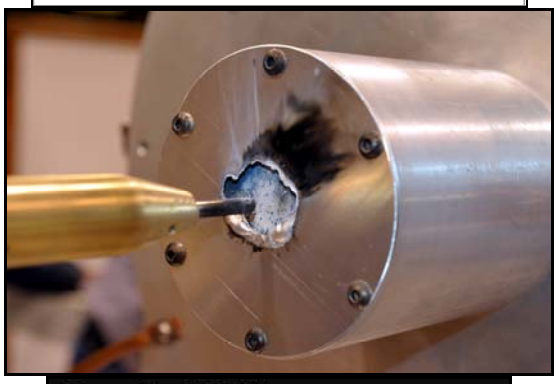

2. Dynamic source impedance experiment-Tektronix 100MΩ probe

The plan here is to vary the source impedance in the measurement system from a short circuit (0.005 ohm CVR), to a nominal load (0.5-1 ohm CVR), to an open circuit (Tektronix probe).

Description: First return stroke, 500ms CCG, second return stroke. 0.050" T6061 Al coupon, 1/4" Tungsten Electrode, 1/4" Gap between electrode and coupon (0.2" between Coupon and Piston Collector) Tektronix P6015 HV probe

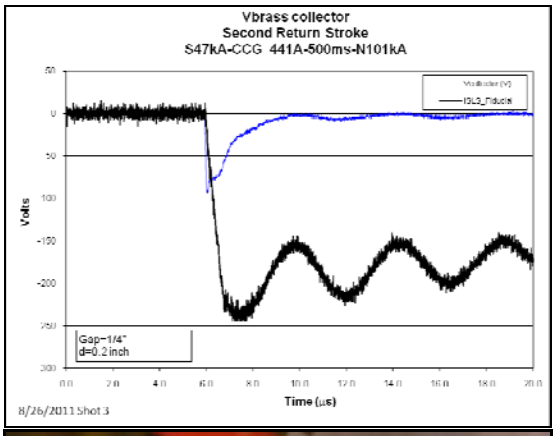

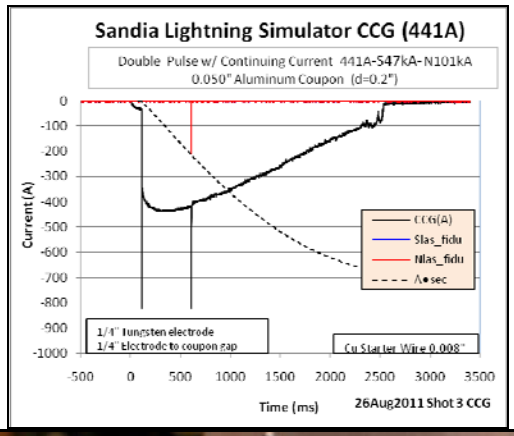

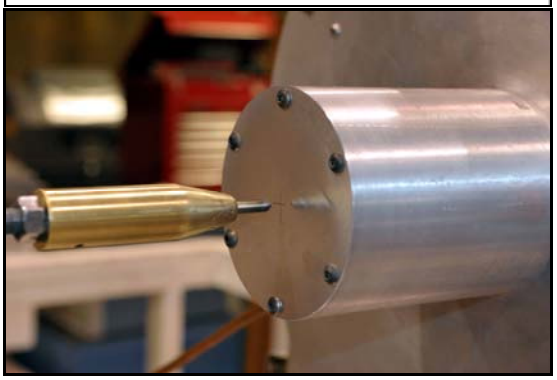

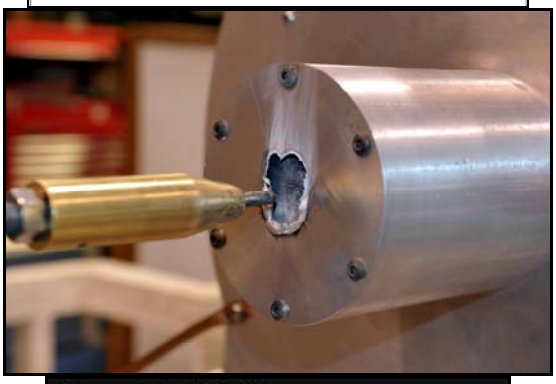

2. Dynamic source impedance experiment-5mΩ CVR

The plan here is to vary the source impedance in the measurement system from a short circuit (0.005 ohm CVR), to a nominal load (0.5-1 ohm CVR), to an open circuit (Tektronix probe).

Description: First return stroke, 500ms CCG, second return stroke. **0.060"** T6061 Al coupon, 1/4" Tungsten Electrode, 1/4" Gap between electrode and coupon (0.2" between Coupon and Piston Collector) 5mΩ CVR

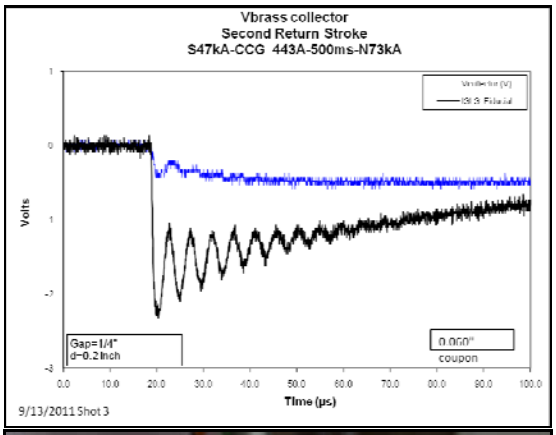

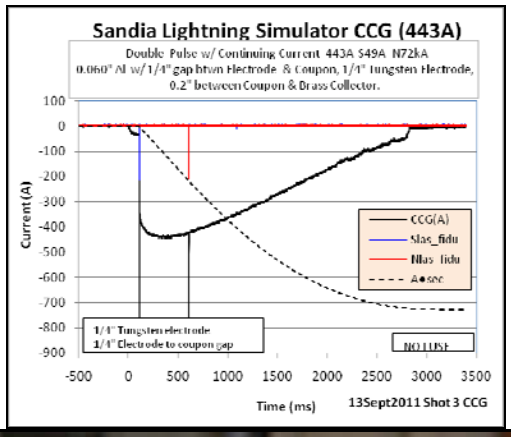

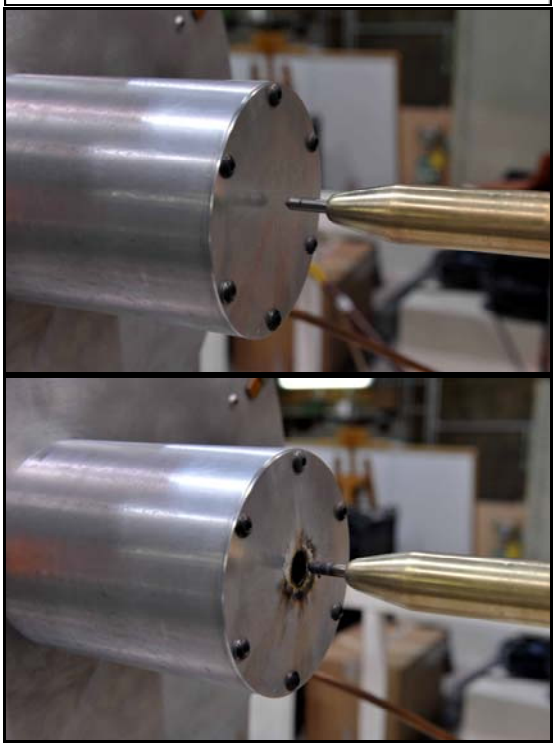

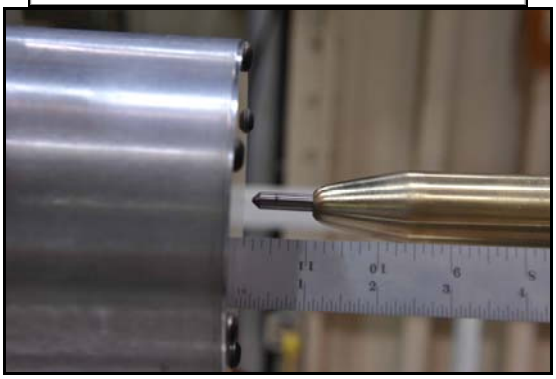

2. Dynamic source impedance experiment-5mΩ CVR

The plan here is to vary the source impedance in the measurement system from a short circuit (0.005 ohm CVR), to a nominal load (0.5-1 ohm CVR), to an open circuit (Tektronix probe).

Description: First return stroke, 500ms CCG, second return stroke. 0.050" T6061 Al coupon, 1/4" Tungsten Electrode, 1/4" Gap between electrode and coupon (0.2" between Coupon and Piston Collector) 5mΩ CVR

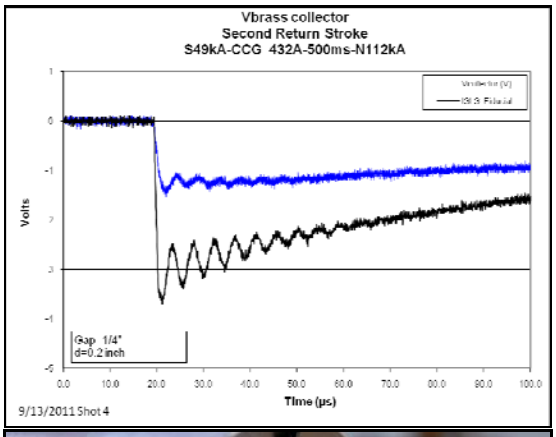

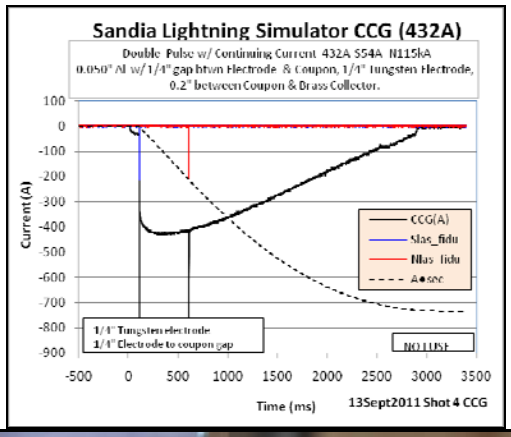

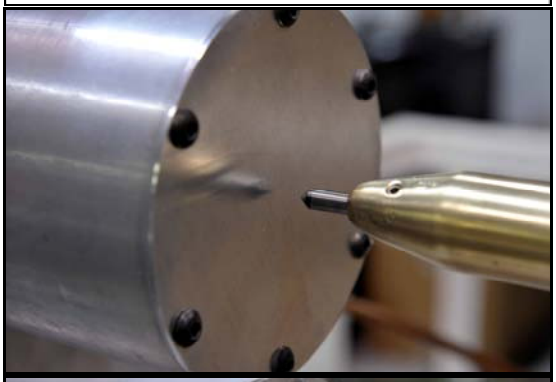

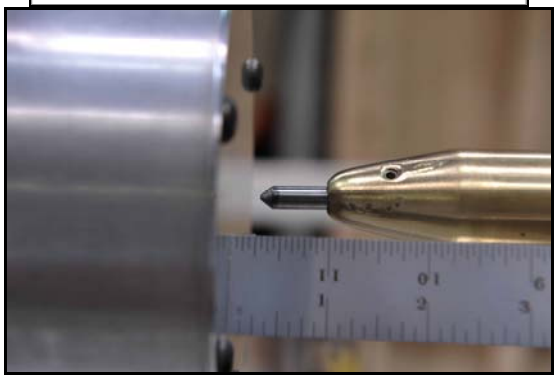

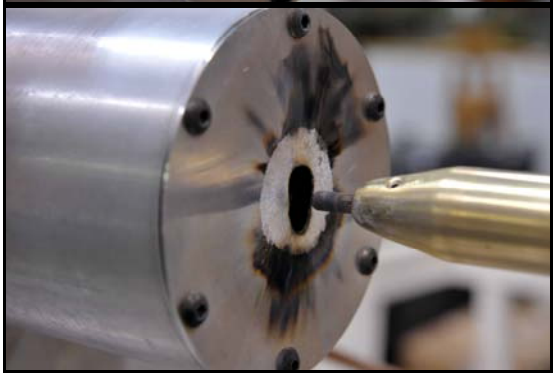

3. Cable connection removed from piston

The plan here is to repeat the original two-return stroke plus continuing current experiments with 500 ms duration but remove the connection of the cable to the piston and leave the piston floating.

Description: First return stroke, 500ms CCG, second return stroke. 0.050" T6061 Al coupon, 1/4" Tungsten Electrode, 1/4" Gap between electrode and coupon (0.2" between Coupon and isolated cable collector) Tektronix P6015 HV probe

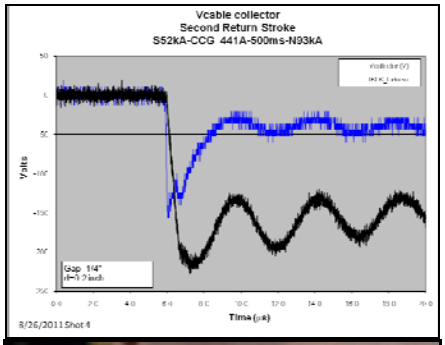

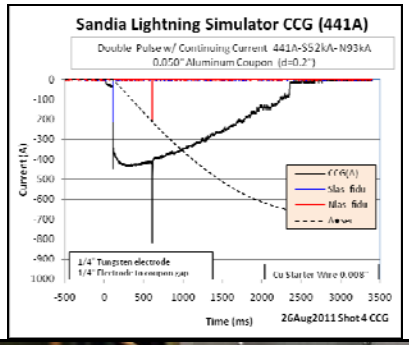

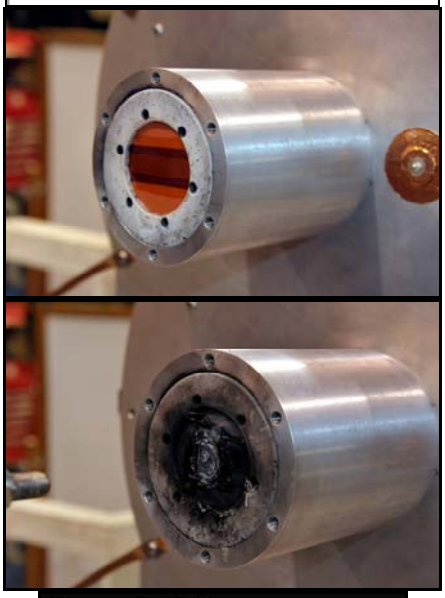

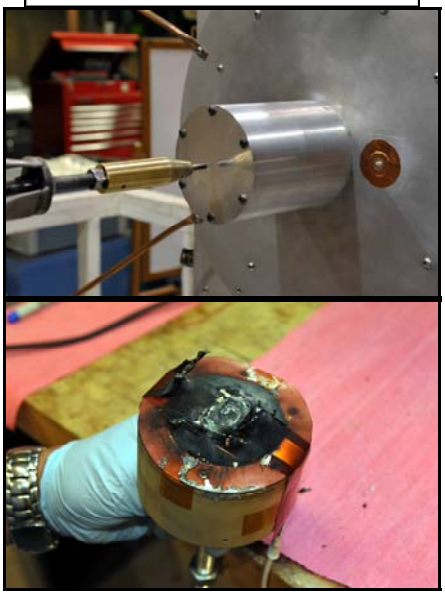

3. Cable connection removed from piston

The plan here is to repeat the original two-return stroke plus continuing current experiments with 500 ms duration but remove the connection of the cable to the piston and leave the piston floating.

Description: First return stroke, 500ms CCG, second return stroke. 0.050" T6061 Al coupon, 1/4" Tungsten Electrode, 1/4" Gap between electrode and coupon (0.2" between Coupon and isolated cable collector) Tektronix P6015 HV probe

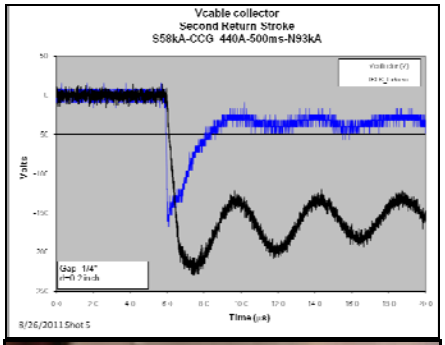

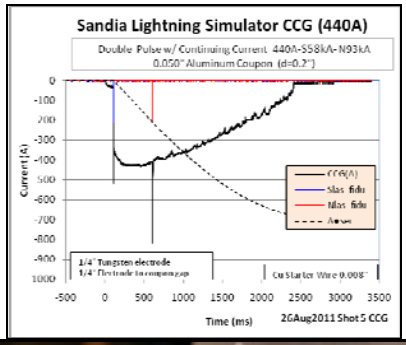

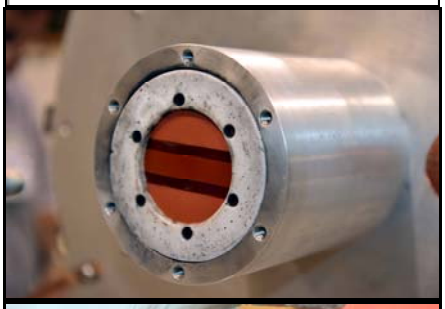

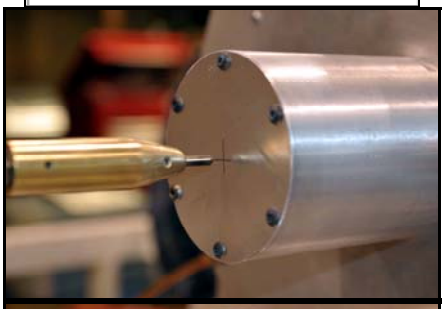

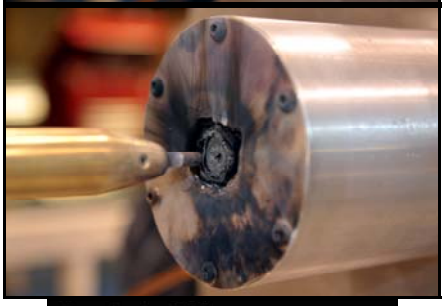

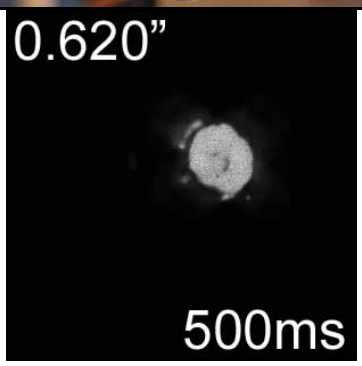

6. Larger discharge gap

The plan here is to increase the discharge gap to one inch and measure the discharge radial development.

Description: First return stroke, 500ms CCG, second return stroke. 0.050" T6061 Al coupon, 1/4" Tungsten Electrode, 1" Gap between electrode and coupon (0.2" between Coupon and Piston Collector) Tektronix P6015 HV probe

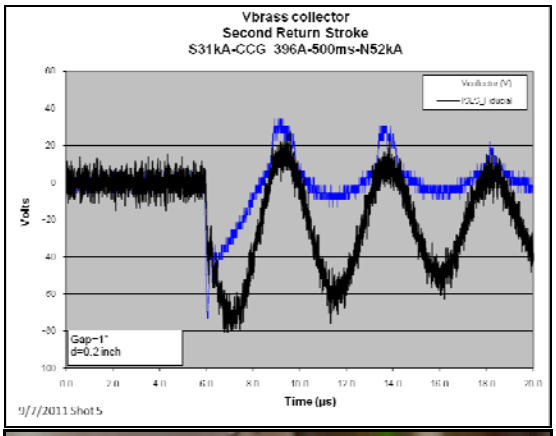

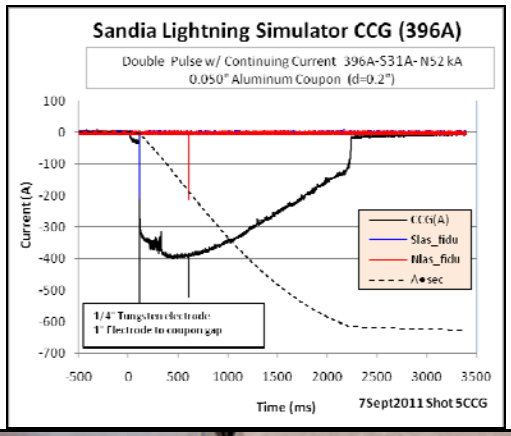

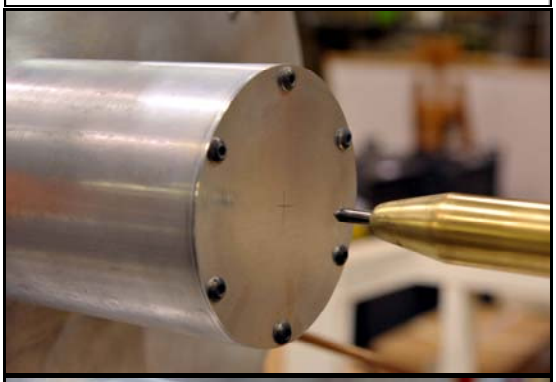

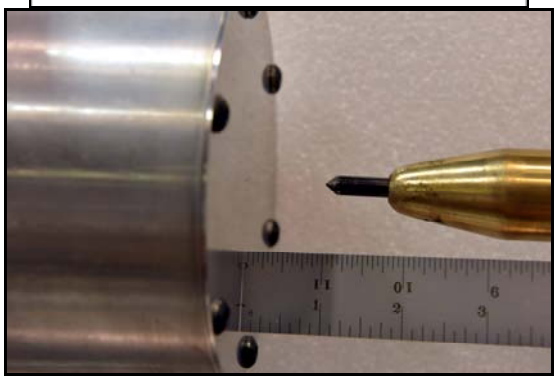

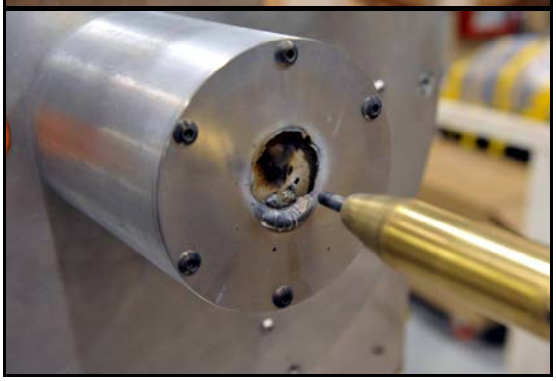

6. Larger discharge gap

The plan here is to increase the discharge gap to one inch and measure the discharge radial development.

Description: First return stroke, 500ms CCG, second return stroke. 0.050" T6061 Al coupon, 1/4" Tungsten Electrode, 1" Gap between electrode and coupon (0.2" between Coupon and Piston Collector) Tektronix P6015 HV probe

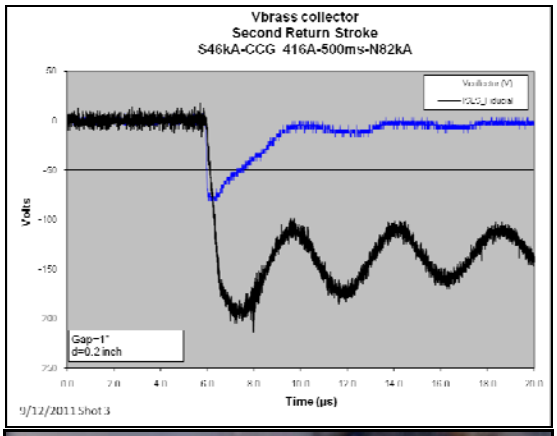

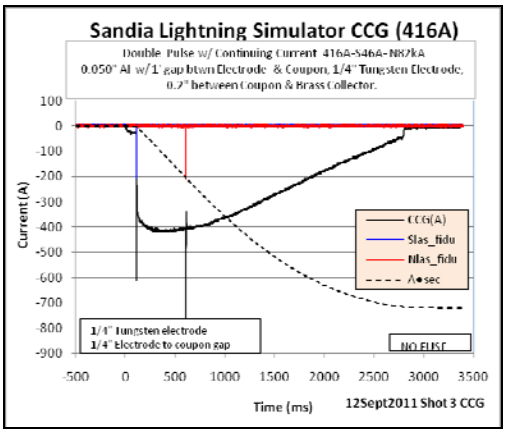

6. Larger discharge gap

The plan here is to increase the discharge gap to one inch and measure the discharge radial development.

Description: First return stroke, 500ms CCG, second return stroke. 0.050" T6061 Al coupon, 1/4" Tungsten Electrode, 1" Gap between electrode and coupon (0.2" between Coupon and Piston Collector) 5mΩ CVR

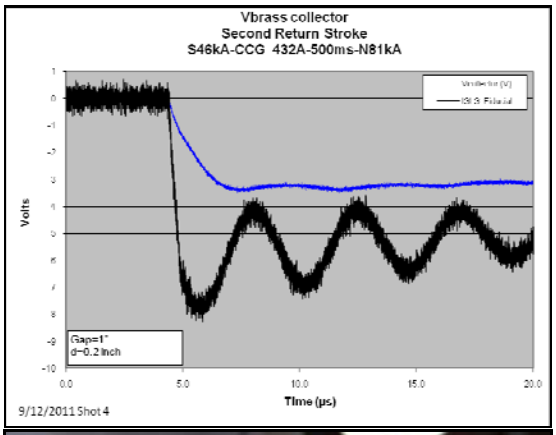

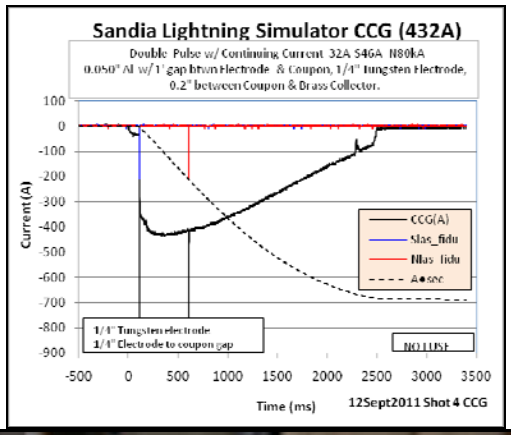

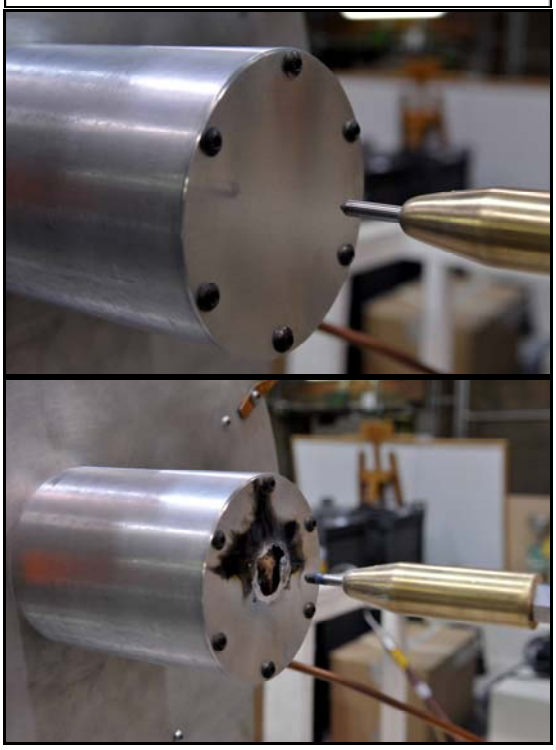

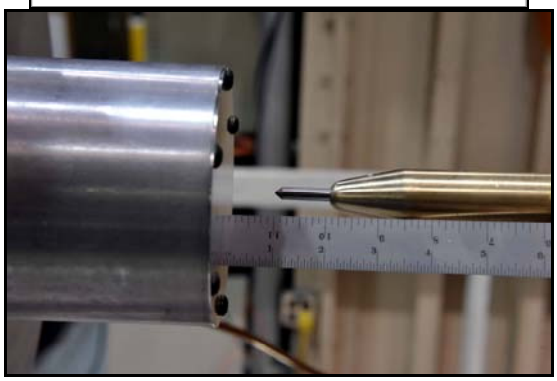

6. Larger discharge gap

The plan here is to increase the discharge gap to one inch and measure the discharge radial development.

Description: First return stroke, 500ms CCG, second return stroke. 0.050" T6061 Al coupon, 1/4" Tungsten Electrode, 1" Gap between electrode and coupon (0.2" between Coupon and Piston Collector) 5mΩ CVR

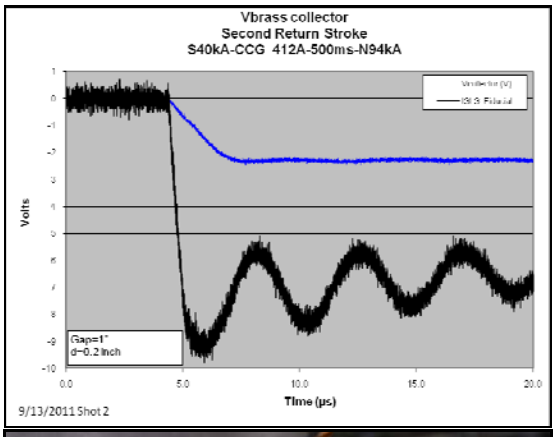

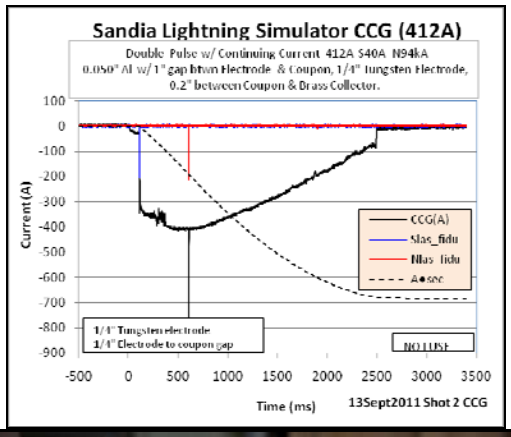

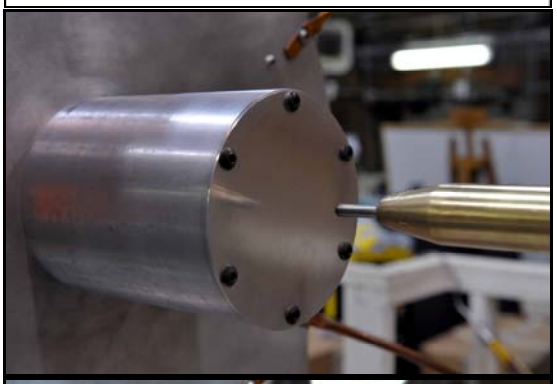

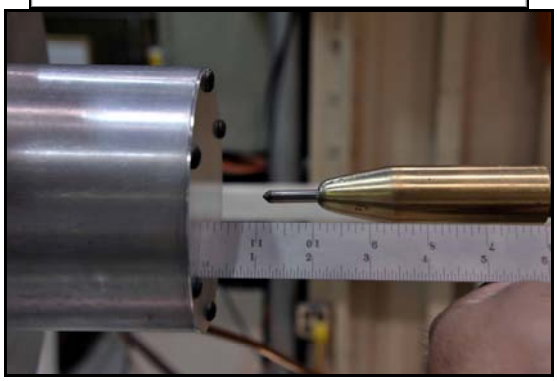

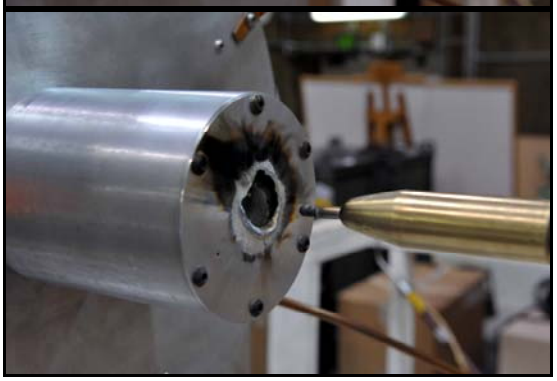

9. Predrilled hole experiments (PTX or SLS?) performed at SLS

The plan here is to repeat the predrilled hole experiments using the SLS with early time recording. **0.5" pre-drilled holes**

Description: 0.050" T6061 Al coupon w/ 0.5" Hole, 1/4" Tungsten Electrode, 1" Gap (Open Circuit) between electrode and coupon (0.2" between Coupon and brass collector) Tektronix P6015 HV probe

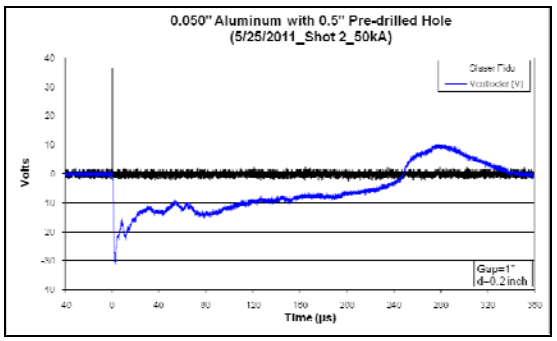

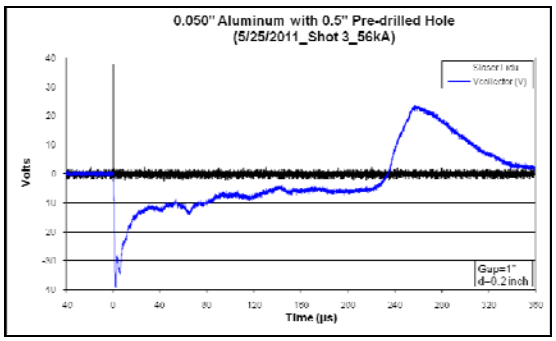

Description: 0.050" T6061 Al coupon w/ 0.5" Hole, 1/4" Tungsten Electrode, 1/4" Gap (Open Circuit) between electrode and coupon (0.2" between Coupon and brass collector) Tektronix P6015 HV probe

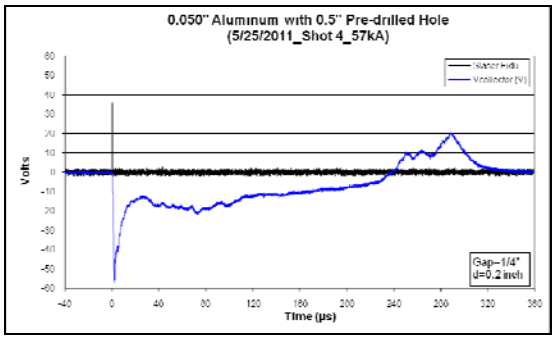

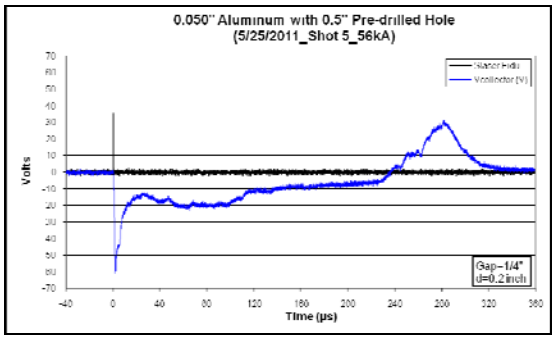

Description: 0.050" T6061 Al coupon w/ 0.5" Hole, 1/4" Tungsten Electrode, 0" Gap (Open Circuit) between electrode and coupon (0.2" between Coupon and brass collector) Tektronix P6015 HV probe

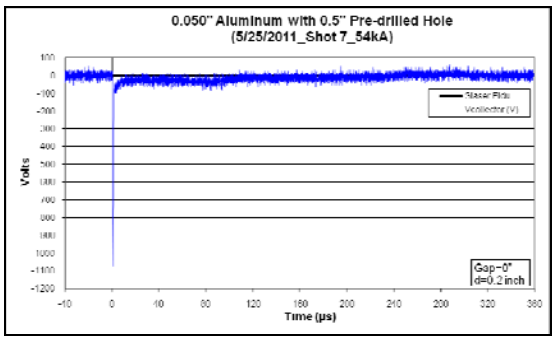

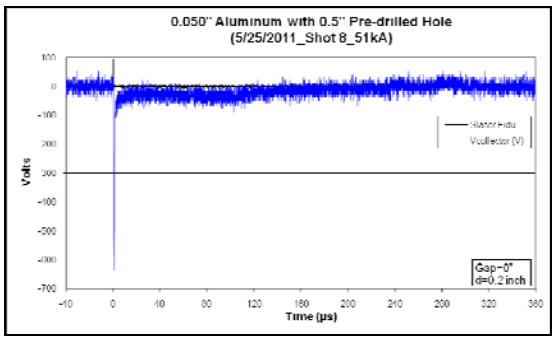

9. Predrilled hole experiments (PTX or SLS?) performed at SLS

The plan here is to repeat the predrilled hole experiments using the SLS with early time recording. **0.5" pre-drilled holes**

Description: 0.050" T6061 Al coupon w/ 0.5" Hole, 1/4" Tungsten Electrode, 0.125" Gap (Open Circuit) between electrode and brass collector (0.2" between Coupon and brass collector) Tektronix P6015 HV probe

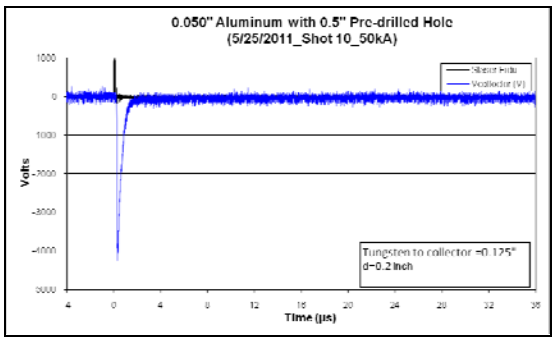

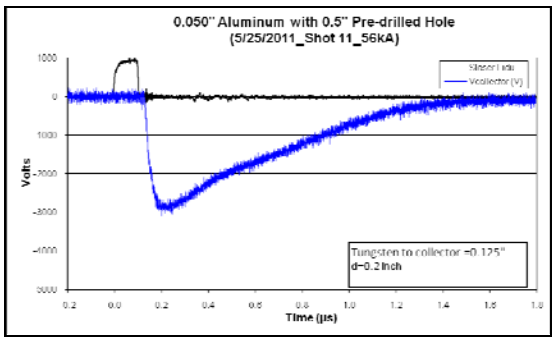

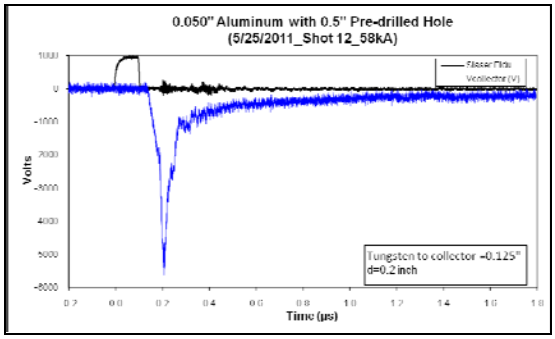

Description: 0.050" T6061 Al coupon w/ 0.5" Hole, 1/4" Tungsten Electrode, 0.0625" Gap (Open Circuit) between electrode and brass collector (0.2" between Coupon and brass collector) Tektronix P6015 HV probe

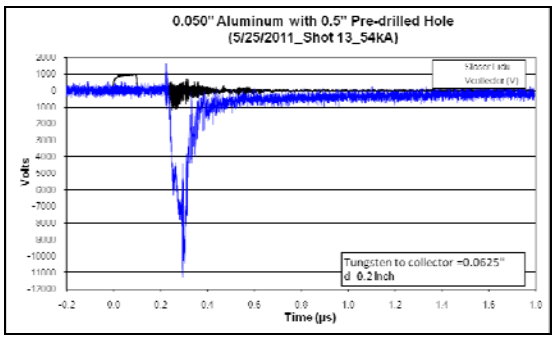

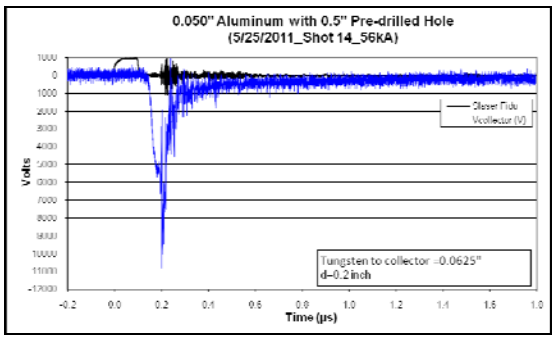

9. Predrilled hole experiments (PTX or SLS?) performed at SLS

The plan here is to repeat the predrilled hole experiments using the SLS with early time recording. **0.7" pre-drilled holes**

Description: 0.050" T6061 Al coupon w/ 0.7" Hole, 1/4" Tungsten Electrode, 1" Gap (Open Circuit) between electrode and coupon (0.2" between Coupon and brass collector) Tektronix P6015 HV probe

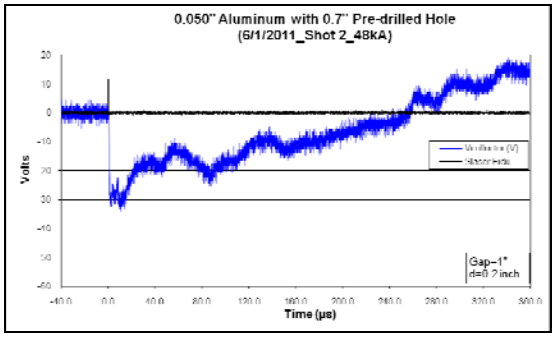

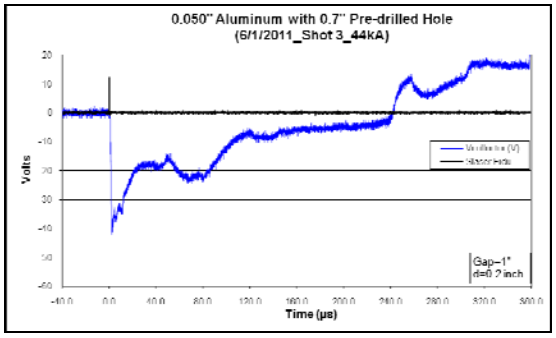

Description: 0.050" T6061 Al coupon w/ 0.7" Hole, 1/4" Tungsten Electrode, 1/4" Gap (Open Circuit) between electrode and coupon (0.2" between Coupon and brass collector) Tektronix P6015 HV probe

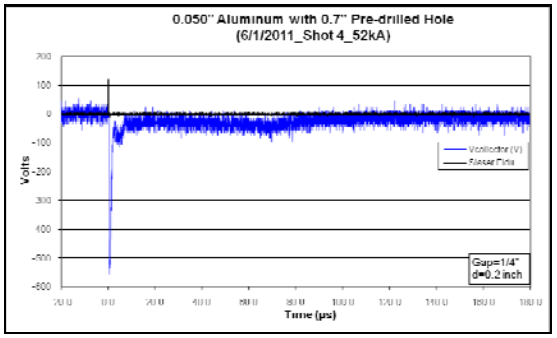

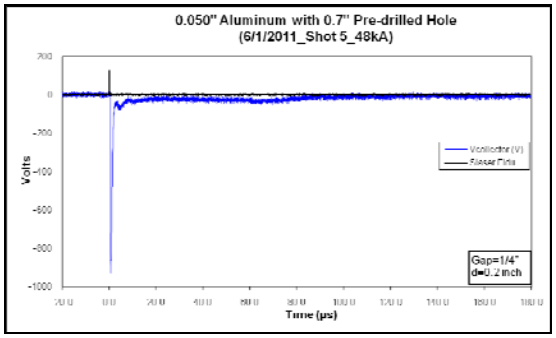

Description: 0.050" T6061 Al coupon w/ 0.7" Hole, 1/4" Tungsten Electrode, 0" Gap (Open Circuit) between electrode and coupon (0.2" between Coupon and brass collector) Tektronix P6015 HV probe

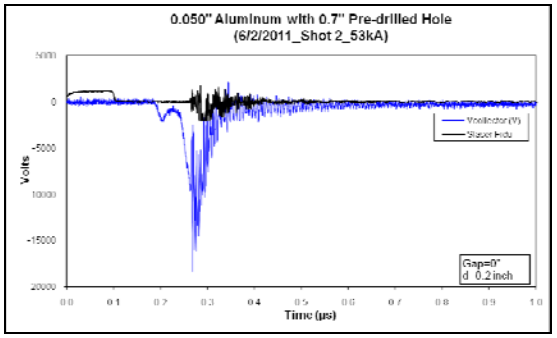

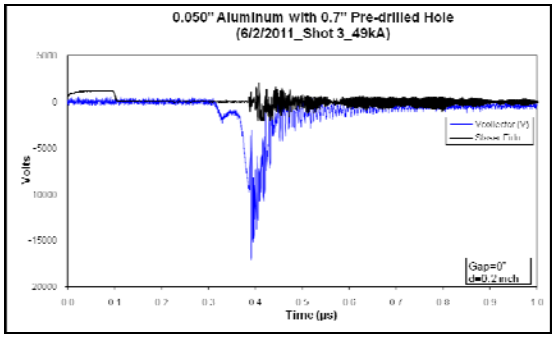

9. Predrilled hole experiments (PTX or SLS?) performed at SLS

The plan here is to repeat the predrilled hole experiments using the SLS with early time recording. **0.7" pre-drilled holes**

Description: 0.050" T6061 Al coupon w/ 0.7" Hole, 1/4" Tungsten Electrode, 0.125" Gap (Open Circuit) between electrode and brass collector (0.2" between Coupon and brass collector) Tektronix P6015 HV probe

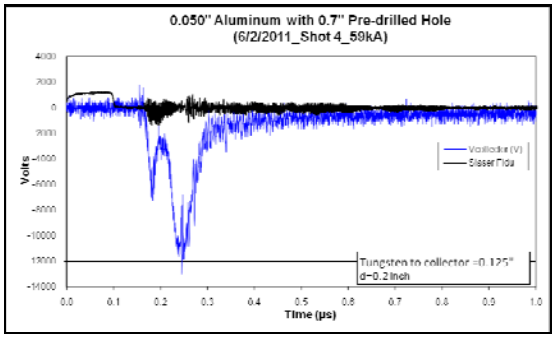

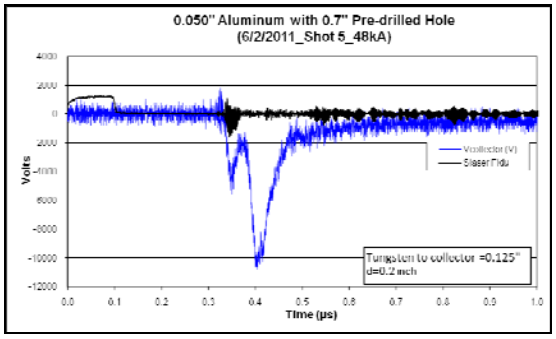

Description: 0.050" T6061 Al coupon w/ 0.7" Hole, 1/4" Tungsten Electrode, 0.0625" Gap (Open Circuit) between electrode and brass collector (0.2" between Coupon and brass collector) Tektronix P6015 HV probe

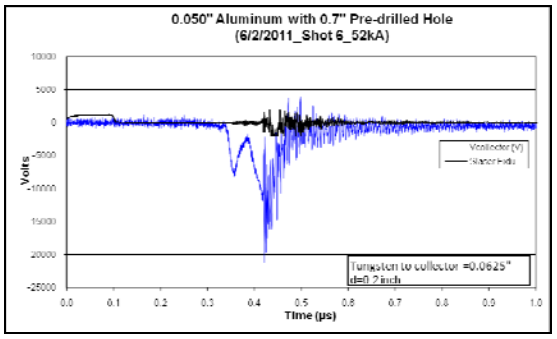

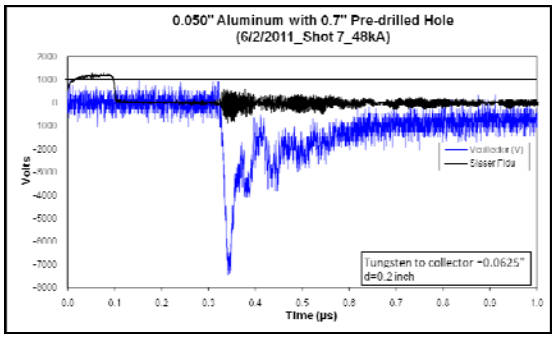

11. Outer radius current probe experiment

The idea here is to construct another current probe with a thick interior region and grooves only at the outer radii. The goal is to have the CCG current terminate on the inner thicker region (without measurement) and to see if the transition into the return stoke rapidly expands the current column to the out grooves. **Tests were conducted to evaluate burnthrough of 0.040" copper and stainless steel coupons at variety of currents and durations.**

Description: Water cooled copper coupon test. 0.040" thick x 5" dia copper disc. 1/4" tungsten electrode with 1/4" gap between electrode tip and copper coupon. 1/16" wide copper tape starter wire. Littelfuse Class K5 NLS-20 fuse. Post shot inspection revealed that the fuse had blown, Fuse Time=90ms Small pin hole in copper plate (water shooting out)

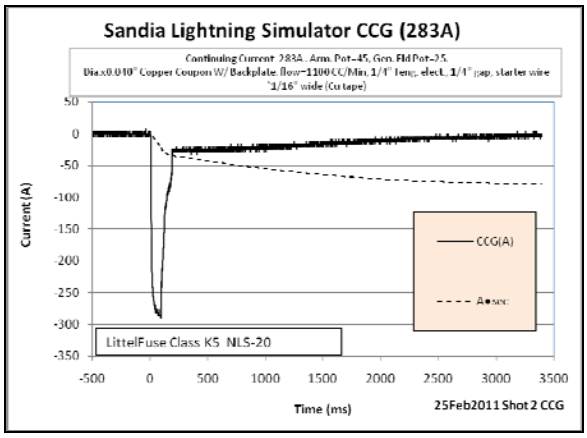

Description: Water cooled copper coupon test. 0.040" thick x 5" dia. copper disc. 1/4" tungsten electrode with 1/4" gap between electrode tip and copper coupon. 1/16" wide copper tape starter wire. Bussman NOS-15 fuse. Post shot inspection revealed that the fuse had blown, Fuse Time= 160 ms. No hole in copper plate

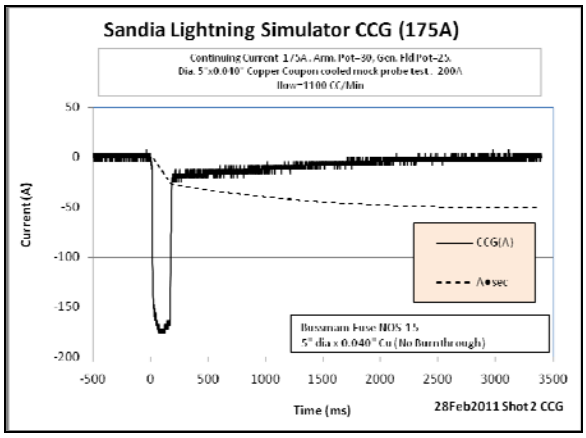

11. Outer radius current probe experiment

The idea here is to construct another current probe with a thick interior region and grooves only at the outer radii. The goal is to have the CCG current terminate on the inner thicker region (without measurement) and to see if the transition into the return stoke rapidly expands the current column to the out grooves. **Tests were conducted to evaluate burnthrough of 0.040" copper and stainless steel coupons at variety of currents and durations.**

Description: Water cooled coupon test. 0.040" thick x 5"x5" Stainless Steel plate. 1/4" tungsten electrode with 1/4" gap between electrode tip and SS coupon. 1/16" wide copper tape starter wire. Bussman NOS-15 fuse. Post shot inspection revealed that the fuse had blown, Fuse Time=215ms Small pin hole in SS plate (water shooting out)

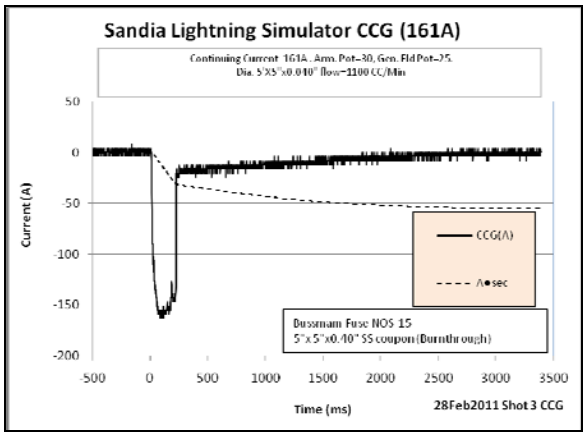

Description: Non cooled coupon test. No cooling fixture used.0.040" thick x 5" dia. copper disc. 1/4" tungsten electrode with 1/4" gap between electrode tip and Cu coupon. 1/16" wide copper tape starter wire (Cu tape adhesive side on Tungsten, Cu tape at coupon-copper side to coupon taped on with Kapton tape. Bussman NOS-15 fuse. Post shot inspection revealed that the fuse had blown, Fuse Time=400ms. A small (0.100" diameter) copper bubble formed on the back side of the copper coupon. No visible puncture

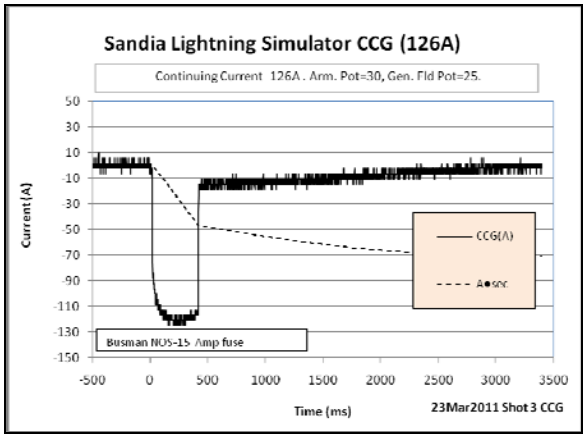

11. Outer radius current probe experiment

The idea here is to construct another current probe with a thick interior region and grooves only at the outer radii. The goal is to have the CCG current terminate on the inner thicker region (without measurement) and to see if the transition into the return stoke rapidly expands the current column to the out grooves. **Tests were conducted to evaluate burnthrough of 0.040" copper and stainless steel coupons at variety of currents and durations.**

Description: Non cooled coupon test. No cooling fixture used.0.040" thick x 5" dia. copper disc. 1/4" tungsten electrode with 1/4" gap between electrode tip and Cu coupon. 1/16" wide copper tape starter wire. (Cu tape adhesive side on Tungsten, Cu tape at coupon-copper side to coupon taped on with Kapton tape. Littelfuse Class K5 NLS-15. Post shot inspection revealed that the fuse had blown, Fuse Time=28ms. No visible puncture

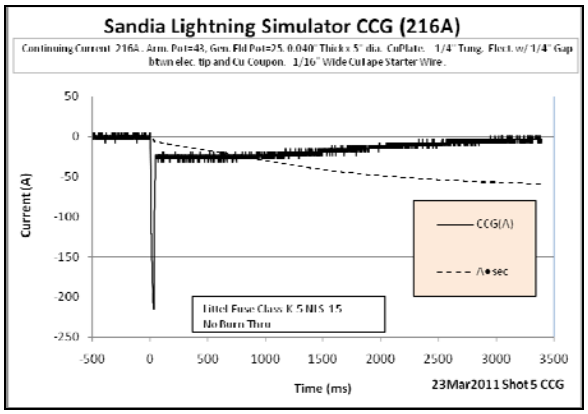

Summary of

Test Equipment Used

in Rounds 1-5

for LDRD

"Field and Charge Penetration by Lightning Burnthrough"

Compiled by: Leonard Martinez, SNL Department 1653
John Jojola, SNL Department 1653
Ed Bystrom, SNL Department 1535
Sandra Montoya, K-Tech Corporation

Revision: Rev 0.

Date: October 2011

Sandia Lightning Simulator (Page 1 of 2)

Lightning Parameters vs. Sandia Lightning Simulator Capabilities

Lightning Parameters	Typical system requirements		Cianos, Pierce [1]		Sandia Lightning Simulator capabilities
	Most severe	50% level	2% level	50% level	
Peak current	200 kA	20 kA	140 kA	20 kA	200 kA, max
Time to peak current	0.2 us	2.0 µs	12 µs	1.8 µs	1 to 5 µs
Current rate of rise	100 kA/us	20 kA/µs	100 kA/µs	22 kA/µs	200 kA/µs, max
Pulse width	200 us	50 µs	170 µs	45 µs	50 – 500 µs
Continuing current amplitude	700 A	140 A	520 A	140 A	100s A
Continuing current duration	500 ms	160 ms	400 ms	160 ms	100s ms
Number of strokes	1 - 12	2	10 -11	2 - 3	1 - 2
Interval between strokes	500 ms	50 ms	320 ms	60 ms	variable
Total flash duration	1 s	200 ms	850 ms	180 ms	variable
Total charge transfer	350 C	15 C	200 C	15 C	variable*
Action integral	3E6 A2 s	5E4 A2 s	-------	------	3E6 A2 s, max, single pulse

[1] N. Cianos, E. T. Pierce, "A Ground Lighting Environment for Engineering Usage," Technical Report 1, Contract L.S. 2817A3, SRI Project 1834, for McDonnell-Douglas Astronautics Corp., Stanford Research Institute, Menlo Park, California, August 1972.

* Charge = 40 C for single pulse, 200 kA peak and 250 C for 500 A / 0.5 s duration continuing current

Sandia Lightning Simulator (Page 2 of 2)

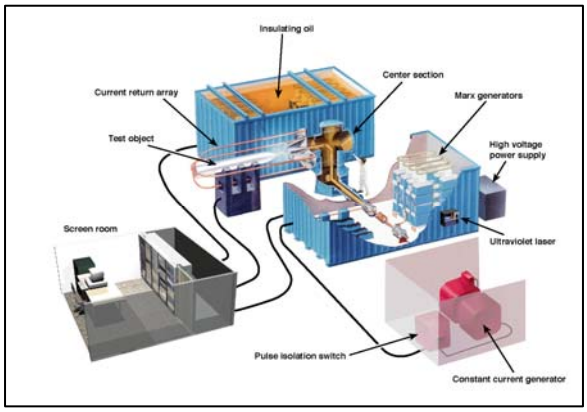

Sandia Lightning Simulator

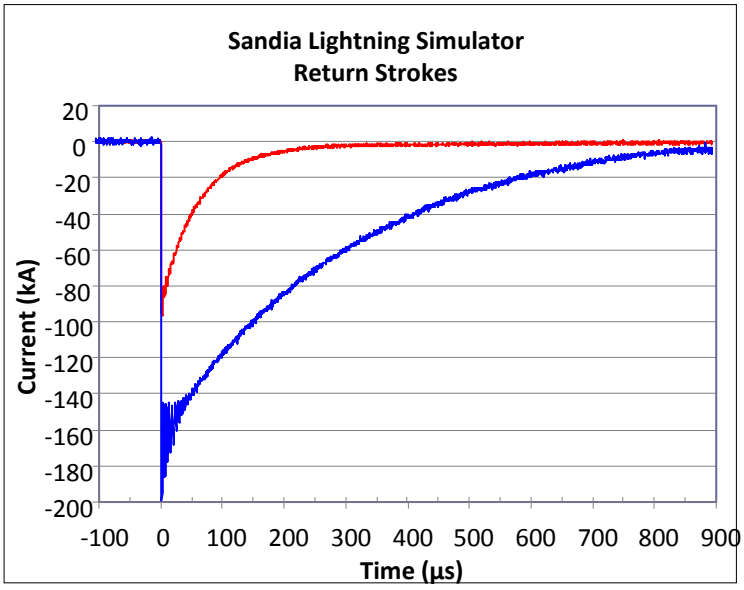

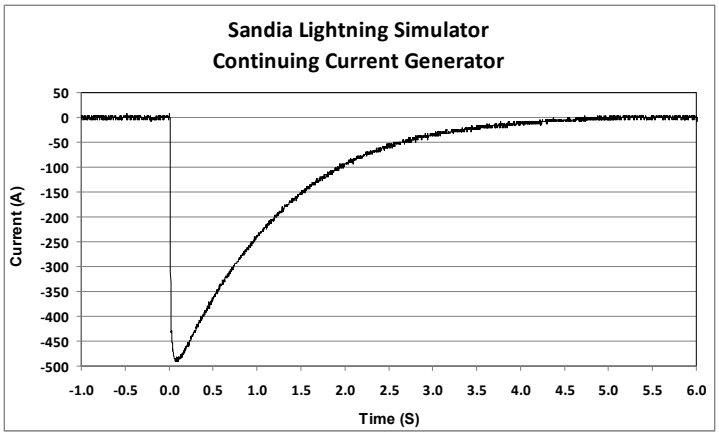

Pantex Lightning Voltage Pulser (Page 1 of 1)

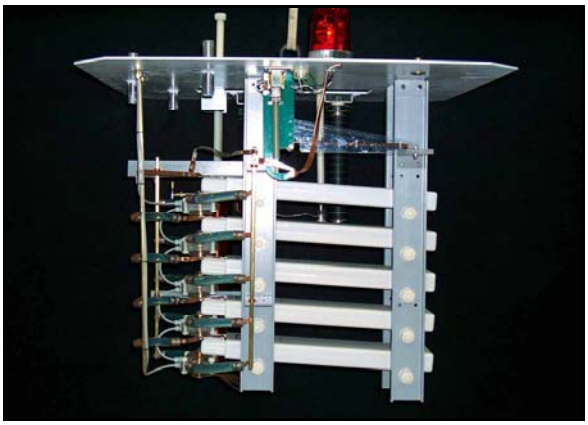

Lightning Voltage Pulser

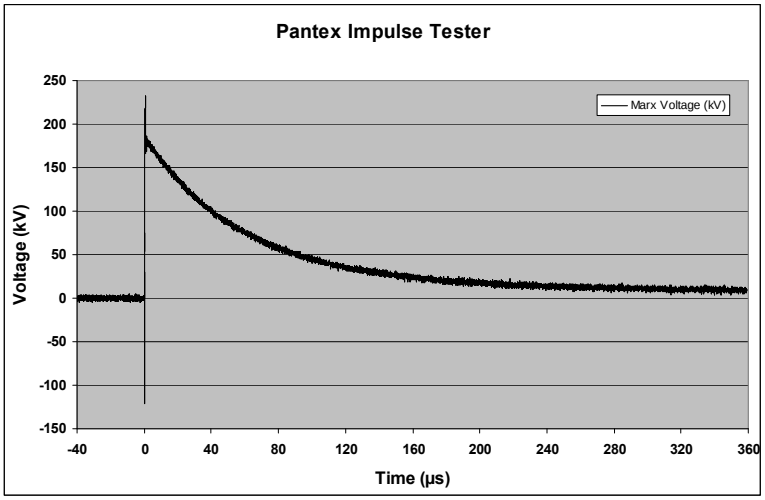

Pantex Lightning Parameters.

- Operating Charge Voltage : 25kV-90kV DC
- Pulse Output/Duration: 125kV-450 kV Peak/800 nS risetime x 50 uS FWHM
- Trigger Generator: TG-70, 70 kV Peak
- Gas Pressure: 0-250 psig, Air and SF6
- Transformer Oil for high voltage insulation: 1000 gals

Velonex 590 Pulser (Page 1 of 1)

Velonex 590

MODEL 590 SPECIFICATION
CONTINUOUS DUAL WAVE (General Description)

The Model 590 Generator produces a waveform which under open circuit conditions provides a 6kV, 1.2 x 50μS exponential signal and under short circuit conditions provides 3kA, 8 x 20μS exponential signal. When operating into an open circuit or short circuit, the waveforms will provide the respective outputs shown above. When operating into any other impedance, the waveform is undefined but will generally lie between the two sets of values gives above. When returning to open or short circuit conditions, the waveforms will return to the values shown. (i.e. the output signal is two directional from Hi Z to Lo Z or vice versa). The repetition rate for the Continuous Dual Mode operation is approximately 0.04Hz or one exponential waveform for every 25 seconds.

CONTINUOUS DUAL WAVE SPECIFICATION

	Open Circuit	Short Circuit
Output Voltage:	Variable by front-panel control up to 6kV maximum (peak value)	-
Output Current:	-	Variable by front-panel control up to 3kV maximum
Rise Time to Peak Value: (30-90% x 1.67)	Approximately 1.2μS	
Rise Time to Peak Value: (10-90% x 1.25)		Approximately 8μS
Decay:	50μS to one-half peak voltage value	20μS from pulse start to on-half peak current value
Repetition Rate:	Approximately 0.04Hz or one exponential waveform for every 25 seconds	
Signal Initiation:	One-Shot; Up to 0.04Hz maximum	

6

Pulse Arrested Spark Discharge (PASD) Pulser (Page 1 of 1)

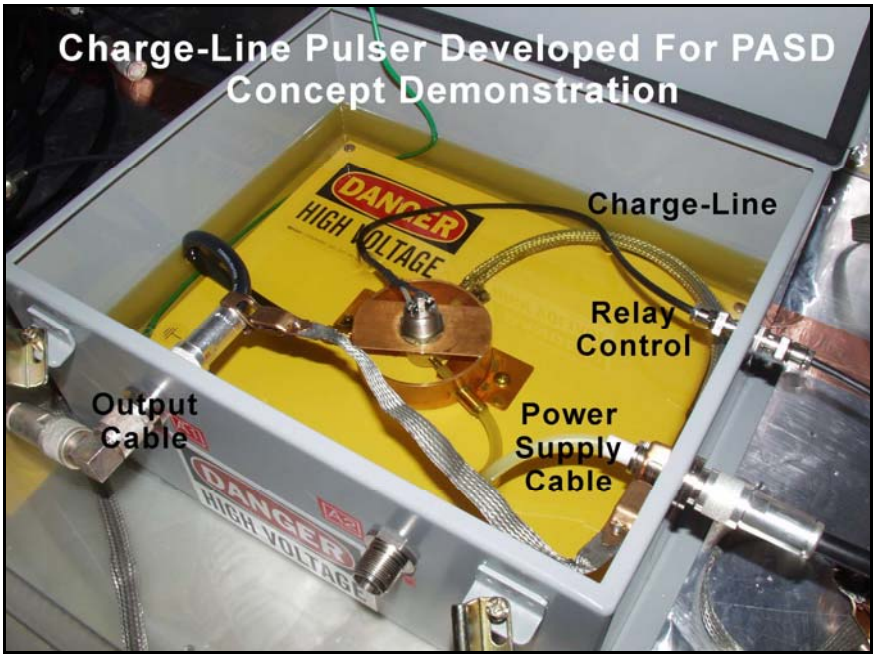

PASD Chargeline Pulser (PASD) unit 25kV 1ns risetime capability.

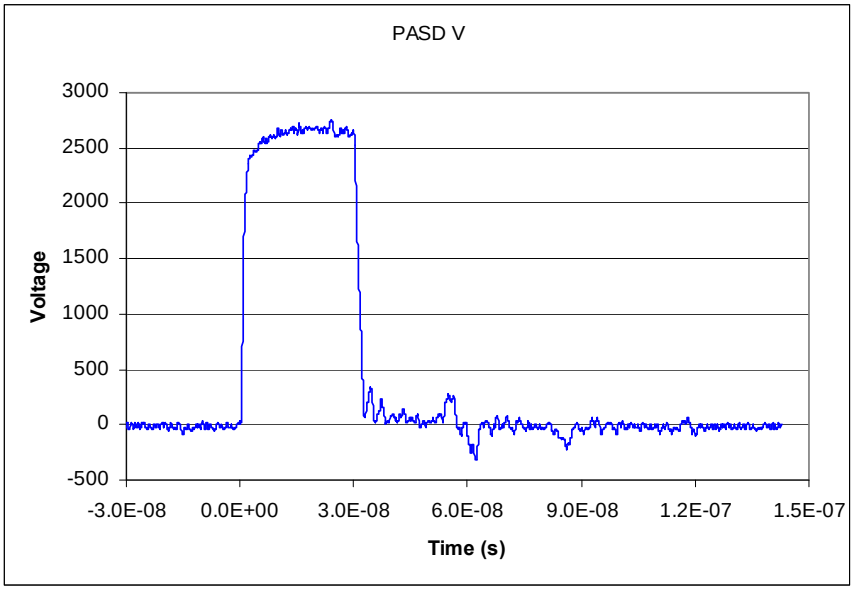

Chargeline Pulse (PASD) 30ns pulse width configuration

Tektronix TDS-7054 Oscilloscope (Page 1 of 4)

Digital Phosphor Oscilloscopes

▶ TDS7000B Series

▶ Characteristics

▶ Vertical System

	TDS7054	TDS7104	TDS7154B	TDS7254B	TDS7404B	TDS7704B
Input Channels	4	4	4	4	4	4
Hardware Analog Bandwidth (–3 dB)	500 MHz	1 GHz	1.5 GHz*1	2.5 GHz*1	4 GHz*1	7.25 GHz*1 (typical), 7 GHz*1 guaranteed
Rise Time 10% to 90% (typical)	800 ps	400 ps	200 ps	130 ps	100 ps	62 ps
Rise Time 20% to 80% (typical)			135 ps	83 ps	72 ps	43 ps
DC Gain Accuracy	1%			±(2% + (2% x offset))		±(2.5% + (2% x offset))
Hardware Bandwidth Limits	250 MHz or 20 MHz			Requires TCA-1 MEG		
Input Coupling	AC, DC, GND			DC, GND		
Input Impedance	1 MΩ ±0.5% or 50 Ω ±1%			50 Ω ±2.5%		
Input Sensitivity, 1 MΩ	1 mV/div to 10 V/div			—		
Input Sensitivity, 50 Ω	1 mV/div to 1 V/div			2 mV/div to 1 V/div		
Vertical Resolution	8-Bit (>11-Bit with averaging)			8-Bit (>11-Bit with averaging)		
Max Input Voltage, 1 MΩ	±150 V CAT I Derate at 20 dB/decade to 9 V_{RMS} above 200 kHz			—		
Max Input Voltage, 50 Ω	5 V_{RMS} with peaks less than ±30 Volts			<1 V_{RMS} for <100 mV/div, <5 V_{RMS} for ≥100 mV/div settings Also determined by TekConnect® accessory		
Offset Range	1 mV/div to 100 mV/div: ±1 V 101 mV/div to 1 V/div: ±10 V 1.01 V/div to 10 V/div: ±100 V			2 mV to 50 mV/div: ±0.5 V 50.5 mV to 99.5 mV: ±0.25 V 100 mV to 500 mV: ±5 V 505 mV to 1 V/div: ±2.5 V		
Channel-to-Channel Isolation Any Two Channels at Equal Vertical Scale Settings	≥100:1 at 100 MHz and ≥30:1 at the rated bandwidth			≥80:1 at 1.5 GHz and ≥15:1 at rated bandwidth		

*1 At ≥10 mV/div.

Note: Typical system bandwidth of TDS7404B with P7240: 4 GHz.

Note: Typical system bandwidth of TDS7404B with P7330: 3.5 GHz.

Note: Typical system bandwidth of TDS7704B with P7260: 6 GHz

Note: Typical system bandwidth of TDS7704B with P7350: 5 GHz.

Tektronix TDS-7054 Oscilloscope (Page 2 of 4)

▶ Time Base System

	TDS7054/TDS7104	TDS7154B/TDS7254B/TDS7404B/TDS7704B
Time Base Range	200 ps/div to 40 s/div	50 ps to 10 s/div
Time Base Delay Time Range	16 ns to 250 s	5 ns to 250 s
Channel-to-channel Deskew Range	±25 ns	±75 ns
Delta Time Measurement Accuracy	±((0.06/sample rate) + (15 ppm x reading)) RMS	±((0.06/sample rate) + (2.5 ppm x reading)) RMS
Trigger Jitter (RMS)	8 ps_{RMS} (typical)	2 ps_{RMS} (typical) (7254B/7154B) 1.5 ps_{RMS} (typical) (7404B) 1.2 ps_{RMS} (typical) (7704B)
Long Term Sample Rate and Delay Time Accuracy	±15 ppm over ≥1 ms interval	2.5 ppm over any ≥100 ms interval

▶ Acquisition System

	TDS7054	TDS7104	TDS7154B/ TDS7254B/ TDS7404B/ TDS7704B
Real-time Sample Rates			
1 channel (max)	5 GS/s	10 GS/s	20 GS/s
2 channels (max)	5 GS/s	5 GS/s	10 GS/s
3-4 channels (max)	2.5 GS/s	2.5 GS/s	5 GS/s
Equivalent Time Sample Rate (max)	250 GS/s	250 GS/s	1 TS/s
Maximum Record Length per Channel with Standard Memory	2 Mb (1-CH.), 1 Mb (2-CH.), 500 Kb (4-CH.)		4 Mb (1-CH.), 2 Mb (2-CH.), 1 Mb (4-CH.)
With Memory Opt. 2M	8 Mb (1-CH.), 4 Mb (2-CH.), 2 Mb (4-CH.)		
With Memory Opt. 3M	16 Mb (1-CH.), 8 Mb (2-CH.), 4 Mb (4-CH.)		
With Memory Opt. 4M			32 Mb (1-CH.), 16 Mb (2-CH.), 8 Mb (4-CH.)
With Memory Opt. 5M			64 Mb (1-CH.), 32 Mb (2-CH.), 16 Mb (4-CH.)

Tektronix TDS-7054 Oscilloscope (Page 3 of 4)

Digital Phosphor Oscilloscopes

▶ TDS7000B Series

▶ Maximum Duration at Highest Real-time Resolution (1-CH)

	TDS7054	TDS7104	TDS7154B/TDS7254B/TDS7404B/TDS7704B
Time Resolution (Single-shot)	200 ps (5 GS/s)	100 ps (10 GS/s)	50 ps (20 GS/s)
Max Duration with Standard Memory	400 µs	200 µs	200 µs
Max Duration with Opt. 2M	1.6 ms	800 µs	400 µs
Max Duration with Opt. 3M	3.2 ms	1.6 ms	800 µs
Max Duration with Opt. 4M			1.6 ms
Max Duration with Opt. 5M			3.2 ms

▶ Acquisition Modes

	TDS7054/TDS7104	TDS7154B/TDS7254B/TDS7404B/TDS7704B
FastAcq Acquisition	Powered by exclusive DPX® acquisition technology, FastAcq optimizes the instrument for analysis of dynamic signals and capture of infrequent events	
Maximum FastAcq Waveform Capture Rate	>200,000 wfms/sec	>400,000 wfms/sec
Waveform Database	Accumulate Waveform Database providing three-dimensional array of amplitude, time and counts	
Sample	Acquire sampled values	
Peak Detect	Captures narrow glitches at all real-time sampling rates	
Minimum Peak Detect Pulse Width	≤1 ns	400 ps
Averaging	From 2 to 10,000 waveforms included in average	
Envelope	From 2 to $2x10^9$ waveforms included in min-max envelope	
Hi-res	Real-time boxcar averaging reduces random noise and increases resolution	
FastFrame™ Acquisition	Acquisition memory divided into segments; maximum trigger rate >265,000 waveforms per second. Time of arrival recorded with each event	

Tektronix TDS-7054 Oscilloscope (Page 4 of 4)

▶ Pinpoint™ Trigger System

	TDS7054	TDS7104	TDS7154B/TDS7254B/TDS7404B/TDS7704B
Sensitivity			
Internal DC Coupled	0.35 div DC to 50 MHz increasing to 1 div at 500 MHz	0.35 div DC to 50 MHz increasing to 1 div at 1 GHz	0.5 div DC to 50 MHz increasing to 1.5 div at 3 GHz TDS7404B/TDS7704B: 2.7 div at 4 GHz (typical)
External (Auxiliary Input)	400 mV from DC to 50 MHz increasing to 750 mV at 100 MHz	250 mV from DC to 50 MHz increasing to 500 mV at 100 MHz	150 mV from DC to 50 MHz increasing to 500 mV at 2.5 GHz
Main Trigger Modes	Auto, Normal and Single		
Trigger Sequences	Main, Delayed by Time, Delayed by Events. All sequences can include separate horizontal delay after the trigger event to position the acquisition window in time		
Trigger Characteristics			
Standard Trigger Types	Edge, Glitch, Runt, Width, Transition Time, Timeout, Pattern, State, Setup/Hold		Edge, Glitch, Runt, Width, Transition Time, Timeout, Pattern, State, Setup/Hold, Window – all except Edge, Pattern and State can be logic qualified by up to two channels
A Event and Delayed B Event Trigger Types	A Event: All above types Delayed B Event: Edge		A Event and Delayed B Event: All above types Reset: Reset if B Event does not occur within specified time, before specified number of events, or before specified State changes
Communications-related Triggers (requires Option SM)	Support for AMI, HDB3, BnZS, CMI, MLT3 and NRZ encoded communications signals. Select among isolated positive or negative one, zero pulse form or eye patterns as applicable to standard		
Serial Pattern Trigger (requires Option ST)			64-Bit serial word recognizer, bits specified in binary (high, low, don't care) or hex format. Trigger on NRZ-encoded data up to 1.25 GBaud
Trigger Level Range			
Internal	±12 divisions from center of screen		
External (Auxiliary In)	±8 V		±5 V
Line	fixed at 0 V		
Trigger Coupling	DC, AC (attenuates <60 Hz), HF Rej (attenuates >30 kHz), LF Rej (attenuates <80 kHz), Noise Reject (reduces sensitivity)		
Trigger Holdoff Range	250 ns minimum to 12 s maximum		

Tektronix TDS-694C Oscilloscope (Page 1 of 1)

TDS 600 Series Characteristics	TDS 654C	TDS 680C	TDS 684C	TDS 694C
Total Channels	4	2 + 2	4	4
Sample Rate (all channels simultaneously)	5 GS/s	5 GS/s	5 GS/s	10GS/s
Real-time Bandwidth	500MHz	1 GHz	1 GHz	3GHz
Maximum Record Length per Channel	15,000 pts	15,000 pts	15,000 pts	120,000pts
Vertical Resolution	1mV/div – 10V/div	1mV/div – 10 V/div	1mV/div – 10V/div	10mV/div – 1V/div
Time Measurement Accuracy	<50ps @ 5GS/s	<50ps @ 5 GS/s	<50ps @ 5GS/s	15 ps @ 10GS/s
Histograms and Measurement Statistics	Std.	Std.	Std.	Std.
Standard Probes	4 P6243	None	None	None
Display Type	7 in. color	7 in. mono	7 in. color	7 in. color
GPIB Port, RS-232 & Centronics	Std.	Std.	Std.	Std.
VGA	Std. Color	Std. Mono	Std. Color	Std. Color
Hard Disk Drive	Opt.	Opt.	Opt.	Opt.

TIME BASE SYSTEM

Time Bases – Main and Delayed.

Time/div Range – 200ps/div to 10 s/div. Except TDS694C: 100ps/div to 10 s/div.

Time Base Accuracy – Over Any Interval >1 ms ±100ppm. Except TDS 694C: Over any interval > 1 ms ± 10ppm.

Time Interval Measurement Accuracy – TDS 654C/680C/684C: ±[(0.2/sample rate) + (100ppm x |Reading|)] single shot. (≈ 50ps @ 5GS/s)
TDS 694C: ±[(0.15/sample rate) + (10ppm x |Reading|)] single shot. (≈ 15ps @ 10GS/s)

Record Length per Channel – 500 to 15,000 pts. Except TDS 694C: 500 to 30,000 pts. (optional: 120,000 pts.)

Trigger Jitter – 8ps RMS (typical).

Pre-Trigger Position – 0% to 100% of Record.

Channel to Channel Deskew Range – ±25 ns.

VERTICAL SYSTEM

Vertical Resolution – 8-Bits (>11-Bits with averaging).

Vertical Sensitivity – 1mV/div to 10V/div. Except TDS 694C: 10mV/div to 1V/div.

Maximum Input Voltage – 300V CAT II; ±400V peak. Derate at 20dB/decade above 1MHz. Except TDS 694C: 5V RMS.

DC Gain Accuracy – ±1.50%. Except TDS 694C: ±1.0%.

Position Range – ±5 divs.

Offset –
±1V from 1 to 99.5mV/div, ±10V from 100mV to 995mV/div, ±100V from 1V to 10V/div.
Except TDS 694C: ±0.5 V from 10 to 50mV/div, ±0.25V from 50.5 to 100mV/div, ±5V from 101mV to 500mV/div, ±2.5V from 505mV to 1V/div.

Bandwidth Selections – 20MHz, 250MHz, and Full. Except TDS 694C: Full only.

Input Impedance Selections – 1 MΩ in parallel with 10pF, or 50 Ω (AC and DC coupling). Except TDS 694C: 50 Ω (DC coupled).

Input Coupling – AC, DC or GND. Except TDS 694C: DC or GND.

AC Coupled Low Frequency Limit (Except TDS 694C) – <10Hz when AC, 1MΩ coupled. <200kHz when AC, 50 Ω coupled.

ACQUISITION MODES

Peak Detect – High frequency and random glitch capture. Captures glitches of 1ns using acquisition hardware at all real-time sampling rates. TDS 694C captures glitches of 100 ps.

Sample – Sample data only.

Envelope – Max/min values acquired over one or more acquisitions.

Average – Waveform data from 2 to 10,000 waveforms (selectable) is averaged.

Single Sequence – Use RUN/STOP button to capture a single triggered acquisition at a time, which may be automatically saved to NVRAM with AutoSave.

TRIGGERING SYSTEM

TRIGGER TYPES

EDGE (Main and Delayed) – Conventional level-driven trigger. Positive or negative slope on any channel or rear panel auxiliary input. Coupling selections: DC, AC, noise reject, HF reject, LF reject.

LOGIC (Main) –
PATTERN: Specifies a logical combination (AND, OR, NAND, NOR) of the four input channels (high, low, don't care). Trigger when pattern stays true or false for a specified time.
STATE: Any logical pattern of channels 1, 2, and 3 (AUX1 on TDS680C) plus a clock edge on channel 4 (AUX2 on TDS680C). Triggerable on rising or falling clock edge.
SETUP/HOLD: Trigger on violations of both setup time and hold time between clock and data which are on two input channels.

PULSE (Main) –
GLITCH: Trigger on or reject glitches of positive, negative, or either polarity. Minimum glitch width is 1.0ns with 200ps resolution.
RUNT: Trigger on a pulse that crosses one threshold but fails to cross a second threshold before crossing the first again.
WIDTH: Trigger on width of positive or negative pulse either within or out of selectable time limits (1ns to 1 s).
SLEW RATE: Trigger on pulse edge rates that are either faster or slower than a set rate. Edges can be rising, falling, or either.

page 2

Tektronix TDS-3054C Oscilloscope (Page 1 of 1)

Data Sheet

Work Where you Need to

The TDS3000C Series packs the power of a DPO in a compact design that is only 5.9 in. (149 mm) deep, freeing up valuable benchtop space. And when you need to move your oscilloscope to another lab, its portable 7 lb. (3.2 kg) design makes for easy transport.

If your work demands even more mobility, then the optional battery pack will give you up to three hours of operation without line power.

TDS3BATC provides you with up to three hours of portable battery operation.

Characteristics

TDS3000C Series Electrical Characteristics

Characteristic	TDS3012C	TDS3014C	TDS3032C	TDS3034C	TDS3052C	TDS3054C
Bandwidth	100 MHz	100 MHz	300 MHz	300 MHz	500 MHz	500 MHz
Calculated Rise Time (typical)	3.5 ns	3.5 ns	1.2 ns	1.2 ns	0.7 ns	0.7 ns
Input Channels	2	4	2	4	2	4
External Trigger Input	Included on all models					
Sample Rate on each channel	1.25 GS/s	1.25 GS/s	2.5 GS/s	2.5 GS/s	5 GS/s	5 GS/s
Record Length	10 kpoints					
Vertical Resolution	9 bits					
Vertical Sensitivity, 1 MΩ	1 mV/div to 10 V/div					
Vertical Sensitivity, 50 Ω	1 mV/div to 1 V/div					
Input Coupling	AC, DC, GND					
Input Impedance	1 MΩ in parallel with 13 pF or 50 Ω					
DC Gain Accuracy	±2%					
Maximum Input Voltage, 1 MΩ	150 V_{RMS} with peaks at ≤400 V					
Maximum Input Voltage, 50 Ω	5 V_{RMS} with peaks at ≤30 V					
Position Range	±5 div					
Bandwidth Limit	20 MHz	20 MHz	20 MHz, 150 MHz	20 MHz, 150 MHz	20 MHz, 150 MHz	20 MHz, 150 MHz
Time Base Range	4 ns to 10 s	4 ns to 10 s	2 ns to 10 s	2 ns to 10 s	1 ns to 10 s	1 ns to 10 s
Time Base Accuracy	±20 ppm over any 1 ms time interval					
Input/Output Interfaces						
Ethernet Port	RJ-45 connector, supports 10Base-T LAN					
USB Port	Front-panel USB 2.0 host port Supports USB flash drive					
GPIB Port	Full talk/listen modes, setting and measurements (Optional with TDS3GV Communications Module)					
RS-232-C Port	DB-9 male connector, full talk/listen modes; control of all modes, settings and measurements Baud rates up to 38,400 (Optional with TDS3GV Communications Module)					
VGA Video Port	DB-15 female connector, monitor output for direct display on large VGA-equipped monitors (Optional with TDS3GV Communications Module)					
External Trigger Input	BNC connector, input impedance >1 MΩ in parallel with 17 pF; max input voltage is 150 V_{RMS}					

Yokagawa DL750 ScopeCorder (Page 1 of 1)

DL750/DL750P/SI1400 Selection

		DL750	DL750P	SL1400
Input Section	Number of input channels	16	16	16
	Logic input	●	●	●
	Long-memory	Max. 1 GW total*1	Max. 1 GW total*1	50 MW total
	DSP channel	●*1	●*1	–
Trigger Section	A wide range of trigger functions	●	●	●
Time Axis	Time axis setting	T/div*2	T/div*2	T*3
Vertical Axis	Voltage-axis sensitivity setting	V/div*4	V/div*4	V*5
Display Function	GIGAZoom ENGINE	●	●	●
	X-Y display	●	●	●
	Snapshot	●	●	●
Acquisition	Dual capture	●	●	–
	Realtime hard disk recording	●*6	●*6	●*6
	Voice memo	●	●	–
Vertical Axis Settings	ALL CH menu	●	●	●
	Linear scaling	●	●	●
Analysis	History memory & history search	●	●	●
	Search & zoom	●	●	–
	Automated measurement of waveform parameters, Statistical processing	●	●	●
	User-defined computation	●*1	●*1	–
	GO/NO-GO determination	●	●	–
Recorder Mode	Recorder mode (T-Y, X-Y)	–	●	●
Screen Image Data Output	Saving and printing the screen image data	●	●	●
Other Functions	Acquisition memory backup	●	●	●
	Action-on-trigger	●	●	●
	Multilingual menu (English/Japanese/Chinese/Korea)	●	●	●
	Multilingual message (eight languages)	●	●	●
Built-in Printer	Built-in printer	104 mm width	204 mm width	204 mm width
Built-in Storage	Floppy disk drive	●*7	●*7	–
	Zip drive	●*7	–	–
	PC card interface	●*7	●*7	●*1
	Internal hard disk	●*1	●*1	●*1
External Storage Interface	USB mass storage device	●	●	●
General Specifications	For AC & DC power input	●*1	–	–

*1: optional *2: The time per one grid square (1 div). The display span is 10 divisions. *3: The length of time within one screen (= The record time)
*4: The voltage value to one grid square (1 div) *5: The voltage across the top and bottom edges of the waveform display area (10 divisions)
*6: with the internal hard disk option *7: Choose one.

Module Selection

Input	Model No.	Sample Rate	Resolution	Bandwidth	Number of Channels	Isolation	Maximum Input Voltage (DC+ACpeak)	DC Accuracy	Note
Analog Voltage	701250	10 MS/s	12-Bit	3 MHz	2	Isolated	600 V*2 250 V*3	±0.5%	high noise immunity
	701251	1 MS/s	16-Bit	300 kHz	2	Isolated	600 V*2 140 V*3	±0.25%	High sensitivity range (10 mV), low noise (±100μVtyp.), and high noise immunity
	701255	10 MS/s	12-Bit	3 MHz	2	Non-Isolated	600 V*4 250 V*3	±0.5%	non-isolation version of model 701250
	701260	100 kS/s	16-Bit	40 kHz	2	Isolated	1000 V*2 850 V*3	±0.25%	with RMS, and high noise immunity
Temperature	701261	100 kS/s (Voltage), 500 S/s (Temperature)	16-Bit (Voltage), 0.1°C (Temperature)	40 kHz (Voltage), 100 Hz (Temperature)	2	Isolated	42 V	±0.25% (Voltage)	thermocouple (K, E, J, T, L, U, N, R, S, B, W, iron-doped gold/chromel)
	701262	100 kS/s (Voltage), 500 S/s (Temperature)	16-Bit (Voltage), 0.1°C (Temperature)	40 kHz (Voltage), 100 Hz (Temperature)	2	Isolated	42 V	±0.25% (Voltage)	thermocouple (K, E, J, T, L, U, N, R, S, B, W, iron-doped gold/chromel), with AAF
	701265	500 S/s (Voltage), 500 S/s (Temperature)	16-Bit (Voltage), 0.1°C (Temperature)	100 Hz	2	Isolated	42 V	±0.08 (Voltage)	thermocouple (K, E, J, T, L, U, N, R, S, B, W, iron-doped gold/chromel), high sensitivity range (1 mV), and low noise (±4 μVtyp.)
Strain	701270	100 kS/s	16-Bit	20 kHz	2	Isolated	10 V	±0.5% (Strain)	Supports strain NDIS, 2, 5, 10 V built-in bridge power supply
	701271	100 kS/s	16-Bit	20 kHz	2	Isolated	10 V	±0.5% (Strain)	Supports strain DSUB, 2, 5, 10 V built-in bridge power supply, and shunt CAL
Analog Voltage, Acceleration	701275	100 kS/s	16-Bit	40 kHz	2	Isolated	42 V	±0.25% (Voltage) ±0.5% (Acceleration)	built-in anti-aliasing filter, Supports built-in amp type acceleration sensors (4 mA/22 V)
Frequency	701280	25 kS/s	16-Bit	resolution 50 ns	2	Isolated	420 V*2 42 V*3	±0.1% (Frequency)	Measurement frequency of 0.01 Hz to 200 kHz, Measured parameters (frequency, rpm, period, duty, power supply frequency, distance, speed)

*1: Probes are not included with any modules.
*2: In combination with 10:1 probe model 700929
*3: Direct input
*4: In combination with 10:1 probe model 701940

11

Nanofast Fiber Optic Link OP300-2A (Page 1 of 5)

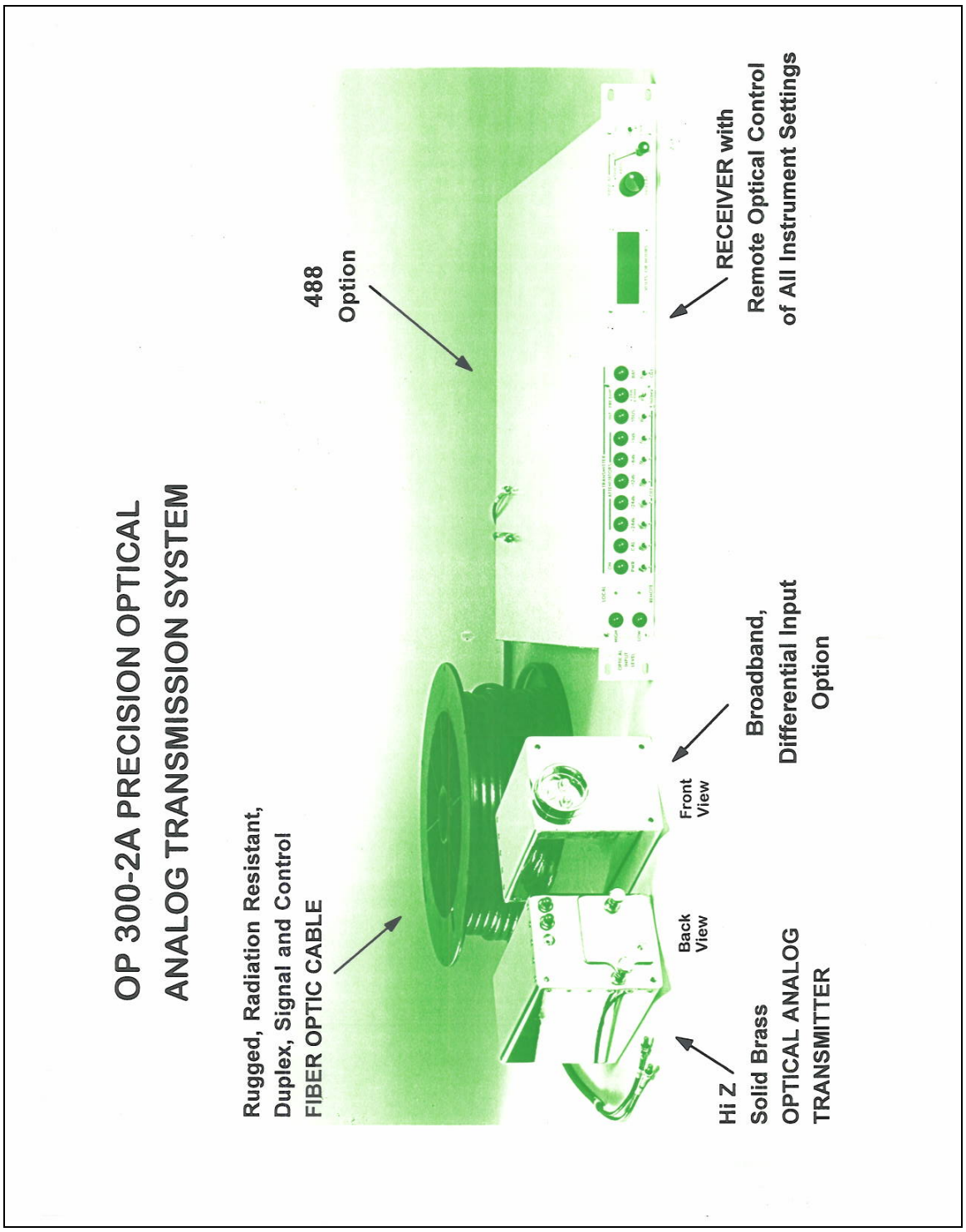

Nanofast Fiber Optic Link OP300-2A (Page 2 of 5)

NANOFAST

OP 300-2A OPTICAL ANALOG TRANSMISSION SYSTEM WITH HIGH FREQUENCY OPTIONS

FUNCTION :	Transmitter accepts single ended or differential 0 to ±160 millivolt signals into 50 ohms, converts signals to a precision optical equivalent waveform and drives the Receiver unit over 150 ft., or other specified length of fiber optic cable. Optional remotely controlled 24 dB (or X16) preamplifier and 3, 6, 12, 24 and 24 dB Attenuators in Transmitter provide full-scale ranges from ±10 mV to ±462 volts. Receiver converts optical input to an electrical output into 50 ohms, equal to the Transmitter input times a system gain of 6 dB, with a full scale of ±.320 V. Alternately, Calibration in volts with remotely selectable FS Ranges from ±10 mV to ±100 V in a 1, 2, 5, 10 sequence, and a FS output of ±100 mV.
FREQUENCY RESPONSE :	Low frequency 3 dB point of 160 Hz and high frequency 3 dB point of 300 MHz, 500 MHz, 750 MHz or 1 GHz as specified.
STABILITY :	Better than 1% over a temperature range from 0 to 120° F and for optical path transmission changes of 50%.
NOISE :	RMS noise down greater than 34 dB with respect to peak signal for 1.2 GHz BW; noise proportionally lower with output filter reduction of bandwidth to 750 MHz, 500 MHz, 250 MHz, etc.
TRANSMITTER SIZE AND POWER :	Basic unit, 4.0" x 3.25" x 7.50". Receiver controlled optical turn on of NiCad battery. Easily replaceable RFI shielded battery pack may be charged both in the transmitter and in a separate 8 battery charger.
RECEIVER :	Standard 1-3/4" h x 19" w rack mounted, with front panel controls, remote optical control of Transmitter and electrical output into 50 ohms. Four digit LED display of Calibrate Check Amplitude, Battery voltage; Operating Time on the Battery etc..
CALIBRATION :	Calibration stable to 1% over a period of one year. Calibrator in Transmitter provides 2 NS rise flat topped 1% accuracy signal turned on at Receiver, and displayed on Receiver 4 digit display.
OPTIONS :	Full Differential Attenuators, Preamp, Amp and Calibrate. Selectable 1, 2, 3, or 4 SMA Inputs. .1 to 10 US Precision Integrators. 488 Read In and Out of settings.

RA-2'

NANOFAST

PERFORMANCE WITH RELIABILITY

416 W. ERIE ST. - CHICAGO, ILLINOIS 60610 - 312-943-4223

RISE TIME AND FREQUENCY RESPONSE OF THE 1 GHz OP 300-2A OPTICAL ANALOG TRANSMISSION SYSTEM ON A 7104 SCOPE

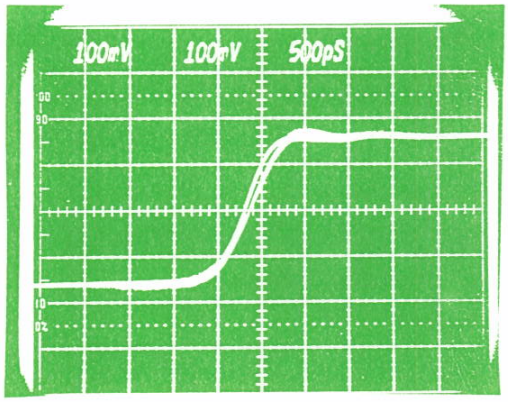

PULSE RESPONSE: SUPERIMPOSED INPUT AND OUTPUT, WITH 550 PICOSECOND RISE INPUT. THE OUTPUT OF CIRCUITRY ADDS 100 PICOSECONDS TO THE RISE. THE OUTPUT IS THE SQUARE ROOT OF THE SUM OF THE SQUARES OF THE .55 NS INPUT AND THE .35 NS RISE OF THE 1 GHz UNIT OR A TOTAL OF .65 NS. THE OUTPUT COMES UP SMOOTHLY WITH VERY LOW OVERSHOOT AND RINGING. 500 PICOSECONDS PER DIV.

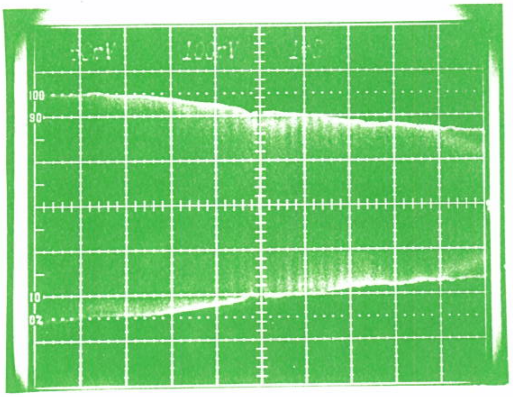

FREQUENCY SWEEP: 1 GHz SWEEP, 100 MHz / DIV WITH SUPERIMPOSED INPUT AND OUTPUT. THE OUTPUT FOLLOWS THE INPUT CLOSELY UNTIL THE 1 GHz POINT WHEN THE OUTPUT FALLS BY 3 dB AND REMAINS AT 3 dB TO 1.2 GHz.

THE SYSTEM IS COMPLETELY INDEPENDENT OF TEMPERATURE, AGING, MOVEMENT OF CABLE AND CONNECTORS, ETC. THERE ARE NO OSCILLATIONS OR LEVEL CHANGES EVEN IF THE FIBER OPTIC CONNECTOR IS MOVED. THE SYSTEM LASTS EFFECTIVELY FOREVER SINCE NO LASERS ARE USED AND THE LED CURRENT DENSITY IS LOW.

Nanofast Fiber Optic Link OP300-2A, 200MHz (Page 4 of 5)

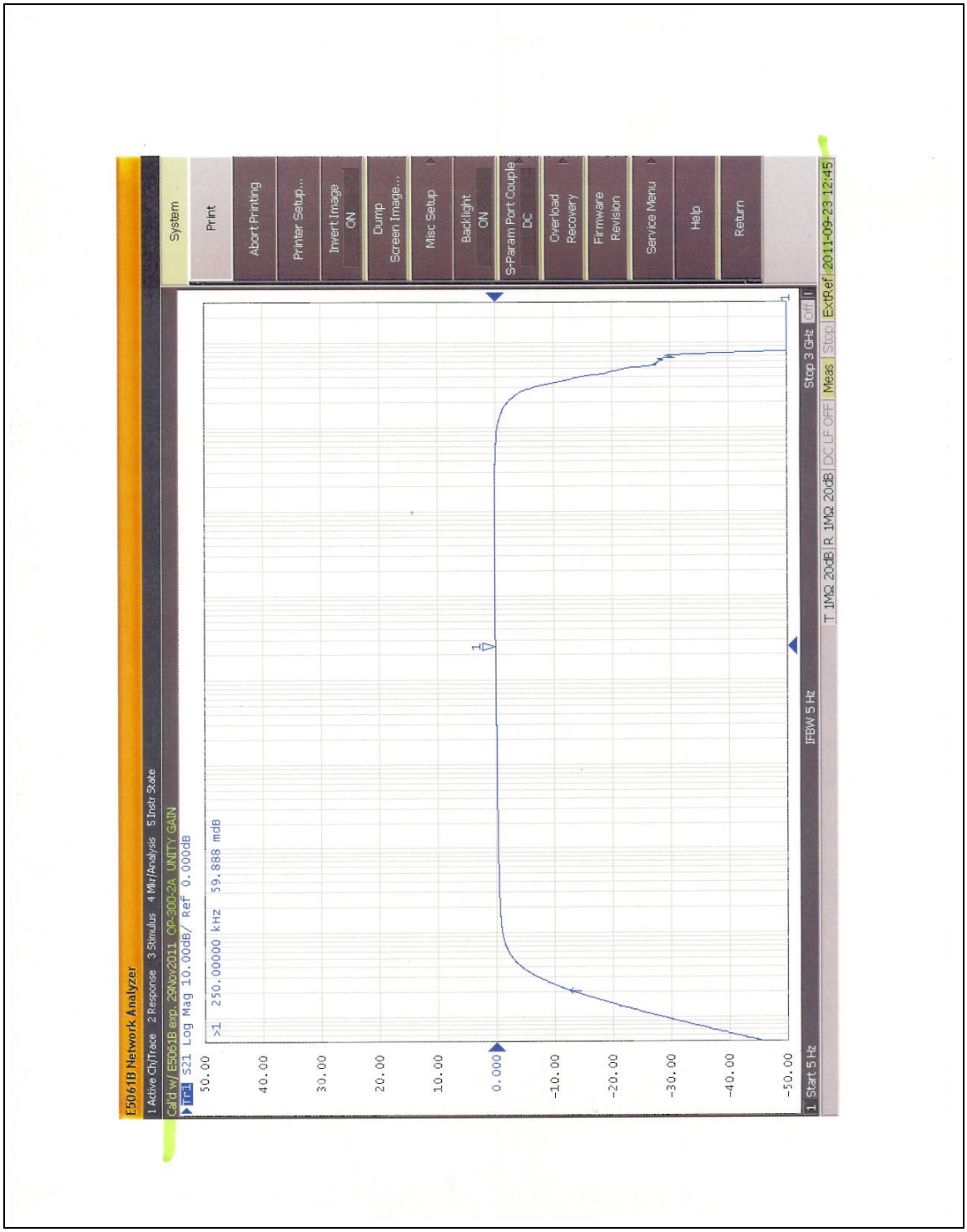

Nanofast Fiber Optic Link OP300-2A, 1000MHz (Page 5 of 5)

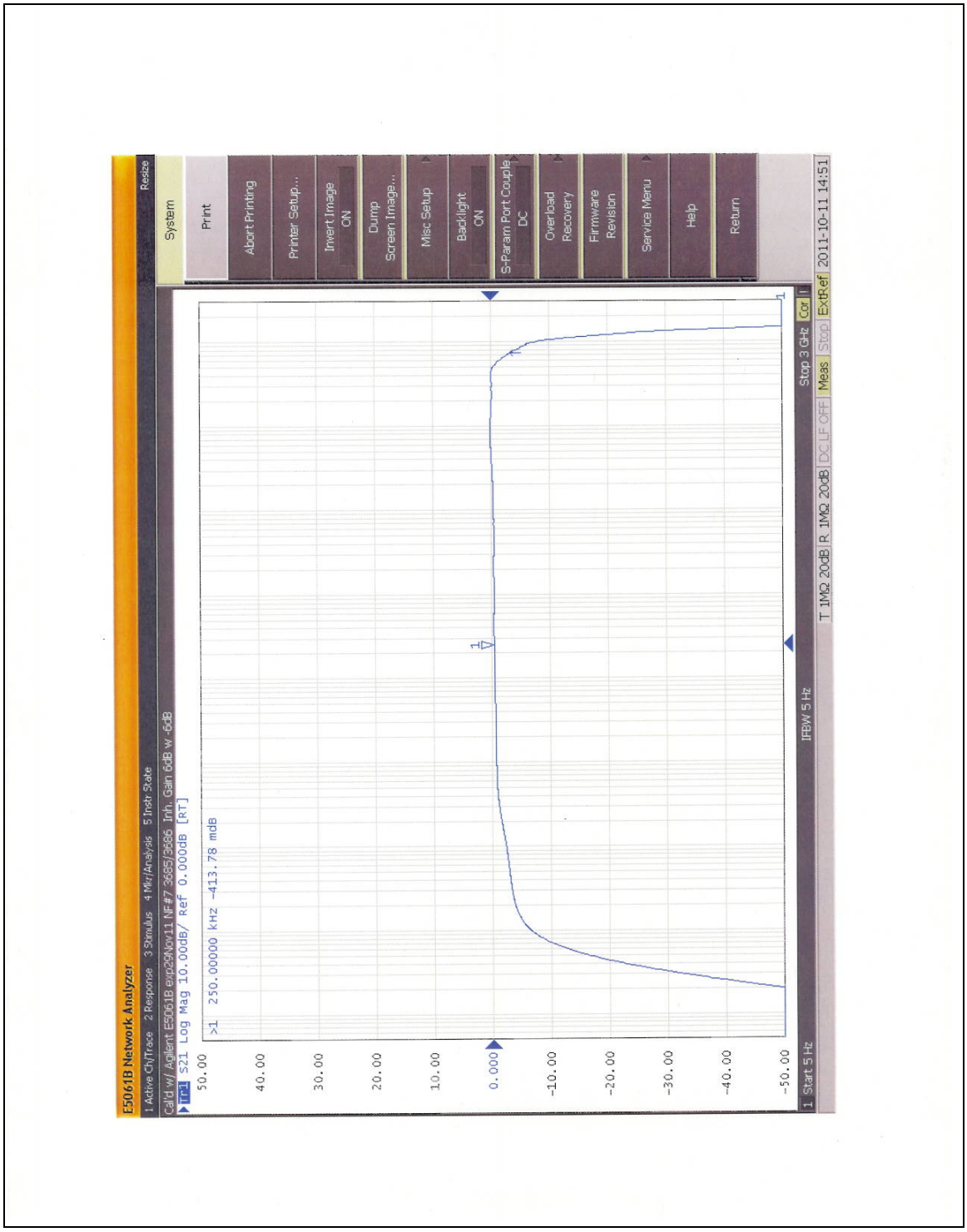

Terahertz Technologies Inc. LTX-5510 Fiber Optic Link 12.5MHz (Page 1 of 6)

Terahertz Technologies Inc.

LTX-5510

"Signal Transporter"

E/O - O/E Converter Pair

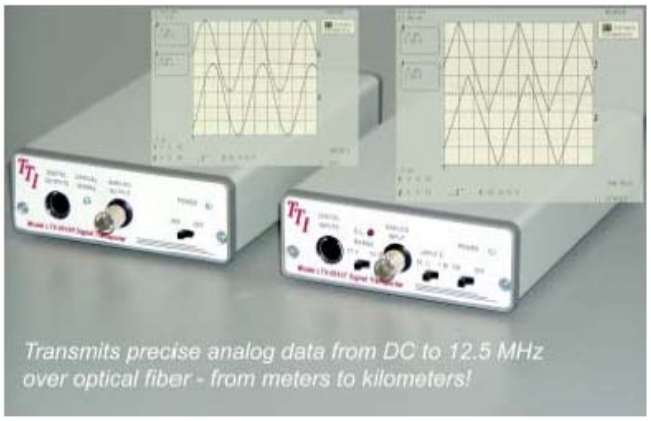

Benefits

- Transmits analog and digital simultaneously
- DC to 12. 5 MHz analog bandwidth
- Two input ranges, +/- 1 V and +/- 5 V
- Analog signal digitized to 12 bit precision
- Four independent digital channels
- DC to 20 MHz digital bandwidth

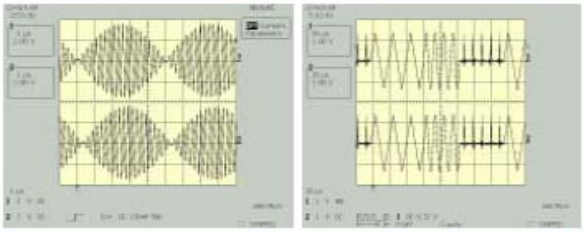

The LTX-5510 enables the precise conveyance of analog plus four channels of digital information over fiber optic links ranging from meters to more than 10 kilometers.

Incoming analog data is digitized to 12-bit precision at 50 mega-samples per second and transmitted over optical fiber at a 1 Gb/s data rate. The receiver acquires this digital data and accurately reconstructs the analog signal at the far end of the fiber optic link.

The analog signal bandwidth is from DC to 12.5 MHz (-3 dB). Two input voltage ranges are provided, +/- 1 Volt and +/- 5 Volts. The input impedance of the transmitter analog channel may be set to 50 ohms or 1 megohm (75 ohms is optional).

Multiplexed along with the analog data, are four independent TTL/CMOS/LVTTL digital signals that may be toggled at rates in excess of 20 MHz.

Two models are available. Selection depends on the fiber type and the length of the fiber optic link that is required. The LTX-5510-850 transmits at 850 nM over multi-mode fiber optic links of up to 500 meters in length, while the LTX-5510-1310 transmits at 1310 nm over single-mode fiber to cover distances in excess of 10 kilometers.

Applications include data acquistion for plasma physics experiments, signal transmission and control of equipment at high voltage potentials, transmission of high quality video, and precise noise-free signal transmission in hostile EMI environments.

Terahertz Technologies Inc. 169 Clear Road Oriskany, NY 13424
Tel: (315) 736-3642 Fax: (315) 736-4078
E-mail: sales@terahertztechnologies.com Website: www.terahertztechnologies.com

LTX-5510 Specifications

TTI reserves the rignt to change specifications w/o notice

Analog Signal Bandwidth	DC to 12.5 MHz (-3dB)
Input Voltage Ranges	+/- 1 V and +/- 5 V Full Scale
Resolution	12 - bits
Transfer Accuracy	+/- 0.1 %
Signal Latency (with one meter of fiber)	~300 nS
Sampling Rate	50 Ms/s
Input Impedance	50 Ohms or 1 Megohm, selectable
Output Drive Capabilty	+/- 5V open circuit, +/- 2 V into 50 Ohms
Output Impedance	50 Ohms
Anti-Aliasing Filter	4 - Pole Chebyshev
Digital Inputs	TTL, LVTTL, CMOS compatible
Digital Outputs	LVTTL (0 - 3.3 V)
Digital Switching Rates	0 - 12 MHz
Digital Signal Edge Uncertainty	+/-10 nS
Laser Wavelength	LTX-5510-850: 850 nm +/- 20 nm, LTX-5510-1310: 1310 nm +/- 20 nm
Optical Transmission Rate	1.0 Gb/s
Loss Budget	0 - 15 dB
Optical Return Loss	> 15 dB
Laser Safety Classification	Class I safety per FDA/CDRH and IEC-825-1 regulations
Typical Transmission Distances (850 nm)	500 M with 50/125 MM fiber, 300 M with 62.5/125 MM fiber
Typical Transmission Distances (1310 nm)	10 KM with 9/125 SM fiber
Fiber Optic Connectors	ST Type standard, FC available on request
LED Indicators Provided	Input Overload (transmitter), Optical Signal - ON (receiver)
Power Supplies	Wall Mount, Universal, US, UK. Continental Europe, and Australian Plugs Included
Power Requirements	95-260 VAC, 50-60 Hz, 16 VA Max
Operating Temperature Range	0 - 40 C
Transmitter Dimensions (mm)	175 L x 104 5 x 40 H
Receiver Dimensions (mm)	175 L x 104 5 x 40 H
Weight Each	0.46 Kg
Standard Warranty	Two years, Components and Workmanship, 30 Day Satisfaction Guarantee

We welcome the challenge of custom applications.
Call, fax, or e-mail us your requirements.

Terahertz Technologies Inc.

Terahertz Technologies Inc.
169 Clear Road
Oriskany, New York 13424 USA
(315) 736-3642 Fax (315) 736-4078
www.terahertztechnologies.com
sales@terahertztechnologies.com

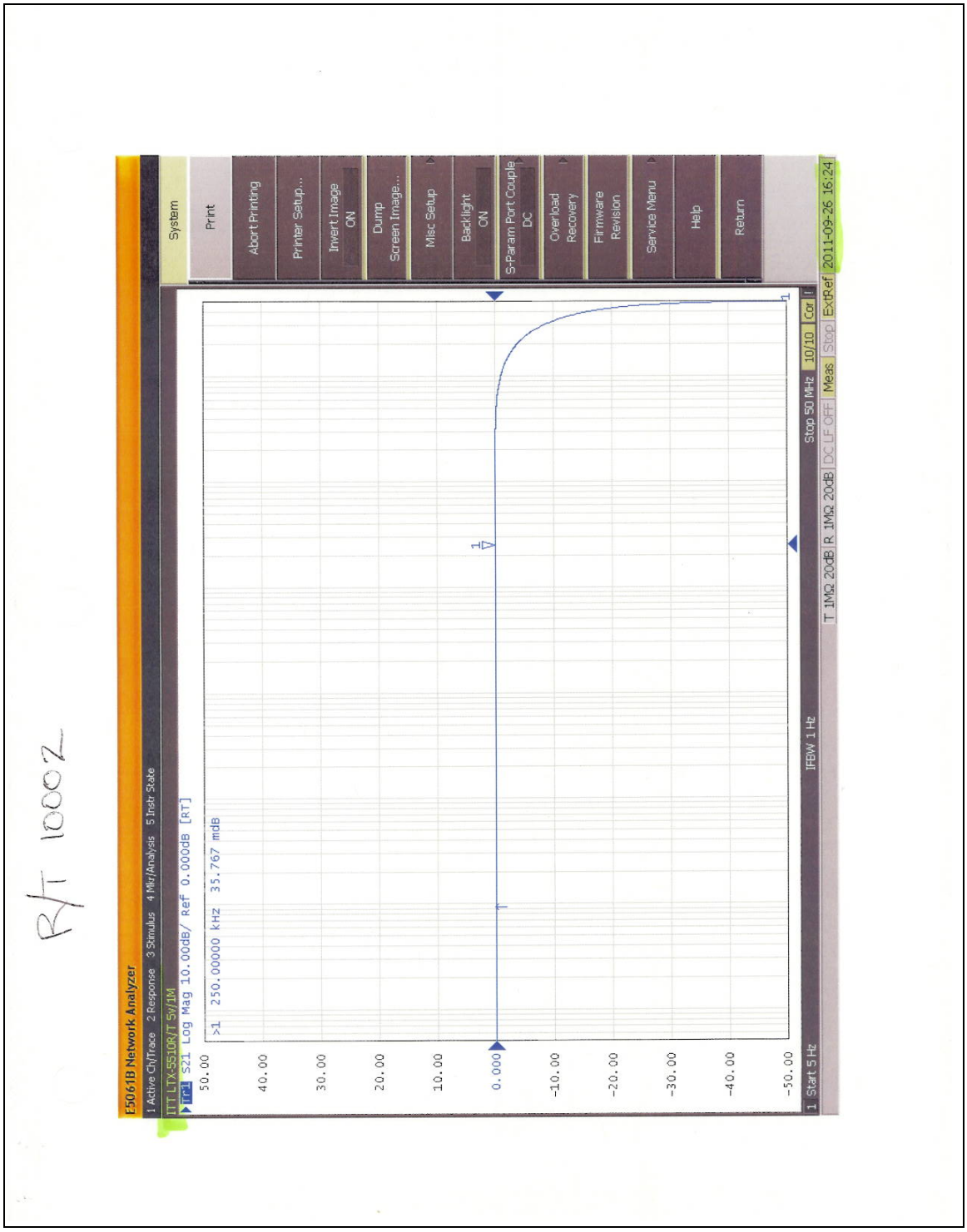
R/T 10002
E5061B Network Analyzer
1 Active Ch/Trace 2 Response 3 Stimulus 4 Mkr/Analysis 5 Instr State
ITT LTX-5510R/T 5w/1M
Tr1 S21 Log Mag 10.00dB/ Ref 0.000dB [RT]
>1 250.00000 kHz 35.767 mdB
50.00
40.00
30.00
20.00
10.00
0.000
-10.00
-20.00
-30.00
-40.00
-50.00
1 Start 5 Hz
IFBW 1 Hz
Stop 90 MHz
T 1MΩ 20dB R 1MΩ 20dB DC LF OFF Meas Stop ExtRef 2011-09-26 16:24
System
Print
Abort Printing
Printer Setup...
Invert Image ON
Dump Screen Image...
Misc Setup
Backlight ON
S-Param Port Couple DC
Overload Recovery
Firmware Revision
Service Menu
Help
Return

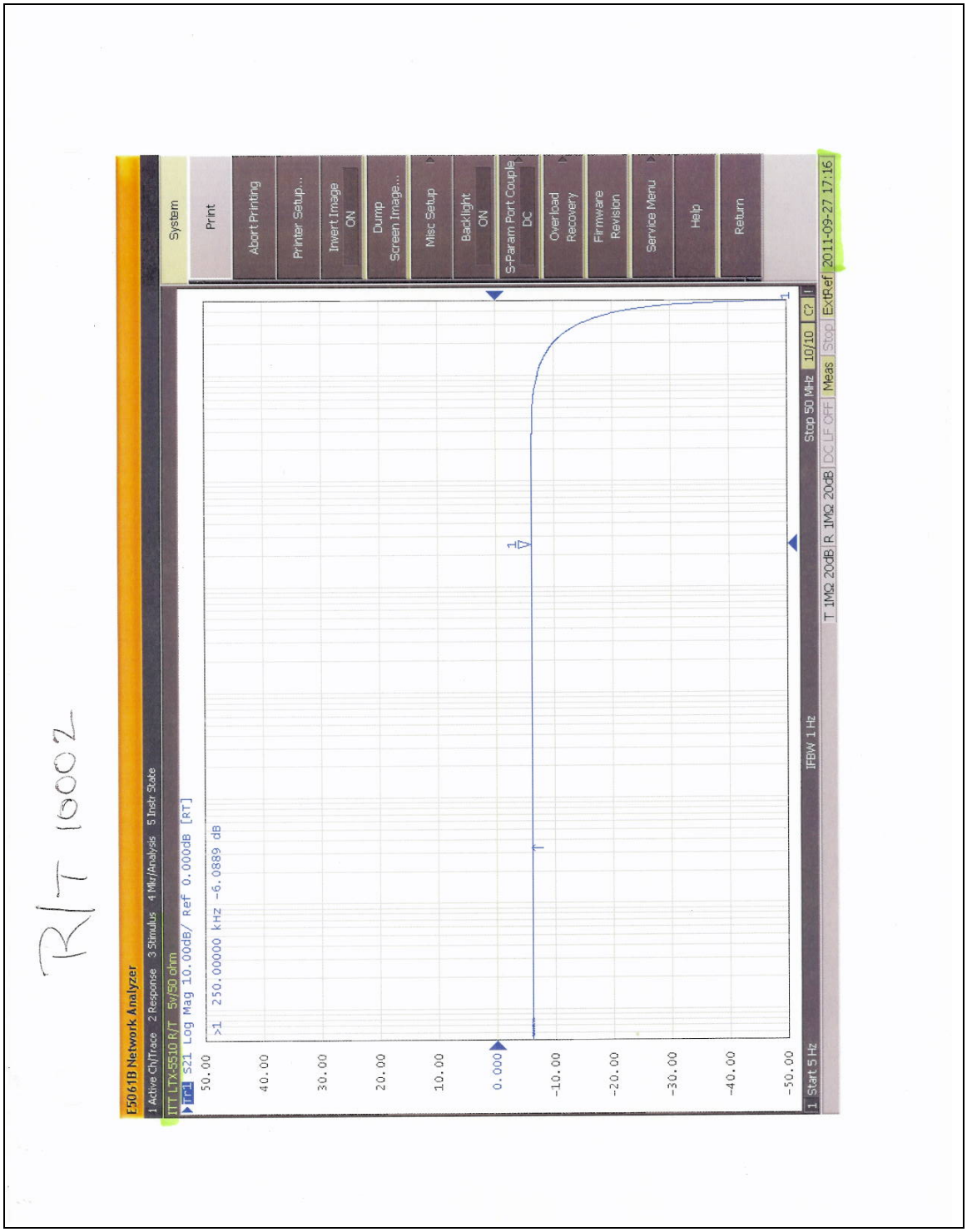
R/T 10002
E5061B Network Analyzer
1 Active Ch/Trace 2 Response 3 Stimulus 4 1Mω/Analysis 5 Instr State
ITT LTX-5510 R/T 5v/50 ohm
>1 250.00000 kHz -6.0889 dB
>1 S21 Log Mag 10.00dB/ Ref 0.000dB [RT]
50.00
40.00
30.00
20.00
10.00
0.000
-10.00
-20.00
-30.00
-40.00
-50.00
1 Start 5 Hz
IFBW 1 Hz
Stop 50 MHz
T 1MΩ 20dB R 1MΩ 20dB DC LF OFF Meas Stop ExtRef 2011-09-27 17:16
System
Print
Abort Printing
Printer Setup...
Invert Image ON
Dump Screen Image...
Misc Setup
Backlight ON
S-Param Port Couple DC
Overload Recovery
Firmware Revision
Service Menu
Help
Return

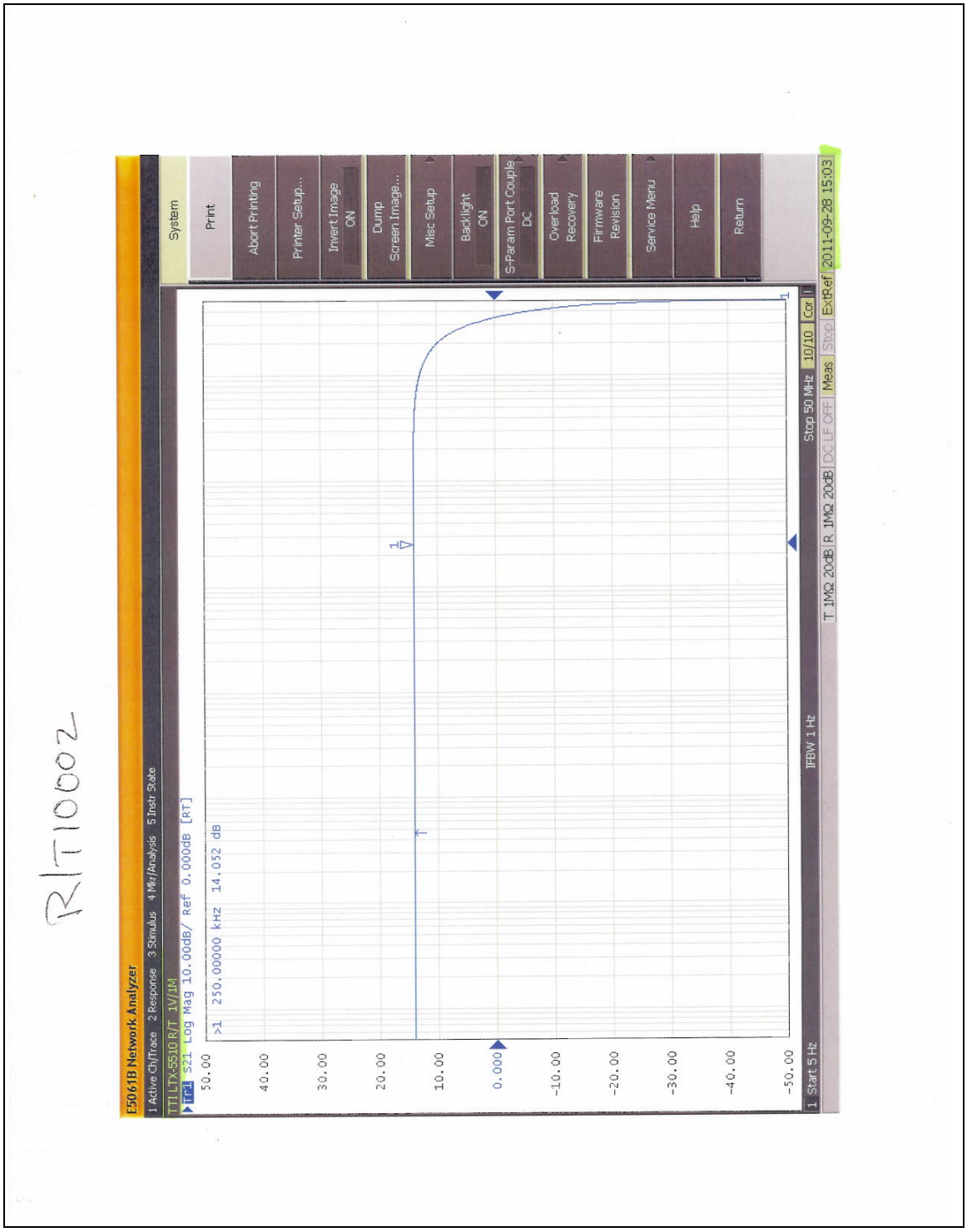
RT10002
E5061B Network Analyzer
1 Active Ch/Trace 2 Response 3 Stimulus 4 Mkr/Analysis 5 Instr State
TTI LTX-5510 R/T 1V/1M
1Pt1 S21 Log Mag 10.00dB/ Ref 0.000dB [RT]
>1 250.00000 kHz 14.052 dB
50.00
40.00
30.00
20.00
10.00
0.000
-10.00
-20.00
-30.00
-40.00
-50.00
1 Start 5 Hz
IFBW 1 Hz
Stop 50 MHz
T 1MΩ 20dB R 1MΩ 20dB DC LF OFF Meas Stop ExtRef 2011-09-28 15:03
System
Print
Abort Printing
Printer Setup...
Invert Image ON
Dump Screen Image...
Misc Setup
Backlight ON
S-Param Port Couple DC
Overload Recovery
Firmware Revision
Service Menu
Help
Return

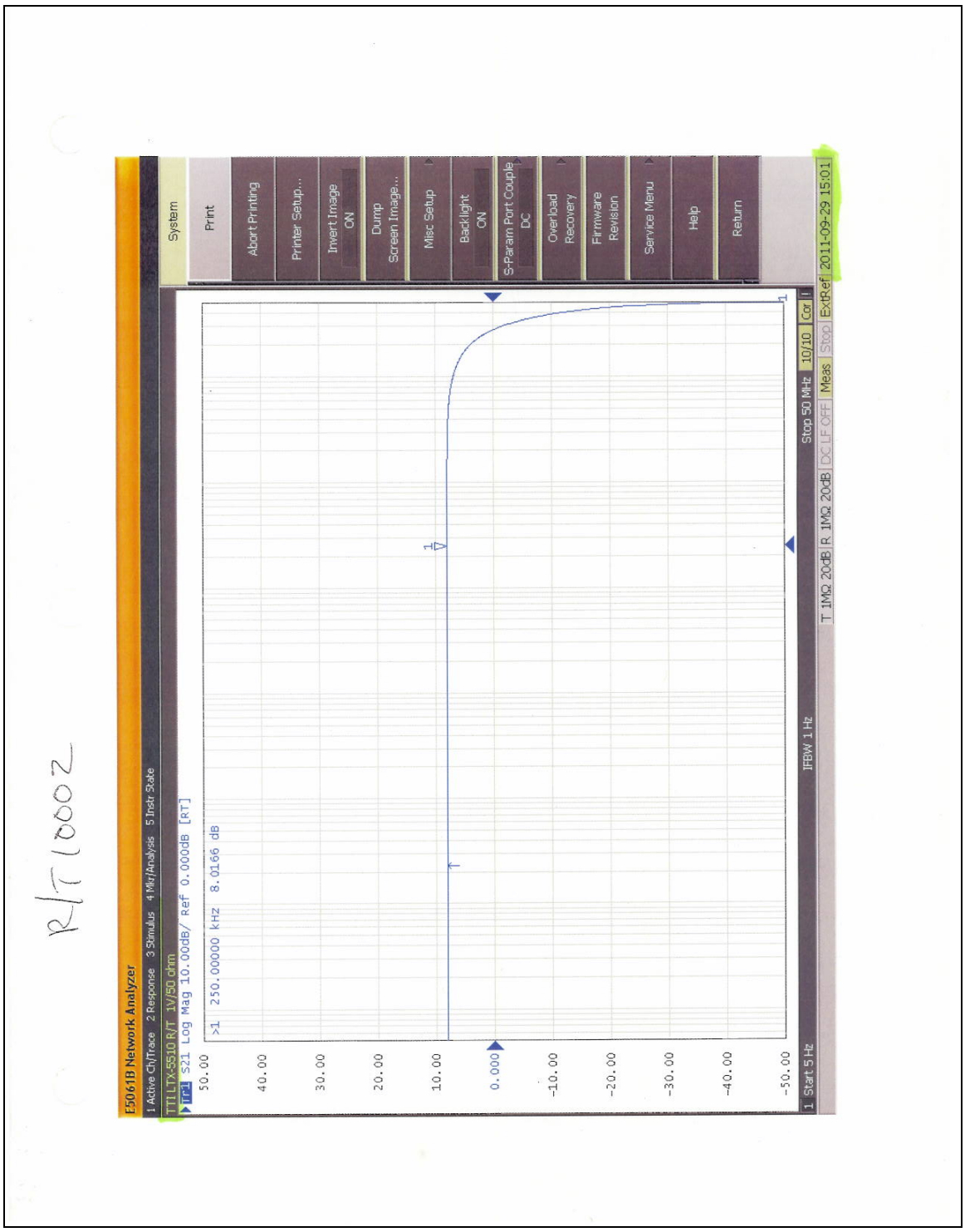
R/T 10002
E5061B Network Analyzer
1 Active Ch/Trace 2 Response 3 Stimulus 4 Mkr/Analysis 5 Instr State
TTI LTX-5510 R/T 1V/50 ohm
Tr1 S21 Log Mag 10.00dB/ Ref 0.000dB [RT]
>1 250.00000 kHz 8.0166 dB
50.00
40.00
30.00
20.00
10.00
0.000
-10.00
-20.00
-30.00
-40.00
-50.00
1 Start 5 Hz
IFBW 1 Hz
Stop 50 MHz
T 1MΩ 20dB R 1MΩ 20dB DC LF OFF Meas Stop ExtRef 2011-09-29 15:01
System
Print
Abort Printing
Printer Setup...
Invert Image ON
Dump Screen Image...
Misc Setup
Backlight ON
S-Param Port Couple DC
Overload Recovery
Firmware Revision
Service Menu
Help
Return

T&M Current Viewing Resistor (CVR) (Page 1 of 6)

T&M® RESEARCH PRODUCTS, INC.
PHONE (505) 268-0316 • 139 RHODE ISLAND ST. NE • ALBUQUERQUE, NEW MEXICO 87108-2298

SERIES A

CURRENT VIEWING RESISTORS

DESCRIPTION

Small terminating type CVR available with BNC, GR, UHF, N, HN, and C connectors. Other connector options available upon request. Standard connections are the "S" input(8-32 stud with threaded case) and BNC output connector.

FEATURES

- Fast Risetime
- Many Connector Options
- Small Size
- Broad Bandpass
- Low Inductance

SPECIFICATIONS

4 Watt Units - 3¼ Inch Case*

Model	Resistance ohms	Bandpass MHz.	Risetime nsec.	Emax joules
A-2-01	.01	400	1	16
A-5-05	.05	2000	0.18	5
A-2-005	.005	200	2	15
A-4-0025	.0025	48	8	30
A-8-001	.001	12	30	70

5 Watt Units - 3⅞ Inch Case*

Model	Resistance ohms	Bandpass MHz.	Risetime nsec.	Emax joules
A-1-05	.05	1200	0.30	20
A-2-025	.025	400	1	40
A-5-1	.10	1200	0.30	10
A-4-005	.005	48	8	60

6 Watt Units - 5 Inch Case*

Model	Resistance ohms	Bandpass MHz.	Risetime nsec.	Emax joules
A-1-1	.10	800	0.45	40
A-2-05	.05	400	1	80
A-5-2	.20	1200	0.30	20

 12-1-90

T&M Current Viewing Resistor (CVR) (Page 2 of 6)

7 Watt Unit - 5½ Inch Case*

Model	Resistance ohms	Bandpass MHz.	Risetime nsec.	Emax joules
A-5-5	.50	800	0.45	15

Standard Resistance tolerance ±4%. Closer tolerance available.
Each unit labeled with exact resistance value accurate to ±0.2%

*Case lenghts are for the SBNC-X-X model type, case lengths for other connections will vary slightly. "S" modification - Current input connection is an 8-32 stud with the case threaded ⅝-24, supplied with two nuts. Unthreaded case available if specified.

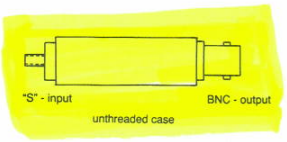

unthreaded case

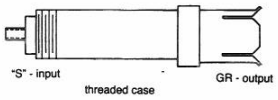

threaded case

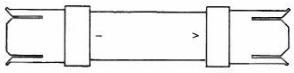
GR - input & output

I = current input end
V = signal output end

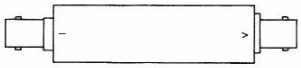
BNC - input & output

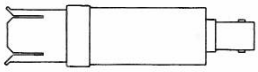

ALL CASES OUTSIDE DIAMETER - ⅝(1.59)

inch(centimeter)

ORDERING INFORMATION

When ordering specify model number, input and output connector or connections, and tolerance.
Example: SBNC-2-01, 4%; NBNC-1-05, 4%

Specifications subject to change without notice.

 12-1-90

T&M RESEARCH PRODUCTS, INC.
139 Rhode Island St. NE
Albuquerque, NM 87108-2298
Phone (505) 268-0316

Page 4

T&M Current Viewing Resistor (CVR) (Page 3 of 6)

T&M® RESEARCH PRODUCTS, INC.
PHONE (505) 268-0316 • 139 RHODE ISLAND ST. NE • ALBUQUERQUE, NEW MEXICO 87108-2298

SERIES F

CURRENT VIEWING RESISTORS

DESCRIPTION

Terminating type CVR with threaded stud and mounting flange input connections.

FEATURES

- Medium Energy Capacity
- BNC Output Connector Stardard
- High Stability at Stated Power Ratings
- Complete Enviromental Protection

SPECIFICATIONS

75 Watt Hi-wattage Units - 8 Inch Overall Length

Model	Resistance ohms	Bandpass MHz.	Risetime nsec.	Emax joules
F-250-1	.02	800	0.45	250
F-500-2	.01	200	2	500
F-1000-4	.005	48	8	1000
F-2000-8	.0025	12	30	2000
F-2500-10	.002	8	45	2500
F-4000-16	.001	3.2	113	4000
F-5000-20	.001	2.2	164	5000
F-8000-32	.000625	1	250	8000
F-10,000-40	.0005	0.58	872	10000

90 Watt Hi-wattage Units - 8 ⅞ Inch Overall Length

Model	Resistance ohms	Bandpass MHz.	Risetime nsec.	Emax joules
F-300-1	.025	800	0.45	300
F-3000-10	.0025	8	45	3000
F-16,000-40	.0008	.58	872	16000

BNC output connector supplied as standard. Other connectors available.
Standard Resistance tolerance ±4%. Closer tolerance available.
Each unit labeled with exact resistance value accurate to ±0.2%

 12-1-90

Page 7

T&M Current Viewing Resistor (CVR) (Page 4 of 6)

CONTINUOUS DUTY RATINGS

Model	Hi-Wattage	Finned Model
8"	75 watt	250 watt
8⅞"	90 watt	300 watt

The Hi-Wattage model is standard. The wattages stated are based on heavy current connections with unconfined mounting. The case temperature should not exceed 140°F(60°C). Additionally the Finned Models require 150 cubic feet(4.2 cubicmeters) per minute air flow over thier cases. The ambient temperature should not exceed 86°F(30°C). Operation above this temperature the wattage rating should be derated accordingly.

3½(8.89) Flange diameter

.71) mounting holes on 2¾(6.99) bolt circle

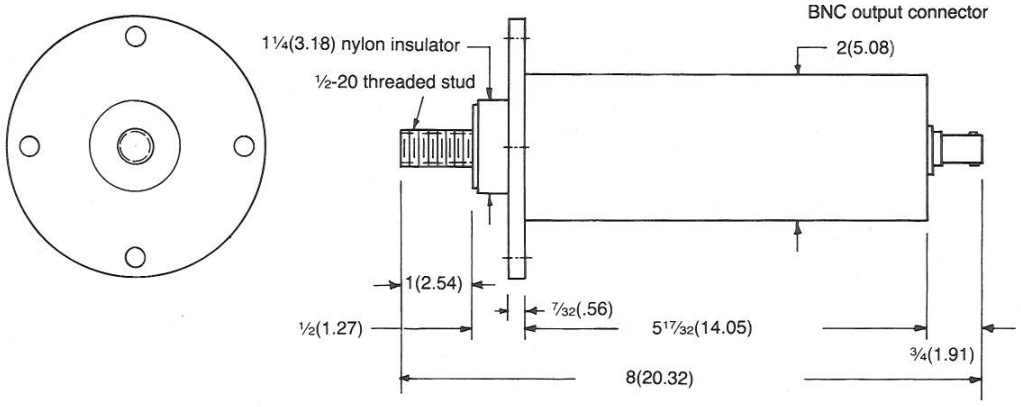

inch(centimeter)

ORDERING INFORMATION

When ordering specify model number, wattage, output connector, and tolerance.
Example: F-5000-20, 75 watts, BNC, 4%.

Specifications subject to change without notice.

 12-1-90

T&M RESEARCH PRODUCTS, INC.
139 Rhode Island St. NE
Albuquerque, NM 87108-2298
Phone (505) 268-0316

Page 8

T&M Current Viewing Resistor (CVR) (Page 5 of 6)

T&M® RESEARCH PRODUCTS, INC.
PHONE (505) 268-0316 • 139 RHODE ISLAND ST. NE • ALBUQUERQUE, NEW MEXICO 87108-2298

SERIES M

CURRENT VIEWING RESISTORS

DESCRIPTION

Terminating type CVR with threaded stud and mounting flange input connections.

FEATURES

- Medium Energy Capacity
- BNC Output Connector Stardard
- High Stability at Stated Power Ratings
- Complete Enviromental Protection

SPECIFICATIONS

1M Models - 20 Watt Hi-wattage Units - 4¾ Inch Overall Length

Model	Resistance ohms	Bandpass MHz.	Risetime nsec.	Emax joules
1M-T10*	.05	1200	0.30	75
1M-05*	.025	400	1	150
1M-1	.02	800	0.45	63
1M-2	.01	200	2	125
1M-4	.005	48	8	250
1M-8	.025	12	30	500
1M-10	.002	8	45	625
1M-16	.00125	3.2	113	1000
1M-20	.001	2.2	164	1250

2M Models - 30 watt Hi-Wattage Units - 6¾ Inch Overall Length

Model	Resistance ohms	Bandpass MHz.	Risetime nsec.	Emax joules
2M-T10*	.1	800	0.45	150
2M-05*	.05	400	1	300
2M-1	.04	400	1	125
2M-2	.02	200	2	250
2M-4	.01	48	8	500
2M-8	.005	12	30	1000
2M-10	.004	8	45	1250
2M-16	.0025	3.2	113	1250
2M-20	.002	2.2	164	2500

*These models slightly longer then stated.
BNC output connector supplied as standard. Other connectors available.
Standard Resistance tolerance ±4%. Closer tolerance available.
Each unit labeled with exact resistance value accurate to ±0.2%

 12-1-90

T&M Current Viewing Resistor (CVR) (Page 6 of 6)

CONTINUOUS DUTY RATINGS

Model	Hi-Wattage	Finned Model
1M	20 watts	75 watt
2M	30 watt	125 watt

The Hi-Wattage model is standard. The wattage for the 1M is 20 watts and the 2M is 30 watts. Both the 1M and 2M are available with cooling fins attached to thier cases. The finned model wattages are 75 watts for the 1M and 125 watts for the 2M. The wattages stated are based on heavy current connections with unconfined mounting. The case temperature should not exceed 140°F(60°C). Additionally the Finned Models require 100 cubic feet(2.8 cubicmeters) per minute air flow over thier cases. The ambient temperature should not exceed 86°F(30°C). Operation above this temperature the wattage rating should be derated accordingly.

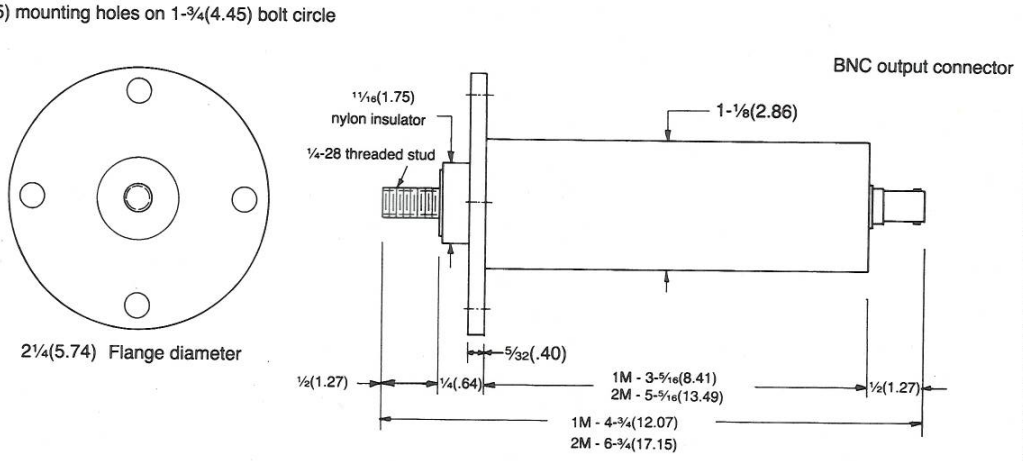

inch(centimeter)

ORDERING INFORMATION

When ordering specify model number, wattage, output connector, and tolerance. **Example:** 1M-20, 20 watts, BNC, 4%.

Specifications subject to change without notice.

 12-1-90

T&M RESEARCH PRODUCTS, INC.
139 Rhode Island St. NE
Albuquerque, NM 87108-2298
Phone (505) 268-0316

Page 6

Pearson Electronics Current Viewing Transformer (CVT) (Page 1 of 1)

PEARSON ELECTRONICS, INC.

PEARSON™ CURRENT MONITOR MODEL 110

Sensitivity	0.1 Volt/Ampere +1/-0%
Output resistance	50 Ohms
Maximum peak current	5000 Amperes
Maximum rms current	65 Amperes
Droop rate	0.8 %/millisecond
Useable rise time	20 nanoseconds
Current time product	0.5 Ampere-second max.*
Low frequency 3dB cut-off	1 Hz (approximate)
High frequency 3dB cut-off	20 MHz (approximate)
I/f figure	1.5 peak Amperes/Hz
Output connector	BNC (UG-290A/U)
Operating temperature	0 to 65 °C
Weight	22 ounces

* Maximum current-time product can be obtained by using core-reset bias as described in the *Application Notes*. 0.2 Ampere-second is typical without bias.

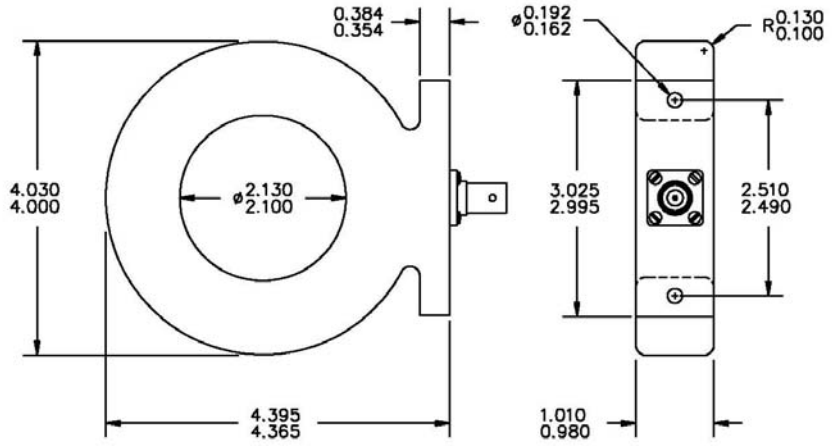

Pearson Electronics, Inc. • 4009 Transport Street • Palo Alto, CA 94303
Telephone 650-494-6444 • FAX 650-494-6716 • www.pearsonelectronics.com

Tektronix P6015A High Impedance Voltage Probe (Page 1 of 2)

Table 1-3: Warranted Electrical Characteristics

Characteristic	Information	
Maximum input voltage		
DC + peak AC[1]	1.5 kV to 20 kV. See frequency derating curve in Figure 1-4. (DC plus peak AC rating is limited to temperatures below 35° C.)	
Peak pulse	40 kV[a] (Never exceed 20 kV rms) Duty cycle derating - 100 ms maximum duration at 10% maximum duty cycle. See duration and duty cycle derating curve in Figure 1-5. Altitude derating - Peak pulse derated linearly from 40 kV at 8000 feet (2440 m) to 30 kV at 15,000 feet (4570 m) altitude. Relative Humidity (RH) derating - Voltage derated with increasing temperature and relative humidity (see Figure 1-7).	
Bandwidth (-3 dB)	Test conditions: Test oscilloscope bandwidth must be ≥100 MHz, Z_{source} = 25 Ω	
10-ft cable	75 MHz	
25-ft cable	25 MHz	
Rise Time[2]		
10-ft cable	≤4.67 ns (calculated from bandwidth)	
25-ft cable	≤14 ns (calculated from bandwidth)	
DC attenuation	1000:1 ±3% (Excluding oscilloscope error)	Test conditions: Oscilloscope input resistance must be 1 MΩ ±2%

1 **Characteristic not checked in manual**

2 **T_r (ns) = .35/BW (MHz)**

Typical and Nominal Characteristics

This section lists the various typical and nominal characteristics that describe the P6015A High Voltage Probe.

Nominal characteristics are determined by design and/or inspection. Nominal characteristics do not have tolerance limits.

Typical characteristics are described in terms of typical or average performance. Typical characteristics are not warranted.

Table 1-5: Typical Electrical Characteristics

Characteristic	Information
Input resistance	100 MΩ ±2%. See Figure 1-8 for typical input impedance curve.
Input capacitance	≤3 pF when probe is properly LF compensated. See Figure 1-8 for typical input impedance curve.
LF compensation range	7 pF to 49 pF
Aberrations	25% p-p for the first 200 ns on a 100 MHz oscilloscope when used with 10 in (25.4 cm) ground lead. <10% p-p typical after first 200 ns; ±5% after the first 400 ns.
Temperature coefficient of DC attenuation	0.006% per degree C[1]
Voltage coefficient of DC attenuation	0.018% per kV
Delay time	10 ft cable: 14.7 ns 25 ft cable: 33.3 ns

1 **Resistor temperature rose 60°C at 20 kV rms over a 30 minute period.**

SNL 50kΩ and 5kΩ Voltage Probes (Page 1 of 1)

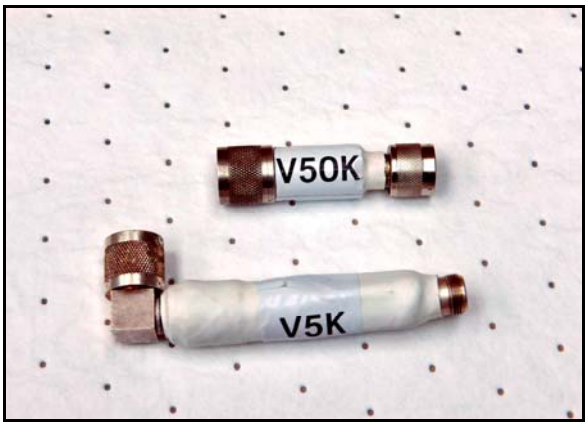

50kΩ and 5kΩ Voltage Probes

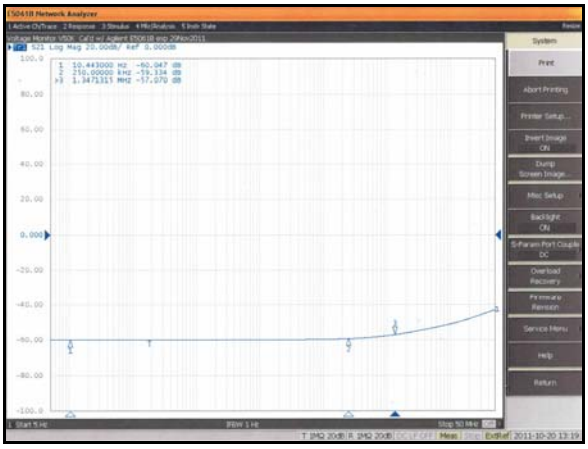

50kΩ Voltage Probe (-60dB, 5Hz-1MHz) terminated into 50Ω

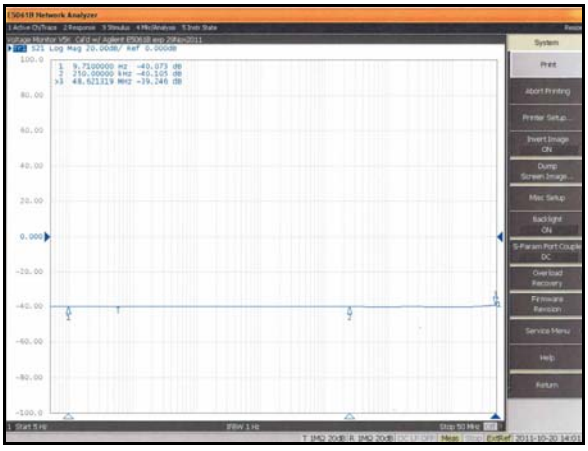

50kΩ Voltage Probe (-40dB, 5Hz-1MHz) terminated into 50Ω

Electric Field Probes, Prodyn AD-10 (Page 1 of 1)

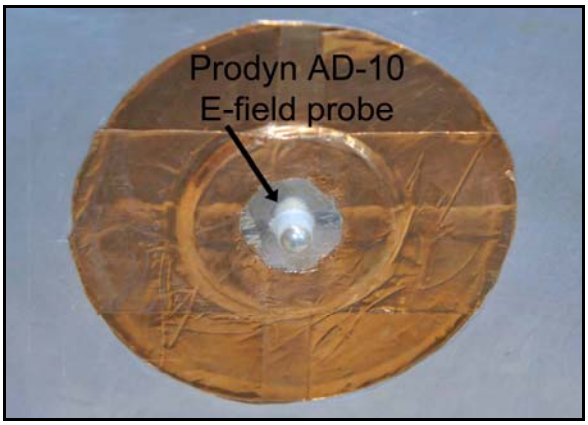

Prodyn Model AD-10

PRODYN's precision high frequency ground plane electric field sensors are designed to measure time rate-of-change of electric displacement over a wide frequency spectrum. They can also be used to measure the time rate-of-change of surface current density. Surface or thru-the-ground plane output configurations are available to allow testing flexibility. Testing has shown the asymptotic sensing element design to have less capacitance and higher upper frequency characteristics compared to older HSD (Hemi-Spherical D-Dot) design. The equation pertinent to these devices is:

$$V_o = R\,A_{eq}\frac{dD}{dt} \quad \text{or} \quad V_o = R\,A_{eq}\frac{d\rho_s}{dt}$$

Where: V_o = sensor output (Volts)

R = sensor characteristic load impedance (50 ohms)

Aeq = sensor equivalent area (m^2)

$\vec{D}$ = Magnitude of electric displacement vector ($D = \varepsilon_o E$ in Coul / m^2)

ρ_s = surface current density (Coul/m^2)

MODEL

Electrical Spec	AD-S(10)	AD-(10)	AD-S(110)	AD-110	AD-S(30)	AD-30(A)	AD-S(60)	AD-60(A)
Equiv. Area (A_{eq})	$1x10^{-4}m^2$	$1x10^{-4}m^2$	$1x10^{-3}m^2$	$1x10^{-3}m^2$	$1x10^{-2}m^2$	$1x10^{-2}m^2$	$1x10^{-1}m^2$	$1x10^{-1}m^2$
Freq. Response (3 db point)	>10GHz	>10GHz	>3.5GHz	>3.5GHz	>1GHz	>1GHz	>400MHz	>400MHz
Risetime (tr 10-90)	<.03ns	<.03ns	<.10ns	<.10ns	<.35ns	<.35ns	<1.0ns	<1.0ns
Maximun Output	±150V	±150V	±1KV	±1KV	±4KV	±4KV	±5KV	±5KV
Output Connector (Female)	SMA	SMA	SMA	SMA	SMA	SMA	Type N	Type N

Electric Field Probes, SNL 4.3mm Monopole (Page 1 of 1)

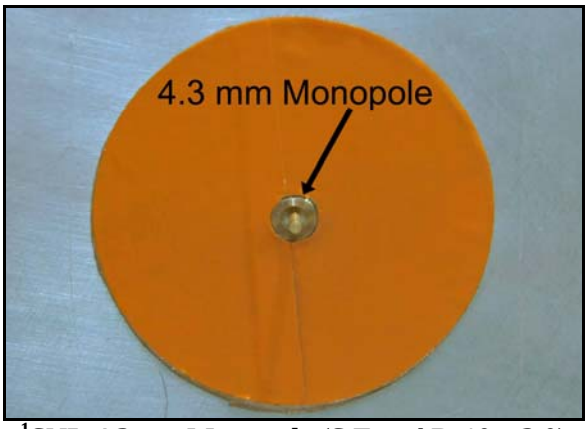

[1]SNL 4.3mm Monopole (S.F. = AD-10 x 2.0)

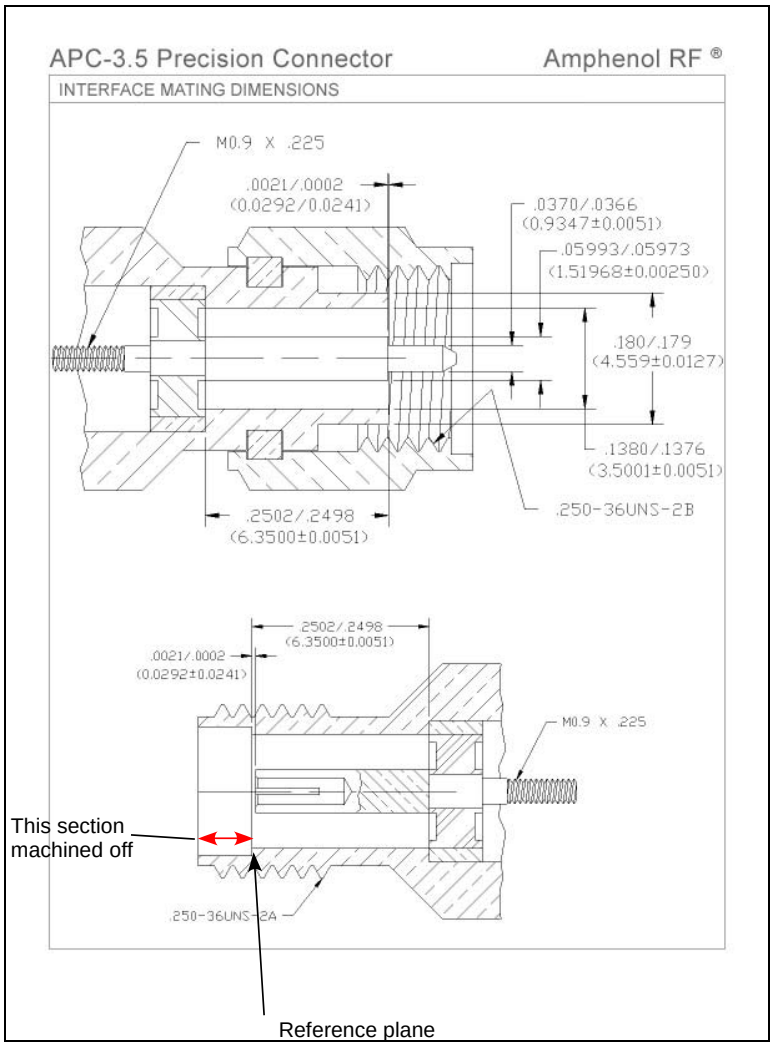

[1] Constructed with APC-3.5 precision connector, Monopole (Mating Pin) extends 4.3mm beyond reference plane

Photometric Camera, Phantom V7 (Page 1 of 1)

Phantom v7.3

800 x 600 at 6,688 frames-per-second, and up to 500,000 fps with the new "turbo mode."

THE UNDISPUTED KING OF SPEED

VRI expands the capabilities of its Phantom v7 Series cameras with the Phantom v7.3. Its full frame 4:3 aspect ratio 14-bit image depth (standard) 800 x 600 active pixel CMOS sensor the camera sports an exception recording rate of 6,688 frames per second at full resolution, and over 190,000 fps (standard mode) or an astounding 500,000 fps (turbo mode) at a reduced resolution adjustable in 32 x 8 pixel increments.

With all the features Phantom camera users have become accustomed to the v7.3 has added a larger memory module option for longer recording times, and a continuous video output HD/SDI interface.

- ***Full frame 4:3 aspect ratio CMOS sensor composed of 800 x 600 pixels***
- ***14-bit image depth (standard)***
- ***6,688 frames per second full resolution, up to 190,000 fps (standard mode), 500,000 fps (turbo mode)***
- ***"CAR" (Continuously Adjustable Resolution) in 32 x 8 pixel increments***
- ***4800 ISO/ASA monochrome, 1200 ISO/ASA color sensitivity equivalency***
- ***Global on-chip shuttering to 2 microseconds, optional 1 µs (standard mode); fixed 1 µs (turbo mode)***
- ***"EDR" Extreme Dynamic Range ™ and Auto Exposure control***
- ***PIV - Particle Image Velocimetry (standard)***
- ***Up to 16 Gigabytes DRAM, 24 Gigabytes non-volatile flash memory (optional)***
- ***IRIG-B timing capture, modulated or unmodulated, IRIG lock w/phase shift***
- ***Continuous video output (NTSC, PAL, HD/SDI 720p, 1080p, 1080i, 1080psf)***
- ***Optional continuous data streaming up to 2000 fps (8-bits)***
- ***Automated multiple session recording for remote unmanned operation***
- ***Gigabit Ethernet or RS232 control***

Datasheet - Subject to Change

Revision: 10.11.2007

Intentionally Left Blank

DISTRIBUTION

Number	Mail Stop	Name	Dept.
1 (electronic)	MS0492	K. C. Chen	0411
1 (electronic)	MS0492	T. Hall	0411
1 (electronic)	MS0405	J. L. Means	0433
1	MS0405	K. O. Merewether	0433
1 (electronic)	MS1139	E. Bystrom	1535
1 (electronic)	MS1181	L. X. Schneider	1650
1 (electronic)	MS1152	M. Caldwell	1652
1 (electronic)	MS1152	R. M. Coats	1652
1	MS1152	R. E. Jorgenson	1652
3	MS1152	L. K. Warne	1652
1 (electronic)	MS1178	M. L. Kiefer	1653
1 (electronic)	MS1152	J. M. Jojola	1653
2	MS1152	L. E. Martinez	1653
1 (electronic)	MS1152	S. L. Montoya	1653
1 (electronic)	MS0447	P. D. Hoover	2111
1 (electronic)	MS0447	E. G. Garavaglia	2111
1 (electronic)	MS0447	M. E. Morris	2111
1 (electronic)	MS0438	T. R. Jones	2810
1 (electronic)	MS0899	RIM - Reports Management	9532
1 (electronic)	MS0359	D. L. Chavez	1911


Sandia National Laboratories